

AD-777 898

**GROSS VOIDED FLAME ARRESTERS FOR
FUEL TANK EXPLOSION PROTECTION**

Terence Dixon

Boeing Aerospace Company

Prepared for:

Air Force Aero Propulsion Laboratory

February 1974

DISTRIBUTED BY:

NTIS

**National Technical Information Service
U. S. DEPARTMENT OF COMMERCE
5285 Port Royal Road, Springfield Va. 22151**

NOTICE

When Government drawings, specifications, or other data are used for any purpose other than in connection with a definitely related Government procurement operation, the United States Government thereby incurs no responsibility nor any obligation whatsoever; and the fact that the government may have formulated, furnished, or in any way supplied the said drawings, specifications, or other data, is not to be regarded by implication or otherwise as in any manner licensing the holder or any other person or corporation, or conveying any rights or permission to manufacture, use, or sell any patented invention that may in any way be related thereto.

ACCESSION for		
NTIS	Write Section	<input checked="" type="checkbox"/>
DDC	Self Section	<input type="checkbox"/>
UNANNOUNCED		<input type="checkbox"/>
JUSTIFICATION		
BY		
DISTRIBUTION/AVAILABILITY CODES		
Dist.	AVAIL. and/or	SPECIAL
A		

Copies of this report should not be returned unless return is required by security considerations, contractual obligations, or notice on a specific document.

UNCLASSIFIED

SECURITY CLASSIFICATION OF THIS PAGE (When Data Entered)

AD 777898

REPORT DOCUMENTATION PAGE		READ INSTRUCTIONS BEFORE COMPLETING FORM
1. REPORT NUMBER AFAPL-TR-73-124	2. GOVT ACCESSION NO.	3. RECIPIENT'S CATALOG NUMBER
4. TITLE (and Subtitle) GROSS VOIDED FLAME ARRESTERS FOR FUEL TANK EXPLOSION PROTECTION		5. TYPE OF REPORT & PERIOD COVERED Final, May 1, 1972 to Oct. 30, 1973
7. AUTHOR(s) TERENCE DIXON		6. PERFORMING ORG. REPORT NUMBER
9. PERFORMING ORGANIZATION NAME AND ADDRESS BOEING AEROSPACE COMPANY SEATTLE, WA 98124		8. CONTRACT OR GRANT NUMBER(s) F33615-72-C-1597
11. CONTROLLING OFFICE NAME AND ADDRESS AIR FORCE AERO PROPULSION LABORATORY WRIGHT-PATTERSON AFB, OH 45433		10. PROGRAM ELEMENT, PROJECT, TASK AREA & WORK UNIT NUMBERS PROJ. 3048, TASK 304807, Work Unit 30480745
14. MONITORING AGENCY NAME & ADDRESS (if different from Controlling Offi. e)		12. REPORT DATE FEBRUARY 1974
		13. NUMBER OF PAGES 502
		15. SECURITY CLASS. (of this report) UNCLASSIFIED
		15a. DECLASSIFICATION DOWNGRADING SCHEDULE
16. DISTRIBUTION STATEMENT (of this Report) APPROVED FOR PUBLIC RELEASE; DISTRIBUTION UNLIMITED		
17. DISTRIBUTION STATEMENT (of the abstract entered in Block 20, if different from Report)		
18. SUPPLEMENTARY NOTES Reproduced by NATIONAL TECHNICAL INFORMATION SERVICE U. S. Department of Commerce Springfield VA 22151		
19. KEY WORDS (Continue on reverse side if necessary, and identify by block number) FLAME ARRESTERS SPARK IGNITION FUEL TANK INCENDIARY IGNITION EXPLOSIONS FLAME PROPAGATION GUNFIRE		
20. ABSTRACT (Continue on reverse side if necessary and identify by block number) In this research test program, new materials were investi- gated for use as flame arresters within gross voided aircraft fuel tankages. The program was developed to reduce the present weight penalties associated with fully packed (10% to 15% voided) fuel tanks, using reticulated polyurethane foam. Previous work demon- strated a low-density, 25-pore-per-inch (PPI) foam explosion sup- pression system with 80% to 90% voiding when the source was (Continued)		

DD FORM 1 JAN 73 1473 EDITION OF 1 NOV 65 IS OBSOLETE

UNCLASSIFIED

SECURITY CLASSIFICATION OF THIS PAGE (When Data Entered)

UNCLASSIFIED

SECURITY CLASSIFICATION OF THIS PAGE(When Data Entered)

(Block 20 Continued)

spark ignition. The ignition sources varied throughout the total program and included a spark, incendiary igniter (developed by AFAPL/SFH) and .50 caliber API gunfire.

An industry search resulted in 40 materials being selected for initial screening tests within a flame tube apparatus. Each material was rated for flame arresting characteristics and air flow pressure drop. As a result of these tests, nine materials were further tested in an 18.0-inch-diameter, variable geometry test apparatus that allowed the incendiary igniter to be used for ignition. Data plots were obtained from both these modes of test that related thickness of material required for burn-through versus flame speed (spark ignition) and initial pressure (spark and incendiary ignition). Resulting from these tests, five materials and combinations of materials were selected for full-scale tests within a simulated fuselage, small wing and large wing tankage in various void configurations.

This program has concluded that fuel tank voiding up to and exceeding 80% is attainable within certain tankage configurations and with specific arrester materials. The ignition source has been shown to be an important consideration.

UNCLASSIFIED

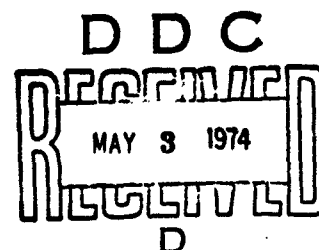
SECURITY CLASSIFICATION OF THIS PAGE(When Data Entered)

ia

GROSS VOIDED FLAME ARRESTERS
FOR FUEL TANK EXPLOSION PROTECTION

Terence Dixon

Approved for public release;
Distribution unlimited.

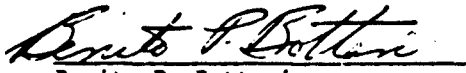


FOREWORD

This report was prepared by Terence Dixon, Damage Mechanisms Group of The Boeing Aerospace Company, Seattle, Washington. The author wishes to thank Doctor J. Romero, who formulated the basic mathematical model. The work reported herein was carried out under contract number F33615-72-C-1597, Project 3048, "Fuels, Lubrication and Fire Protection," Task 304807, "Aerospace Vehicle Fire Protection," work unit 30480745, "Gross Voided Flame Arresters for Fuel Tank Explosion Protection" and was administered by the Fire Protection Branch, Air Force Aero Propulsion Laboratory, Air Force Systems Command, Wright-Patterson Air Force Base, Ohio with A. J. Ferrenberg (AFAPL/SFH) as Project Engineer.

This report describes the results of work conducted during the period May 1, 1972 to October 30, 1973.

This technical report has been reviewed and is approved.


Benito P. Botteri
Chief, Fire Protection Branch
Fuels and Lubrication Division

ABSTRACT

In this research test program, new materials were investigated for use as flame arresters within gross voided aircraft fuel tankages. The program was developed to reduce the present weight penalties associated with fully packed (10% to 15% voided) fuel tanks, using reticulated polyurethane foam. Previous work demonstrated a low-density, 25-pore-per-inch (PPI) foam explosion suppression system with 80% to 90% voiding when the source was spark ignition. The ignition sources varied throughout the total program and included a spark, incendiary igniter (developed by AFAPL/SFH) and .50 caliber API gunfire.

An industry search resulted in 40 materials being selected for initial screening tests within a flame tube apparatus. Each material was rated for flame arresting characteristics and air flow pressure drop. As a result of these tests, nine materials and combinations of these materials were further tested in an 18.0-inch-diameter, variable geometry test apparatus that allowed the incendiary igniter to be used for ignition. Data plots were obtained from both these modes of test that related thickness of material required for burn-through versus flame speed (spark ignition) and initial pressure (spark and incendiary ignition). Resulting from these tests, five materials and combinations of materials were selected for full-scale tests within a simulated fuselage, small wing and large wing tankage in various void configurations.

This program has concluded that fuel tank voiding up to and exceeding 80% is attainable within certain tankage configurations and with specific arrester materials. The ignition source has been shown to be an important consideration.

CONTENTS

	<u>Page</u>
SECTION I - INTRODUCTION	1
SECTION II - SUMMARY	5
SECTION III - PROGRAM DESCRIPTION	15
SECTION IV - TASK I MODE 1A TEST PROGRAM	19
1.0 Test Apparatus: 4.0-Inch Flame Tube	19
2.0 Industry Search and Material Tested	23
3.0 Instrumentation	33
4.0 Ignition System	35
5.0 Test Procedure	35
6.0 Results and Discussion of Results	40
7.0 Conclusions and Recommendations	49
SECTION V - TASK I MODE IB TEST PROGRAM	53
1.0 Test Apparatus	53
2.0 Material Description	57
3.0 Instrumentation	59
4.0 Ignition System	59
5.0 Test Procedure	63
6.0 Results and Discussion of Results	68
7.0 Conclusions and Recommendations	85
SECTION VI - TASK I MODE II TEST PROGRAM	89
1.0 Material Description	89
2.0 Test Configuration	89
3.0 Instrumentation	90
4.0 Ignition Systems	95
5.0 Test Procedure	95
6.0 Results and Discussion of Results	96
7.0 Conclusions and Recommendations	111
SECTION VII - MATERIAL PROPERTY DETERMINATION	113

Preceding Page Blank

4

CONTENTS (Continued)

	<u>Page</u>
SECTION VIII - ANALYSIS	117
1.0 General Overpressure Derivation	117
2.0 Steady State Mathematical Model	119
3.0 Dynamic Mathematical Model	121
SECTION IX - TASK II TEST PROGRAM	159
1.0 Material Description	159
2.0 Test Configuration General	159
3.0 Instrumentation	173
4.0 Ignition Systems	183
5.0 Test Procedure	183
6.0 Results and Discussion of Results	201
7.0 Conclusions and Recommendations	223
SECTION X - TASK III TEST PROGRAM	225
1.0 Material Description	225
2.0 Test Configuration	226
3.0 Instrumentation	227
4.0 Ignition Systems	227
5.0 Test Procedure	227
6.0 Results and Discussion of Results	227
7.0 Conclusions and Recommendations	259
APPENDIX A TASK I TEST DATA	261
APPENDIX B TASK II TEST DATA	417
APPENDIX C TASK III TEST DATA	455
REFERENCES	502

TABLES

<u>Table</u>		<u>Page</u>
I	Data Summary Table for Selected Materials	69
II	Mixing Bomb Sampler Pressure Data	81
III	Instrumentation Listing	94
IV	Displacement Data	114
V	Density and Retention Data JP5	115
VI	Fuselage Tankage, Instrument List	184
VII	Small Wing Tankage Instrument List	185
VIII	Large Wing Tankage Instrument List	186
A-I	4.0-Inch Flame Tube Data Summary	262
A-II	Carbon Fiber Pressure Drop Data	281
A-III	25-PPI Pressure Drop Data	290
A-IV	GAF (Standard Felt) Pressure Drop	292
A-V	20-Mesh Stainless Steel Screen Pressure Drop Data	294
A-VI	35-Mesh Stainless Steel Screen Pressure Drop Data	296
A-VII	Custom Material 7611XP Pressure Drop Data	298
A-VIII	10-Oz Glass Cloth Pressure Drop Data	300
A-IX	3M Scotch Brite Pressure Drop Data	302
A-X	KCF-100 Carbon Fiber Cloth Pressure Drop Data	304
A-XI	KCF-100 Standard Carbon Fiber Cloth Pressure Drop Data	306
A-XII	10-PPI Foam Pressure Drop Data	308
A-XIII	Hough Industries HL 1106 and HL 1110 Pressure Drop Data	310
A-XIV	25 PPI Research Foam Pressure Drop Data	313
A-XV	Variable Geometry Tank Test Data	315
A-XVI	Data Correlation of Volume Relationships	324
A-XVII	Variable Geometry Tank Burn Time Data	391
A-XVIII	Fuselage Tank Test Data Summary	400
B-I	Fuselage Tank Test Data Summary	418
B-II	Small Wing Tankage Test Data Summary	427
B-III	Large Wing Tankage Test Data Summary	443

TABLES (Continued)

<u>Table</u>		<u>Page</u>
C-I	Fuselage Tank Test Data Summary	456
C-II	Small Wing Tankage Test Data Summary	474
C-III	Large Wing Tankage Test Data Summary	493

ILLUSTRATIONS

<u>Figure</u>		<u>Page</u>
1	Program Flow Chart	16
2	Arrester Concept Aircraft Application and Variable Geometry Test Apparatus	17
3	4.0 Inch Flame Tube Test Schematic	20
4	4.0 Inch Flame Tube Test Apparatus	21
5	Photo-Cell Locations for 4.0 Inch Flame Tube Tests	22
6	Air Flow Pressure Drop Apparatus Schematic	24
7	Instrumentation Schematic	34
8	4.0 Inch Flame Tube Instrumentation Listing	34
9	Mode 1A Screening Tests 4.0 Inch Flame Tube	36
10	Variations of Fuel-to-Air (Volume) Ratios	37
11	Typical Data Traces	41
12	Typical Pressure Versus Time Traces for Various Bomb Ignition Locations	42
13	Arrester Material Pressure Drop Data Summary	48
14	Variable Geometry Test Apparatus	54
15	Variable Geometry Test Apparatus (Foam Installation)	55
16	Variable Geometry Flame Tube Test Schematic	56
17	Variable Geometry Test Apparatus Sectional Layout	58
18	Instrumentation Flow Diagram	60
19	Incendiary Igniter Firing Circuit	61
20	Igniter Assembly	62
21	Igniter Charge Housing	62
22	Typical Arrester Installation in the Variable Geometry Apparatus	64
23	Control Console	67
24	Typical Variable Geometry Pressure Traces	72
25	Typical Variable Geometry Pressure Traces	73
26	Typical Pressure Versus Time Trace for 12 x 8-Inch Diameter Bomb	82
27	Bomb Sampler Pressure Ratio Versus F/A Ratio	83
28	Bomb Sampler Pressure Ratio and F/A Ratio Versus Time Data	84

ILLUSTRATIONS (Continued)

<u>Figure</u>		<u>Page</u>
29	Variations of Percent Void and V_R/V_C With Arrestor Thickness (Lined Wall)	91
30	Fuselage Tank System Schematic	92
31	Fuselage Tank Test Assembly	93
32	Lined Wall Configuration (Dry)	97
33	Lined Wall Configuration (Wetted with JP5)	98
34	Fuselage Tank (Lined Wall) Material Screening Tests (I)	99
35	Fuselage Tank (Lined Wall) Material Screening Tests (II)	100
36	Fuselage Tank (Lined Wall) Material Screening Tests (III)	101
37	Fuselage Tank (Lined Wall) Wet with JP-5 Variations in Fuel/Air Ratio (I)	102
38	Fuselage Tank (Lined Wall) Wet with JP-5 Variations in Fuel/Air Ratio (II)	103
39	Typical Bomb Sample Data	105
40	Typical Bomb Sample Data, 25 PPI (Wet)	106
41	Variation of Bomb Sample Pressure Rise for Different Materials	107
42	Variation of Fuselage Tank Overpressure for Different Materials at Various Fuel-to-Air Ratios	108
43	Pressure Ratio vs Relief to Combustion Volume Ratio - Fuselage Tank (Lined Wall)	109
44	Fuselage Tank Data Summary Mode II Test	111
45	Steady State Mathematical Model Volume Ratio V_R/V_C Versus Pressure Ratio $P_C/P_{Initial}$	122
46	Steady State Mathematical Model Percent Voic V_C/V_T Versus Pressure Ratio $P_C/P_{Initial}$	123
47	Computer Flow Diagram	135
48	Dynamic Model Volume Versus Pressure for Data for 53% Orifice (Spark Ignition)	140
49	Dynamic Model Volume Versus Pressure Data for 53% Orifice (Incendiary Ignition)	141
50	Dynamic Model Volume Versus Pressure Data for 10% Orifice (Spark Ignition)	142
51	Dynamic Model Volume Versus Pressure Data for 10% Orifice (Incendiary Ignition)	143

ILLUSTRATIONS (Continued)

<u>Figure</u>		<u>Page</u>
52	Variable Geometry Test Data versus Transient Model Data	144
53	Fuselage Tank (Lined Wall) Dynamic Model Pressure Plots	146
54	Dynamic Model Pressure Ratio versus Relief-to-Combustion Ratio	147
	Listing A	148
	Listing B	151
	Listing C	155
55	Hot Wire Foam Cutting	160
56	Variations of Percent Void and V_R/V_C with Arrestor Thickness (Top Wall)	162
57	Variation of Percent Void and Relief Depth (Voided Top Wall)	164
58	Variation of Percent Void, Penalty Percent Void and Relief Void Depth	165
59	Small Wing Tankage Test Configuration	167
60	Variations of Percent Penalty Void with Arrestor Thickness (Voided Top Wall)	169
61	Variation of Percent Void with Arrestor Thickness (Voided Top Wall)	170
62	Variations of Percent Void and V_R/V_C with Arrestor Thickness (Voided Top Wall)	171
63	Variations of Percent Void and V_R/V_C with Arrestor Thickness (Egg Crate)	174
64	Large Wing Tankage Test Configuration	176
65	Variation of Percent Void and V_R/V_C with Arrestor Thickness (Lined Wall)	177
66	Variations of Percent Void and V_R/V_C with Arrestor Thickness (Egg Crate Center Only)	180
67	Variations of Percent Void and V_R/V_C with Arrestor Thickness (Total Egg Crate)	182
68	Incendiary Igniter/Spark Plug Firing Circuit	187
69	Bomb Firing Circuit	188
70	Gun Firing Circuit	189
71	.50 Caliber Gun	190
72	Test Schematic Fuselage Tank	191

ILLUSTRATIONS (Continued)

<u>Figure</u>		<u>Page</u>
73	Test Schematic Small Wing Tank	192
74	Test Schematic Large Wing Tank	193
75	Percent Void Versus Pressure Ratio Data Plots, Fuselage Tank (Top Wall and Voided Top Wall)	203
76	Percent Void Versus Pressure Ratio Data Plots, Fuselage Tank (Voided Top Wall)	204
77	Percent Void Versus Pressure Ratio Data Plots, Fuselage Tank (Voided Top Wall)	205
78	Percent Void Versus Pressure Ratio, Summary Data Plot, Fuselage Tank (Top Wall and Voided Top Wall)	206
79	Relief to Combustion Volume Ratio Versus Pressure Ratio, Fuselage Tank (Top Wall and Voided Top Wall)	207
80	Fuselage Tank Data Summary	208
81	Percent Void Versus Pressure Ratio Proof Pressure Data Plots, Small Wing Tank (Voided Top Wall)	210
82	Percent Void Versus Pressure Ratio Data Plot, Small Wing Tank (Voided Top Wall)	211
83	Percent Void Versus Pressure Ratio Data Plot, Small Wing Tank (Voided Top Wall)	212
84	Percent Void Versus Pressure Ratio Summary Data Plot, Small Wing Tank (Egg Crate)	213
85	Small Wing Tank Data Summary	214
86	Percent Void Versus Pressure Ratio Summary Data Plot (Large Wing Tank)	219
87	Percent Void Versus Pressure Ratio Summary Data Plot (Large Wing Tank)	220
88	Large Wing Tank Data Summary	221
89	Variations of Percent Void and V_R/V_C with Arrester Thickness (Voided Lined Wall)	228
90	Percent Void Versus Pressure Ratio Summary Data Plot, Fuselage Tank (Voided Lined Wall)	221
91	Percent Void Versus Pressure Ratio Summary Data Plot, Fuselage Tank (Voided Top Wall)	232
92	Summary Data Plot Fuselage Tank, Voided Top Wall	233
93	Percent Void Versus Pressure Ratio Summary Data Plot, Fuselage Tank (Voided Top Wall)	234
94	Fuselage Tank Data Summary	235

ILLUSTRATIONS (Continued)

<u>Figure</u>		<u>Page</u>
95	Percent Void Versus Pressure Ratio Summary Data Plot, Small Wing Tank Egg Crate Configuration	237
96	Percent Void Versus Pressure Ratio Summary Data Plot, Small Wing Tank Voided Top Wall Configuration	239
97	Percent Void Versus Pressure Ratio Summary Data Plot for Small Wing Tank Voided Top Wall Configuration	240
98	Percent Void Versus Pressure Ratio Summary Data Plot for Small Wing Tank Voided Top Wall Configuration	241
99	Small Wing Tank Data Summary	242
100	Percent Void Versus Pressure Ratio Summary Data Plot Large Wing Tank (Lined Wall)	246
101	Percent Void Versus Pressure Ratio Summary Data Plot Large Wing Tank	247
102	Percent Void Versus Pressure Ratio Summary Data Plot Large Wing Tank	248
103	Large Wing Tank Data Summary	249
104	Arrester Material Net Weight Penalty	254
105	Arrester Material Operational Weight Penalty	255
106	Screen Material Installation Penalties	256
A-1	Quartz Fiber and Glass Cloth Arrester Material Data	271
A-2	KCF Carbon Fiber Cloth Screen Data	272
A-3	GAF Felt Type 2A-5A and 8A Arrester Material Data	273
A-4	3M Scotch Brite GAF Felt (Standard and KCF Felt Carbon Fiber Arrester Material Data	274
A-5	25-PPI Foam with Variations	275
A-6	Honeycomb and 400 P.E. Screen Arrester Material Data	276
A-7	10-PPI and 15-PPI Foam Arrester Material Data	277
A-8	Custom Material 7611XP with Various Supporting Material, Arrester Data	278
A-9	20-Mesh and 35-Mesh Stainless Steel Screen Arrester Material Data	279
A-10	25-PPI and Honeycomb Post-Test Photograph	280
A-11	20-Mesh and 35-Mesh Stainless Steel Screen Post-Test Photograph	282
A-12	GAF, KCF, and 3M Felt Materials Post-Test Photograph	283

ILLUSTRATIONS (Continued)

<u>Figure</u>		<u>Page</u>
A-13	10-PPI Foam Post Test Photograph	284
A-14	15-PPI Foam Post Test Photograph	285
A-15	25-PPI Combined with 20-Mesh Stainless Steel Screen Post-Test Photograph	286
A-16	25-PPI Foam Post-Test Photograph	287
A-17	KCF Carbon Fiber Cloth Screens Post-Test Photograph	288
A-18	Carbon Fiber ΔP Data Plots	289
A-19	25-PPI Foam ΔP Data Plots	291
A-20	GAF (Standard Felt) ΔP Data Plots	293
A-21	20-Mesh Stainless Steel Screen ΔP Data Plots	295
A-22	35-Mesh Stainless Steel Screen ΔP Data Plots	297
A-23	Custom Material 7611XP ΔP Data Plots	299
A-24	10-Oz Glass Cloth ΔP Data Plots	301
A-25	3M Scotch Brite ΔP Data Plots	303
A-26	KCF-100 Carbon Fiber Cloth ΔP Data Plots	305
A-27	KCF-100 Standard Carbon Fiber Cloth ΔP Data Plots	307
A-28	10-PPI Foam ΔP Data Plots	309
A-29	Hough Industries HL 1106 ΔP Data Plots	311
A-30	Hough Industries HL 1110 ΔP Data Plots	312
A-31	25 PPI Research Foam ΔP Data Plots	314
A-32	Arrester Thickness Versus Initial Pressure Data Plots for 10-Oz Glass Cloth and GAF Felt (Standard) Material	325
A-33	Arrester Thickness Versus Initial Pressure Data Plots for 3M Scotch Brite	326
A-34	Arrester Thickness Versus Initial Pressure Data Plots for 3M Scotch Brite	327
A-35	Arrester Thickness Versus Initial Pressure Data Plots for 3M Scotch Brite	328
A-36	Arrester Thickness Versus Initial Pressure Data Plots for 20 Mesh-016 Stainless Steel Screen	329
A-37	Arrester Thickness Versus Initial Pressure Data Plots for GAF Felt (Type 2A)	330
A-38	Arrester Thickness Versus Initial Pressure Data Plots for 25-PPI Foam with Two Layers of 20-Mesh -016 Stainless Steel Wire Screen on Each Side	331

ILLUSTRATIONS (Continued)

<u>Figure</u>		<u>Page</u>
A-39	Arrester Thickness Versus Initial Pressure Data Plots for Quartz Fiber Type 594/38-9073 10 Layers on the Front Face with 25-PPI Foam and 4-Mesh Support Screen	332
A-40	Arrester Thickness Versus Initial Pressure Data Plots for Quartz Fiber Type 594/38-9073 10 Layers with Two Layers of 20-Mesh -016 Stainless Steel Wire Screen	333
A-41	Arrester Thickness Versus Initial Pressure Data Plots for 25-PPI Foam	334
A-42	Arrester Thickness Versus Initial Pressure Data Plots for 25-PPI Foam	335
A-43	Arrester Thickness Versus Initial Pressure Data Plots for 25-PPI Foam	336
A-44	Arrester Thickness Versus Initial Pressure Data Plots for 25-PPI Foam	337
A-45	Arrester Thickness Versus Initial Pressure Data Plots for 25-PPI Foam Wetted with JP5	338
A-46	Arrester Thickness Versus Initial Pressure Data Plots for 15-PPI Foam	339
A-47	Arrester Thickness Versus Initial Pressure Data Plots for 25-PPI Foam with Two Layers of 20-Mesh -016 Stainless Steel Wire Screen	340
A-48	Arrester Thickness Versus Initial Pressure Data Plots for Quartz Fiber Type 495/38-9073 with 4-Mesh Support Screen	341
A-49	Arrester Thickness Versus Initial Pressure Data Plots for Quartz Fiber Type 594/38-9073 with 4-Mesh Support Screen	342
A-50	Variation of 25 PPI-Foam Arrester Thickness with Combustion Volume	343
A-51	Volume Ratio Versus Pressure Ratio Data Plots for GAF Felt Type 2A	344
A-52	Volume Ratio Versus Pressure Ratio Data Plots for GAF Felt Type 2A	345
A-53	Volume Ratio Versus Pressure Ratio Data Plots for GAF Felt Standard	346
A-54	Volume Ratio Versus Pressure Ratio Data Plots for 3M Felt with Two 20-Mesh -016 Stainless Steel Screens on the Front Face Only	347
A-55	Volume Ratio Versus Pressure Ratio Data Plots for 3M Felt Scotch Brite	348

ILLUSTRATIONS (Continued)

<u>Figure</u>		<u>Page</u>
A-56	Volume Ratio Versus Pressure Ratio Data Plots for 3M Felt Scotch Brite	349
A-57	Volume Ratio Versus Pressure Ratio Data Plots for 3M Felt Scotch Brite	350
A-58	Volume Ratio Versus Pressure Ratio Data Plots for Quartz Fiber 594/38-9073 with 4-Mesh Retaining Screen	351
A-59	Volume Ratio Versus Pressure Ratio Data Plots for Quartz Fiber 594/38-9073 with 4-Mesh Retaining Screen	352
A-60	Volume Ratio Versus Pressure Ratio Data Plots for Quartz Fiber 594/38-9073 with 4-Mesh Retaining Screen	353
A-61	Volume Ratio Versus Pressure Ratio Data Plots for Quartz Fiber 594/38-9073 with 20-Mesh Retaining Screen	354
A-62	Volume Ratio Versus Pressure Ratio Data Plots for Quartz Fiber 594/38-9073 with Two Layers of 20 Mesh -016 Stainless Steel Screen	355
A-63	Volume Ratio Versus Pressure Ratio Data Plots for 25-PPI Foam with 4-Mesh Retaining Screen	356
A-64	Volume Ratio Versus Pressure Ratio Data Plots for 25-PPI Foam with 4-Mesh Retaining Screen	357
A-65	Volume Ratio Versus Pressure Ratio Data Plots for 25-PPI Foam with 4-Mesh Retaining Screen	358
A-66	Volume Ratio Versus Pressure Ratio Data Plots for 25-PPI Foam with 4-Mesh Retaining Screen	359
A-67	Volume Ratio Versus Pressure Ratio Data Plots for 25-PPI Foam with 4-Mesh Stainless Steel Retaining Screen, Various F/A Ratios	360
A-68	Volume Ratio Versus Pressure Ratio Data Plots for 25-PPI Foam with 20-Mesh -016 Stainless Steel Screen-- Two Layers on the Front Face Only	361
A-69	Volume Ratio Versus Pressure Ratio Data Plots for 25-PPI Foam with 10 Layers of Quartz Fiber Type 594/38-9073 on the Front Face--4-Mesh Support Screen	362
A-70	Volume Ratio Versus Pressure Ratio Data Plots for 25-PPI Foam with Two Layers of Stainless Steel Screen on Each Side	363
A-71	Volume Ratio Versus Pressure Ratio Data Plots for 25-PPI Foam with Two Layers of Stainless Steel Screen on Each Side	364
A-72	Volume Ratio Versus Pressure Ratio Data Plots for 20-Mesh -016 Stainless Steel Screen	365

ILLUSTRATIONS (Continued)

<u>Figure</u>		<u>Page</u>
A-73	Volume Ratio Versus Pressure Ratio Data Plots for 10-Pz Glass Cloth with 3/16 HRH 327 Honeycomb 1-1/4 Inch Thick	366
A-74	Volume Ratio Versus Pressure Ratio Data Plots for 15-PPI Yellow Foam	367
A-75	25-PPI Foam Combustion Face, Run 003	368
A-76	25-PPI Foam Relief Face, Run 003	369
A-77	25-PPI Foam Combustion Face, Run 005	370
A-78	25-PPI Foam Relief Face, Run 005	371
A-79	25-PPI Foam Combustion Faces Runs 033, 034, 035, 036, 037, 038	372
A-80	25-PPI Foam Relief Faces Runs 033, 034, 035, 036, 037, 038	373
A-81	25-PPI Foam Combustion Faces Runs 021, 022, 023, 024, 028, 029	374
A-82	25-PPI Foam Relief Faces Runs 021, 022, 023, 024, 028, 029	375
A-83	25-PPI Foam Combustion Faces Runs 014, 015, 016, 017, 019, 020	376
A-84	25-PPI Foam Relief Faces Runs 014, 015, 016, 017, 019, 020	377
A-85	25-PPI Foam Combustion Faces Runs 008, 009, 010, 011, 012, 013	378
A-86	25-PPI Foam Relief Faces Runs 008, 009, 010, 011, 012, 013	379
A-87	Various Test Samples (Prior to Test)	380
A-88	GAF Felt (Type 2A) Following Combustion	381
A-89	3M Scotch Brite Combustion Faces	382
A-90	3M Scotch Brite Relief Faces	383
A-91	GAF Felt (Standard) Combustion Faces	384
A-92	GAF Felt (Standard) Relief Faces	385
A-93	GAF Felt (2A) Combustion Faces	386
A-94	GAF Felt (2A) Relief Faces	387
A-95	Quartz Fiber Type 594/38-9073 10 Layers and 25-PPI Foam Backed with Two Layers of Stainless Steel, 20-Mesh -016 Screen	388

ILLUSTRATIONS (Continued)

<u>Figure</u>		<u>Page</u>
B-6	Typical Pressure Traces for Fuselage Tank (Top Wall) Runs 46 and 47	425
B-7	Typical Pressure Traces for Fuselage Tank (Top Wall) Run 48	426
B-8	Typical Small Wing Tank Pressure Traces, Voided Top Wall, Runs 49B and 52E	428
B-9	Typical Small Wing Tank Pressure Traces, Voided Top Wall, Runs 53 and 54	429
B-10	Typical Small Wing Tank Pressure Traces, Voided Top Wall, Runs 55 and 56	430
B-11	Typical Small Wing Tank Pressure Traces, Voided Top Wall, Runs 57 and 58	431
B-12	Typical Small Wing Tank Pressure Traces, Voided Top Wall, Runs 68 and 69	432
B-13	Typical Small Wing Tank Pressure Traces, Voided Top Wall, Runs 70 and 71	433
B-14	Typical Small Wing Tank Pressure Traces, Voided Top Wall, Run 59	434
B-15	Typical Small Wing Tank Pressure Traces, Egg Crate Configuration, Runs 50A and 51	435
B-16	Typical Small Wing Tank Pressure Traces, Egg Crate Configuration, Runs 60 and 61	436
B-17	Typical Small Wing Tank Pressure Traces, Egg Crate Configuration, Runs 62 and 63	437
B-18	Typical Small Wing Tank Pressure Traces, Egg Crate Configuration, Runs 64 and 66	438
B-19	Typical Small Wing Tank Pressure Traces, Egg Crate Configuration, Run 67	439
B-20	Voided Top Wall (Run 53)	440
B-21	Voided Top Wall (Run 54)	441
B-22	Egg Crate-Runs 61 and 62	442
B-23	Large Wing Tank Data Traces, Lined Wall (Runs 72 and 73A)	444
B-24	Large Wing Tank Data Traces, Lined Wall (Runs 74 and 75)	445
B-25	Large Wing Tank Data Traces, Lined Wall (Run 76)	446
B-26	Large Wing Tank Data Traces, Lined Wall (Run 77)	447

ILLUSTRATIONS (Continued)

<u>Figure</u>		<u>Page</u>
A-96	Quartz Fiber Type 594/38-9073 10 Layers Backed with 25-PPI Foam (Note: Foam Burnt Away)	389
A-97	Damaged 4 Mesh Support Screen on Completion of Run 123	390
A-98	Typical Fuselage Tank Pressure Traces, Line Wall Configuration, 25-PPI Dry	404
A-99	Typical Fuselage Tank Pressure Traces, Lined Wall Configuration, 25-PPI Wet with JPS	405
A-100	Typical Fuselage Tank Pressure Traces, Lined Wall Configuration, 25-PPI Wet with JP5	406
A-101	Typical Pressure Traces for 39% Void Fuselage Tank (Lined Wall) Wet with JP5	407
A-102	Typical Pressure Traces for 39% Void Fuselage Tank (Lined Wall) (Dry)	408
A-103	Typical Pressure Traces for 39% Void Fuselage Tank (Lined Wall) (Dry)	409
A-104	Typical Pressure Traces for 39% Void Fuselage Tank (Lined Wall) (Dry)	410
A-105	Typical Pressure Traces for 39% Void Fuselage Tank (Lined Wall) 25 PPI (Wet)	411
A-106	Typical Pressure Traces for 39% Void Fuselage Tank (Lined Wall) Wet with JP5	412
A-107	Typical Pressure Traces for 39% Void Fuselage Tank (Lined Wall) Wet with JP5	413
A-108	Typical Pressure Traces for 39% Void Fuselage Tank (Lined Wall) 25-PPI Foam - 10 Layers of Quartz	414
A-109	Typical Pressure Traces for 39% Void Fuselage Tank (Lined Wall)	415
B-1	Typical Pressure Traces for Fuselage Tank (Top Wall) Runs 36 and 37	420
B-2	Typical Pressure Traces for Fuselage Tank (Top Wall) Runs 38 and 39	421
B-3	Typical Pressure Traces for Fuselage Tank (Top Wall) Runs 40 and 41	422
B-4	Typical Pressure Traces for Fuselage Tank (Top Wall) Runs 42 and 43	423
B-5	Typical Pressure Traces for Fuselage Tank (Top Wall) Runs 44 and 45	424

ILLUSTRATIONS (Continued)

<u>Figure</u>		<u>Page</u>
B-27	Typical Large Wing Tank Pressure Traces, Central Egg Crate (Runs 78 and 79)	448
B-28	Typical Large Wing Tank Pressure Traces, Total Egg Crate (Runs 80 and 82)	449
B-29	Typical Large Wing Tank Pressure Traces, Total Egg Crate (Run 83)	450
B-30	Typical Large Wing Tank Pressure Traces, Total Egg Crate (Runs 84 and 84A)	451
B-31	Typical Large Wing Tank Pressure Traces, Total Egg Crate (Runs 85 and 85A)	452
B-32	Typical Large Wing Tank Pressure Traces, Total Egg Crate (Run 86)	453
B-33	Typical Large Wing Tank Pressure Traces, Run 87, Total Egg Crate	454
C-1	Typical Pressure Traces for Fuselage Tank Voided Top Wall Runs 98 and 99	457
C-2	Typical Pressure Traces for Fuselage Tank Voided Top Wall Runs 98 and 99	458
C-3	Typical Pressure Traces for Fuselage Tank Voided Top Wall Runs 101 and 102	459
C-4	Typical Pressure Traces for Fuselage Tank Voided Top Wall Runs 103 and 104	460
C-5	Typical Pressure Traces for Fuselage Tank Voided Top Wall Run 105	461
C-6	Typical Pressure Traces for Fuselage Tank Voided Lined Wall Runs 106 and 107	462
C-7	Typical Pressure Traces for Fuselage Tank Voided Lined Wall Run 108	463
C-8	Typical Pressure Traces for Fuselage Tank Voided Top Wall Runs 109 and 110	464
C-9	Typical Pressure Traces for Fuselage Tank Voided Top Wall Runs 111 and 112	465
C-10	Typical Pressure Traces for Fuselage Tank Voided Top Wall Run 113A	466
C-11	Typical Pressure Traces for Fuselage Tank Voided Top Wall Run 114	467
C-12	Typical Pressure Traces for Fuselage Tank Voided Top Wall Run 115	468

ILLUSTRATIONS (Continued)

<u>Figure</u>		<u>Page</u>
C-13	Typical Pressure Traces for Fuselage Tank Voided Top Wall Run 116	469
C-14	Typical Pressure Traces for Fuselage Tank Voided Top Wall Run 117	470
C-15	Typical Pressure Traces for Fuselage Tank Voided Top Wall Run 111A	471
C-16	Typical Pressure Traces for Fuselage Tank Voided Top Wall Run 118	472
C-17	Typical Pressure Traces for Fuselage Tank Voided Top Wall Run 119	473
C-18	Typical Pressure Traces for Small Wing Tankage Egg Crate Run 121	475
C-19	Typical Pressure Traces for Small Wing Tankage Egg Crate Run 122	476
C-20	Typical Pressure Traces for Small Wing Tank Voided Top Wall Run 123A	477
C-21	Typical Pressure Traces for Small Wing Tank-Run 124 and 125-3M Felt-Voided Top Wall	478
C-22	Typical Pressure Traces for Small Wing Tank Voided Top Wall Run 126	479
C-23	Run 126A	480
C-24	Typical Pressure Trace for Small Wing Tank-Runs 127 and 128-3M Felt-Voided Top Wall	481
C-25	Typical Pressure Traces for Small Wing Tank-Runs 129 and 130 3M Felt Voided Top Wall	482
C-26	Typical Pressure Traces for Small Wing Tank Run 131 3M Felt Voided Top Wall	483
C-27	Typical Pressure Traces for Small Wing Tank Run 132 3M Felt Voided Top Wall	484
C-28	Typical Pressure Traces for Small Wing Tank Runs 133 25-PPI + Quartz Voided Top Wall	485
C-29	Typical Pressure Traces for Small Wing Tank Runs 135 and 136 25-PPI + Quartz Voided Top Wall	486
C-30	Typical Pressure Traces for Small Wing Tank Voided Top Wall 25-PPI Foam + 2 Layers Stainless Steel	487
C-31	Typical Pressure Traces for Small Wing Tank V.T.W. 25-PPI Foam + 2 Layers Screen	488

ILLUSTRATIONS (Continued)

<u>Figure</u>		<u>Page</u>
C-32	Typical Pressure Traces for Small Wing Tank V.T.W. 25-PPI Foam + 2 Layers Screen	489
C-33	Typical Pressure Traces for Small Wing Tank V.T.W. 25-PPI Foam + 2 Layers Screen	490
C-34	Typical Pressure Traces for Small Wing Tank V.T.W. 25-PPI Foam + 2 Layers Screen	491
C-35	Typical Pressure Traces for Small Wing Tank V.T.W. 25-PPI Foam + 2 Layers Screen	492
C-36	Typical Pressure Traces for Large Wing Tank Lined Wall Runs 88 and 89	494
C-37	Typical Pressure Traces for Large Wing Tank Lined Wall Run 90	495
C-38	Typical Pressure Traces for Large Wing Tank Lined Wall Run 91	496
C-39	Typical Pressure Traces for Large Wing Tank Lined Wall Runs 92 and 93	497
C-40	Typical Pressure Traces for Large Wing Tank Lined Wall Run 94	498
C-41	Typical Pressure Traces for Large Wing Tank Lined Wall Run 95	499
C-42	Typical Pressure Traces for Large Wing Tank Lined Wall Run 96	500
C-43	Typical Pressure Traces for Large Wing Tank Lined Wall Run 97	501

SECTION I

INTRODUCTION

Vulnerability of the ullage in an aircraft fuel tank relates directly to the flammability of the vapor present when an ignition source is introduced. Flammability is the process of fuel combustion requiring fuel to be vaporized, then mixed with oxygen, followed by reaction that is activated by an ignition source. Whether the reaction will propagate depends on whether the vapor composition at the time and place of ignition is within the flammability limits.

This hazard potential is greatly increased by reduction of the lean limit caused by dynamic aircraft responses and tank penetration by incendiary munitions that locally heat the fuel vapor.

The Air Force has successfully implemented a 10-pores-per-inch (ppi) orange polyurethane foam material in the fuel tanks of a number of combat aircraft for protection against internal fire and explosion resulting from ground fire or other stray ignition sources. The success of the concept to date has been demonstrated by more than three years of continuous use in both "lead the fleet" systems and combat aircraft.

Present technology installations with 10-ppi foam inerted systems have been limited to only fully packed (85% to 90% foam) applications, with associated penalties to the system. The penalty to the fuel system includes about 2.5% displacement and 1.0% to 1.5% fuel retention. There is also a weight penalty: the dry weight of the foam is 1.86 lb/ft³ or 0.24 lb/gal. When the 2.5% fuel displacement is accounted for, the overall weight penalty to a full tank is about 0.06 to 0.08 lb/gal of tankage, based on JP-4 (Reference 1).

The reduction of foam volume and associated weight penalty reduction by either coring the foam or by gross voiding techniques is now being seriously considered for retrofit on existing aircraft and for application to future aircraft. Lower-density material is also being considered.

Voiding is a feasible approach to possible weight and volume reductions of the present foam inerting system; however, tests to date have been limited in most cases to small-scale configurations with only selected concepts. The use of voiding in tanks where tank operating pressures are above atmospheric will require greater foam thickness, which may be a limiting factor in some concepts.

Previous work by MCAIR, in cooperation with Scott Paper Co., demonstrated a low-density reticulated polyurethane foam explosion suppression system with 80% to 90% voiding with a spark ignition source (contract F33615-71-C-1191).

Gross voiding techniques appear to be better suited for use with 20- to 25~~4~~ppf foams and provide a better potential for voiding up to 50%, and possibly even the 80% levels (Reference 1).

Basically, the concept is one of structural or foam isolation. Within aircraft wing tanks, for instance, where the structure offers natural compartmentization with intercommunicating openings between cells, foam is used to isolate each cell so as to allow pressure communication and at the same time arrest the propagating flame front. Pressure generated within the combustion cell is relieved through the foam, and the burnt and unburnt gases are expanded within the total tankage, resulting in a greatly reduced maximum overpressure.

The basic drawback is that these concepts require special hardware for compartmenting the tank unless it has been compartmented in its original design; also, special techniques are required for attaching the arrester to the tank interior. The use of uncomplicated gross voiding appears to be the most promising technique utilizing currently used arresting materials for reducing weight.

In fuselage tanks, the voiding technique presently being considered is coring; this reduces the material required by approximately 40%, uses the foam for its own support, and requires no internal bracings except, of course, to protect functional fuel system components. However, this technique has certain inherent limitations associated with installations and fabrication, particularly as voiding percentage increases.

Installation techniques need to be developed that do not degrade ease of access to the fuel cells or performance of the total fuel system. Aircraft down-time increased as a consequence of fully packed foam installations. Entrance to the fuel tank is severely hindered. Intelligence and experience are also required in the disassembly and reassembly of the foam "jig-saw puzzle." Maintenance is further complicated by the need for a complete system functional check on final closing of the tanks.

This program was initiated to develop advanced flame arrester concepts that optimize the arresting material and voiding concepts to improve the protection of aircraft fuel tanks with respect to explosions induced by small arms fire. It has been noted that flames of relatively low speed can propagate through the 10-ppi polyurethane foam in thicknesses greater than 12 inches, while higher-velocity flames are stopped by considerably less of the same material (Reference 2). Also, there is some evidence to indicate that slowly moving flame fronts and pressure waves may, in some cases, cause sufficient mixing of gases within the tank to allow unburnt combustible gases to be pushed from the foam and thus add to the combustion. Flame speeds and the mixing process are effected by the type of ignition source utilized and tank configuration. Most previous research performed in this area has utilized a spark or arc discharge ignition source. It has been shown that for certain voiding concepts, particularly the "compartmenting" technique, the ability of the voided flame arrester system to protect the fuel tank from excessive overpressures is greatly affected by the type of ignition source. In order to more closely simulate the type of ignition for which the Air Force currently has the greatest concern, the Aero Propulsion Laboratory (Fire Protection Branch) has developed and tested an ignition source which more nearly simulates gunfire than spark or arc ignition (reference 3). This ignition source has been used in this program with proof testing of each configuration with .50 caliber API gunfire.

SECTION II

SUMMARY

For convenience, the program was divided into three tasks:

TASK I

This effort was directed at defining and optimizing a second generation flame arrester material. This task was directed at separating the fundamental physical parameters affecting the arrester performance from the influences of tank configuration and geometry that affect flame properties.

At program inception, concern was felt for the type of tests that each material would be subjected to. We required that the screening tests would adequately subject the materials to all conditions expected during flame suppression within an aircraft tank. To achieve this required segregation of test parameters, Task I was further subdivided into two modes as follows:

Mode I--These screening tests evaluated the ability of a material to resist burn-through. The major phases in these tests were:

Mode IA

- Industry search for suitable materials
- 4.0-inch-flame tube tests

Mode IB

- Variable geometry tests

Mode II--These screening tests evaluated the ability of arresters to minimize the peak pressure attained in a 40% voided fuselage test tankage. The major phases in this mode were:

- Peak pressure tests with various concepts within a 100-gallon fuselage tank
- Material property determination
- Mathematical model development

Preceding page blank

TASK II

Task II was directed at evaluating and optimizing voiding techniques using 25-ppi reticulated polyurethane foam. Separate voiding concepts were proposed and tested for simulated fuselage tanks, small wing tanks, and large wing tanks.

TASK III

The objective of this portion of the program was to combine the technology developed in Tasks I and II and to test and evaluate advanced flame arrester voiding concepts combined with the optimized materials.

MODE IA

Industry Search for Suitable Materials—A letter that briefly described the intent of the program was forwarded to 48 companies that were believed capable of supplying possible candidate materials. We obtained replies to this correspondence from approximately 80% of those contacted.

4-Inch-Flame Tube Tests—These tests qualitatively rated each arrester material against the others, in a 4.0-inch-flame tube configuration. This configuration was so designed that the observed flame speed could be controlled from 50.0 to 1,000 inches per second within an environment approaching constant pressure. The flame speed was controlled by varying orifices at the combustion and relief end of the tube, and in part, of course, by the pressure drop through the arrester material itself. This apparatus, it was thought, while adequately screening each material, would indicate at an early date in the program the dependence of materials on the speed at which the flame is attempting to propagate through the arrester. This velocity has been shown to be an important part of the mechanism by which a flame front is extinguished. Some arresters performed well at low flame speeds while allowing higher flame speeds to propagate through, and others arrested fast-moving flame fronts and allowed slow-moving flames to pass through. As an extension to these early screening tests, the pressure drop through each material using shop air at room temperature was determined. These data allowed a comparison and rating of each material with the others to be represented as a velocity

head loss, i.e., a "K" factor. The pressure drop obtained for each material was considered an important parameter in determining a good arrester material, if the material was to be utilized in the continuing program. The success criterion was the ability of the material to suppress fast-moving and/or slow-moving flame fronts with minimum pressure drop or low K factors. This would allow immediate pressure communication to the relief volume and would not result in excessive pressure rise in the combustion volume. This combination, it was thought, would result in an arrester material capable of being used in aircraft fuel tanks.

MODE IB

Variable Geometry Tests--The 4-inch-flame tube configuration did not adequately describe the conditions in an aircraft fuel tank during an explosion or fire created by an incendiary projectile. Consequently, the materials chosen as a result of Mode IA tests underwent further exhaustive tests in a variable geometry configuration that allowed a condition more representative of those occurring during an incendiary activated fire. This apparatus, which more realistically approached that of an aircraft installation, consisted of an 18-inch-diameter combustion chamber that allowed the gases created during the combustion process to relieve through the arrester and orifice into a relief volume. Both the relief volume and orifice size were capable of being varied. The criteria for success in this apparatus were twofold:

- Adequate pressure communication between the two chambers so as not to allow too high a pressure to occur within the combustion chamber.
- Adequate suppression of the flame front.

The ignition source for this phase of Mode I was the AFAPL/SFH incendiary igniter, which used IM-11 incendiary powder. This igniter represented more closely the type of ignition that occurs from an incendiary bullet. Tests were conducted on some materials using spark ignition.

During tests in the 4-inch-flame tube, flame speed was the only recorded parameter. Tests within the variable geometry allowed records of pressure within each of the two chambers to be recorded on a transient basis and dis-

played on an appropriate trace recorder. A viewing port in the relief volume used for high-speed movies allowed visual evidence that a flame occurred on the other side of the arrester. This of course was apparent on the pressure traces as a secondary pressure rise.

The test data obtained during these tests showed that expanding gas velocity or the velocity of the flame front attempting to pass through the arrester as well as combustion volume are important considerations. This can be shown by the fact that 25-ppi foam required a 4-inch thickness to arrest an explosion at an initial pressure of 2-psi. Stainless steel screens alone would not arrest a flame front. However, a combination of both at a 2-psi initial pressure required only 1 to 2 inches of foam and two screens on either side to arrest a flame front in an identical situation. This was attributed to the fact that the flame front initially attempting to propagate through the foam is at a high gas velocity and the foam arrests this fast-moving flame.

However, at a certain moment the increasing relief volume pressure and the decaying combustion volume pressure equalize. If this occurs while there is still a fire, the slow-moving flame, capable of propagating through and burning the foam, is now arrested by the screens. Early tests during Mode IA showed that indeed slow flames were not allowed to propagate through certain thicknesses of screens. Consequently, the screens attached to the front and rear faces of the foam become the arresting material, which finally extinguishes the flame front.

During a large portion of the tests, especially with the GAF and 3M materials, large holes in the arrester materials were frequently found; however, no resulting relief volume ignition occurred. This was thought unusual and was attributed to the inerting effects of the products of combustion, and the expanding hot gases not retaining enough energy after burning and melting through the material to initiate a reaction.

The sensitivity of arrester thickness required for arrest with respect to initial over-pressures is high when small combustion volumes are used. At 0 psig, 2 to 3 inches of 25 (PPI) polyurethane foam are required. At 1 psig, 10 to 12

inches are required to arrest an incendiary burn. This high pressure dependence decreases in severity as combustion volume increases. Early tests with the 1.0-cubic-foot combustion volume showed that an incendiary ignition with 10.0 inches of foam still allowed an explosion to occur within the relief volume. However, a delay of 3 to 4 seconds separated the ignition event from the fire observed at the relief volume viewing port. The arrester was not damaged but had sustained the usually blackened stain and relief side burning.

It was observed and can be stated, from the large amount of material burnt and observed to be melted and blown into the relief volume during most tests, that these gases largely contribute to local inerting on the relief side of the foam. Finally, if a flame did propagate through a hole created in the arrester, no combustible gas is present at the time and place of the ignition and the reaction terminates.

This probability of burn-through and possible secondary explosion does not allow the data to be presented by a sharply defined curve. Consequently, the graphical data defining arrest and burn-through are represented by a shaded area.

This probability was not as noticeable in tests with screen or other non-flammable materials; the ignition delay experienced is caused solely by the arresting mechanism -attributed to geometry.

MODE II

Peak Pressure Tests--It has been shown that within the fuselage configuration with a lined wall voiding concept, 25-ppi reticulated polyurethane foam wetted with JP5 showed a higher pressure rise for a spark-initiated explosion than for one initiated with the incendiary igniter. Also, for the voided top wall configuration the explosions initiated with a .50 caliber API projectile fired through 1/4-inch aluminum 6061-T6 plate at a muzzle velocity \approx 2,300 feet per second, the pressure rise was lower than in those produced by the incendiary igniter.

A possible explanation for this difference in pressure rise is presented in the main body of the report. In summary, it has been suggested that the lower pressure rises obtained when using the incendiary igniter to initiate an explosion is related to:

- o the mechanism of incendiary reaction
- o the apparent rate of burn in the combustion volume.

The data indicate that the following materials were conducive to reducing maximum over-pressure:

- o 3M felt (Scotch Brite)
- o 25 ppi foam
- o 25-ppi foam and Astroquartz 594
- o 25 ppi foam and 20-mesh -016 stainless steel screen

These materials based upon results of Mode IA, 4.0-inch-flame tube and Mode IB, variable geometry test program, were acceptable as materials for inclusion in the Task III portion of the program.

Material Property Determinations--The results of the property determinations conducted per MIL-B83054 on 13 material samples indicate that the 3M Scotch Brite material and the 25-ppi foam have a high fuel retention figure (4.5% and 6% respectively).

Mathematical Model Development--A dynamic mathematical model was developed and modified throughout the test program to reflect test data. However, modifications were minimal and centered on establishing the correct "K" factor for each material. The model inherently couples pressure and temperature rise to the mass flow through the orifice and relief volume pressure rise implicitly. These parameters could only be affected by changing the time at which peak pressure was observed to occur in the combustion volume. All the other parameters are determined and modified by the program because they all depend on each other.

The mathematical model predicts the pressure and temperature increases within the combustion and relief volume, both during spark and incendiary-initiated

explosions. The model was found in accordance with the test data generated as a result of Mode IB testing and in general with that of Mode II. However, the program was not modified to reflect the pressure changes resulting from various ignition sources. These pressure variations experienced during tests within the fuselage tankage will require a higher degree of sophistication in present modeling to describe observed phenomena.

The results of all Task I work have shown:

- Flame speed at the time and place of arrest is an important parameter
- Material burning contributes to arresting characteristics of foams and felts
- Combustion volume affects the thickness of arrester required to arrest a flame front
- The ignition source directly affects the pressure rise time within a combustion volume
- Differences in rise time contribute to varying gas mass flow rates through an arrester
- The arrester cross-section area and total relief area affect the velocity of expanding burnt and unburnt gases contributing to changing arrester characteristics.

TASK II

All test configurations were tested with 25-ppi reticulated polyurethane foam. The initial test void condition was determined using steady state model relief to combustion ratio versus overpressure data. Further tests with increases in the percent void were each determined from the data obtained during the preceding tests. Testing was centered on obtaining data relating to the defined over-pressure criteria of 10 psig.

The tabulated data summarize pertinent data for each test conducted, taken directly from the detailed test data sheets. It was apparent from the preceding task that the ignition mode and pressure rise times were important. Conse-

quently, included in this report is a direct copy of all data traces for each test condition. Each trace records an arrest or a burn-through and the ignition mode.

The relationship of percent penalty void to absolute pressure ratio is graphically shown for each test. Penalty void is defined as the ratio of the total tank void volume versus the total volume. The data are presented in tabular and graphical form, with a bar chart for each tankage.

In all cases of burn-through, several pressure peaks were recorded. Each is shown in the data traces and plotted as an over-pressure ratio in the graphical data.

It is noted that throughout this program the over-pressure is correlated with percent penalty void, as this relates directly to aircraft applications. Each void configuration was initially standardized so that its application in any cell of each configuration would not affect the total penalty void of each tankage. The only exception is with the three-cell large wing tank central egg crate concept. In this instance the data are plotted as the center cell egg crate penalty void.

In all tests the intent was to obtain sufficient data to allow a determination to be made of relative performance of each concept.

A correlation with the dynamic mathematical model is made only with data obtained from the lined wall configuration. The required program routine changes required to describe some of the more exotic voiding concepts tested within the small and large wing tankages were considered beyond the scope of this program.

It was found that the most acceptable voiding technique using 10-psig overpressure criteria applicable for a fuselage tankage was the voided top wall, up to Ω 53% total voiding. The small wing tankage showed that 85% to 90% voiding is

possible with a voided top wall concept with spark ignition, reducing to 77% with the incendiary igniter and to 73% with .50 caliber API. The large wing tankage lined wall concept allowed voiding up to 75% to be achieved at 0 psig with an incendiary ignition source.

The voiding concepts recommended for testing in Task III are as follows:

- Fuselage Tankage
 - Voided Top Wall
 - Voided Lined Wall
- Small Wing Tankage
 - Egg Crate
 - Voided Top Wall
- Large Wing Tankage
 - Lined Wall.

TASK III

The test program was conducted in a similar manner to that conducted previously in Task II. The initial test void condition was determined using relief-to-combustion ratio versus over-pressure, as predicted from the mathematical model. Further tests with increases in the percent void were each determined from the data obtained during the preceding tests. Testing was centered on obtaining data relating to the defined pressure rise criteria of 10 psi.

Each void configuration was initially standardized as in Task II so that its application in any cell of each configuration would not affect the total penalty void of each tankage. In this task the void configurations obtained from Task II were tested using various other materials that were proved acceptable as a result of Task I. These materials were:

- o 3M Scotch Brite
- o G.A.F. Polyester Fiber, type 2A
- o 25 ppi foam and 016 Stainless Steel
- o 25 ppi foam and Astroquartz, type 594.

In all tests, the intent was to obtain sufficient data to allow a determination to be made of relative performance of each concept.

The data are presented in tabular and graphical form with a summary bar chart for each tankage.

The tabulated data summarize pertinent data for each test conducted, taken directly from the detailed test data sheets. Included in the data is a direct copy of all data traces taken for each test condition. Each trace records an arrest or a burn-through and the ignition mode.

The relationship of percent penalty void to absolute pressure ratio is graphically shown in the report for each test.

The voiding concepts tested that showed greatest promise in their application to aircraft tankages are as follows:

- Fuselage
 - Voided top wall
- Small Wing
 - Egg crate
 - Voided top wall
- Large Wing
 - Lined wall.

These voiding concepts should be further exhaustively tested in full-scale configurations that represent more closely aircraft installations.

SECTION III PROGRAM DESCRIPTION

TEST OBJECTIVES

A program flow chart is shown in Figure 1.

Task I was aimed at defining and optimizing a second generation flame arrester material. The program was directed at separating the fundamental physical parameters affecting the arrester performance from the influences of fuel tank configuration and geometry that affect flame properties.

This initial phase was separated into the following modes:

Mode I: Screening tests to evaluate the material's ability to prevent burn-through-- To achieve these screening evaluations, this mode was further subdivided into programs, A and B, as follows:

Mode IA: 4.0-Inch Flame Tube Tests--This fixed geometry apparatus allowed a determination of the flame speed at which burn-through occurred for various arrester materials and thicknesses. The igniter source for all Mode IA tests was a high energy sparkplug with modifications that allowed the probes to extend into the tube.

Mode IB: Variable Geometry Tube--By use of AFAPL/SFH incendiary igniter, this apparatus determined the resistance of arrester materials to burn-through. Variations in combustion volume, relief volume, and relief area were obtained. The conceptual development of this apparatus is shown in Figure 2.

Mode II

These screening tests allowed an evaluation of the ability of the arrester materials (chosen from Mode IB tests) to minimize the pressure obtained in a lined-wall, 40% voided, 100-gallon fuselage configuration test tank.

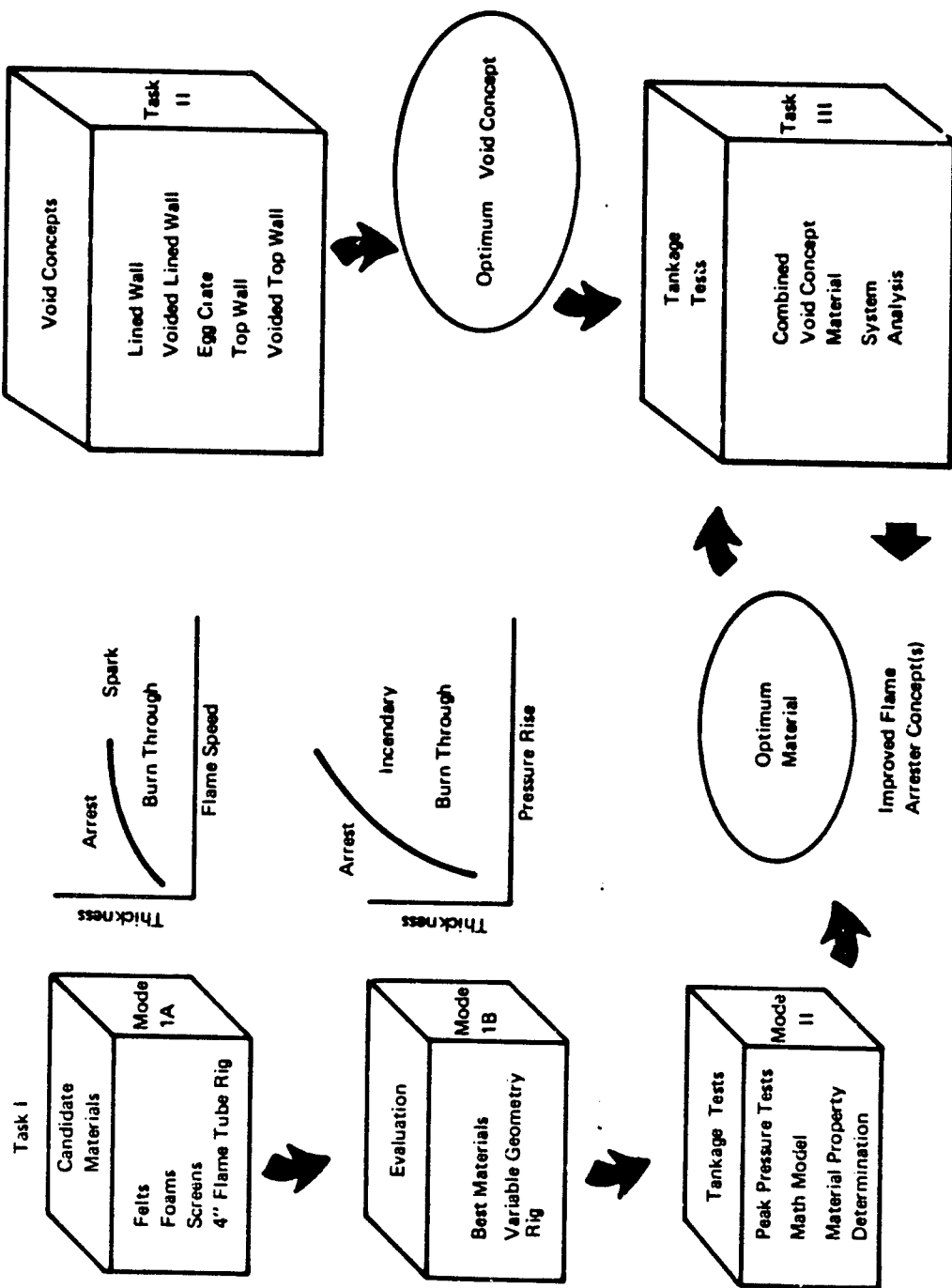
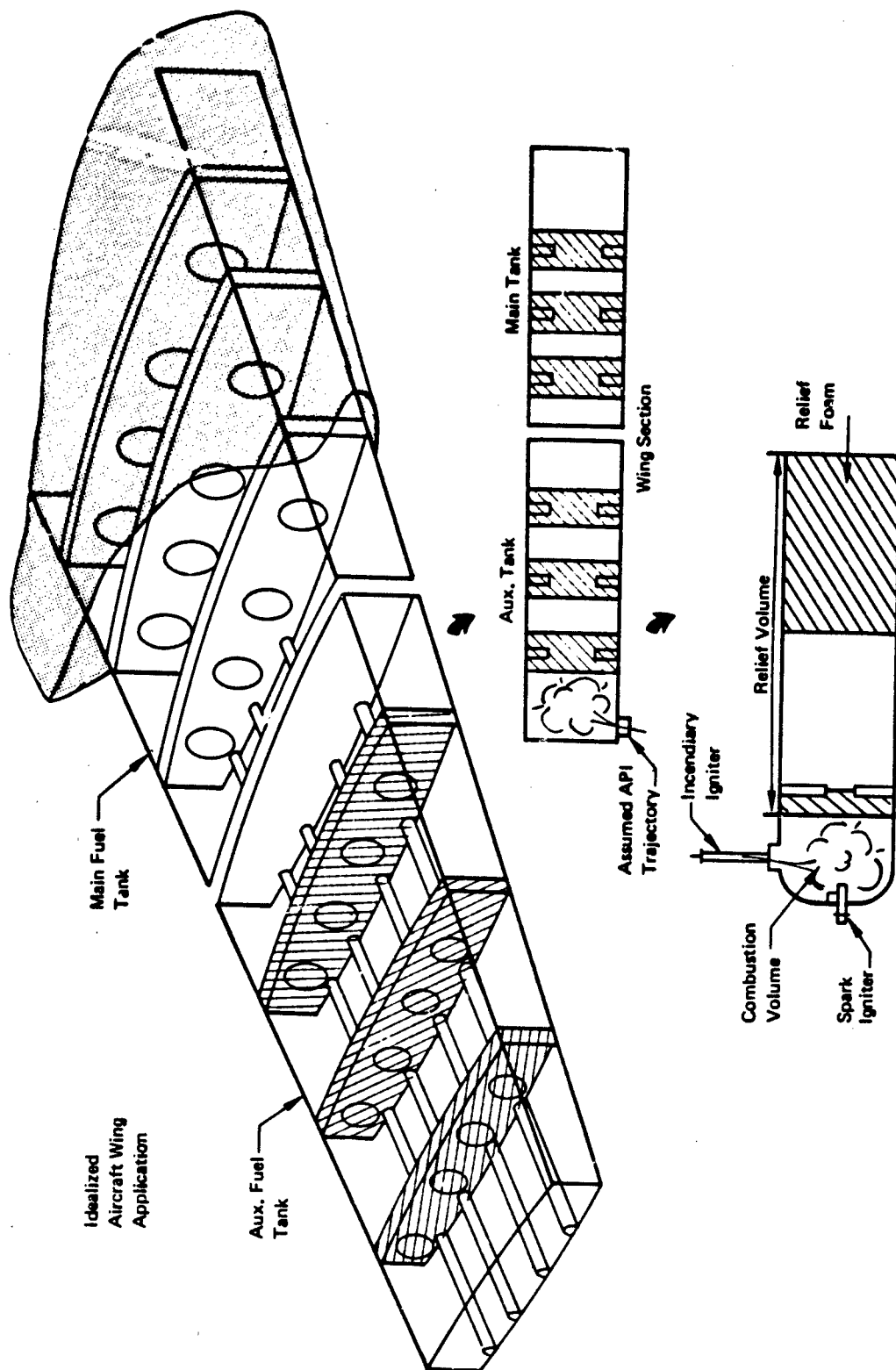


Figure 1: Program Flow Chart



Variable Geometry Test Apparatus

Figure 2: Arrestor Concept Aircraft Application and Variable Geometry Test Apparatus

Task II is concerned with evaluation and optimization with respect to achieving maximum percent void with various voiding concepts. Tests were conducted on various tankage configurations.

The objective of Task III was to combine the technology developed in Tasks I and II and to evaluate, by testing, advanced arrester voiding concepts combined with the optimized materials.

SECTION IV
TASK I MODE IA TEST PROGRAM

1.0 TEST APPARATUS: 4.0-INCH-FLAME TUBE

The test setup shown schematically in Figure 3 consisted basically of an 8.5-cubic foot mixing chamber, a propane supply, and the 4-inch-diameter flame tube assembly. A small mixture test bomb was used to check the gas mixture for the proper fuel-to-air ratio by igniting a fixed volume (0.3 cubic feet) of mixture and noting the pressure rise. The mixture bomb was hydrostatically tested at 350 psig: the maximum expected test pressure was 125 psig.

Mixing Tank—An 8.5-cubic foot mixing tank was used to mix the propane and air in the proper ratio prior to introducing the mixture to the bomb and the flame tube. The tank working pressure is 330 psig; the tank was hydrostatically tested to 500 psig.

4-Inch Flame Tube—The flame tube, Figure 4, consisted of two 60-inch sections of 4-inch-diameter pyrex glass tubing mounted horizontally on a stand with an aluminum test section clamped and sealed between the sections. Aluminum adapter plates were attached to the upstream and downstream ends of the tube for installation of flame speed control orifice plates and to seal the tube for evacuation during filling. The upstream adapter plate contained provisions for introducing the gas mixture and the spark igniter. The spark igniter was a modified automotive spark plug powered by a 15-kv transformer. Normal output voltage, however, was adjusted to 8 kv by varying the input voltage.

Ten photodiodes (Texas Instruments P/N H-35) were positioned on the upper surface of the flame tube to measure the flame speed. Reflective foil was taped to the outside of the tube opposite the photodiodes to reflect as much light as possible into them. The locations of these diodes in the flame tube are detailed in Figure 5.

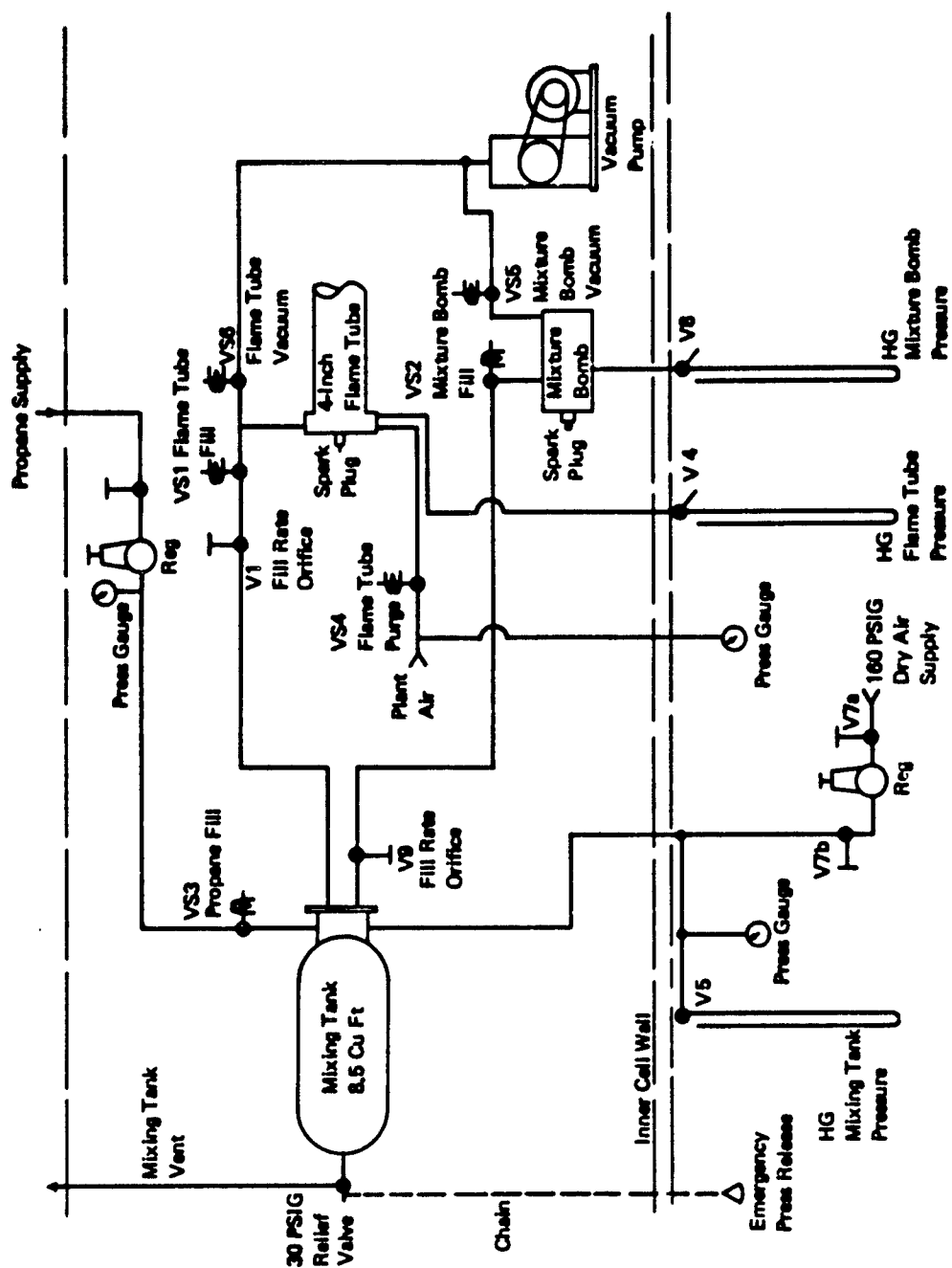


Figure 3 : 4.0 Inch Flame Tube Test Schematic

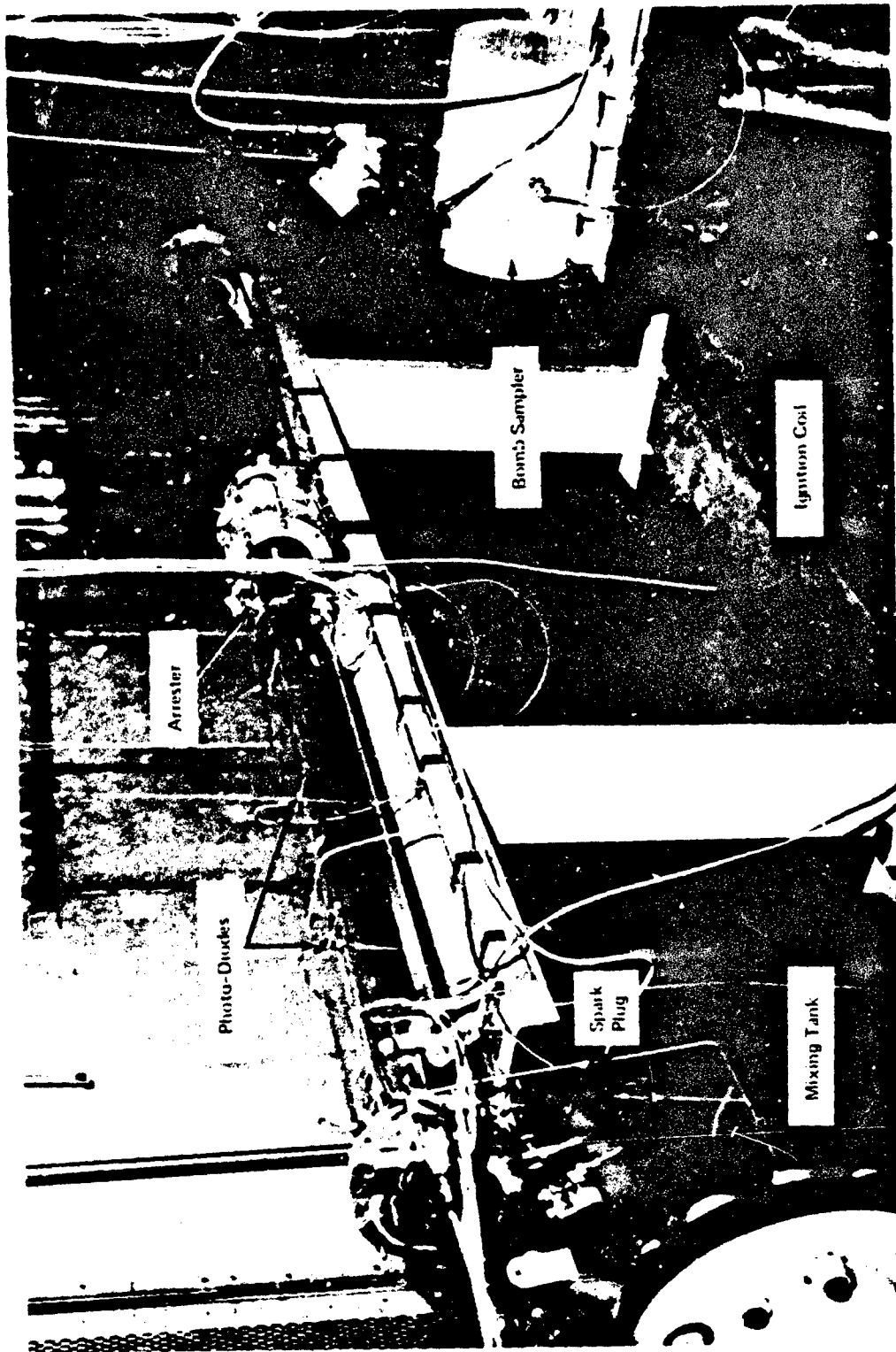
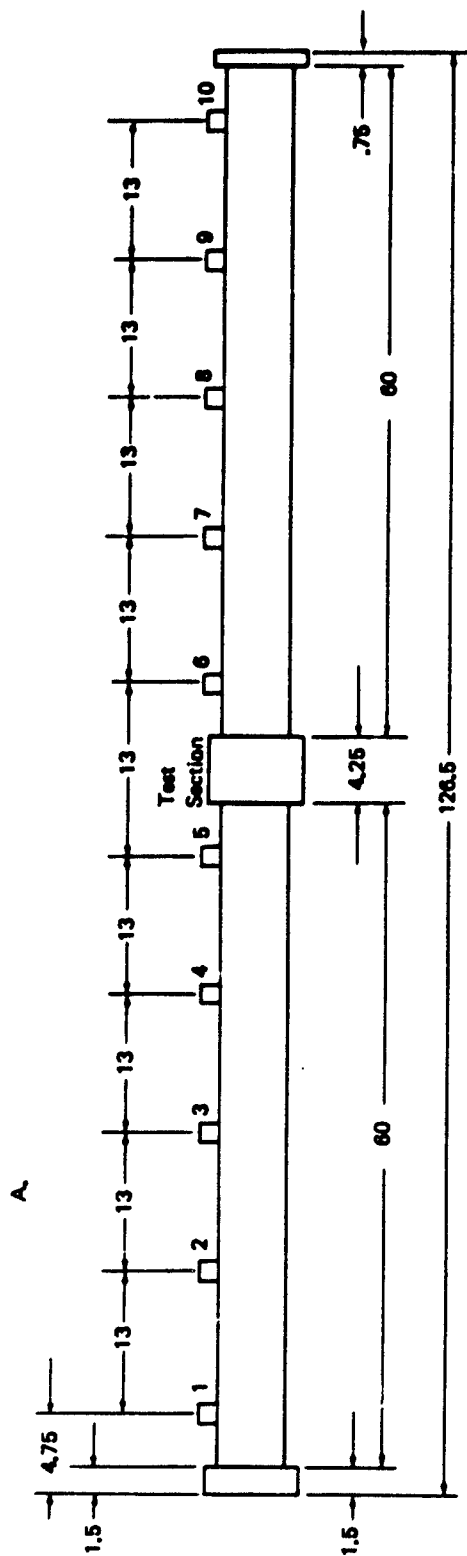
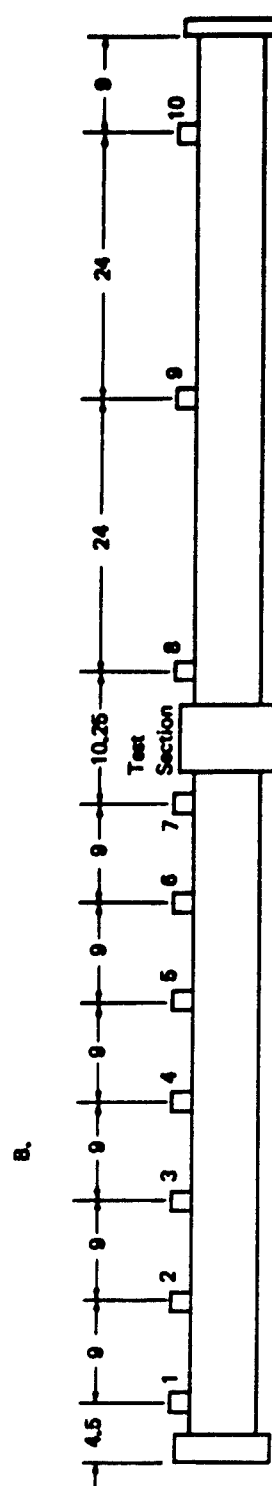


Figure 4: 4.0 Inch Flame Tube Test Apparatus



22



Notes: Figure "A" shows photodiode locations for runs 1-22 .
Figure "B" shows photodiode locations for runs 23 on.

Figure 5: Photo-Cell Locations for 4.0 Inch Flame Tube Tests

Air Flow Pressure Drop

The test setup used to determine the pressure drop characteristics with air at NTP is shown schematically in Figure 6. An ASME nozzle calibrated flow tube measured airflow rates through the arrester material. The pressure drop across the arrester was measured with a 50-inch mercury manometer.

2.0 INDUSTRY SEARCH AND MATERIAL TESTED

To procure new materials an industry search was conducted. The following letter was sent to approximately 50 companies thought capable of infusing new materials to the task of arresting flames:

Subject: Gross Voided Flame Arresters for Aircraft Fuel
Tanks - Contract No. F33615-72-C-1597

Gentlemen:

In conjunction with the subject contract, Boeing is presently conducting an industry search for candidate materials--either new or presently available--to function as a "flame arrester" within aircraft fuel tanks. Candidate materials must be compatible with liquid hydrocarbon fuels.

This inquiry is being forwarded to a large number of manufacturers of possible materials and is therefore general in nature. Data is requested on any of the material types listed below which you may manufacture, or on any other materials you believe may be of interest.

Materials of Interest:

- 1) Screens
 - a) Polyester
 - b) Stainless Steel
 - c) Polyester Teflon Coated Metal
- 2) Wire Mesh (stacked for depth)
 - a) Stainless Steel Wire
 - b) Polyester Wire
 - c) Teflon Wire
 - d) Knitted Nylon (Balls or Tubes)
 - e) Knitted Teflon (Balls or Tubes)

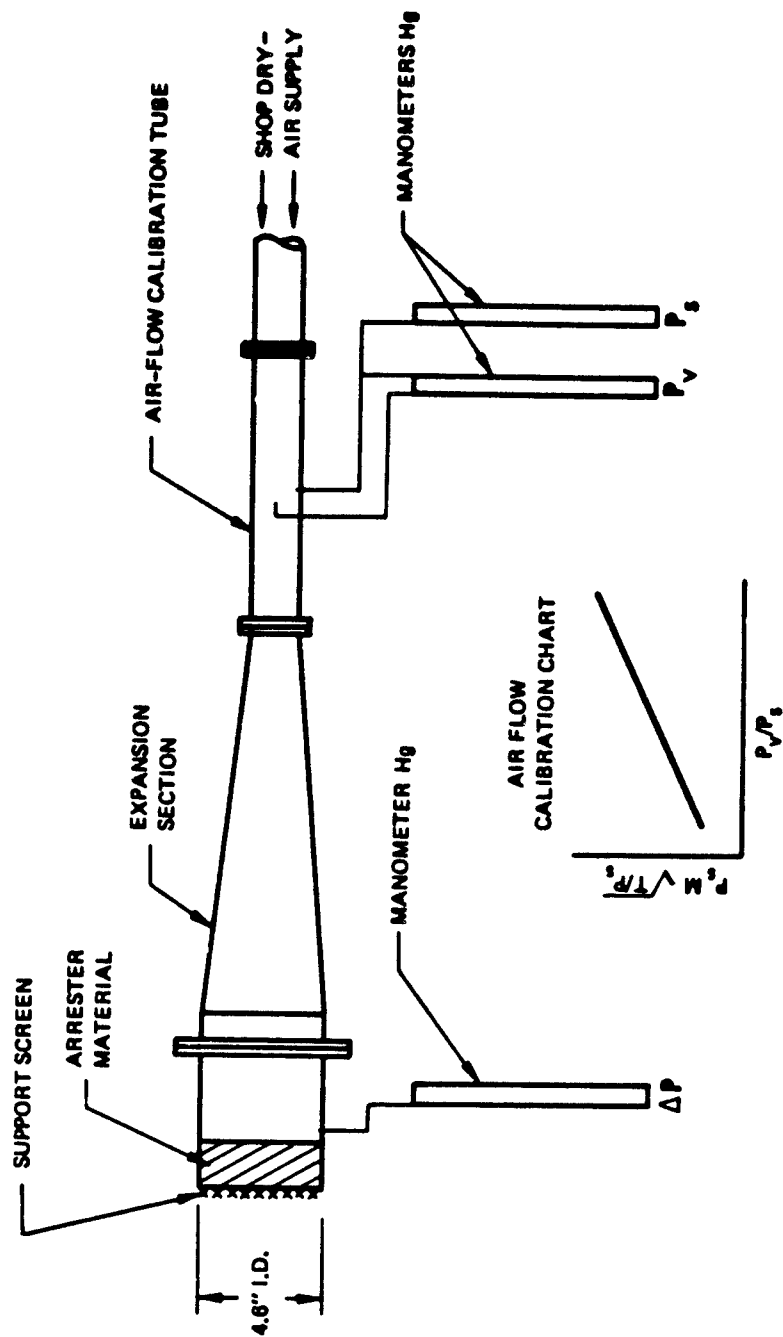


Figure 6: Air Flow Pressure Drop Apparatus Schematic

- 3) Honeycomb Construction
 - a) Nomex
 - b) Stainless Steel Lisk Disks (or others)
 - c) Fiberglas (Sine waves, tubes, etc.)
 - d) Aluminum Tube Core
- 4) Polyester, Nonwoven
 - a) Scotch Brite
 - b) Variations of Scotch Brite
- 5) Reticulated Polyurethane Foam
 - a) 25 Pores per inch
 - b) 15 Pores per inch
 - c) 10 Pores per inch
 - d) Foam Spheres
 - e) Foam Tubes (Hollow and Solid)

Should you be interested in our consideration of one or more of your products, the following information should be forwarded to the undersigned:

- 1) Delivery lead time
- 2) Availability of material variations and range of dimensional variations available
- 3) Cost (single piece and bulk lot price)

Where available, the following details as to physical characteristics of each candidate material are requested: Denier, Density, Physical Strength (Stiffness, Brittleness, etc.), Fuel Retention, Equivalent Porosity (Fuel Flow Pressure Drop), Volume Displacement, Thermal Conductivity, Hydrolytic Stability, Melting Point, Specific Heat, Fiber Size, Deterioration (Fuel Exposure to JP-5), Humidity Exposure, Flammability.

If you feel that a product (or products) presently being manufactured and available (or to be available in the near future) is applicable as a flame arrester material, details, brochures and samples of same are requested in response to this inquiry. Your response should be addressed as follows:

The Boeing Company
Aeronautical and Information Systems Division
P. O. Box 3999
Seattle, Wash. 98124
Attention: D. L. Duncan
Org. 2-4565
Mail Stop 40-14

Your early response, or indication of intent not to respond to this request is greatly appreciated.

Very truly yours,

THE BOEING COMPANY
Aeronautical and Information Systems Division

The companies contacted were:

Avco Corp.
Lowell Industrial Park
Lowell, Mass. 01851

Babcock & Wilcox Co.
Old Savannah Rd.
Augusta, Ga. 30903

Brunswick Corp.
69W. Wash. St.
Chicago, Ill. 60602

Carborundum Co.
P. O. Box 337
Niagara Falls, N.Y. 14302

Commonwealth Felt Co.
76 Summer St.
Boston, Mass. 02110

Connecticut Hard Rubber Co.
407 East St.
New Haven, Conn. 06509

Continental Felt Co.
22 W. 15 St.
New York City, N.Y. 10011

Custom Materials Inc.
279 Billerica Road
Chelmsford, Mass. 01824

C. H. Dexter
One Elm St.
Windsor Locks, Conn. 06096

Eagle-Picher Industries, Inc.
American Building
Cincinnati, Ohio 45202

Electrical Specialty Co.
213 E. Harris Avenue
So. San Francisco, Calif. 94080

Fabricon Products
1721 W. Pleasant Avenue
River Rouge, Mich. 48218

Ferro Corp.
3512 -20 Helms Ave.
Culver City, Calif. 90230

Fiberglas Canada Ltd.
48 St. Clair Ave. W.
Toronto, Ont.

Fiber Glass Industries, Inc.
Homestead Pl.
Amsterdam, N.Y. 12010

Firestone Coated Fabrics Div.
Akron, Ohio

Firestone Coated Fabrics Co.
Magnolia, Ark.
Attn: Mr. Phil Webb

GAF Corp.
Industrial Products Div.
109 Glenville Station
Greenwich, Conn. 06830

General Technologies Corp.
1821 Michael
Paraday Dr.
Reston, Va. 22070

B. F. Goodrich Industrial Prod. Co.
500 S. Main St.
Akron, Ohio 44318

Goodyear, GL4-4097-213-583-3083
Tire & Rubber Co.
Akron, Ohio

Hampden Brass & Aluminum Co.
262 Liberty St.
Springfield, Mass. 01101

Hitco
1600 W. 135th St.
Gardena, Calif. 90249

Huyck Felt Co.
Washington St.
Rensselaer, N.Y. 12144

Johns-Manville
22 East 40th St.
New York City, N.Y. 10016

Kintex, Inc.
575 Kennedy Road
Buffalo, N.Y. 14227

Kreha Corp. of America
116 E. Alondra Blvd.
Gardena, Calif. 90248

Masland Durable Leather Co.
Amber & Willard Sts.
Phila., Pa. 19134

Minnesota Mining & Manufacturing Co.
3M Center, Attn: J. G. Simmon
St. Paul, Minn. 55101

Monsanto
800 North Lindbergh Blvd.
St. Louis, Mo. 63166

Owens-Corning Fiberglas Corp.
P. O. Box 901
Toledo, Ohio 43601

Pellon Corp.
221 Jackson St.
Lowell, Mass. 01852

Pittsburgh Corning Corp.
One Gateway Center
Pittsburgh, Pa. 15222

James H. Rhodes & Co.
48-02, 29 St.
L.I.C., New York 11101

Rodgers Foam Corp.
114 Central St.
Somerville, Mass. 02145
Attn. Mr. Al Fuller

Ruco Div.
Hooker Chemical Corp.
New So. Rd.
Hicksville, N.Y. 11802

Joseph T. Ryerson & Son, Inc.
Box 8000-A
Chicago, Ill. 60618

Schramm Fiberglass Prod. Co.
2849 Montrole Avenue
Chicago, Ill. 60618

Scott Paper Co.
Foam Division
Chester, Pe-n.

Star Textile and Research Inc.
Saratogo St.
Cohoes, New York 12047

J. P. Stevens & Co., Inc.
Stevens Tower, 1135 Avenue of
the Americas
New York, N.Y. 10036

Strathmore Paper Co.
60 Front St.
West Springfield, Mass. 01089

Supreme Industrial Prod. Co.
367 No. Karlov Avenue
Chicago, Ill. 60624

Thermal American Fused Quartz Co.
Rt. 202 & Change Bridge Rd.
Montville, N. Y. 07045

Uniroyal
Mishawaka, Inc.

Western Felt Works
4115 Odgen Ave.
Chicago, I-1. 60623

Westpoint Pepperell
111 W. 40 St.
New York City, N.Y. 10018

Zurn Industries, Inc.
5533 Perry Highway
Erie, Pa. 16512

A reply was received from approximately 80% of the contacted manufacturers. As a result of these inquiries applicable materials were selected and purchased.

A complete list of purchased materials follows. Those that have been tested within the 4-inch-flame tube are indicated with an asterisk.

1. KREHA Corp.

- * KCF - 100-10 Mesh Cloth
- * KCF - 100 Standard Cloth Square Weave
- KCF - 100 Tow
- KRECA Foam (Mini-Sample)
- * KCF - 100 Feet - 50 Felt

2. Custom Materials Inc.

*#7611 XP Black Foam 25 PPI

This material is a 25-ppi foam, coated with "Velostat," which reduces static hazards during handling and processing of static-sensitive materials because it provides a conductive path to ground.

3. Hexcel Products Inc.

- * HRH 327 (E) 3/16 Spec. No Bms 8-125 (Black) Class I Type III P.
1/16 inch
- * HRP 3/16 GF11-40 (Brown)
- * HRP 1/8 GF11-40 (Brown)

4. *Titanium Honeycomb 1/8"

5. *10-PPI Orange Reticulated Polyurethane Foam

6. *15-PPI Yellow Reticulated Polyurethane Foam

7. *25-PPI Black Reticulated Polyurethane Foam

8. *25-PPI Red Reticulated Polyurethane Foam

9. TET-Kressilk (Screens)

 * Stainless Steel *35 - 011

 30 - 013

 24 - 014

 *20 - 016

 Propyltex 5-30 - 590

 *5-25 - 710

 5-20 - 840

 710 PE

 630 PE

 530 PE

 400 PE

 8-20-20

 8-25-23

 8-34-32

10. *3M Corp. Felt Standard (Scotch Brite)

11. *GAF Corp. Felt Standard

12. GAF Felts (Experimental) Wex 1215

 *2A Density 1.8 Denier 40

 *5A Density 1.36 Denier 40

 *8A Density 1.00 Denier 40

13. *Snuffer Tube Concept

 Proposed by Boeing

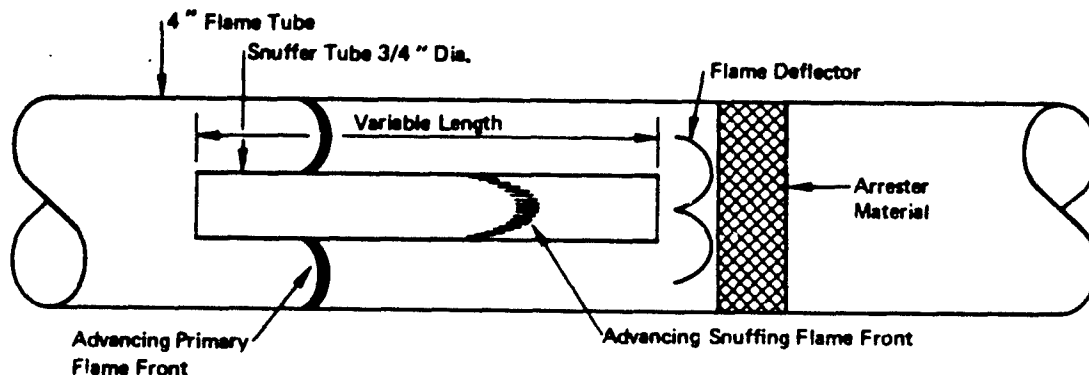
 *6".0 Long

DESCRIPTION OF PROPOSED SNUFFER TUBE AND EXTINGUISHING PHILOSOPHY

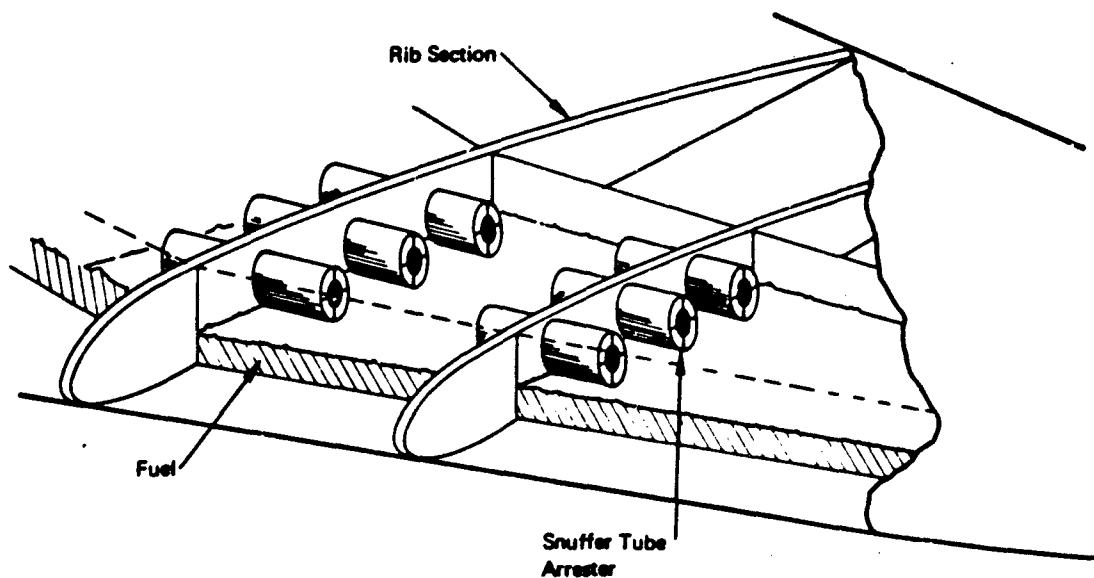
The parameters involved in extinguishing an explosion are combustion volume relief area, arrester thickness, ignition source, and rate of burn. These latter conditions relate to the gas velocity expanding through the arrester. The snuffer tube was introduced to the test program in an attempt to control the speed of the flame front at the arrester.

This concept would create a condition where the flame speed in the snuffer tube would be greater than that in the annular space. The flame front direction in the snuffer tube reverses, collides with the advancing flame front in the annular space and arrest occurs. This concept would be used in conjunction with an arrester material.

This concept was thought practical if this self-extinguishing flame front resulted in conditions at the arrester face that allowed the use of a substantially reduced arrester material thickness.



The application of this concept within an aircraft tankage, if shown acceptable, could be used in conjunction with a flame arrester in an aircraft wing tank as shown below.



The advantages of this particular concept would be a reduction of pressure drop through the arrester material due to increased efficiency of flame arrest.

14. Hough Industries Arrester (Reference3)

- * 010 Sample
- * 006 Sample

15. Fiberglass Cloth

- * 5 oz
- * 10 oz

16. J. P. Stevens Co.

- * Quartz Fiber Style 594
- Quartz Fiber Mat

Material request made to the GAF Corporation resulted in the purchase of nine materials that varied from their standard polyester fiber. This material was coded WEX 1215 and each 40-square-foot sample was supplied approximately 4 inches thick, with the binder material compatible with JP4 and JP5 fuels.

PROPERTIES OF WEX 1215 SAMPLES

Sample No.	Density (lb/ft ³)	Denier	Fiber Type	Porosity (% voids)	Fuel Retention, 3-min drain (wt %)	Fuel Displacement (% vol)
1A	1.80	25	Kodel Type 231	97.9	130	2.1
2A	2.3	50	Kodel Type 431	97.4	118	2.6
3A	1.1	15	Kodel Type 231	98.7	173	1.3
4A	1.2	25	Kodel Type 231	98.6	203	1.4
5A	1.3	50	Kodel Type 431	98.5	146	1.5
6A	1.1	15	Kodel Type 231	98.7	166	1.3

7A	0.9	25	Kodel Type 231	98.9	224	1.1
8A	1.2	50	Kodel Type 431	98.6	149	1.4
9A	1.0	15	Kodel Type 231	98.8	202	1.2

The general properties of these samples are:

Fiber	Kodel Polyester
Binder	M3 Melamine Formaldehyde
Fiber	Specific Heat - 0.32 cal/gm/ °C
Hydrolytic Qualities	Long-Time Stability in the Presence of Moisture at 212°F
Fuel Resistance (JP4-JP5)	Completely Stable

3.0 INSTRUMENTATION

Ten photodiodes (Texas Instruments H-35) are positioned on the upper surface of the tubes and spaced so that the flame speed can be measured. A reflective foil is taped on the opposite side of the tube to reflect as much light as possible into the photodiodes.

Test instrumentation consists of two basic parts. The first is for setup and control of the test conditions and consists of pressure measuring instruments; second is for obtaining data during the test. It consists of the photodiodes to measure flame speed, thermocouples upstream and downstream of the test section, and high-speed movie coverage of the most promising materials under test.

A block schematic of the instrumentation system used in Mode 1A testing is shown in Figure 7 and a listing is included as Figure 8.

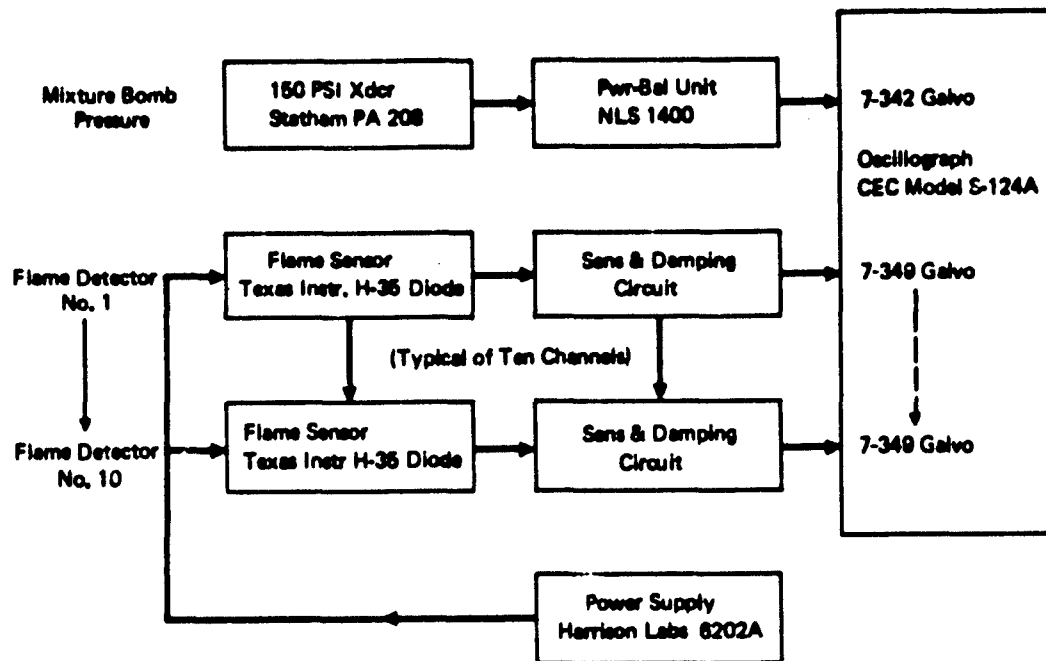


Figure 7 : Instrumentation Schematic

Variable to be Measured			Range		Accuracy Required % FS	Frequency of Variable (CPS)	Sample Rate Required (SPS)	Oscil	Remarks
Item No.	Sym	Description	Min	Max					
1-10	PD1 PD10	Photo Diodes T.J. H35					Cont	✓	Flame Speed Measurement
13	PS1	Sample Test Bomb Pressure	0 PSIA	180 PSIA	± 2%	Steady			Existing From 2288 TP
14	VS1	110V AC Solenoid Valve	-	-					Test Control
15	VS2	110V AC Solenoid Valve	-	-					Test Control
16	VS3	110V AC Solenoid Valve	-	-					Test Control
17	VS4	110V AC Solenoid Valve	-	-					Test Control
18	VS5	110V AC Solenoid Valve	-	-					Test Control
19	VS6	110V AC Solenoid Valve	-	-					Test Control
20	M	Acoustic Mixer							Verifies
21	IG1	Ignition Source							Sample Test Bomb Existing from 2288 TP
22	IG2	Ignition Source							New - Event Marker

Figure 8: 4.0 Inch Flame Tube Instrumentation Listing

4.0 IGNITION SYSTEM

The spark igniter is a modified automotive spark plug powered by a 15-kv maximum transformer. Normal output voltage, however, is adjusted to approximately 8 kv by variation of the input voltage. A similar transformer energized the spark plug within the mixing chamber bomb sampler.

5.0 TEST PROCEDURE

Test Section Buildup -- A typical test section buildup is shown schematically in Figure 9. As shown, the flame arrester sample was placed in the downstream end of the test section. For arrester samples less than 4 inches thick, spacer sleeves were used to support the upstream face. For selected runs, a 4-mesh stainless steel support screen was placed on the downstream side of the sample.

To minimize "organ pipe resonance" interference with the flame front propagation rate, an annular cross-section of acoustic material approximately 10 inches long was placed at the downstream end of the flame tube (References 5 and 6).

Preparation of Air-Fuel Mixture -- A 4.5% propane air mixture was used for runs in this phase of the program. Mixing was accomplished through the partial pressures of the component gases as shown in Figure 10. The propane was added to the mixing tank through Valve VS3 and the tank partial pressure monitored on a mercury manometer by opening Valve V5. After Valves VS3 and V5 were closed, air was added to the tank through Valves V7a and V7b. Tank pressure was monitored on a 0-to 60-psig pressure gauge. Valves V7a and V7b were then closed. A 4-inch-diameter speaker with a 1-inch diameter orifice plate was used for in-tank mixing. The speaker was not energized until all personnel had cleared the test cell.

Evacuation of the Flame Tube -- Thin neoprene disks (1/16 inch) were attached with vacuum grease to the end flanges of the flame tube. Metal end plates were manually held over these neoprene disks as the vacuum pump was turned on and valves VS5 and VS6 were opened. As the vacuum in the flame tube

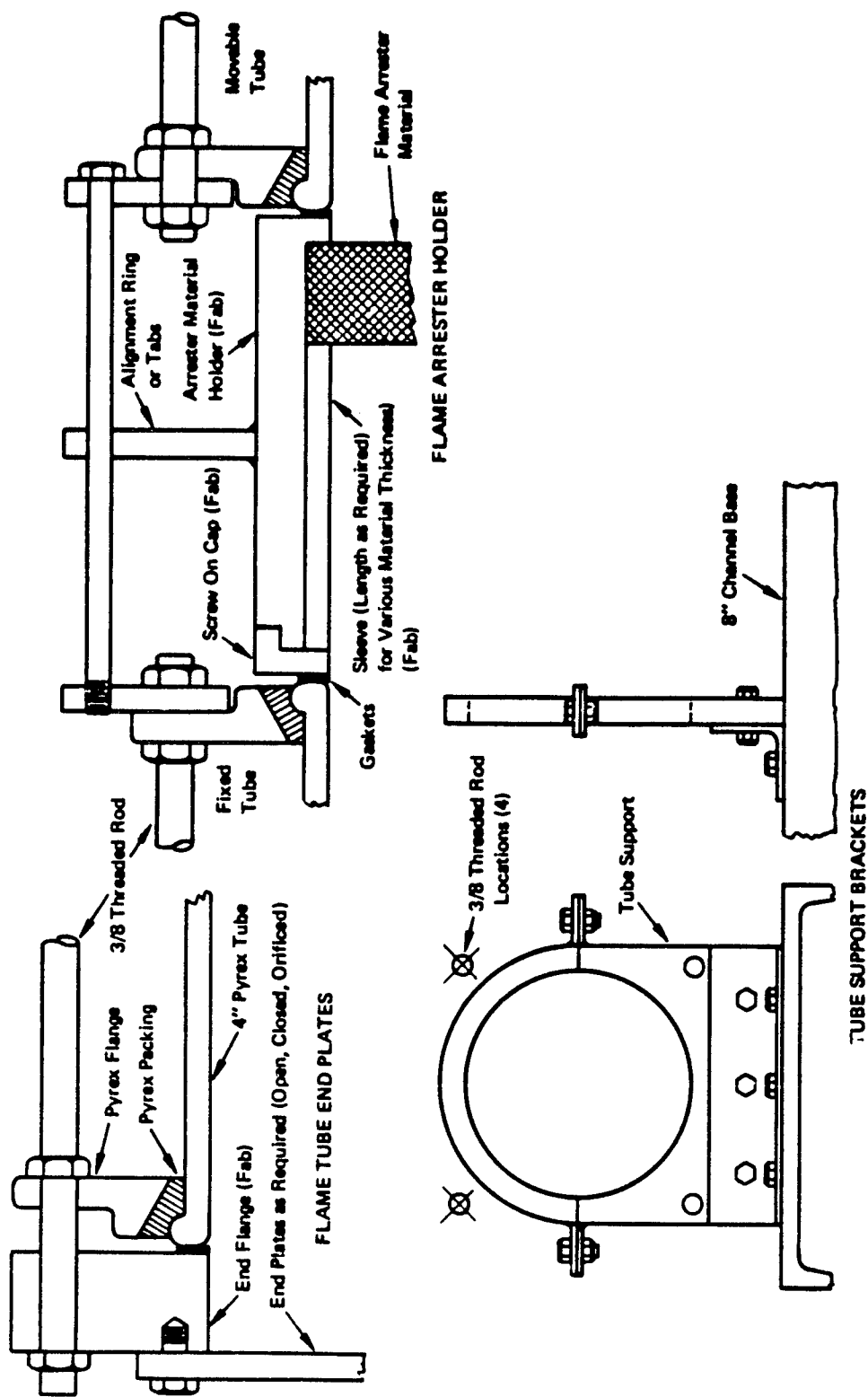


Figure 9 : Mode 1A Screening Tests 4.0-Inch Flame Tube

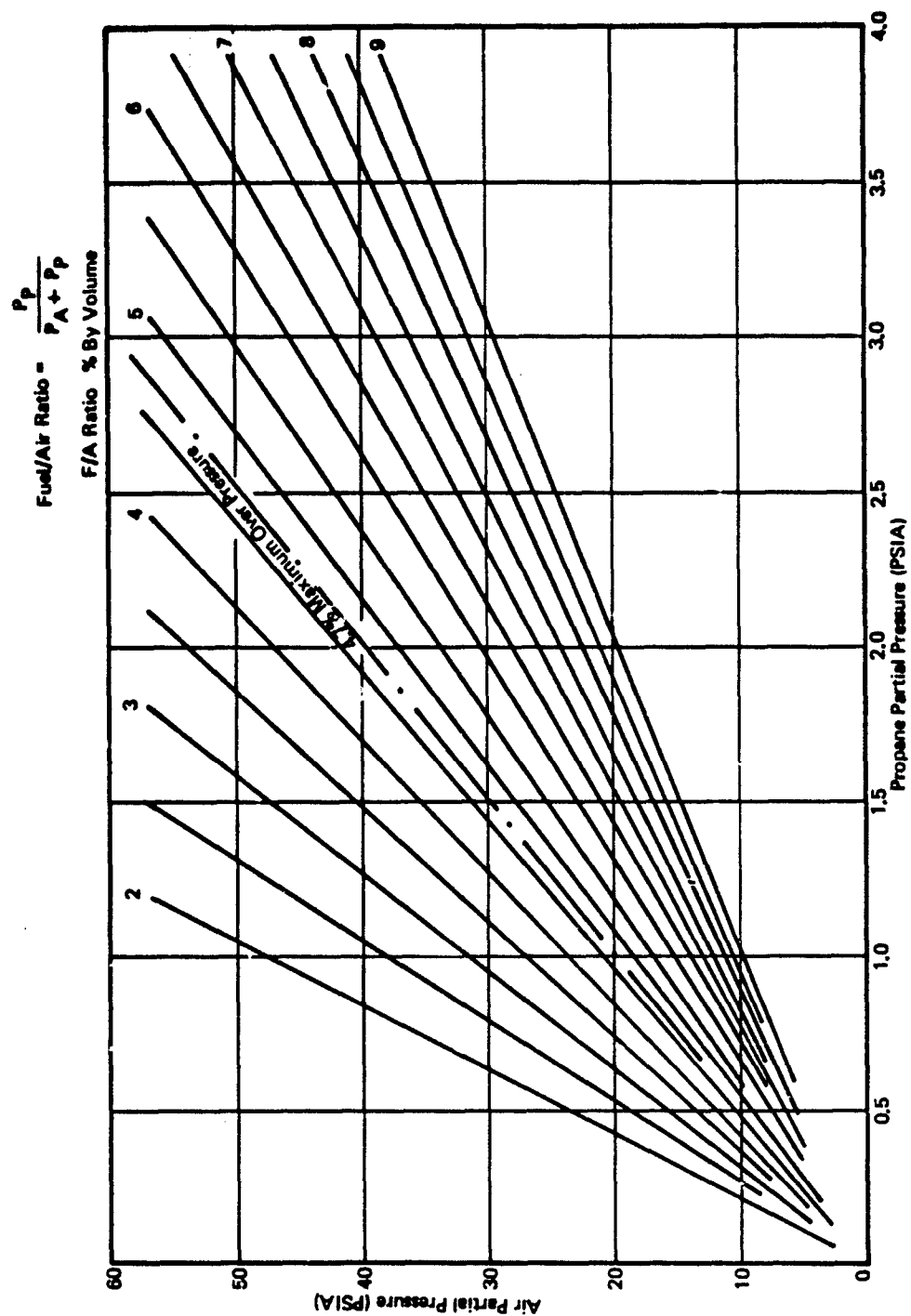


Figure 10: Variations of Fuel-to-Air (Volume) Ratios

increased, these metal plates were self-supporting. Opening Valve VS5 allowed the mixture bomb and flame tube to be evacuated simultaneously. Both chambers were evacuated to -14.5 psig, with the vacuum monitored on mercury manometers through Valves V4 and V8.

After both the flame tube and mixture bomb had been evacuated, the vacuum pump was turned off and Valves VS5 and VS6 closed.

Filling the Flame Tube and Mixture Bomb -- The fuel air mixture was introduced to the flame tube and mixture bombs through Valves VS1 and VS2, respectively. Both chambers were brought up to ambient pressure. As the pressure in the flame tube approached ambient, the metal end plates dropped off, leaving only the neprene disks over the tube end. Mercury manometers, through Valves V4 and V8, were used to monitor the chamber pressures. All valves were then closed.

Firing the Mixture Bomb -- Prior to the evacuation of the mixture bomb, the 150-psig pressure transducer on the mixture bomb was set for zero and span calibration, and the oscillograph was set for paper speed of 16 inches/second. The oscillograph was turned on and, immediately thereafter, the mixture bomb fire switch was depressed. After approximately 2 seconds the oscillograph was turned off.

The maximum height of the bomb pressure trace was measured and, using the sensitivity of 100 psi per inch, converted to pressure. A pressure rise of greater than 90 psi indicated a proper fuel-air mixture.

If the mixture proved unsatisfactory, the flame tube and mixture bomb were evacuated to -14.5 psig. The mixing tank was vented to ambient through the manual control arm on the 30-psig relief valve. The tank was then purged several times and a new combustible "batch" was mixed.

Firing the Flame Tube -- The oscillograph was turned on and the flame tube FIRE switch immediately depressed. The oscillograph was left on until all evidence of flame in the tube had disappeared.

Following the firing of the flame tube, the vacuum pump was again turned on, Valve VS5 was opened to evacuate the bomb, and the mixing tank was vented to ambient pressure through the 30-psig relief valve.

Test Data -- The oscillograph record with 0.01-second timing lines and the photodiode output traces, denoting passage of the flame front, together with the measurement data on the photodiode locations, allowed the flame front velocity in the tube to be calculated.

The observed linear flame speed was controlled by the use of orifice plates positioned at each end of the tube. The fastest flame speed was obtained by closing the ignition end and fully opening the other; the slowest by fully opening the ignition end and closing the other end. Due to the nature of the tests, pressure was not a recorded parameter. In all tests the required flame speed was obtained with one end of the tube fully opened, consequently, the pressure rise would be related to the pressure drop along the tube and across the arrester material and has generally been considered to be very low.

The flame speed orifice plates used in the program were as follows:

<u>Diameter</u> <u>(in.)</u>	<u>Area</u> <u>(%)</u>
4	100
3.795	90
3.347	70
2.828	50
2.19	30
1.26	10
1.09	7.5
0.89	5

6.0 RESULTS AND DISCUSSION OF RESULTS

The flame speed comparison tests for different materials allowed a quantitative rating of each material. The graphical and tabular results relating the observed flame speed with the thickness of arrester material required for arrest are shown numerically in Table A-I and Figures A-1 through A-9, (Appendix A).

A trace of typical data obtained for each of the 288 flame tube tests is shown in Figure 11. It is noted that the observed flame speed is calculated from the time taken for the flame to pass Photocells 3 and 5 for Runs 1 through 22 and 4 and 7 for Runs 23 through 288 (Reference Figure 11). The relocation of photocells was made to allow a more in-depth review of the flame speed before the arrester is encountered.

A typical bomb sample data trace is shown in Figure 12. These data show the slight increase in pressure and reduced burning time associated with locating the spark ignition source 4.0 inches into the 10.0-inch-long chamber. A calculation of the flame speed for correlation with the mathematical model follows.

Assuming that maximum bomb overpressure occurs when the flame front propagating spherically from the ignition source hits the end wall, then it follows that the average flame speed relative to the walls is given by:

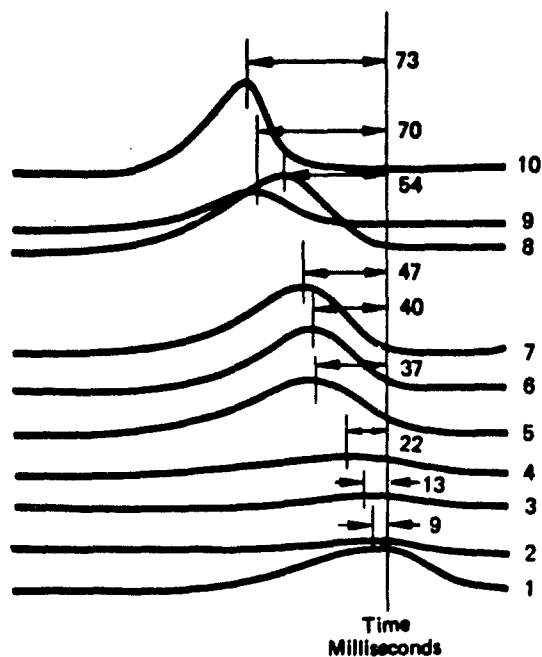
$$\begin{aligned} S_A &= XLC/t \\ &= 10 / (12 \times 0.102) = 8.17 \text{ (fps)} \end{aligned}$$

where XLC = length of explosion chamber (inches)

t = time of pressure rise (seconds)

Similarly with the ignition source located 4.0 inches into the chamber:

$$S_A = \frac{(10-4)}{12 \times .69} = 7.25 \text{ fps}$$



RUN 164
(Immediate Burn Through)

$$\begin{aligned} \text{Average Flame Speed} &= \frac{\text{Distance Inches 4 - 7}}{\Delta \text{ Time 4 - 7}} \\ &= \frac{27}{.047 - .025} = 1080 \end{aligned}$$

$$\begin{aligned} \text{Average Flame Speed} &= 1080 \text{ Ins/Sec} \end{aligned}$$

RUN 162
(Arrest)

$$\begin{aligned} \text{Average Flame Speed} &= \frac{\text{Distance Inches 4 - 7}}{\Delta \text{ Time 4 - 7}} \\ &= \frac{27 \text{ Ins.}}{.485 - .295} = 142 \text{ Ins./Sec} \end{aligned}$$

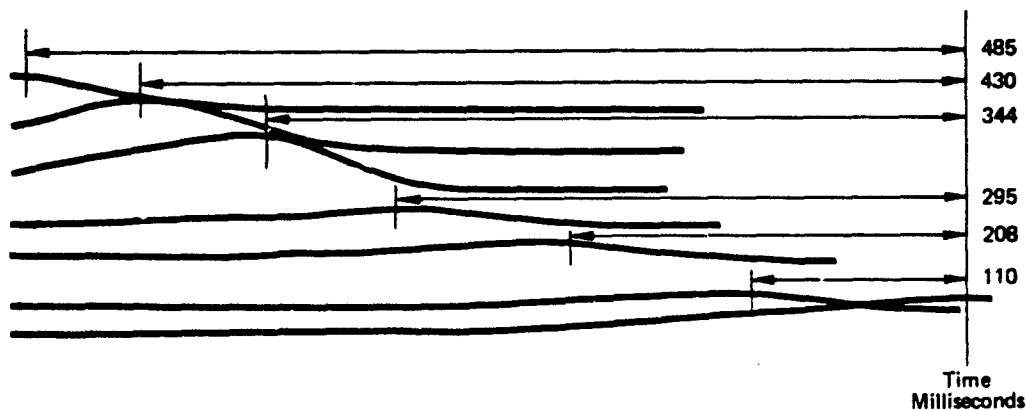
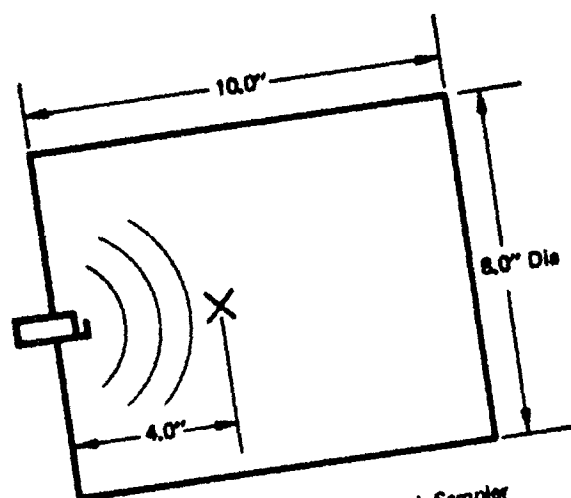


Figure 11: Typical Data Traces



Dimensions of 4.0" Flame Tube Bomb Sampler

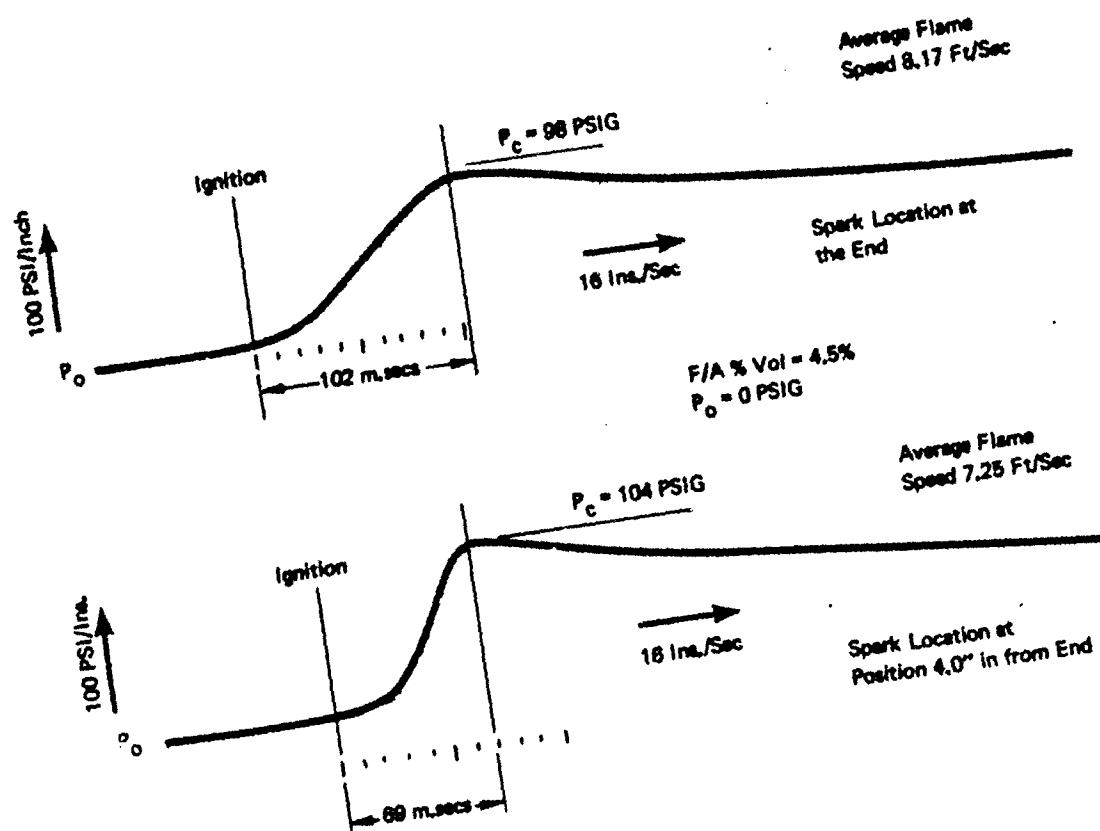


Figure 12: Typical Pressure Versus Time Traces for Various Bomb Ignition Locations

Reference 7, page 528, indicates that the apparent flame speed lies between 9 and 12 fps assuming

- 1) The ratio of molecular volumes before and after ignition $M = 1.04$
- 2) The fundamental flame speed S_0 about 1.25 fps
- 3) Flame temperature T_e between $1,300^\circ\text{K}$ and $2,300^\circ\text{K}$

The burn-through data resulting from these tests allowed the following materials to be selected, based upon their flame-arresting qualities only.

The materials are listed (not in any order of preference) as follows:

- 3M Scotch Brite
- GAF Felt (Standard)
- GAF Felt (Type 2A)
- KCF Carbon Fiber
- Velstat 4611 x P Coated Foam
- Astroquartz Fiber Type 594 (10 Layers)
- Astroquartz Fiber Type 594 (6 Layers)
- Stainless Steel Screen, 20 Mesh, .016
- Stainless Steel Screen, 35 Mesh, .011

The arresting qualities of various materials were enhanced by selectively combining various arresters. For instance, the velocity of flame required for burn through 25-ppi foam could be increased by installing stainless steel screens at the front and rear of the sample.

It is interesting to note that the test results obtained with the 15-ppi and 10-ppi reticulated polyurethane foam (Figure A7) shows that the 10-ppi foam produced very erratic data, becoming stabilized only when the pore size increased to 15 ppi and 25 ppi.

The 15-ppi foam allowed flame speeds less than 350 inches per second to pass through but arrested the high flame speeds. These data essentially substantiate the results of Reference 2, in which flame speed was considered an important consideration in the mechanism by which reticulated polyurethane foam arrested a moving flame front.

Photographs of material samples showing the extent of damage for various test conditions are shown in Figures A-10 through A-17.

The material selection results from the burn-through tests were then further evaluated for acceptable pressure drop characteristics.

The pressure drop across these selected materials was determined using dry shop air at 70°F (530°K). The results have been tabulated in Tables A-II through A-XIV and graphically represented in Figures A-18 through A-31.

The airflow versus pressure drop data taken were intended primarily for qualitative use. Consequently, all test data were taken within 10 to 20 seconds of establishing an airflow condition.

Pressure Drop Analysis and Data

The pressure loss in a fluid system caused by factors other than fluid friction is normally expressed as a resistance coefficient (K) and is defined as the number of velocity heads lost for flow through a given obstruction (Reference 7).

Pressure drop in feet of fluid, Δh
 is given by $\Delta h = K h_v = K \left(\frac{v^2}{2g} \right)$
 converting units

$$\Delta P \text{ (lb/in.}^2\text{)} = K \frac{\rho v^2}{2 \times 144 \times g} \quad (1)$$

The weight of fluid flowing W is given by $W = \rho A v$
transposing and squaring

$$v^2 = \frac{W^2}{\rho^2 A^2} = \frac{16 W^2}{\rho^2 \pi^2 D^4} \quad (1A)$$

substituting equation (1A) into (1) and standardizing units

$$\Delta P \text{ (lb/in.}^2\text{)} = \frac{16 \times K \times W^2 \times 144^2}{2 \times 144 \times \pi^2 \times \rho \times D^4 \times g \times 3,600}$$

where D = tube diameter in feet.

$$\text{Pressure drop } \Delta P = K \times \frac{0.0133 W^2}{D^4} \quad (2)$$

It is convenient to express variations of K for typical obstructions as a function of Reynolds $N^0 = (R_e)$

$$R_e = \frac{V D}{\mu} \quad (2A)$$

where μ = viscosity (for air at NTP)
= $1.427 \times 10^{-4} \text{ ft}^2/\text{sec}$

Rewriting Equation (2A) and normalizing units compatible with Equation (2) results in

$$R_e = 23,500 \frac{W}{D} \quad (3)$$

P = lb/in.²

W = mass flow in lbs/min

D = diameter in inches

ρ = density (0.076 lb/ft³ for air)

g = gravitational constant (lb(m)-ft/lb(f) - sec²)

v = velocity in fps.

The values of K have been calculated from this data using Equation (2) and have been graphically represented for each material as a function of Reynolds number using Equation (3).

It would be expected that the velocity head loss K will reduce as Reynolds number increases until a constant value of K is obtained. However, it is generally shown in the data pertinent to foams and felts that compressability of the arrester material allows the K value to increase prior to establishing a theoretical value that remains constant. These data allow comparisons of degree of pressure drop for each material tested.

In the real world, however, the arrester will be compressed as the expansion and expulsion of hot combustion gases through the material occurs as a result of an explosion. This compression will be immediate and will continue until the pressure drop is high enough to achieve the following conditions.

Maximum overpressure is reached, determined by

- Arrester thickness
- Relief area
- Pressure drop (K factor)
- Arrester tensile strength

The key was to find an arrester that did not allow fast or slow moving flame fronts to propagate through, that also had low-pressure drop characteristics, i.e., a low K factor.

The pressure drop through the apparatus and holding screen with no arrester installed would not indicate a pressure drop for the highest airflow tested, and would be considered so low that its influence on the test data could be ignored.

The test data taken indicated that the foam and felt materials offered a large wetted area to the airflow and that compression of the material while holding an air flow setting influenced the pressure drop, resulting in pressure drop data that vary with time.

Data from Reference 2 using 10-ppi orange foam for the arrester indicated that an airflow in excess of 8 to 9 pounds per minute would compress the foam, and at 15 pounds per minute it would have been compressed to 42% of its original thickness. The material pressure drop data are summarized in Figure 13, allowing easy comparison for each material.

The airflow pressure drop data were obtained by passing dry air through a 4.0-inch-thick material sample. The correlation of velocity head loss (K factor) with Reynolds number, resulting in a constant value of K, inherently assumes that the material does not compress or has compressed to some maximum value. When the material has compressed its full amount, only then could K remain constant.

The thickness of material chosen for the airflow pressure drop analysis was commensurate with that applicable to this total program. Obviously if a relatively thick sample had been chose, say 12 inches, the K factor would continue to increase as the material continued to compress, until a maximum physical thickness was reached, determined by material density. At this condition the velocity head loss (K) would indeed be constant, but would be of a higher value than that obtained from a thinner sample, depending upon the original material thickness and density and porosity.

From this summary curve the following materials resulted in acceptably low pressure drops.

- 011 Stainless Steel Screens, 35 Mesh
- 016 Stainless Steel Screens, 20 Mesh
- KCF-100 No. 10 Mesh Screen
- Quartz-Fiber Type 594
(Note that these samples were supplied by Hough Industries, Inc.)
- 3M Felt (Std)
- 25-PPI Foam
- Custom Material 7611 XP Foam
- 10-PPI Foam
- GAF Felt (Std)

Following tests conducted with the Astroquartz samples H1110 and H1106 supplied by Hough Industries, Inc., tests were conducted on 5-ounce and 10-ounce glass cloth.

It is noted that two screens of 10 OZE glass cloth were sufficient to arrest all flame speeds that the apparatus could produce; however, with reference to Figure 13 the pressure loss is rather high. It is hypothesized that

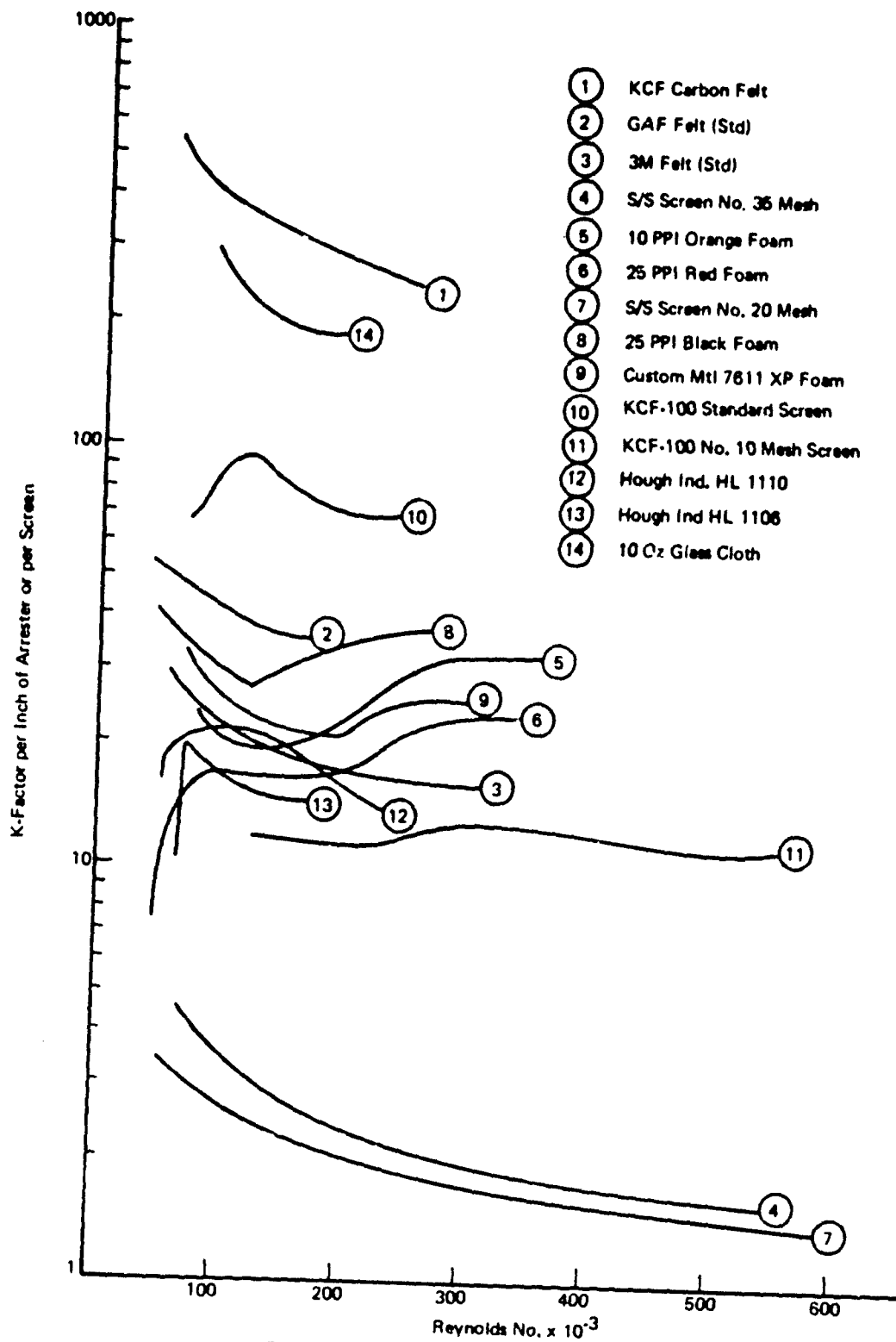


Figure 13: Arrestor Material Pressure Drop Data Summary

given time to develop this type of arrester, an open weave mesh could be obtained, such that the pressure drop approaches a K factor per screen of Ω 5 and that four or five could be assembled so that the K factor approached that of 1 inch of 25-ppi reticulated polyurethane foam. The snuffer tube concept was tested in conjunction with 2 layers of 20 mesh stainless steel screen. The flame speed was varied between 173 ins/sec and 475 ins/sec. Previous tests had concluded this to be an area of burn-through and any improvement in flame arresting capability at these conditions could be attributed to the use of a snuffer tube. Tests 180 and 181 with the snuffer tube resulted in immediate burn-through and further tests were not undertaken.

Figure A-7 shows the variations in arrester thickness and flame speed for the 15 ppi foam. These data show a relationship between flame speed and arrester thickness. Data resulting from tests with the 20 mesh -016 stainless steel screens shown in Figure A-9, indicate that for a combined arrester thickness, up to 4 screens, the area of arrest was reverse to that obtained for the 15 ppi foam.

Correlation of test data obtained from these two materials was thought permissible as their pore sizes appear to be similar, reference Figures A-11 and A-14.

7.0 CONCLUSIONS AND RECOMMENDATIONS

It is concluded that flame speed is an important parameter in ascertaining the capabilities of arrester materials to stop a propagating flame front.

Metal screens arrested slow moving flames and allowed higher flame speeds to propagate through, while generally the fibrous arresters (i.e., foams, felts, etc.) arrested fast-moving flame fronts and allowed slow-moving flames to pass through.

The data would indicate that when the number of screens was increased to 4 or more, the assembled screens arrested all the flame speeds tested. Reducing the screen mesh to a 35-011 resulted in the same characteristic curve as shown in Figure A-9. These results show that a threshold of arrester thickness occurs, beyond which a particular material will arrest all flame speeds. The test data obtained would indicate that the material type, pore size (affecting the quenching distance), thickness, and flame speed at the time of arrest are all influencing parameters.

This application could be adopted and generalized around the techniques developed from the Space Lattice Wing Base Development Program proposed by the Boeing Aerospace Company (Reference 9) submitted to the Air Force Materials Laboratory, June 1972.

Vibratory flame travel was audibly noted during most tests where a very slow or very fast moving flame front was propagated. Tests with the foam materials usually result in a severely damaged and burnt back face if a burn-through occurs.

It has been concluded as a result of all flame tube and associated air flow pressure drop tests that the following materials and variations of assembly and combinations of these materials show promise as flame arresters:

- 3M Scotch Brite
- GAF Felt (Standard)
- GAF Felt (Type 2A)
- 25-ppi Foam
- 15-ppi Foam
- 5-ounce Glass Cloth (Fiberglass)
- Astroquartz Type 594
- 016 Stainless Steel 20-Mesh Screen

Consequently these materials, and combinations of them, were further evaluated in the variable geometry test rig during the ensuing program.

A new material suitable for use as a flame arrester has been developed by J.R.L. Associates of 46 Saranac Avenue, Lake Placid, New York 12946 (518-523-9066). The process treats a special alloy aluminum sheet in such a way that, after being coiled, the material resembles a semi-rigid cellular foam or sponge. Material samples have been requested. However, this material/process was developed too late to be included in the present program.

The cost of this material is estimated to be \$3.00 per cubic foot, its weight is 3 lbs./ft.³.

While weight and assumed retention penalties appear to prohibit use within fully packed tankage, its application within gross voided tankages could be practical.

It is recommended that this material be subjected to tests similar to those undertaken during Task I of this program to establish pertinent arresting and pressure drop characteristics. These data will allow a determination of the application of the material in gross voided tankages.

SECTION V

TASK I MODE IB TEST PROGRAM

1.0 TEST APPARATUS

Overall views of the mode IB test set-up within the hazardous cell are shown in Figures 14 and 15. In Figure 15 the combustion chamber is shown with a foam specimen in the test section. The major items in the set-up are identified in Figure 14, from left to right, as the mixing chamber, 18-inch flame tube assembly, flame tube vacuum pump (upper right), and the mixture bomb (lower right). A schematic of the test set-up showing the interconnecting plumbing and test instrumentation is included as Figure 16. The 8.5-cu-ft mixing tank was the same as used in Mode IA testing. This tank, however, was retested hydrostatically to 860 psig to allow higher batch mixing pressures.

18-inch Variable Volume Flame Tube

The 18-inch flame tube was fabricated from 18-inch diameter, schedule 10, mild steel pipe. The maximum working pressure was determined to be 252 psia.

Following fabrication, a stresscoat analysis was performed on the 18-inch flame tube to locate areas of high stress. The stresscoat has a strain threshold of 24 ksi, assuming a modulus of elasticity of 30×10^6 psi.

When the tube was hydrostatically tested to 250 psig, no cracks were detected in the coating. Considering the accuracy of the technique, the stresses on the flame tube shell and welds were considered to be less than 30 ksi at the maximum test pressure.

The factors of safety were therefore calculated to be:

Yield: 1.27 to 1.96 factors @ 250 psig

Ultimate: 2.00 to 3.12 factors @ 250 psig

Preceding page blank

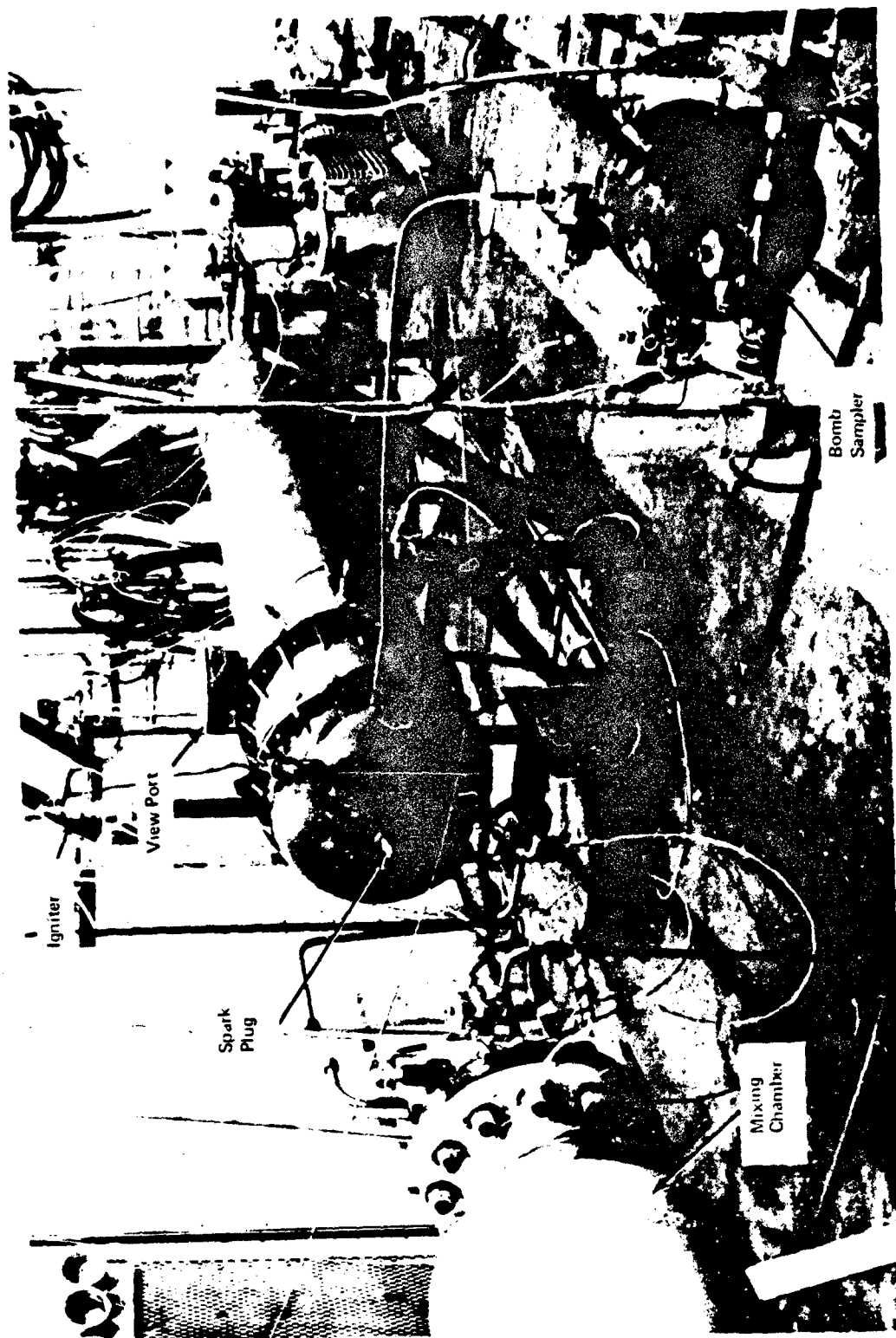


Figure 14: Variable Geometry Test Apparatus



Figure 15: Variable Geometry Test Apparatus (Foam Installation)

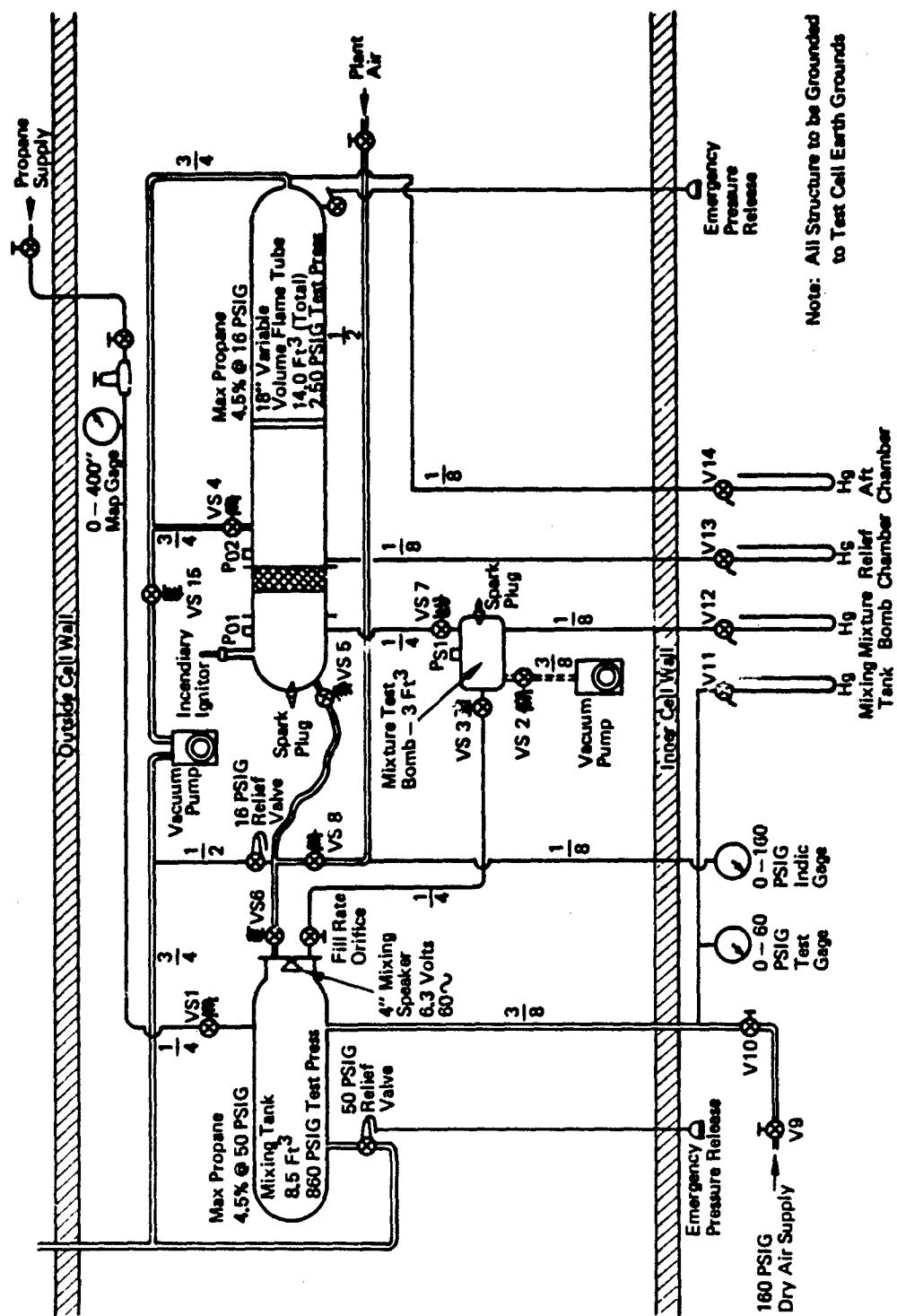


Figure 16: Variable Geometry Flame Tube Test Schematic

This assembly was designed for a maximum total volume of 14.4 cubic feet and was fitted with a variable partition. For test runs in Mode IB, the partition was set for a maximum volume of 12.8 cubic feet. A cross section of the 18-inch-flame tube is shown in Figure 17.

The principal components of the flame tube include:

- 1) Combustion chamber head, Volume: 0.955 cubic feet
- 2) Test section, 7.6 inches long, volume: 1.575 cubic feet
- 3) Test section, 11.2 inches long, volume: 1.576 cubic feet
- 4) Test section, 4.0 inches long, volume: 0.574 cubic feet
- 5) Main section volume: 9.1 cubic feet (as used in Mode IB testing). This section contained the variable partition, viewing window, relief volume, and relief foam. The flame tube support structure was attached to this section.

Nominal combustion volumes of 1.0, 1.5 and 2.0 cubic feet could be set by using the (1) section, (1) and (4) sections, and (1) and (2) sections, respectively. The flame arrester specimens were installed in either the 11.2-inch, 7.5-inch, or the 4.0-inch section, depending on the specimen thickness.

2.0 MATERIAL DESCRIPTION

The materials tested at various thicknesses during the test program are listed as follows:

25-ppi Red Foam
15-ppi Yellow Foam
3M Scotch Brite Felt
GAF Standard Felt
GAF Type 2A Felt
016 Stainless Steel 20-Mesh Screen
5-ounce Glass Cloth
Astroquartz Type 594

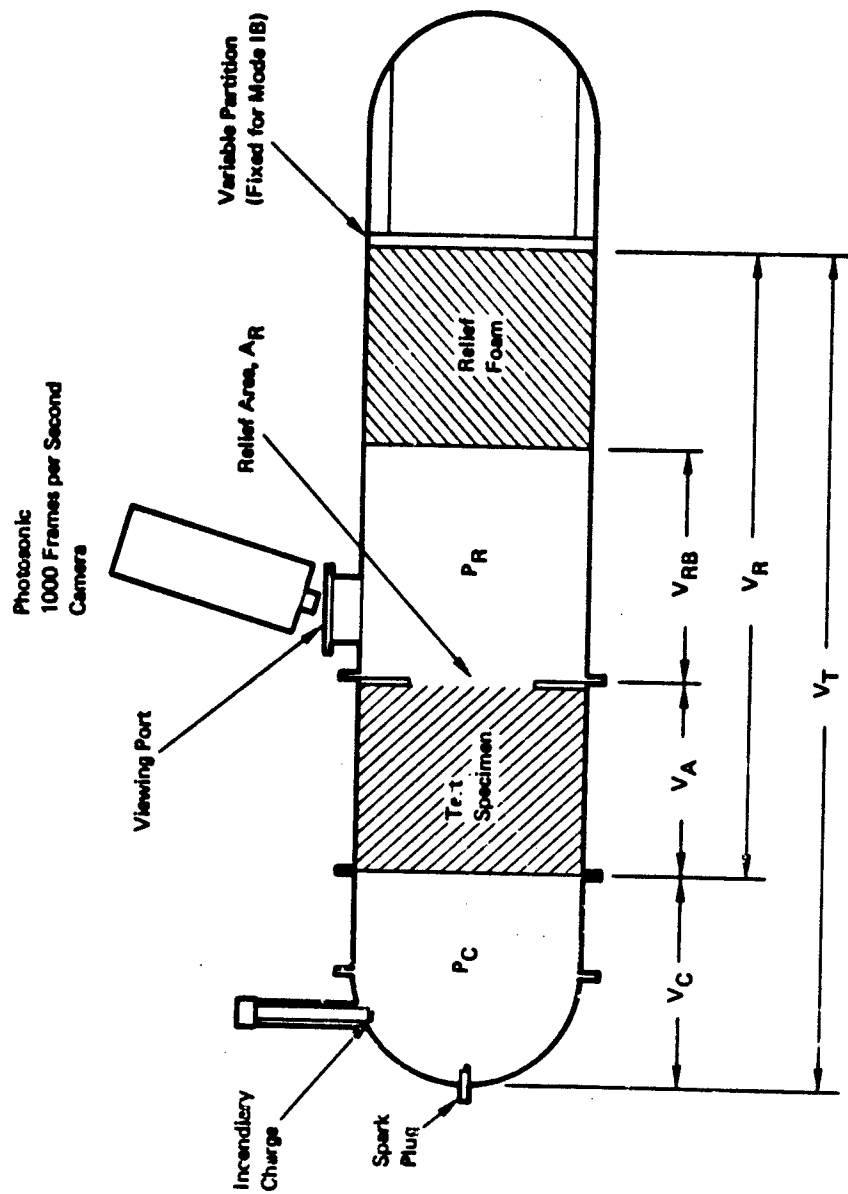


Figure 17: Variable Geometry Test Apparatus Sectional Layout

Tests were conducted with various combinations of the above materials in an attempt to improve flame arresting characteristics.

25-ppi Foam and Stainless Steel Screens
(Various Combinations)

25-ppi Foam and Astroquartz
(Various Combinations)

Astroquartz and Stainless Steel Screen

3M Scotch Brite Felt and Stainless Steel Screen

3.0 INSTRUMENTATION

The instrumentation consisted of two basic parts: the first part, for set-up and control of the test conditions, consists of pressure-measuring instruments; the second part was for obtaining data during the test.

A block schematic of the instrumentation system used is shown in Figure 18.

High-speed movies (1000 frames per second) were taken with a Photo-Sonics, Inc. 16 mm 1B-100 camera loaded with Ektachrome 7240 EF, ASA 160 film. The aperture was set at f 1.5.

4.0 IGNITION SYSTEM

The incendiary ignition circuit is shown in Figure 19. For 95% of all tests the AFAPL incendiary igniter was used. This device is shown in Figures 20 and 21. The incendiary powder composition as supplied by the Air Force (AFAPL) is as follows (Reference 10):

50/50 magnesium/aluminum	48%
50 Barium nitrate	50.5%
Asphaltum	1.5%

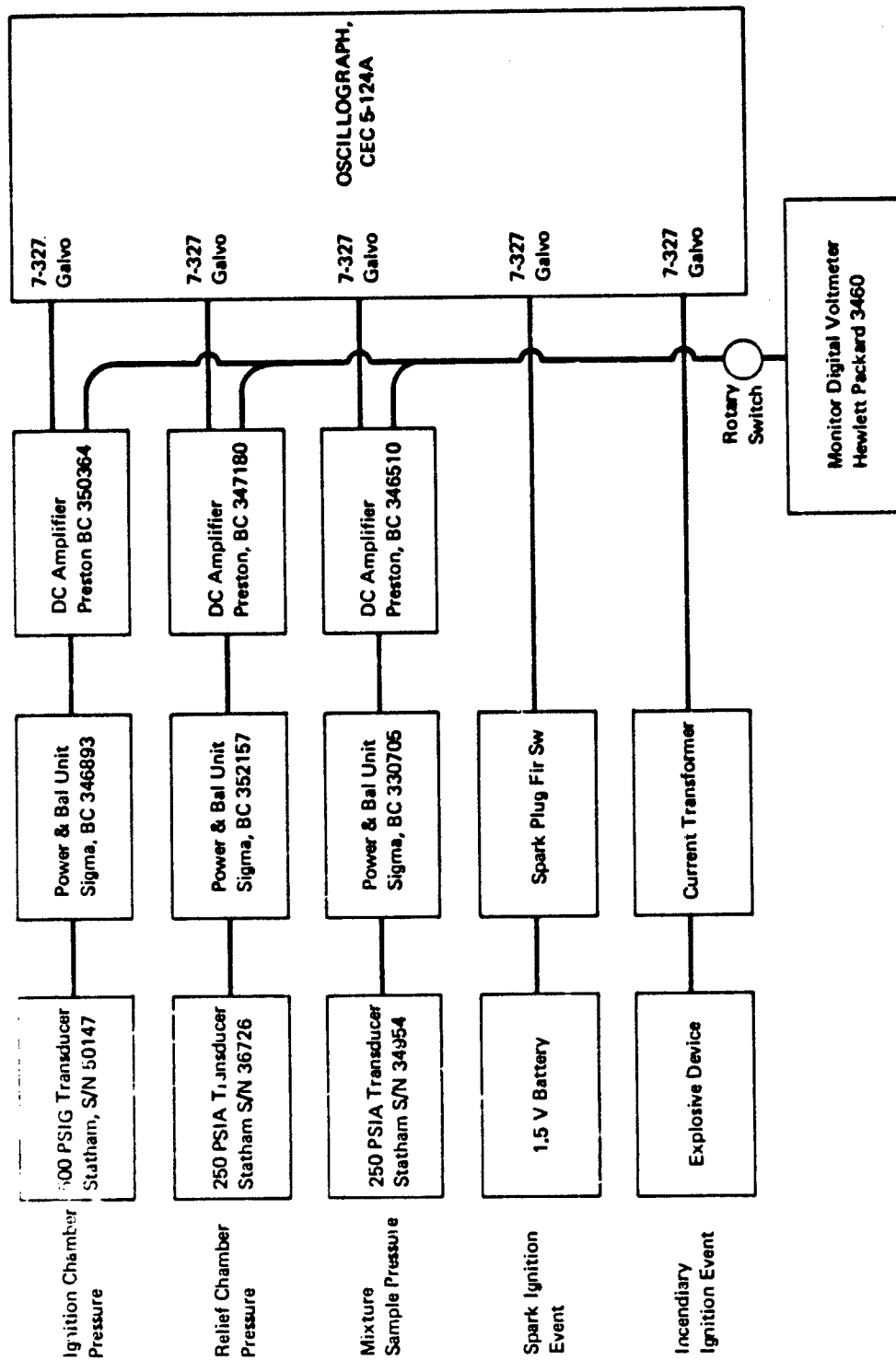


Figure 18: Instrumentation Flow Diagram

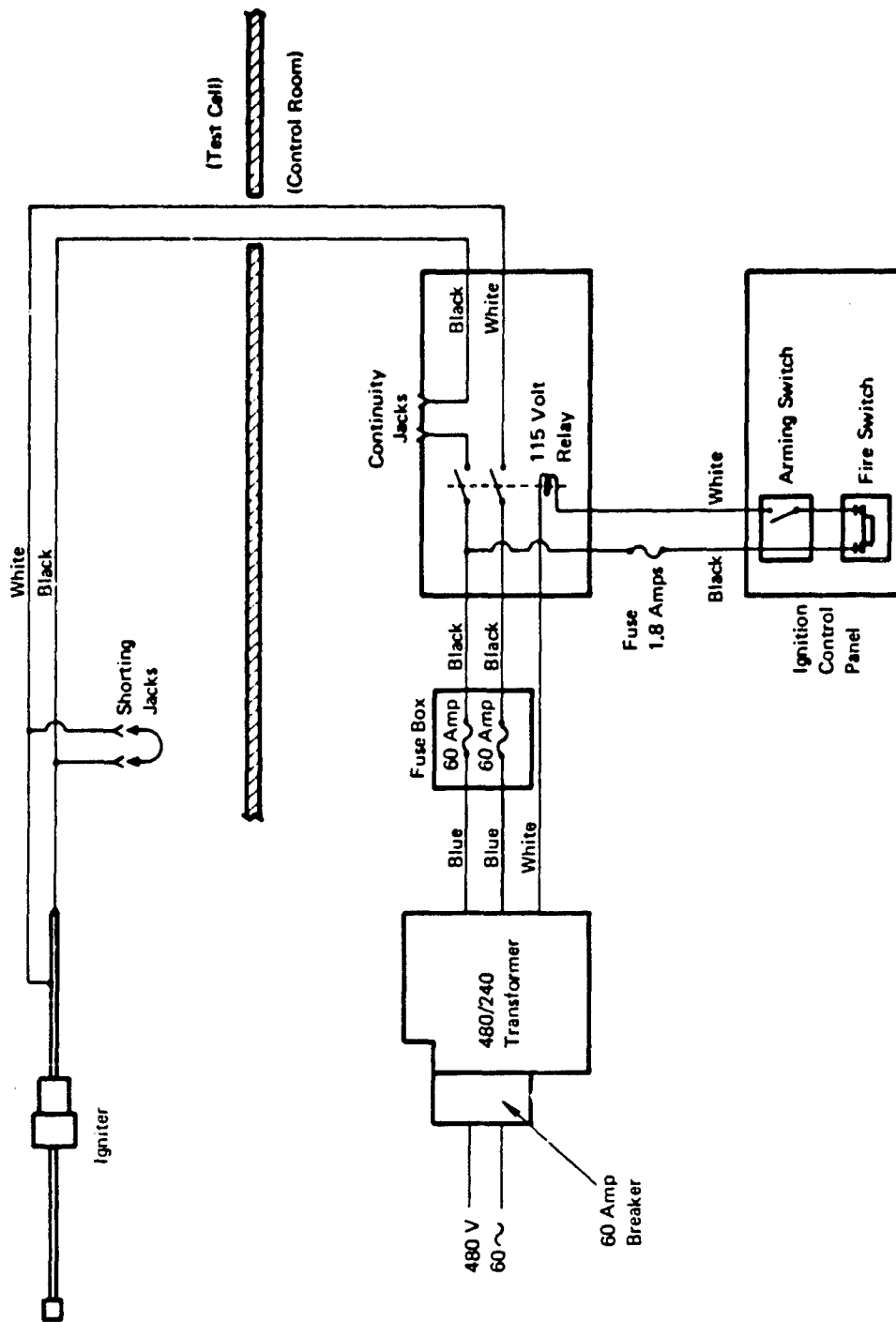


Figure 19: Incendiary Igniter Firing Circuit

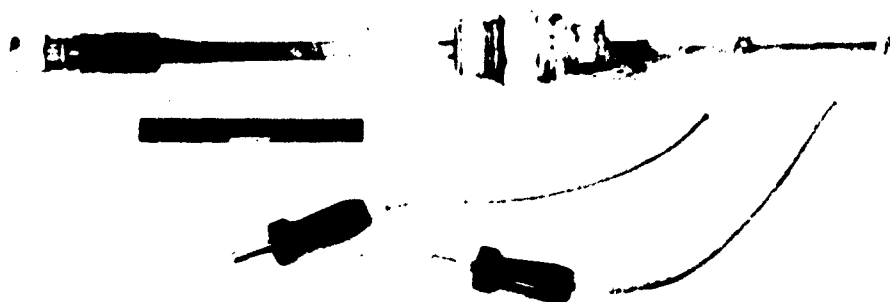
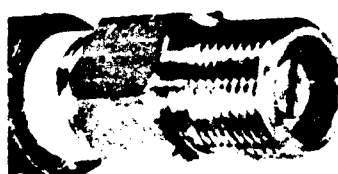


Figure 20: Igniter Assembly



Housing



Nut

Burst Disk



Figure 21: Igniter Charge Housing

The size of charge was approximately 30 to 40 grains per firing, depending upon the condition of the igniter used.

For tests with a spark ignition, a high-energy coil was used. The system was identical to that used during the preceding 4.0-inch-flame tube tests.

5.0 TEST PROCEDURE

Test Section Buildup -- Prior to installation of a test specimen, any remains of the previous specimens were wire-brushed from the chamber walls and the sample retaining screen, and the viewing window in the test chamber was wiped clean.

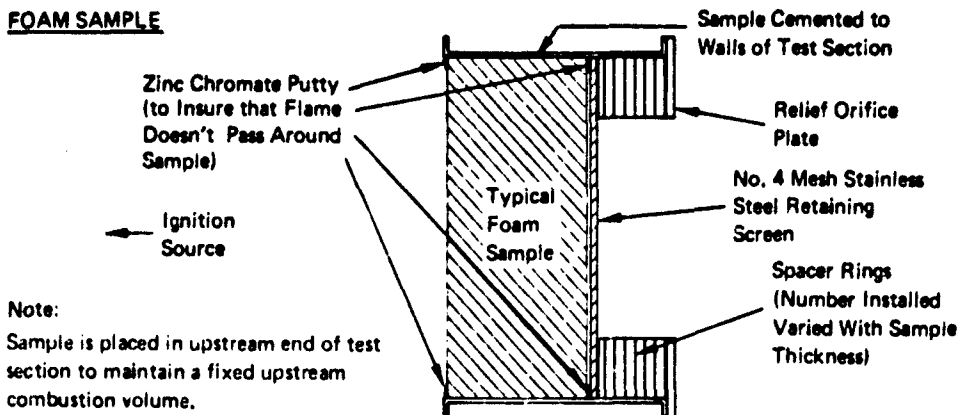
To maintain a controlled combustion chamber volume, the upstream face of the test specimen was located within 1/4 inch of the upstream test section mounting flange. In cases where the test specimen length was less than that of the test section, annular steel spacers were used between the relief-area orifice plate and the downstream face of the test specimen. A four-mesh stainless steel retaining screen was placed on the downstream side of the specimen.

To conserve materials, smaller-diameter test specimens were used for some runs with the 10% relief area orifice. In these instances the 8-inch-diameter specimens were installed in annular plywood spacers, stacked to the length of the sample, with an eight-inch inside diameter. These specimens were sealed in place as described above.

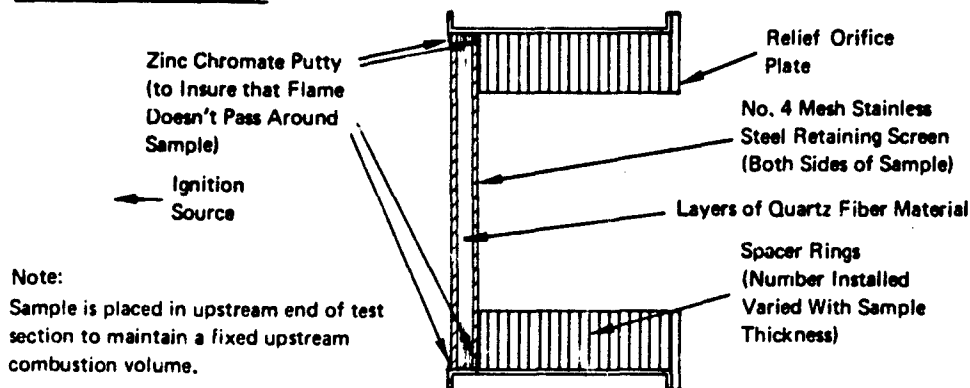
Typical test section buildups for large-and small-diameter arrester specimens are shown in Figure 22.

Preparation of the Propane/Air Mixture -- The mixing chamber was purged by opening the 160-psig dry air supply line. Valves V9 and V10 were then closed (reference system schematic, Figure 16) and the tank was then vented to ambient. This procedure was repeated three times.

FOAM SAMPLE



QUARTZ FIBER SAMPLE



SMALL DIAMETER FOAM SAMPLE

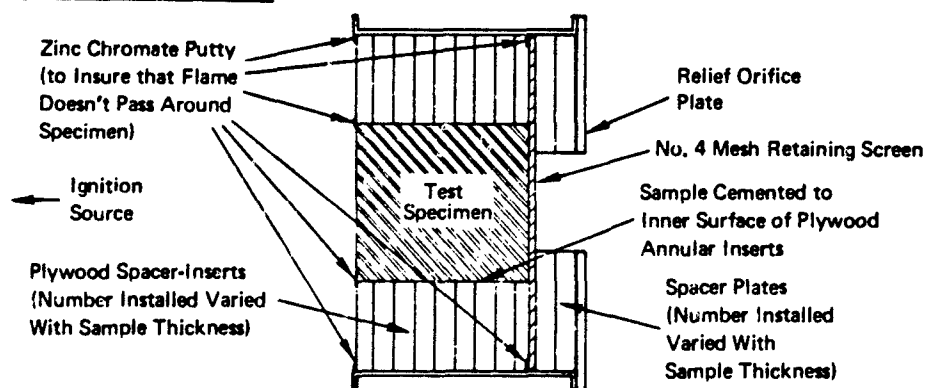


Figure 22: Typical Arrestor Installation in the Variable Geometry Apparatus

Following the final purge, the propane-air mixture was prepared using the partial pressure curves shown in Figure 10. As an example, to prepare a 4.7 volume percent mixture at 45 psig from a purged evacuated tank at approximately 0.2 psia, a partial pressure of 2.8 psia of propane would be introduced to the mixing tank through the propane supply valve, Valve VS1. Opening Valve V11 allowed this pressure to be monitored on a mercury monometer. After closing Valves VS1 and V11 the mixing tank was brought up to 45 psig with the dry air supply valves, V9 and V10. The final tank pressure was monitored with a 0-to 60- psig pressure gauge.

The mixing chamber contained a 4-inch-diameter speaker with orifice plate used to mix the propane and air. For safety reasons, this speaker was not operated until personnel had left the test cell.

Instrumentation Setup -- Prior to each test run, and before sealing, the flame tube was sealed by insertion of the incendiary ignitor assembly; each of the three pressure transducers was set for zero and span. Identified as PC, PR, and PB, they measure gauge pressure in the combustion chamber, relief chamber, and mixture test bomb.

Incendiary Igniter Installation and Safety Checklist -- For all runs involving incendiary ignition, preparation of the device was accomplished by a qualified ordnance technician. Installation of the device was witnessed by the test engineer, and the checklist was completed and signed by both. This checklist included such items as the resistance check of the igniter, check for hazardous current and verification that the firing plug is installed, and that all personnel are cleared from the test cell. The Boeing Fire Department was notified prior to each ordnance firing.

For runs using spark ignition, a dummy igniter assembly was installed in the flame tube.

Loading the Flame Tube and Mixture Bomb -- The flame tube and mixture test bomb were simultaneously evacuated to -14.5 psig by turning on the flame tube vacuum pump and opening Valves VS15 and VS7. The vacuum was monitored either by the DVM readout of the pressure transducers or by opening Valves

V12, V13, and V14 and monitoring the mercury manometers. Valve VS15 was then closed and the vacuum pump turned off. With Valve VS7 still open, the fuel-air mixture was introduced to the flame tube and mixture bomb by opening Valves VS5 and VS6. The pressures in both the mixture bomb and flame tube were then brought up to the desired initial pressure. All valves were then closed.

Firing the Mixture Bomb -- The oscillograph, set for a paper speed of 16 inches per second, was turned on, and after approximately 1/2 second the mixture bomb ignition switch was activated. The oscillograph was then turned off. The maximum height of the mixture bomb pressure trace was measured and the pressure rise calculated using the calibrated sensitivity of 50 psi per inch. If the pressure rise was satisfactory, a satisfactory mixture was assumed. A view of the control panel and oscillograph is shown in Figure 23.

Firing the Flame Tube -- After the ordnance technician had signed the checklist as "ready to fire," a 5-second countdown was conducted prior to firing.

If high-speed photographs were required for the test run, the remotely-controlled Photo-Sonic, 1000 frames per second camera with the aperture wide open at f 2 was turned on at 3 seconds. Ektachrome Type 7141 film was used and development was pushed one stop. The oscillograph, set for 16 inches per second paper speed, was turned on 2 seconds before ignition.

The ordnance technician fired the igniter at 0 seconds.

Approximately 3 seconds after the firing, the oscillograph and camera were turned off. The oscillograph traces were then examined for indication of proper firing. If the firing appeared satisfactory, both the flame tube and mixture bomb were evacuated to -14.5 psig by turning on the flame tube vacuum pump and opening Valves VS7 and VS15. At the same time the mixing tank pressure was relieved to ambient by opening the 50-psig relief valve.



Figure 23: Control Console

Following the evacuation of the flame tube and mixture bomb, the vacuum pump was turned off and Valve VS15 closed. The flame tube and bomb were brought back to ambient pressure with plant air through Valve VS8.

The ordnance technician and test engineer then entered the test cell, removed the igniter assembly, and inspected it for evidence of proper firing. The test cell was then declared "safe." The 60-amp fuses in the firing circuit were replaced.

For runs requiring spark ignition, the firing of the flame tube was accomplished by the test engineer. A similar countdown was conducted and the same postfiring safety precautions were followed.

6.0 RESULTS AND DISCUSSION OF RESULTS

Tests were completed on all the materials and combination of materials shown listed in Section 2.0. The major test variables were:

- Arrester material
- Initial pressure
- Combustion volume V_C 1.0, 1.5 and 2.0 ft³ (nominal)
- Relief to combustion volume ratio V_R/V_C of 5, 7 and 10 (nominal)
- Ignition Mode: incendiary igniter or spark
- Area of relief (10% or 53% of the cross sectional area)

For data correlation of volume relationships, see Table A-16.

All the test data is sequentially summarized in tabular form and included as Table A-XV. A data collation of volume relationships is shown in Table A-XVI.

The results are graphically represented in two ways: First, arrester thickness required for flame arrest versus initial pressure. These data are shown in Figures A-32 through A-50 for various relief areas and combustion volumes. A summary listing is shown as Table I. Second, the actual relief-to-combustion ratio (V_R/V_C) is plotted with all observed peak combustion to initial absolute pressure ratio ($P_C/P_{initial}$). These data are shown in

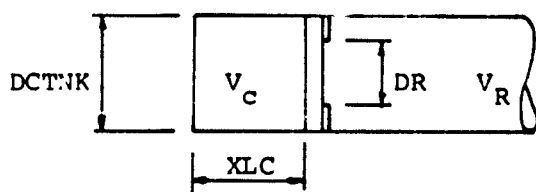
Table 1: Data Summary Table for Selected Materials

Material and/or Combination (Dry)	Thickness Required for Arrest Combustion Volume $V_C = 2.0 \text{ Ft}^3$											
	Incendiary						Spark					
	Initial Pressure (PSIG)						Initial Pressure (PSIG)					
	10%			53%			10%			53%		
	0	6	10	0	6	10	0	6	10	0	6	10
1) 25 PPI Foam	6	4	4	6.5	6	6	6	14	0.5	12.0	-	-
2) 3 M Sinterbrite	3	8	6.5	8.0	7.0	>10.0	-	-	-	-	-	-
3) GAF (Std)	3	7	-	-	-	-	-	-	-	-	-	-
4) GAF (2A)	4.0	6.0	-	-	5.0	7.0	-	-	-	-	-	-
5) Quartz Fiber	>10 L	>10 L	21 L	31 L	>10 L	>10 L	>10 L	>10 L	21 L	3: L	-	-
6) 20 Mesh S/Steel - C16 Screen	-	-	>10 L	>10 L	-	-	-	-	-	-	-	-
7) 25 PPI & 20 Mesh Screen	4.0	10.0	<1.0	<1.0	<1.0	<1.0	-	-	-	-	-	-
8) 25 PPI & 10 Layers Quartz	>4.0	-	<1.5	<4.0	-	-	-	-	-	-	-	-
9) Quartz Fiber & 2 Layers of 20 Mesh Screens	-	-	10.0 L	<5.0 L	-	-	-	-	-	-	-	-
10) 15 PPI Foam	-	-	>11.0	>11.0	-	-	-	-	-	-	-	-

Note: 'L' Refers to Layers

Figures A-51 through A-74 for various combustion volumes (V_C), relief areas (A_R), and initial pressures ($P_{initial}$). The relief area as shown in all the data is the surface area of the relief hole related as a percentage of the cross sectional area of the tube.

It was thought desirable to relate the relief area (allowing gases to expand into the relief volume from the combustion volume) to some parameter involving the combustion volume. It was decided to involve the total combustion surface area.



Note:

$DCTNK = 17.5 \text{ ins} = \text{Constant}$

Combustion surface area is given by S/A

$$S/A \text{ (ft}^2\text{)} = \frac{\pi}{4 \times 144} \left[D_R^2 + DCTNK^2 + (70 \times XLC) + DCTNK^2 \right]$$

$$\text{Relief area } A_R \text{ ft}^2 = \frac{\pi \times D_R^2}{4 \times 144}$$

Relating A_R as a percentage of S/A is given by

$$A_T\% = \frac{D_R^2 \times 100}{17.5^2 + (70 \times XLC) + 17.5^2 - D_R^2}$$

Calculating S/A and $A_R\%$ for the test parameters involved in the variable geometry test rig results in the following table.

RELIEF DIAMETER D_R (in.)					
XLC (in.)	Combustion Vol (ft ³)	5.5 in. (10%)		12.75 in. (53%)	
		S/A (ft ²)	$A_T\%$	S/A (ft ²)	$A_T\%$
8.0	1.0	6.23	2.648	5.508	16.096
11.2	1.5	7.451	2.214	6.73	13.174
14.4	2.0	8.673	1.902	7.9518	11.1501

The sensitivity of arrester thickness required for arrest with respect to initial over-pressure and combustion volumes is of a surprisingly high slope (Figure A-50). Overpressures as little as 1 psig require thicknesses in excess of 10.0 inches to arrest an incendiary burn. Run 016 showed that an incendiary ignition with 10.0 inches of foam still allowed an explosion to occur within the relief volume; however, a delay of 3 to 4 seconds separated the ignition event from the low-intensity fire observed at the relief volume viewing port. All tests have resulted in a black stain extending a considerable distance into the arrester, and in the majority of cases blackening is observed on the relief side regardless of whether ignition within the relief volume had occurred. See Figures A-75 through A-97.

The times at which significant events occurred during each test condition were recorded and tabulated as shown in Table A-XVII.

This could indicate that ignited incendiary permeated the arrester propelled by expanding gases. This blackening and/or staining of the arrester material was most pronounced for the 1.0-cubic-foot combustion volumes, and the small 10% relief area.

In all tests where burn-through occurred, the burning within the relief volume simulates a spark ignition with respect to pressure rise time as recorded on the traces, samples of which are shown in Figures 24 and 25. Except for runs 61 through 75, inclusive, all tests were completed with the material dry.

For the portion of tests wetted with JP5 or Jet A fuel it was noted that in runs 65, 66, and 67 the arrester material was badly damaged and had sustained large holes that would have normally resulted in a secondary explosion within the relief volume.

It was postulated that hot gas resulting from combustion volume ignition expanding through the arrester and orifice vaporized a portion of the liquid fuel in which the arrester was soaked prior to test. Vaporization contributed to local richening of the fuel/air relationship during the explosion, resulting in a mixture downstream of the arrester too rich to burn. Three tests -- 71, 72, and 73 -- were conducted to resolve this problem

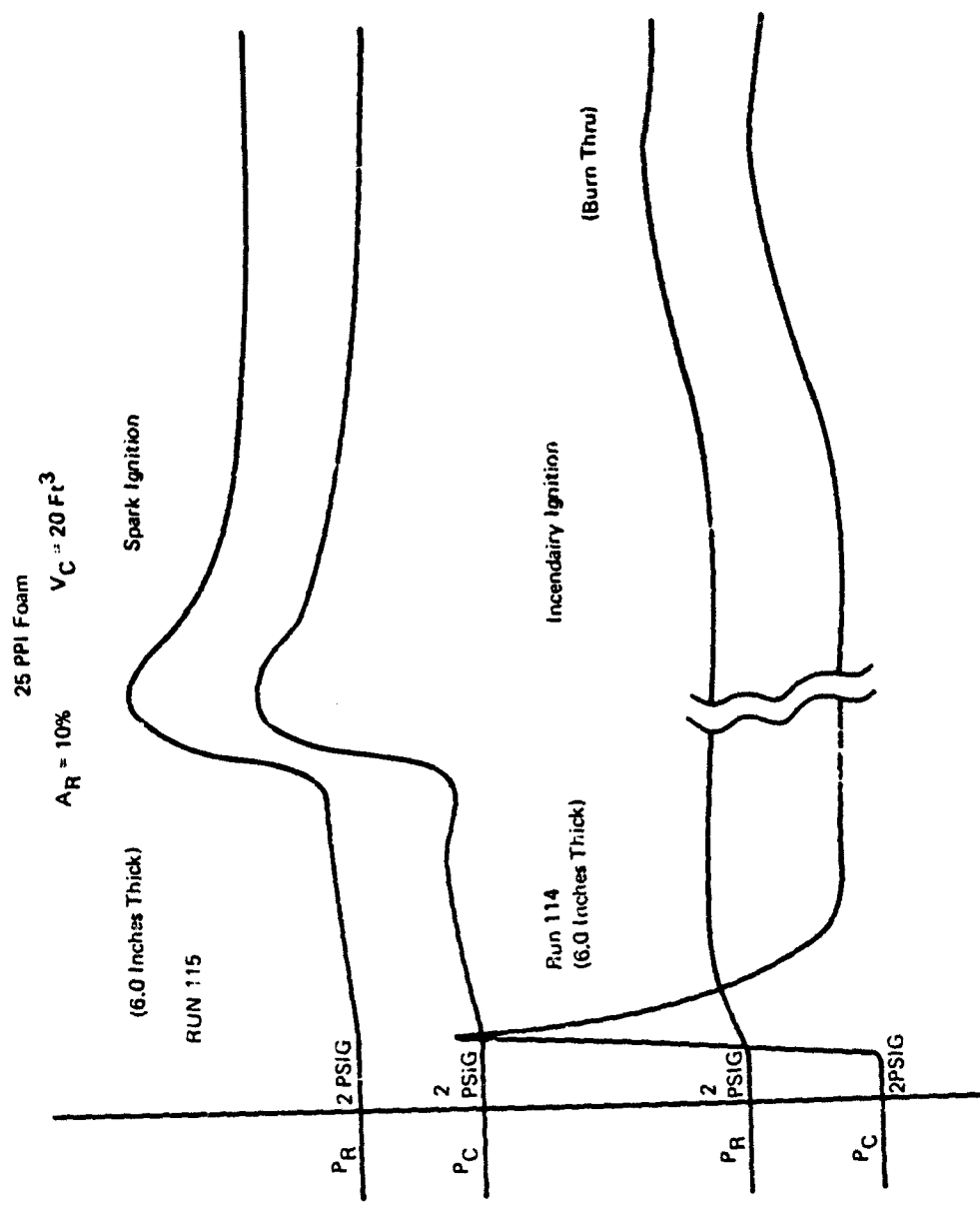


Figure 24: Typical Variable Geometry Pressure Traces

25 PP: F_{max}

A_g 53"

V_C 2.0 Ft³

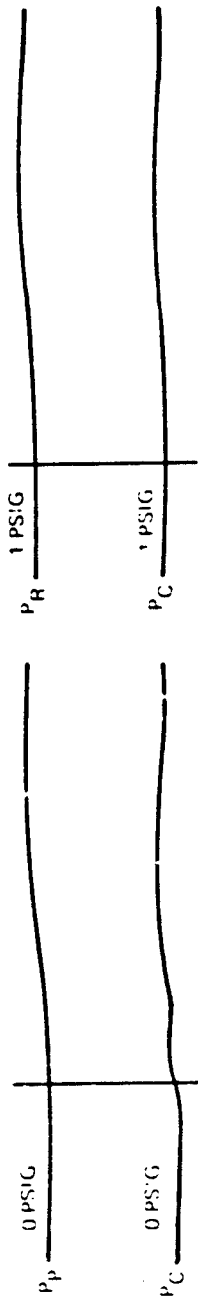
(11.0 n. Thick)

(4.0 n. Thick)

SPARK IGNITION

RUN NO. 160

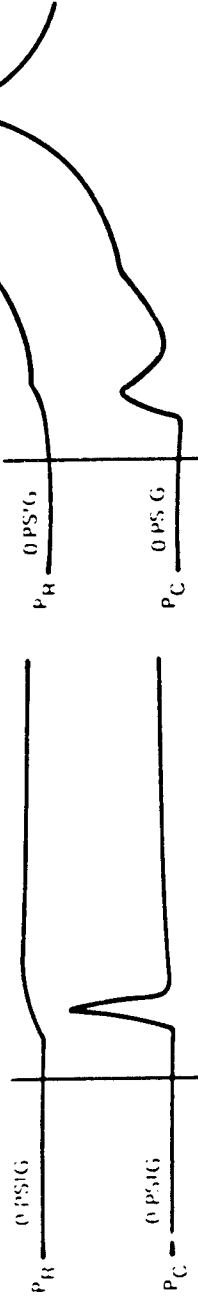
RUN NO. 134



INCENDIARY IGNITION

RUN NO. 140

RUN NO. 020



(Burn Thru)

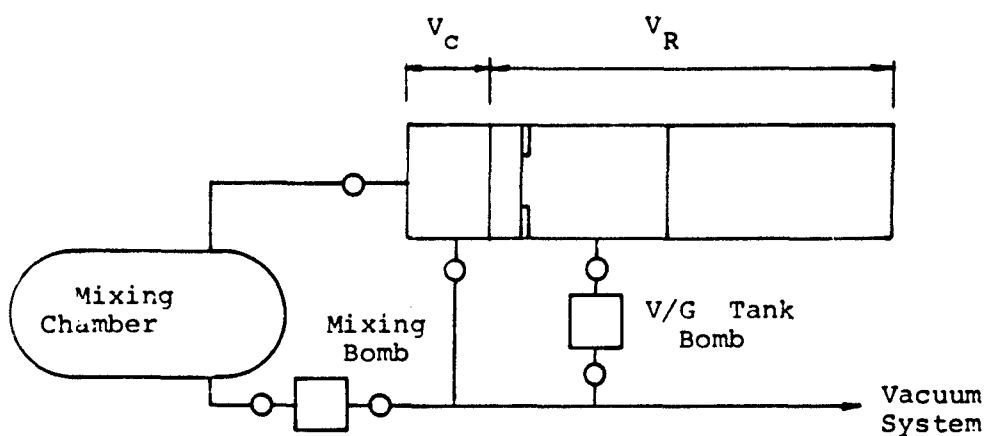
Figure 25: Typical Variable Geometry Pressure Traces

and determine how lean the propane-air mixture should be to ensure that after addition of fuel light ends, a maximum pressure explosive mixture in the relief volume would result.

Test Conditions:

- 2.0 inches of 25-ppi Red Foam
- Wetted with Jet A
- Not glued in, held with 0.046 screen, 4 meshes per inch

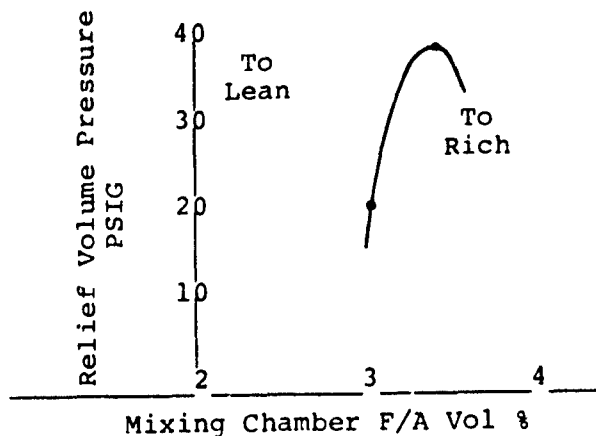
SYSTEM SCHEMATIC



Data

Run	Initial Mixture	Mixing Bomb	V/G Tank Bomb	VC Pressure	VR Pressure
<u>No.</u>	<u>F/A</u> <u>%</u>	<u>(psig)</u>	<u>(psig)</u>	<u>(psig)</u>	<u>(psig)</u>
071	3.0	77	73	5.25	21.5
072	3.5	88	85.5	5.75	38.5
073	4.0	96.5	94.5	11.75	No Burn- through

Data Plot



NOTE: Hot expanding gases vaporize liquid fuel on the arrester and contribute to a lean mix of tank fuel/air to produce a maximum-pressure burning mixture in the relief volume.

Tests conducted with the fuel-to-air ratio both rich and lean lend further credibility to the proposed mechanism by which a flame is arrested by reticulated polyurethane foam. This mechanism is in part attributed to the burning and melting of the material producing gases that expand through the arrester into the relief volume and contribute to local inerting. Some data with lean fuel-to-air ratios, 3.5% by volume, showed that slight backface burning of the arrester foam had taken place, indicating burn-through, although the pressure trace data did not indicate an increase in pressure.

Most tests with a rich mixture (6.5% by volume) badly damaged the arrester, in some instances burning half the material completely through; yet combustion within the relief volume was not initiated. In all cases of this kind the relief volume viewing port was clouded with burnt material.

These data would indicate that the capability of a foam material to arrest a flame front is not really a go-no-go situation. A probability exists, depending on the amount of arrester material burned.

Ignition Theory

A relief volume ignition theory is formulated from the test data and observed ignition phenomena.

Event Description

1-2: With the ignition switch on, power is supplied to the igniter incendiary powder. Heat and pressure are built up within the igniter until the 0.046-inch thick (average) plexiglass burst disc is ruptured, allowing the incendiary charge to expand into the combustion chamber.

2-3: The incendiary plume immediately causes a fluctuation and pressure increase in the combustion chamber pressure. This pressure increases rapidly to a maximum dependent only on the relief area and pressure drop through the arrester material. At the same instant a pressure rise is effected within the relief volume, depending upon the relief area. If the relief volume was very small $V_R/V_C \leq 0.2$ then this too would influence the pressure rise.

3-4: Upon reaching maximum pressure in the combustion volume, a pressure decrease ensues. At the same time, pressure continues to increase within the relief volume; this process continues, P_C decreasing and P_R increasing until pressure is equalized. The time at which this occurs depends upon the relief volume and pressure drop through the orifice and arrester material.

Ignition Phenomena (Incendiary Igniter)

2-3: The incendiary plume expands into the fuel-air mixture (optimized for maximum overpressure 4.7% by volume). Ignition of the gases is immediate, and complete combustion and expansion is within 5 to 10 milliseconds. Hot unburnt and burnt gases are expanded through the relief orifice and arrester material into the relief volume. However, the expansion is so rapid that pressure rises on both sides of the relief area and arrester. The pressure drop across the orifice and arrester increases as burning in the combustion chamber continues until all combustible gases in the combustion chamber are reacted (see Figure A).

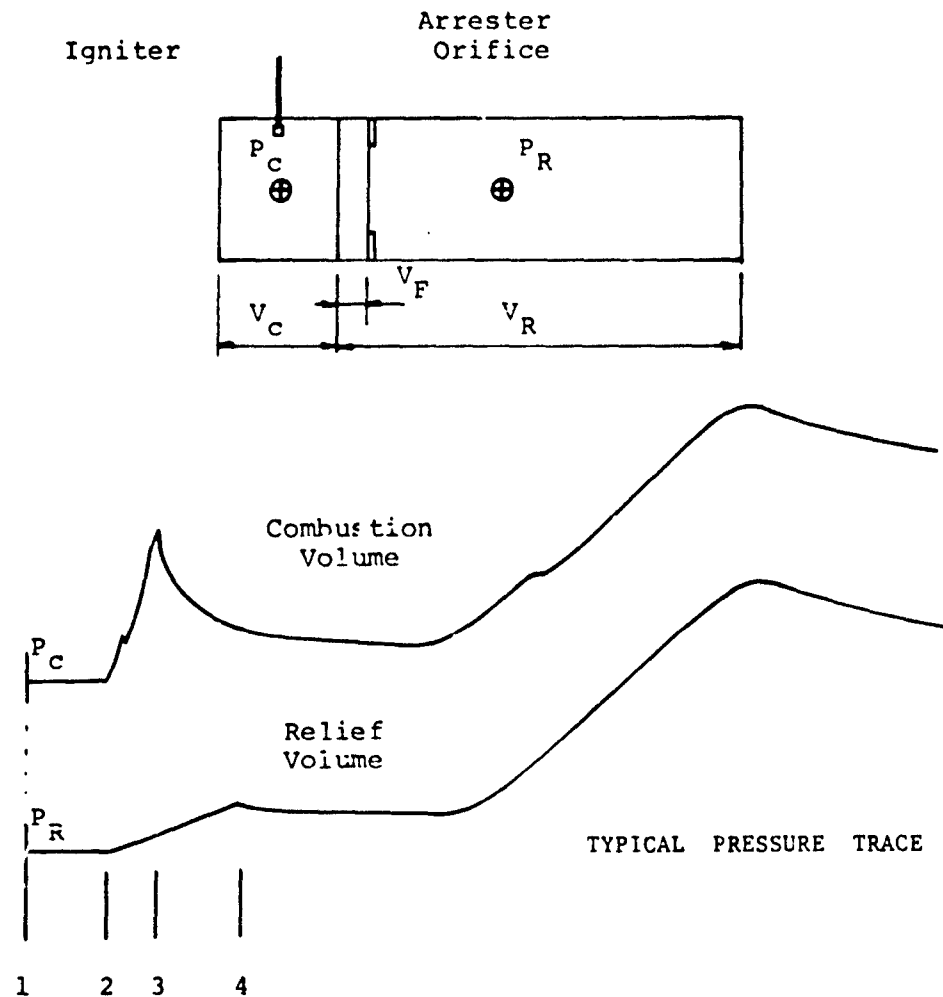


Fig. A

3-4: Pressure decay begins and continues until equilibrium, with essentially no more burning in either chamber (burning is defined here as that resulting in a pressure increase).

However, as shown in Figure B, during the time between events 2 and 3 a pressure drop is maintained across the arrester, driving a cone of hot gases, burnt or unburnt, from the combustion chamber into the relief chamber. Postulating that the active life of an DM-II incendiary particle is less than 10 milliseconds, before event 4, all particles should have reduced their individual energy levels to zero and therefore do not contribute further. It is presumed that their energy was expended in scorching the arrester face.

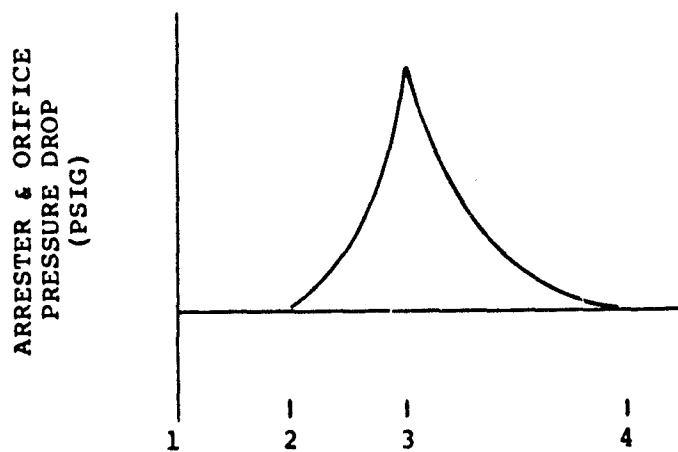


Fig. B.

The mechanization by which ignition occurs in the relief volume is baffling, to say the least. Three possibilities are immediately apparent; their working hypotheses are:

- 1) The cone of hot gases expanding into the relief volume retains sufficient heat energy to initiate a reaction. The cone of high velocity hot gases expanding into a relatively quiescent combustible mixture will produce vortices that encourage mixing and energy interchange.



Further, it could be this jet of hot gases passing through the foam that produces the blackening of the arrester material characteristic of all tests conducted.

- 2) In all tests completed, ignition in the relief volume was preceded by the events of condition 4 resulting in the pressure drop reducing to zero. It is assumed that at this condition a flame or flame front exists that is attempting to expand normally. This requires an order of magnitude increase in

time to propagate when compared to an incendiary ignition. This slow burning process is still taking place in the combustion chamber in the small amount of combustible gases remaining when pressure equilibrium occurs at event 4. Possibly, combustible gases could permeate the arrester in a reverse flow and begin feeding the feeble flame front remaining in the combustion chamber. This slow-moving flame could now pass through the arrester, accelerating, as burned gas again produces a slight positive pressure drop, driving the slow-moving flame through and into the relief volume where normal burning and associated pressure increases occur similar to spark ignition.

- 3) Pressure rises in the combustion volume in approximately 10 milliseconds average for the runs completed, and leaves no time for normal burning to initiate and propagate. This immediate expansion is accredited to the normal expansion of the gases created by incendiary particles and subsequent burning and rapid temperature increase of the reaction within the expanding incendiary flame. The immediate expansion creates a pressure drop across the foam. The ensuing gas velocity, created by the expanding hot gases endeavoring to establish equilibrium, could transport burning incendiary particles through the arrester with sufficient momentum for them to penetrate. Sufficient energy could be retained by the particles to initiate a reaction on the relief side. It is noted that this burning within the relief volume simulates a spark ignition with respect to pressure rise time as recorded on the pressure traces.

Movies of previous studies within Boeing regarding the life of various incendiary mixtures indicate that the IM-II incendiary mix reacts and dies very quickly: ≤ 10 milliseconds. This is a shorter time period than the average time to pressure equalization.

Bomb Sample Data

The fuel/air ratio that resulted in a maximum over-pressure was determined by test. The bomb sample dimensions and a typical pressure rise data trace are shown in Figure 26. These data are shown in Table II and are graphically represented in Figures 27 and 28.

Some tests with the 50% orifice and the arrester wetted with JP5, the pressure drop across the arrester dislodged arrester samples from their mounted position and forced them through the orifice into the relief volume. On each occasion the foam prior to wetting was securely glued in position. The glue being applied on the outer edge and on the orifice contact surface. On each occasion arrester material was left glued to the surfaces, indicating that the ultimate tensile strength of the material was exceeded and that tearing occurred.

During some tests with the quartz fiber screening material supported in the tube with a four-mesh screen, the combustion process was accompanied with a loud report. On one run the supporting screen was badly damaged (Figure A-97).

Pressure rise data show that peak pressure is reached within the 2.0-cubic-foot volume in approximately 8 to 10 milliseconds. Assuming that the "flame front" travels the 14.4-inch length of the combustion chamber within this time, then the speed of travel (average), assuming planar propagation, is given as

$$\text{Flame speed} = \frac{14.4 \text{ in.}}{12 \text{ in./ft} \times 0.008 \text{ sec}} = 150 \text{ ft/sec}$$

The speed of sound in the unburned mixture is calculated from

$$C = \sqrt{\gamma g R T}$$

γ = ratio of specific heats

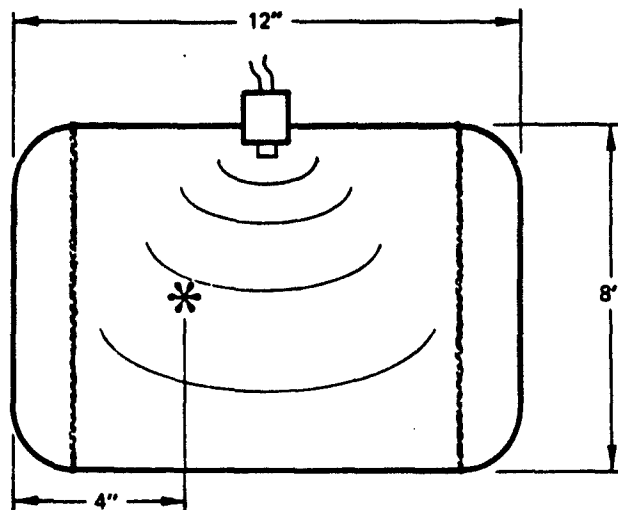
g = 32.2 ft lb (F)/lb (m) sec²

R = gas constant

T = gas temperature O_R

Table II: Mixing Bomb Sampler Pressure Data

Run No	Fuel/Air Volume %	Initial Pressure		Final Pressure		P_c/P_{In}	Rise Time M. Secs.
		PSIG	PSIA	PSIG	PSIA		
1	7.0	0	14.7	74	88.7	6.03	650
3	7.0	0	14.7	75	89.7	6.102	610
4	7.0	0	14.7	64	78.7	5.353	1100
5	6.0	0	14.7	57	104.7	7.12	170
6	6.0	0	14.7	91.5	105.2	7.22	160
7	5.5	0	14.7	98	112.7	7.666	117
8	5.5	0	14.7	93.5	108.2	7.36	118
9	5.0	0	14.7	100	114.7	7.8	96
10	5.0	0	14.7	98	112.7	7.666	98
11	4.59	0	14.7	99	113.7	7.735	107
12	4.59	0	14.7	96.5	111.2	7.564	126
13	4.0	0	14.7	94	108.7	7.394	116
14	3.5	0	14.7	83	97	6.598	140
15	3.0	0	14.7	70	84	5.714	220
063	4.0	1	15.7	104	118.7	7.56	97
063	4.0	1	15.7	102.5	117.2	7.46	110
16	4.0	0	14.7	96.5	111.2	7.564	115
064	4.5	3	17.7	135	149.7	8.45	102
068	4.5	0	14.7	104	118.7	5.07	92
165	6.5	3.0	17.7	103	117.7	6.65	340
166	6.5	6.0	20.7	117.5	132.2	6.386	560
167	6.5	3.0	17.7	96.5	111.2	6.28	500
168	6.5	2.0	16.7	93	107.7	6.45	450
169	6.5	4.0	18.7	103	117.7	6.29	500
170	6.5	6.0	20.7	127	141.7	6.845	340
171	6.5	3.0	17.7	99	113.7	6.423	410
172	6.5	6.0	20.7	127	141.7	6.845	341
173	3.5	0	14.7	85	99.7	6.78	157
174	3.5	4	18.7	114.5	129.2	6.91	170
175	3.5	6	20.7	132.0	146.7	7.087	165
176	3.5	2	16.7	100.5	115.2	6.89	160
177	3.5	6	20.7	150	164.7	7.956	111
178	3.5	0	14.7	98.5	113.2	7.7	110



Dimension of 18" Variable Geometry Bomb Sampler

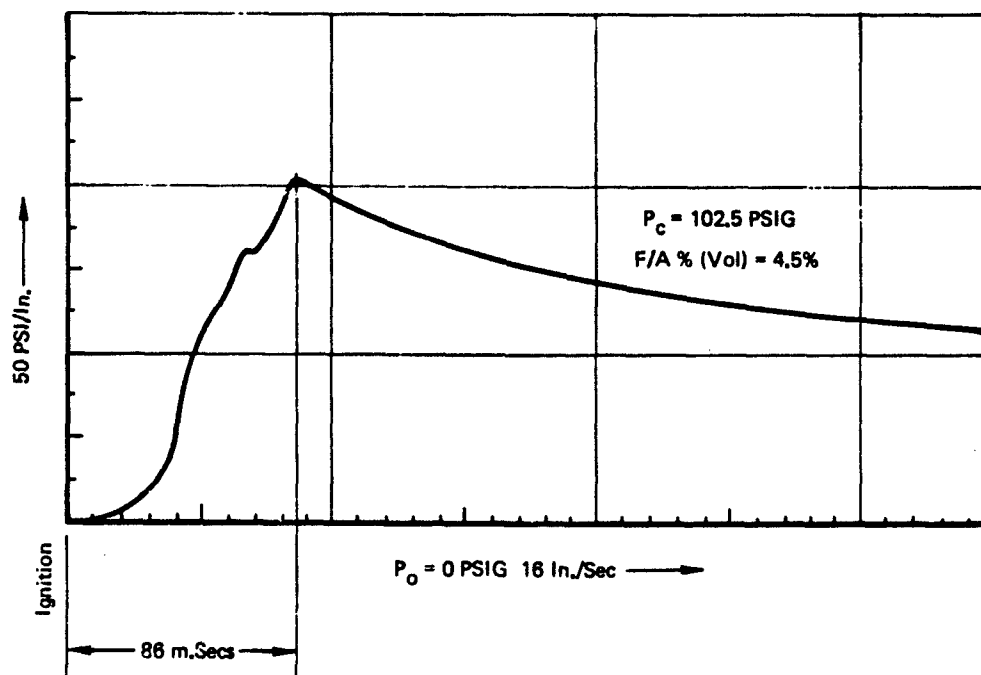


Figure 26: Typical Pressure Versus Time Trace for 12" x 8" Diameter Bomb

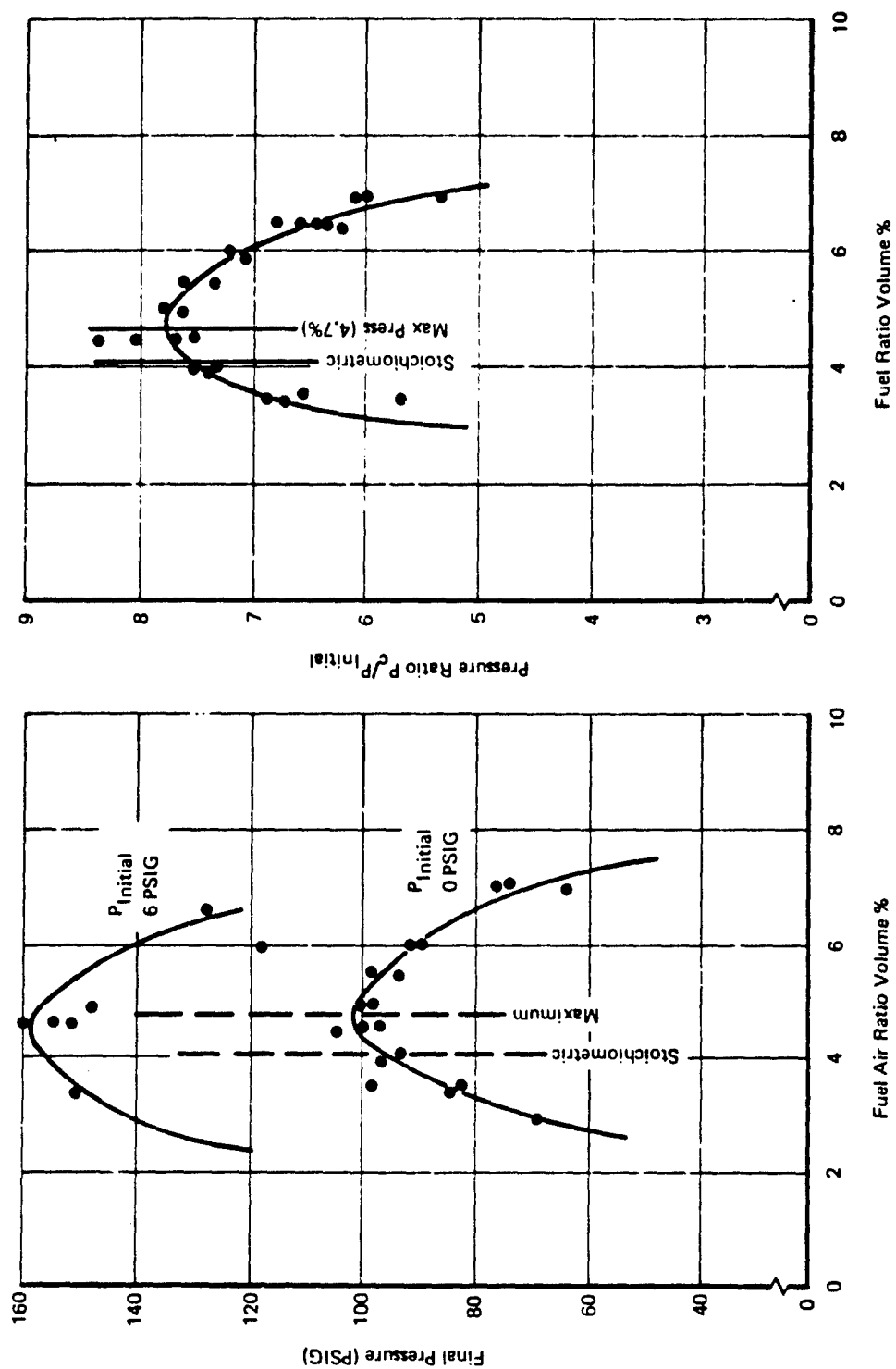


Figure 27: Bomb Sampler Pressure Ratio Versus F/A Ratio

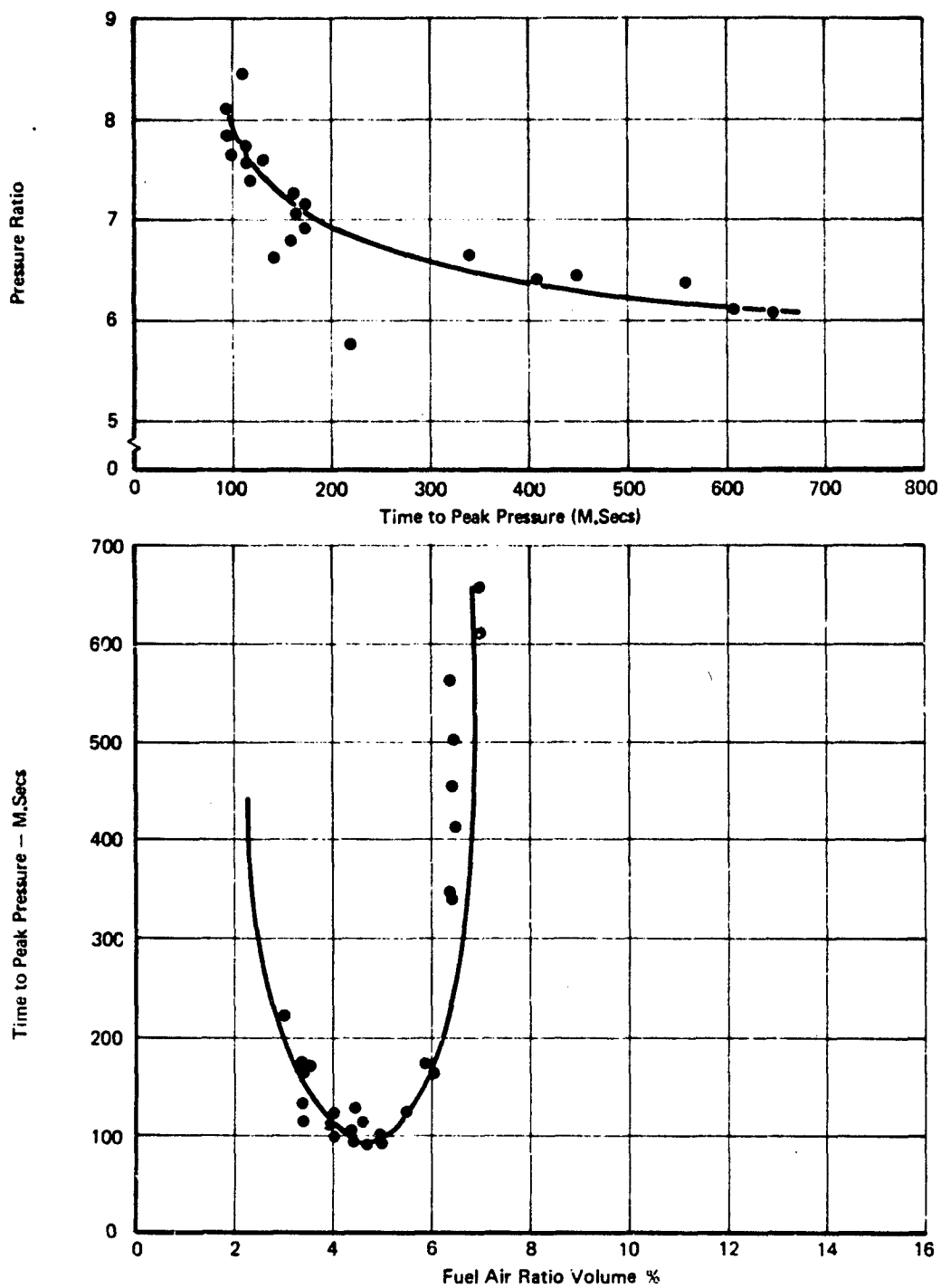


Figure 28: Bomb Sampler Pressure Ratio & F/A Ratio Versus Time Data

It is assumed that for a propane-air mixture

$$\gamma = 1.37, R = \frac{1545.43}{29} = 53.3 \text{ ft lb (m)/lb (F)} ^\circ\text{R}$$

$$T = 520^\circ \text{ R}$$

$$C = \sqrt{1.37 \times 32.2 \times 53.3 \times 520}$$

$$= 1,118 \text{ ft/sec}$$

The observed flame speed (average) during an explosion in the 2.0-cubic-foot volume as calculated above, is shown to be an order of magnitude less than that causing detonation and consequently the loud report associated with Runs 118 and 122 is unexplained.

It is possible that repeated use of the four-mesh stainless steel supporting screens resulted in fatiguing the welds and that fracture occurred.

7.0 CONCLUSIONS AND RECOMMENDATIONS

It appears that the incendiary ignition (within the 1-cubic-foot combustion volume) overwhelms the combustible gases with regard to the rate of expansion of the explosive plume. Pressure rises in the combustion volume in approximately 6 to 8 milliseconds average, and leaves no time for normal burning to initiate and propagate. This immediate expansion is credited to the normal expansion of the gases created by incendiary particles and subsequent burning and rapid temperature increase of the reaction within the expanding incendiary flame.

The combustion chamber subjected to burning incendiary material is blackened, but incurs none of the severe foam melting and burning that has been experienced on the relief volume side. It has been observed that the front face burning is more severe when an arrest occurs than when the relief volume ignites indicating a burn-through. It is noted from the data that the extent of relief volume burning is influenced by the thickness of the foam and the relief area; this burning penetrates into the foam as much as 3 to 4 inches with a 15-inch-diameter burn.

With respect to the hypotheses on ignition phenomena formulated from the test results, the following is concluded:

Hypothesis 1 -- Ignition by hot gases is the easiest to explain if the expanding gases reach a sufficiently high temperature. However, some long delays experienced prior to secondary ignition defy this hypothesis. Delays of from 1/2 to 4 seconds separate the events of event 4 and the occurrence of relief volume secondary ignition.

A correlation of the volume and temperature of hot gases expanded into the relief volume would help determine the minimum energy required to be transported to cause ignition by this mechanism. However, temperature was not a recorded parameter during the program.

Hypothesis 2 -- This hypothesis is presently compatible with all the data, except in cases where the arrester has a low pressure drop; event 4 is immediately followed by the secondary relief volume ignition, possibly indicating that a reverse flow of combustible gas is not required.

Hypothesis 3 -- All tests to date have resulted in a black stain's extending a considerable distance into the foam and in the majority of cases blackened foam is observed in the relief side, regardless of whether there was ignition in the relief volume. This could indicate that ignition in the incendiary permeated the foam propelled by expanding gases, and in a large number of cases could have retained sufficient energy to ignite the combustible gas in the relief volume.

It has been generally noted that arrests have occurred with the foam and felt materials where posttest examination revealed that large holes had been burnt through. This suggests that in the case of combustible arresters, the burning of material contributes to locally inert the relief volume; consequently, it is probable that given another type of geometry, secondary relief side ignition (burn-through) could have resulted.

Fire trying to propagate through the arrester is possibly being extinguished due to high-velocity passage through the arrester. As pressure equilibrium is approached, the rapid expansion of the fire or flame front is reduced and allows the final slow-moving flame to pass through the arrester. Again, passage produces blackening of the arrester material, although melting or severe damage to the front face occurred only on a few occasions. Whenever there was a burn-through, the pressure rise time has been that attributed to normal spark ignition. The arrester material was damaged on the relief face, usually burning and melting the material to a depth of one to two inches. The depth and extent of damage appears to be related to the thickness of the arrester used. The pressure traces, however, did not always show a pressure lag between P_C or P_R , which would indicate a pressure drop through the arrester; it is as though combustion is initiated simultaneously on both sides of the arrester.

The tests completed during runs 61 through 75 with the material wet, show that a change in the fuel/air ratio in the relief volume occurs during the explosion. Hot gases expanding through the arrester material vaporize a portion of the fuel, these fuel light ends then contribute to a local richening of the fuel/air ratio in the relief volume.

The test data allow the following conclusions to be determined.

- 1) The thickness of arrester material required increases with increasing initial pressure.
- 2) It has been shown that the thickness of arrester material required to arrest a propagating flame front decreased as combustion volume was increased from 1.0 cubic foot to 2.0 cubic feet.
- 3) Reducing the relief area requires an increase in 25 ppi arrester material to arrest a propagating flame front.
- 4) Reducing the relief area, in all tests, corresponded with increases in the final combustion volume overpressure.

Unless stipulated otherwise in the tabulated or graphical data, all tests were completed with the arrester material dry.

From the test data obtained during tests within the variable geometry test apparatus, the following materials have been selected for further investigation during the Mode II portion of this task:

25-ppi Reticulated Polyurethane Foam

3M Scotch Brite

GAF Polyester Fiber, Type 2A

25-ppi Foam and 016 Stainless Steel Screen, 20 Mesh

25-ppi Foam and Astroquartz, Type 594

The 240 Volt A.C. power supply utilized for activation of the incendiary igniter required the replacement of the 60 ampere fuze after each test. This electrical configuration allowed successful igniter firing each time, and will be used for the remaining Task I, Task II and Task III tests. It was considered more cost effective to replace the fuze after each test than to repeat the test due to an igniter fizzle, and/or failure to operate.

SECTION VI
TASK I MODE II TEST PROGRAM

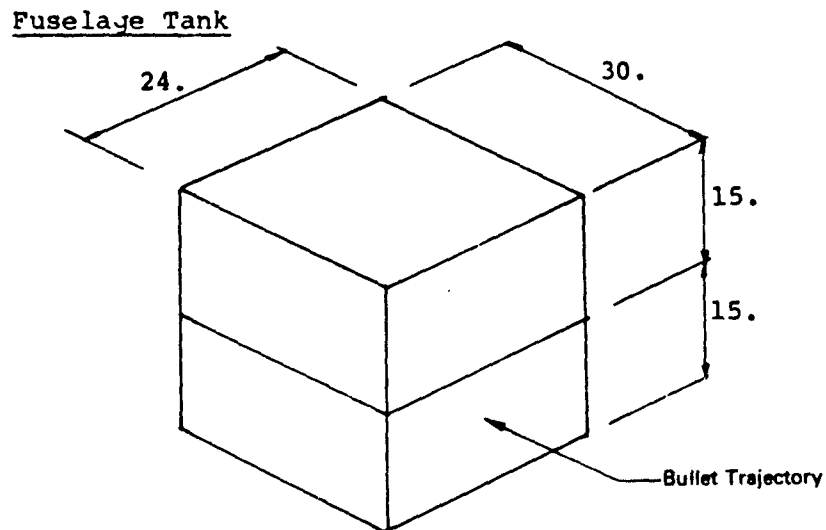
1.0 MATERIAL DESCRIPTION

Resulting from Mode IB variable geometry tests, the following materials were considered for continuing evaluation during Mode II screening tests. These tests were completed in the fuselage test apparatus, in a lined wall voiding configuration.

- 25-ppi Foam (Red)
- 3M Felt
- GAF Felt, Type 2A
- 25-ppi Foam and 016 Stainless Steel Screen, 20 Mesh
- 25-ppi Foam and 10 Layers of Quartz Fiber, Type 594

2.0 TEST CONFIGURATION

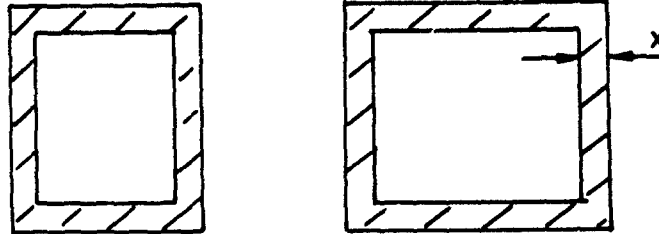
The geometry of fuselage tank assembly is shown here: Dimensions are in inches.



All tests were conducted with a lined wall configuration. The percent voiding was achieved by varying the arrester thickness glued to the inside of the tankage.

Lined Wall

Note: X = Arrester Thickness



Variations of percent void with arrester thickness are calculated as follows:

$$V_{\text{Total}} = V_T = 30 \times 30 \times 24 = \underline{21,600 \text{ in}^2}$$

$$V_{\text{Combustion}} = V_C = (30 - 2X)(30 - 2X)(24 - 2X)$$

$$V_{\text{Relief}} = V_R = V_T - V_C$$

$$\text{Percent Void (Penalty)} = V_C / V_T \times 100$$

$$V_C / V_T \text{ (Penalty)} = \frac{(21600 - 4680X + 336X^2 - 8X^3) \times 100}{21600}$$

$$V_R / V_C = \frac{4680X - 336X^2 + 8X^3}{21600 - 4680X + 336X^2 - 8X^3}$$

Variations of percent void and V_R / V_C for changes in arrester thickness X are shown in Figure 29.

A schematic of the test apparatus is shown in Figure 30 and a photograph of the overall test installation is included as Figure 31.

3.0 INSTRUMENTATION

Table III is a listing of all pertinent instrumentation used in obtaining test data.

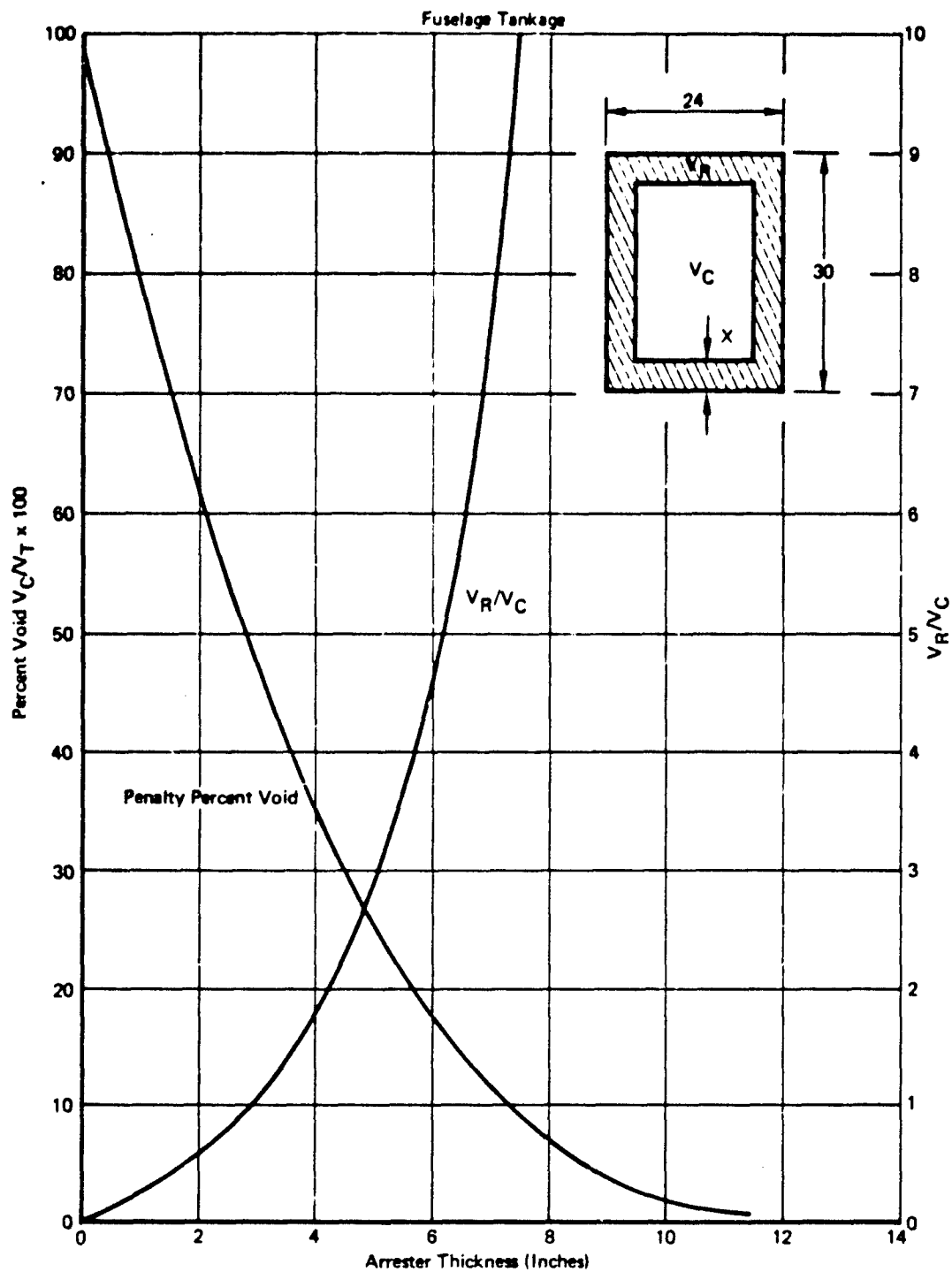


Figure 29: Variations of Percent Void and V_R/V_C with Arrestor Thickness (Lined Wali)

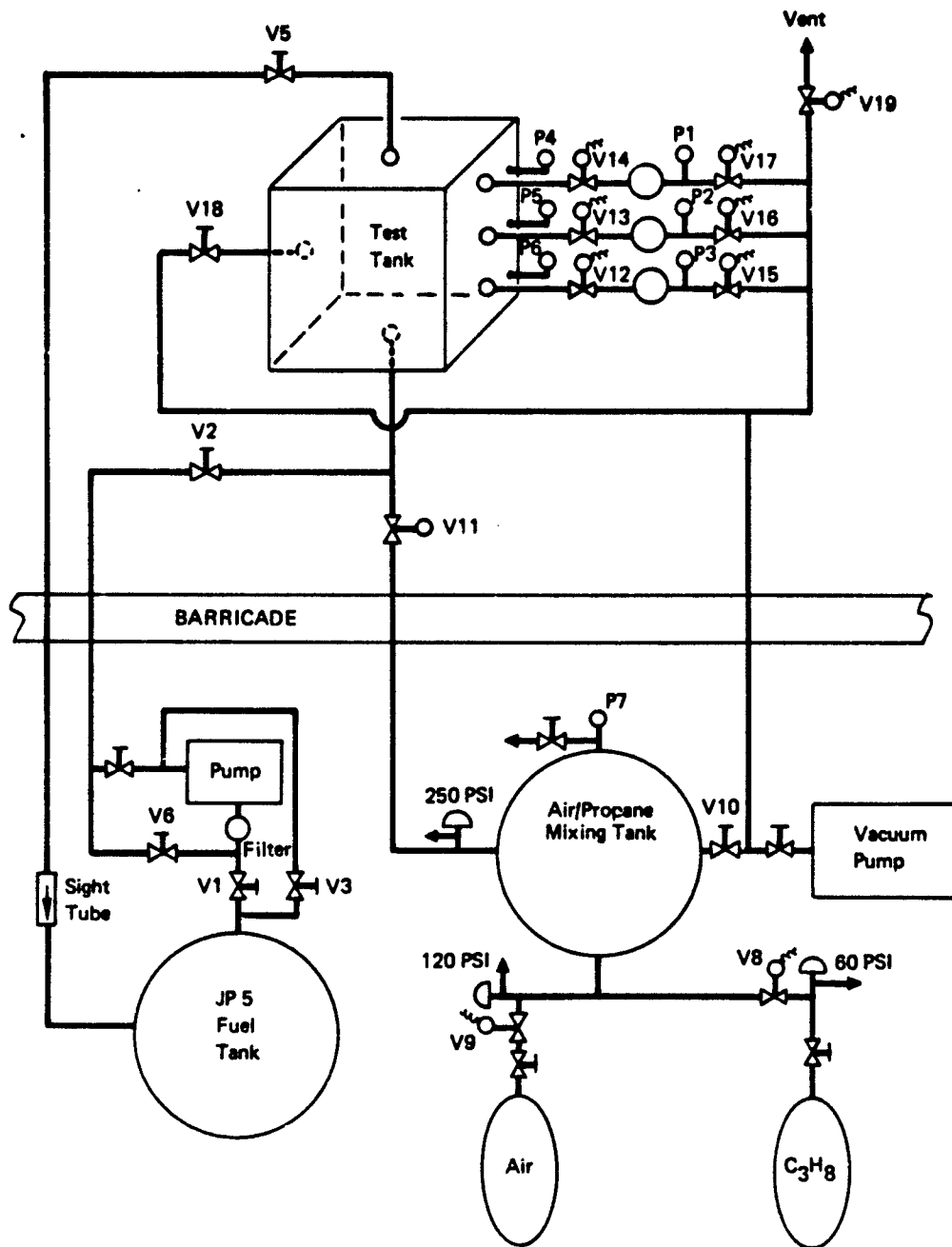


Figure 30: Fuselage Tank System Schematic

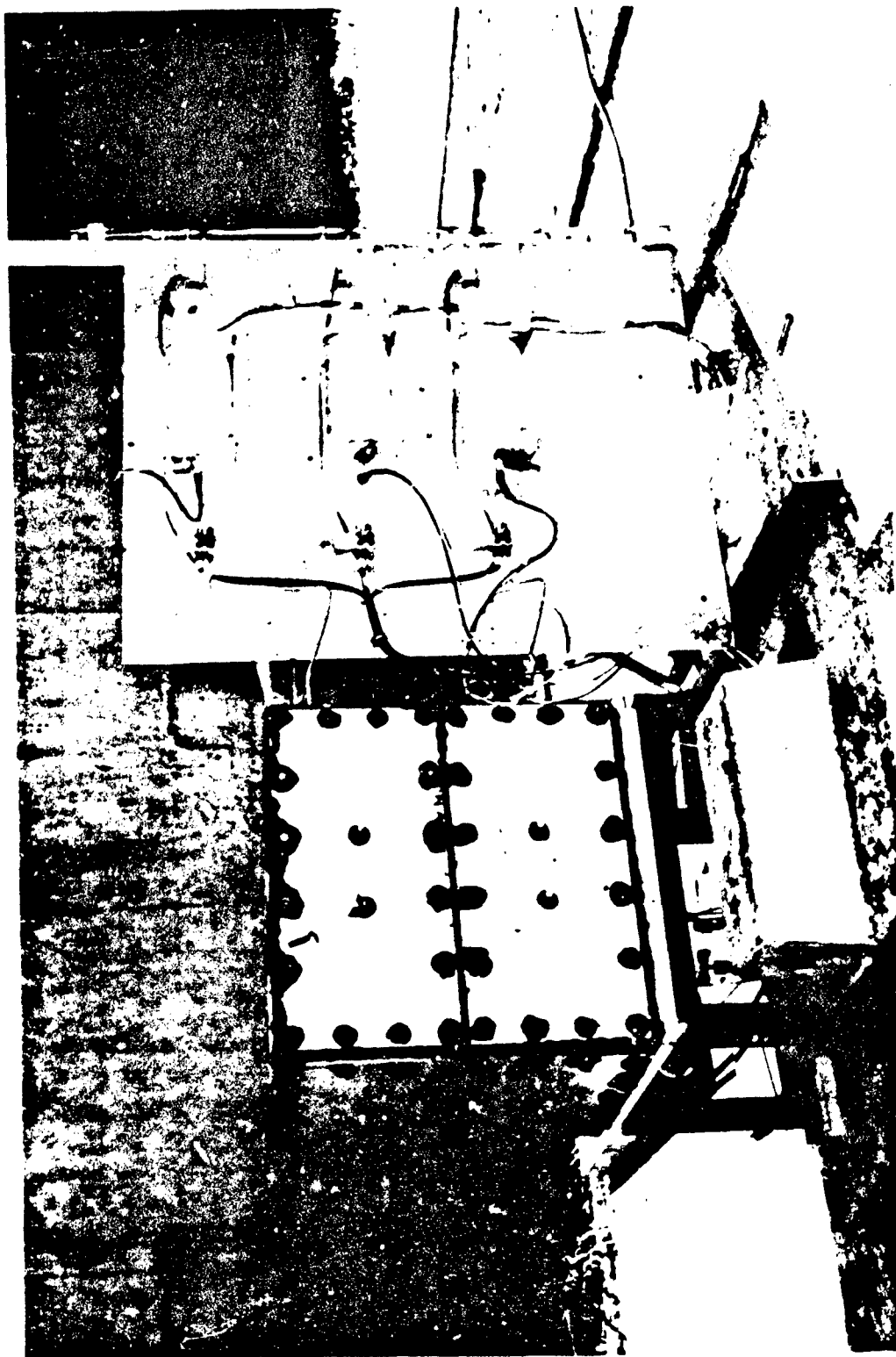


Figure 31: Fuselage Tank Test Assembly

Table III: Instrumentation Listing

Measurement		Transducer			Balance Channel	Amplifier Channel	Osc Signal Cond.	TADC No. 1 Input Channel	Osc Channel	Calibration				Sensitivity	
No.	Location	Type - Ser. No.	Full Scale Range	Excit Volt						Rc Equiv (PSI)	DVm Sqr for RC (Volts)	Galvo Set for RC (in.)	DVM (PSI/V)	Osc'g (PSI/in.)	
P ₁	Upper Bomb	Taber 624950	300A	10.0	34	1	—	—	1	—	—	40% - 2.40	—	50	
							1	1	—	80% = 2.40	2.40V	—	100		
P ₂	Middle Bomb	Taber 624952	300A	10.0	35	2	—	—	2	—	—	40% = 2.40	—	50	
							2	2	—	80% = 2.40	2.40	—	100	—	
P ₃	Lower Bomb	Station 4837	2500	5.0	36	3	—	—	3	—	—	80% = 1.422	—	50	
							3	3	—	80% = 71.1	0.711	—	100	—	
P ₄	Upper Tank	Station 22727	100A	6.0	37	4	—	—	4	—	—	80% = 2.52	—	10	
							4	4	—	80% = 25.15	0.2515	—	100	—	
P ₅	Middle Tank	Station 2637	50A	6.0	38	5	—	—	21	—	—	80% = 2.62	—	10	
							5	5	—	80% = 26.15	0.2615	—	100	—	
P ₆	Lower Tank	Station 9629	100A	6.0	39	6	—	—	22	—	—	40% = 3.12	—	10	
							6	6	—	40% = 31.35	0.3135	—	100	—	
I ₁	Igniter Fir. Pulse	Current	XFMR	—	—	7/8	7/8	—	23	—	—	—	—	Event Only	
I _G	Gun Fir. Pulse	✓	✓	—	—	9	9	—	24	—	—	—	—	Event Only	
P ₇	Mixing Tank	Bin 27535	504	10.0	41	7	—	7	—	80% = 40.2	0.4022	—	100	—	

4.0 IGNITION SYSTEMS

The two ignition systems for this phase of the Task I program were identical to those used for the earlier Mode IB program: high-energy spark and incendiary igniter.

5.0 TEST PROCEDURE

The test procedure for all tankage configurations was identical. The void configuration was fabricated and installed in the tankage. The arrester material was wetted with JP5 fuel, thus: fuel was pumped from the storage tank into the test tank (using a small centrifugal type pump) until full. The fuel was then pumped out of the test tank and back into storage. The dummy igniter used to seal the tank during filling was removed and all residual fuel allowed to drain.

The AFAPL-SFH incendiary igniter was loaded with powder and the resistance checked to approximately 0.2 ohms. After about 3 to 4 minutes the test igniter was installed, sealing the tank.

The test tankage and all three bomb samplers were evacuated to approximately 0.4 psia with an oil seal mechanical vacuum pump. A premixed, pressurized propane-air mixture was introduced into the test tank which was filled to a positive pressure approximately 1.0 to 1.5 psig above that required for the test. Valves were then opened allowing samples to be withdrawn from three locations into three bomb samplers and the pressure in the complete manifolded system reduced to that required for the test condition. Each bomb sample was then isolated with appropriate valving and ignited with the spark assembly. The pressure time data were recorded prior to each test run. If the pressure was considered adequate for the fuel mixture introduced, the test tankage was ignited and its pressure time history recorded.

For all tests the ignition of the test tankage followed that of the bomb samples by not more than 45 seconds on each test run. Sufficient data were taken to allow a curve of pressure rise versus percentage void to be plotted.

6.0 RESULTS AND DISCUSSION OF RESULTS

Tests within the fuselage configuration with a lined wall voiding concept using 25-ppi reticulated polyurethane foam, wet with JP5 or dry, indicated a higher pressure rise for a spark-initiated explosion than for one initiated with the incendiary igniter. Also, for the fuselage tank voided, top-wall configuration, tested in TASK II the explosions initiated with a .50 caliber API shot through 1/4-inch aluminum plate at a muzzle velocity of approximately 2,300 feet per second, the resulting pressure rise was lower than those produced by the incendiary igniter.

The fuselage tank test data are summarized in Table A-XVIII. Data traces are included for reference as Figures A-98 through A-109. The difference in pressure rise time within a 39% voided lined wall configuration is shown in Figure A-101. The rise times are 17 milliseconds for the incendiary igniter and 130 milliseconds for a spark ignition.

The lined wall fuselage tankage data plots relating the percent void with absolute overpressure ratio are shown in Figures 32 through 38. Superimposed on each plot is the dynamic mathematical model prediction. It is noted that this model is conservative in that the pressure ratio predictions are generally higher than those obtained from test. This is due in part to the present inability of the model to change the inputted pressure drop K factor as arrester thicknesses and percent void within the fuselage tank are changed. This program change could be easily achieved at a later date. The predicted pressure ratio plotted, results from a pressure drop K factor of 60 (approximately equal to 5.0 inches of 25-ppi foam) being used and this K factor remaining constant for all percent void variations.

The variation in absolute overpressure with different ignition sources is shown in Figures 32 and 33. Large variations in overpressure with the arrester material dry or wetted with JP5 are shown to exist.

A comparison of overpressures obtained with various arrester materials is shown in Figures 34, 35, and 36. The effect of varying the fuel air ratio on tank overpressure for three different materials is shown in Figures 37 and 38.

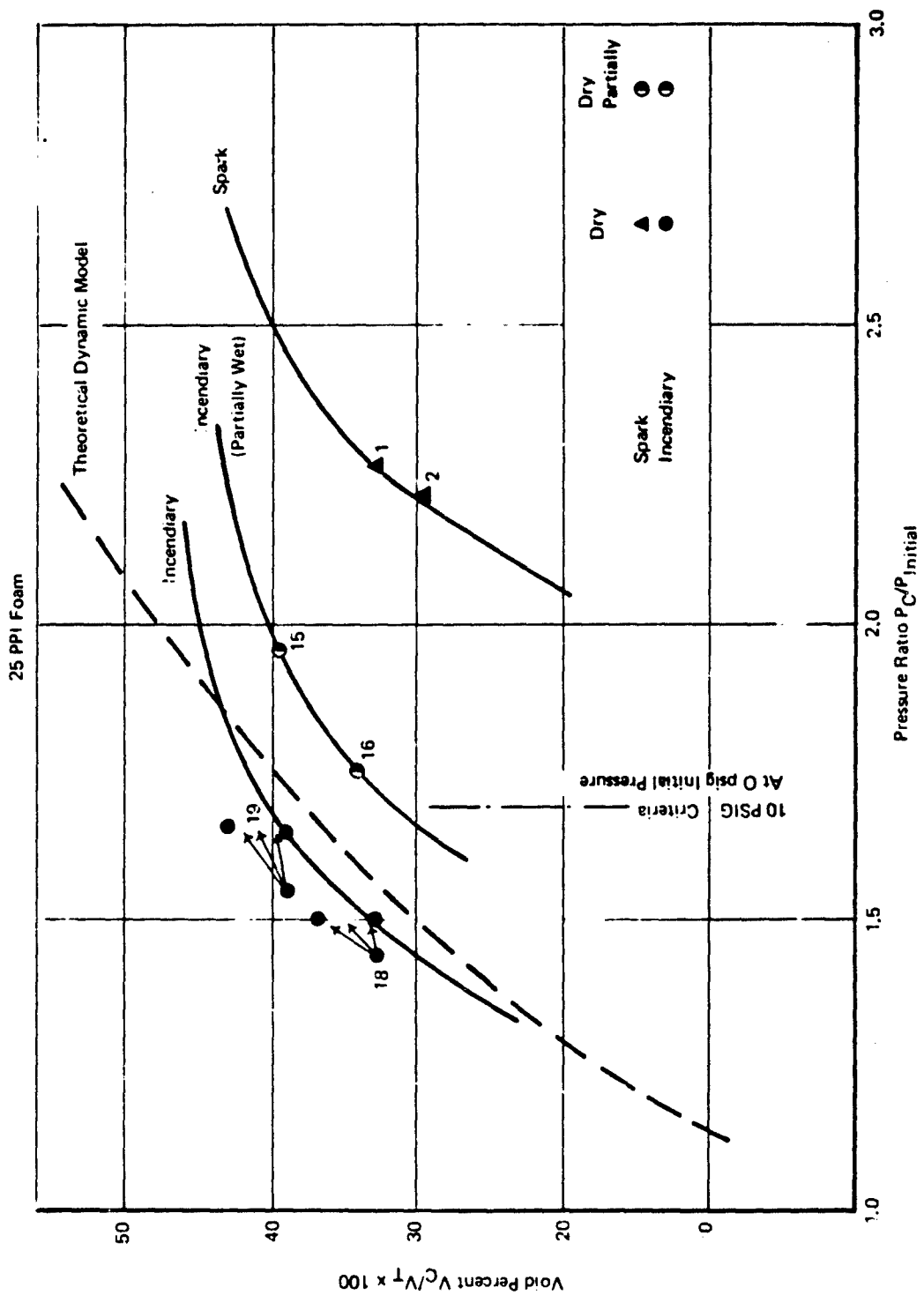


Figure 32: Lined Wall Configuration (Dry)

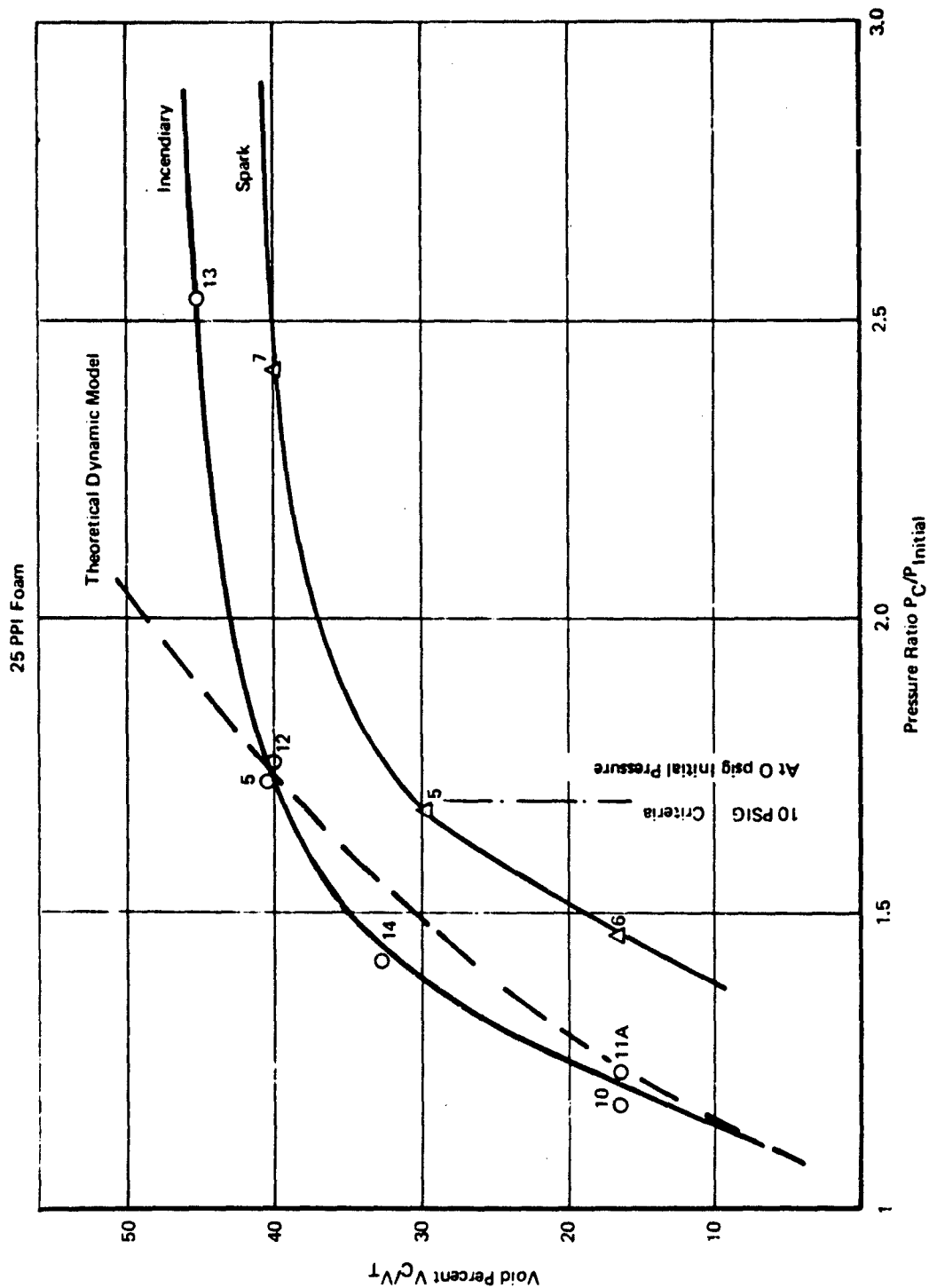


Figure 33: Lined Wall Configuration (Wetted with JP5)

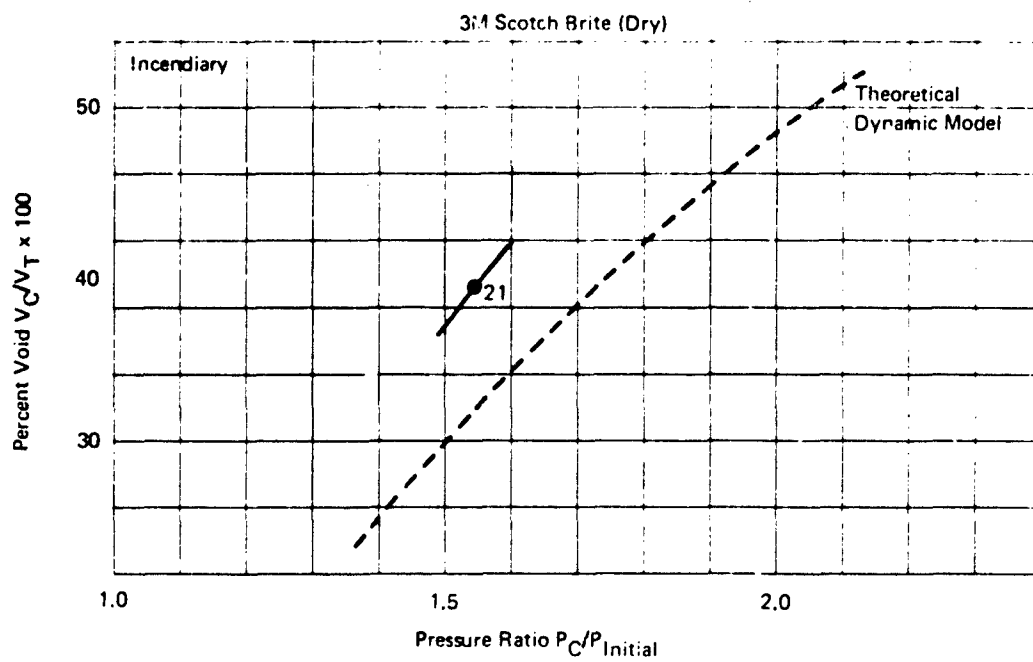
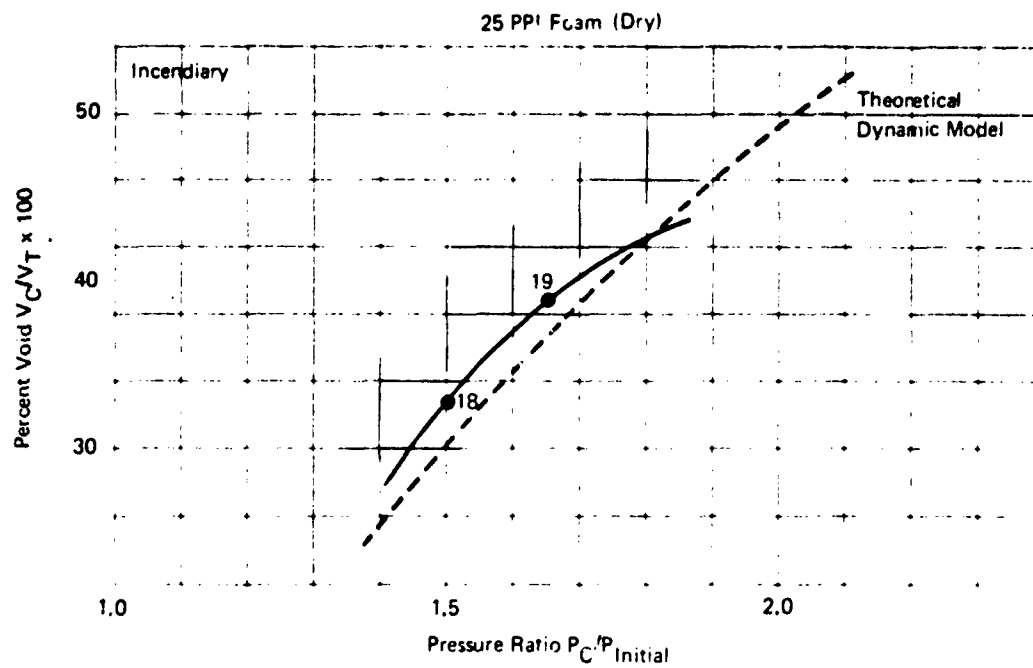


Figure 3-4: Fuselage Tank (Lined Wall) Material Screening Tests (I)

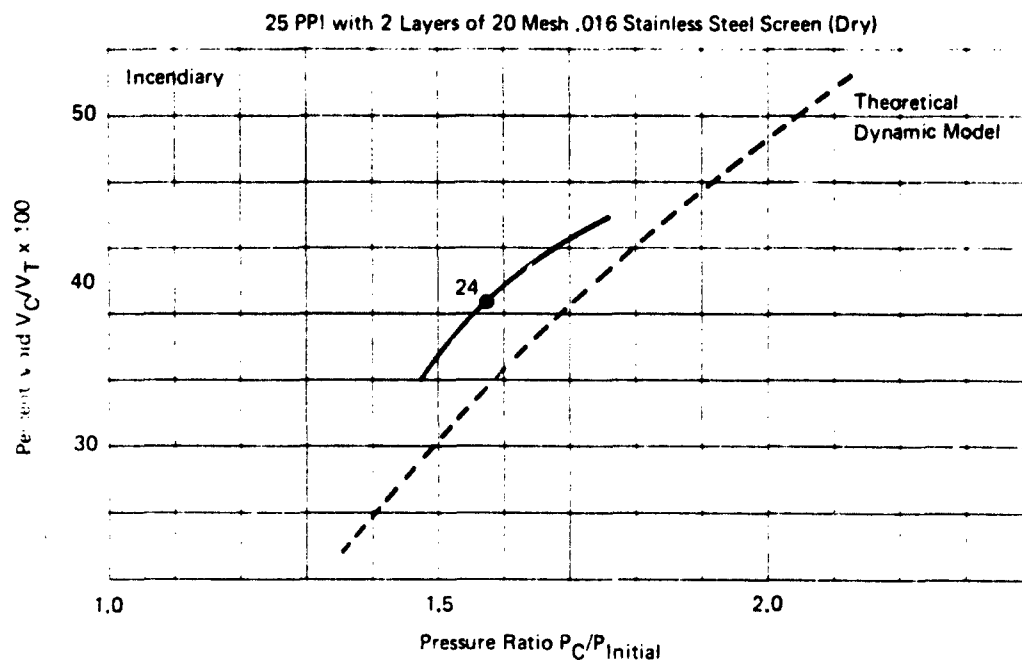
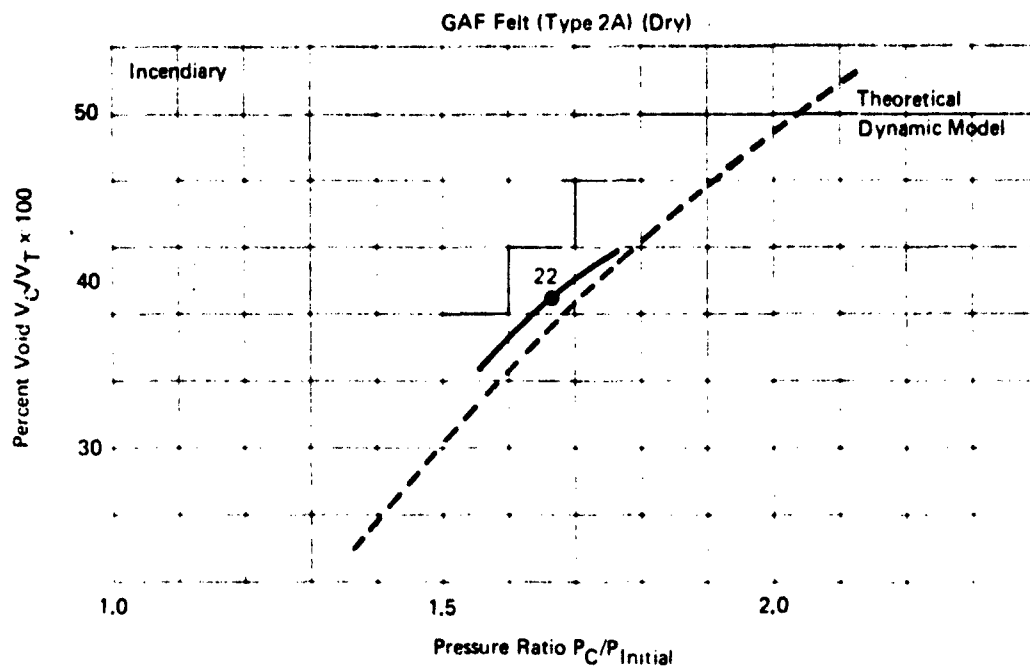


Figure 35: Fuselage Tank (Lined Wall) Material Screening Tests (II)

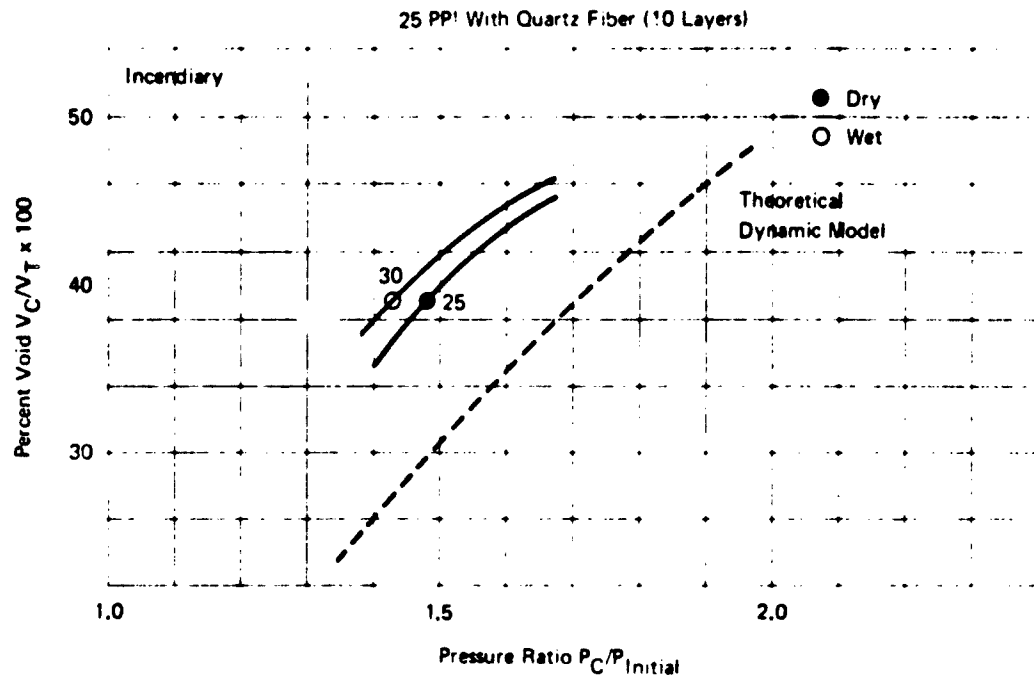
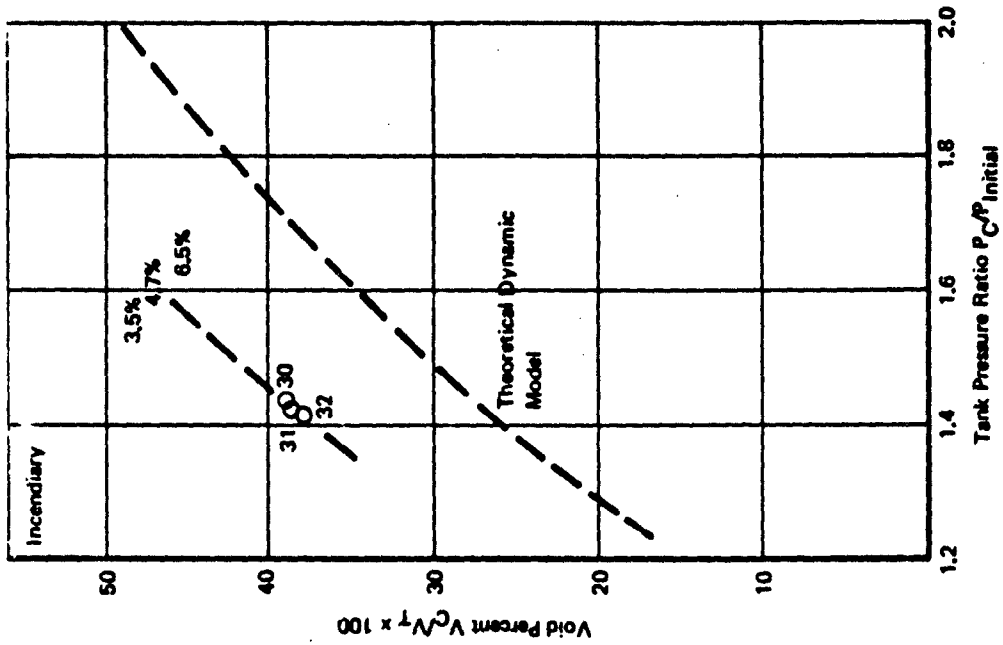


Figure 36: Fuselage Tank (Lined Wall) Material Screening Tests (III)

25 MPa Foam - 10 Layer
of Quartz Fiber 594



25 MPa Foam

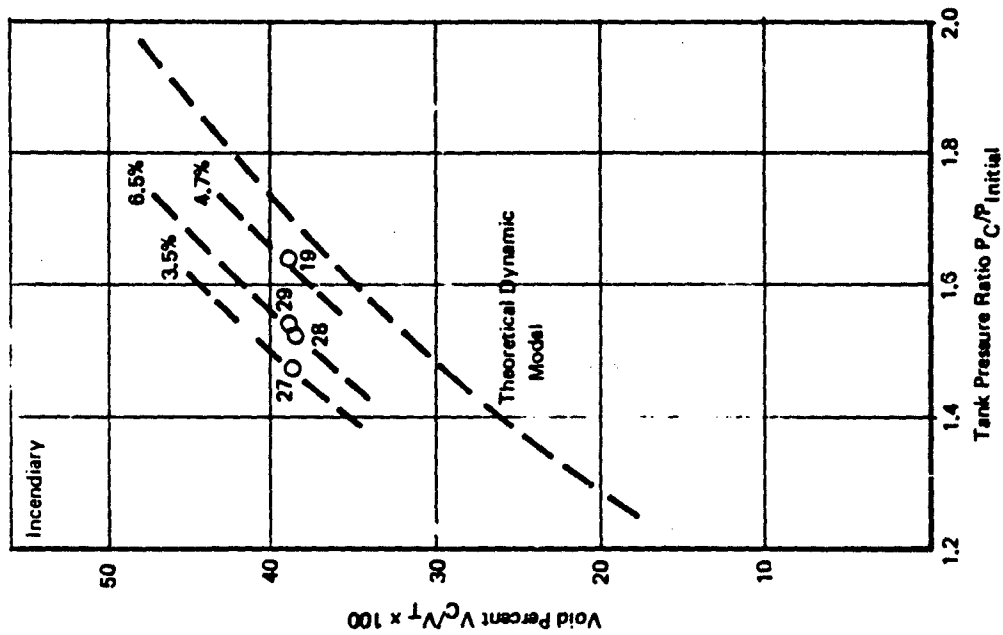


Figure 37: Fuselage Tank (Lined Wall) Wet with JPS Variations in Fuel/Air Ratio (I)

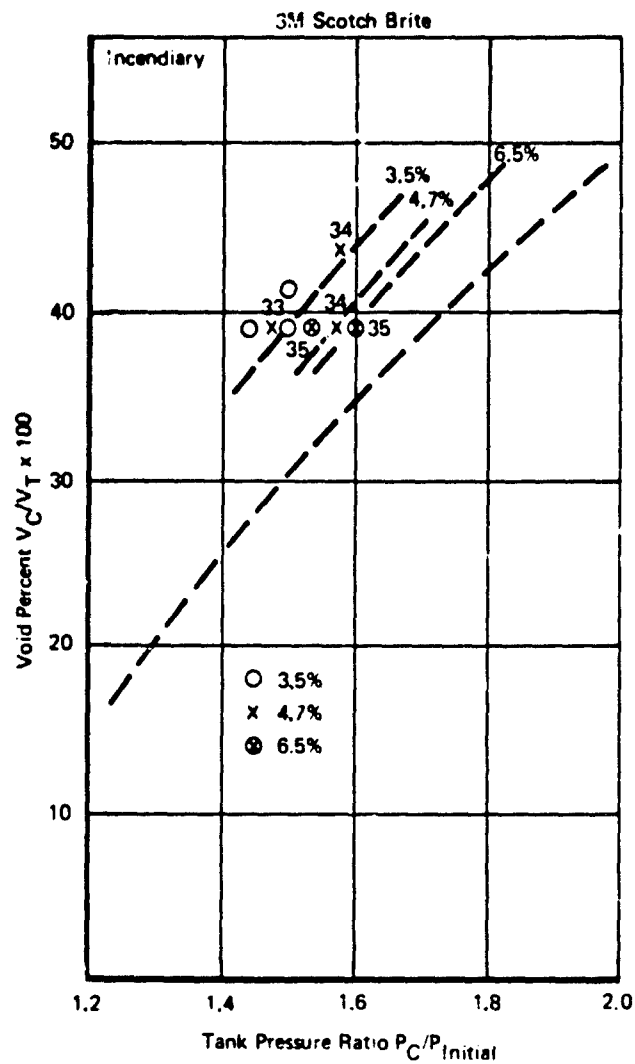


Figure 38: Fuselage Tank (Lined Wall) Wet with JP5 Variations in Fuel/Air Ratio (II)

Typical bomb sample data for a 33% voided lined wall, with the arrester material (25-ppi foam) wet and partially wetted with JP5 is shown in Figure 39. Variations of bomb sample overpressure with fuel-to-air ratio and the overpressures obtained in the fuselage tankage containing different materials are shown in Figures 40 and 41. The tankage overpressures obtained in a 39% voided lined wall configuration with different fuel-to-air ratios are compared in Figure 42 for three different materials.

The data shown graphically in Figures 40 and 41 are for information only. They indicate that the bomb sampler location and installed material influenced, to a slight degree, the sampler overpressures obtained. This overpressure is of course influenced by the fuel/air ratio of the sample withdrawn. It is possible that fuel droplets as well as C_3H_8 vapor were pulled through the sample line. The extent of droplet contamination is determined by the fuel retention properties of the arrester material. Subsequent droplet vaporization and possible water condensation in the line and sampler would influence the pressure rise data.

The overpressures obtained within the fuselage tank shown in Figure 42 indicate that, for this void configuration, the 25 PPI foam and astroquartz combination resulted in a lower overpressure than the other materials. It is interesting to note that overpressure increase is directly related to an increase in K factor when determined for a low Reynolds number, reference Figure 13.

A summary of all data obtained during tests of a lined wall configuration are shown in Figure 43, where the absolute overpressure ratio is related to the ratio of relief and combustion volume.

The pressure rise and rise time in a voided container has been shown to vary as the volume of explosive mixture reacted.

This phenomenon was not as noticeable in the variable geometry tests, partly because of the smaller combustion volume variations but mostly because of the small volume of arrester material used and the comparatively smaller relief area allowing pressure communication.

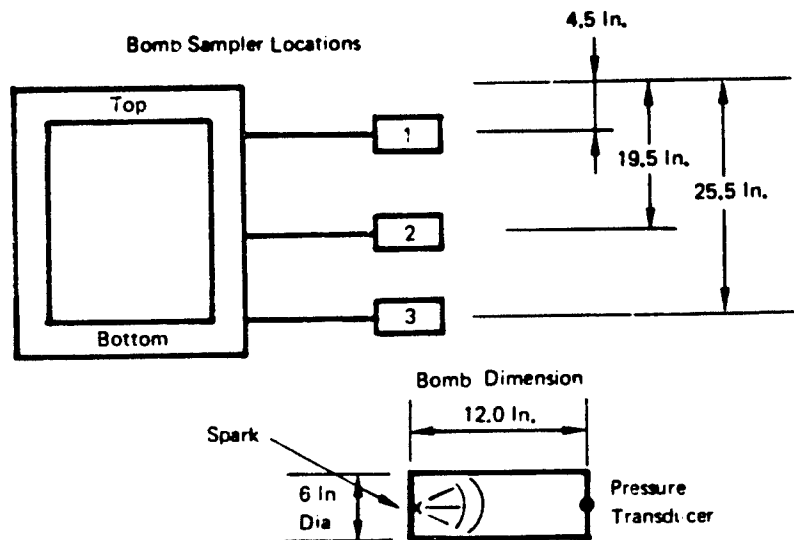
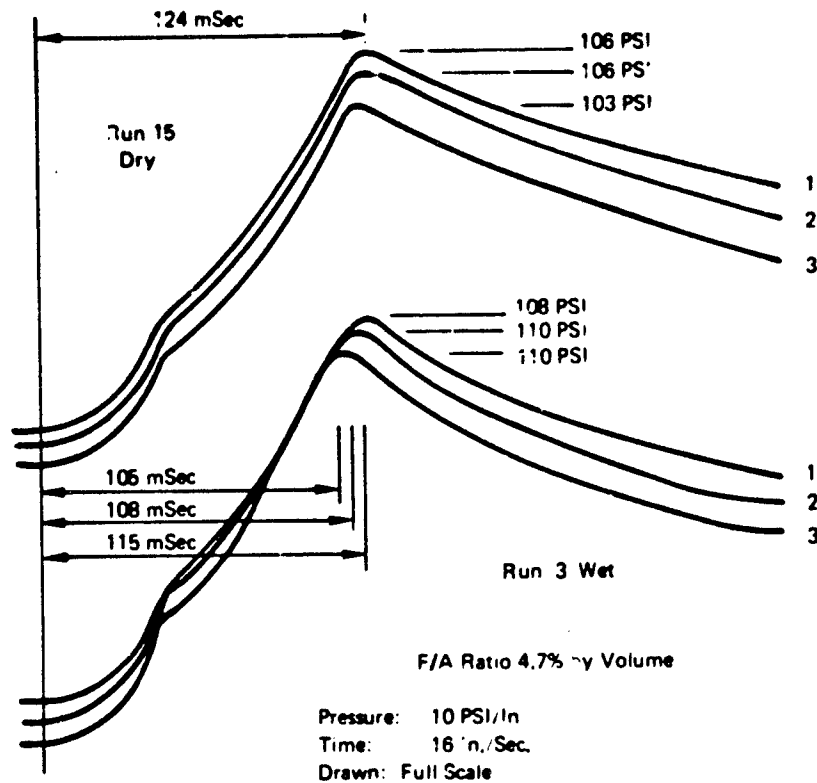


Figure 39: Typical Bomb Sample Data

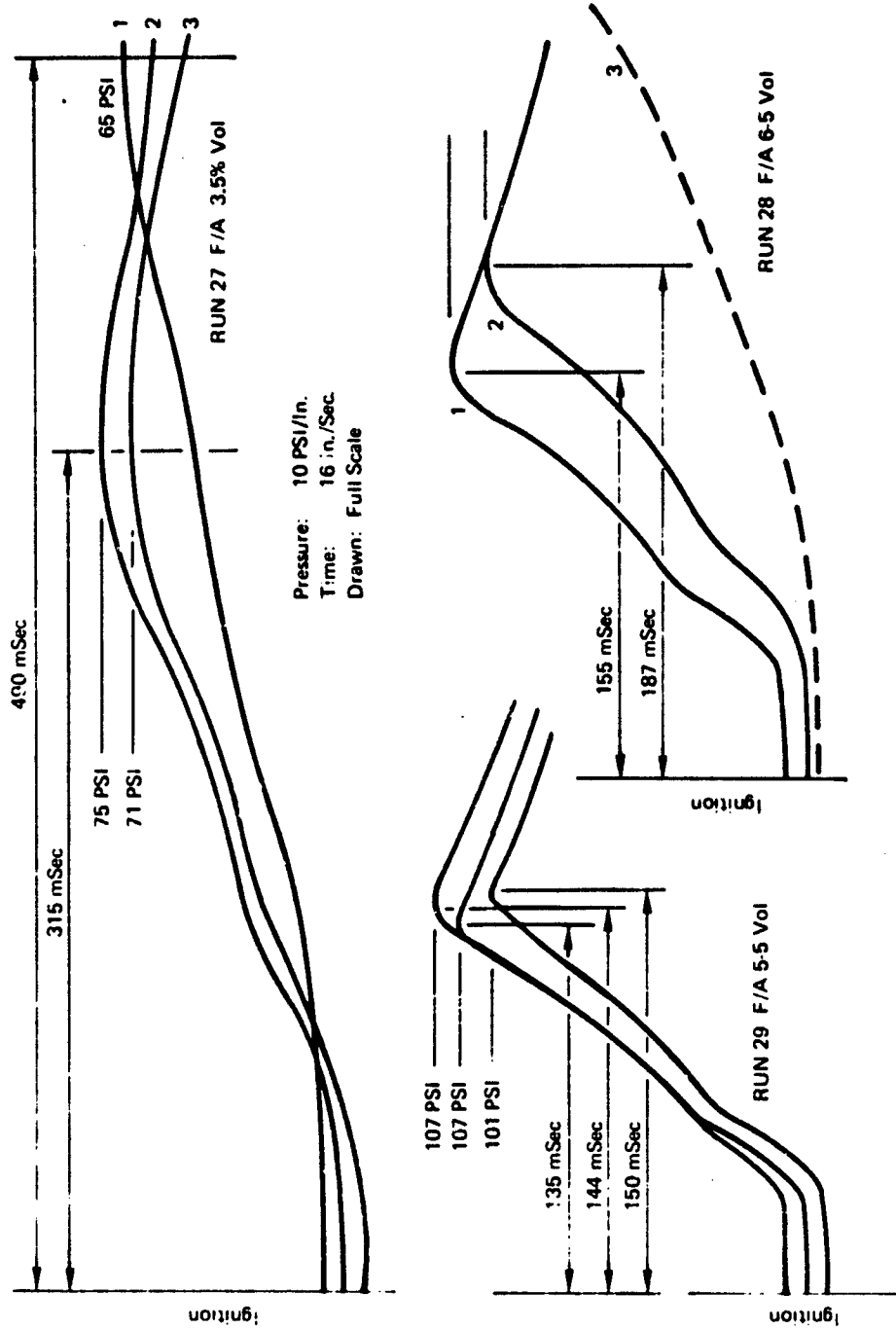


Figure 40: Typical Bomb Sample Data, 25-PPI (Wet)

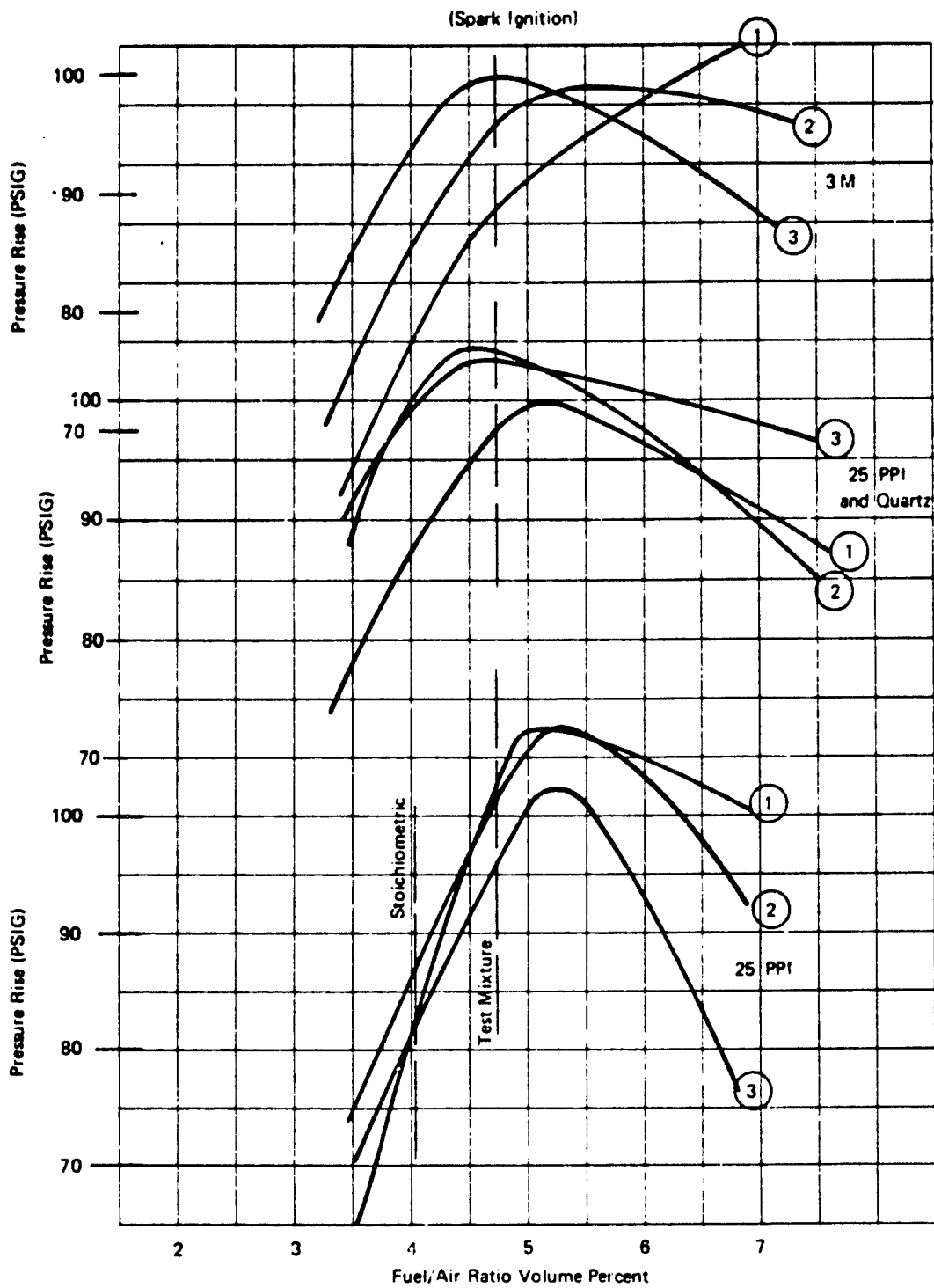


Figure 41: Variation of Bomb Sample Pressure Rise for Different Materials

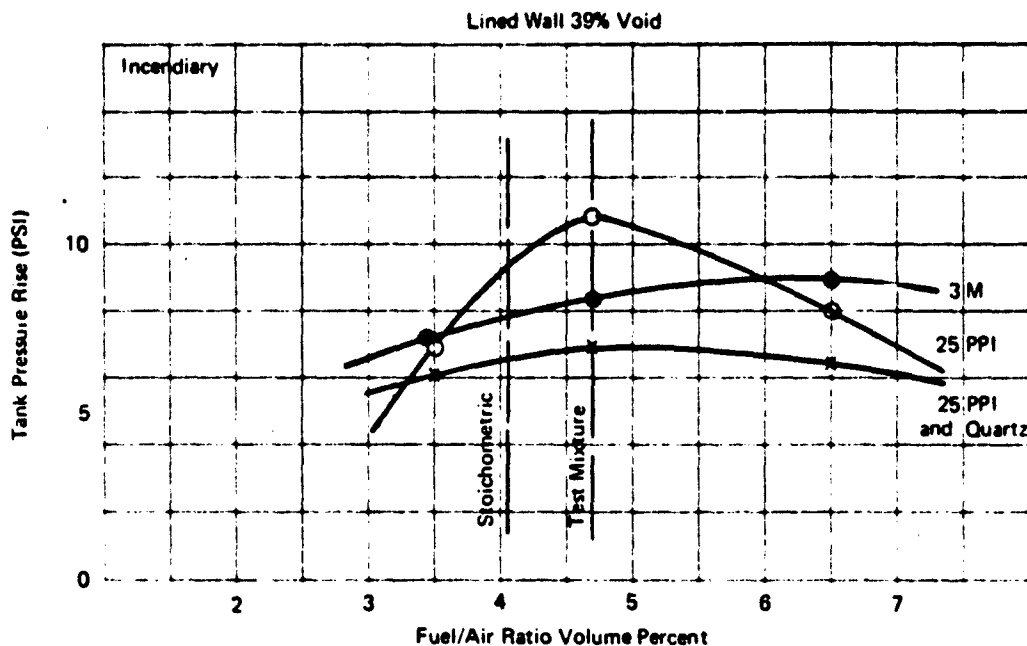


Figure 42: Variation of Fuselage Tank Overpressure for Different Materials at Various Fuel-to-Air Ratios

For those tests undertaken with the material wet, the lower pressures obtained could be attributed to C_3H_8 going into solution, and so weakening the fuel-air ratio.

The lower pressures that occurred with the igniter can be attributed to a reduction in available explosive mixture. This reduced amount of available explosive C_3H_8 -air mixture is attributed to two phenomena during an explosion initiated by incendiary mixture:

- 1) C_3H_8 -air mixture's being pushed into the foam
- 2) C_3H_8 -air mixture's being diluted with product of incendiary mixture combustion

The following has been extracted from Reference 10 T.O. 11A-1-34 Military Explosives in an attempt to explain observed phenomena.

The incendiary composition of IM-11 is considered as intermediate between thermite compositions, which produce no gases, and tracer compositions, which do.

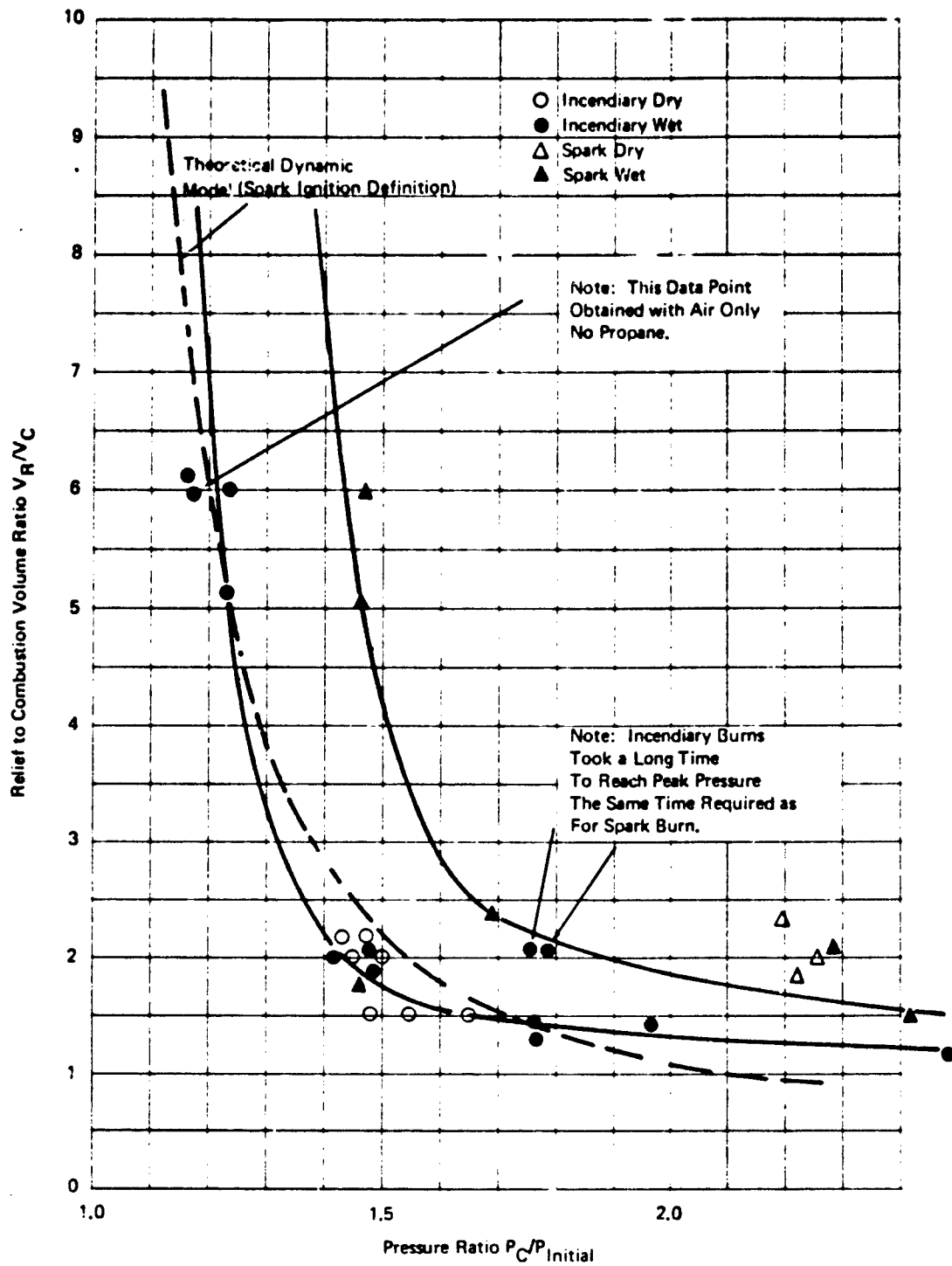


Figure 43: Pressure Ratio vs Relief to Combustion Volume Ratio – Fuselage Tank (Lined Wall)

IM-11 composition:

50/50 magnesium/aluminum	48%
Barium nitrate	50.5%
Asphaltum	1.5%

The incendiary compositions are purposely not oxygen-balanced and are provided an excess of metal particles, most of which burn to their oxides in the air after expulsion from the projectile. Essentially, the only gas produced for the oxidizer-fuel types of incendiary compositions is nitrogen.

It is further noted that all incendiary reaction temperatures are above 5,400°F and that the reaction mixture is oxygen deficient. If this is true then continued burning of the incendiary particles will locally enrich the explosive mixture by using available oxygen in extending the life of the ignition source. This has been previously noted to be approximately 8 to 10 milliseconds for IM-11.

The overpressure design criterion of 10 psig pressure rise results in the following relationship of initial pressure and final absolute pressure ratio:

<u>PSIG</u>	<u>Pc/P_{initial}</u>
0	1.68
2	1.6
4	1.534
5	1.5

The data summary table shown in Figure 44 indicates that the materials giving the lowest pressure in a lined wall configuration are 3M material, 25-ppi and quartz fiber (10 layers), and 25-ppi and stainless steel screen.

In conjunction with the results of all Mode 1A and Mode 1B tests the above materials and variations of material association will be used for all Task III testing.

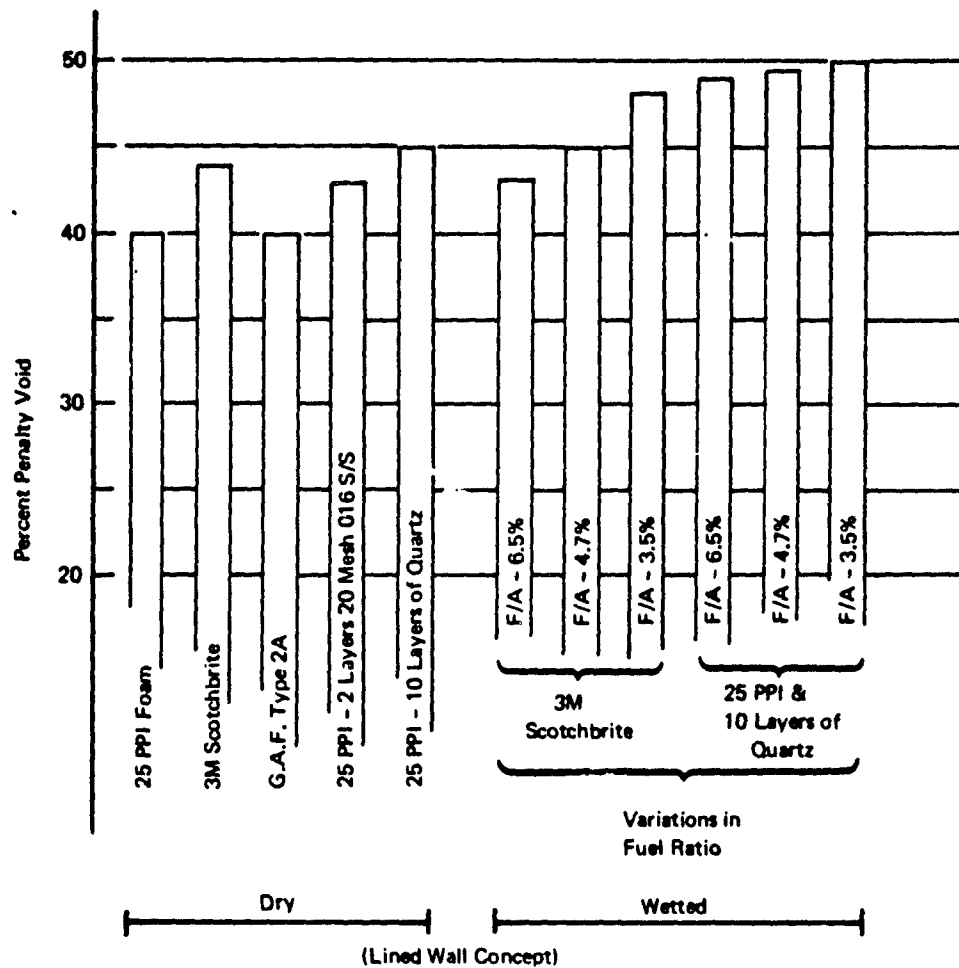


Figure 44: Fuselage Tank Data Summary Mode II Test

NOTE:

The penalty void shown is based upon 10 psig overpressure.

7.0 CONCLUSIONS AND RECOMMENDATIONS

The initial pressure rise experienced when the incendiary round is fired (as indicated on all the pressure traces and shown dramatically during run No. 10, when the igniter was fired into a voided tank containing air only) is responsible for driving a certain percentage of the available gas into the arrester and diluting the C_3H_8 explosive mixture with inertant (N_2) such as to change the mixture ratio.

An explosive mixture of C_3H_8 is pushed into the arrester material during an explosion. The mathematical model data shown in Figure 45 indicate that, for a particular unvented void configuration, the overpressure is related to the amount of explosive mixture reacted.

The test data has shown that within an unvented tankage a spark initiated explosion resulted in a higher pressure rise than that achieved with an incendiary igniter. The rise time for the spark is shown in Figure A-99 to be 175 msec and Figure A-100 shows the rise time for the incendiary to be 10 to 40 msec. It is apparent from these data that the ignition source influences the volume of explosive mixture reacted.

The incendiary burn pressure rise, as well as the forcing of unreacted gas into the foam, reduces the available volume of C_3H_8 -air mixture by replacing a certain percentage with products of its own combustion. It is this change that is the major cause of a lower final pressure in any particular voiding configuration.

A large difference in final absolute overpressure ratio is observed when an incendiary or spark is used to initiate an explosion in a lined wall concept with the arrester material dry or wetted with JP5 fuel. The tests with a dry arrester resulted in a higher pressure rise.

SECTION VII
MATERIAL PROPERTY DETERMINATION

The critical properties of the most promising materials with regards to aircraft installation penalties have been determined per MIL-B-83054. These properties are as follows:

Density	Paragraph 4-7-2
Displacement	Paragraph 4-7-8
Retention	Paragraph 4-7-9

The test fluid was MIL-T-5624 grade JP5 fuel. The specific gravity of this fluid at 60/60 was determined by test to be 0.8105.

The measurement of weight on the smaller samples was taken on a Mettler PIGON (Scientific Products Inc.). For the larger samples required by the specification the weights were recorded on a Harvard Trip Balance manufactured by Ohaus Scale Corp., Union, N. J.

The results are shown in Tables IV and V.

The volume displaced shown tabulated in Table IV was determined from the following equation:

$$\text{Volume displaced \%} = \frac{\text{NL (increase)} \times 100}{\text{Original volume (NL)}}$$

The density tabulated in Table V, Column (1), was determined from the following equation:

$$\text{Density lb/ft}^3 = \frac{\text{Weight (gms)} \times 0.002205 \text{ (lb/gm)}}{\text{Volume (ft}^3\text{)}}$$

The retention percent tabulated in Table V, Column (2), was determined from the following equation:

$$\% \text{ Retention} = \frac{\text{Weight (wet-dry) (gm)} \times 100 \times 1 \text{ cm}^3/\text{gm}}{\text{Volume (in}^3\text{)} \times 16.39 \text{ (cm}^3/\text{in}^3\text{)} \times \text{specific gravity}}$$

Table IV: Displacement Data

Material	Original Level M L *	Final Level M L	Δ M L	% Vol Displaced
25 PPI (Red)	900	918	18	2%
15 PPI (Yellow)	900	920	20	2.22%
10 PPI (Orange)	900	922	23	2.55%
3 M (Std) (1)	900	930	30	3.33%
3 M (Std) (2)	900	930	30	3.33%
GAF (Std)	900	927	27	3.0%
GAF (2A)	900	922	22	2.44%

* Milliliters

Table V: Density and Retention Data JP5

Material	Sample Dimen, in	Vol in ³	Vol ft ³	Weight (gm)		Density Lb Ft ³		Retention Percent
				Dry	Wet	Dry	Wet	
25 PPI (Red)	6x6x5	180	.1041	67.99	209.88	1.44	4.44	5.93
25 PPI (Red)	7x7x7	354	.199	129	404	1.43	4.49	5.84
	7x7x7	354	.199	129	382	1.43	4.25	5.36
15 PPI (Yellow)	6x6x5	180	.1041	69.11	128.95	1.46	2.73	2.502
	7x6x5	210	.1215	79.86	132.73	1.45	2.409	1.859
10 PPI (Orange)	6x6x5	180	.1041	90.71	204.14	1.92	4.32	4.74
	6x6x5	188	.1041	89.44	166.37	1.893	4.009	3.157
3 M (Std)	6x6x4	171	.099	121.76	228.75	2.71	5.095	4.709
	6x6x2-7/8	103.5	.0599	74.71	149.05	2.75	5.487	5.4
GAF (Std)	6x6x5	198	.1146	101.21	204.25	1.94	3.93	3.91
	6x6x3	117	.0677	54.73	124.18	1.78	4.045	4.468
GAF (2A)	6x6x7	252	.1458	139.90	260.01	2.11	3.93	3.587
	6x6x3	126	.073	71.60	34.08	2.16	4.05	3.73
GAF (5A)	6x6x6	234	.135	114.57	234.45	1.87	3.83	3.856
	6x6x3	117	.0677	58.04	140.44	1.89	4.574	5.30
GAF (8A)	6x6x5	198	.1146	93.39	183.21	1.797	3.525	3.414
	6x6x2	99	.057	46.14	95.05	1.785	3.677	3.719
* 20 Mesh .016 Screen	4" Dia x .032	.509	.000294	30.936	32.6	232.02	244.5	24.60
* 35 Mesh .011 Screen	4" Dia x .022	.35	.000202	21.635	25.91	236.16	282.83	91.94
* Fiberglass 10 oz .01	5x5x.04	1.0	.000579	10.25	16.29	39.035	62.037	45.46
	3 Layers							
* Quartz Fiber 594	4x4x.075	1.2	.000694	9.32	20.16	29.6118	64.05	68.00
	10 Layers							
Custom Material: XP 7611	6x6x2	72	.0466	36.04	111.63	1.907	5.910	7.903

* NOTE:

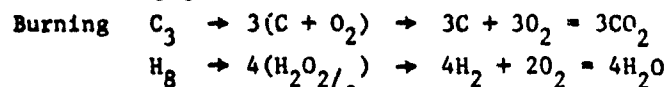
The density and percent retention appear prohibitive. However, the materials were being considered for application within highly voided configurations and should not be discarded on the basis of their properties as shown.

SECTION VIII ANALYSIS

1.0 GENERAL OVERPRESSURE DERIVATION

Calculation of Overpressure Ratio K for a Stoichiometric Propane Air Mixture

Propane (C_3H_8) and air mixture



It can be shown that $N_2 = 3.76 O_2$ by weight



Molecular weights of the gases involved

$$C = 12$$

$$H_2 = 2$$

$$O_2 = 32$$

$$N_2 = 28$$

$$\text{Air-to-fuel ratio} = \frac{(5 \times 32) + (5 \times 28 \times 3.76)}{(3 \times 12) + 4 \times 2} = 15.6/1 \text{ (By Weight)}$$

$$\text{Further F/A (Vol \%)} = \frac{V_{\text{fuel}} \times 100}{V_{\text{fuel}} + V_{\text{air}}} = \frac{100}{1 + V_{\text{air}}/V_{\text{fuel}}} \quad (1)$$

$$P_F V_F = WRT_F = (1.) R_{O/F} \cdot T_F \quad (1A)$$

$$P_A V_A = WRT_A = (15.6) R_{O/A} \cdot T_A \quad (1B)$$

for equilibrium $P_A = P_F$ and $T_F = T_A$ combining 1A and 1B.

$$V_{\text{air}}/V_{\text{fuel}} = 15.6 M_F/M_A \quad (2)$$

Preceding page blank

Substituting Equation (2) in (1).

$$F/A \text{ Vol } \% = \frac{100}{1 + \left(\frac{15.6 \times 44}{28.97} \right)} = 4.05\%$$

The assumptions of simple heating will be adhered to, so that no notice will be given the changes in chemical composition, molecular weight, and specific heat.

From Reference 10 the stagnation-temperature rise across the propagating flame front is given as

$$T_{O_2} - T_{O_1} = \Delta T = \frac{\Delta H}{CP} \left(\frac{M_F}{M_F + M_A} \right)$$

where ΔH -- is the heat of reaction of the fuel in BTU/Lb.

CP -- is the heat capacity of the fuel/air mixture at constant pressure BTU/Lb°F

assuming no external energy added, the total mass of combustible stoichiometric mixture 1 pound of fuel plus 15.6 pounds of air.

$$\text{Total pounds burnt} = \underline{16.6}$$

The heat of reaction for propane is given as 19,930 Btu/lb (Reference 11) and the average specific heat during the process is assumed to be 0.32 Btu/lb°F

$$\text{therefore } \Delta T = \frac{19,930}{16.6 \times 0.32} = 3,750^\circ R$$

and consequently,

$$\frac{T_{O_2}}{T_{O_1}} = P_C/P_1 = \frac{4,270}{520} = 8.22$$

2.0 STEADY STATE MATHEMATICAL MODEL

Calculation of Overpressure, with Variations of the Relief Volume - This simple mathematical model configuration is essentially a two-cell model, which assumes immediate and complete pressure communication, while arresting the fire and/or flame front.



Burning all the combustible mixture in the combustion volume V_C immediately and expanding only burnt gases into V_R will result in the maximum allowable overpressure, assuming no restriction in the expansion of the gases in V_R .

Final pressure in V_C assuming no expansion into V_R

$$P_2 = P_1 K \quad P_1 = \text{initial pressure PSIA}$$

$$K = T_2/T_1 = 8.22 \quad (\text{See Section 1.0 for derivation})$$

$$\text{pressure rise} = P_2 - P_1 = P_1 K - P_1 = P_1 (K-1)$$

Assuming an isothermal process $PV = \text{const.}$ and assuming static equilibrium conditions, the maximum total tank pressure is correlated as follows:

$$P_2 V_C + P_1 V_R = P_C V_T \quad \text{where } V_T = V_C + V_R$$

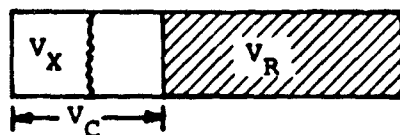
substituting $P_2 = P_1 K$

$$P_1 (K V_C + V_R) = P_C V_T$$

$$P_C/P_1 = V_C/V_T (K + V_R/V_C) \quad \text{maximum overpressure} \quad (1)$$

However, in practice the expanding gases push some of the unreacted gases through the foam into the relief volume. Consequently, not all of the combustion volume energy is converted to pressure energy by the burning process.

The following model was developed in Reference 2. An isothermal process allows the gas to expand unrestricted from V_C into V_R and assumes no pressure loss through the arrester.



Equating conditions at the beginning and end of the reaction, V_X is the volume of V_C that combusts.

$$K P_1 V_X = P_C V_C \quad (1A)$$

at condition 1 (flame front as shown)

$$K P_1 V_X + P_1 (V_C - V_X) + P_1 V_R = P_2 V_T \quad (1B)$$

at condition 2 flame front expands to the foam face.

$$P_C V_C + P_C V_R = P_2 V_T \quad (1C)$$

equating Equations (1B) and (1C)

$$K P_1 V_X - P_1 V_X + P_1 V_C + P_1 V_R = P_C V_C + P_C V_R$$

Substituting Equation (1A) to eliminate V_X

$$P_1 V_X = P_C V_C / K \text{ into the above}$$

$$P_C V_C - P_C V_C / K + P_1 V_C + P_1 V_R = P_C V_C + P_C V_R$$

$$P_1 (V_C + V_R) = P_C (V_C / K + V_R)$$

rearranging

$$P_C / P_1 = \frac{V_C + V_R}{V_C / K + V_R} = \frac{V_T K}{V_T K - V_C (K-1)}$$

$$\text{finally } P_C/P_1 = \frac{K(V_R/V_C + 1)}{KV_R/V_C + 1} \quad \text{minimum overpressure} \quad (2)$$

The calculated absolute pressure ratio for maximum and minimum overpressures as calculated from Equations (1) and (2) are related to volume ratio and percent void as shown in Figures 45 and 46.

3.0 DYNAMIC MATHEMATICAL MODEL

3.1 Transient Analysis

A transient analysis was formulated for a tank that is being pressurized by the products of combustion of a flammable mixture, while allowing pressure communication through an orifice into a relief volume.

Two models were formulated for a spark and incendiary activated burn. Both models are identical except for the definition of flame propagation.

The pressure response within the tank can be characterized by a burning phase followed by an emptying phase. The burning phase lasts until all the vapor has been burned and the flame has traversed the combustion volume. At completion of the burning phase, the internal pressure within the combustion volume has reached its peak value; the pressure then decays during the emptying phase as burnt gases relieve through the aperture into the relief volume, whose pressure increases until pressure equilibrium is reached.

The model is illustrated in Figure A, showing tank conditions shortly after ignition. On one side of the flame front, unburnt gas is present: P_U , V_U , T_U , M_U . On the other side, combustion is complete and products are formed: P_B , V_B , T_B , M_B .

Since the study involves normal explosions and the flame velocity is small compared to the velocity of sound, the following conditions and/or assumptions are postulated.

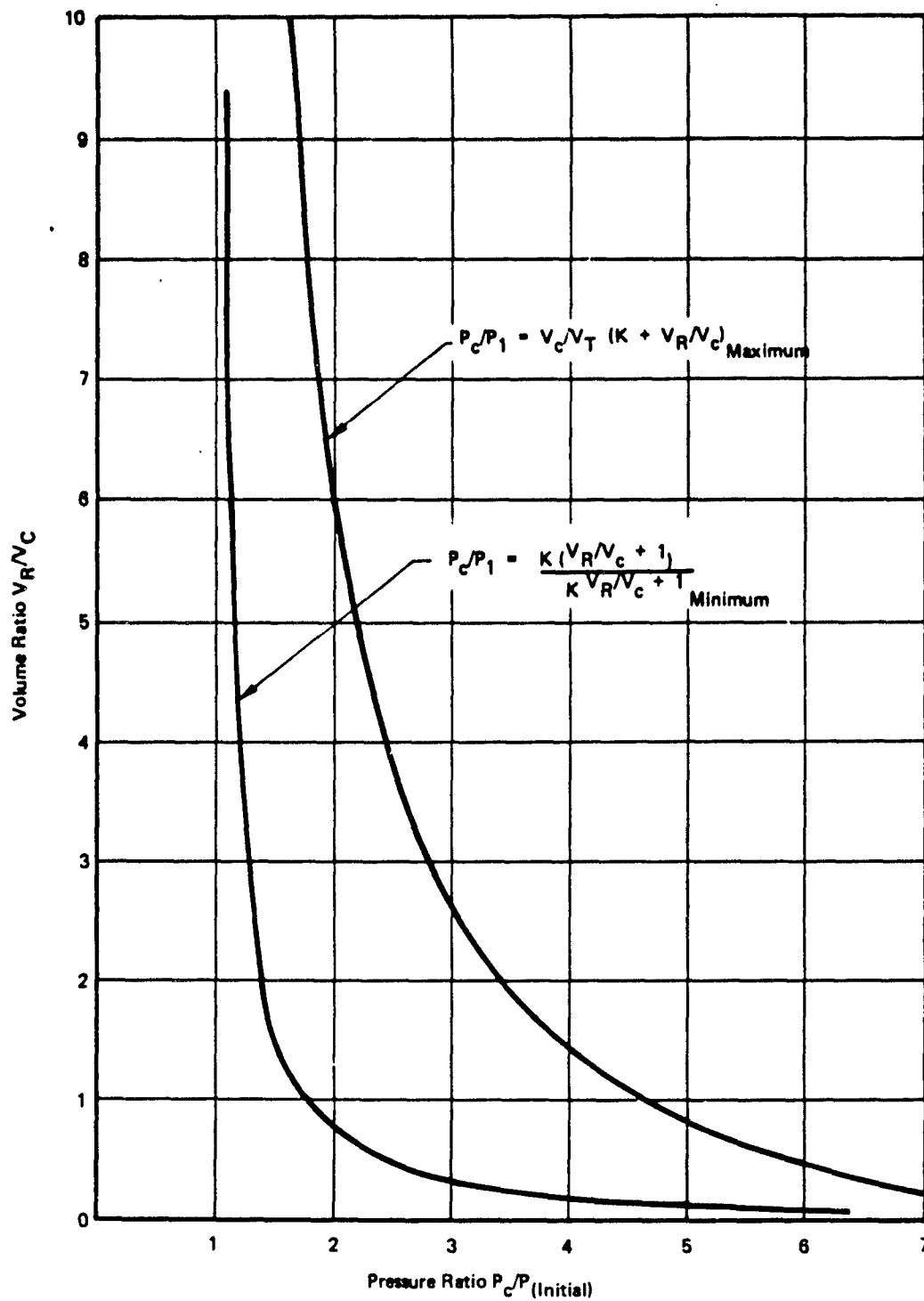


Figure 45: Steady State Mathematical Model Volume Ratio V_R/V_C Versus Pressure Ratio $P_C/P_{Initial}$

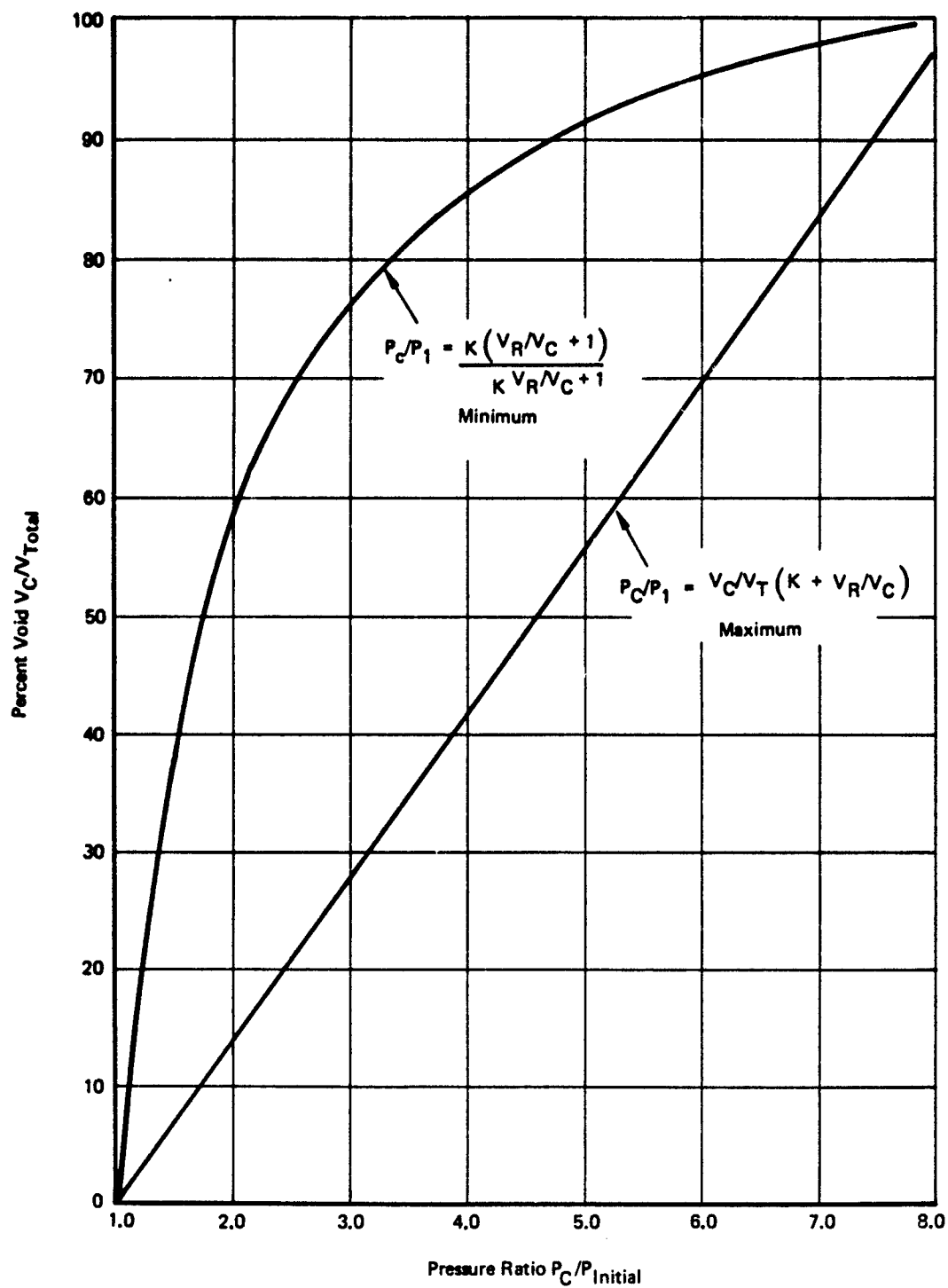


Figure 46: Steady State Mathematical Model Percent Void V_C/V_T versus Pressure Ratio $P_C/P_{Initial}$

- 1) The pressure field sets up rapidly in unconfined volumes, thus

$$P_B(t) = P_U(t) = P(t)$$

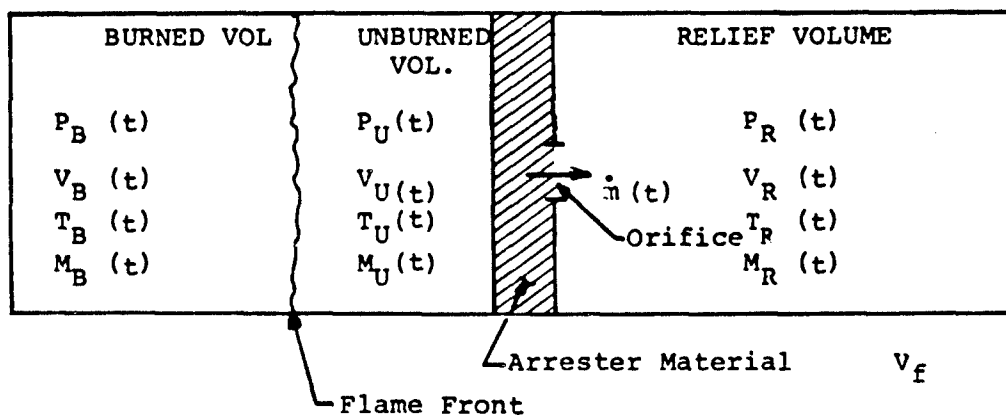
- 2) There is a pressure drop across the arrester material and orifice equal to ΔP , thus

$$P_R(t) = P(t) - \Delta P(t)$$

NOTE: $\Delta P(t)$ is a function of mass flowrate.

- 3) There is isentropic compression of the unburned gas and the relief volume gases as pressure increases during burning.
- 4) Total and static qualities are equivalent.

Figure A MODEL SCHEMATIC



2.1.1 Burning Phase

Combustion Volume

The rate of mass depletion in the combustion volume is given by

$$\frac{dM(t)}{dt} = -\dot{m} \quad (1)$$

where $M(t) = M_B(t) + M_U(t)$

$$= \frac{P_B(t) V_B(t)}{R_B T_B(t)} + \frac{P_U(t) V_U(t)}{R_U T_U(t)} \quad (2)$$

Since $P_B(t) = P_U(t) = P(t)$ (3)

and $V_U(t) = V_T - V_B(t)$ (4)

where V_T = burned volume + unburned volume = combustion volume.

Substituting Equations (3) and (4) into (2), then:

$$M(t) = \frac{P(t) V_B(t)}{R_B T_B(t)} + \frac{P(t) [V_T - V_B(t)]}{R_U T_U(t)}$$

expanding

$$M(t) = \frac{P(t) V_B(t)}{R_B T_B(t)} + \frac{P(t) V_T}{R_U T_U(t)} - \frac{P(t) V_B(t)}{R_U T_U(t)}$$

Rewriting

$$M(t) = \frac{P(t)}{R_U T_U(t)} \left[V_T - V_B(t) + \left(\frac{R_U}{R_B} \right) \left(\frac{T_U(t)}{T_B(t)} \right) V_B(t) \right] \quad (5)$$

differentiating Equation (5) with respect to time.

$$\begin{aligned} \frac{dM(t)}{dt} = & \frac{P(t)}{R_U T_U(t)} \left\{ - \frac{dV_B(t)}{dt} + \left(\frac{R_U}{R_B} \right) \left[\frac{T_U(t)}{T_B(t)} \frac{dV_B(t)}{dt} + V_B(t) \frac{d}{dt} \left(\frac{T_U(t)}{T_B(t)} \right) \right] \right\} \\ & + \left[V_T - V_B(t) + \left(\frac{R_U}{R_B} \right) \left(\frac{T_U(t)}{T_B(t)} \right) V_B(t) \right] \frac{1}{R_U} \left[\frac{dP(t)}{dt} \frac{1}{T_U(t)} - \frac{P(t)}{T_U^2(t)} \frac{dT_U(t)}{dt} \right] \end{aligned} \quad (6)$$

Rewriting

$$\begin{aligned} \frac{dM(t)}{dt} = & \frac{P(t)}{R_U T_U(t)} \left\{ \left[\left(\frac{R_U}{R_B} \right) \left(\frac{T_U(t)}{T_B(t)} \right) - 1 \right] \frac{dv_B(t)}{dt} + \left(\frac{R_U}{R_B} \right) v_B(t) \frac{d}{dt} \left(\frac{T_U(t)}{T_B(t)} \right) \right\} \\ & + \frac{P(t)}{R_U T_U(t)} \left\{ \left[v_T + \left(\frac{R_U}{R_B} \right) \left(\frac{T_U(t)}{T_B(t)} \right) v_B(t) - v_B(t) \right] \right. \\ & \left. \left(\frac{1}{P(t)} \cdot \frac{dP(t)}{dt} - \frac{1}{T_U(t)} \frac{dT_U(t)}{dt} \right) \right\} \end{aligned} \quad (7)$$

Substituting Equation (7) into Equation (1)

$$\begin{aligned} -\dot{m} = & \frac{P(t)}{R_U T_U(t)} \left\{ \left[\left(\frac{R_U}{R_B} \right) \left(\frac{T_U(t)}{T_B(t)} \right) - 1 \right] \frac{dv_B(t)}{dt} + \left(\frac{R_U}{R_B} \right) v_B(t) \frac{d}{dt} \left(\frac{T_U(t)}{T_B(t)} \right) \right\} \\ & + \frac{P(t)}{R_U T_U(t)} \left\{ \left[v_T + \left(\frac{R_U}{R_B} \right) \left(\frac{T_U(t)}{T_B(t)} \right) v_B(t) - v_B(t) \right] \right. \\ & \left. \left(\frac{1}{P(t)} \cdot \frac{dP(t)}{dt} - \frac{1}{T_U(t)} \frac{dT_U(t)}{dt} \right) \right\} \end{aligned} \quad (8)$$

let

$$E = v_T + \left[\left(\frac{R_U}{R_B} \right) \left(\frac{T_U(t)}{T_B(t)} \right) - 1 \right] v_B(t) \quad (9)$$

then substituting Equation (9) into (8) and rewriting.

$$\begin{aligned} \frac{1}{P(t)} \frac{dP(t)}{dt} - \frac{1}{T_U(t)} \frac{dT_U(t)}{dt} = & \\ -\dot{m} = & \frac{P(t)}{R_U T_U(t)} \left\{ \left[\left(\frac{R_U}{R_B} \right) \left(\frac{T_U(t)}{T_B(t)} \right) - 1 \right] \frac{dv_B(t)}{dt} + \left(\frac{R_U}{R_B} \right) v_B(t) \frac{d}{dt} \left(\frac{T_U(t)}{T_B(t)} \right) \right\} \\ & + \frac{P(t)}{R_U T_U(t)} E \end{aligned} \quad (10)$$

rewriting equation (10)

$$\frac{dP(t)}{dt} = \frac{P(t)}{T_U(t)} \frac{dT_U(t)}{dt} - \left\{ \frac{R_U T_U(t) \dot{m} + P(t) \left\{ \left[\left(\frac{R_U}{R_B} \right) \left(\frac{T_U(t)}{T_B(t)} \right) - 1 \right] \frac{dV_B(t)}{dt} + \left(\frac{R_V}{R_B} \right) V_B(t) \frac{d}{dt} \left(\frac{T_U(t)}{T_B(t)} \right) \right\}}{E} \right\} \quad (11)$$

there is evidence to indicate that the compression of the unburned gas in the tank is isentropic (Reference 12). If this is assumed, then

$$T_U(t) = T_{1U} \left(\frac{P(t)}{P_1} \right)^{\frac{\gamma_{U-1}}{\gamma_U}} = K_{1U} P(t)^{\frac{\gamma_{U-1}}{\gamma_U}} \quad (12)$$

$$\text{where } K_{1U} = T_{1U}/P_1^{\frac{\gamma_{U-1}}{\gamma_U}} \quad (13)$$

In Equation (12) the subscript 1 refers to initial conditions.

Differentiating Equation (12)

$$\frac{dT_U(t)}{dt} = K_{1U} \left(\frac{\gamma_{U-1}}{\gamma_U} \right) P(t)^{-\frac{1}{\gamma_U}} \frac{dP(t)}{dt} \quad (14)$$

The temperature rise in the burned gas can be approximated by

$$T_B(t) = T_U(t) + \frac{\Delta H}{C_{P_B}} \quad (15)$$

rewriting

$$\frac{T_U(t)}{T_B(t)} = 1 - \frac{\Delta H}{T_B(t) C_{P_B}} \quad (16)$$

differentiating Equation (16)

$$\frac{d}{dt} \left(\frac{T_U(t)}{T_B(t)} \right) = \frac{\Delta H}{C_{P_B}} \frac{1}{T_B^2(t)} \frac{dT_B(t)}{dt} \quad (17)$$

Differentiating Equation (15) gives the following

$$\frac{dT_B(t)}{dt} = \frac{dT_U(t)}{dt} \quad (18)$$

Substituting Equation (18 into (17)

$$\frac{d}{dt} \left(\frac{T_U(t)}{T_B(t)} \right) = \frac{\Delta H}{C_{P_B}} \frac{1}{T_B^2(t)} \frac{dT_U(t)}{dt} \quad (19)$$

substituting Equation (14 into (19)

$$\frac{1}{dt} \left(\frac{T_U(t)}{T_B(t)} \right) = \frac{\Delta H}{C_{P_B} T_B(t)} \left(\frac{\gamma_{U-1}}{\gamma_U} \right) P(t)^{-1/\gamma_U} \frac{dP(t)}{dt} \quad (20)$$

Substituting Equations (14) and (20) into Equation (11) and rewriting

$$\begin{aligned} E \left[1 - \frac{P(t)}{T_U(t)} \cdot K_{L_U} \left(\frac{\gamma_{U-1}}{\gamma_U} \right) P(t)^{-1/\gamma_U} \right] \frac{dP(t)}{dt} + R_U T_U(t) \dot{m} = \\ - \left(\frac{R_U}{R_B} \right) \left(\frac{T_U(t)}{T_B(t)} - 1 \right) \left[\frac{P(t)}{dt} \frac{dV_B(t)}{dt} \right. \\ \left. - \left[P(t) \frac{R_U}{R_B} \frac{V_B(t)}{C_{P_B}} \frac{\Delta H}{T_B^2(t)} \left(\frac{\gamma_{U-1}}{\gamma_U} \right) P(t)^{-1/\gamma_U} \frac{dP(t)}{dt} \right] \right] \quad (21) \end{aligned}$$

Substituting Equation (12) into Equation (21) and rewriting

$$E \left[1 - \left(\frac{\gamma_{U-1}}{\gamma_U} \right) + \frac{R_U}{R_B} \left(\frac{\Delta H}{C_{P_B}} \right) \left(\frac{\gamma_{U-1}}{\gamma_U} \right) K_{L_U} \left(\frac{1}{T_B^2(t)} \right) V_B(t) P(t) \frac{\gamma_{U-1}}{\gamma_U} \right]$$

$$\frac{dP(t)}{dt} = - R_U T_U(t) \dot{m} - P(t) \left[\left(\frac{R_U}{R_B} \right) \left(\frac{T_U(t)}{T_B(t)} - 1 \right) \right] \frac{dV_B(t)}{dt} \quad (22)$$

further rewriting results in

$$\frac{dP(t)}{dt} = \frac{- R_U T_U(t) \dot{m} - P(t) \left[\left(\frac{R_U}{R_B} \right) \left(\frac{T_U(t)}{T_B(t)} - 1 \right) \right] \frac{dV_B(t)}{dt}}{E \left[1 - \left(\frac{\gamma_{U-1}}{\gamma_U} \right) + \left(\frac{R_U}{R_B} \right) \left(\frac{\Delta H}{C_{P_B}} \right) \left(\frac{\gamma_{U-1}}{\gamma_U} \right) \left(K_{L_U} \right) \left(\frac{1}{T_B^2(t)} \right) V_B(t) P(t) \frac{\gamma_{U-1}}{\gamma_U} \right]} \quad (23)$$

The major unknowns in Equation (23) are the volume V_B and its rate of change and in the mass flow relieving the combustion pressure through the arrester material and orifice.

The mass flow depends on orifice area, arrester pressure drop, and whether the flow is choked or unchoked. For the pressure ranges of interest it is estimated that both choked and unchoked flow will occur.

For choked flow, the mass flow rate \dot{m} is:

$$\dot{m} = \frac{K_2 A_o P_B}{\sqrt{T_B}} \quad (24)$$

where A_o is the area of the aperture (relief area), and K_2 is a factor that depends on the vapor properties and on C_d , the coefficient of discharge

$$K_2 = C_D \left(\frac{\gamma_B g_c}{R_B} \right)^{1/2} \cdot \left(\frac{2}{\gamma_{B+1}} \right)^{\frac{\gamma_{B+1}}{2(\gamma_{B+1}-1)}} \quad (25)$$

For unchoked flow:

$$\dot{m} = K_6 A_o P_B \sqrt{\frac{1}{T_B} \left[\left(\frac{P_R}{P_B} \right)^{\frac{2}{\gamma_B}} - \left(\frac{P_R}{P_B} \right)^{\frac{\gamma_{B+1}}{\gamma_B}} \right]} \quad (26)$$

where

$$K_6 = C_D \left(\frac{2 \gamma_B g_c}{R_B (\gamma_{B+1})} \right)^{\frac{1}{2}} \quad (27)$$

P_R is the pressure in the relief volume at time (t).

It is convenient to relate C_D to an equivalent velocity head loss K factor.

From Reference 7:

$$K = \frac{1}{C_D^2}$$

rewriting

$$C_D = \frac{1}{\sqrt{K_D}} \quad (28)$$

The velocity head loss through the arrester material K_A found by test allows the total losses to be expressed conveniently by summing both velocity head losses.

$$\text{Total } C_D = \frac{1}{\sqrt{K_A + K_D}} \quad (29)$$

$V_B(t)$ is a function of the burning rate

$\frac{dV_B(t)}{dt}$ is a function of the burning rate

As seen from Figure A, these quantities depend on the speed of the flame front and its shape.

However, flame phenomena are complicated, influenced by laminar to turbulent transitions, gas conditions, and tank geometry. There is no suitable analytical expression for these phenomena and the solution presently must rely on experimental observations.

Relief Phase

During the burning phase, unburnt and burnt gases are expanded through the relief area into the relief volume.

$$\frac{dM_{R(t)}}{dt} = \dot{m} \quad (30)$$

$$M_{R(t)} = \frac{P_{R(t)} V_R}{R T_{R(t)}} \quad \text{as } V_R \text{ is constant with time.}$$

$$\frac{dM_{R(t)}}{dt} = \frac{V_R}{R} \left[\frac{1}{T_{R(t)}} \frac{dP_{R(t)}}{dt} - \frac{P_{R(t)}}{T_{R(t)}^2} \frac{dT_{R(t)}}{dt} \right] \quad (31)$$

rewriting

$$\frac{dM_{R(t)}}{dt} = \frac{V_R}{T_{R(t)} R} \left[\frac{dP_{R(t)}}{dt} - \frac{P_{R(t)}}{T_{R(t)}} \frac{dT_{R(t)}}{dt} \right] \quad (32)$$

remembering that $P_{R(t)} = P(t) - \Delta P(t)$

$$\frac{dM_{R(t)}}{dt} = \frac{V_R}{T_{R(t)} R} \left[\frac{dP(t)}{dt} - \frac{d\Delta P(t)}{dt} - \frac{[P(t) - \Delta P(t)]}{T_{R(t)}} \frac{dT_{R(t)}}{dt} \right] \quad (33)$$

assuming isentropic compression as during the burning phase.

$$T_{R(t)} = T_{1R} \left(\frac{P_{R(t)}}{P_1} \right)^{\gamma_R - 1/\gamma_R} = K_{1R} P_{R(t)}^{\gamma_R - 1/\gamma_R} \quad (34)$$

Note $K_{1U} = K_{1R}$

and $\gamma_U = \gamma_R$

$$T_{R(t)} = K_{1R} [P(t) - \Delta P(t)]^{\gamma_R - 1/\gamma_R} \quad (35)$$

differentiating Equation (35)

$$\frac{dT_{R(t)}}{dt} = K_{1R} \left(\frac{\gamma_R - 1}{\gamma_R} \right) [P(t) - \Delta P(t)]^{-1/\gamma_R} \left[\frac{dP(t)}{dt} - \frac{d\Delta P(t)}{dt} \right] \quad (36)$$

rewriting

$$\frac{dT_{R(t)}}{dt} = K_{1R} \left(\frac{\gamma_R - 1}{\gamma_R} \right) P_{R(t)}^{-1/\gamma_R} \frac{dP_{R(t)}}{dt} \quad (37)$$

Substituting Equations (35) and (37) into Equation (32)

$$\frac{dM_{R(t)}}{dt} = \frac{V_R}{R K_{1R} [P(t) - \Delta P(t)]^{\gamma_R - 1/\gamma_R}} \left[\frac{dP(t)}{dt} - \frac{d\Delta P(t)}{dt} - \left(\frac{\gamma_R - 1}{\gamma_R} \right) \left(\frac{dP(t)}{dt} - \frac{d\Delta P(t)}{dt} \right) \right] \quad (38)$$

Substituting Equation (38) into (30) and transposing

$$\frac{dP(t)}{dt} - \frac{d\Delta P(t)}{dt} = \frac{\gamma_R R_R K_{LR} \dot{m}}{V_R} \left[P(t) - \Delta P(t) \right]^{\gamma_R - 1/\gamma_R} \quad (39)$$

as $P_{R(t)} = P(t) - \Delta P(t)$

Equation (39) can be written

$$\frac{dP_{R(t)}}{dt} = \frac{\gamma_R R_R K_{LR} \dot{m}}{V_R} \left[P_{R(t)} \right]^{\gamma_R - 1/\gamma_R} \quad (40)$$

3.2 Computer Program General Description

Based upon the analysis previously described in Section 3.1, a tank overpressure program was developed. This program integrates the transient equations for predicting the pressure history inside a tank with a relief area during combustion. Two ignition sources are described: spark and incendiary.

It is assumed that a flame front propagates from the area of ignition, increasing the internal pressure of the tank. Concurrently, depressurization of the combustion tank occurs as gases expand through the relief area and arrester material into the relief volume. A peak pressure occurs at termination of burning, that is to say, when the assumed flame front traverses the length of the combustion volume.

Data are input to the program by eight data cards, which include general constants, tank dimensions, and fuel-air properties for both burned and unburned gases. The program primary output is the resulting overpressure as a function of time. The major unknown in the analysis is the flame speed, which must be input from available data or test results.

The program automatically determines whether the flow through the relief area is choked or unchoked, based on a pressure ratio criterion, and uses appropriate equations for mass flow calculations.

The program is written in WATFOR language for use on the 360 computer. A flow diagram indicating the logic and analysis steps is shown in Figure 47. A listing of input data and a program listing are included as part of Section 3.4.

Program limitations are reflected in that the geometry description is limited to the variable geometry test tank of circular cross section. Also, the program does not account for the decay of combustion pressure and relief volume pressure rise, attempting to reach equilibrium after combustion ceases; nor does it account for decay of internal pressure due to heat transfer through the walls of the tankage. However, it is believed that the effect of heat transfer on maximum pressure during the burn will be negligible because of the relatively slow heat transfer rates compared to the pressure rise time.

NOMENCLATURE

A_0	=	Area of aperture
C_p	=	Specific heat
g_c	=	Gravitational conversion factors
ΔH	=	Heat of combustion
K_{1U}	=	$T_{IU}/P_{IU} \frac{\gamma_U - 1}{\gamma_U}$
K_6	=	$\sqrt{\frac{2 \gamma_B g_c}{R_B (\gamma_B - 1)}}$
K_2	=	$\sqrt{\frac{\gamma_B g_c}{R_B} \times \left(\frac{2}{\gamma_B + 1}\right) \frac{\gamma_B + 1}{2(\gamma_B - 1)}}$
M	=	Mass of gas in tank at any time
\dot{m}	=	Rate of emptying through aperture
P	=	Tank pressure
P_{am}	=	Ambient pressure
R	=	Gas constant
T	=	Gas temperature
t	=	Time
V	=	Volume

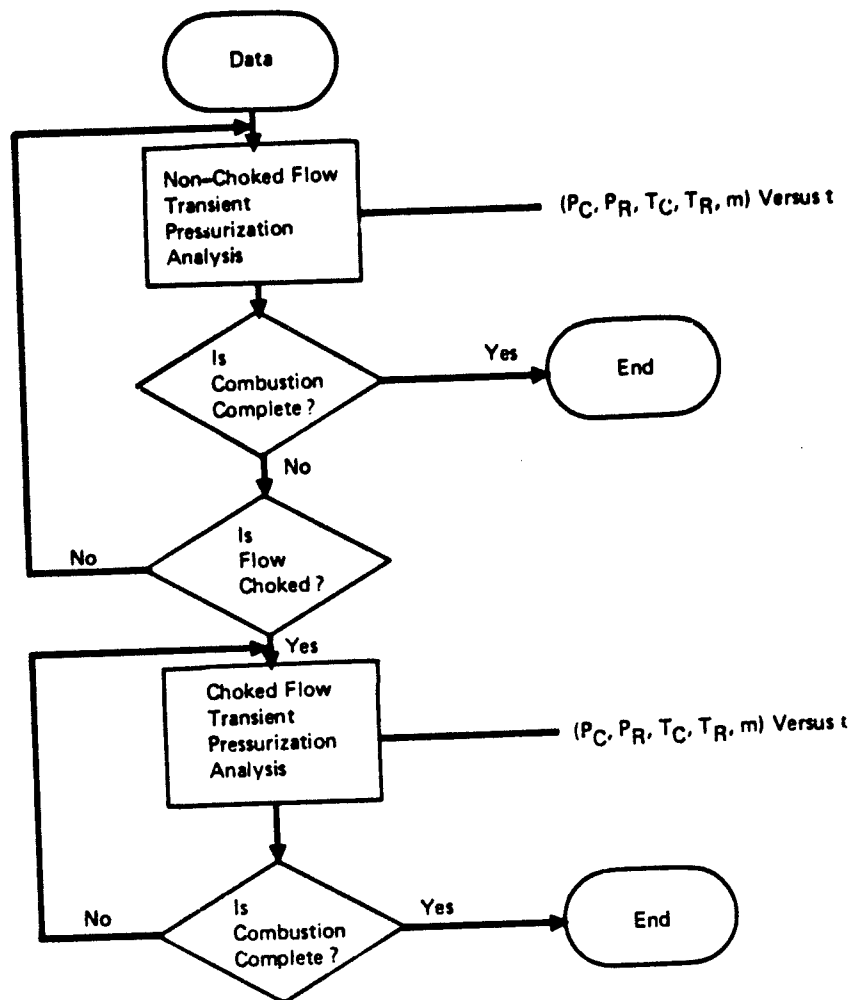


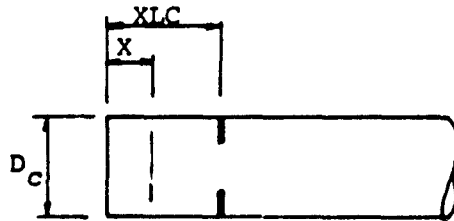
Figure 47: Computer Flow Diagram

Subscripts

i	=	Initial conditions
U	=	Unburned gas
B	=	Combustion products
T	=	Total

DEFINITION OF VOLUME BURNT AS USED IN THE PROGRAMS

Spark Ignition



The volume burnt VBT is given by

$$VBT = \frac{\pi D_c^2}{4 \times 144} X$$

where X for any given time is $X = UF \times t$

where UF is the assumed flame speed.

$$VBT = \frac{\pi}{4 \times 144} \cdot D_c^2 \cdot UF \cdot t \quad (1)$$

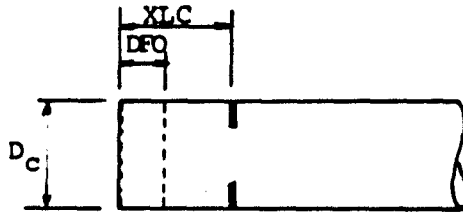
Differentiating

$$DVBT = \frac{\pi}{4 \times 144} \cdot D_c^2 \cdot UF \quad (2)$$

The final time of the combustion is given by

$$TPF = \frac{XLC}{12 UF} \quad (3)$$

Incendiary Ignition



Time to final burn is given by

TPF = Time for incendiary plume to burn DFO + Time for remainder of burn

$$TPF = \frac{DFO}{24UI} + \frac{XLC - DFO}{24 \times UF} \quad (4)$$

where UI is the apparent incendiary expansion and UF is the burn speed in the remaining gases.

$$VBT_1 = \frac{2 \pi D_c^2 X}{4 \times 144} \quad \text{where } X = UI.t$$

$$VBT_2 = \frac{2 \pi D_c^2}{4 \times 144 \times 12} \left(\frac{DFO}{12} + \left[X - \frac{DFO}{2} \right] \right)$$

$$\text{Total Volume} = VBT_1 + VBT_2$$

$$= \frac{2\pi D_c^2 DFO}{4 \times 144 \times 24} + \frac{2\pi D_c^2 UF}{4 \times 144} \left(T_{\text{Total}} - \frac{DFO}{24 UI} \right)$$

$$VBT = \frac{2\pi D_c^2}{4 \times 144} \left[\frac{DFO}{24} + U Ft - \frac{UF \cdot DFO}{24 UI} \right] \quad (5)$$

differentiating

$$DVBT = \frac{2\pi D_c^2 UF}{4 \times 144} \quad (6)$$

NOMENCLATURE

UI	-	Apparent velocity of burn of incendiary cone
XK	-	Overall foam discharge coefficient
XK ϕ	-	Orifice discharge coefficient
PI	-	Initial chamber pressure (LBF/FT ²)
TIU	-	Initial temperature of unburned gas (°R)
D ϕ	-	Diameter of orifice (in.)
DCTNK	-	Cylindrical diameter of combustion chamber (in.)
DRTNK	-	Cylindrical diameter of reservoir chamber (cyl) (in.)
XLC	-	Length of combustion chamber (cyl.) (in.)
XLR	-	Length of reservoir chamber (cyl.) (in.)
D ϕ	-	Diameter of initial incendiary plume (in.)
UF	-	Apparent flame speed (ft/sec)
DHHC	-	Heat of fuel combustion (BTU/LB-MOLE)
XMF	-	Molecular weight of fuel (LBM/LB-MOLE)
CPCX	-	Heat capacity of fuel (BTU/LB-MOLE-°R)
XNI	-	Molecular fraction of fuel in vapor
XMA	-	Molecular weight of air (LBM/LB-MOLE)
CPA	-	Heat capacity of air (BTU/LB-MOLE-°R)
X, Y, Z	-	Constants in chemical equation
$\text{C}_3\text{H}_8 + 5\text{O}_2 = 3\text{CO}_2 + 4\text{H}_2\text{O}$		
CVN ₂	-	Heat capacity of H ₂ (BTU/LB-MOLE-°R)
CVO ₂	-	Heat capacity of O ₂ (BTU/LB-MOLE-°R)
CVCO ₂	-	Heat capacity of CO ₂ (BTU/LB-MOLE-°R)
CVH ₂ O	-	Heat capacity of H ₂ O (BTU/LB-MOLE-°R)
GC	-	Gravity conversion factor (LBM-FT/LBF-SEC ²)
R	-	Gas constant (BTU/LB-MOLE)

3.3 Dynamic Model Data

It has been observed during the test program that the time to peak pressure is influenced by the following parameters:

- Combustion volume (geometry)
- Initial pressure
- Rate of gas expansion through the relief area into the relief volume
- Fuel-to-air ratio.

Presently the dynamic mathematical model couples the pressure rise time or time to peak pressure directly to the combustion volume.

The initial flame speed U_i and the final flame speed U_f assumed to exist for an incendiary burn have been determined so as to produce maximum over-pressures and pressure rise times as produced during the test program within the variable geometry tank. These "calculated" flame speeds used are not observed flame speeds in a strict sense. To relate the fundamental and observed flame speeds to all four variables was considered beyond the present scope of the test program. These could, however, be coupled to the program at a later date.

It is shown in the graphical presentation of the transient model data, that for a spark ignition, K factors up to 70 have no appreciable effect on tank overpressures, for a relief orifice of 53% (0.852 ft^2) or greater. However, an incendiary ignition influences the pressure rise quite sharply under the same conditions, Figures 48 and 49.

It is further noted that when the orifice size is reduced to 10% (0.167 square feet), pressure influences seen for a spark ignition (Figure 50) are sharply increased when an incendiary igniter is used, as shown in Figure 51 where even a K factor of 20 increases P_c/P_{initial} by a factor of 6.

Compressibility of these types of materials could be accounted for by varying the K factor as combustion pressure increases, or could be achieved by pressure drop definition, as shown in Reference 13.

A typical plot of pressure rise versus time as found by test is compared to that calculated by the dynamic model, as shown in Figure 52.

**Dynamic Model Data 53% Orifice
Spark Ignition**

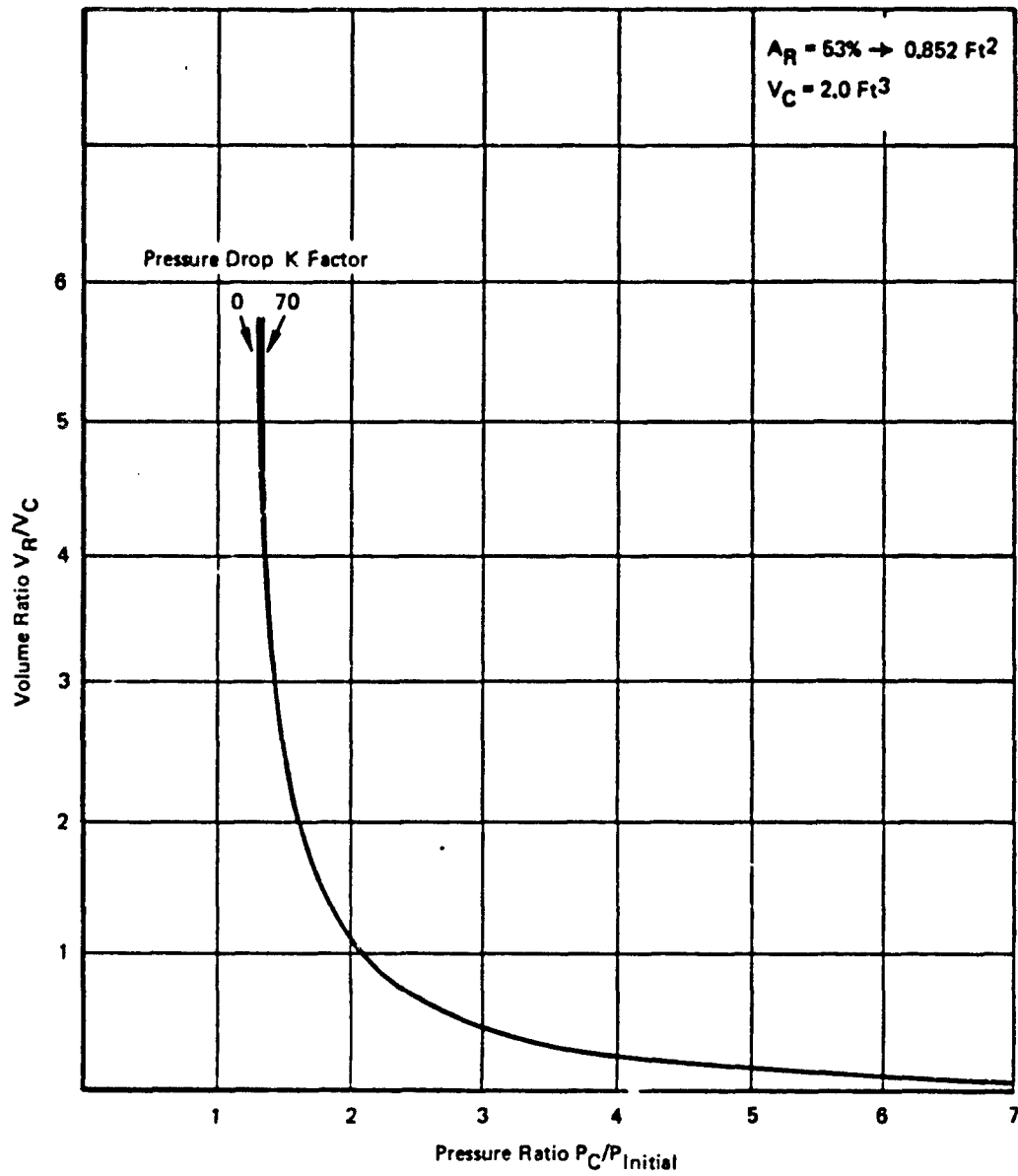


Figure 48: Dynamic Model Volume Versus Pressure Data for 53% Orifice (Spark Ignition)

**Dynamic Model Data 53% Orifice
Incendiary Ignition**

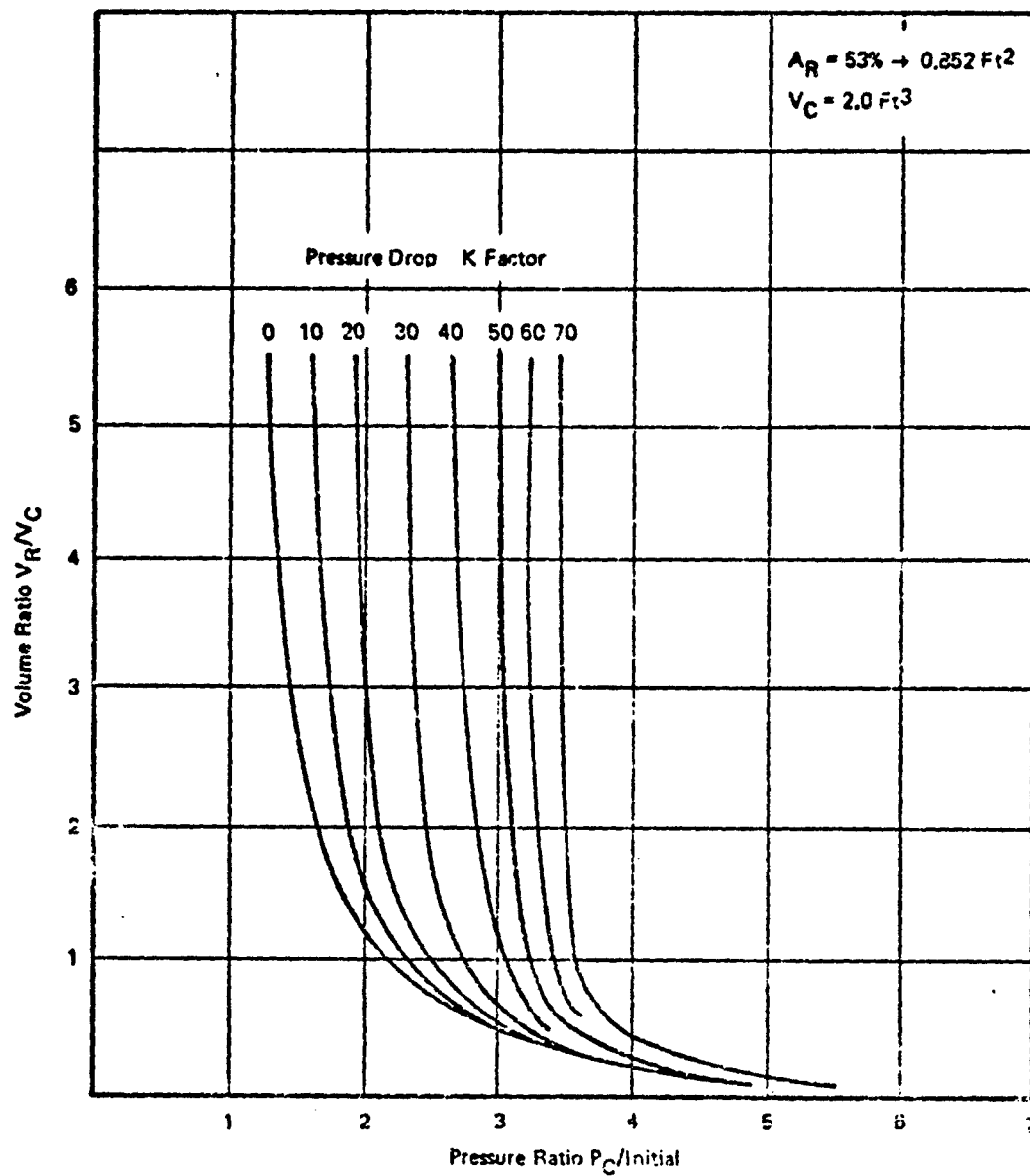


Figure 49: Dynamic Model Volume Versus Pressure Data for 53% Orifice (Incendiary Ignition)

*Dynamic Model Data 10% Orifice
Spark Ignition*

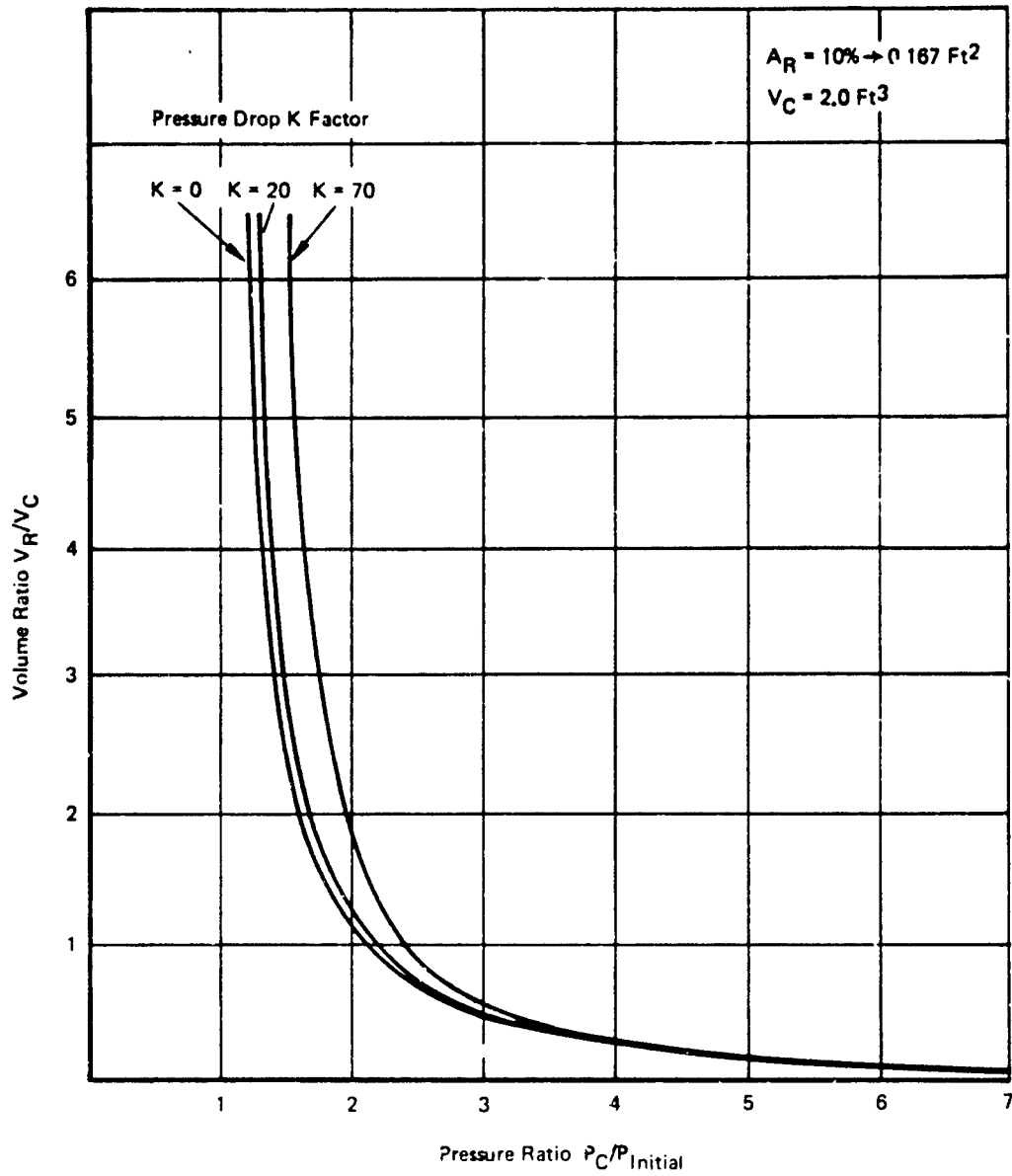


Figure 50: Dynamic Model Volume Versus Pressure Data for 10% Orifice (Spark Ignition)

**Dynamic Model Data 10% Orifice
Incendiary Ignition**

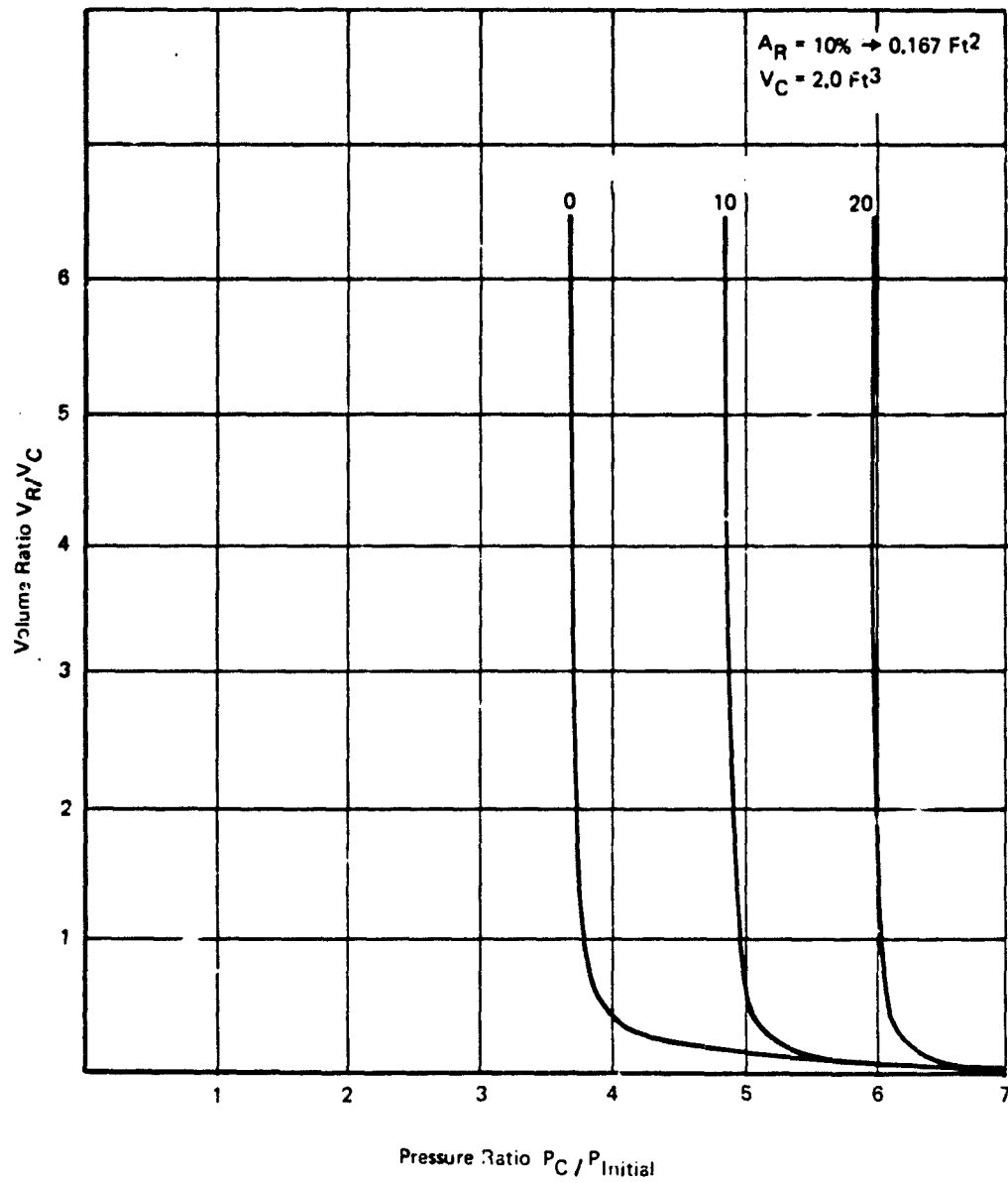


Figure 5-1: Dynamic Model Volume Versus Pressure Data for 10% Orifice (Incendiary Ignition)

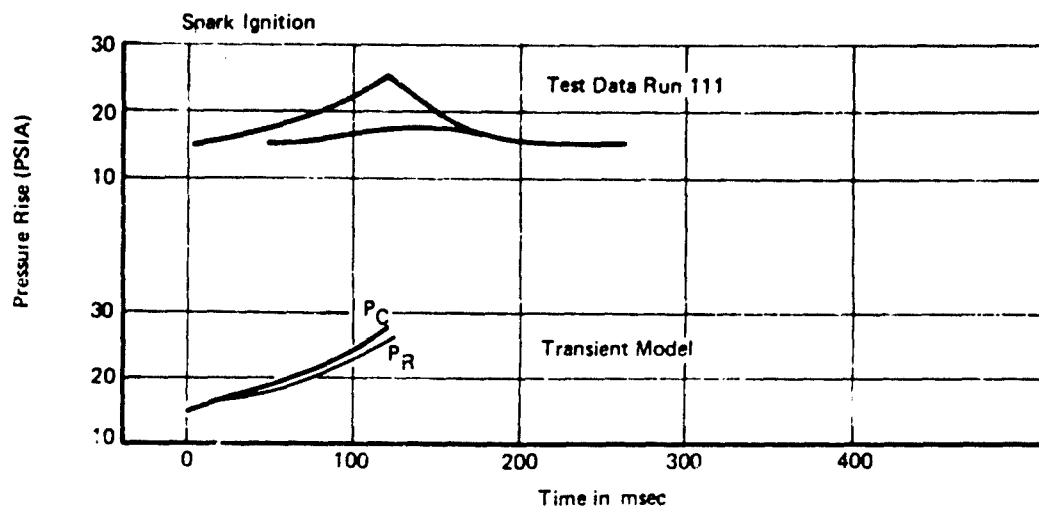
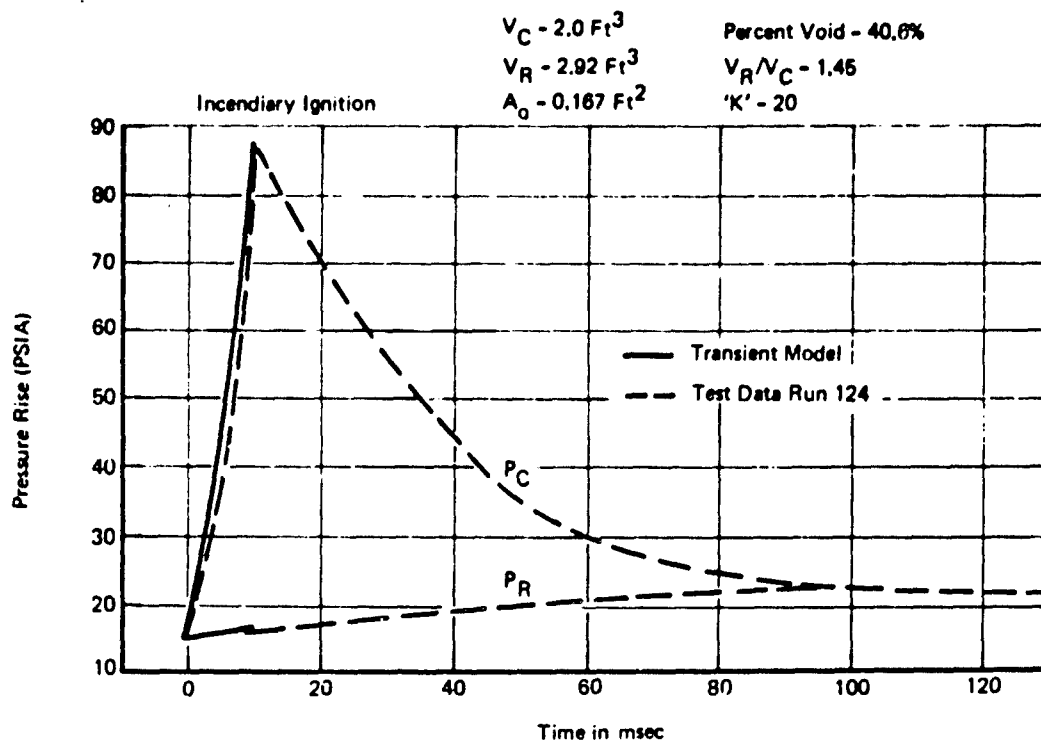


Figure 52: Variable Geometry Test Data vs Transient Model Data

A description of the fuselage tankage with a lined wall configuration installed was programmed. The resulting tank pressures for various percent voids are plotted in Figure 53. A data presentation relating the ratio of relief and combustion volume to the ratio of absolute final and initial pressure is shown in Figure 54. The curve is shown in Figure 43 with data superimposed.

3.4 Program Flow Diagram and Listing

A flow diagram of the Dynamic Mathematical model integration and computational steps is shown in Figure 47.

Three listings are included.

Listing (A)--Variable Geometry Pressure Rise for a Spark Ignition Source

Listing (B)--Variable Geometry Pressure Rise for an Incendiary Ignition Source

Listing (C)--Fuselage, Small Wing, or Large Wing Pressure Rise for a Spark or Incendiary Ignition Source

It is generally noted that the program presently requires a major change to the computational routines as the configuration description is changed.

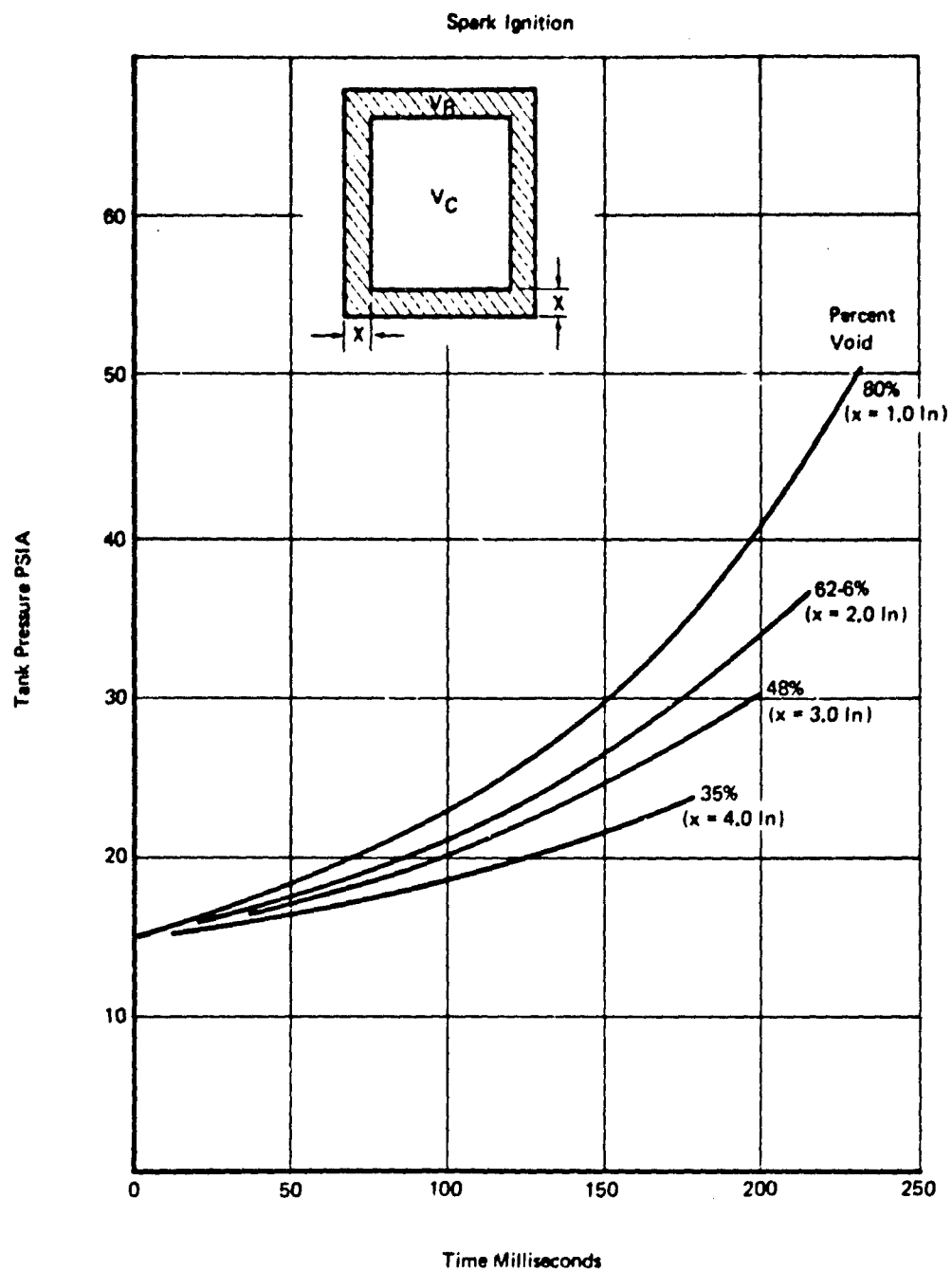


Figure 53: Fuselage Tank (Lined Wall) Dynamic Model Pressure Plots

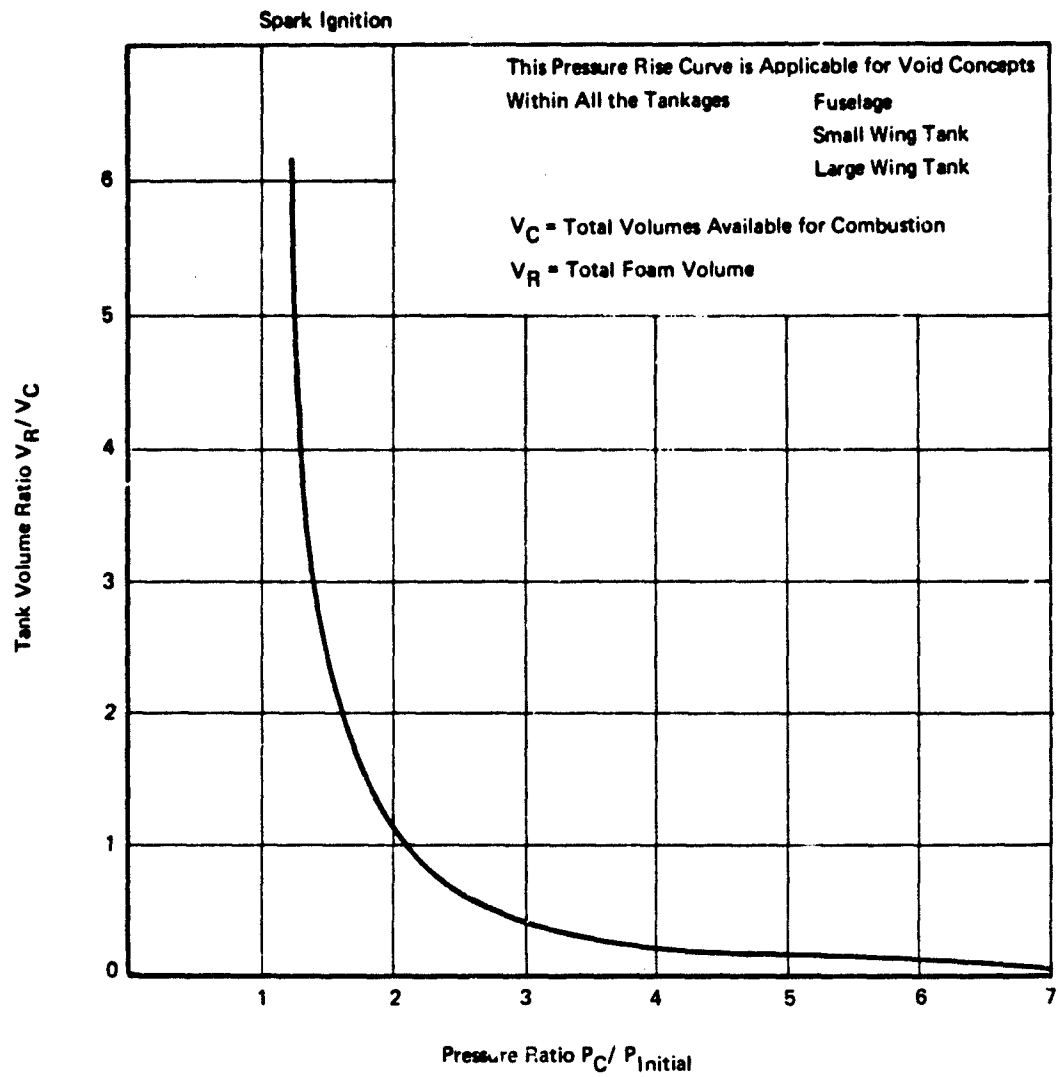


Figure 54: Dynamic Model Pressure Ratio Versus Relief-to-Combustion Ratio

LISTING A

148

LISTING A (Continued)

```

XK6#0021002.FG00000/0RU#00U-1.***
01#00H/CVR***0-1.*/00000000
CP#00
PC#00
XK10#0010
TDF#XLC/0UF#12.*
001#-2./00U.1.***0-(U/00U-1.**)
WRITE06,12*
WRITE06,14*
WRITE06,14* VT,VR,VOLRAT,KEV0LP,KAREAP
WRITE06,12*
WRITE06,13*
TP#0.
XC01#PI
XC02#PI
CALL SYSTEM01,0,0,P,X0,2*
5 V0T#3.141593*0CTNK**2.*UF#1/04.*144.*
0V2T#3.141593*0CTNK**2.*UF/04.*144.*
TUT#XK10#PI***00U-1.*/00*
T0TATUT,0H/CVB
TU0TE#1.-0H/0T0T*CVB*
S#0P02*/001***02./00*-0P02*/001***00U.1.*/00*
IF05.LE.0.* 5#0000000001
S1#SORT001.-000/AC***2.*#01.-000/AC***2.*0P02*/001***02./00***
X#00T#XK5*00XKN*51*001**SORT001/00*
A#-RU#TUT*X#001
R#001** 0RU/0R**0TU0TE-1.***0V0T
C#00U/0R***0 V0T/0T0T**2.***001***00U-1.*/00*
0#0V0T.0RU/0R***0TU0TE-1.***0V0T
001#00A-0*/001.-00U-1.*/00*.01*0**0*
002**00000000XK10#X#001*002***0002-1.*/0R**/VR
10 CALL ST0P005,TP#
0001#001*/144.
0001#002*/144.
WRITE06,14* 10,01001,02PS1,02PS1,0UT,101,001*,002*,TU010
02001*/002*
IF010.00.TPF# GO TO 100
IF010.001
IF010.01.TPF# TP#TP#
IF000.01.001* GO TO 10

```

LISTING A (Concluded)

```

X001*#P01*
X002*#002*
T7/TP-.001
CALL SYGTFM01,TZ,D,P,X0,2*
6 VRT#3.141593*001K**2.*0F*1/04.*144.*
DVRT#3.141593*001K**2.*0F/04.*144.*
TUT#XV10*001**00GU-1.**/GU*
TUT#TUT.DH/CVB
TUOTR#1.-DH/RTBT*CVB*
YMDOT#XK2*AO*KN*P01*/SORT#TUT*
A#-RU*TUT*X'DOT
R#P1K*RU/RP**0TUOTB-1.**DVBT
C*RU/RP**EVBT/RT**2.***P01**00GU-1.**/GU*
E#VT.0RU/RP**0TUOTB-1.**VBT
001*00A-P*/001.-00GU-1.**/GU*.01*C**L*
D-2*#0GR/VR**RR*KK1R*XXDOT:P02**00GR-1.**/GR*
11 CALL STEP 006,TP*
PIP5I#P01*/144.
P2PSI#P02*/144.
WRITE06,14* TP,PIP5I,P2PSI,TUT,RTBT,D01*,D02*,TUOTR
IF0TP.EQ.TPF* GO TO 100
TP#TP..0005
IF0TP.GI.TPF* TP#TPF
GO TO 11
100 CONTINUE
15 STOP
END
**EXECUTE
**EOJ
/*

```

150

LISTING B

```
// 7MGR21WX00,02*,0TERRY DIXON# 655-2869 M/S 40-A1
// EXEC WATFOR
//GO,SYSIN DD *
*JOB
C      .TIME#600
      EXPLOSION PRESSURE RISE INCENDIARY
      DIMENSION XC02*,PM2*,DM2*
      CALL ACCUR01*
      12 FORMATN////*
      13 FORMAT06X,2HTP,12X,5HP1PSI,10X,5HP2PSI,11X,3HTUT,11X,3HTBT,11X,
        C4H001*,11X,4H002*,10X,5HTU0TR*
      16 FORMAT012X,2HVC,12X,2HVR,12X,6HVOLRAT,9X,6HREVOLP,9X,6HRAREAP*
      14 FORMAT08F15,4*
      DATA XK,XKO/01,02,0/
      DATA PI,TIU/2116,0530,/
      DATA DO,DCTNK,DRTNK,XLC,XLR/5.54,17.5,17.5,14.4,72.0/
      DATA DFO,UF,UI/4.055,100,/
      DATA DHHC,XMF,CPCX,XNI/96F6,44.000,15.00,0045/
      DATA XMA,CPA,X,Y,Z/29.00,6.95,5.03,04,/
      DATA CVN2,CVN2,CVC02,CVH20/8.00,8.00,22.00,11.10/
      DATA GC,R/22,174,1,00/
      DFO#DFO/02,012,*
      YY#DCTNK/12,
      AC#3,141593#00**2,04,0144,*
      AC#3,141593#DCTNK**2,04,0144,*
      XMURAR#XNI*XMF,01,-XNI**XMA
      PU#1545,43/XMURAR
      XNT#01,-XNI*,XNI#0Y,Z-X*
      CPURAP#XNI*CPCX,01,-XNI**CPA
      GU#1,01,-R/CPUPAR*
      CVR#CVN2*0,79*01,-XNI*,CVC02*00,21*01,-XNI*-X*XNI*,CVC02*Y*XNI
      C,CVH20*Z*XNI
      GR#1,01,-R/CVP*
      XY2#00GU*GC/RU***.5**02,0GU,01,*****0GU,01,02,00GU-1,***
      DO 100 L#01,71,10
      XLR#FL0ATNL*
      DOINT,XLR
      XKN#1,00XK,XKO***0,5*
      VT#3,141593#DCTNK**2,*XLC/04,01728,*
      VP#3,141593#DPTNK**2,*XLR/04,01728,*
      VOLRAT#VP/VT
```

LISTING 5 (Continued)

```

REVOLP#VR*100./DVP.VT*
RPFAP#MAN*100./AC
NH#XNI#NHHC/XNT
XK1U#TUT#PI**CGU-1./GU**
XMBRAR#27.82.84.*Y.1R.*Z-37.*X-27.82**XNI
RP#1549.41/XMBRAR
XK6#SOR#2.*GU*GC#/#U#CGU-1.***
Q1#DH/CVR**CGU-1./GU**XK1U
GR#GU
RR#RU
XK1R#XK1U
TPF#DFO/#24.*UI**.#XLC-#FO*/#24.*UF**
PR1#2./CGU.1.***#-GU/#GU-1.**
PRINT#CPUBAR.GU.CVB.G8.XK2.DH.XK1U.XMBRAR.XK6.TPF.PR1.RU.RB
C,Q1
WRITE#6,12*
WRITE#6,16*
WRITE#6,14* VT,VR,VOLRAT,REVOLP,RAREAP
WRITE#6,12*
WRITE#6,13*
TP#0.
XC#1#PI
XC#2#PI
CALL SYSTEM#0,0,0,P,X0,2*
5 RAD#UIT
IFRAD.GE.RF0# GO TO 20
VBT#3.1415#DCTNK**2**UI*Y/28R.
NVRT#3.1415#DCTNK**2**UI/28R.
GO TO 30
20 VBT#3.1415#DCTNK**2*/28R.#DFO/24.*#UF*Y**#UF#DFO*/#24.*UI***
NVRT#3.1415#DCTNK**2**UF/28R.
30 TUT#XK1U#PI**CGU-1./GU*
TUT#TUT.#H/CVR
TUOTR#1.-DH/#TUT#CVR*
S#P#2#/#PI***#2*/GU**#P#2*/#PI***#CGU.1./GU*
IFDS.LE.0.* S#.#00000001
XMDOT#XK6#AC#XKN#PI**SQRTS/TUT*
A#-RU#TUT#XMDOT
R#PI** RU/RA**#TUTR-1.***DVRT
C#RU/RA**# VBT/#TUT**2.***#PI***#CGU-1./GU*

```

LISTING B (Continued)

```

E#VT,ORU/RA**TUOTR-1,**VAT
DE1**AA-R*/aa1.-aaGU-1.*/GU*.01*C**E*
Da2**aaGR**RR**XK1R**XMDOT**Pa2**aaGR-1.*/GR**/VR
10 CALL STEPaa5,TP*
  P1PS1#Pa1*/144.
  P2PS1#Pa2*/144.
  WRITEaa6,14* TP,P1PS1,P2PS1,TUT,TBT,Da1*,Da2*,TUOTR
  PR#Pa1*/Pa2*
  IFaTP.EQ.TPF* GO TO 100
  TP#TP..0001
  IFaTP.GT.TPF* TP#TPF
  IFaPR.LT.PR1* GO TO 10
  Xaa1**Pa1*
  Xaa2**Pa2*
  TZ#TP..0001
  CALL SYSTEMBT,TZ.D.P.X0.2*
  6 RADRU1*
  IFaRAD.GE.RFO* GO TO 22
  VRT#3.1415**BODCTNK**2**UI*/288.
  DVRT#3.1415**BODCTNK**2**UI/288.
  GO TO 32
22 VRT#3.1415**BODCTNK**2*/288.**BODFO/24.*.aUF*Y*-aaUF*BDFN*/aa24.*UI***
  DVRT#3.1415**BODCTNK**2**UF/288.
  32 TUT#XK1U#Pa1***aaGU-1.*/GU*
  TBT#TUT.DH/CVB
  TUOTR#1.-DH/aTBT*CVB*
  XMDOT#XK2*AO*XKN*Pa1*/SORTaTUT*
  A#-RU#TUT*XMDOT
  R#Pa1**ORU/RB**aaTUOTR-1.**DVAT
  C#ORU/RA**aaVAT/aTBT**2.**aaPa1***aaGU-1.*/GU*
  E#VT,ORU/RB**aaTUOTR-1,**VAT
  aa1**AA-R*/aa1.-aaGU-1.*/GU*.01*C**E*
  aa2**aaGR/VR**RR**XK1R**XMDOT**Pa2**aaGR-1.*/G1*
  11 CALL STEP aa6,TP*
    P1PS1#Pa1*/144.
    P2PS1#Pa2*/144.
    WRITEaa6,14* TP,P1PS1,P2PS1,TUT,TBT,Da1*,Da2*,TUOTR
    IFaTP.EQ.TPF* GO TO 100
    TP#TP..0001
    IFaTP.GT.TPF* TP#TPF

```

LISTING B (Concluded)

GO TO 11
100 CONTINUE
15 STOP
END
*EXECUTE
*FOJ
/*

```
// 7MGR21W 00,00*,@FERRY DIXON# 655-2869 M/S 40-A1
// EXEC WA-FOR
//GO,SYSIN ON *
*JOB
C      ,TIME#2400
EXPLOSION PRESSURE RISE CO-PLANAR SPARK FUSELAGE
CALL ACCUR#1*
12 FORMAT#7,///**
13 FORMAT#6X,2HTP,1ZX,5HP1PSI,1OX,5HP2PSI,11X,3HTUT,11X,3HTBT,11X,
CAM#01*,11X,4HDD2*,1OX,5HTUOTR*
14 FORMAT#8F15,4*
DATA XK,XKO/60.,2.0/
DATA PI,TIU/2116.,530./
DATA UF/100./
DATA AA,BP,CC,THK/24.,30.,30.,4.,25/
DATA DHHC,XMF,CPCX,XNI/.96F6,44.000,15.00.,0.5/
DATA XMA,CPA,X,Y,Z/29.00,6.95,5.53.,4./
DATA CVN2,CVC02,CVC02,CVH20/8.00,8.00,22.00,11.10/
DATA GC,R/32,174,1.99/
XNURAR#XNI*XMF.#1.-XNI**XMA
RU#1545-43/XMURAR
XNT#01.-NI*.XNI#BY.Z-X*
CPURAR#XNI*CPCX.#1.-XNI**CPA
GU#1./#1.-R/CPUPAR*
CVR#CVN2*0.79#01.-XNI*.CVN2*0.21#01.-XNI*-X*XNI*.CVC02*Y*XNI
C.CVH20*Z*XNI
GR#1./#1.-R/CVR*
XK?#00GU*GC/RU***.5***#2./#GU.1.***#00GU-1.*/*#2.*#GU-1.***
DO 100 L#03,15,1
THK#FLOATEL*
PRINT,THK
XKN#1./#0X.XKO***0.5*
DH#XNI*DMHC/XNT
XKIU#TIU/PII**#00GU-1.*/#GU**
XMRRAR#27.82.#44.*Y.1R.*Z-32.*X-27.82***XNI
RP#1545.43/XMRRAR
XV6#SQRT#02.*GU*GC*/#RU*#00GU-1.***
GI*GDH/CVR**#00GU-1.*/#GU**XKIU
GD#GU
RR#RU
```

LISTING C (Continued)

```

XK1R*XXK1U
VTOT#AA*RR*CC/1728.
EXI#AA 02.*THK*
EXII#RR-02.*THK*
EXIII#CC-02.*THK*
XLC#FXIII
VCOMR#FXI#EXII#EXIII/1728.
VT#VCOMR
VRELF#VTOT-VCOMB
VPVC#VRELF/VCOMR
PVCVT#VCOMB#100./VTOT
COSUAR#0AA*XLC*2.*.0AA*RR*2.*
A0#COSUAR/144.
PRINT,VTOT,VCOMB,VRELF,VPVC,PVCVT,A0
TPF#XLC/DUF#12.*
PR1#02./0GU.1.***0-GU-1.***
PRINT,CPURAR,0GU,CVB,GR,XK2,VT,VR,DH,XK1U,XMURAR,XMBBAR,XK6,TPF,PR1
WRITE06,12*
WRITE06,12*
WRITE06,13*
TP#0.
X001#PI
X002#PI
CALL SYSTE#0T,0.,D,P,X0,2*
5 VRT#EXI#EXII#UF#T/144.
DVRT#EXI#EXII#UF/144.
TUT#XK1U#P01***0GU-1.*./GU*
TRT#TUT,DH/CVB
TUOTR#1.-DH/0TBT#CVB*
S00P02*/P01***02./GU*-0P02*/P01***00GU.1.*./GU*
IFS.LF.0.* S#000000001
XMDOT#XK6*AA*0XK#P01**SORT0S/TUT*
A#-RU*TUT*XMDOT
R#P01** 0RU/RR**0TUOTB-1.**0VAT
C#0RU/RR**0 VAY/0TBT**2.***P01***00GU-1.*./GU*
E#VT.0RU/RR**0TUOTB-1.**0VAT
D01#0A-B*/001.-00GU-1.*./GU*.Q1#C**E*
D02#0GP*RR*XK1R*XMDOT#P02***0GR-1.*./GR**/VRELF
10 CALL STP005,TP*
P1P01#P01*/144.

```

LISTING C (Concluded)

```

DPSI#P22*/144.
WRITE#6,14* TP,P1PSI,P2PSI,TUT,TAT,D01*.D02*,TUOTA
D#P01*/P02*
IFTP#EQ.TPF* GO TO 100
TP#T0.005
IFTP#GT.TPF* TP#TPF
IFBPR#LT.PRI* GO TO 10
X001#P01*
X002#P02*
T7#TP=005
CALL SYSTEM#T2.D.D.X0.2*
6 VRT#FXI*FXII*UF#T/144.
NVRT#FXI*FXII*UF/144.
TUT#XKIU#P01***D0GU-1.*.*/GU*
TP#TUT.CM/CVR
TUOTA#1.-DH/ETPT#CVR*
XMDCT#XK2*AO*XXN#P01*/SORT#TUT*
A#PU*TUT*XMCT
P#P01**BRU/RR**TUOTA-1.**DVAT
C#P0U/RR**BVRT/RTAT**2.**P01***D0GU-1.*.*/GU*
F#VT.BRU/RR**TUOTA-1.**VAT
D01*#0A-F*/M1.-M0GU-1.*.*/GU*.01*(*F*
D02*#0G0/VR**RR#XK1P*XMCT#P02***D0GR-1.*.*/GR*
11 CALL STOP 066,TP*
DPSI#P01*/144.
D001#D02*/144.
WRITE#6,14* TP,P1PSI,P2PSI,TUT,TAT,D01*.D02*,TUOTA
IFTP#EQ.TPF* GO TO 100
TP#T0.001
IFTP#GT.TPF* TP#TPF
GO TO 11
100 CONTINUE
15 STOP
END
*EXECUTE
*EOJ
/*

```

SECTION IX
TASK II TEST PROGRAM

1.0 MATERIAL DESCRIPTION

The material used for all Task II testing was 25-ppi reticulated polyurethane foam, manufactured by Scott Paper Company and distributed by Firestone Corporation.

Shown in Figure 55 is a sample of foam 4.0 inches thick being cut by the not wire apparatus. This hot wire cutting technique was utilized throughout a major portion of Task I and all of Tasks II and III.

2.0 TEST CONFIGURATION GENERAL

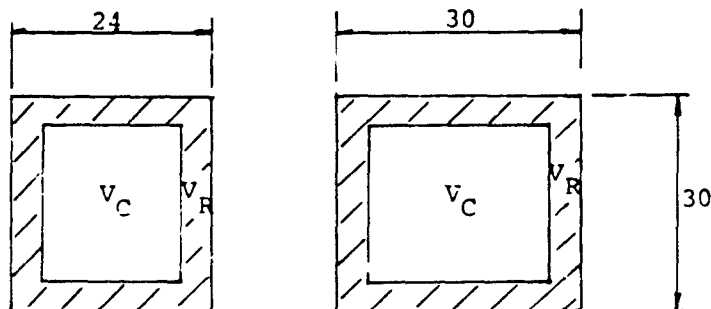
Test configurations were obtained by assembling six 30- by 24- by 15-inch steel cubes, supplied by AFAPL, into three different configurations.

The relationship of percent penalty void V_C/V_T versus other pertinent arrester dimensions is included in this report for each voiding concept as follows.

2.1 Fuselage Tankage

This configuration assembly is shown in Section VI, Mode II testing. A photograph of the test assembly is shown in Figure 31, (Section VI).

2.1.1 Lined Wall



Preceding page blank



Figure 55: Hot Wire Foam Cutting

$$V_T = 30 \times 30 \times 24 = 21,600 \text{ in.}^3$$

$$V_C = (30 - 2x) \times (30 - 2x) \times (24 - 2x) = 21600 - 4680x + 336x^2 - 8x^3$$

$$V_R = V_T - V_C$$

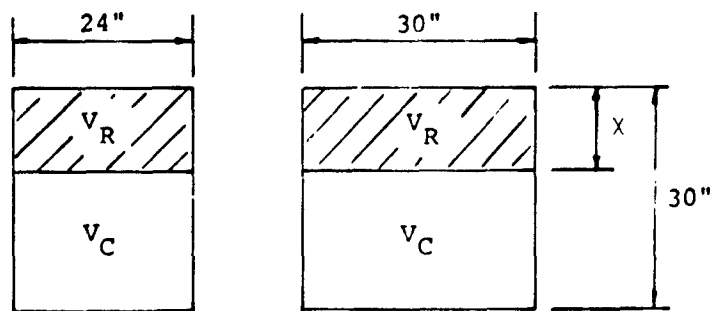
$$\text{Percent penalty void} = V_C/V_T \times 100$$

$$= \frac{(21600 - 4680x + 336x^2 - 8x^3)}{21600} \times 100$$

$$V_R/V_C = \frac{4680 - 336x^2 + 8x^3}{21600 - 4680x + 336x^2 - 8x^3}$$

Variations of percent void and V_R/V_C with arrester thickness are shown in Figure 29.

2.1.2 Top Wall



$$V_T = 30 \times 24 \times 30 = 21,600 \text{ in.}^3$$

$$V_C = 30 \times 24 \times (30 - x) = 21,600 - 720x$$

$$V_R = V_T - V_C = 720x$$

$$\text{Percent penalty void} = V_C/V_T \times 100 = \frac{(21,600 - 720x)}{21,600} \times 100 \quad (1)$$

$$V_R/V_C = \frac{720x}{21,600 - 720x}$$

Variations of percent void and V_R/V_C with arrester thickness are shown in Figure 56.

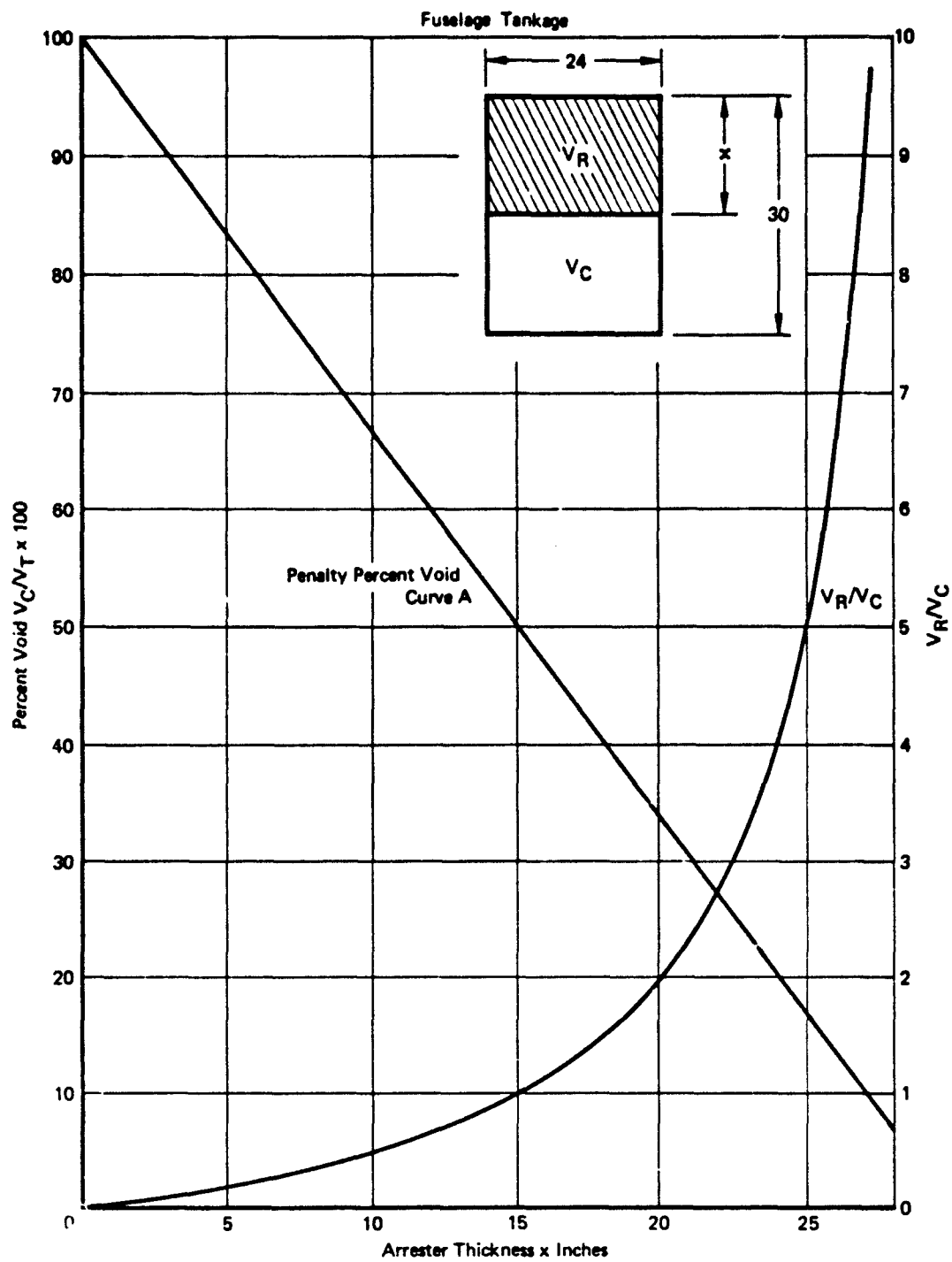


Figure 56: Variations of Percent Void and V_R/V_C with Arrestor Thickness (Top Wall)

2.1.3 Voided Top Wall

$$V_T = 30 \times 24 \times 30 \text{ in.}^3$$

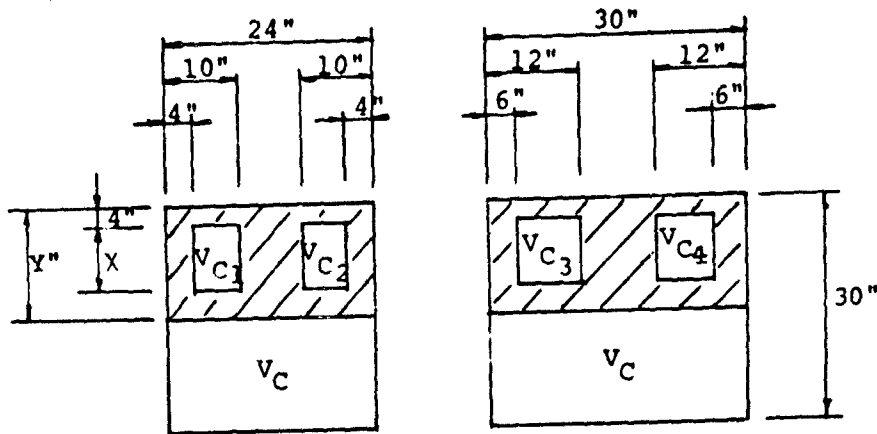
$$= 21,600 \text{ in.}^3$$

$$V_C = 30 \times 24 \times (30-y) \text{ in.}^3$$

$$= 21,600 - 720y$$

$$V_R = V_T - V_C = 720y$$

$$\sum_{i=1}^4 V_{C_i} = 6 \times 6 \times 4 \times x = 144x$$



$$\text{Percent relief void} = \frac{\sum_{i=1}^4 V_{C_i} \times 100}{V_R} = \frac{14,400x}{720y} = 20x/y \quad (1)$$

$$\text{Percent void} = \frac{V_C \times 100}{V_T} = \frac{21,600 - 720y}{21,600} \quad (2)$$

$$\text{Percent penalty void} = \frac{\sum_{i=1}^4 V_{C_i} + V_C}{V_T} \times 100$$

$$= \frac{(144x + 21,600 - 720y)}{21,600} \times 100 \quad (3)$$

$$V_R/V_C = \frac{720y}{21,600 - 720y} \quad (4)$$

Variations of percent void with respect to changes in the x and y dimensions are shown in Figure 57 and Figure 58. The variation of arrester thickness y and V_R/V_C is identical to the top wall configuration shown in Figure 56.

Fuselage Tank Test Configuration (Voided Top Wall)

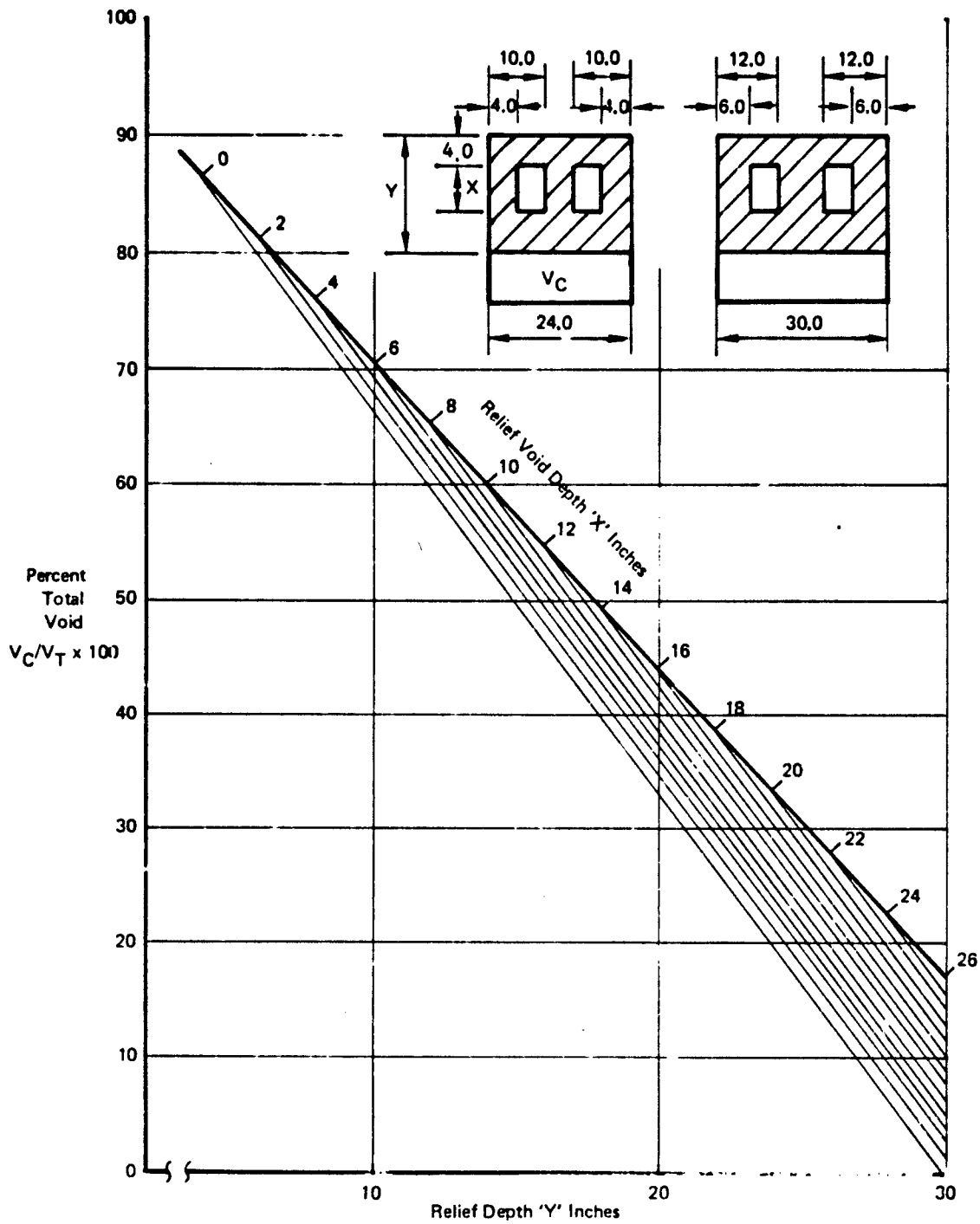


Figure 57: Variation of Percent Void and Relief Depth (Voided Top Wall)

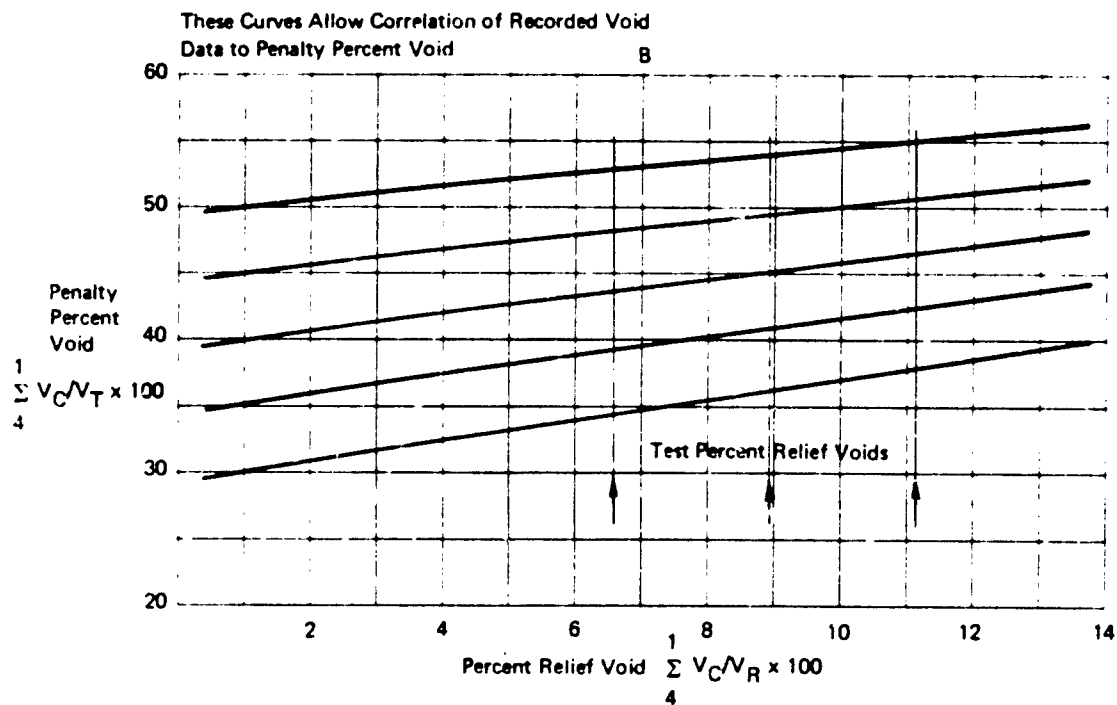
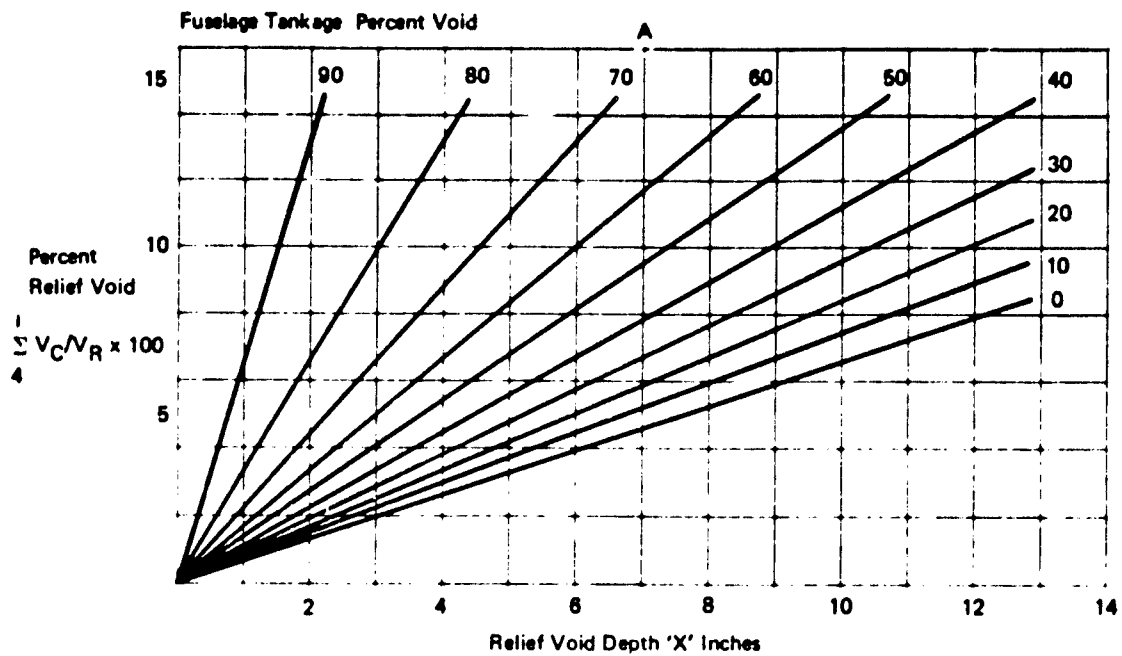
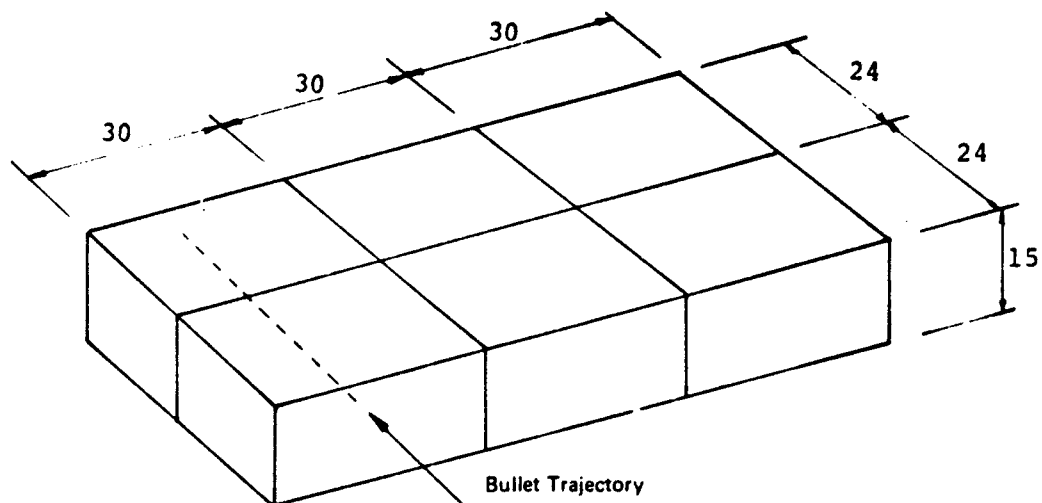


Figure 58: Variation of Percent Void, Penalty Percent Void and Relief Void Depth

2.2 Small Wing Tankage

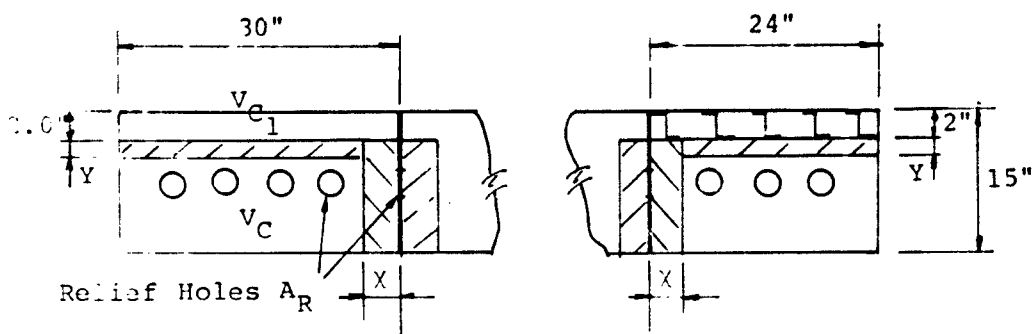
The test cubes were assembled in the following manner.



A photograph of the test assembly is shown in Figure 59.

The relationship of percent penalty void $V_C/V_T \times 100$ versus other pertinent arrester dimension are included in this report for each voiding concept as follows.

2.2.1 Voided Top Wall



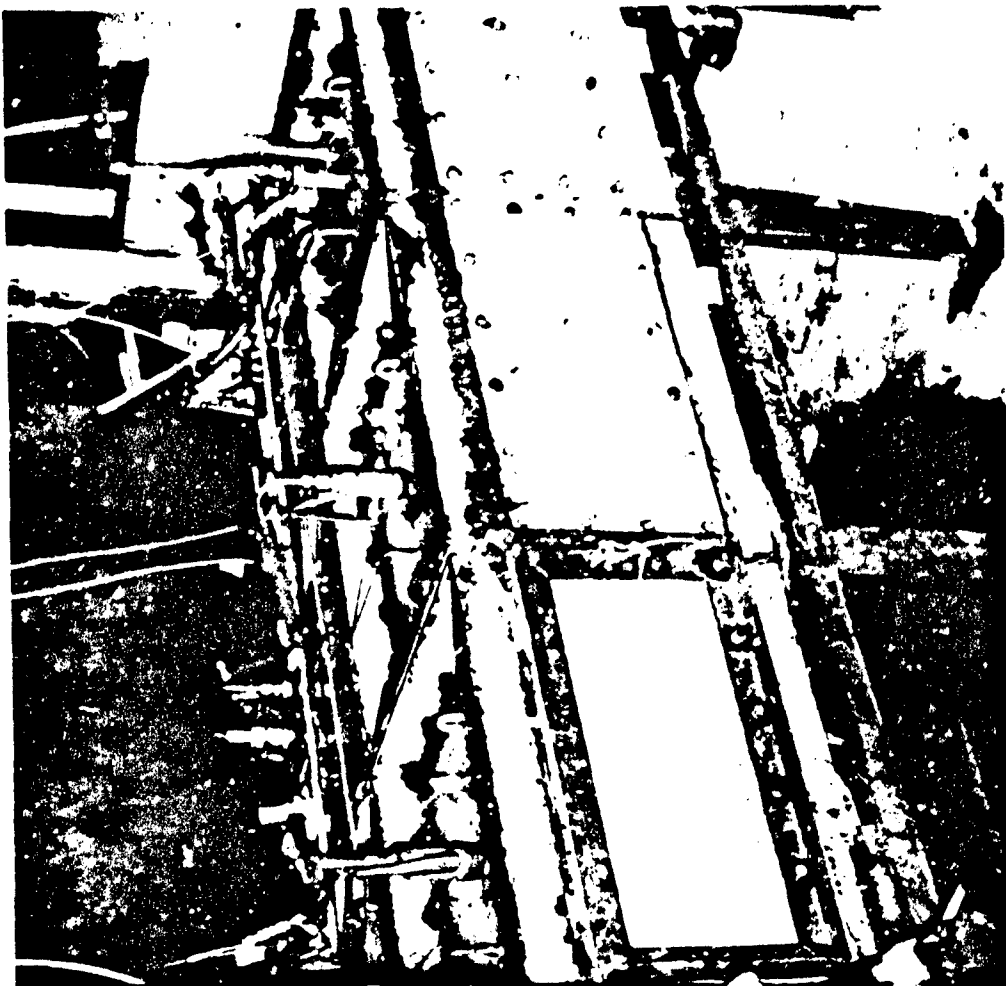


Figure 55: Small Wing Tankage Test Configuration



$$\text{Total relief area (30 x 15) plate} = \frac{\pi \times 2.65^2}{4} \times 4 = 22.2 \text{ in.}^2$$

$$\text{Total relief area (24 x 15) plate} = \frac{\pi \times 2.65^2}{4} \times 3 = 16.6 \text{ in.}^2$$

$$\text{Percent relief area (30 x 15) plate} = A_R/A_T = \frac{22.2 \times 100}{30 \times 15} = 4.93\%$$

$$\text{Percent relief area (24 x 15) plate} = A_R/A_T = \frac{16.6 \times 100}{24 \times 15} = 4.61\%$$

$$V_{C1} = 30 \times 24 \times 2 = 1440 \text{ in.}^3$$

$$V_C = (13 - y)(30 - x)(24 - x) = 9360 - 701x + 13x^2 - 720y + 54xy - yx^2$$

$$V_T = 30 \times 24 \times 15 = 10,800 \text{ in.}^3$$

$$\text{Percent Void} = \frac{V_C \times 100}{V_T} = \frac{(9360 - 701x + 13x^2 - 720y + 54xy - yx^2) 100}{10,800}$$

$$\text{Penalty Percent Void} = \frac{(V_C + V_{C1}) 100}{V_T}$$

$$= \frac{(9360 - 701x + 13x^2 - 720y + 54xy - yx^2) + 1440 \times 100}{10,800}$$

$$V_R/V_C = \frac{V_T - V_C}{V_C}$$

$$= \frac{(10,800 - 9360 + 701x - 13x^2 + 720y - 54xy + yx^2)}{9360 - 701x + 13x^2 - 720y + 54xy - yx^2}$$

$$V_R/V_C \text{ Total Assembly} = \frac{V_{\text{Total Assembly}} - V_C}{V_C}$$

$$= \frac{(800 \times 6) - 9360 + 701x - 13x^2 + 720y - 54xy + yx^2}{9360 - 701x + 13x^2 - 720y + 54xy - yx^2}$$

Variations of percent void and V_R/V_C for various arrester thicknesses are shown in Figures 60, 61 and 62; Figure 62 is for $x = y$.

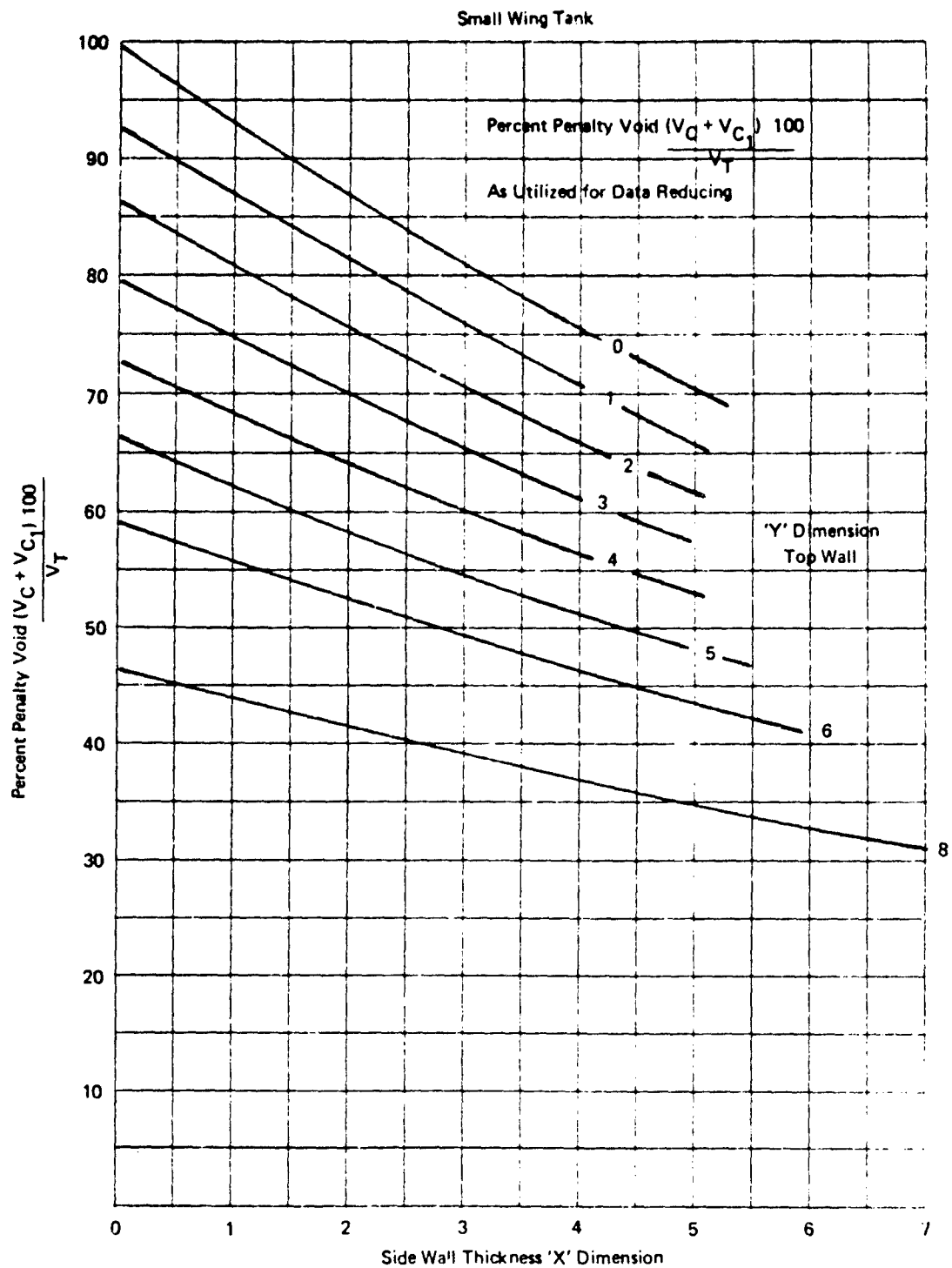


Figure 60: Variations of Percent Penalty Void With Arrestor Thickness (Voided Top Wall)

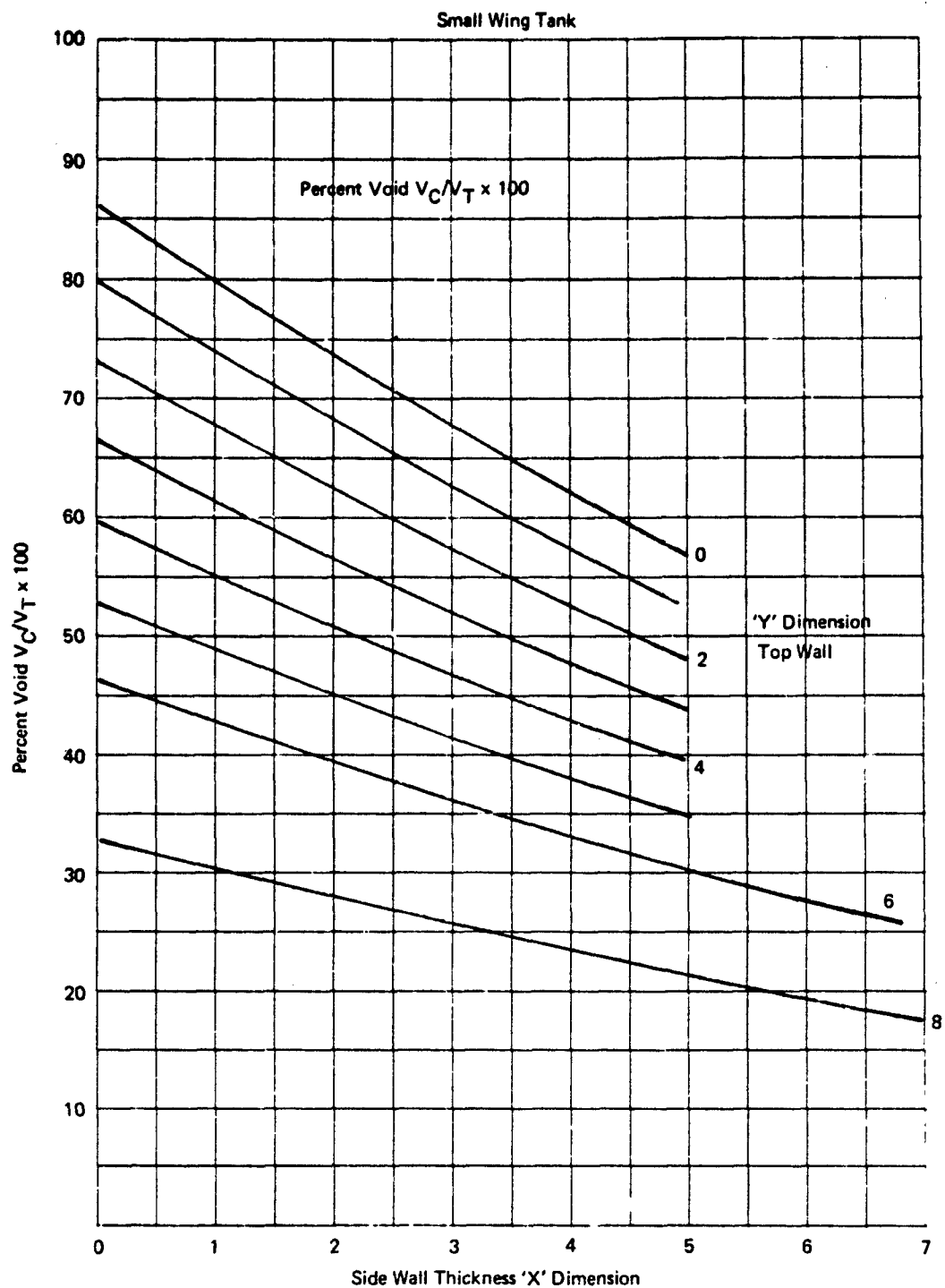


Figure 61: Variations of Percent Void with Arrestor Thickness (Voided Top Wall)

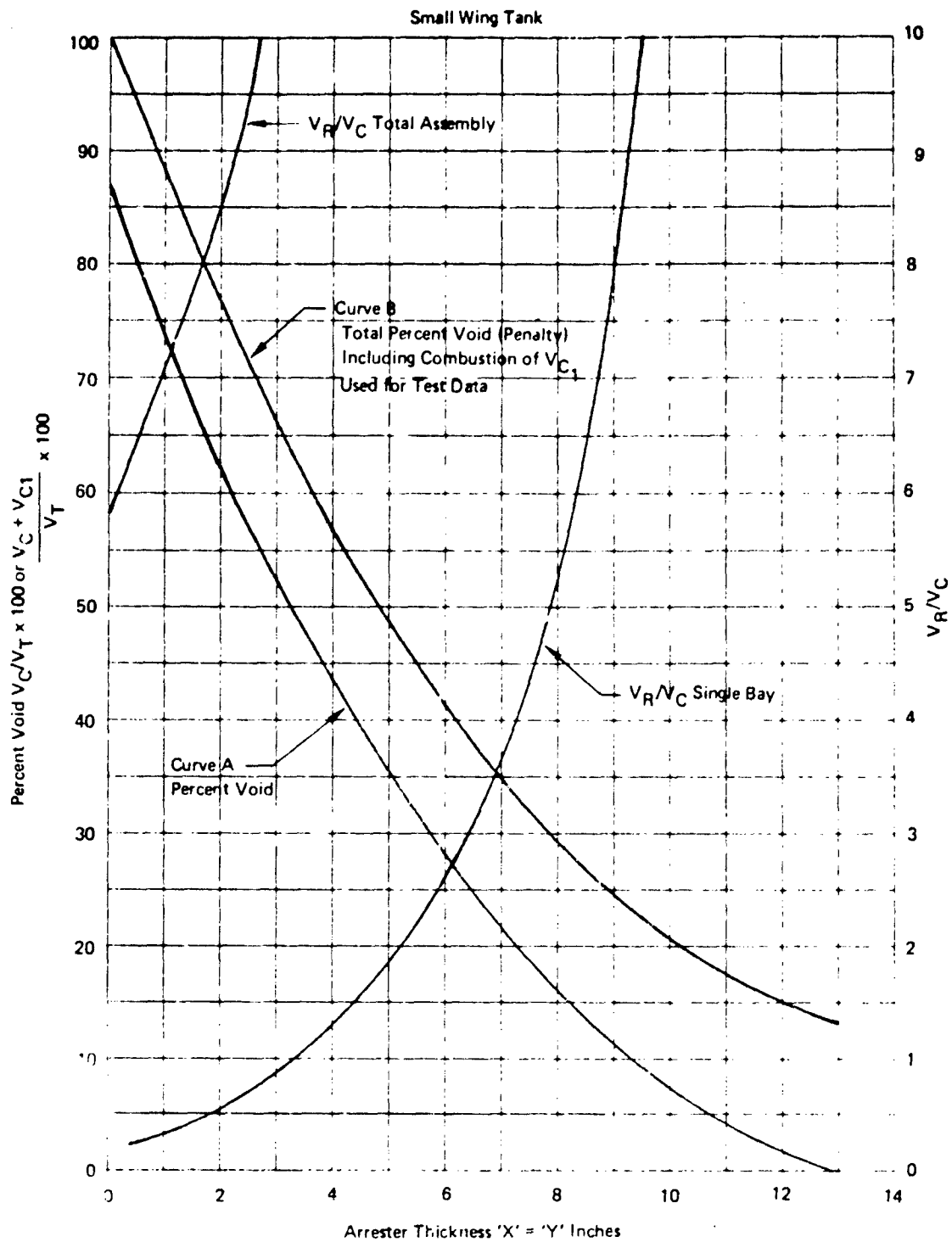


Figure 62: Variations of Percent Void and V_R/V_C with Arrestor Thickness (Voided Top Wall)

2.2.2 Egg Crate Configuration

$$V_T = 30 \times 24 \times 15 = 10,800 \text{ in.}^3$$

$$V_C = (30 - 4x) \times (24 - 4x) \times (15 - 2x)$$

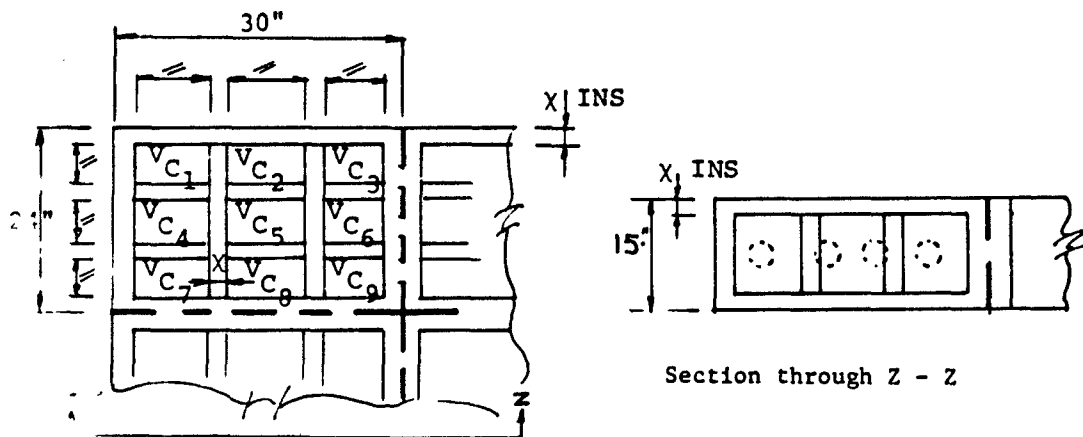
$$= 10,800 - 4,680x + 672x^2 - 32x^3$$

$$\text{Percent penalty void} = \frac{\frac{1}{9} \sum V_C \times 100}{V_T}$$

$$= \frac{(10,800 - 4,680x + 672x^2 - 32x^3) \times 100}{10,800} \quad (1)$$

$$V_R/V_C = \frac{\frac{9}{V_T - 1} \sum V_C}{\frac{1}{9} \sum V_C} = \frac{4680x - 672x^2 + 32x^3}{10,800 - 4680x + 672x^2 - 32x^3} \quad (2)$$

Single Bay



$$V_R/V_C = \frac{\frac{1}{9} \sum V_C}{\frac{1}{9} \sum V_C} = \frac{V_{\text{Total Assy}} - \frac{1}{9} \sum V_C}{\frac{1}{9} \sum V_C} = \frac{(10,800 \times 6) - (10,800 - 4680x + 672x^2 - 32x^3)}{10,800 - 4680x + 672x^2 - 32x^3}$$

Total Assembly

Variations of percent void and V_R/V_C for various arrester thicknesses are shown in Figure 63.

V_R/V_C for ignition of a single combustion volume V_{C1}

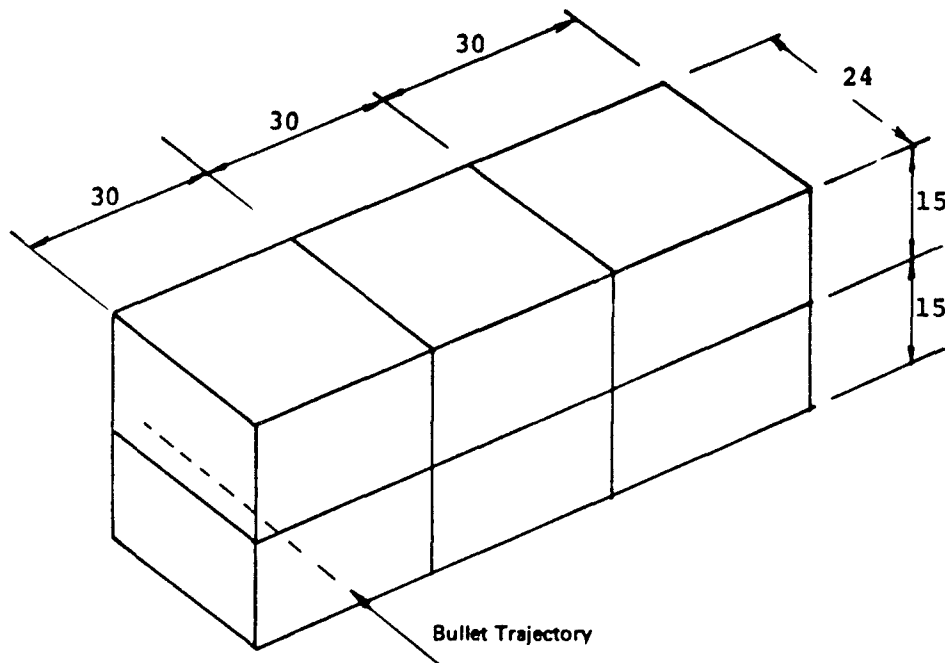
$$V_R/V_C \text{ Single Volume} = \frac{V_{\text{Total}} - V_{C1}}{V_{C1}}$$

$$V_R/V_C \text{ Single Volume} = \frac{(10,800 \times 6) - \frac{(10,800 - 4680x + 672x^2 - 32x^3)}{9}}{\frac{10,800 - 4680x + 672x^2 - 32x^3}{9}}$$

The range of values in which this V_R/V_C (Single Volume) results, falls within . 0 and 53 min. These values are high and correspond to a very low pressure ratio $P_C/P_{\text{Initial}} = 1.03$ over this range.

2.3 Large Wing Tankage

For large wing tankage simulation, the test cubes were assembled thus:



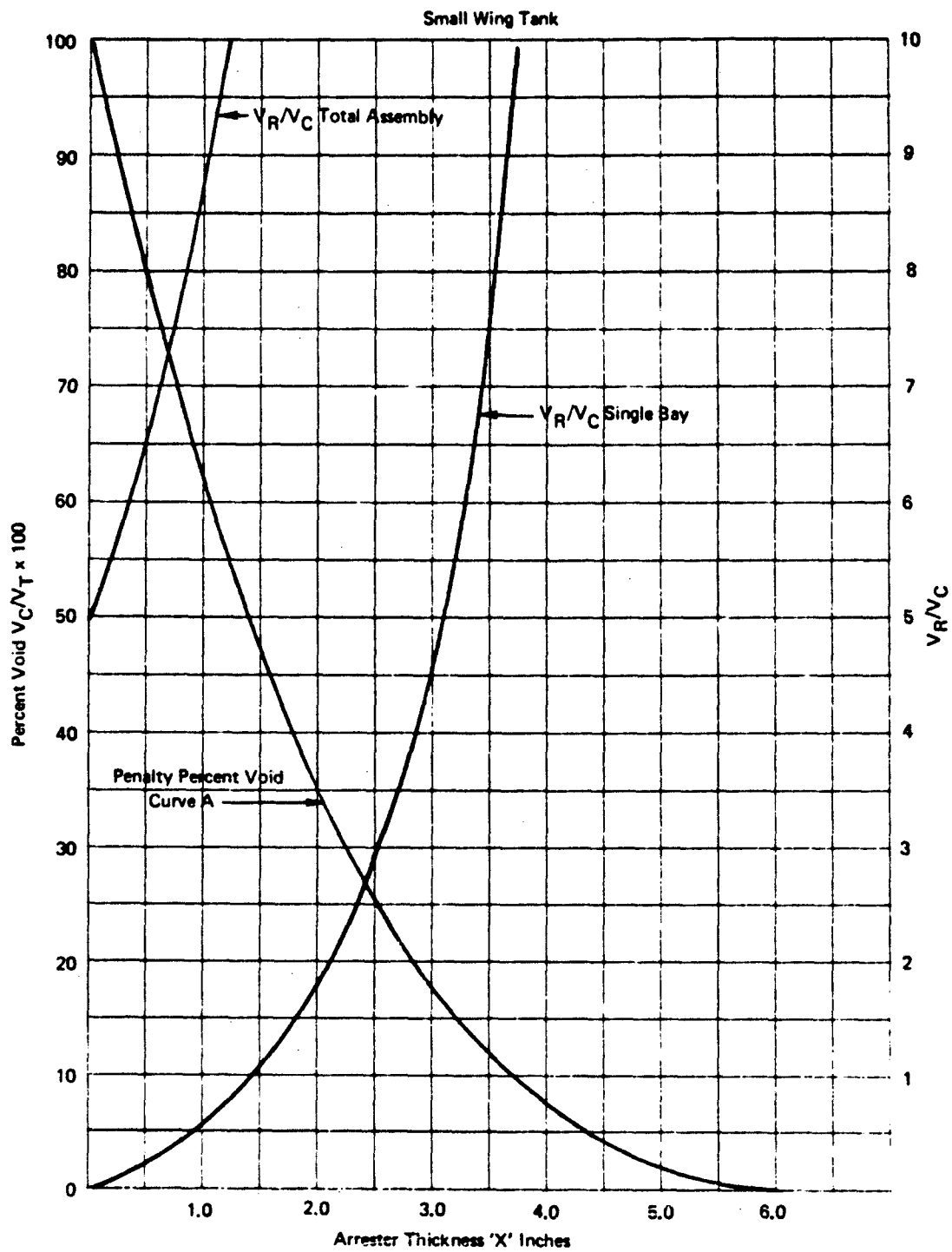
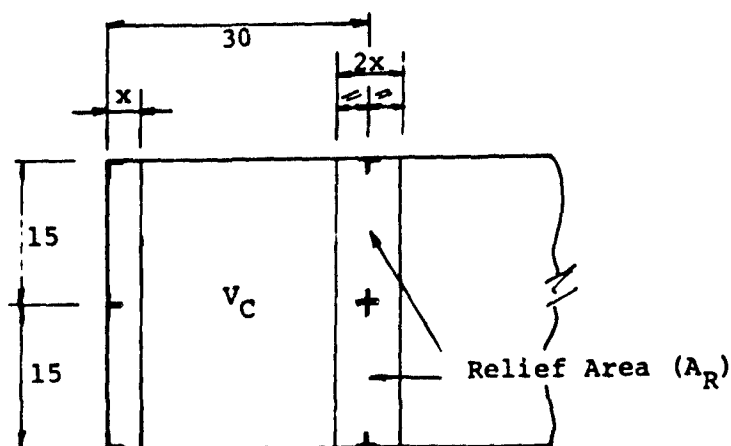


Figure 63: Variation of Percent Void and V_R/V_C with Arrestor Thickness (Egg Crate)

The test assembly is shown in Figure 64.

The relationship of percent penalty void $V_C/V_T \times 100$ versus other pertinent arrester dimensions is included in this report for each voiding concept as follows.

2.3.1 Lined Wall Configuration



Variations of percent void and V_R/V_C for various arrester thicknesses are shown in Figure 65.

$$\text{Total relief area} = A_R = (24 - 6) \times (15 - 4) \times 2 = 396 \text{ in.}^2$$

$$\text{Total area} = A_T = 24 \times 15 \times 2 = 720 \text{ INS}^2$$

The total relief area allowing pressure communication into the adjacent cell is given as:

$$\text{Percent relief area} = A_R/A_T \times 100 = \frac{396 \times 100}{720} = 55\%$$

$$V_C = (30 - 2x) \times 30 \times 24 = 21,600 - 1,440x$$

$$\text{Percent penalty void} = V_C/V_T \times 100 = \frac{(21,600 - 1440x) 100}{21,600} \quad (1)$$

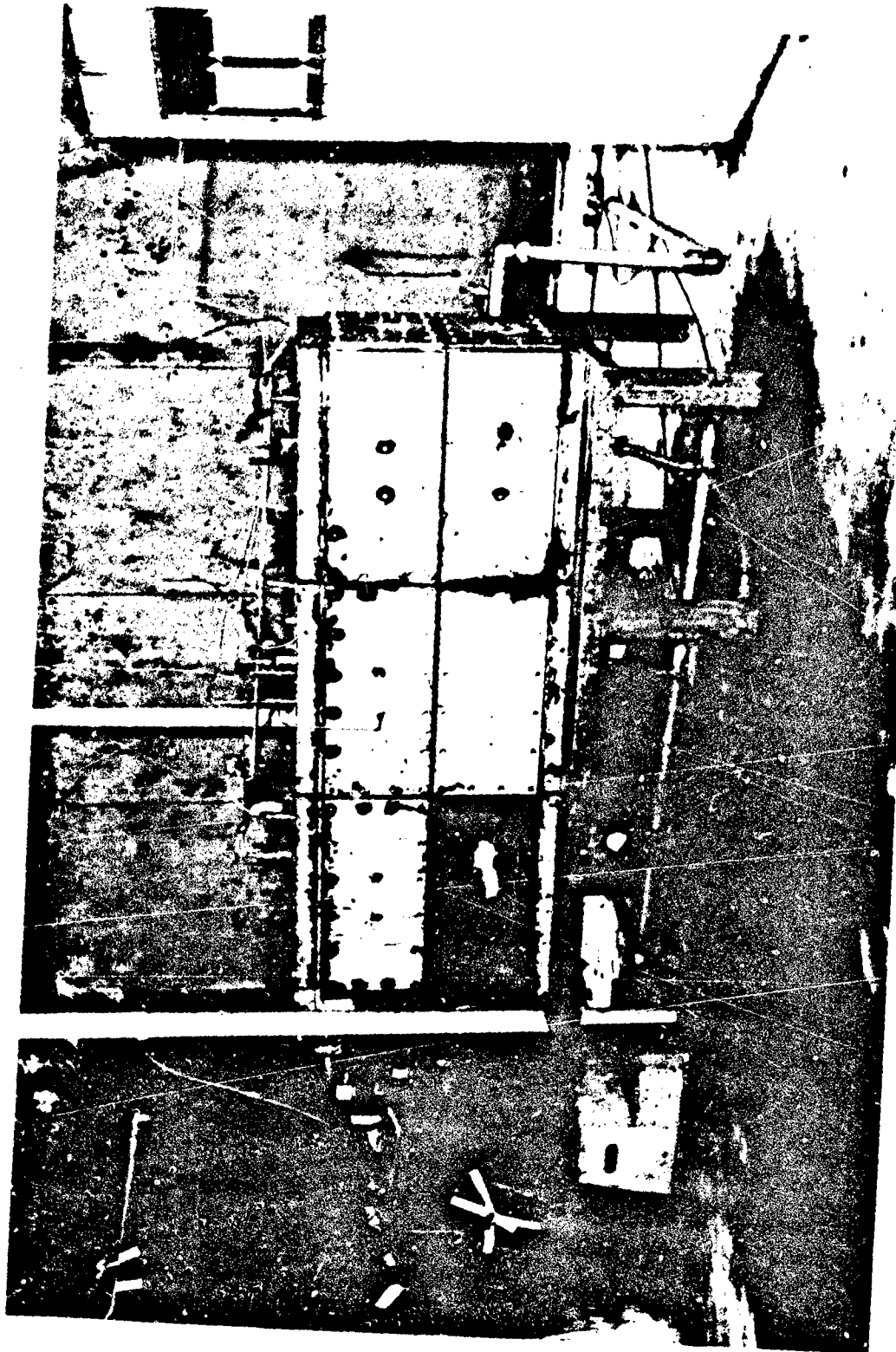


Figure 64: Large Wing Tankage Test Configuration

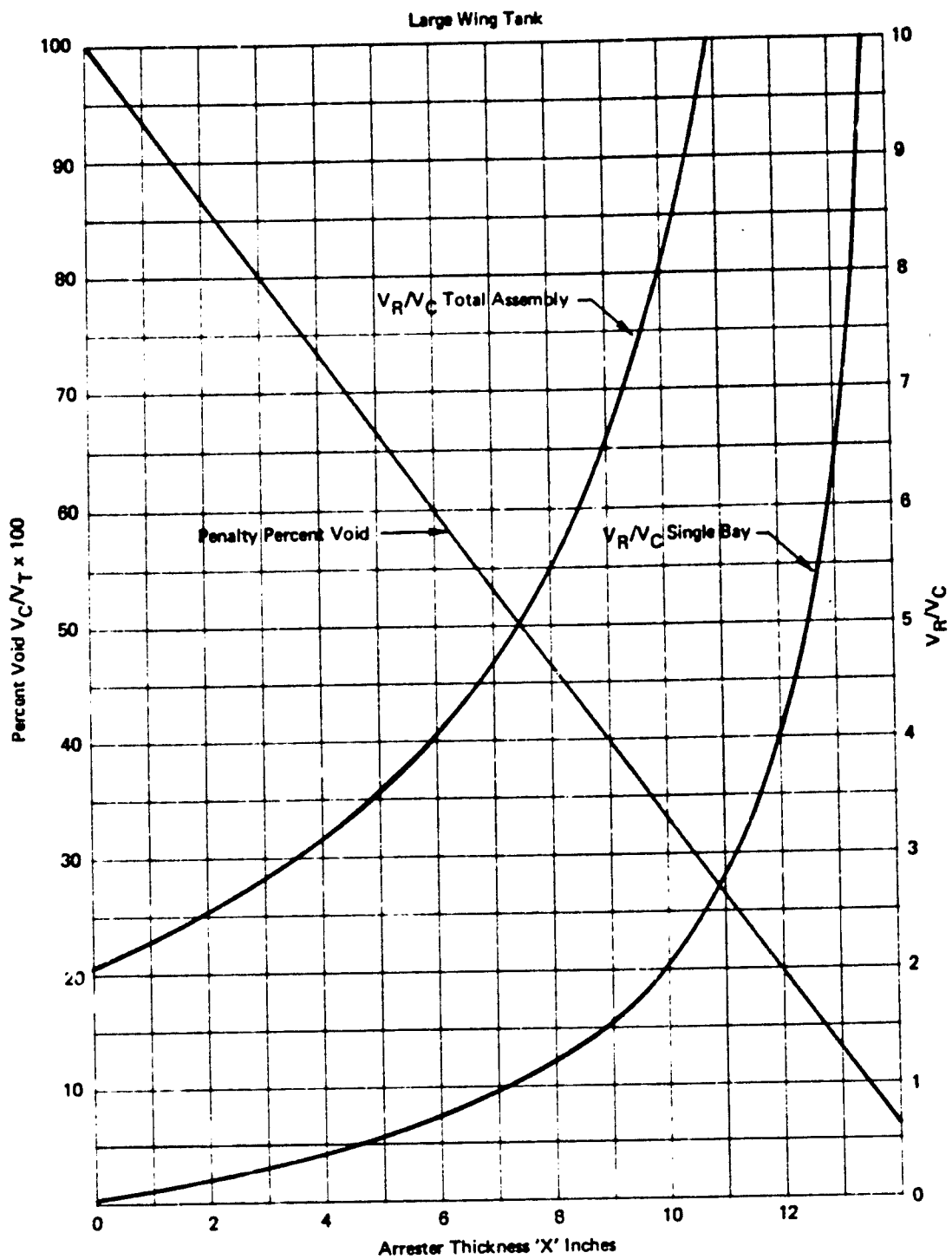


Figure 65: Variations of Percent Void and V_R/V_C with Arrestor Thickness (Lined Wall)

The relationship of relief to combustion volume for a single bay is given as:

$$V_R/V_C = \frac{V_T - V_C}{V_C} = \frac{1440x}{21,600 - 1440x}$$

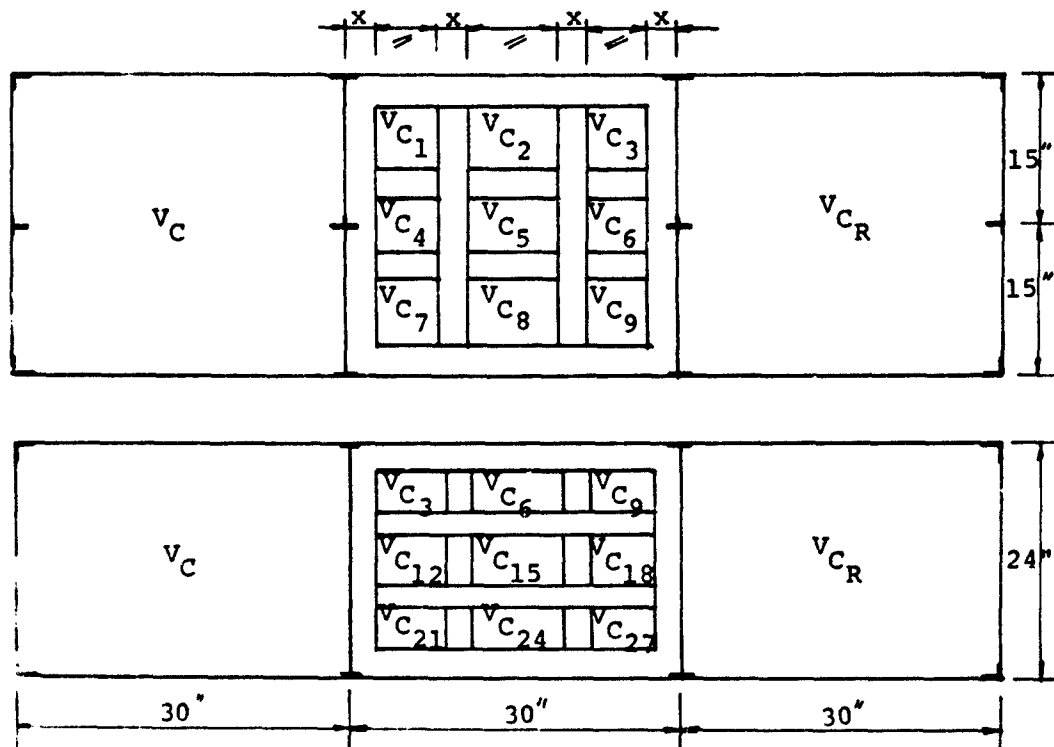
(Single bay)

The relationship of relief to combustion volume for the total assembly is given as:

$$V_R/V_C = \frac{V_{\text{Total Assy}} - V_C}{V_C} = \frac{(21,600 \times 3) - (21,600 - 1440x)}{21,600 - 1440x}$$

Total assembly

2.3.2 (Center Only) Egg Crate



$$\sum_{27} V_C = (30 - 4x) \times (24 - 4x) \times (30 - 4x)$$

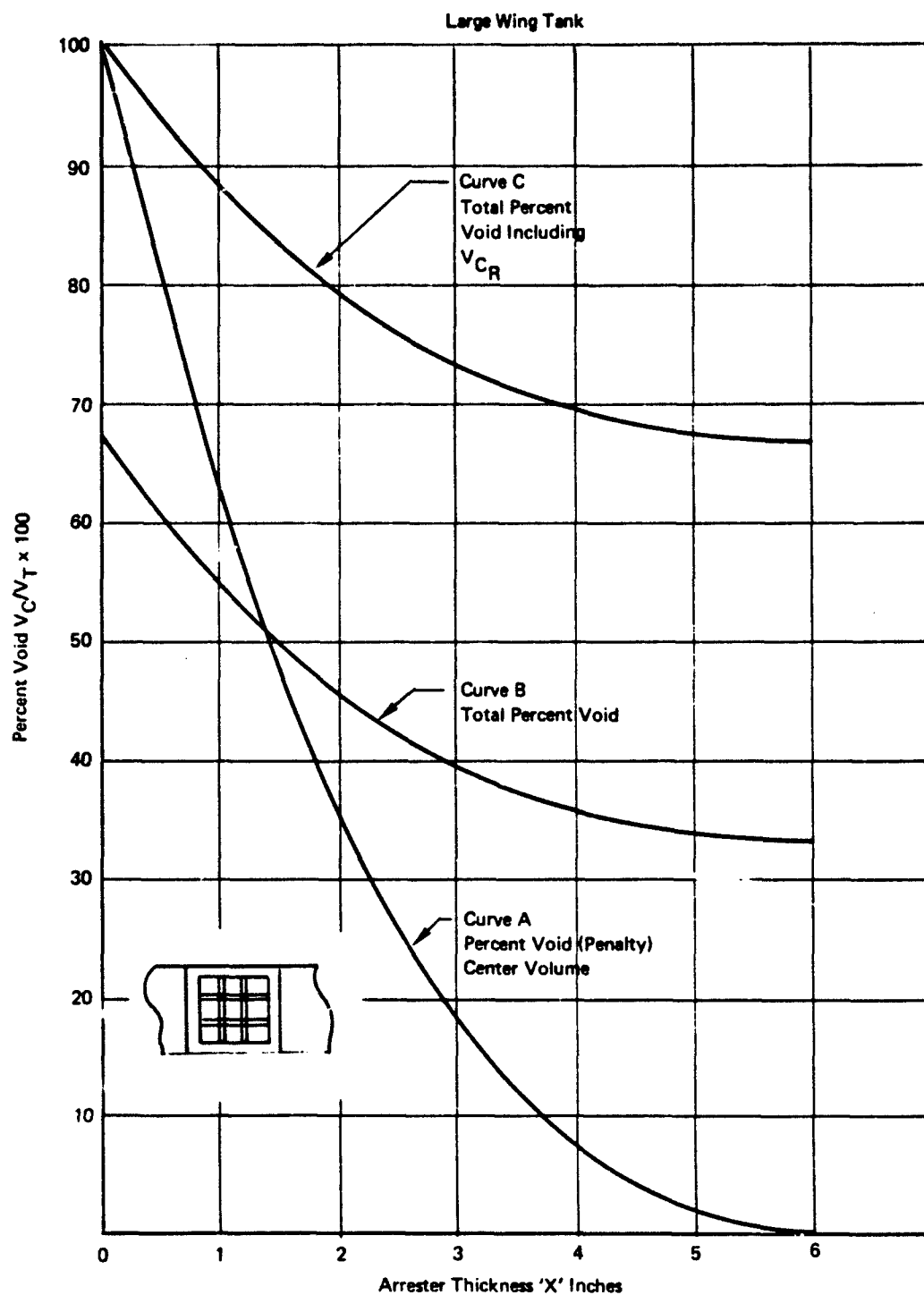


Figure 66: Variations of Percent Void and V_R/V_C with Arrestor Thickness (Egg Crate Center Only)

$$\sum_8^1 V_C = (30 - 3x) \times (24 - 3x) \times (30 - 3x).$$

$$\text{Percent Penalty Void} = \frac{\sum_8^1 V_C \times 100}{21,600}$$

$$\text{Percent Penalty Void} = \frac{(21,600 - 7,020x + 756x^2 - 27x^3)}{21,600} \times 100$$

The relationship of relief to combustion volume for a Curve A is given as:

$$V_R/V_C = \frac{\left(\frac{V_T - \sum_8^1 V_C}{\sum_8^1 V_C} \right) = \frac{(7020x - 756x^2 + 27x^3)}{21,600 - 7020x + 756x^2 - 27x^3}}$$

The relationship of relief to combustion volume for the total assembly assuming no burn-through is given as:

$$V_R/V_C = \frac{V_{\text{Total}} - \sum_8^1 V_C}{\sum_8^1 V_C} = \frac{(21,600 \times 3) - (21,600 - 7020x + 756x^2 - 27x^3)}{21,600 - 7020x + 756x^2 - 27x^3}$$

Total Assy $\sum_8^1 V_C$

Variations of percent void and V_R/V_C for various arrester thicknesses x are shown in Figure 67.

V_R/V_C for ignition of a single combustion volume V_{C1}

$$V_R/V_C \text{ Single Volume} = \frac{V_{\text{Total}} - V_{C1}}{V_{C1}}$$

$$= \frac{(21,600 \times 3) - \frac{(21,600 - 7020x + 756x^2 - 27x^3)}{8}}{\frac{(21,600 - 7020x + 756x^2 - 27x^3)}{8}}$$

V_R/V_C Single Volume

The range of values that this V_R/V_C (Single Volume) results in, falls within α and 23. These values are high and correspond to a very low pressure ratio. $P_{C/P}$ value as predicted by the dynamic mathematical model, this ratio has essentially a constant value of $P_{C/P}^{\text{initial}} = 1.03$ over this range.

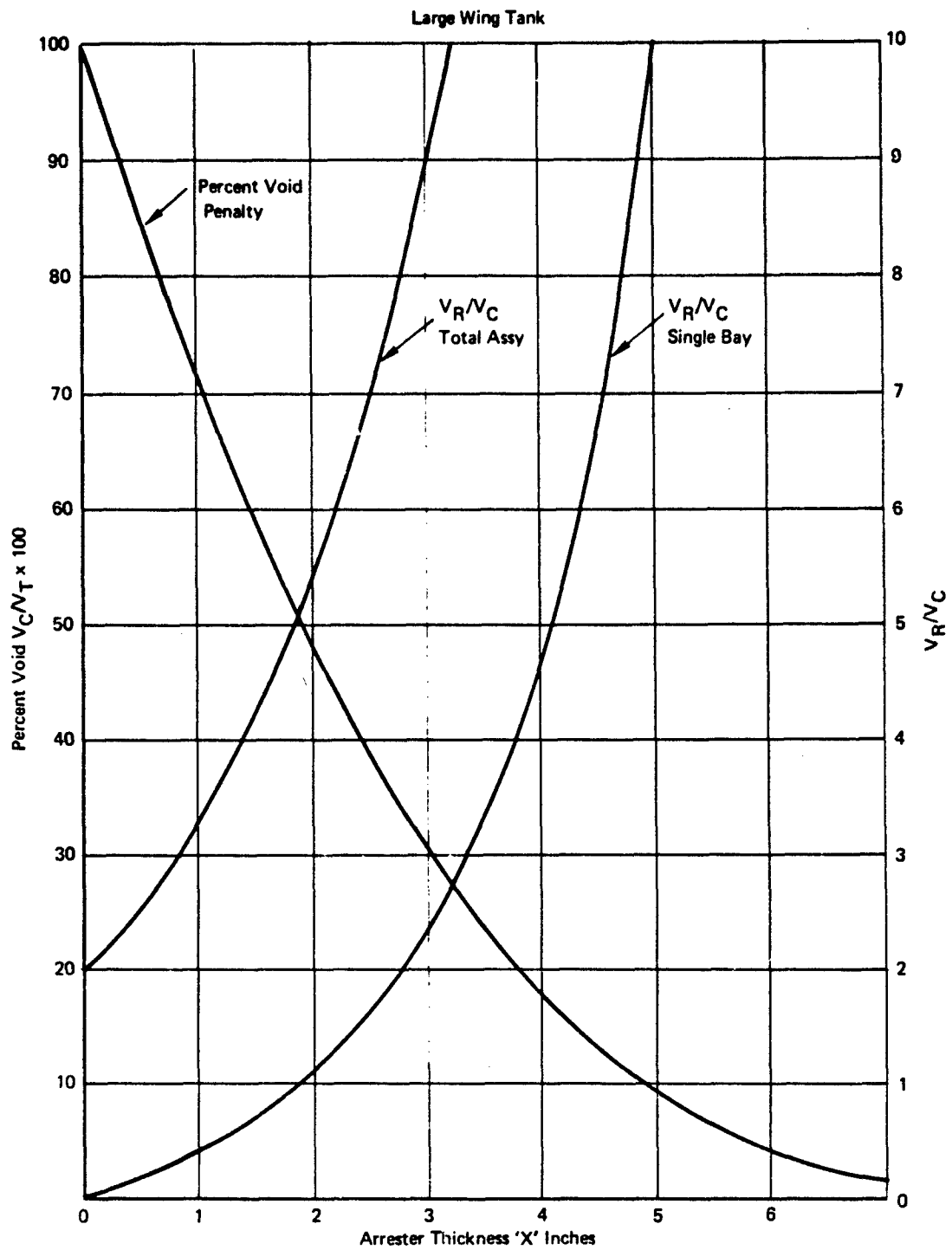


Figure 67: Variations of Percent Void and V_R/V_C with Arrestor Thickness (Total Egg Crate)

3.0 INSTRUMENTATION

The instrumentation in general is identical to that utilized for the Task I program.

A listing is included for each of the major configurations.

3.1 Fuselage Tankage, Table VI

3.2 Small Wing Tankage, Table VII

3.3 Large Wing Tankage, Table VIII

4.0 IGNITION SYSTEMS

The ignition systems are those utilized for the Task I program, with the addition of a separate circuit to activate the breech of the .50 caliber gun. These circuits are detailed in Figures 68, 69, and 70, as follows:

- Incendiary igniter/spark plug firing circuit, Figure 68
- Bomb firing circuit, Figure 69
- Gun firing circuit, Figure 70

The gun assembly is shown in Figure 71.

5.0 TEST PROCEDURE









5.1 General

The test procedure is summarized in Section VI (Mode II testing), Paragraph 5.0.

system schematic for each configuration is shown in Figures 72, 73, and 74, as follows:

- Fuselage tankage, Figure 72
- Small wing tankage, Figure 73
- Large wing tankage, Figure 74.











Table VI: Fuselage Tank Instrument List

SYMBOL	DESCRIPTION	FREQ. RESP. (Hz)	RANGE	ACCURACY	MONITOR	RECORDER
P 1	Pressure, Mixture Sampling Bombs, Upper Level	100	0-200 PSIA	± 5%	X	 Visicorder
P 2	Pressure, Mixture Sampling Bombs, Middle Level	100	0-200 PSIA	± 5%	X	 Visicorder
P 3	Pressure, Mixture Sampling Bombs, Lower Level	100	0-200 PSIA	± 5%	X	 Visicorder
P 4	Pressure, Test Tank, Upper Level	100	0-50 PSIA	± 5%	X	 Visicorder
P 5	Pressure, Test Tank, Middle Level	100	0-50 PSIA	± 5%	X	 Visicorder
P 6	Pressure, Test Tank, Lower Level	100	0-50 PSIA	± 5%	X	 Visicorder
P 7	Pressure, Mixing Tank	0	0-50 PSIA	± 1%	X	 Visico
I ₁ GN	Current in Ignition Firing Circuit	N.A.	Event Indication Only	N.A.		 Visicorder



Paper speed 16 IPS; timing lines 0.01 sec.

Table VII : Small Wing Tank Instrument List

SYMBOL	DESCRIPTION	FREQ. RESP. (Hz)	RANGE	ACCURACY	MONITOR	RECORDER
P 1	Pressure, Mixture Sample Bombs, Cell 1	100	0-200 PSIA	± 5%	X	Visicorder 
P 2	Pressure, Mixture Sample Bombs, Cell 2	100	0-200 PSIA	± 5%	X	Visicorder 
P 3	Pressure, Mixture Sample Bombs, Cell 6	100	0-200 PSIA	± 5%	X	Visicorder 
P 11	Pressure, Test Tank, Cell No. 1	100	0-50 PSIA	± 5%	X	Visicorder 
P 12	Pressure, Test Tank, Cell No. 2	100	0-50 PSIA	± 5%	X	Visicorder 
P 13	Pressure, Test Tank, Cell No. 3	100	0-50 PSIA	± 5%	X	Visicorder 
P 14	Pressure, Test Tank, Cell No. 4	100	0-50 PSIA	± 5%	X	Visicorder 
P 15	Pressure, Test Tank, Cell No. 5	100	0-50 PSIA	± 5%	X	Visicorder 
P 16	Pressure, Test Tank, Cell No. 6	100	0-50 PSIA	± 5%	X	Visicorder 
P 7	Pressure, Mixing Tank	0	0-50 PSIA	± 1%	X	
I ₁ GN	Current in Ignition Firing Circuit	N.A.	Event Indication Only	N.A.		Visicorder 






 Paper speed 16 IPS: timing lines 0.01 sec.

Table VIII: Large Wing Tank Instrument List

SYMBOL	DESCRIPTION	FREQ. RESP. (Hz)	RANGE	ACCURACY	MONITOR	RECORDER
P 1	Pressure, Mixture Sample Bomb, Cell 1	100	0-200 PSIA	± 5%	X	 Visicorder
P 2	Pressure, Mixture Sample Bomb, Cell 2	100	0-200 PSIA	± 5%	X	Visicorder
P 3	Pressure, Mixture Sample Bomb, Cell 3	100	0-200 PSIA	± 5%	X	Visicorder
P 11	Pressure, Test Tank, Cell No. 1	100	0-50 PSIA	± 5%	X	Visicorder
P 12	Pressure, Test Tank, Cell No. 2	100	0-50 PSIA	± 5 ± 5%	X	Visicorder
P 13	Pressure, Test Tank, Cell No. 3	100	0-50 PSIA	± 5%	X	 Visicorder
P 7	Pressure, Mixing Tank	0	0-50 PSIA	± 1%	X	Visicorder
I _{IGN.}	Current in Ignition Firing Circuit	N.A.	Event Indication Only	N.A.		 Visicorder

 Paper speed 16 IPS: timing lines 0.01 sec.



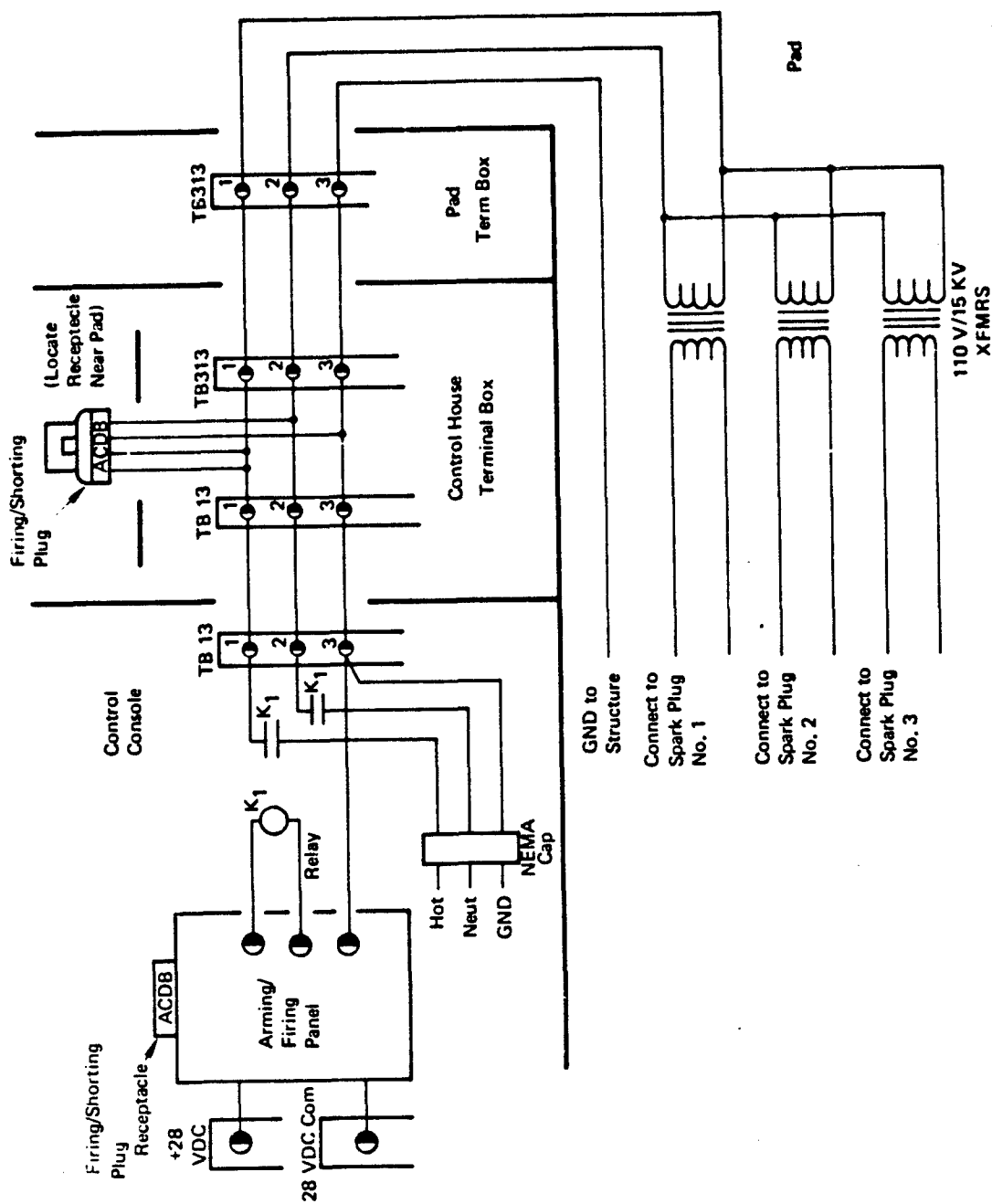


Figure 69 : Domb Firing Circuit

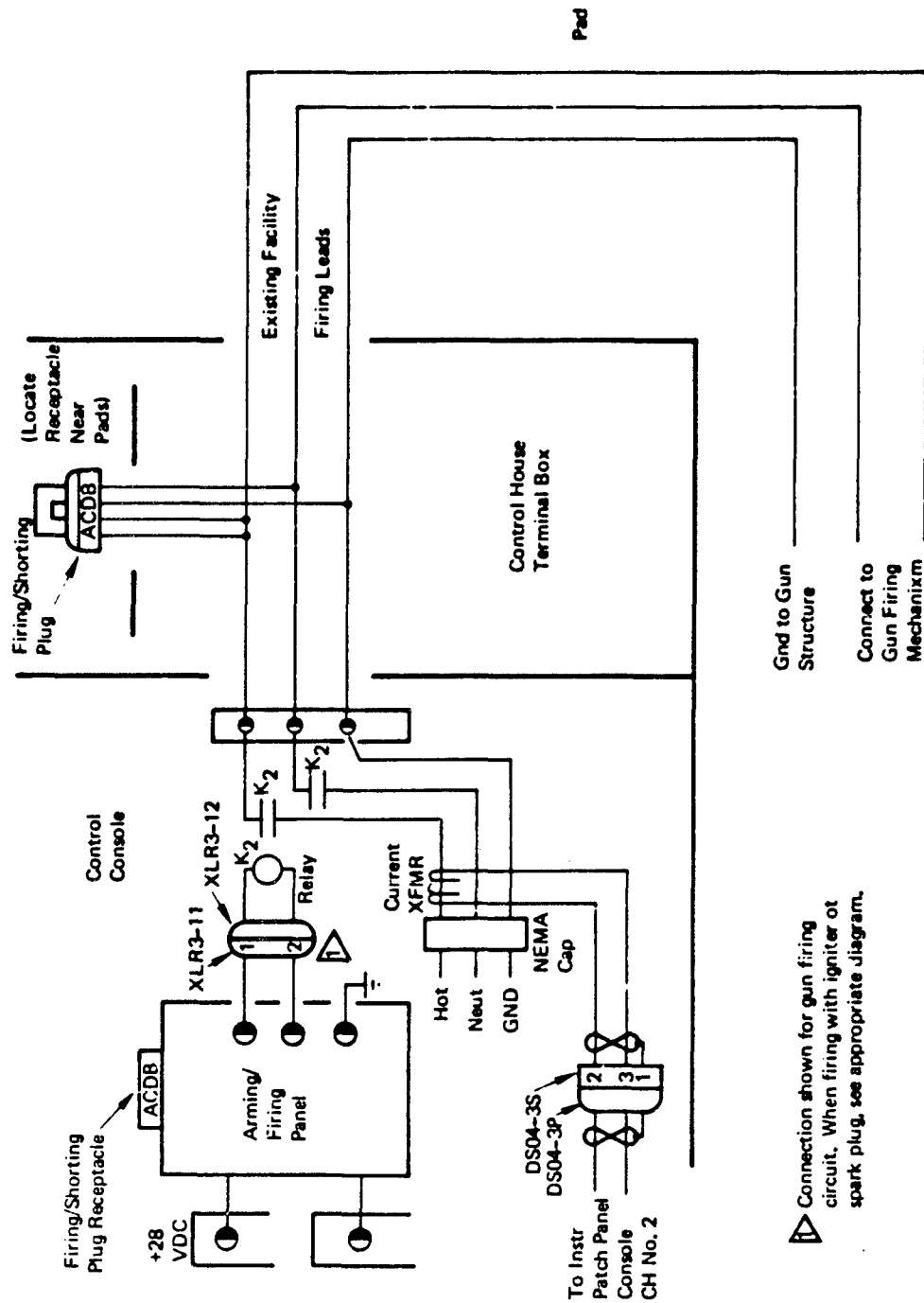


Figure 70: Gun Firing Circuit

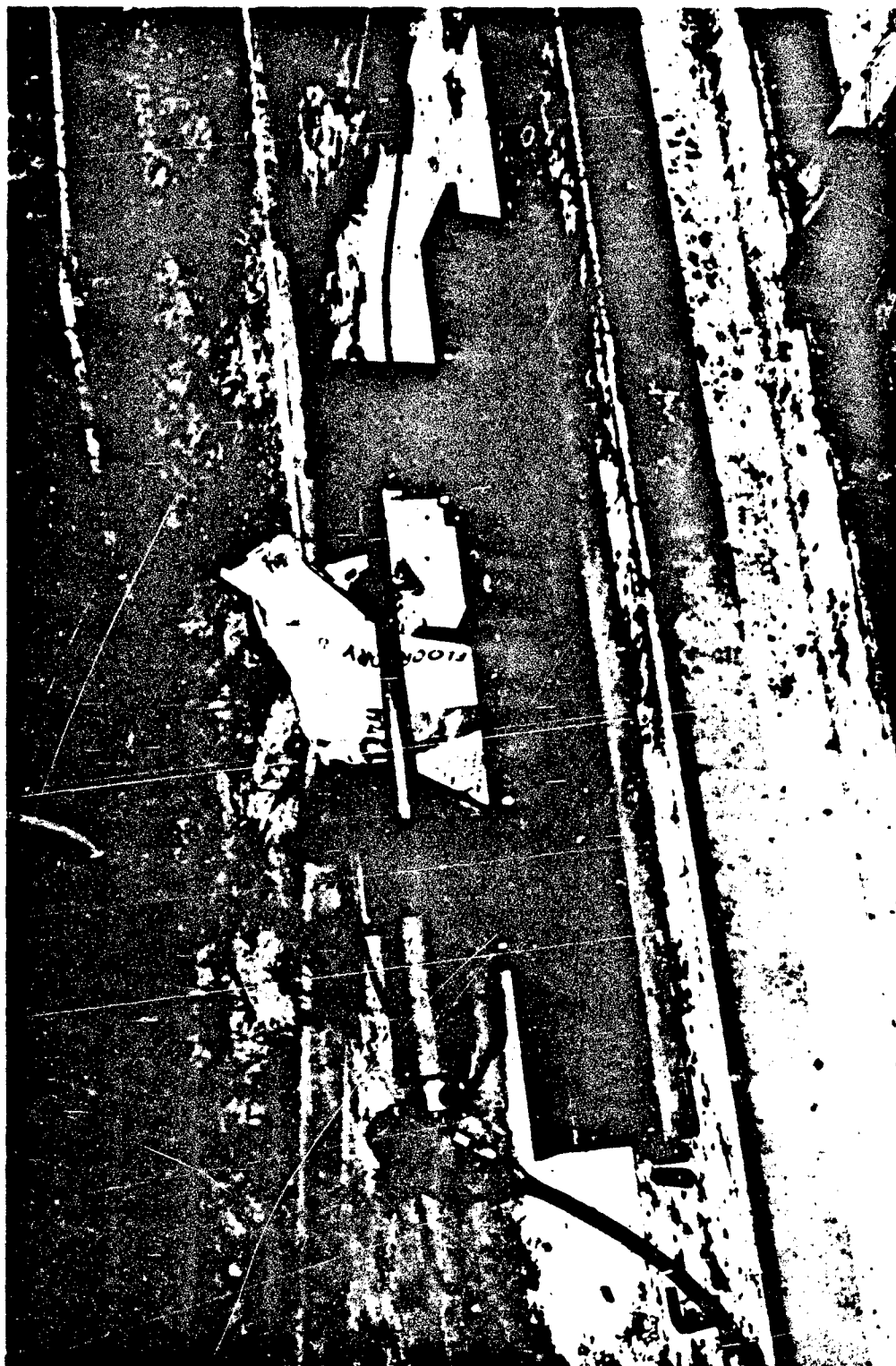


Figure 71: .50 Caliber Gun

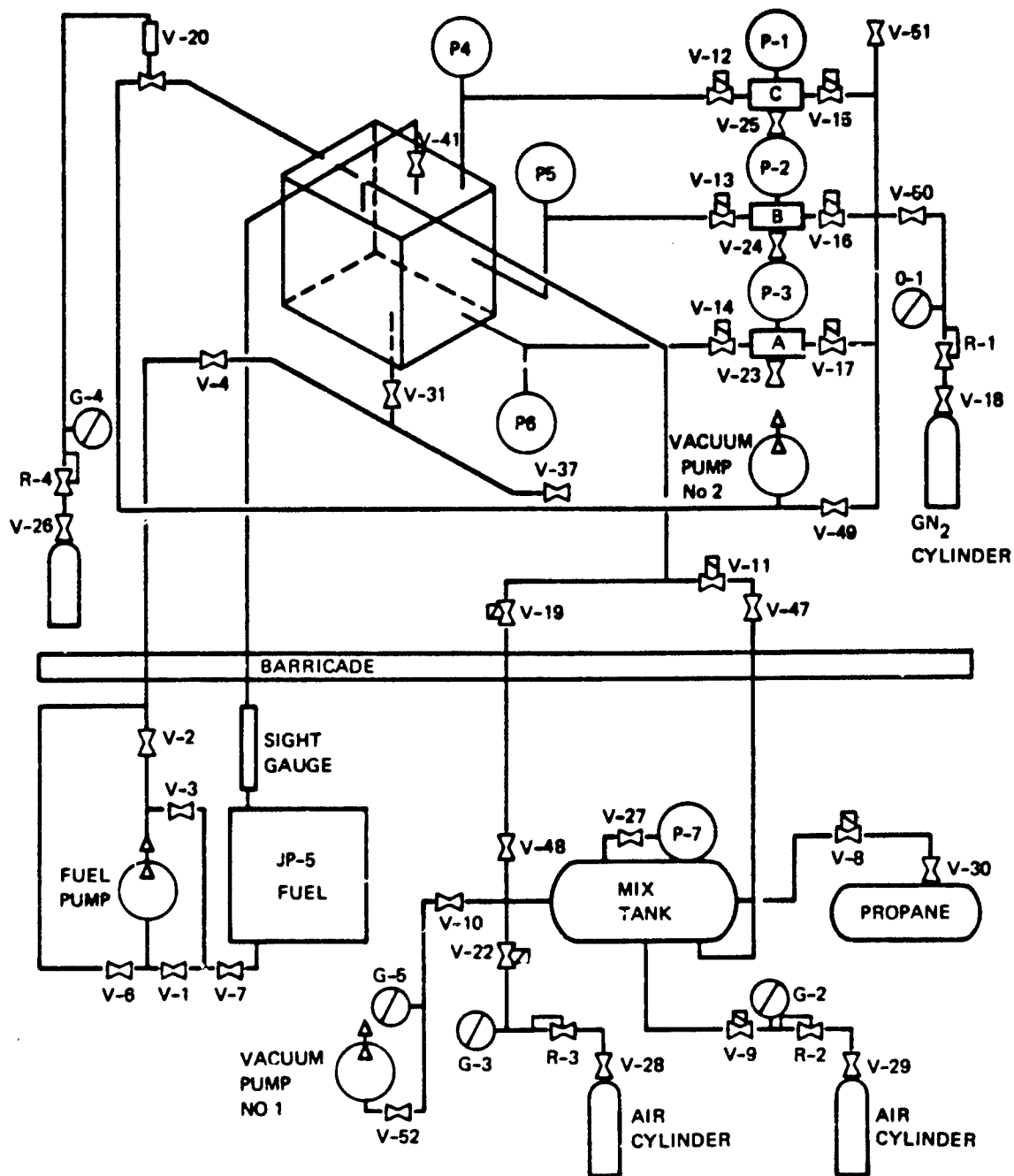


Figure 72: Test Schematic Fuselage Tank

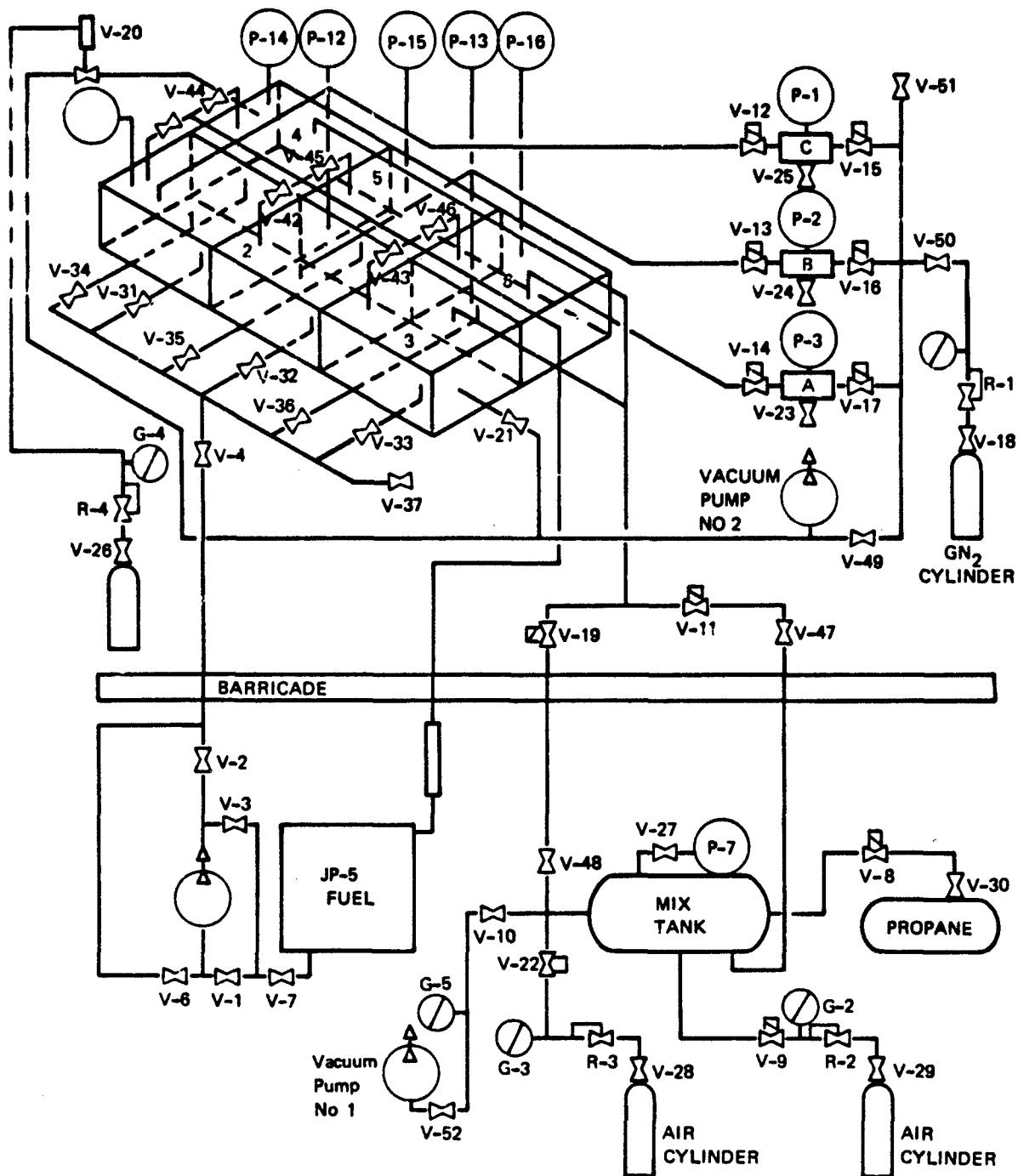


Figure 73: Test Schematic Small Wing Tank

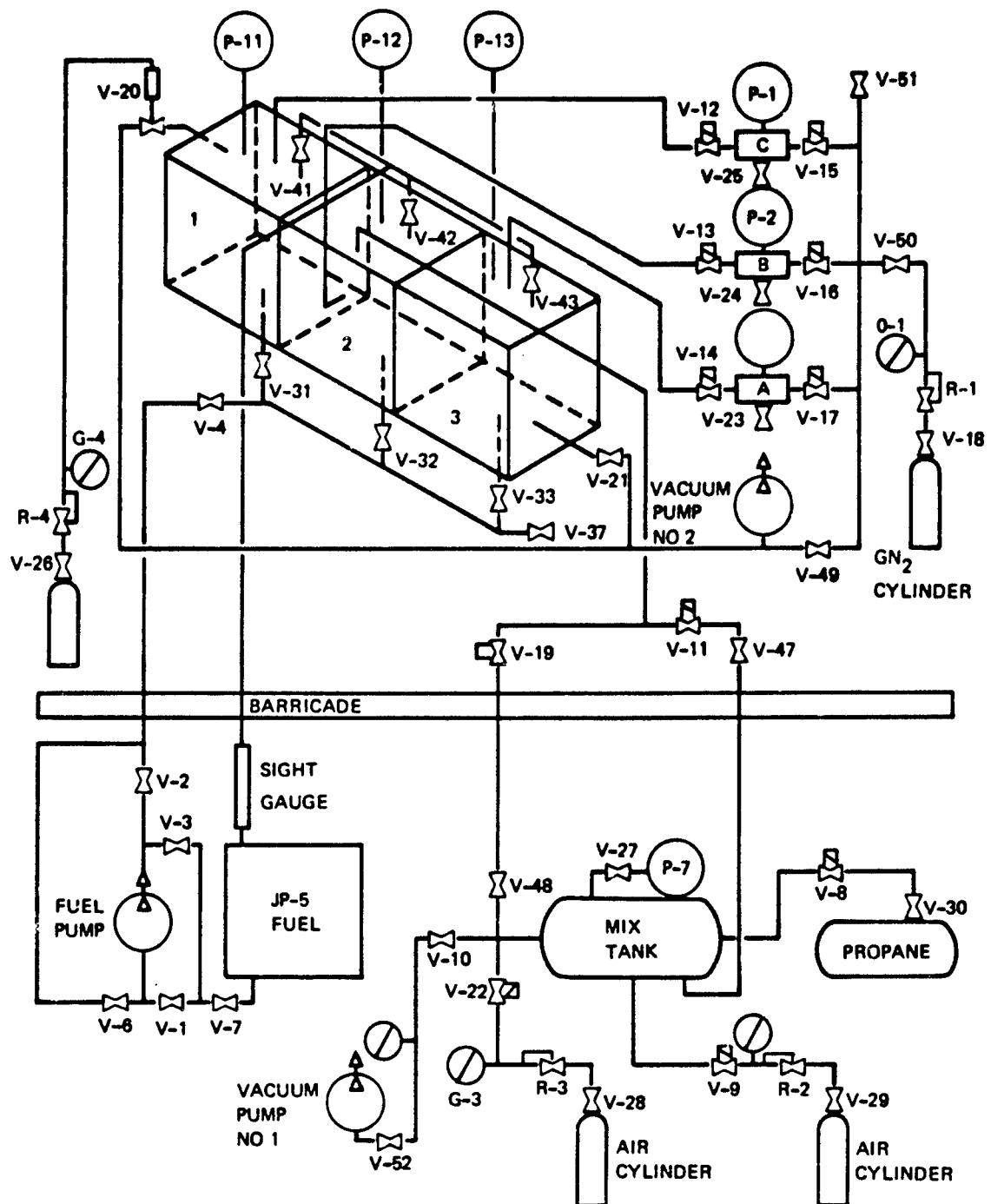


Figure 74: Test Schematic Large Wing Tank

The fuselage schematic was slightly modified from that used for all early tests in Mode II. This modification allowed for a faster refueling and defueling and for the easy purging of residual fuel from the sampling bombs and lines.

5.2 Detailed Procedural Checklist

The following is the detailed safety and procedural steps completed prior to initiating a test firing. This procedure was adopted for all Mode II and Task II tests.

5.2.1 Basic Facility (Safe Condition)

Area control lights green.

All valves closed.

Tank and sample bomb firing circuits in safe mode with shorting plugs in receptacles outside control house and arm, fire and key switches off.

Vacuum pumps off.

Fuel pump off.

Propane supply off.

Mix tank air supply off.

Sample bomb GN_2 purge supply off.

V-20 GN_2 supply off.

5.2.2 Basic Facility (Ready Condition)

Area control lights "YELLOW" inner and outer perimeters.

All valves closed except as specified below.

Tank and sample bomb firing circuits in safe mode with shorting plugs in receptacles outside control house and arm, fire and key switches off.

Vacuum pumps off.

Fuel pump off.

Propane supply on.

Mix tank air supply on.

Sample bomb GN_2 purge supply on.

V-20 GN_2 supply on.

5.2.3 Mix Tank

Open valves V-10, V-47, V-48 and V-52.

Start vacuum pump 1 and evacuate mix tank until P7 indicates less than 1/2 psia.

- 1) Close V-10 and V-52 and record vacuum and decay rate.

Vacuum _____ psia

Decay rate _____ psi/min.

- 2) Determine and record desired propane-air mix, propane partial pressure and final mix pressure.

Propane-air mix _____ %

Propane partial pressure _____ psi

Final mix pressure _____ psia

- 3) Place pad in "RED" and notify Fire Department.
- 4) Bleed in required propane using V-8.
- 5) Bleed in air using V-9 and V-22 to get final mix pressure.
- 6) Place pad in "YELLOW" and notify Fire Department.

5.2.4 Camera and Firing Circuits

- 1) If movie camera is to be used check operation by holding in microswitch in camera body and having camera switch in control house operated. Motor will operate if circuit is activated.
- 2) Load movie film magazine in camera.
- 3) Check firing circuit by pulling shorting plug and installing in control console, turning key and arm switches on and turning on fire switch. If circuit is activated, a meter across the firing leads at the pad will indicate 110 volts.
- 4) Circuit check verified.
- 5) Turn off fire, arm, and key switches and insert shorting plug in receptacle outside control house.

5.2.5 Sample Bomb Vacuum Check

- 1) Start Vacuum Pump 2.
- 2) Open Valves V-15, V-16, V-17, and V-49 to evacuate sample bombs.
- 3) After 5 minutes close Valves V-15, V-16, V-17 and V-49.
- 4) Monitor P1, P2 and P3 to determine vacuum integrity of bombs.

P1 _____ psig
Decay rate _____ psi/min
P2 _____ psig
Decay rate _____ psi/min
P3 _____ psig
Decay rate _____ psi/min

5.2.6 Test Tank

- 1) Arrester material installed.

Configuration _____

- 2) Top and/or side plates installed. Torque bolts and nuts by hand only to minimize stripping threads.
- 3) Fuel fill/drain manifold underneath tank installed. All connections tight and valves closed.
- 4) Vent manifold on top of tank installed. All connections tight and valves closed.
- 5) Sample bomb lines installed. All connections tight and valves closed.
- 6) Vacuum manifold installed. All connections tight and valves closed.
- 7) Dummy igniters installed.
- 8) Check pressure integrity of tank (if necessary) by pressurizing and recording decay rate. The tank is pressurized by bleeding bomb purge gas into the tank through valves V-50 and V-12 through V-17. When the desired pressure has been reached on P1 close Valves V-12 through V-17 and V-50.

Pressure attained _____ psig

Decay rate _____ psi/min

- 9) Vent tank by opening valve V-41. Close V-41 when tank pressure drops to atmospheric.
- 10) Check vacuum integrity of tank by opening Valves V-20 and V-21 to pull a vacuum. Close Valves V-20 and V-21 when P1 indicates a stable vacuum. Record vacuum and decay rate.

Vacuum attained _____ psig

Decay rate _____ psi/min

- 11) Open V-41 through V-46 to vent tank to atmosphere.

5.2.7 Fuel Fill and Detank

- 1) Call Fire Department and wait for truck. When it arrives put outer perimeter in "RED."
- 2) Check that V-7 is open.
- 3) Open V-31 through V-36 and V-4.
- 4) Open V-1 and V-2.
- 5) Turn on fuel pump to start fuel flow. The flow may be throttled as needed with V-2 or V-4.
- 6) When tank is full, as indicated by fuel in vent sight tube, turn off fuel pump and close V-2 and V-1.
- 7) Detank by opening V-6 and V-3 and turning fuel pump on.
- 8) When tank is empty close V-6, turn off fuel pump and close V-3.
- 9) Close V-4, V-31 through V-36 and V-41 through V-46.
- 10) Place inner perimeter in "YELLOW." If test uses a spark or incendiary igniter proceed with Section 5.2.8. If it is a gunfire test proceed with Section 5.2.9.

5.2.8 Spark or Incendiary Igniter Installation

- 1) Remove dummy igniter from tank.
- 2) If spark igniter is to be used, install spark igniter assembly, making sure it is properly inserted in the quick-disconnect fitting.
- 3) If incendiary igniter is to be used load about 30 grains of 1M-11 mix into igniter assembly.
- 4) Check that igniter resistance is 0.2 ohms. Adjust compression nut if necessary.
- 5) Install assembly into tank making sure it is properly inserted into the quick-disconnect fitting.

5.2.9 Sample Bomb Purge

- 1) Open V-20 and V-21 to pull vacuum on tank.
- 2) Open V-15, V-16, V-17 and V-50 to pressurize bombs A, B, and C.
- 3) Open V-23 for 30 seconds to drain any residual fuel, then close V-23.
- 4) Open V-24 for 30 seconds, then close V-24.
- 5) Open V-25 for 30 seconds, then close V-25.
- 6) Open V-14 for 1 minute to purge bomb A sample line, then close V-14.
- 7) Open V-13 for 1 minute, then close V-13.
- 8) Open V-12 for 1 minute, then close V-12.
- 9) Close V-50 and open V-49 to evacuate the sample bombs. If the test uses a spark or incendiary igniter, proceed with Section 5.2.10. If it is a gunfire test proceed with Section 5.2.11.

5.2.10 Igniter Hookup

- 1) Fire Department at control house.
- 2) Outer perimeter in "RED."
- 3) Firing circuits key, arm, and fire switches off.
- 4) Shorting plugs in receptacle outside of control house.
- 5) The test engineer and ordnance technician go to pad to hookup firing circuit. All other personnel in control house.
- 6) Close V-21.
- 7) Check firing circuit for stray voltage or current. If none is found connect firing leads to igniter.
- 8) Test engineer and ordnance technician return to control house.
- 9) Put inner perimeter in "RED."

5.2.11 Gun Loading and Hookup

- 1) Fire Department at control house.
- 2) Outer perimeter in "RED."

- 3) Firing circuits key, arm, and fire switches off.
- 4) Shorting plugs in receptacle outside of control house.
- 5) The test engineer and ordnance technician will go to the pad to load the gun and hook up the firing circuit. All other personnel in control house.
- 6) Check that gun is aimed properly and no obstructions are in the barrel.
- 7) Close V-21.
- 8) Load gun with .50 caliber API round and 20 MM electrically primed case loaded with 500 grains of powder.
- 9) Check firing circuit for stray voltage or current. If none is found connect firing leads to gun.
- 10) Test engineer and ordnance Technician return to control house.
- 11) Put inner perimeter in "RED."

5.2.12 Explosive Mix Loading

- 1) Check that tank vacuum indicated by P1 is at desired level.
Record pressure _____ psig
- 2) Instrumentation checklist complete.
- 3) Close V-15, V-16, V-17, and V-20.
- 4) Open V-11 and V-19 as desired to pressurize tank to _____ psig.
Then close V-11 and V-19.
- 5) Wait 2 minutes. Maintain pressure as needed.
- 6) Check P1, P2 and P3 to make sure an adequate vacuum is in the sample bombs.
- 7) Open V-12, V-13 and V-14 for 1 minute, then close them.

5.2.13 Firing

- 1) Notify personnel that firing is imminent.
- 2) Install shorting plugs in control console and turn on key and arm switches.
- 3) Give 5-second countdown and fire bombs.
- 4) Observe whether P1, P2, and P3 are over 90 psig and whether pressure rise time is less than 200 milliseconds.

- 5) If P1, P2, and P3 are ready, start 5-second countdown and fire tank.
- 6) Put inner perimeter in "YELLOW."
- 7) Test engineer, fireman and ordnance technician inspect pad.
- 8) Put outer perimeter in "YELLOW."
- 9) Return area to "READY" condition.
- 10) Read, tabulate, and plot data.

6.0 RESULTS AND DISCUSSION OF RESULTS

All test configurations were tested with 25-ppi reticulated polyurethane foam. The initial test void condition was determined using steady state model relief-to-combustion ratio versus overpressure data. Further tests with increases in the percent void were each determined from the data obtained during the preceding tests. Testing was centered on obtaining data relating to the defined overpressure criterion of 10 psig. For concepts consisting of one or more voids, for example "egg crate," a 3.0 inch diameter hole was cut, interconnecting the voids, to duplicate multiple ignition similar to gunfire. The data are presented in tabular and graphic form, with a summary bar chart for each tankage.

The tabulated data summarize pertinent data for each test conducted, taken directly from the detailed test data sheets. It was apparent from the preceding program that the ignition mode and pressure rise times were important considerations. Consequently, included in this report is a direct copy of all data traces for each test condition. Each trace records an arrest or a burn-through and the ignition mode.

The relationship of percent penalty void to absolute pressure ratio is shown for each test.

In all cases where a burn-through occurred several pressure peaks were recorded; each is shown in the data traces and plotted as an overpressure ratio in the graphic data.

It is noted that throughout this program the overpressure is correlated with percent penalty void, as this relates directly to aircraft applications. Each void configuration was initially standardized so that its application in any cell of each configuration would not affect the total penalty void of each tankage. The only exception is with the three-cell large wing tank central egg crate concept. In this instance the data is plotted as the center cell egg crate penalty void.

The concluding bar charts allow an immediate voiding assessment of each concept relative to the others. In all tests the intent was to obtain sufficient data to allow a determination to be made of the relative performance of each concept.

A correlation with the dynamic mathematical model is made only with data obtained from the lined wall configuration. The required program routine changes required to describe some of the more exotic voiding concepts tested within the small and large wing tankages were considered beyond the scope of this program.

6.1 Fuselage Tankage Configuration

Pressure rise data traces are shown in Figures B-1 through B-7. The configuration description and combustion overpressure data are included as Table B-I. The relationship of penalty void with absolute overpressure ratio found by tests are shown plotted in Figures 75 through 79. The prediction of the dynamic mathematical model is shown only for the fuselage tests.

A summary bar chart allowing assessment of each void concept with the others shown in Figure 80.

6.1.1 Lined Wall

The recorded data is shown in Table B-I. The percent penalty void versus absolute overpressure ratio data plots are shown in Figure 29, reference Section VI, Mode II tests.

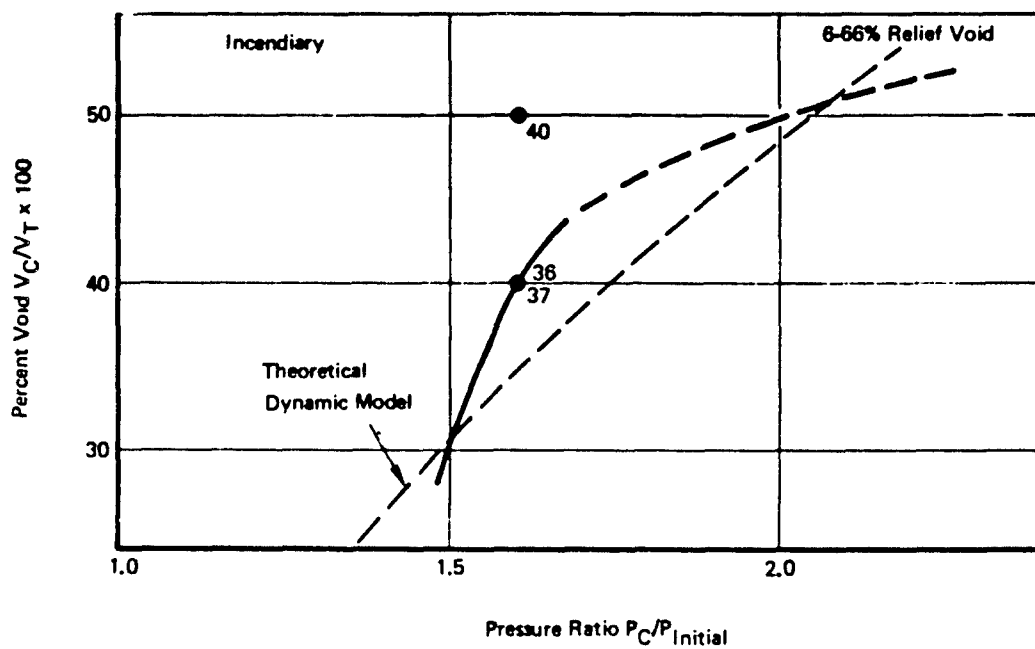
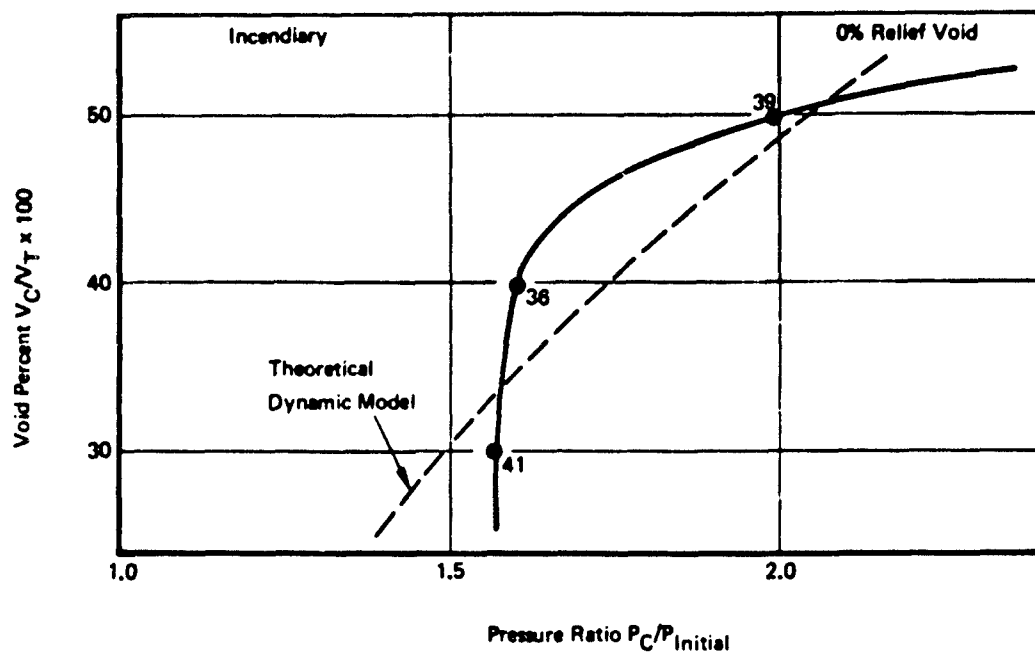


Figure 75: Percent Void Versus Pressure Ratio Data Plots,
Fuselage Tank (Top Wall and Voided Top Wall)

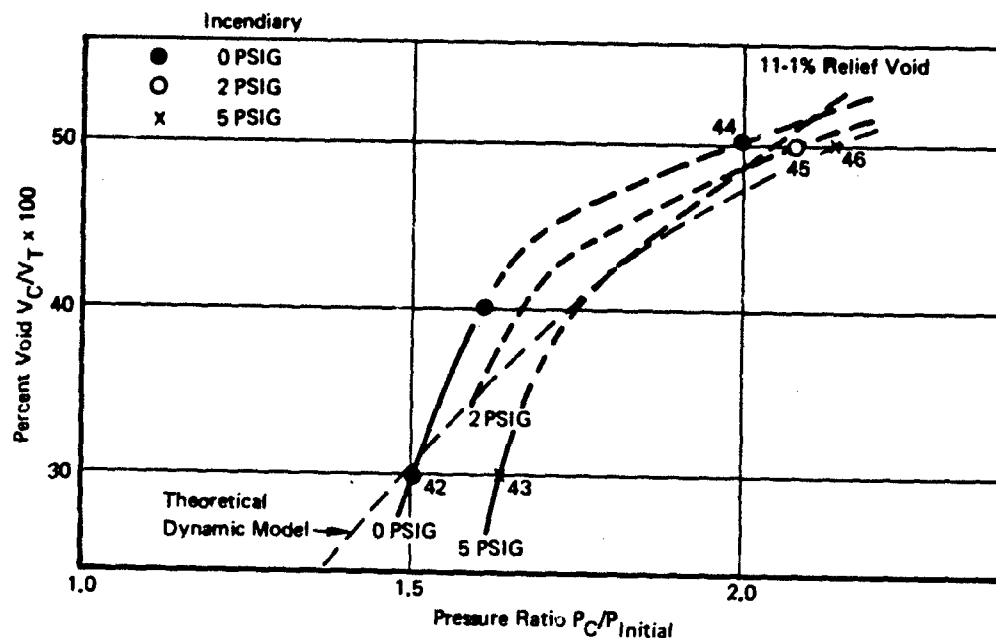
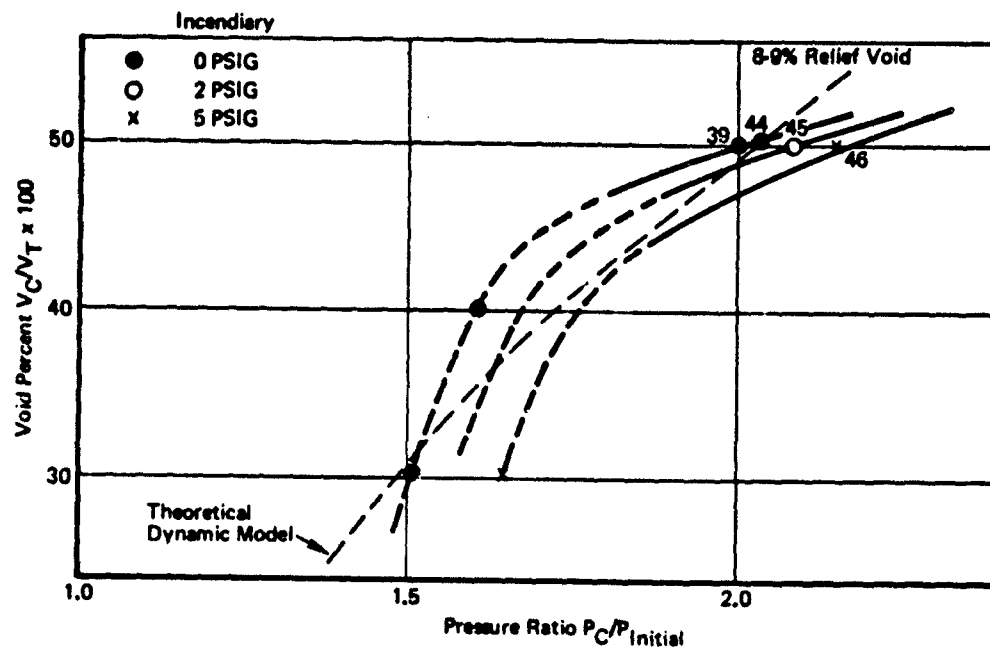


Figure 76: Percent Void Versus Pressure Ratio Data Plots,
Fuselage Tank (Voided Top Wall)

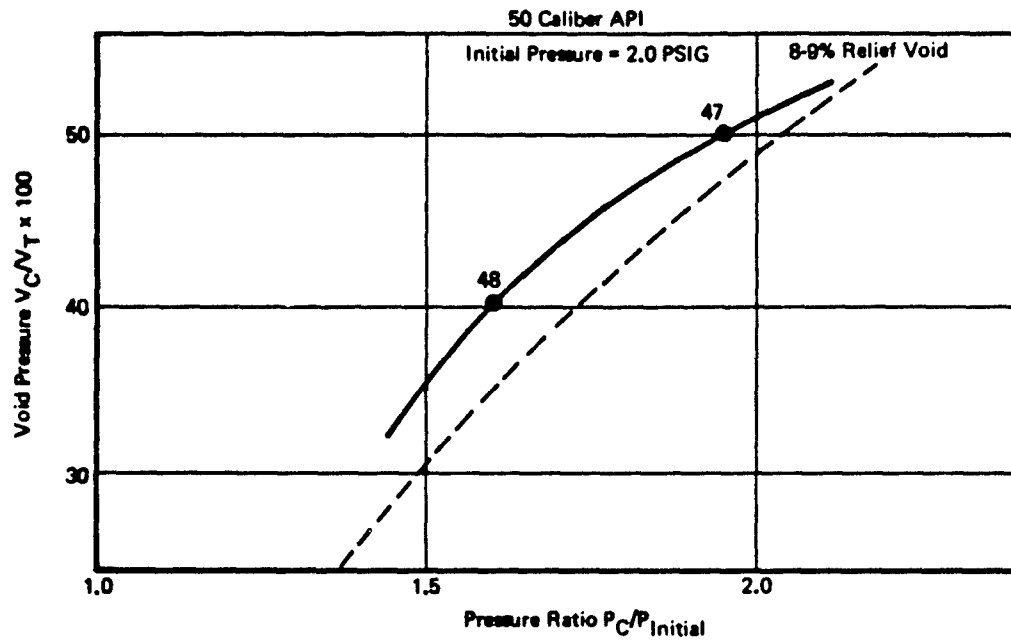


Figure 77: Percent Void Versus Pressure Ratio Data Plots,
Fuselage Tank (Voided Top 1/3 all)

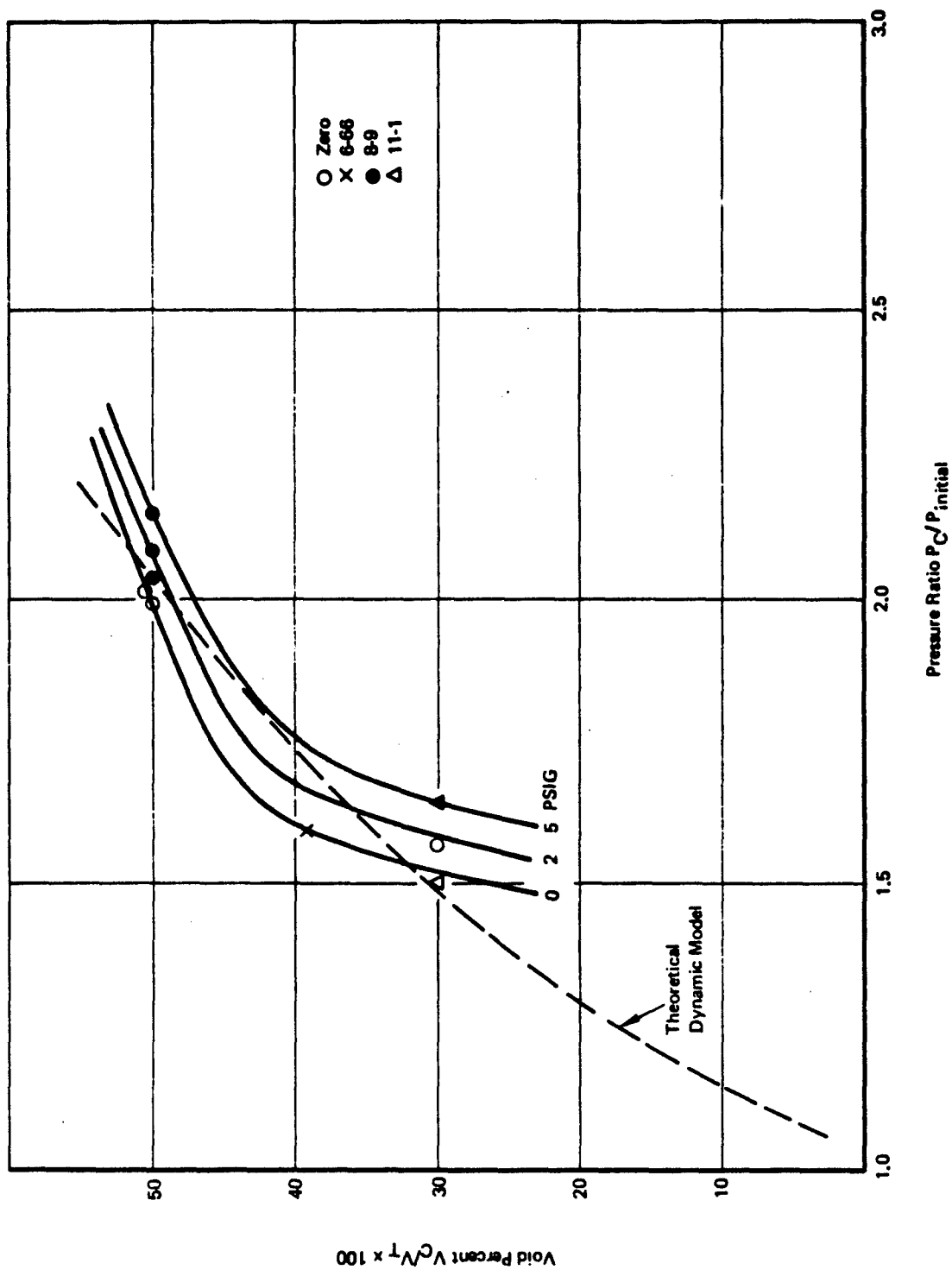


Figure 78: Percent Void Versus Pressure Ratio, Summary Data Plot, Fuselage Tank (Top Wall and Voided Top Wall)

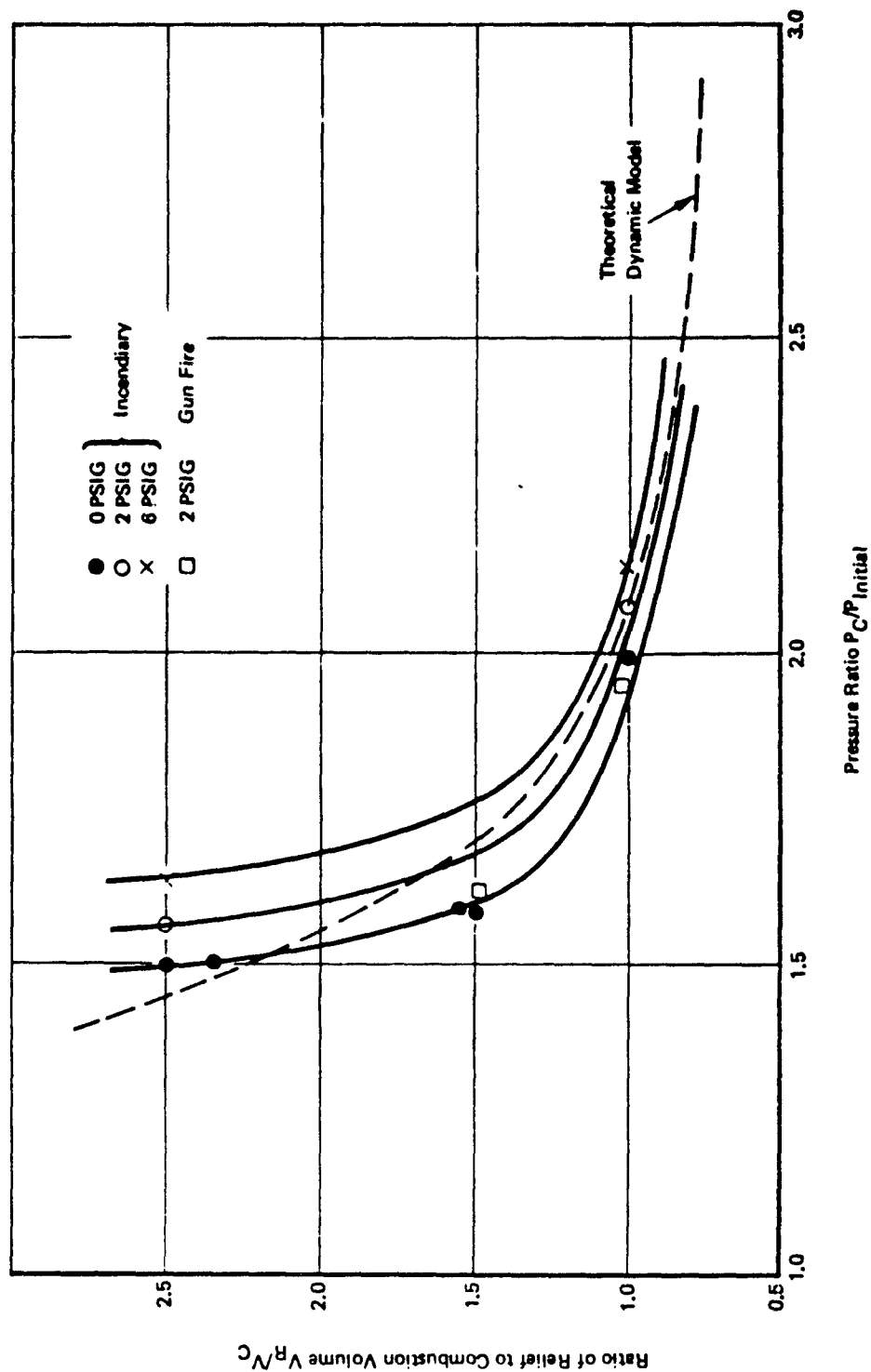


Figure 79: Relief to Combustion Volume Ratio Versus Pressure Ratio, Fuselage Tank (Top Wall and Voided Top Wall)

Note:-
The penalty void shown is based upon 10 PSIG overpressure.

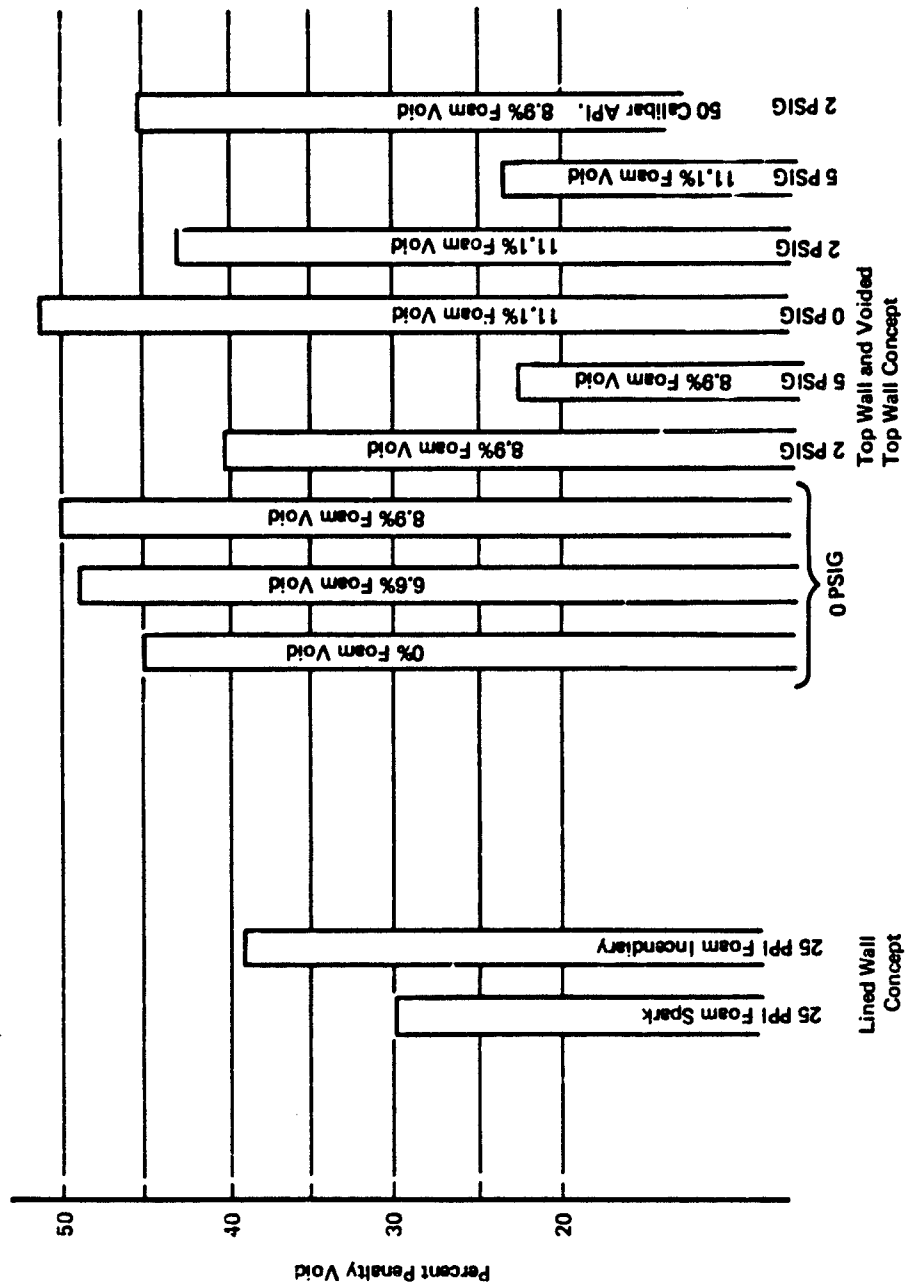


Figure 80: Fuselage Tank Data Summary

The largest percent void obtainable was 39% with incendiary ignition. The data show that when ignition is completed with a spark the percent void obtained is reduced to only 30%. This implies that with a lined wall concept a spark ignition results in higher overpressures than those resulting from an incendiary ignition.

6.1.2 Top Wall and Voided Top Wall

The top wall configuration data plots are shown in Figures 75 through 79. The correlation with the dynamic mathematical model data is not satisfactory, because the mathematical model pressure rise is coupled implicitly with pressure rise time. This rise time was assumed to be constant at 15 milliseconds for each test. Data traces, however, show large variations in the time of pressure rise, varying from 2 to 20 milliseconds for an incendiary ignition. A correlation of the ratio of relief and combustion volumes with absolute pressure is shown in Figure 79. A summary data plot showing the effect of increasing the initial pressure is shown in Figure 80.

It is noted that for all relief voids tested (up to 11.1%) no burn-through appeared, and the pressure rise was attributed to a zero relief voided top wall.

6.2 Small Wing Tank

The pressure rise data traces are shown in Figures B-8 through B-19. The configuration descriptions and combustion overpressure data are included as Table B-II. The relationships of penalty void with absolute overpressure ratio found by test are shown plotted in Figures 81 through 84.

A summary bar chart allowing assessment of each void concept with the others is shown in Figure 85.

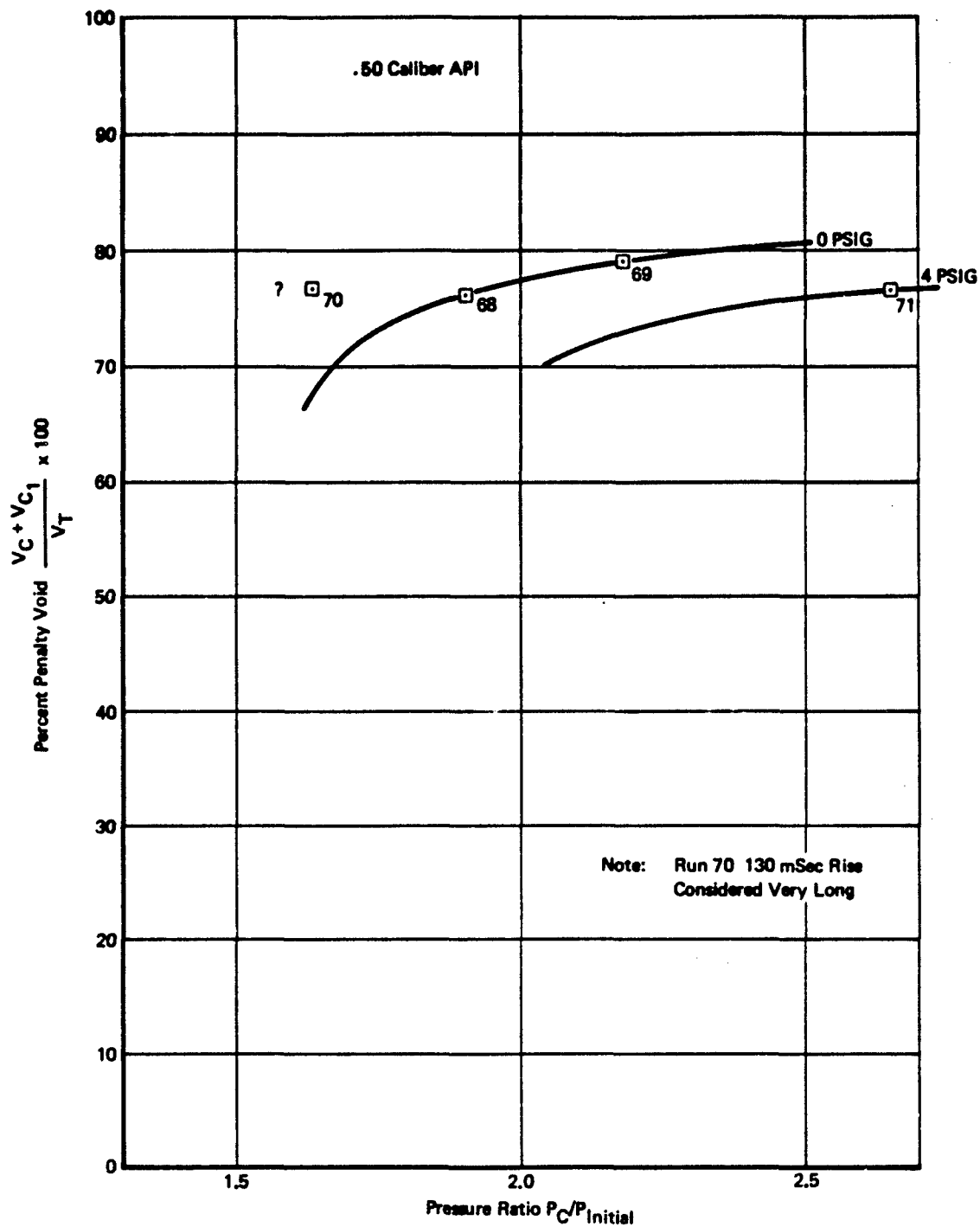


Figure 81: Percent Void Versus Pressure Ratio Proof Pressure Data Plots, Small Wing Tank (Voided Top Wall)

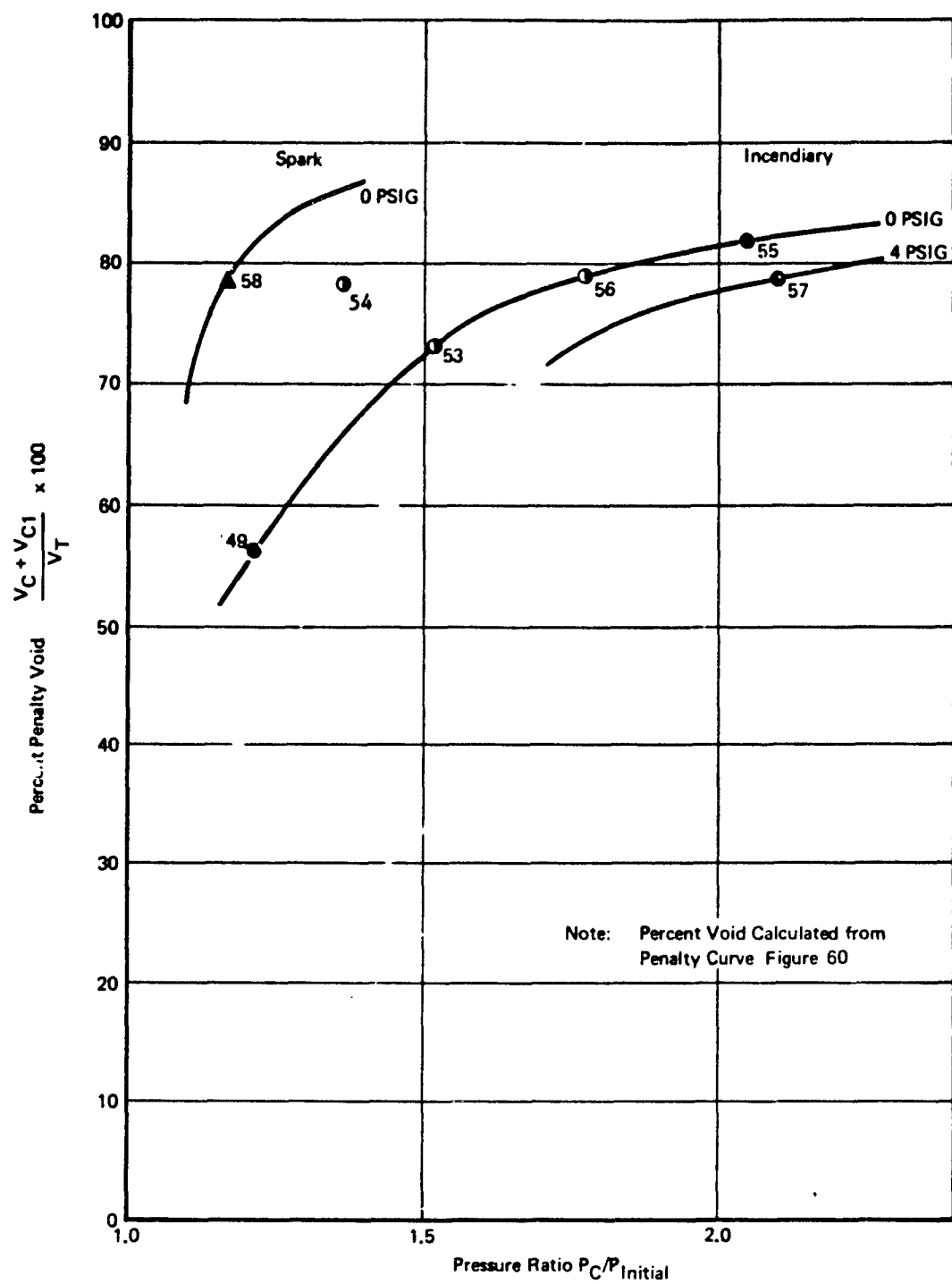


Figure 82: Percent Void Versus Pressure Ratio Data Plot, Small Wing Tank (Voided Top Wall)

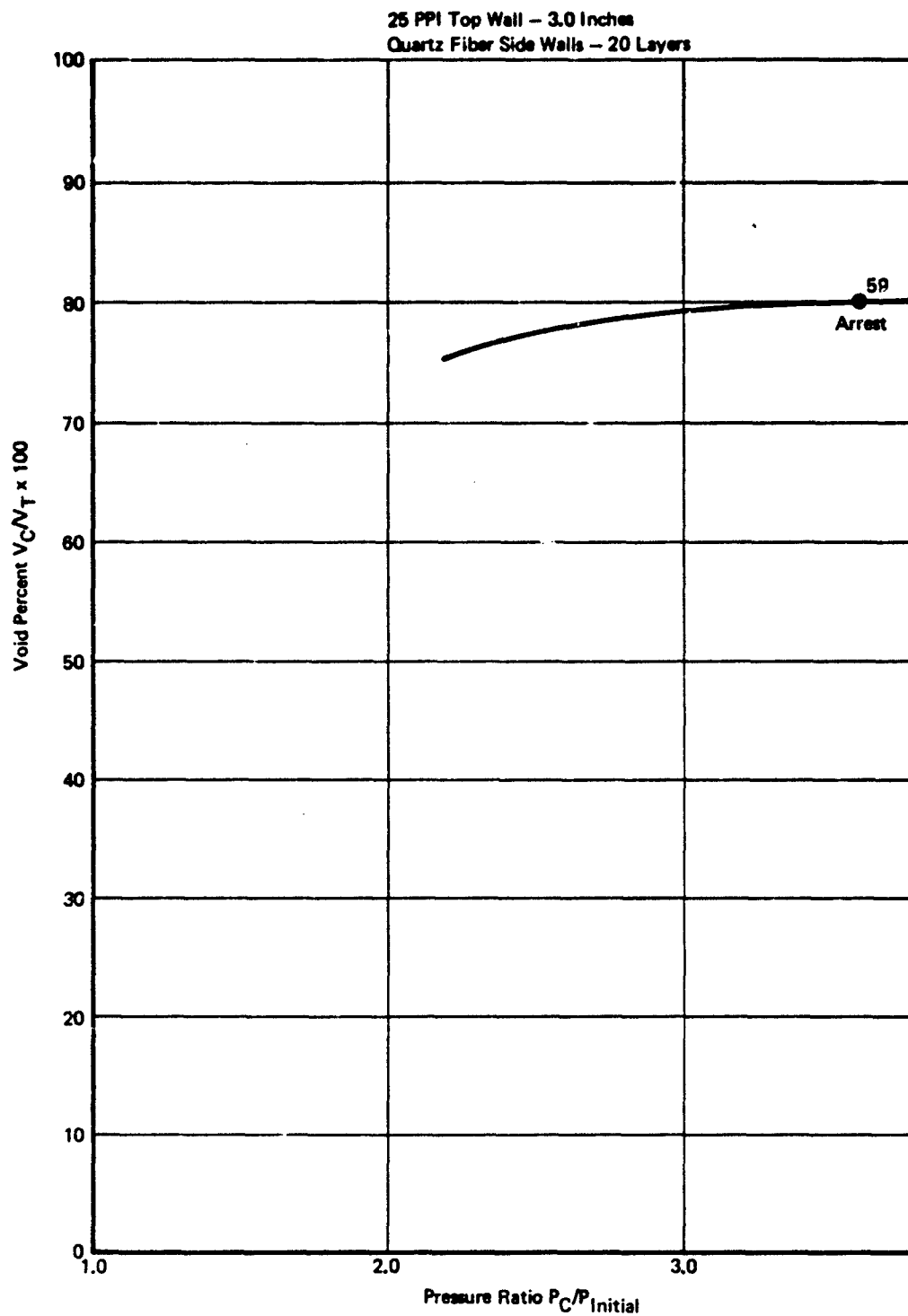


Figure 83: Percent Void Versus Pressure Ratio Data Plot, Small Wing Tank (Voided Top Wall)

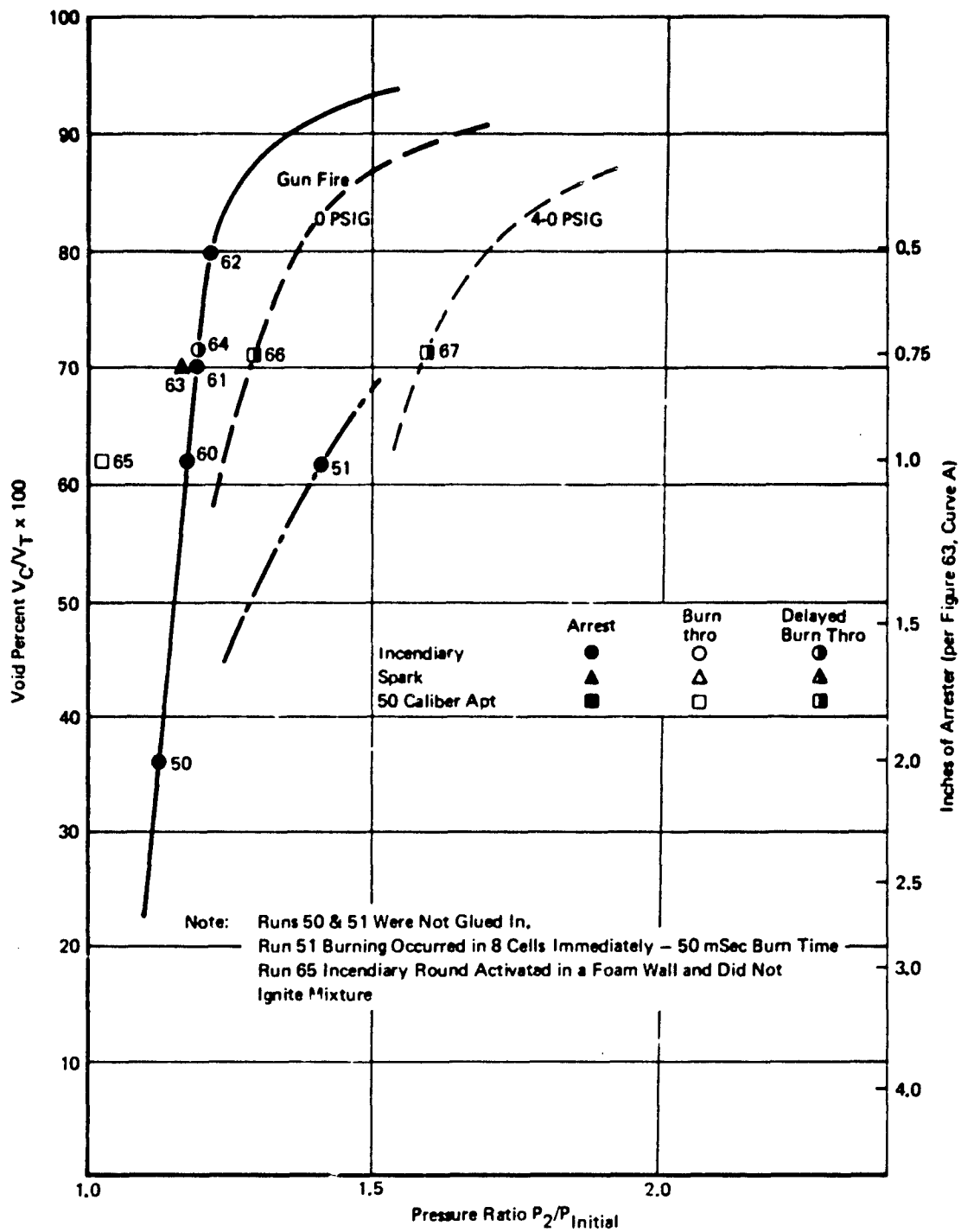


Figure 84: Percent Void Versus Pressure Ratio Summary Data Plot, Small Wing Tank (Egg Crate)

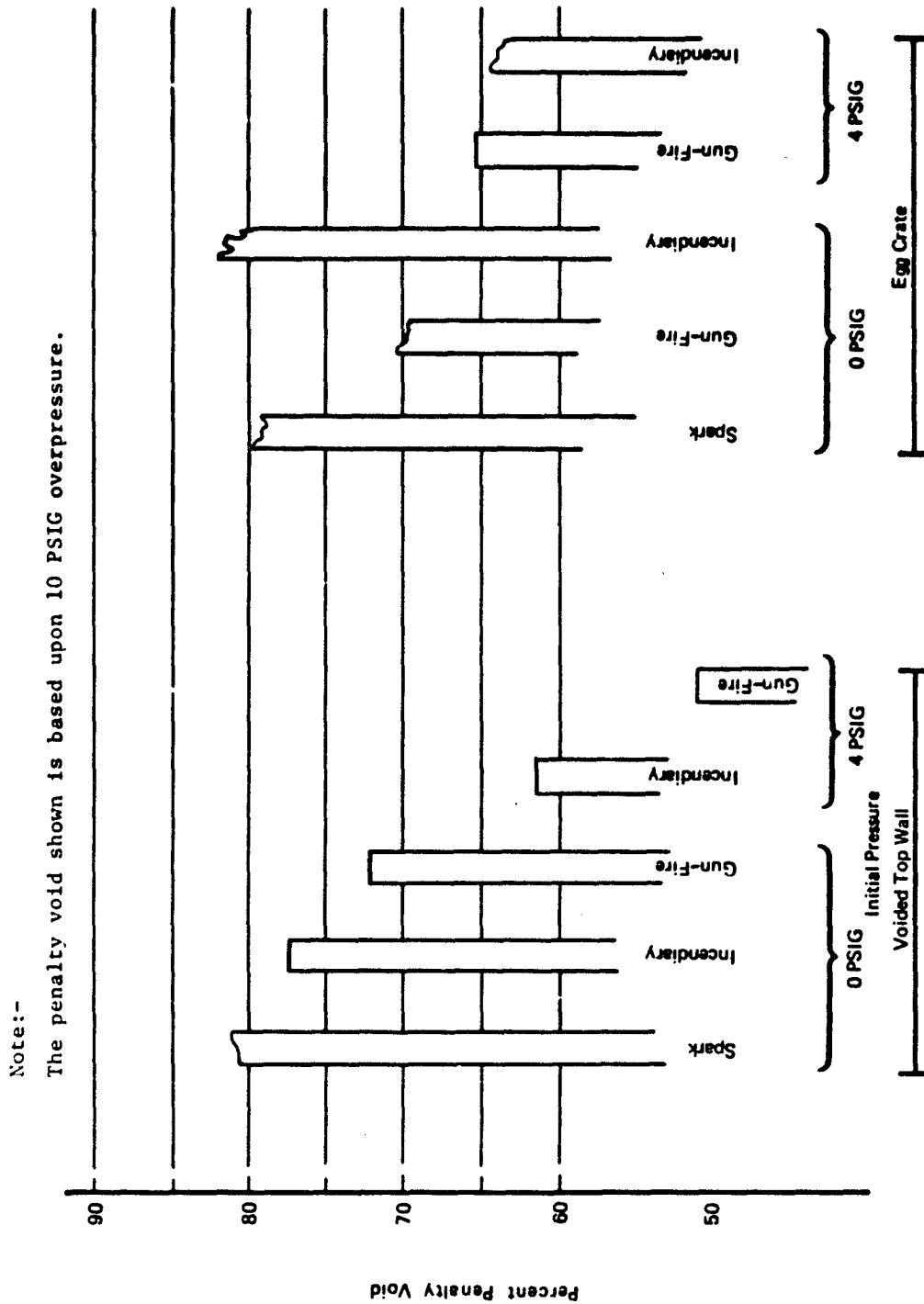


Figure 85: Small Wing Tank Data Summary

6.2.1 Voided Top Wall

All tests to date indicate that the top wall relief volume V_{c1} was not ignited. The foam thickness was reduced to a minimum of 1.0 inch during early tests and was then held constant for all further tests. This top wall sustained a black stain on the combustion side during all tests. The side walls were also blackened, and for all tests on materials less than 4.0 inches thick, the 25-ppi foam had sustained a "blow hole" at each rib-lightening hole. On the side walls that did not sustain a burn hole, a black stain was observed that permeated through the arrester directly in front of each hole.

Posttest photographs of the voided test wall for Runs 53 and 54 are shown in Figures B-20 and B-21.

It is not likely that burn-through occurs in the top void because of the immediate pressure communication created by the large surface area. The top wall black stain and/or burning is similar to and substantiates the data obtained during tests within the variable geometry apparatus, where it was shown that the arrester thickness required varied with the velocity of the flame attempting to propagate through. It was observed on conclusion of Run 52 with 2.0-inch top and side walls that the flame did not propagate into V_{c1} . However, the 2.65-inch-diameter relief holes allowed the low combustion pressure of 5.7 psig to carry the flame into the adjacent cells. The 25-ppi foam was burnt completely away, leaving a 1-1/2- to 2.0-inch diameter hole right through 4.0-inch-thick side walls.

All data traces are included for reference in Figures B-8 through B-14. Summary data plots relating to percent void with pressure ratio are shown in Figures 81 through 83.

6.2.2 Egg Crate Configuration

For all egg crate tests, holes were burned through the side walls at each 2.65-inch-diameter relief hole. Except for two tests, there was secondary ignition in the other wing cells. When there was no ignition, the pressure record was that generally expected for the percent void in each of the adjacent cells. Pressure communication was immediate for each trace, requiring 150 to 400 milliseconds to peak.

The pressure traces of each percent voiding tested are shown in Figures B-15 through B-19. The test results showed that increasing the percent void did not substantially increase the initial absolute pressure ratio. The data are shown in Figure 84.

These results are accounted for by the flame front created by incendiary and/or spark ignition: it was contained within the center volumes of the egg crate. It is noted that for all tests, two 3.0-inch diameter holes in the walls of the center egg crate allowed communication into the two adjacent cells. It was intended to reproduce gunfire ignition by setting off three voids in a direct line.

It is worthy of comment, however, that in all cases evidence of burning was apparent in all nine cells; a blackened stain permeated the foam in all areas. This blackening could have been caused by hot incendiary particles and/or hot reacted gases. These gases (as reported earlier here) expanding through foam barriers effectively locally inert the adjacent propane/air mixture during the life time of the ignition source. The pressures recorded are those resulting from the ignition of a very small percentage of the gas within the combustible volume.

Posttest photographs of the 3/4-inch and 1/2-inch wall thickness egg crate per Runs 61 and 62 are shown in Figure B-22.

This assumption is verified by the results obtained during Mode IB testing within the variable geometry apparatus. It was shown that maximum pressure

rise within the combustion volumes with a relatively large relief area (53%) was a function of the combustion volume. The influencing parameters on pressure rise for small combustion volumes were noted as follows, notwithstanding the restricting effect of the orifice (A_R):

Large Relief Area ($A_R = 53\%$)

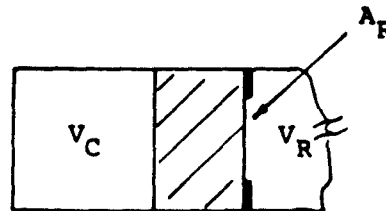
Major relief area (A_R)

Minor arrester volume

Small Relief Area ($A_R = 10\%$)

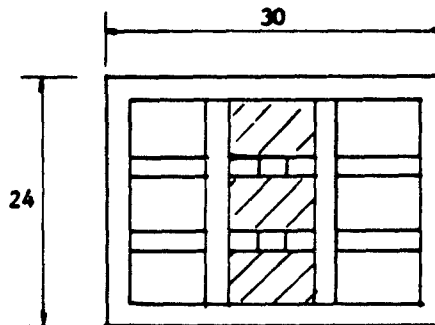
Major arrester volume

Minor relief area (A_R)



This is attributed to the overwhelming effect of an incendiary ignition in a relatively small volume.

The three center voids result in a total maximum combustible volume for the maximum void tested 80% (0.5 inch foam thickness) as follows:



$$\frac{[30 - (0.5 \times 4)] \times [24 - (0.5 \times 4)]}{3 \times 1728} \text{ft}^3 = 0.119 \text{ft}^3$$

This is a very small volume and, provided the fire is contained within this volume, all other volumes will not be ignited during the short duration that the ignition source is active. High-speed movies show this to be approximately 5 to 10 milliseconds.

6.3 Large Wing Tank

The pressure rise data traces are shown in Figures B-23 through B-33. The configuration description and combustion over-pressure data are included as Table B-III.

The relationship of penalty void with absolute over-pressure ratio found by test are shown plotted in Figures 86 and 87.

A summary bar chart allowing assessment of each void concept with the others is shown in Figure 88.

6.3.1 Lined Wall Configuration

The pressure traces of each percent voiding tested are shown in Figures B-23 through B-26. The data is plotted as percent void versus absolute pressure ratio in Figure 86.

Following Runs 72, 73, and 73A, no visual evidence of burn-through was found. The pressure traces indicated that the secondary ignition could be the result of pressure decay, allowing propane mixture to reverse-flow back into the combustion cell where reignition occurred.

The foam was not severely damaged during Runs 74 and 75, although posttest examination showed that the upper surface had dislodged and possibly allowed the flame to propagate into the center cell.

Posttest examination following Run 77 showed the usual black stain had permeated through two layers of 1.0-inch-thick foam. It was observed that no hole was burnt into or through the foam, but, again, a secondary fire was initiated in the center cell after 1,450 seconds. This was apparent from the sizzled state of the foam in the center cell and the resulting pressure rise of 9.5 psi recorded on the data trace. Again ignition energy of some kind (hot, expanding gases, flame passing through the foam, etc.) passed through the foam and ignited the center cell without damaging the arrester.

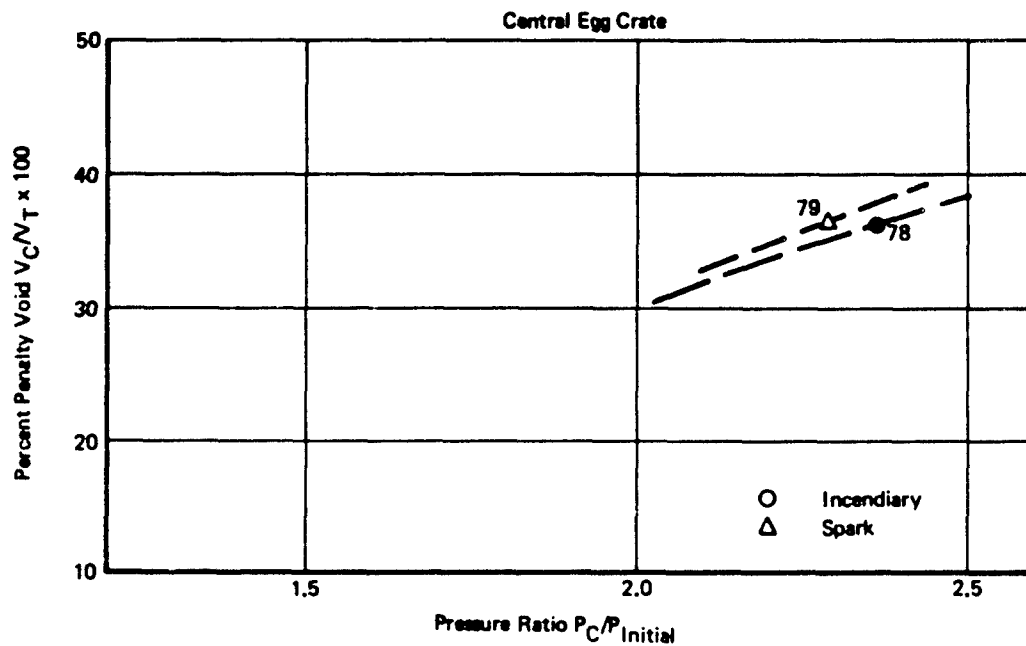
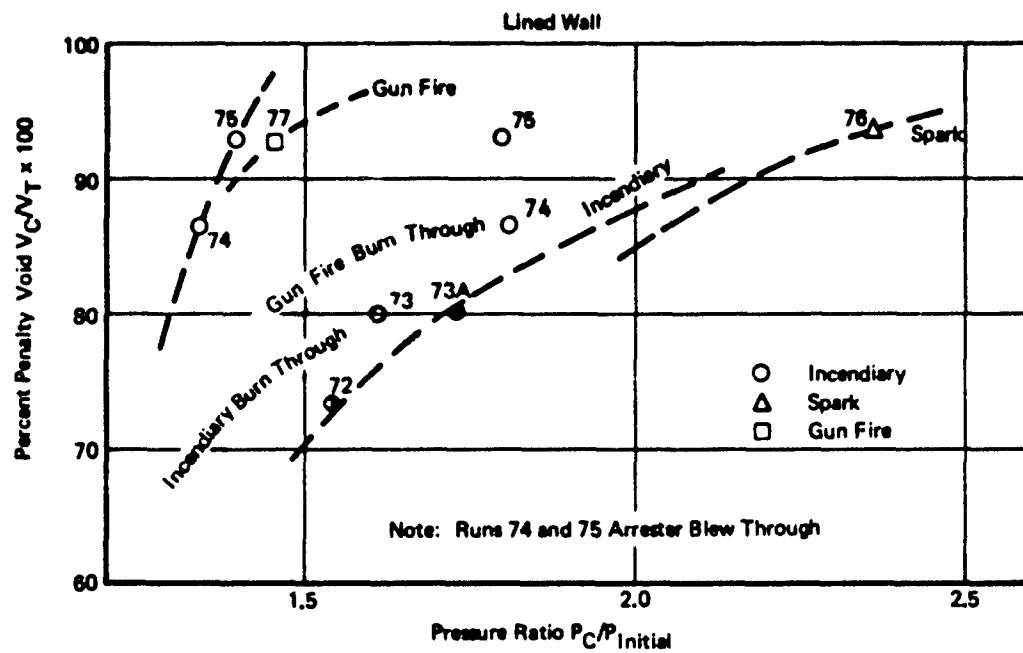


Figure 86: Percent Void Versus Pressure Ratio Summary Data Plot (Large Wing Tank)

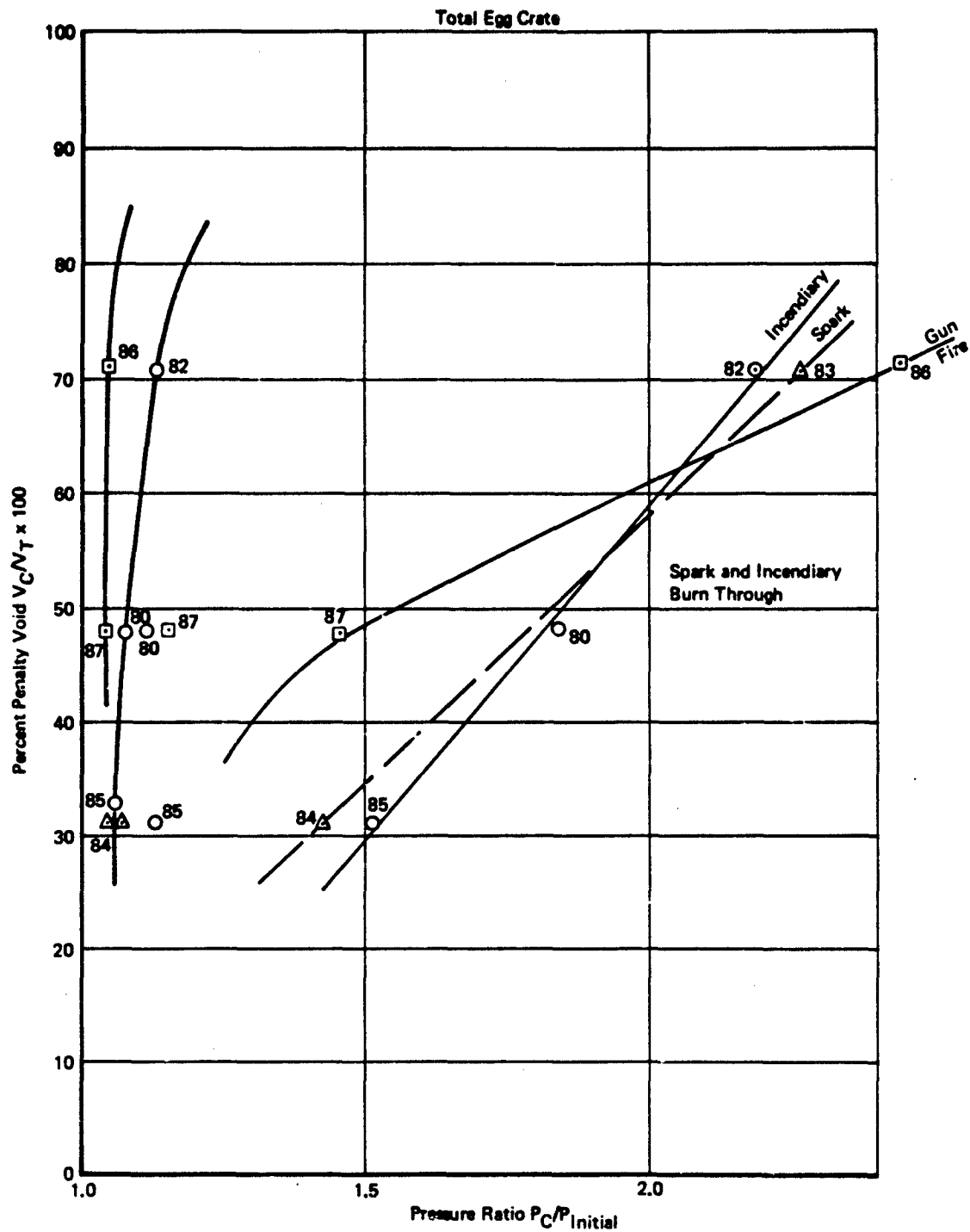


Figure 87: Percent Void Versus Pressure Ratio Summary Data Plot Large Wing Tank

Note:-
The penalty void shown is based upon 10 PSIG overpressure.

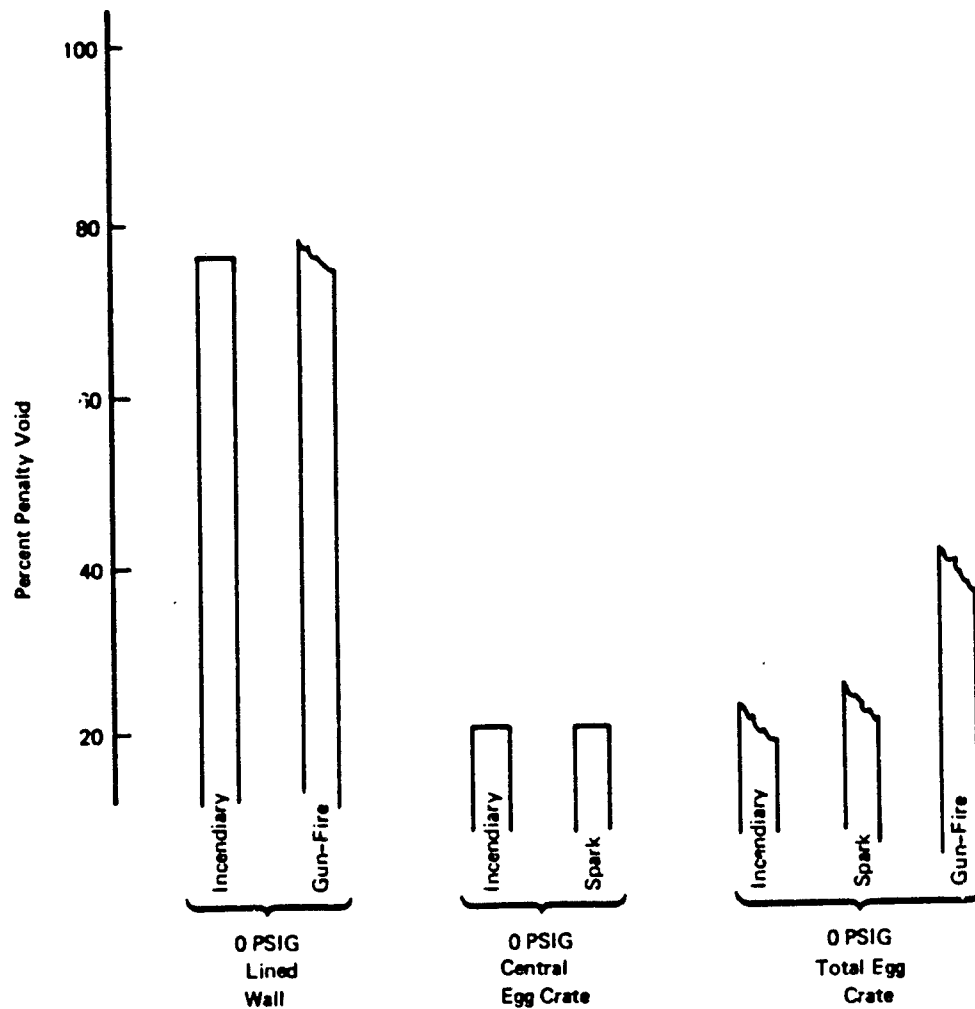


Figure 88: Large Wing Tank Data Summary

The configuration description and combustion over-pressure data are included as Table B-III.

6.3.2 Central Egg Crate

Only two tests were completed with this assembly, one with a spark and one with incendiary ignition. The pressure traces are shown in Figure B-27. The data is plotted as percent penalty void versus absolute pressure ratio in Figure 86.

The configuration description and combustion over-pressure data are included as Table B-III.

Over-pressures 20.2 and 17.2 psi were excessive. The pressure drop across the total central egg crate during Run 78 with the incendiary ignition resulted in the complete assembly's being partially rammed into Cell 3. It is noted that for both tests the total assembly was not glued into the center cell.

6.3.3 Total Egg Crate

The pressure traces are shown in Figures B-28 through B-33. The data are plotted as percent penalty void versus absolute pressure ratio in Figure 66. The configuration description and combustion over-pressure data are included as Table B-III.

The results are similar to those obtained during the small wing tank egg crate tests. Three distinct pressure rises were seen on the traces, with apparent burn-through into the other cells. The incendiary and spark ignition do not produce the usual large over-pressure differences. Voiding possibilities appear to be commensurate with those of the lined wall concept.

Ignition was allowed in two of the lower cells simultaneously by cutting a hole in the dividing wall, allowing the incendiary to activate equally into both cells.

7.0 CONCLUSIONS AND RECOMMENDATIONS

During the initial check tests with the small wing and large wing tank configuration, problems were encountered with the GFE equipment. It was not possible to get a vacuum tight tankage because of the non-machined surfaces, cork gaskets, and 456 nuts and bolts. Leakage between each dividing plate had to be sealed. In addition, some nuts that were welded in place to facilitate easy assembly were stripped of their threads and had to be replaced.

In all small wing tank configurations with an approximate total relief area of 5%, up to 4.0 inches of foam was required to stop the flame/fire from passing into the next bay. Thicknesses less than this resulted in a hole burnt through.

Tests within the large wing tank with an approximate total relief area of 55% required only 2.0 inches of foam to achieve arrest with an incendiary igniter. Thickness less than this either burnt through allowing flame communication, or burnt through by other mechanism that created a blackened stain in its passage through. It was noticed that immediate burn-through occurred rarely, and generally pressure equalization had to occur before flame passage was allowed. This phenomenon is similar to that described in Mode IB variable geometry tests.

The results of all Task II work have shown that:

- Flame speed at the time and place of arrest is an important parameter.
- Material burning contributes to arresting characteristics of foams and felts.
- Combustion volume affects the thickness of arrester required to arrest a flame front.
- The ignition source directly affects the pressure rise time within a combustion volume.
- Differences in rise time contribute to varying gas mass flow rates through an arrester.
- The arrester cross-section area and total relief area affect the velocity of expanding burnt and unburnt gases, contributing to changing arrester characteristics.

The voiding concepts recommended for testing in Task 3 are as follows:

- Fuselage Tankage
 - Voided Top Wall
 - Voided Lined Wall
- Small Wing Tankage
 - Egg Crate
 - Voided Top Wall
- Large Wing Tankage
 - Lined Wall

SECTION X

TASK III TEST PROGRAM

1.0 MATERIAL DESCRIPTION

The arrester materials and combinations of materials tested at various thickness during the test program are listed as follows for each configuration:

Fuselage Tankage

- 3M Scotch Brite felt
- 25-ppi foam and 10 layers of quartz fiber type 594 on the explosion face
- 25-ppi foam and 10 layers of quartz fiber backed with two layers of 20 mesh-016 stainless steel screen on the explosion face

Small Wing Tankage

- 25-ppi foam with 10 layers of quartz fiber type 594 on the explosion face
- 3M Scotch Brite felt
- 25-ppi foam and two layers of stainless steel screen on the explosion face

Large Wing Tankage

- 25-ppi foam with ten layers of quartz fiber type 594 on the explosion face
- 3M Scotch Brite felt
- 2 layers of 20 mesh-016 stainless steel screen with ten layers of quartz fiber type 594

2.0 TEST CONFIGURATION

2.1 General

Except for the voided lined wall, the geometries of all configurations and voiding concepts are identical to those assembled for use in Task II. These configurations are described in Section IX, paragraph 2.0.

2.2 Voided Lined Wall

The ten layers of quartz fiber type 594 material was supported and centrally located within the fuselage tankage by 25-ppi foam. The supporting foam was voided by cutting a 10-inch square section from each of the six precut segments as follows:

$$\text{Relief Void} = \sum_{1}^6 V_c = 6 \times 10 \times 10 \times x = 600 x \text{ in.}^3$$

$$\text{Combustion Volume} = V_c = (30 - 2x)(30 - 2x)(24 - 2x)$$

$$V_c = 21600 - 4680x + 336x^2 - 8x^3$$

$$\text{Total Volume} = V_T = 24 \times 30 \times 30 = 21,600 \text{ in.}^3$$

$$\text{Relief Volume} = V_T - V_c = V_R$$

$$V_R = 4680x - 336x^2 + 8x^3$$

$$\text{Percent Relief Void} = \frac{\sum_{1}^6 V_c \times 100}{V_R} = \frac{600 \times 100}{4680 - 336x + 8x^2}$$

$$\text{Percent penalty void} = \frac{\frac{216}{(V_c + \sum_{1}^6 V_c)} \times 100}{V_T}$$

$$= \frac{[(21600 - 4680x + 336x^2 - 8x^3) + 600x]}{21,600} 100$$

Variations of percent penalty and percent relief void for changes in the dimension of χ are shown in Figure 89.

3.0 INSTRUMENTATION

The instrumentation was identical to that utilized for Task II, and is described in Section IX Paragraph 3.0.

4.0 IGNITION SYSTEMS

The test ignition systems were identical to those described in Section IX, Paragraph 4.0.

5.0 TEST PROCEDURE

The test procedure was identical to that described in Section IX, Paragraph 5.0.

6.0 RESULTS AND DISCUSSION OF RESULTS

A test matrix describing the total Task III test program, relating materials and combination of materials tested within each voiding concept is as follows:

Fuselage Tankage

Voided Top Wall

- 3M Scotch Brite
- 25-ppi foam and quartz fiber
- 25-ppi foam and quartz fiber supported by stainless steel screen

Voided Lined Wall

- 25-ppi foam and quartz fiber
- 3M Scotch Brite

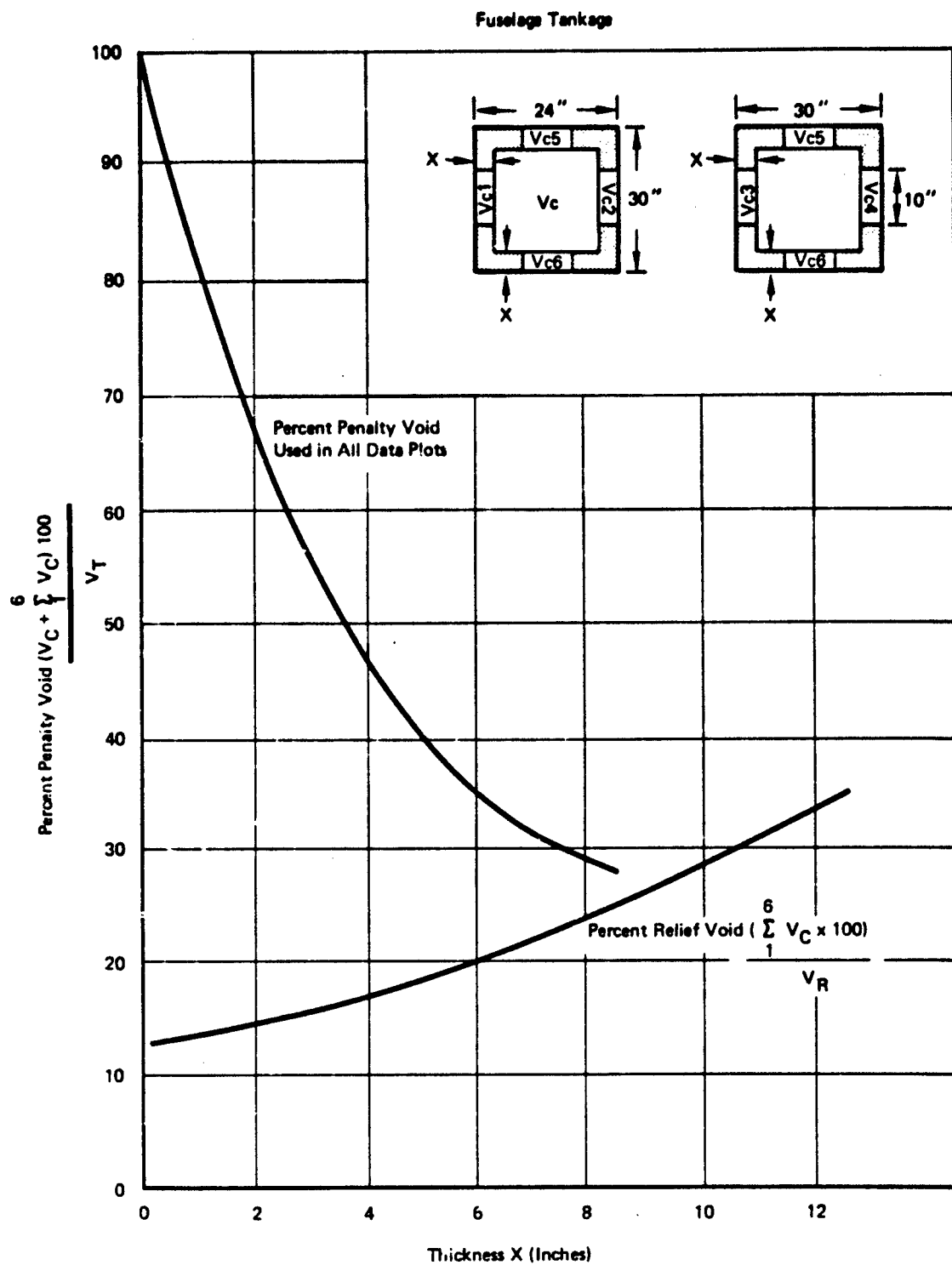


Figure 89: Variations of Percent Void and V_R/V_C With Arrestor Thickness (Voided Lined Wall)

Small Wing Tankage

Egg Crate

- 3M Scotch Brite

Voided Top Wall

- 3M Scotch Brite
- 25-ppi foam and quartz fiber
- 25 ppi foam and stainless steel screen

Large Wing Tankage

Lined Wall

- 3M Scotch Brite
- 25-ppi foam and quartz fiber
- quartz fiber and stainless steel screen

The test program was conducted in a similar manner to that undertaken in Section VI and Section IX. The initial test void condition was determined using relief to combustion ratio versus overpressure as predicted from the mathematical model. Further tests with increases in the percent void were each determined from the data obtained and plotted during the preceding tests. Testing was centered upon obtaining data relating to the defined pressure rise criteria of 10 psi.

The data is presented in tabular and graphical form with a summary bar chart for each tankage.

The tabulated data summarizes pertinent data for each test conducted and is extracted directly from the detailed test data sheets. Included in the data is a direct copy of all pressure rise data traces taken for each test condition. Each trace records an arrest or a burn-through, the ignition mode, and the pressure rise as a function of time.

The relationship of percent penalty void to absolute pressure ratio is graphically shown for each test.

The percent penalty void relates the total void in each tankage to the volume of the total tankage.

The volume of arrester material installed within each tankage is given as:

Arrester volume (percent) = 100 - percent penalty void.

This parameter allows direct correlation of all test data to a system penalty for a particular voiding concept.

Each void configuration was initially standardized as in Task II, Section IX, such that its application in any cell of each configuration would not affect the total penalty void of each tankage.

In all tests the intent was to obtain sufficient data to allow a determination to be made of relative performance of each concept.

The concluding bar charts allow an immediate voiding assessment of each concept relative to each other.

6.1 Fuselage Tankage Configuration

The pressure rise data traces are shown in Figures C-1 through C-17.

The configuration description and combustion overpressure summary data are included as Table C-1. The relationship of penalty void with absolute overpressure ratio found by test are shown in Figures 90 through 93.

A summary bar chart allowing assessment of each void concept with each other is shown in Figure 94.

6.1.1 Voided Top Wall

The effect of rise time on the final overpressure is shown in Figure C-1.

The relief void was increased from 8.9% run 100 to 11.1% run 101 and produced

25 PPI Foam and 10 Layers of Quart. Fiber Type 594.

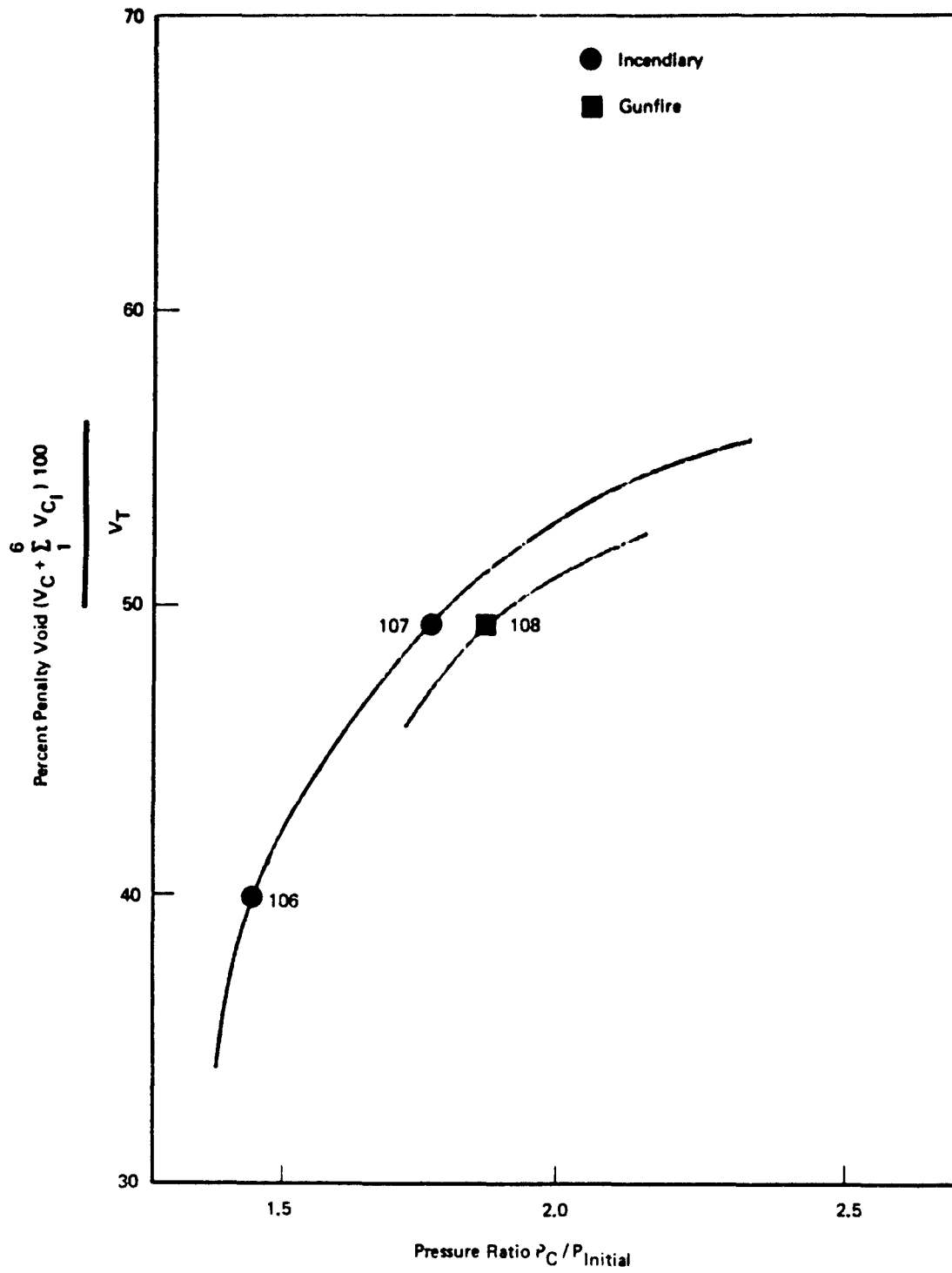


Figure 90: Percent Void Versus Pressure Ratio Summary Data Plot
Fuselage Tank (Voided Lined Wall)

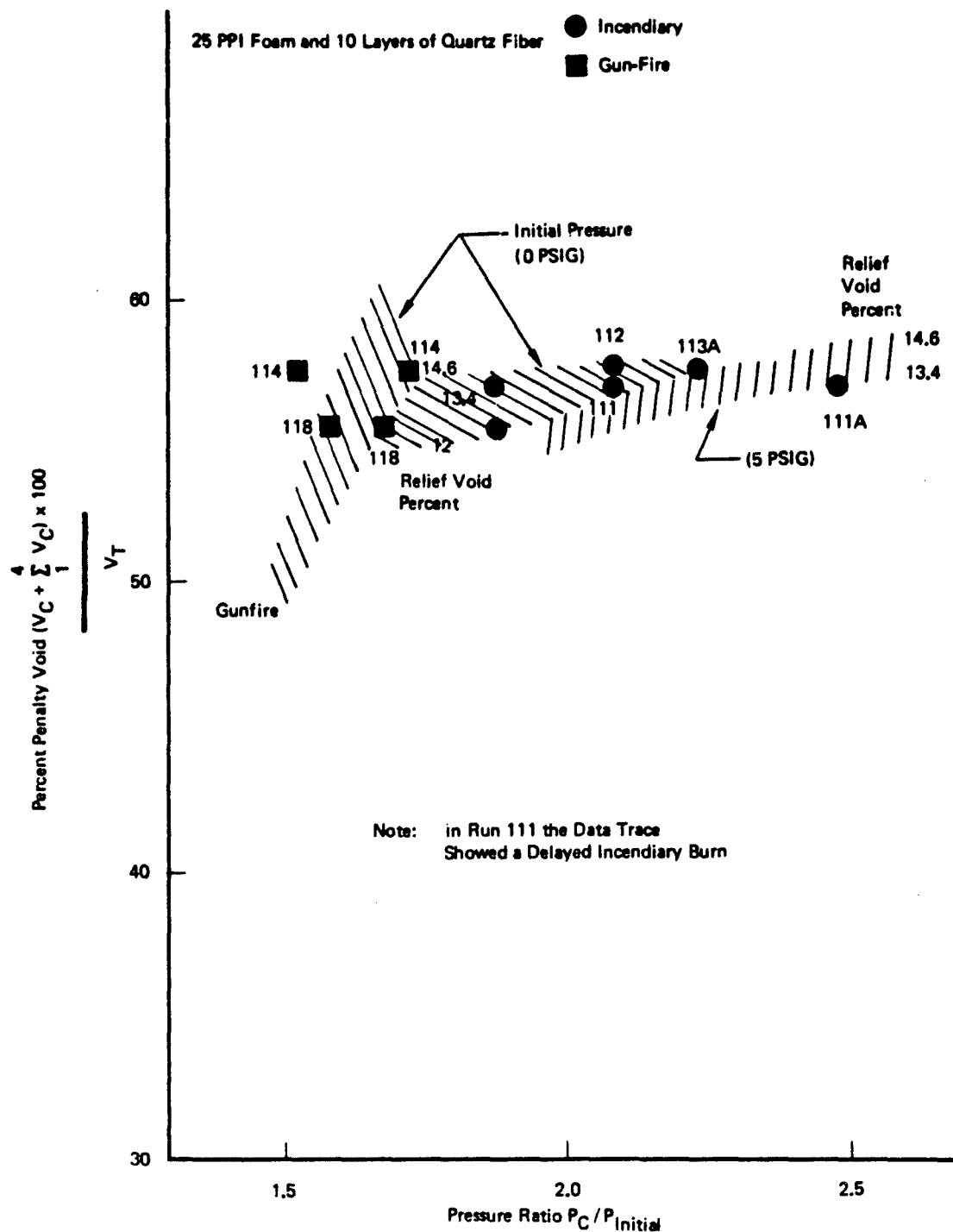


Figure 91: Percent Void Versus Pressure Ratio Summary Data Plot
Fuselage Tank Voided Top Wall

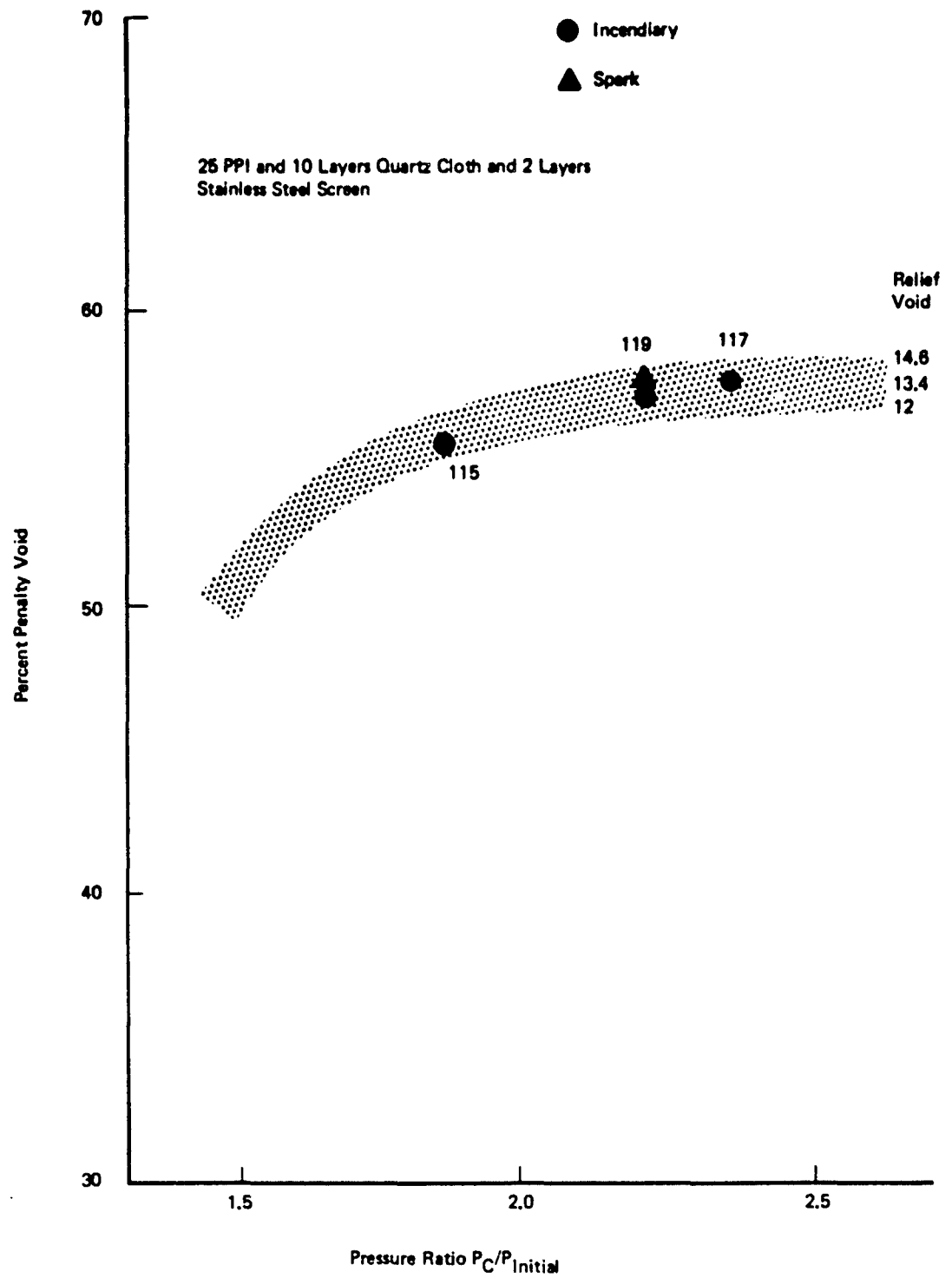


Figure 92: Summary Data Plot Fuselage Tank, Voided Top Wall

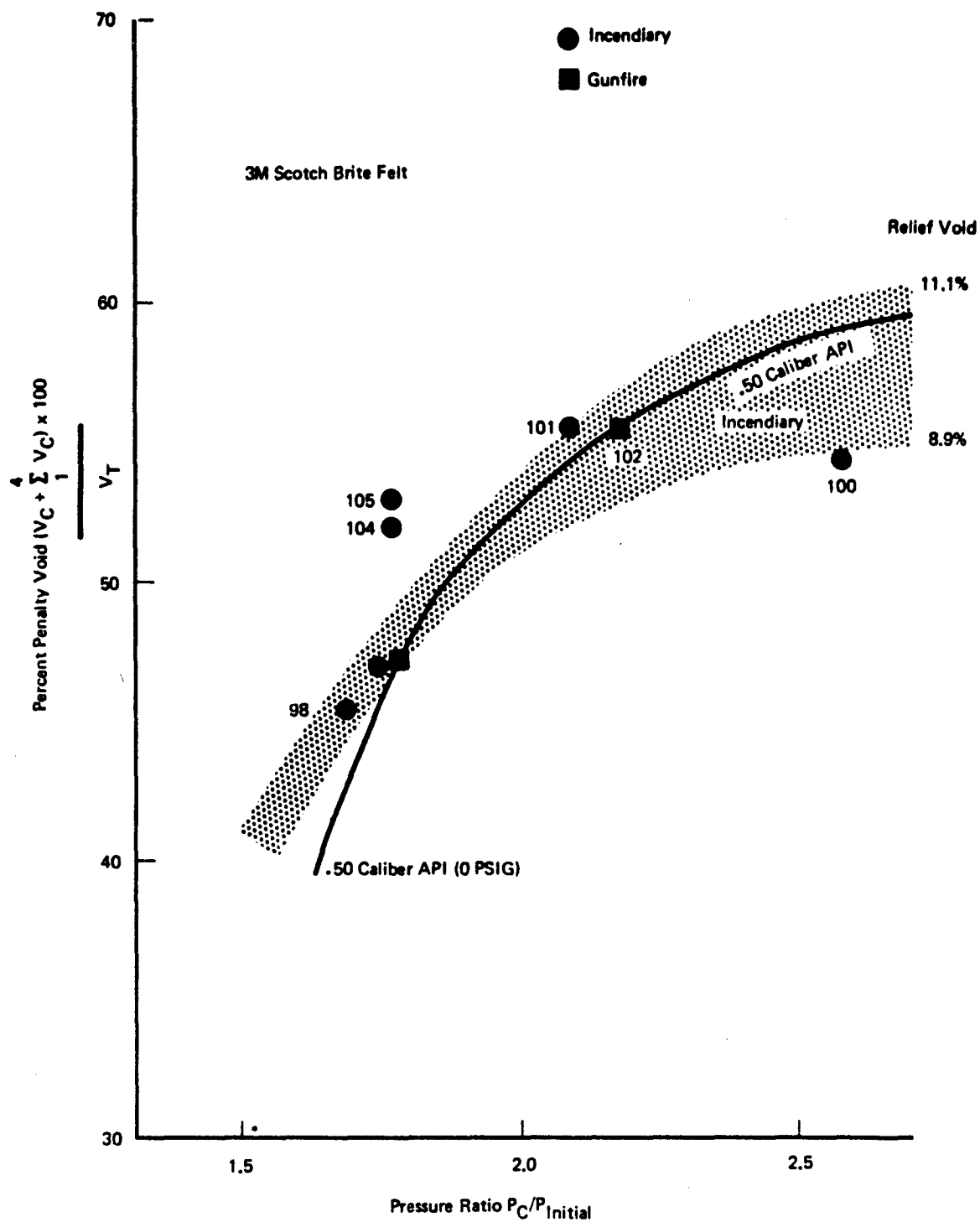


Figure 93: Percent Void Versus Pressure Ratio Summary Data Plot
Fuselage Tank (Voided Top Wall)

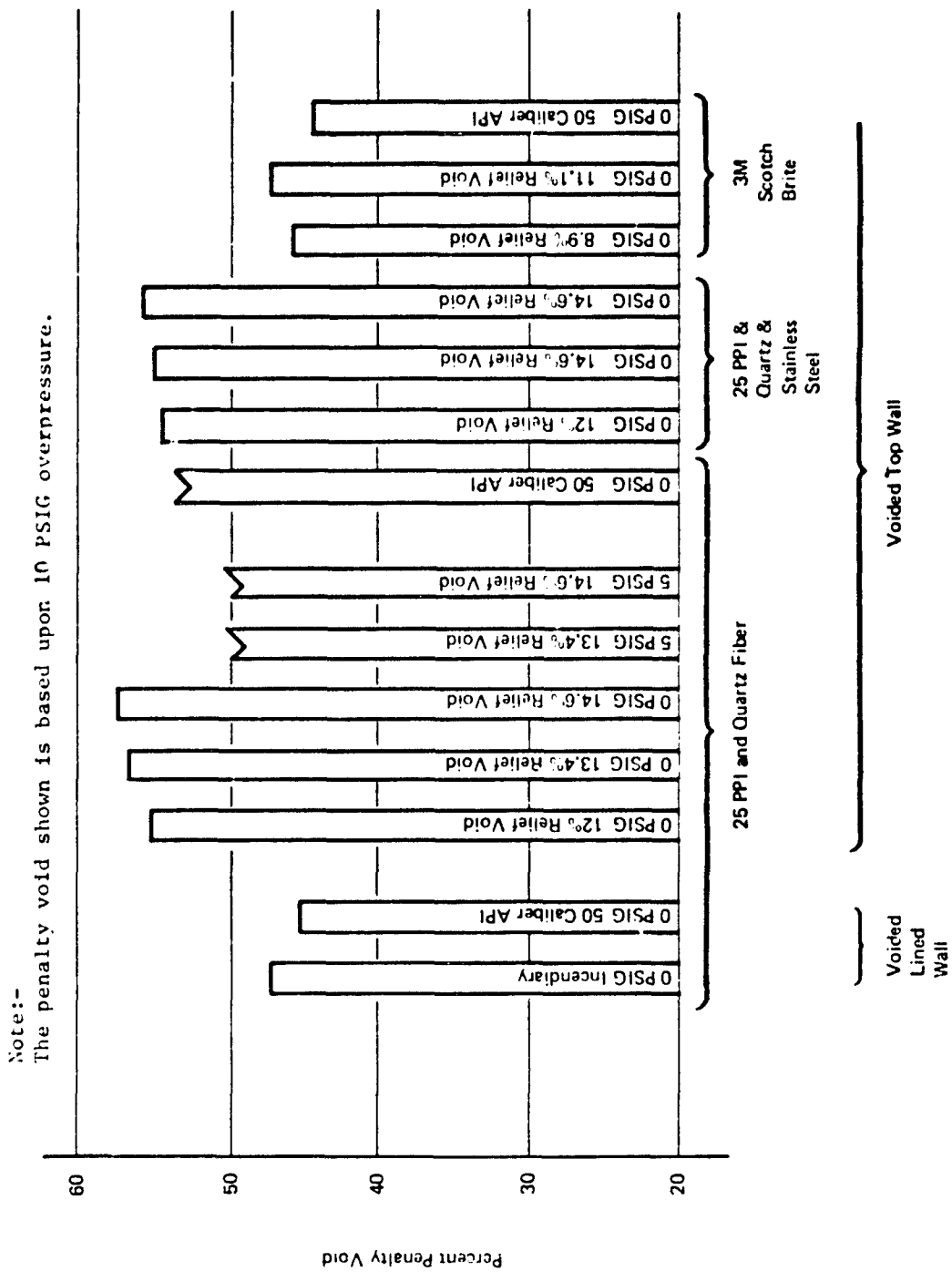


Figure 94: Fuselage Tank Data Summary

a longer pressure rise time and a correspondingly lower final pressure. This decrease in overpressure is related directly to a decrease in the arrester thickness allowing pressure communication from the combustion volume into each relief void. This thickness reduced from 4.0 inches for the 8.9 relief void to 2.6 inches for the 11.1 relief void. The change in overpressure rise time could be attributed to the decrease in the pressure drop of the arrester material into each void volume. It is noted, however, that a repeat test with the 11.1 percent relief void using a .50 caliber API as an ignition source, run 101, was successful in reducing the pressure rise time and increasing the maximum pressure to that attained early with the incendiary ignition run 100, shown in Figure C-2.

A low magnitude secondary burn is indicated in nearly all the test conditions indicative of the propane-air mixture being reignited as the pressure decay allowed unreacted gas to expand from the top wall into the combustion volume. This secondary burn occurred generally 100 to 150 milliseconds after ignition. Damage to the arrester material did not occur, although in all tests the upper surface was scorched and deeply blackened.

Post-test examination of the 25-ppi foam arrester protected by two layers of 20-mesh stainless steel screens showed that in run 117 the screen was badly blackened and damaged. In run 115 and 116 the flame and/or fire had not burned into each void area, but the overpressures in a 57% penalty void were excessive at 18 and 20 psi, as shown in runs 116, 117 and 118 shown in Figures C13, C14 and C16.

The tests conducted with the 3M Scotch Brite material resulted in the higher pressure rises being obtained and producing, as a consequence, low voiding percentages (Figure 93). Variations in overpressure for changes in arrester material were generally not noteworthy in magnitude as shown in the summary data plot (Figure 94).

6.1.2 Voided Lined Wall

The results of tests with the quartz fiber type 594 are shown in Figures C16 and C17. Increasing the combustion volume from penalty void of 40%, run 106, to 49%, run 107, resulted in a more positive burn; that is to say, the rise time was reduced from 80 milliseconds to 60 milliseconds. The rate of change of pressure with respect to time was of a higher magnitude. The proof pressure test conducted with a .50 caliber API on the 49% voided tankage resulted in a higher pressure rise in a longer time period (98 milliseconds). See Figure C17. The rate of change of pressure with respect to time was similar to test run 106 conducted on the 40% voided tankage.

6.2 Small Wing Tankage

The pressure rise data traces are shown in Figures C-18 through C-35. The configuration descriptions and combustion over-pressure data are included as Table C-II. The relationship of penalty void with absolute over-pressure ratio found by test is shown in Figures 95 through 98.

A summary bar chart allowing assessment of each void concept with each other is shown in Figure 99.

6.2.1 Egg Crate

This configuration was assembled using the 3M Scotch Brite material. Tests conducted on a 7.5% voided tankage, run 120 and 120A, resulted in no burn through. The three center cells in which the incendiary was discharged were badly blackened and resulted in a low overpressure of 0.6 psi.

Increasing the percent void to 36% increased the resulting pressure rise to 2.2 psi (see Figure C18). This pressure and resulting pressure drop across the relief orifices resulted in badly blackened material in front of each relief hole. This staining was similar to that occurring in similar tests

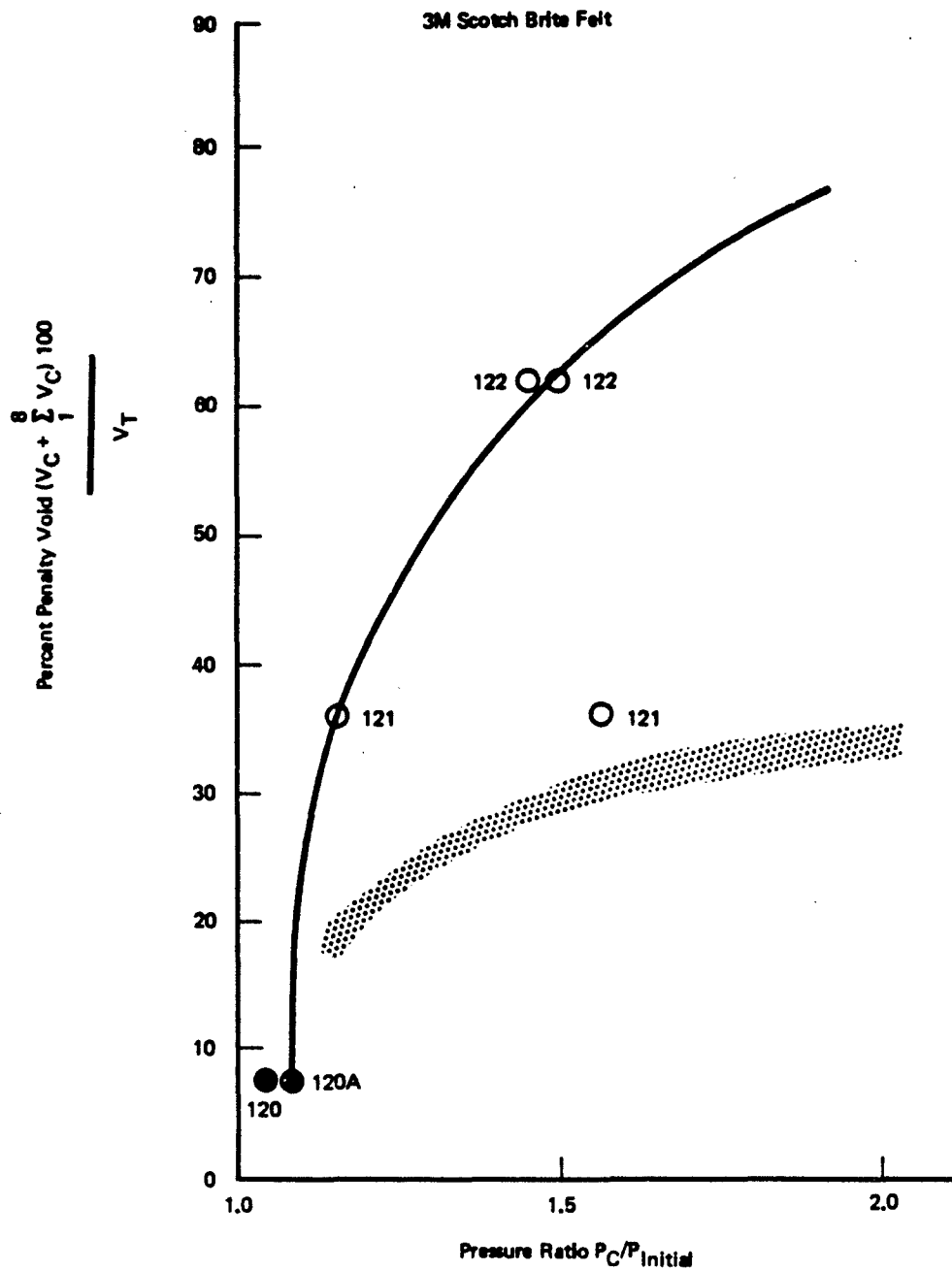


*Figure 95: Percent Void Versus Pressure Ratio Summary Data Plot,
Small Wing Tank Egg Crate Configuration*

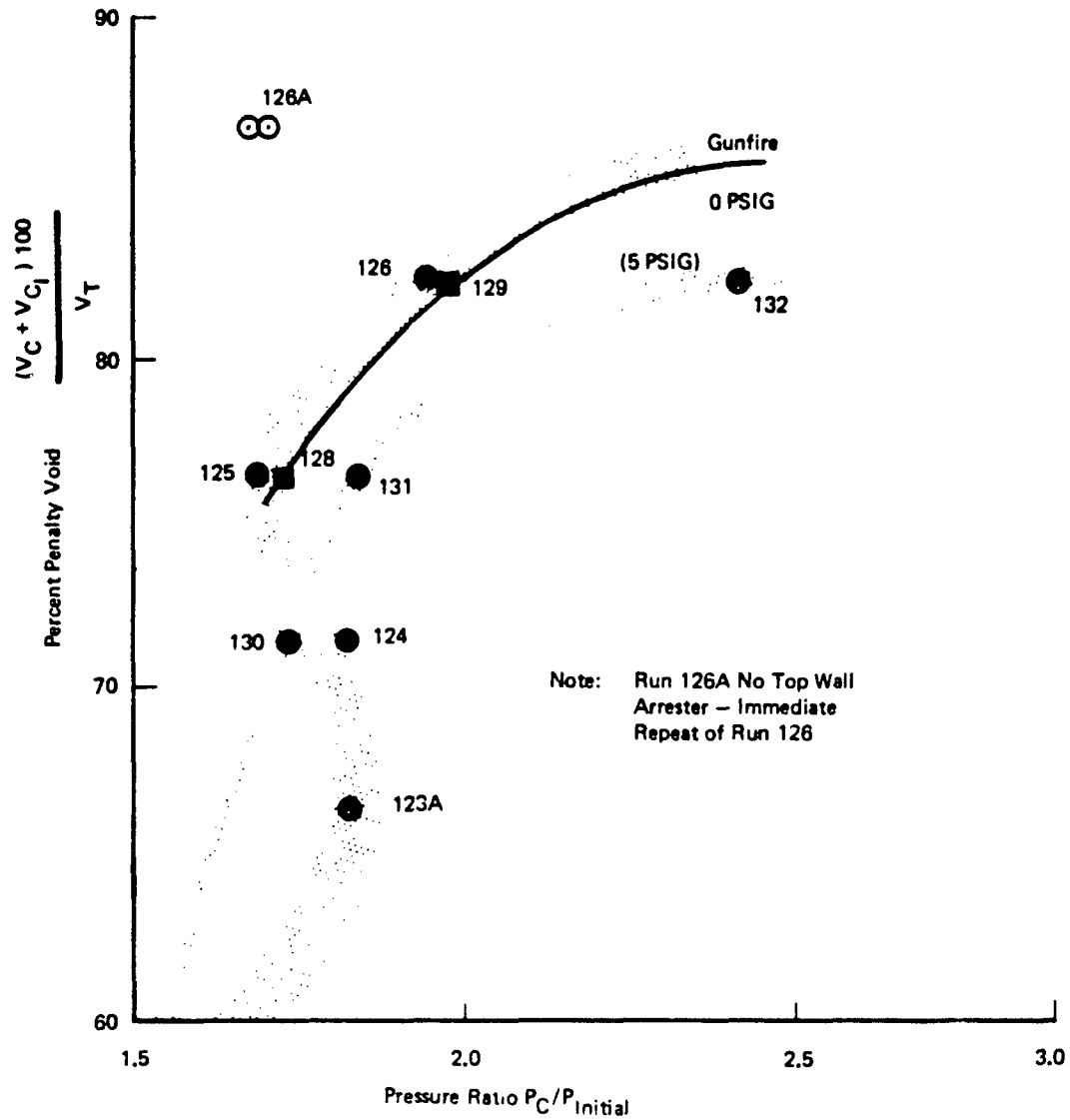


Figure 96: Percent Void Versus Pressure Ratio Summary Data Plot, Small Wing Tank Voided Top Wall Configuration

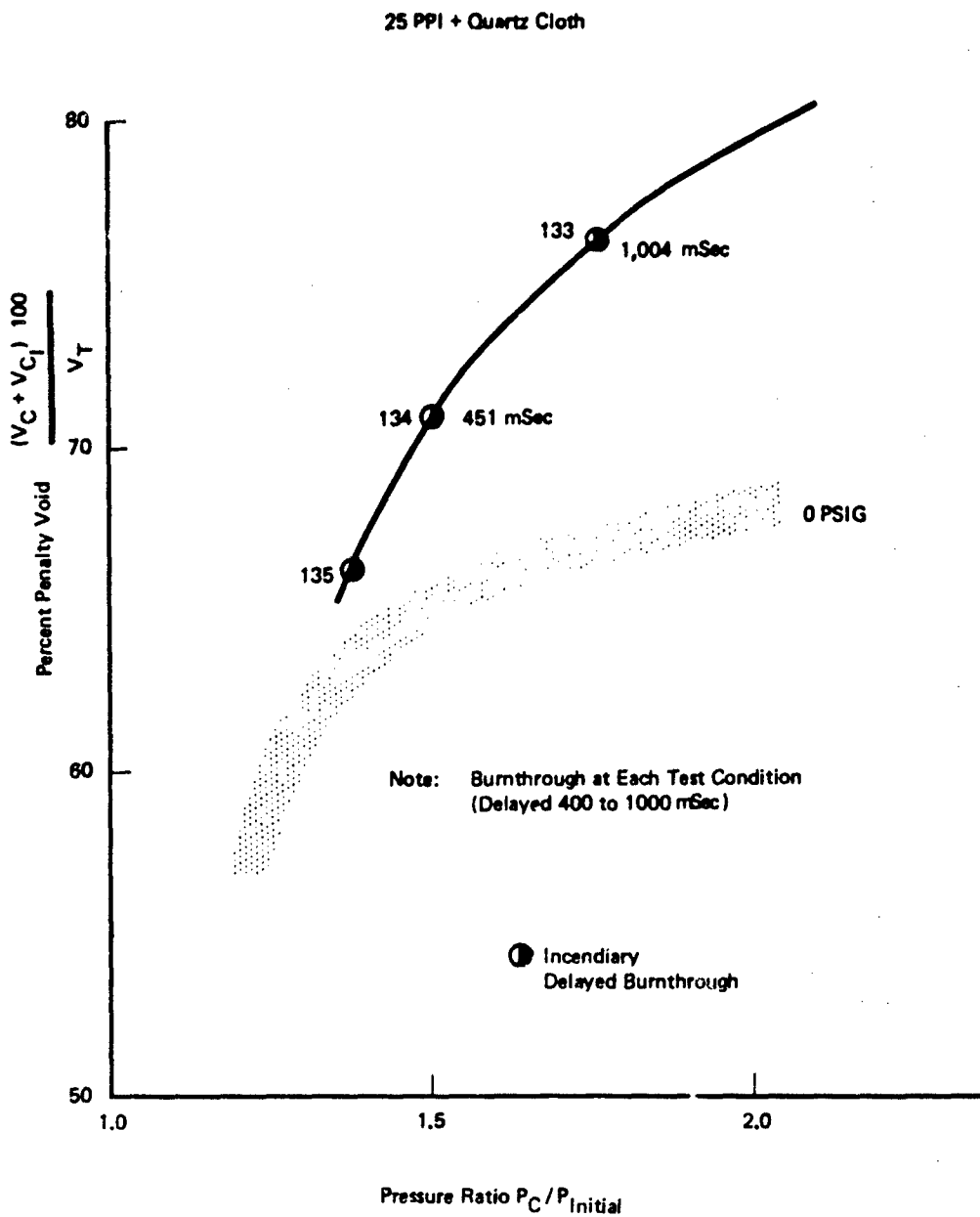


Figure 97: Percent Void Versus Pressure Ratio Summary Data Plot
for Small Wing Tank Voided Top Wall Configuration

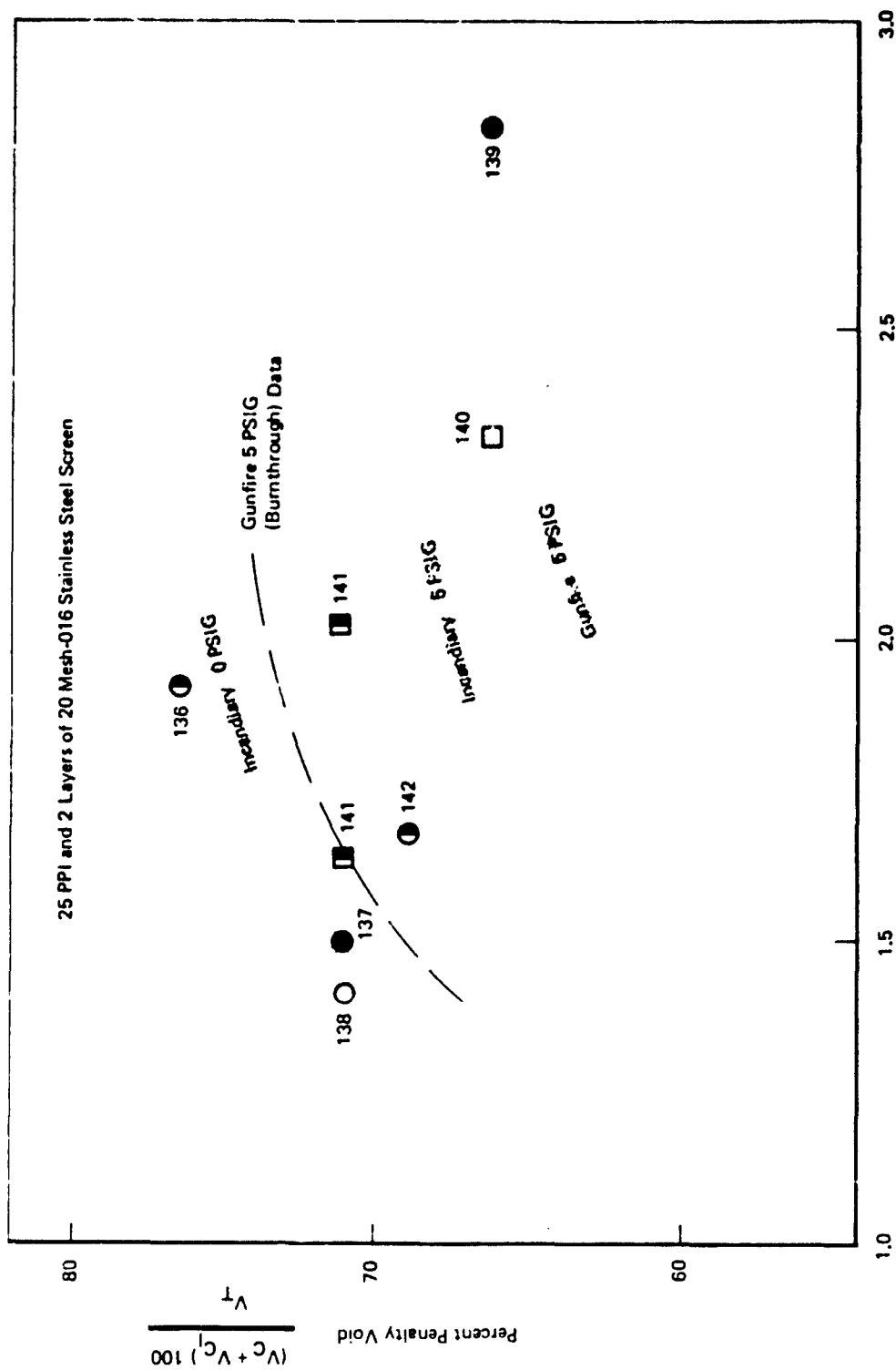


Figure 99: Percent Void Versus Pressure Ratio Summary Data Plot for Small Wing Tank Voided Top Wall Configuration

Note:-

The penalty void shown is based upon 10 PSIG overpressure.

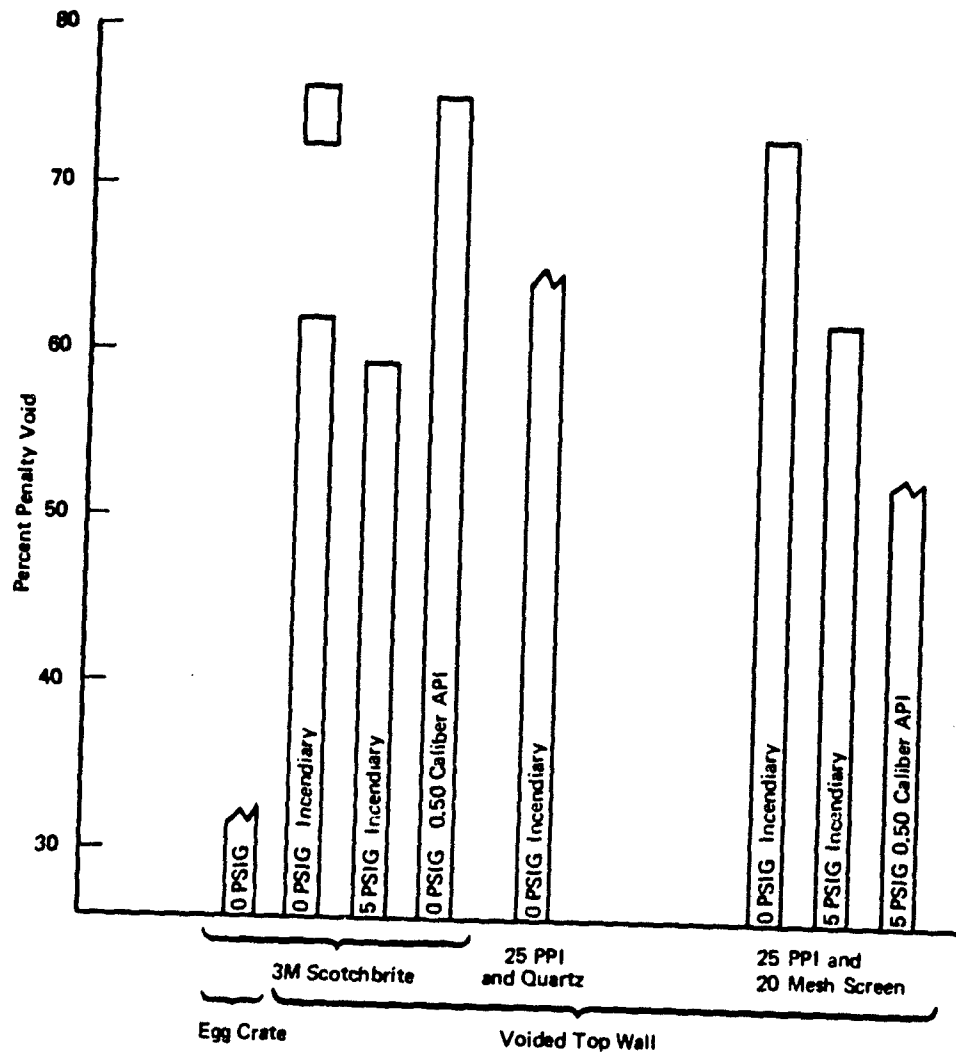


Figure 99: Small Wing Tank Data Summary

with 25-ppi foam. The arrester was not damaged, but burn-through had resulted. Burn-through was indicated on the data tracer, and post-test examination showed the arrester material in the adjacent cells was burnt. Run 122, shown in Figure C19, conducted on a 62% voided configuration, resulted in a 6.5-psi overpressure and the expanding gases badly blackened and charred the three central ignition cells, completely burning away the upper portion of one wall. The material in front of each relief hole was completely burned away by the expanding gases. The arrester sections cut to fit within the tankage in front of all the relief holes resulted in damage similar to that experienced with 25-ppi foam.

It is concluded that with this material and configuration, the approximate maximum voiding available is 30% at 0 psi initial pressure. This void approximates 2-1/4 inches of material on each side of relief holes.

6.2.2 Voided Top Wall

Test runs 123A and 124 were undertaken with a 4.0" side wall and a 2.0", 1.0" top wall respectively. Each test resulted in the top wall being badly charred and blackened but not damaged. Post-test observations and inspection of the pressure traces shown in Figure C-20 and C-21 did not indicate that burn-through into the top stringer section or into the adjacent cells had occurred. However, in both runs the side walls protecting the relief holes were blackened on the combustion surface and had sustained a black stain that permeated through the material. A section cut through the arrester on completion revealed the usual conical stain opposite each of the seven relief holes.

An increase in voiding was obtained by reducing the thickness of arrester material on either side of the relief holes. Runs 123A and 124 were undertaken with 4.0 inches of material on either side of the holes. This resulted in a total arrester thickness of 8.0 inches.

The data summary curve for the voided top wall configuration using 3M Scotch Brite material appears confusing (Figure 96). An explanation based on test

observation and the results of the air flow pressure drop tests conducted in Task I is as follows: During the explosion, the pressure drop is at such a high level due to transient squashing of the material. The data traces show a pressure rise of approximately 12 psi occurred for both runs 123A and 124. Post-test examination showed little damage to the arrester material. Increasing the percent void by reducing the material thickness to 3.0 inches resulting in a total of 6.0 inches available for arresting the flame front (run 125) resulted in material damage occurring. Approximately 80% of the material at each relief hole was burnt away. It can be assumed, therefore, that during the explosion the pressure drop across the arrester reached a peak value lower than that previously obtained, and then reduced as the explosion continued to burn away the material at each hole. This lower pressure drop resulted in a lower maximum overpressure of 10 psi. It is noted that the resulting damage did not produce a burn-through into the adjacent cells.

Increasing the void to 82% by reducing the material thickness to 2.0 inches, giving a total of 4.0 inches for arrest, resulted in a pressure rise of 13.8 psi, run 129A shown in Figure C-25. The post-test examination again showed the arrester material to be severely burned and a communicating hole blown through at each relief hole. The higher pressure rise recorded is assumed to have resulted from burning substantially more propane-air mixture. As the percent void increases, the combustion volume also increases. As stipulated earlier in the program, the pressure rise is influenced by the volume of gases burnt in relation to the arrester relief volume.

It is this decrease in arrester pressure drop during the explosion resulting in partial or complete burn-through, depending upon original thickness, coupled with an increase in combustion volume that produced the apparent erratic pressure rise data as shown in the summary survey (Figure 96).

Burn through could occur at any voiding above 75%, due to the fact that tests at voids in excess of this percent void resulted in burn holes into the adjacent

cells. Ignition of the adjacent cell did not occur until voidings as high as 80% were reached. It is considered that if voidings above this are contemplated, the statistical probability of sustaining a burn-through would be very high.

Runs 133, 134 and 135 using 3.0 inches, 4.0 inches and 5 inches of 25-ppi foam on each side of the relief holes backed with 10 layers of 25-ppi quartz fiber type 594 burnt through on each occasion. The delayed burn-through occurred approximately 1 second after the combustion volume pressure decayed, and again allowing pressure equalization. From this it was concluded that installing quartz fiber on the front faces of the side walk, protecting direct flame communication into the adjacent cells, did not help in arresting the propagating flame, the data being substantially identical to that obtained during Task II testing in the same configuration. Further testing with the quartz fiber was discontinued.

Similar tests conducted with 2 layers of 20 mesh - 016 stainless steel screen on the front faces showed that voiding in excess of 70% at 0 psig initial pressure was attainable.

6.3 Large Wing Tankage

The pressure rise data traces are shown in Figures C-36 through C-43. The configuration description and combustion over-pressure data are included as Table C-III.

The relationship of penalty void with absolute over-pressure ratio found by test are shown in Figures 100 through 102.

A summary bar chart allowing assessment of each void concept with each other, is shown in Figure 103.

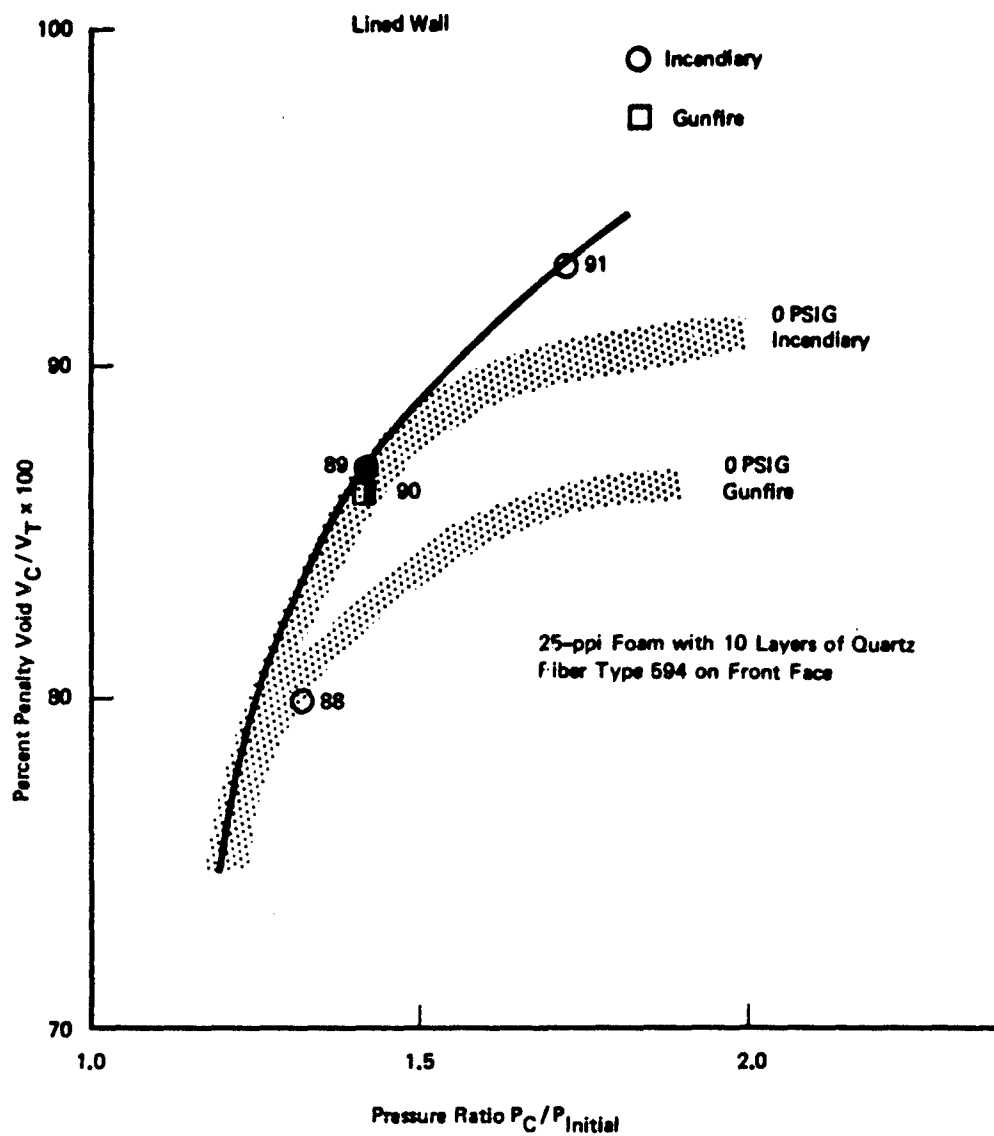


Figure 100: Percent Void Versus Pressure Ratio Summary Data Plot
Large Wing Tank (Lined Wall)

2 Layers of 20 Mesh-016 Stainless Steel Screen with 10 Layers of Quartz Fiber
Type 594 on the Front Face

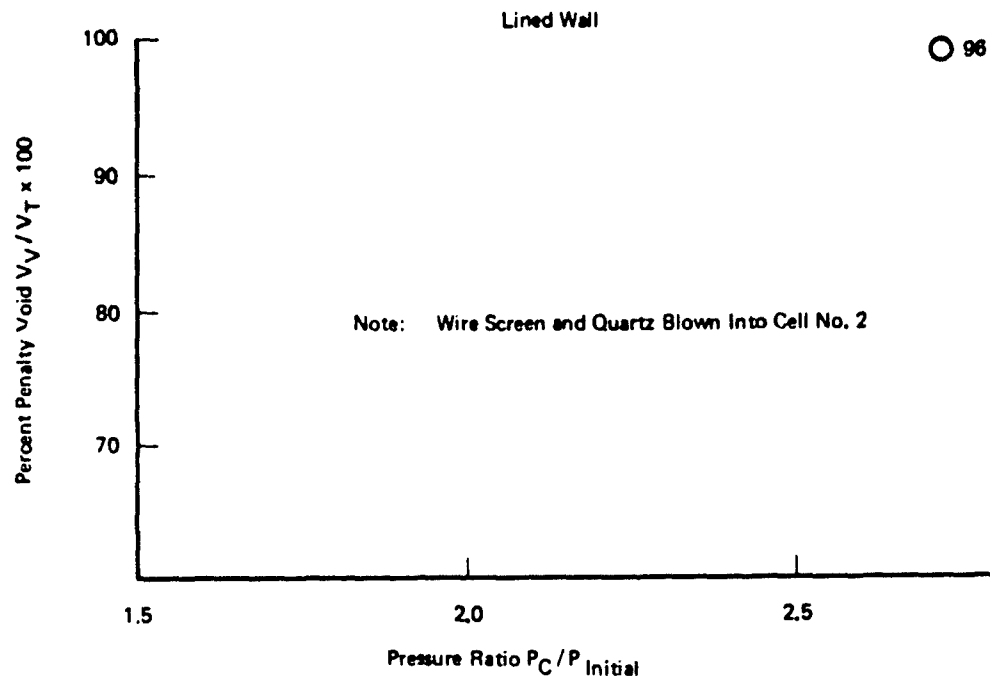


Figure 101: Percent Void Versus Pressure Ratio Summary Data Plot –
Large Wing Tank

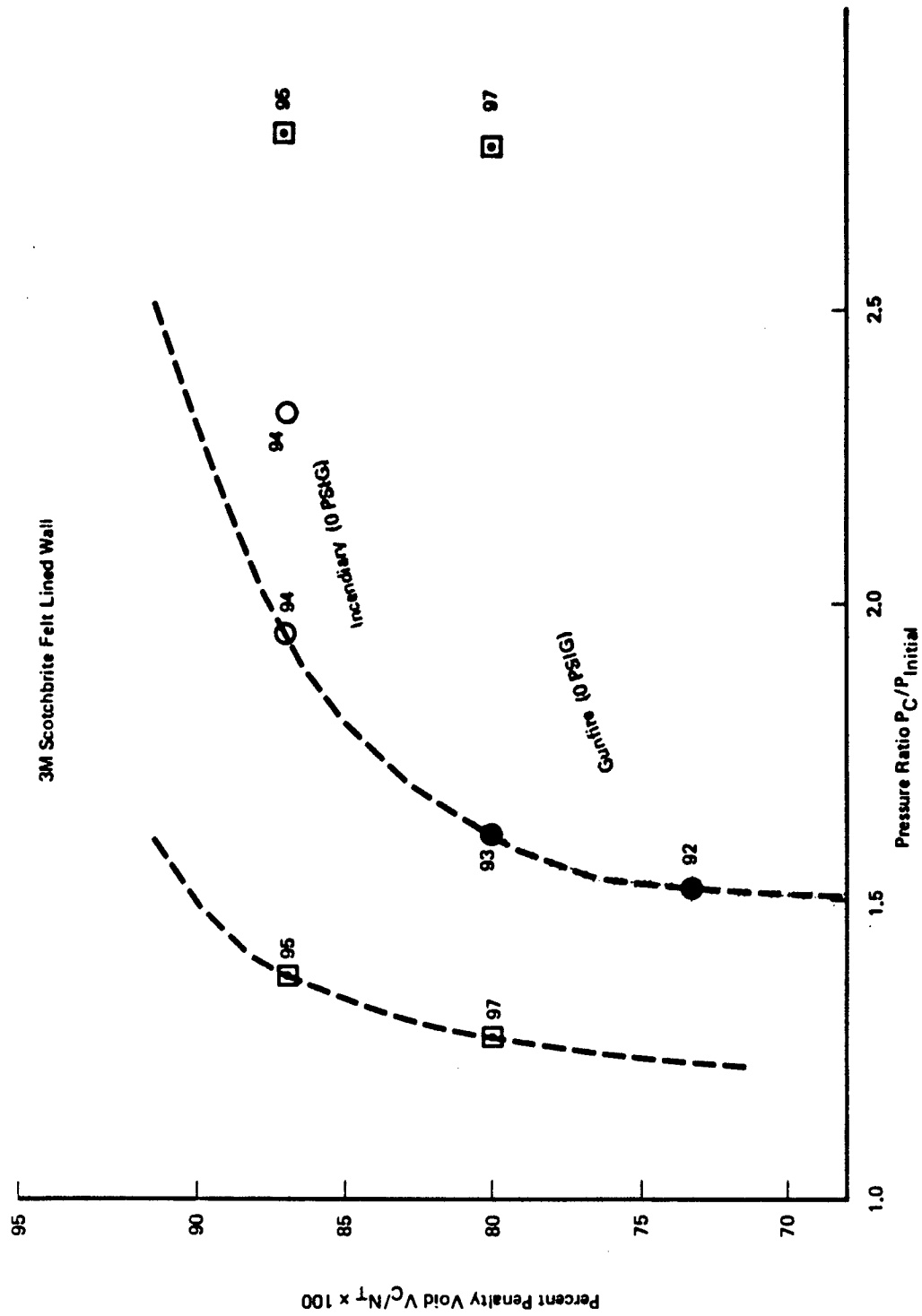


Figure 102: Percent Void Versus Pressure Ratio Summary Data Plot—Large Wing Tank

Note:-

The penalty void shown is based upon 10 PSIG overpressure.

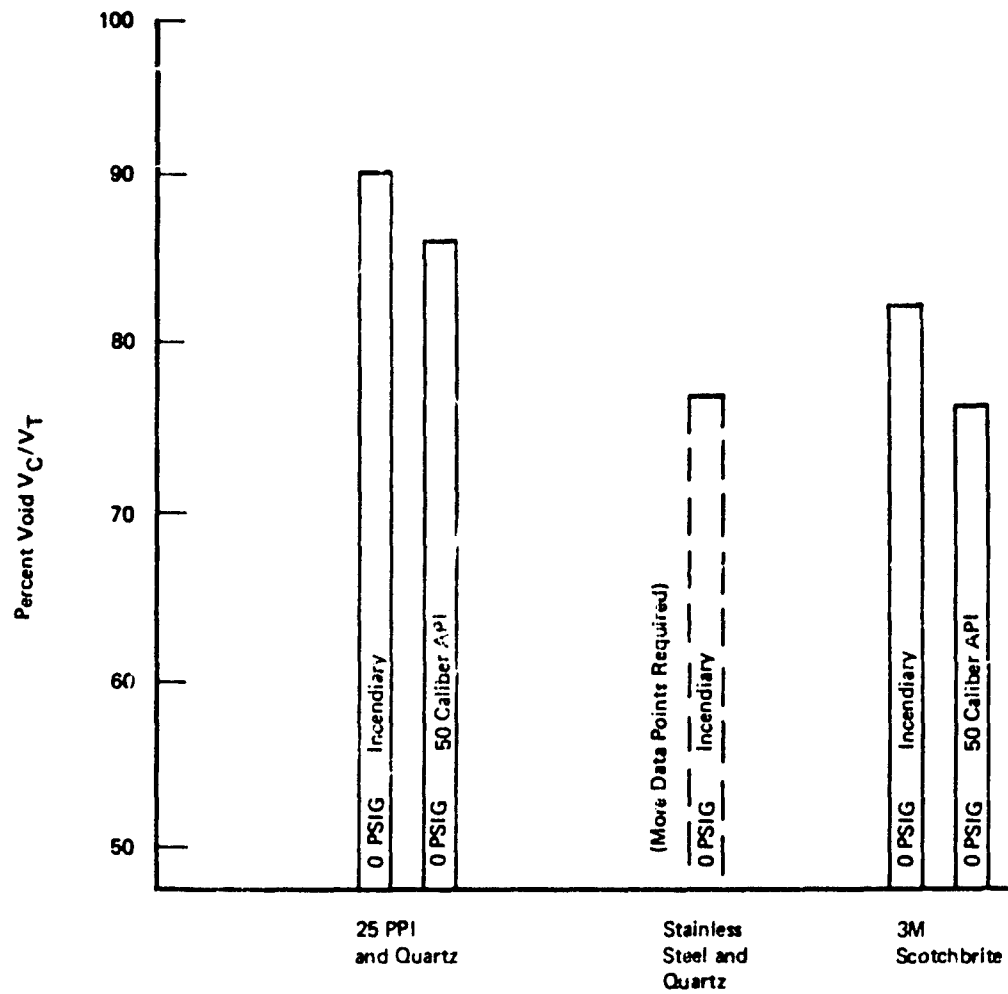


Figure 103: Large Wing Tank Data Summary

6.3.1 Lined Wall

The highest percent void obtainable with a .50 caliber API as an ignition source was not accurately defined for both material combinations tested. More data in this particular configuration would be most desirable. Examination of the particular data traces runs 90, 95 and 97 have allowed a provisional determination of the maximum voiding obtainable. Further testing it is noted could lower the voiding shown in Figures 100 and 102.

Run 96 shown in Figure 101, using 2 layers of 20 mesh-016 stainless steel with 10 layers of quartz fiber type 594 resulted in a excessive overpressure and severe damage to the arrester. The wire screen and quartz were torn from their supports and blown into the adjacent cell. Burn-through as indicated on the pressure trace was immediate. The high pressure rise and subsequent blow-through indicate that during the explosion the mass flow attempting to expand through the arrester is high, producing an excessive pressure drop across the arrester material.

The gunfire data presented in Figure 102 for an initial pressure of 0 psig is estimated as a result of the condition of the material during post-test examination. More data points with this ignition source are desirable.

6.4 Penalty

The material property determinations conducted in Section VII resulted in retention, weight and displacement data for all materials tested in the majority of Task I and all of Task II and Task III. This data allows comparative penalties to be determine for typical configuration and voiding concepts.

Present installation practice, using the 10-ppi orange reticulated polyurethane foam, is to fully pack the tankage except for voiding around components. This voiding results in total voiding of approximately 10%, depending on the type of

tankage. The installation incurs a 2% to 6% compression of the arrester material to ensure a well fitting installation so that flame paths do not exceed 0.050 inch.

From Tables IV and V the following data are extracted.

6.4.1 10 PPI (Orange) Foam - Baseline Arrester Material

$$\begin{aligned}\text{Dry Weight} &= 1.9 \text{ lbs/ft}^3 \text{ (average)} \\ &= 1.9 \text{ lbs/ft}^3 \times 0.1337 \text{ ft}^3/\text{gal.} = 0.254 \text{ lbs/gal.}\end{aligned}$$

Correcting for installation, 10% voiding and 6% (maximum) compression, results in a weight reduction of 4%. Final installed weight penalty reduces to

$$0.254 \times 0.96 = 0.244 \text{ lbs/gallon}$$

Fuel Displacement: 2.55%

Assuming 6.5 lbs/gallon of fuel, the total displacement is
 $.0255 \times 6.5 \text{ lbs/gal.} \times 0.96 = 0.159 \text{ lbs/gallon}$

Fuel Retention: 4% (Average)

Assuming 6.5 lbs/gallon of fuel, the total retention is given by:
 $.04 \times 6.5 \text{ lbs/gal} \times 0.96 = 0.25 \text{ lbs/gallon.}$

The net weight increase of a tankage installed with fully packed 10 PPI foam is given as follows:

- Increase in Net Weight = Dry Weight - Displacement
 $= 0.244 - 0.159 = .085 \text{ lbs/gallon}$

The operational increase in weight will include the retention penalty.

- Increase in Operational Weight = Net Weight Increase + Retention
 $= 0.085 + 0.25 = 0.335 \text{ lbs/gallon}$

Weight and volume penalties are somewhat severe at 0.085 lbs/gallon, when large volume tankages are considered in conjunction with further unusable fuel of 0.25 lbs/gallon.

The total unusable fuel directly affecting range capabilities on volume limited aircraft is the fuel displaced plus the fuel retained = $0.159 + 0.25 = 0.409$ lbs/gallon.

These penalties will be reduced when gross voiding techniques developed during this test program are fully evaluated. These techniques now being evaluated use as a baseline a reticulated polyurethane foam with 25 ppi. From Tables IV and V the following data are extracted.

6.4.2 25 PPI (Red) Foam

The following data is not corrected for fully packed voiding and compression.

Dry Weight	= 1.44 lbs/ft^3	= 0.193 lbs/gallon
Fuel Displacement	= 2%	= 0.13 lbs/gallon
Fuel Retention	= 5.8%	= 0.377 lbs/gallon
Increase in Net Weight		= 0.063 lbs/gallon
Increase in Operational Weight		= 0.44 lbs/gallon

The net weight increase of 0.63 lbs/gallon for a fully packed tankage is less than that for the 10-ppi foam. However, the operational weight increases from 0.335 to 0.44 lbs/gallon. A minimum voiding of approximately 24% has to be obtained to equal the operational weight penalty of the fully packed 10-ppi tankage.

6.4.3 3M Scotch brite Felt

The following data is not corrected for fully packed voiding and compression:

Dry Weight	= 2.71 lb/ft^3	= 0.362 lb/gal
Fuel Displacement	= 3.33%	= 0.216 lb/gal
Fuel Retention	= 5.1%	= 0.332 lb/gal
Increase in Net Weight		= 0.146 lb/gal
Increase in Operational Weight		= 0.478 lb/gal

Using this material the weight and volume penalties are further increased in severity from .085 lbs/gallon for the 10 PPI foam to 0.146 lbs/gallon. The operational weight is also increased from 0.335 to 0.478 lbs/gallon. A minimum voiding of 30% has to be obtained to equal the operation weight penalty of the fully packed 10-ppi tankage, reference Figures 104 and 105.

6.4.4 Screen Materials

With reference to the material property determinations in Section XII, the percent retention and density values for the screen materials are very high. However, the presence of these arrester materials in any tankage voiding configuration will be associated with a very high percent void if it is considered separately. This voiding will be in the order of 98% (Figure 106).

The fuel displacement data for the Quartz Fiber and Stainless Steel screen was not determined by test.

6.4.5 Tankage Penalties

It is noted that the weight increase net or operational is very high for the stainless steel screen material. For practical usage the volume factor has to be in the order of 0.01 to 0.02. Further penalty evaluation may require the data to be presented on a material square foot basis.

The test program has concluded that the following voiding concepts and materials produced the greatest allowable percent voiding in the test tankages.

- Fuselage Tankage -- Voided Top Wall
Material: 25 ppi + 10 layers of quartz fiber
- Small Wing Tank -- Egg Crate and Voided Top Wall
Material: 3M, 25 ppi + stainless steel screen

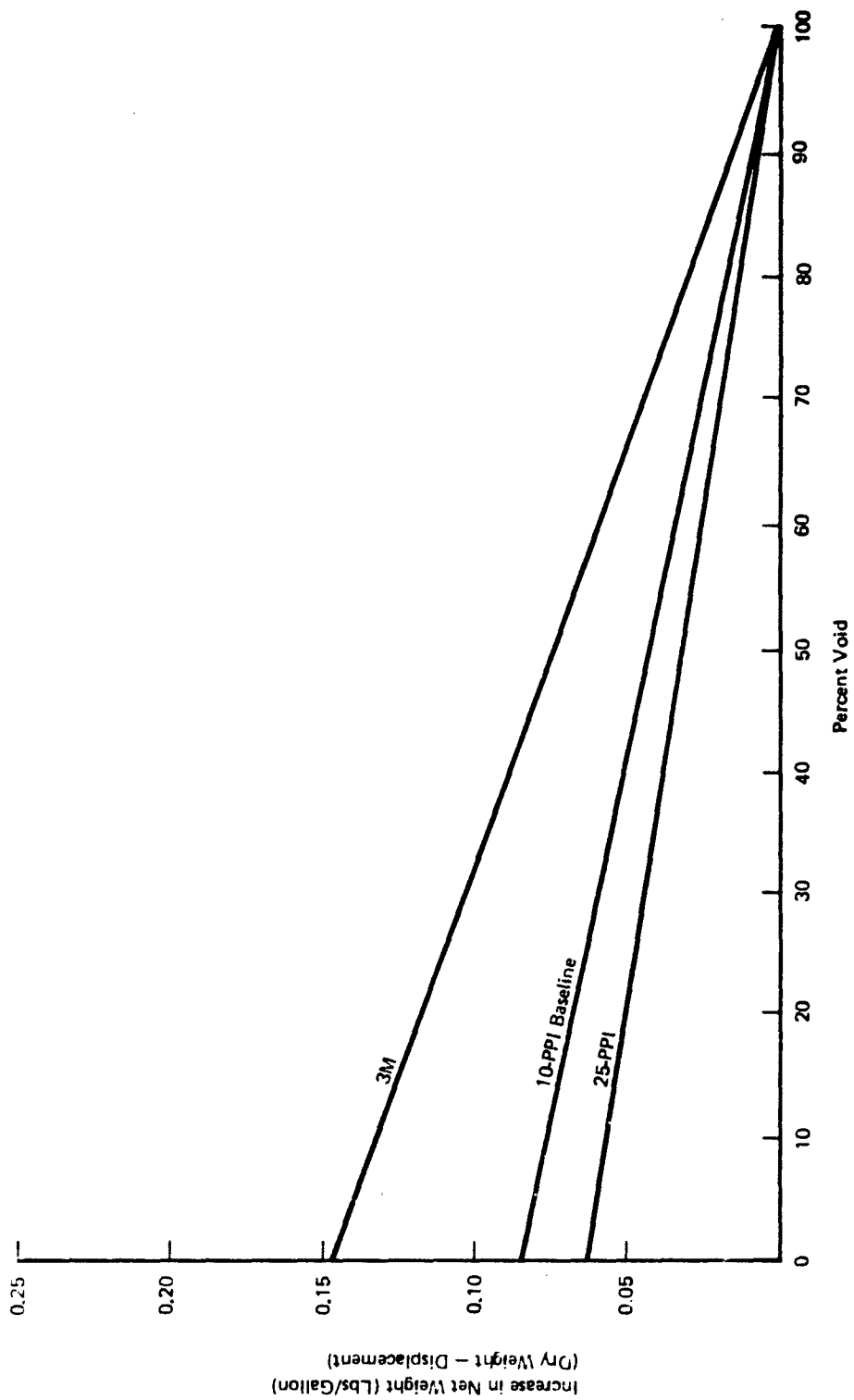


Figure 104: Arrestor Material Net Weight Penalty

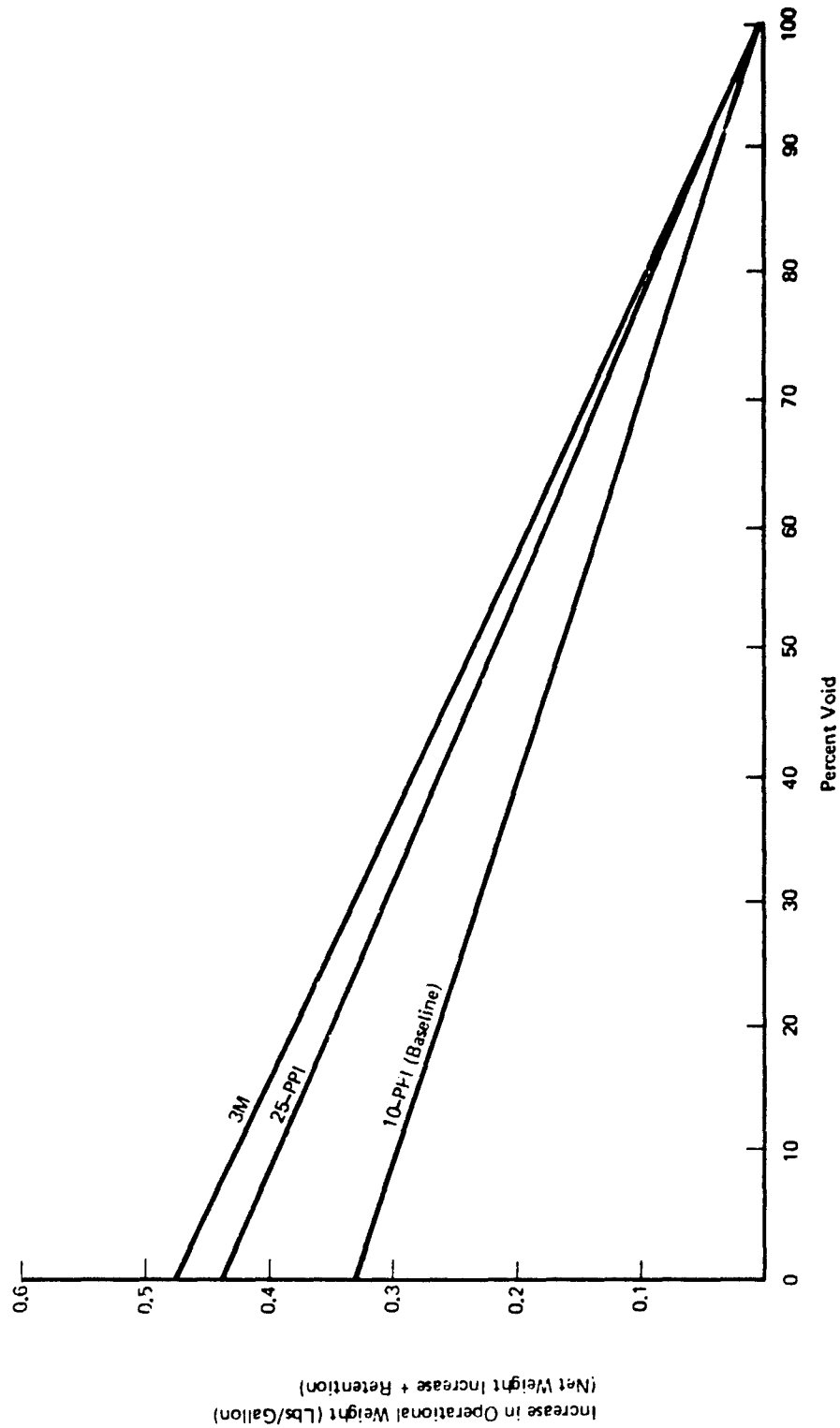


Figure 105: Arrestor Material Operational Weight Penalty

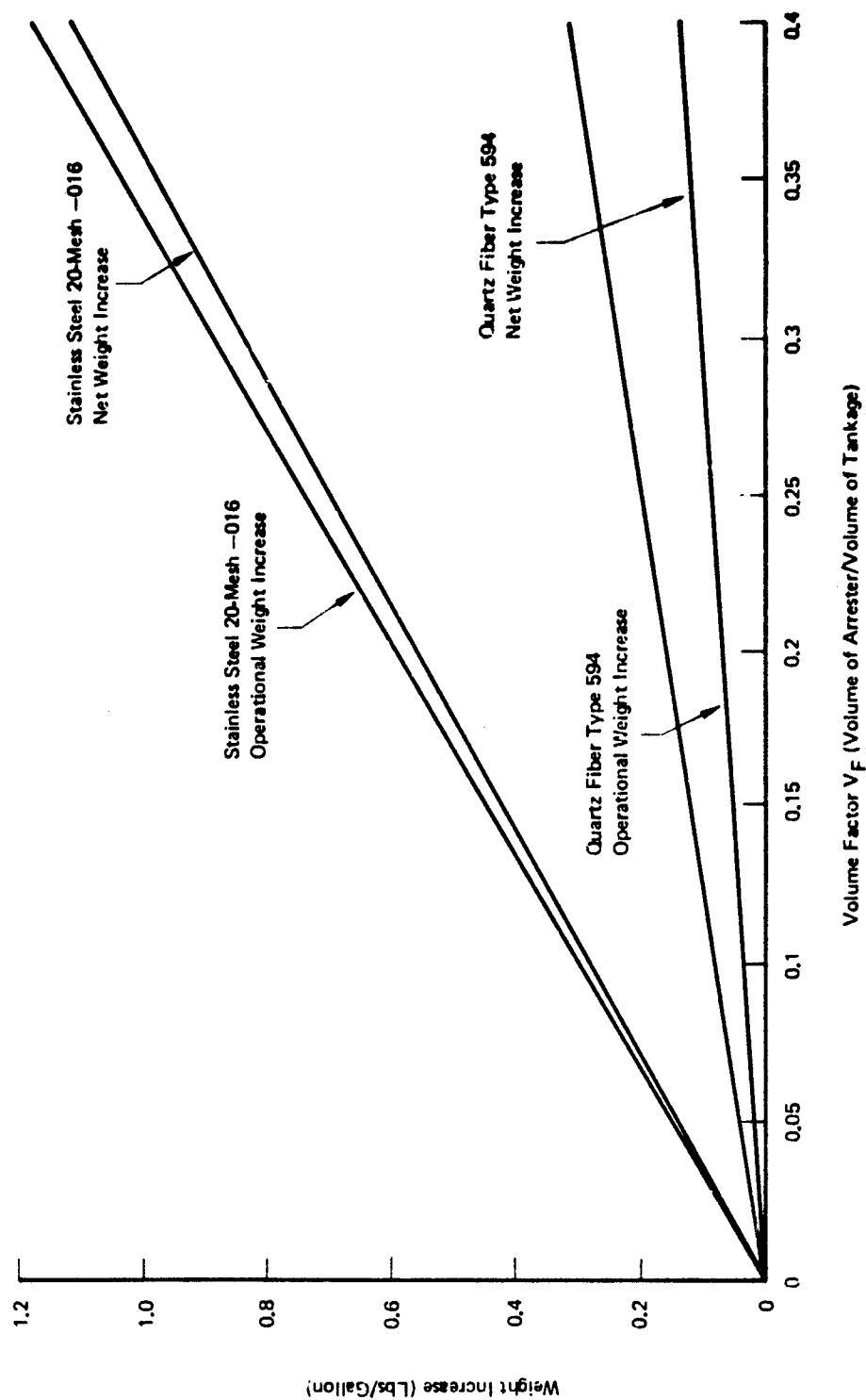
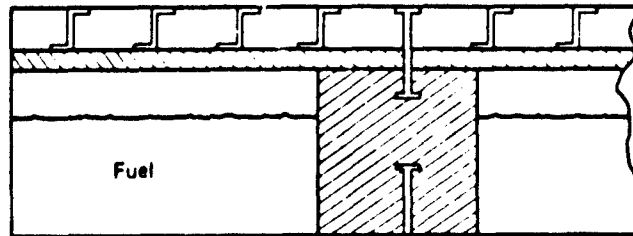


Figure 106: Screen Material Installation Penalties

● Large Wing Tank -- Lined Wall

Material: 25 ppi + 10 layers of quartz fiber

It is noted that the major advantage of the voided top wall concept is that the major portion of the void is filled with fuel. The maximum percentage void only occurs when the tankage is empty.



A detailed appraisal of the weight penalties for each installation has not been undertaken. The results of such an analysis would be applicable only to the test tankages and would not reflect the actual penalties when installed in an aircraft configuration.

The large wing tank, lined wall concept could be adapted to that of the voided top wall. The design constraint will involve the relief area allowing pressure communication into the adjacent bays.

The arrester material will be located on either side of the wing rib structure. With quartz fiber on the tank inner surface, the problem would be in the attachment of the arrester material to the tank structure. The use of attachment plates or fully utilizing the structural rigidity of screens could be utilized, but would add to the weight of the voiding system.

The air flow pressure drop has been shown to be generally similar for the 10 ppi, 25 ppi and 3M Scotch Brite, with 10 layers of quartz fiber producing a slightly higher pressure flow relationship. It is anticipated that fuel flow will result in each arrester material relating to each other in a similar way. Consequently airplane systems with fully packed 10-ppi foam have been active in service and proven acceptable. The gross voiding of material with similar pressure drop characteristics would prove to be no problem. Fuel flow tests are required for the quartz fiber material if serious consideration for aircraft installation is given. Air flow pressure drop tests conducted as part of Task I showed this material to have a higher pressure drop than other materials considered in Task III.

6.4.6 System Effects

The fuel level effects and installation considerations of arrester materials evaluated during this program are identical with those discussed in Reference 1.

The high percentage void egg crate installations tested did not lend themselves easily to a simple interlocking assembly. Unless each section was interlocked and glued, the explosion initiated with .50 caliber API on the incendiary igniter would severely distort the assembled geometry. This gluing of the egg crate outer walls and inner sections will involve a penalty weight of glue, possibly limiting the maximum practical voiding.

7.0 CONCLUSIONS AND RECOMMENDATIONS

Test on the fuselage tank with a voided top wall configuration were conducted up to a maximum of 11.1 percent relief void. Post-test examination revealed that burn through into the relief voids had not occurred during any test. It is possible that changes to the voiding geometry could result in obtaining higher relief void, and consequently a higher penalty void.

Task II and Task III of this program were initially planned and detailed with definite void concepts that indicated promise as a result of applying the basic design parameters that resulted from all Task I testing. Consequently at Task II and Task III program inception the number of test conditions available within the constraints of the budget were distributed throughout both tasks on a void concept basis. It was thought that these tests allocated for each void concept and tankage configuration would be sufficient to adequately describe relationship of over-pressure versus percent void and produce definite relationships and design trends. To a large degree this objective was obtained, however in all configurations tested more data points would have been desirable to further define voiding limits and fully understand the complicated phenomena occurring and to more fully relate all the variables that influence pressure rise within an individual void concept.

The data obtained within these maximum run number constraints, was very revealing and indicated certain courses of action, allowing some concepts to be found acceptable.

The voiding concepts tested that showed greatest promise in their application to aircraft tankages are as follows:

- Fuselage
 - Voided top wall
- Small Wing
 - Egg crate
 - Voided top wall

- Large Wing
Lined wall

These voiding concepts should be further exhaustively tested in full scale configurations that represent more closely aircraft installation.

The test results obtained during Task I testing being basic in nature will prove to be invaluable tools in determining preliminary applicability of concepts prior to serious consideration.

This program has shown that understanding the basic mechanism by which a propagating flame is arrested and the influence of various materials are important considerations requiring further exploratory investigation.

It has been shown that the following materials show promise as flame arresters within certain gross voiding configurations.

- 25 Pores per inch Reticulated Polyurethane Foam.
- 3M Scotch Brite Felt
- Various combinations of
 - 20 mesh 016 stainless steel screen
 - Quartz Fiber type 594
 - 25-ppi foam

It is noted that the purchase price of the Quartz Fiber (trade name ASTROQUARTZ type 594) was prohibitive. Consequently it is suggested that further development of the Fiber Glass Cloth within the Space Lattice concept as suggested in Task I Section IV could be of immediate benefit. Presently the air flow pressure drop through commercially available fiber glass cloth is very high. Reducing the pressure drop by developing a more open weave is desirable.

APPENDIX A
TASK I TEST DATA

Table A.1: 4.0-Inch. Flame Tube Data Summary, Runs 1 through 33

Material	Run	Flame Tube Configuration		Thickness	Bomb Pressure Rise	Flame Speed	Burn Through	
		% Open/Ignition	% Open/Relief				Yes	No
Custom mtl 5 7611 x P velstat	1	100	100	4 New	80	89.6		x
	2	100	100	4 Used	90			x
	3	100	100	4 Used	88	65.0		x
	4	50	100	4 Used	-	76.5		x
	5	50	0	4 Used	-	53.0		x
	6	100	0	4 Used	-	56.5		x
	7	0	100	4 Used	95	2600		
10 PPI RPF	8	100	100	4 New	84	108	x	
	9	50	100	4 Used	-	130	x	
	10	0	100	4 Used	93	434		x
	11	25	100	4 Used	-	162		x
	12	50	100	4 Used	92	86.6	x	
	13	50	100	3 1/2 New	93	81.2	x	
	14	25	100	3 1/2 Used	-	145	x	
	15	25	100	3 1/2 Used	-	-	x	
	16	25	100	3 1/2 Used	-	260	x	
	17	0	100	3 1/2 Used	-	434		x
	18	13	100	3 1/2 Used	-	322		x
	19	13	100	3.0 New	-	325	x	
	20	0	100	3.0 Used	-	1300		x
	21	0	100	2.5 Used	-	433		x
	22	100	100	6.5 4" New	-	68		x
	23	100	0	2 1/2" Used	104	65.8		x
	24	100	0	2.5 Used	-	544	x	
	25	0	100	2.5 New	105	2600		x
	26	13	100	2.5 Used	-	360	x	
	27	13	100	3.0 New	-	360	x	
	28	7	100	3.0 Used	105	575	x	
	29	0	100	2.0 New	-	600		x
	30	7	100	2.0 Used	-	482	x	
	31	0	100	1.0 New	104	1590	x	
	32	0	100	1.0 Used but undamaged	-	562	x	
	33	0	100	1.5 New	-	540	x	

Table A-1: (Continued) Runs 34 through 65

Material	Run No.	Flame Tube Configuration		Thickness	Bomb Pressure Rise	Flame Speed	Burn Through	
		% Open/Ignition	% Open/Relief				Yes	No
10 PPI	34	0	100	1.5 New	104	562		x ?
	35	0	100	1.5 Used	-	562		x
25 PPI Black	36	100	100	4.0 New	-	50.0		x
	37	100	0	4.0 Used	-	52.0		x
	38	100	100	2.0 New	-	52.5		x
	39	100	0	2.0 Used	-	79.5		x
	40	100	100	1.0 New	-	96.5		x
	41	100	0	1.0 Used	-	90.0		x
	42	100	100	0.6 New	104	104.0		x
	43	100	0	0.6 Used	-	84.5		x
with screens	44	50	100	0.5 New	108	81.8		x
	45	7	100	0.5 Used	-	410.0	Delayed	
3:1	46	100	0	2.0 New 2-1" Layers	-	51.9		x
	47	100	0	1.0 Used (left layer)	-	57.5		x
GAF Felt	48	100	0	1.25 New (2 layers)	-	52.0		x
	49	100	0	.52 New	90 & 90	39.0		x
	50	100	0	.62 New	102	?		x
	51	100	0	.62 Used	109	Very slow ?		x
	52	100	0	.62 Used	-	45.8		x
3M	53	100	0	.50 New	Post: Run 105	Very Slow		x
	54	100	100	.50 Used	-	54.1		x
	55	25	100	.50 Used	-	180.0		x
GAF Felt	56	25	100	.62 New	105	142.0		x
	57	13	100	.62 New	-	159.0		x
	58	7	100	.62 New	-	159.0	Delayed	
	59	7	100	1.25 New	-	300.0		x
	60	0	100	1.25 New	-	2450		
with screens	61	0	100	1.25 New	-	540		x
3M	62	13	100	.50 New	-	270	Delayed	
15 PPI	63	50	100	4.0 New	-	37.4		x
	64	100	100	4.0 Used	-	71.5	Delayed	
	65	50	100	4.0 New	Post Test	90	x	

Table A-1: (Continued) Tests 66 through 98

Material	Run No.	Flame Tube Configuration		Thickness	Bomb Pressure Rise	Flame Loss	Burn Through	
		% Open / Ignition	% Open / Relief				Yes	No
15 PPI 4 Red	66	25	100	4.0 New	105	159.0	x	
	67	7	100	4.0 New	-	300	x	
w/aft screen	68	0	100	4.0 New	-	492		x
25 PPI 4 Red	69	0	100	4.0 New	-	483		x
	70	13	100	4.0 New	-	270		x
	71	100	0	4.0 New	-	52		x
	72	100	0	2.0 New	-	51		x
	73	100	0	1.0 New	-	56.2		x
Screens both sides	74	100	0	.5 New	-	62.9		x
	75	25	100	.5 New	-	225	Delayed	
	76	50	100	.5 New	102	193	Delayed	
	77	70	100	.5 New	102	123		x
15 PPI 3 Yellow	78	7	100	1.0 New	-	520	x	
	79	3.25	100	4.0 New	101	260	x	
	80	1.75	100	4.0 New	-	245		x
	81	1.75	100	4.0 New	109	473		x
w/aft screen	82	1.75	100	4.0 New	-	420		x
	83	3.5	100	4.0 New	-	346	x	
	84	0	100	3.0 New	-	820	x	
w/aft screen	85	0	100	3.0 New	-	540		x
w/aft screen	86	3.5	100	3.0 New	-	385		x
	87	7.0	100	3.0 New	-	500		
	88	100	100	6.0 New 4.0 + 2.0	-	54.0	x	
	89	50	100	6.0 New 4.0 + 2.0	-	61.0	x	
	90	25	100	6.0 New 4.0 + 2.0	-	150	x	
	91	13	100	6.0 New 4.0 + 2.0	-	229	x	
	92	3.5	100	6.0 New 4.0 + 2.0	104	482	x	
	93	0	100	6.0 New 4.0 + 2.0	102	519		x
25 PPI 4 Red	94	100	100	2" New w/aft screen	105	42		x
	95	0	100	1" New w/aft screen	-	970	x	
	96	50	100	1" New w/aft screen	-	142		x
	97	25	100	1" New w/aft screen	-	194		x
	98	13	100	1" New w/aft screen	-	300	Delayed	

Table A-1: (Continued) Runs 99 through 131

Material	Run No.	Flame Tube Configuration		Thickness	Bomb Pressure Rise	Flame Speed	Burn Through	
		% Open/Ignition	% Open/Relief				Yes	No
25 PPI Red	99	0	100	2.0 New	-	1350	x	
w/aft screen	100	0	100	2.0 New	-	575		x
Screens both sides	101	0	100	0.5 New	-	1225	x	
	102	0	100	4.0 New	-	685	x	
w/aft screen	103	0	100	4.0 New	-	770		x
Screens both sides	104	7	100	0.5 New	-	450	x	
40 PPI 7611 XP	105	0	100	2.0 New w/aft screen	-	770		x
Screens both sides	106	0	100	0.5 New	-	1080		x
Screen both sides	107	0	100	0.5 New	109	1120		x
Screen both sides	108	0	100	0.25 New	-	1500	x	
Aft screen	109	100	0	0.5 New	-	71.5		x
Aft screen	110	100	0	0.25 New	-	57.5		x
Screen both sides	111	25	100	0.25 New	-	338		x
Screen both sides	112	7	100	0.25 New	-	562	x	
5-20-840 Cloth screen	113	7	100	4 Layers	-	422	x	
No 20 Mesh SS screen	114	7	100	4 Layers	-	550	x	
	115	7	100	3 Layers	-	660	x	
	116	7	100	8 Layers	109	346		x
	117	7	100	5 Layers	106	294		x
	118	7	100	4 Layers	-	365		x
	119	0	100	4 Layers	-	1180		x
	120	0	100	4 Layers	-	820		x
	121	50	100	3 Layers	-	211		x
	122	50	100	3 Layers	-	167	Delayed	
	123	100	0	4 Layers	-	34		x
	124	100	0	3 Layers	-	52		x
	125	100	0	New 2 Layers	-	59		x
	126	100	100	Used 2 Layers	-	127		x
	127	70	100	Used 2 Layers	-	314		x
	128	50	100	New 2 Layers	103	237	x	
No. 35 Mesh	129	0	100	3 Layer	106	1124		x
	130	0	100	1 Layer	-	2250	x	
	131	0	100	2 Layer	-	1590	x	

Table A-1: (Continued) Runs 132 into gth 164

Material	Run No.	Flame: Tube Configuration			Thickness	Bomb Pressure Rise	Flame Speed	Burn Through	
		% Open / Ignition	% Open / Relief					Yes	No
No. 35 Mesh SS screen	132	50	100		2 Layers New	-	140.5	Delayed	
	133	7	100		2 Layers New	-	435	x	
	134	13	100		2 Layers Used	-	169		x
	135	100	100		1 Layer New	105	46.7		x
	136	50	100		1 Layer Used	-	199	x	
1/8 Yellow honeycomb	137	50	100		4.0 in. New	-	173	x	
	138	100	0		4.0 in. Used	-	60		x
	139	100	100		4.0 in. Used	-	109	x	
3/16 Black honeycomb	140	100	0		4 1/2 in. New	-	55	x	
	141	0	100		4 1/2 in. Used	-	276	x	
	142	13	100		4 1/2 in. Used	105		Delayed	
1/8" Yellow honeycomb	143	0	100		4.0 in. Used	-	1350	x	
	144	100	0		2.90 in. Used	107	58		x
No. 35 Mesh SS screen	145	70	100		1 Layer	-	164	x	
No. 20 Mesh SS screen	146	100	100		1 Layer	-	172	x	
No. 20 Mesh SS screen	147	100	0		1 Layer	-	58		x
15 PPI yellow foam	148	100	100		1"	-	73	x	
15 PPI yellow foam	149	3.5	100		2" New	-	409		x
15 PPI yellow foam	150	7	100		2" Used	-	386		x
15 PPI yellow foam	151	7	100		5" New	-	386	x	
15 PPI yellow foam	152	0	100		6" Half & Half	-			
15 PPI yellow foam	153	0	100		6" New	-	530		
15 PPI yellow foam	154	0	100		1" New	105			
15 PPI yellow foam	155	0	100		1" with screen	106	1285		x
KCF	156	50	100		3 Layers KCF	-	52	x	
KCF	157	50	100		1 Layer	-	174		x
KCF	158	50	100		1 Layer	-	54		x
KCF	159	100	0		1 Layer	-	54		x
400 PE screen	160	50	100		15 Layers	-	47		x
400 PE screen	161	25	100		15 Layers	-			x
400 PE screen	162	25	100		15 Layers	-	142		x
400 PE screen	163	25	100		11 Layers	105	166		x
400 PE screen	164	0	100		6 Layers	-	1080		x

Table A-1: (Continued) Runs 165 through 197

Material	Run No.	Flame Tube Configuration		Thickness	Bomb Pressure Rise	Flame Speed	Burn Through	
		% Open / Ignition	% Open / Relief				Yes	No
400 PE screen	165	7	100	6	103	422	x	
400 PE screen	166	1.7	100	6	107			x
400 PE screen	167		100	6		135	x	
400 PE screen	168	0	100	6		1125		x
400 PE screen	169	1.7	100	6		330		x
25 PPI red 20 Mesh SS	170	1.7	100	2.0" Screen both sides	109	225		x
25 PPI red 20 Mesh SS	171	1.7	100	2.0" Screen both sides		338		x
25 PPI red 20 Mesh SS	172	0	100	2.0" Screen both sides		575		x
25 PPI red 20 Mesh SS	173	100	0	2.0" Screen both sides		555		x
25 PPI red 20 Mesh SS	174	100	0	1.0" Screen both sides	104	52.5		x
25 PPI red 20 Mesh SS	175	3.5	100	1.0" Screen both sides		334		x
25 PPI red 20 Mesh SS	176	0	100	1.0" Screen both sides		693	x	
25 PPI red 20 Mesh SS	177	100	0	4" Screen both sides	106	52.5		x
25 PPI red 20 Mesh SS	178	1.75	100	4" Screen both sides	105	466		x
25 PPI red 20 Mesh SS	179	1.75	100	1.0" Screen both sides		422		x
20 Mesh Screen & Tube	180	25	100	4" Screen both sides		475	x	
20 Mesh Screen & Tube	181	50	100	2		173	x	
20 Mesh screen	182	50	100	2		185	x	
20 Mesh screen	183	50	100	3		168	Delayed	
20 Mesh screen	184	50	100	3		176		x
20 Mesh screen	185	50	100	3		169		x
20 Mesh screen	186	50	100	3		179	x	
20 Mesh screen	187	50	100	3	102	154	x	
25 PPI red 20 Mesh SS	188	50	100	1.0"		125		x
Yellow foam	189	50	100	4.0"	103	92	x	
25 PPI Red foam	190	50	100	0.4"	110	197	x	
25 PPI Red foam	191	50	100	1.0"		248		x
25 PPI Red foam	192	25	100	1.0"		360	x	
25 PPI Red foam	193	70	100	0.4		154		x
25 PPI Red foam	194	50	100	0.4		187	x	
25 PPI Red foam	195	0	100	3.0"		1122		x
10 PPI Orange foam	196	13	100	3.5"	104	250	x	
Red foam	197	13	100	2.0"	106	211		x

Material	Run No.	Flame Tube Configuration		Thickness	Bomb Pressure Rise	Flame Speed	Burn Through	
		% Open / Ignition	% Open / Relief				Yes	No
Red Foam	198	0	100	2.0"	-	540		x
Red Foam	199	0	100	1.6"	-	540		x
20 Mesh Screen	200	70	100	2	-	152	x	
20 Mesh Screen	201	50	100	3	-	170	x	
20 Mesh Screen	202	25	100	3	-	342		x
20 Mesh Screen	203	25	100	2	-	284	x	
20 Mesh Screen	204	25	100	2	-	338	x	
20 Mesh Screen	205	25	100	2	-	346	x	
20 Mesh Screen	206	0	100	1"	104	550	x	
Red Foam	207	0	100	1"	104	614		x
Red Foam	208	0	100	1"	-	491		x
Red Foam	209	0	100	1/2	-	1500		x
Red Foam	210	25	100	3/4"	-	50		x
Red Foam	211	100	100	3/4"	-	38		x
Red Foam	212	100	0	3/4"	-	59		x
Red Foam	213	70	100	1/2"	-	143		x
Red Foam	214	17	100	1/2"	102	587	x	
Red Foam	215	3.5	100	1/2"	106	510	x	
Red Foam	216	3.5	100	1/2"	-	392		x
Red Foam	217	7	100	1/2"	-	365	x	
Red Foam	218	25	100	1/2"	-	351	x	
Titanium honeycomb	219	0	100	1.1"	-	1121	x	
Titanium honeycomb	220	25	100	1.1"	-	328	x	
Titanium honeycomb	221	50	100	1.1"	-	117	x	
Titanium honeycomb	222	100	100	1.1"	-	59	x	
Red Foam	223	7	100	1"	-	318		x
Red Foam	224	0	100	1"	105			x
Black Foam	225	0	100	1/2"	107	643		x
Black Foam	226	100	100	1/2"	-	93		x
Black Foam	227	100	100	1/4"	-	123		x
Black Foam	228	0	100	1/4"	-	1500	x	
Black Foam	229	13	100	1/4"	-	297	x	
15 PPI Yellow Foam	230	13	100	1"	-	300	x	

Table A-1: (Continued) Runs 231 through 263

Material	Run No.	Flame Tube Configuration		Thickness	Bomb Pressure Rise	Flame Speed	Burn Through	
		% Open / Ignition	% Open / Relief				Yes	No
KCF-100 Standard	231	50%	100%	2 Layers	104	384		x
KCF-100 Standard	232	7	100	2 Used	-	392		
KCF-100 Standard	233	7	100	1 Used	-	180		x
KCF-100 Standard	234	13	100	1 New	-	73		x
GAF 2A Felt	235	13	100	3.0	-	104		x
GAF 2A Felt	236	13	100	2.0	-	113		x
GAF 2A Felt	237	7	100	1 1/2	94	436		
KCF-100 Standard	238	25	100	1 New Layer	109	152		x
KCF-100 Standard	239	13	100	1 Used	-	245		x
KCF-100 Standard	240	7	100	1 Used	-	450		
KCF-100 Standard	241	7	100	1 New	-	386	x	
KCF-100 Standard	242	7	100	2 Layers 1 New, 1 Used	-	291		x
KCF-100 Standard	243	0	100	2 Layers 1 New, 1 Used	-	1080	x	
2-A Felt	244	0	100	3 - Complete Thickness	-	730		
2-A Felt	245	0	100	3 - 1/2 Honeycomb	-	750		x
2-A Felt	246	0	100	1/2 - 1/2 Honeycomb	-	1590		
5-A Felt	247	13	100	3 - Complete Thickness	-			x
5-A Felt	248	0	100	3 - 1" Honeycomb	105	870		x
5-A Felt	249	13	100	1 - 1" Honeycomb	105	326		
5-A Felt	250	13	100	1 - Double Honeycomb	-	135	x	
5-A Felt	251	25	100	1 - Double Honeycomb	104	168		x
5-A Felt	252	25	100	1 - Double Honeycomb	107	168	x	
5-A Felt	253	100	100	1 - Double Honeycomb	-	63	x	
5-A Felt	254	100	100	1 New Honeycomb	-	39		x
8-A Felt	255	100	100	3 - Complete New Thickness	-	40		x
8-A Felt	256	0	100	New	-	1040		x
8-A Felt	257	100	100	1 - Double Honeycomb	-	52		x
8-A Felt	258	25	100	1 - Double Honeycomb	-	135		x
8-A Felt	259	0	100	1 - Double Honeycomb	103	1228		x
2-A Felt	260	25	100	1" New - 2 Honeycomb	-	193		x
2-A Felt	261	0	100	1 Used	103	960		x
5-A Felt	262	13	100	1" New 2 Honeycomb	-	326		x
5-A Felt	263	0	100	1 Used	-	1120		x

[illegible]

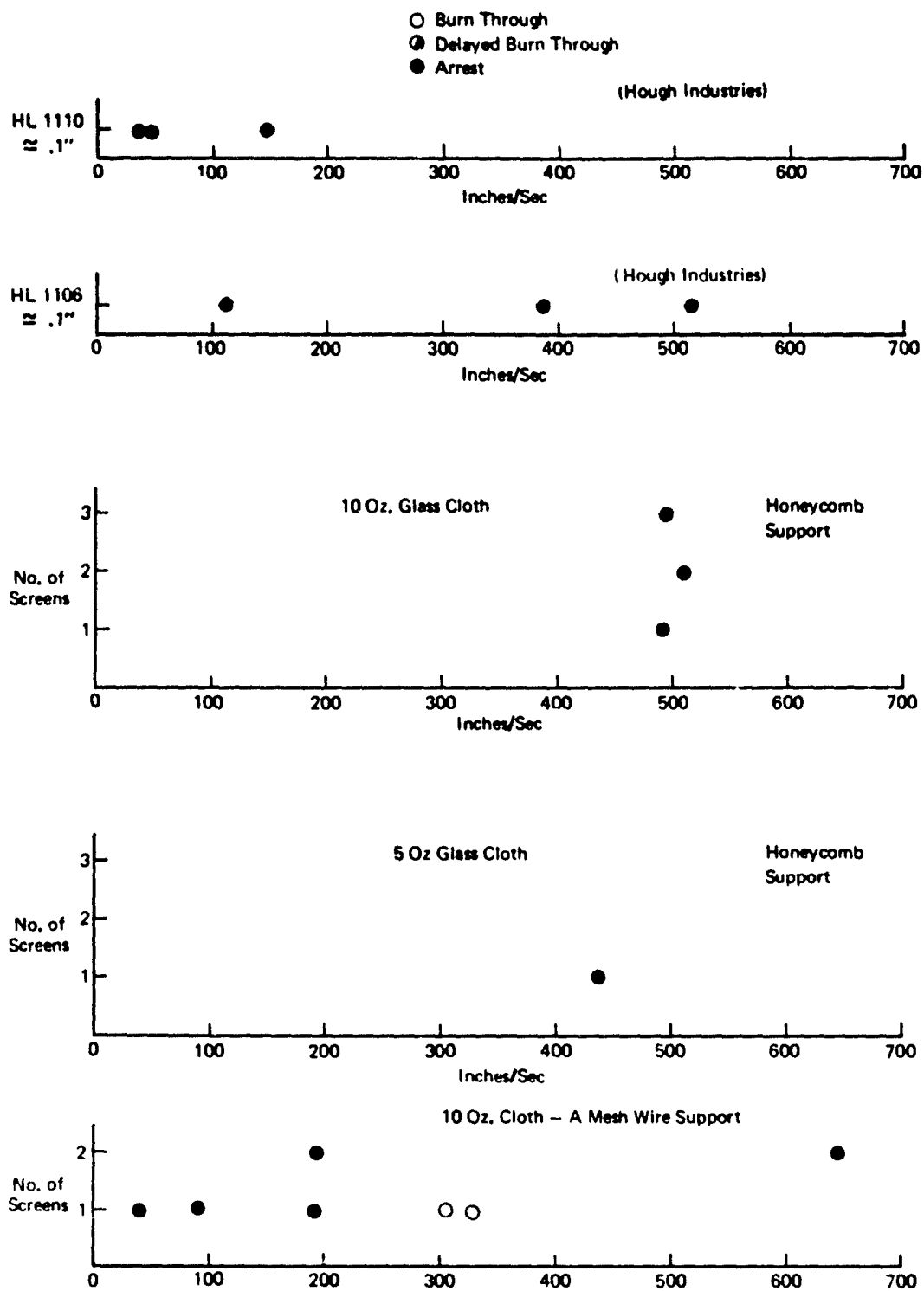


Figure A-1: Quartz Fiber and Glass Cloth Arrester Material Data

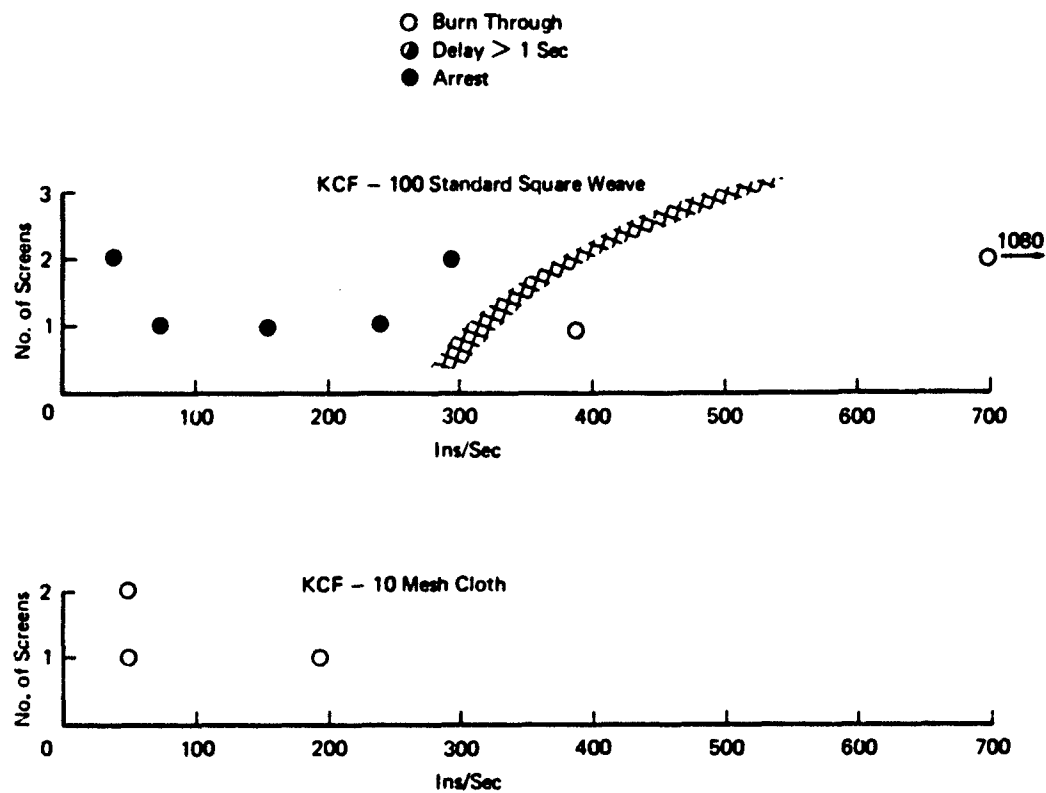


Figure A-2: KCF Carbon Fiber Cloth Screen Data

- Burn Through
- Delay > 1 Sec
- Arrest

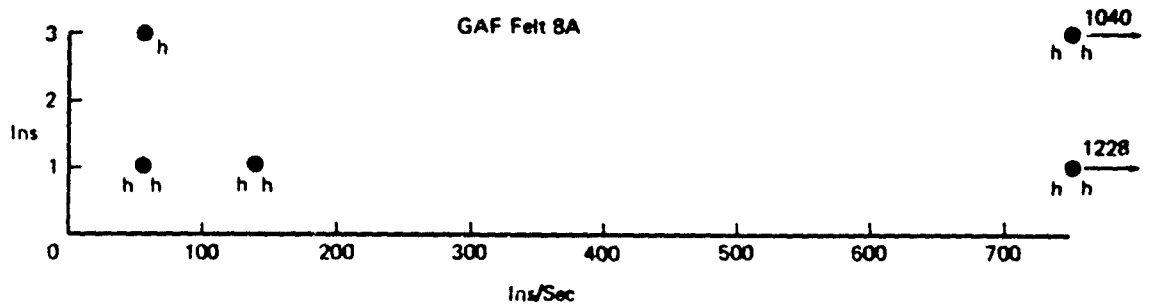
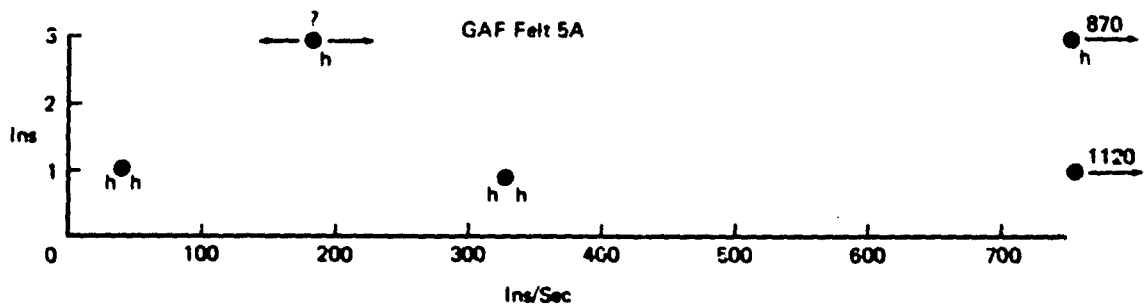
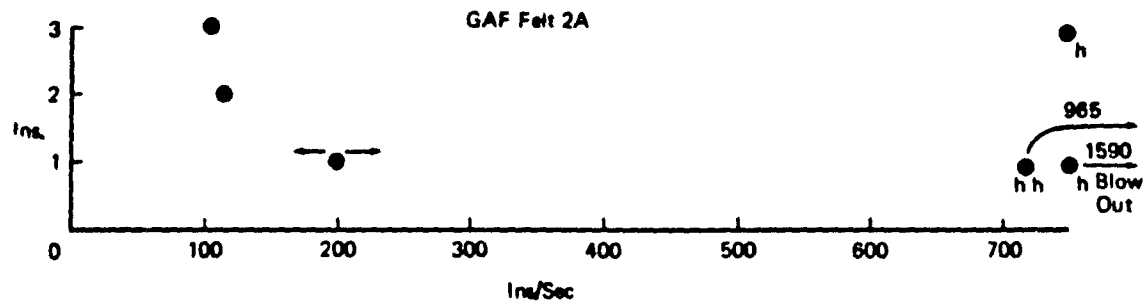
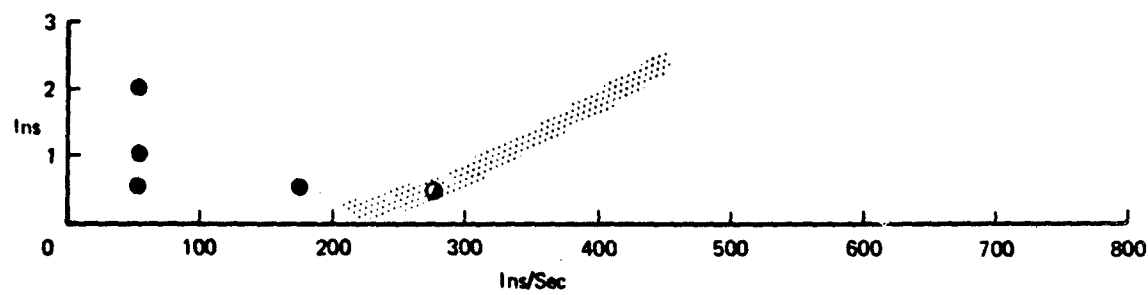


Figure A-3: GAF Felt Type 2A-5A and 8A Arrestor Material Data

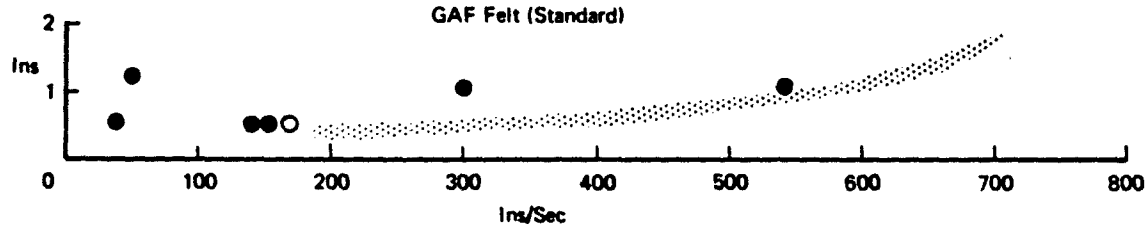
7

- Burn Through
- Delay > 1 Sec
- Arrest

3M Felt (Standard)



GAF Felt (Standard)



KCF Felt in 3/8" Layers (Carbon Fiber)

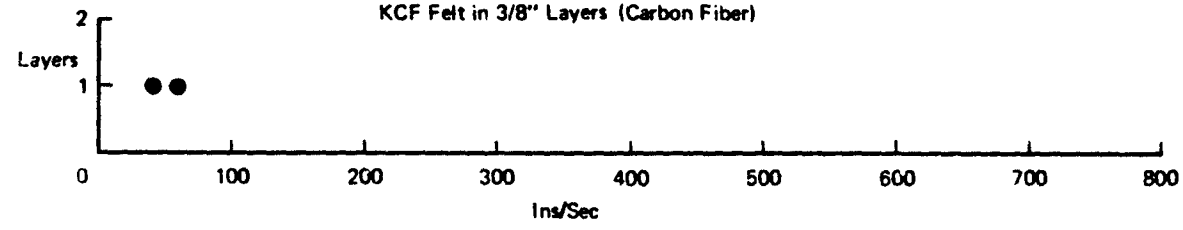


Figure A-4: 3M Scotch Brite GAF Felt (Standard) and KCF Felt Carbon Fiber Arrestor Material Data

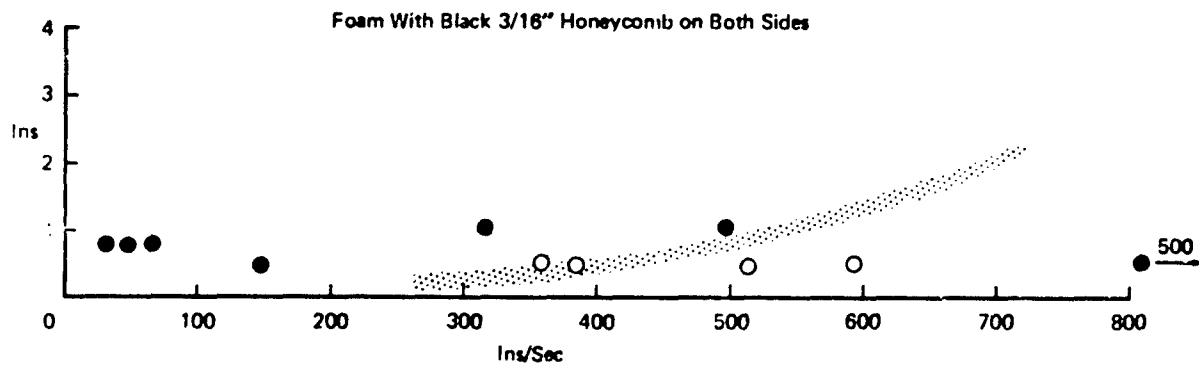
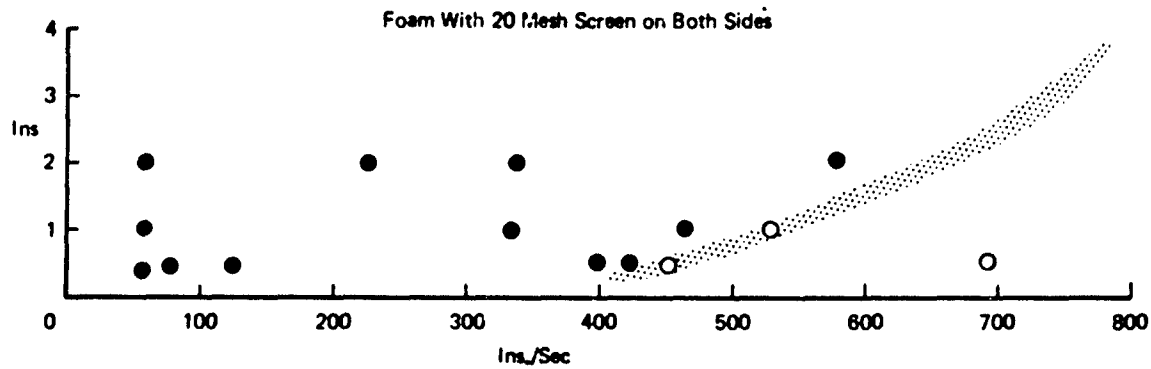
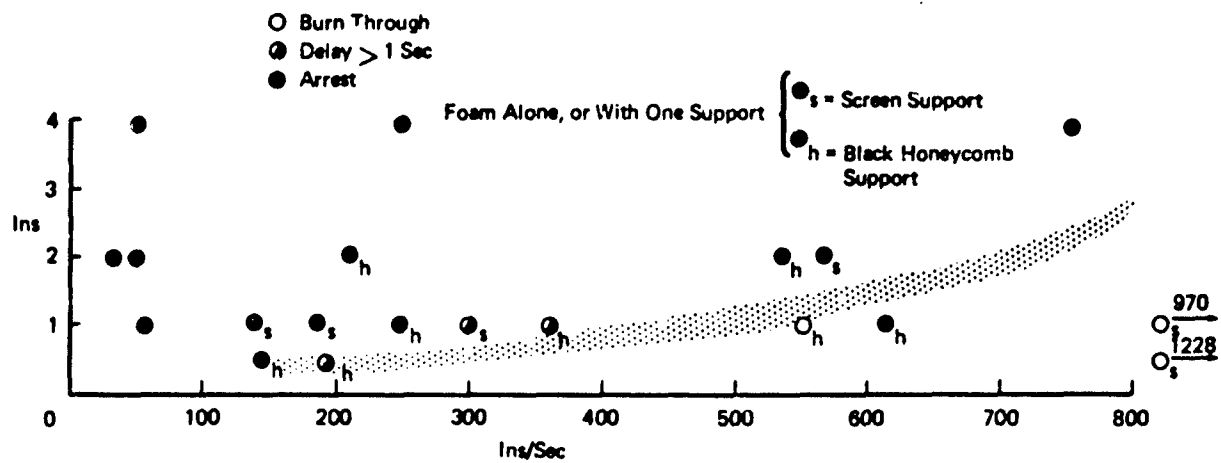


Figure A-5: 25-PPI Red Foam With Variations

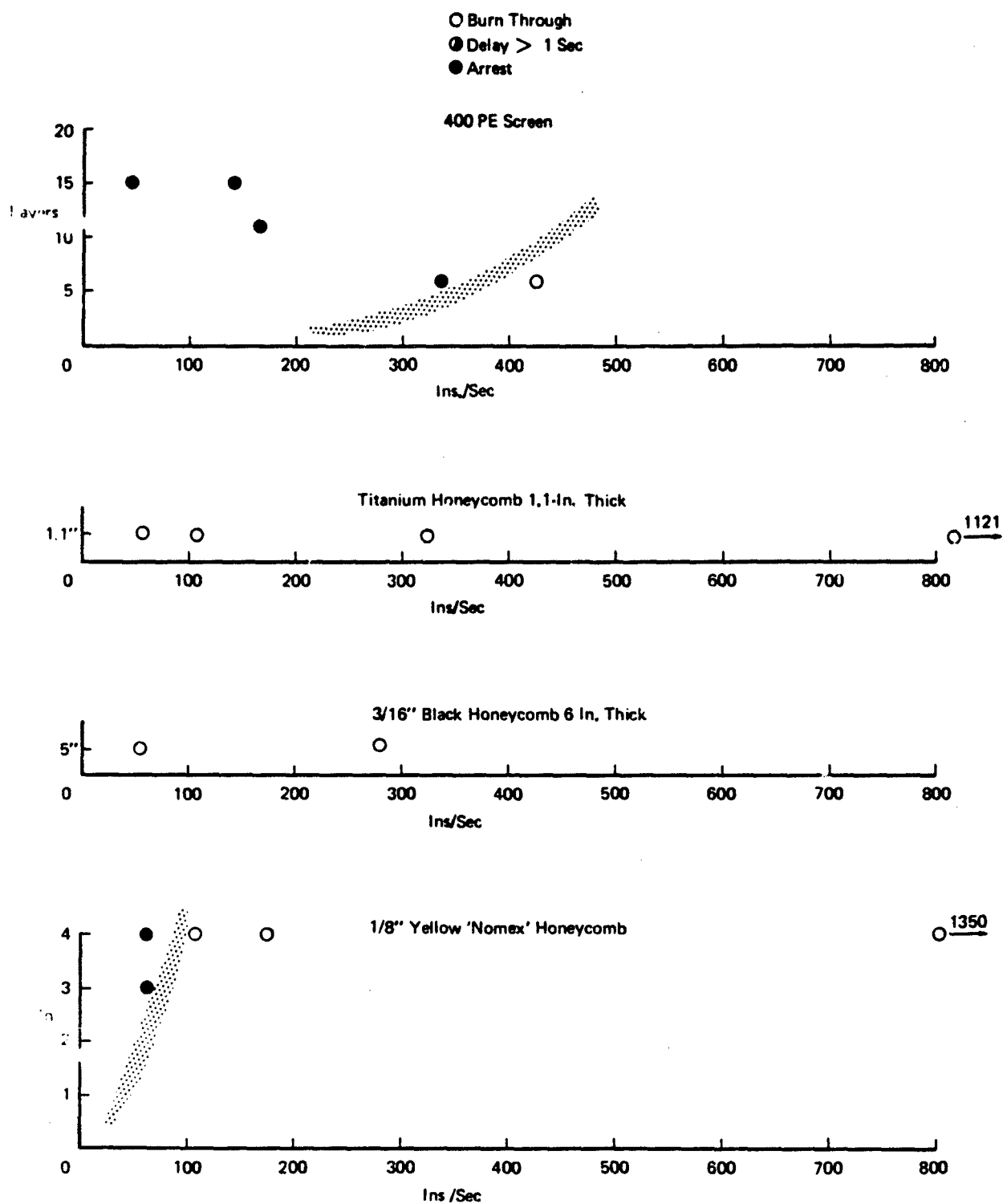


Figure A-6: Honeycomb and 400-PE Screen Arrestor Material Data

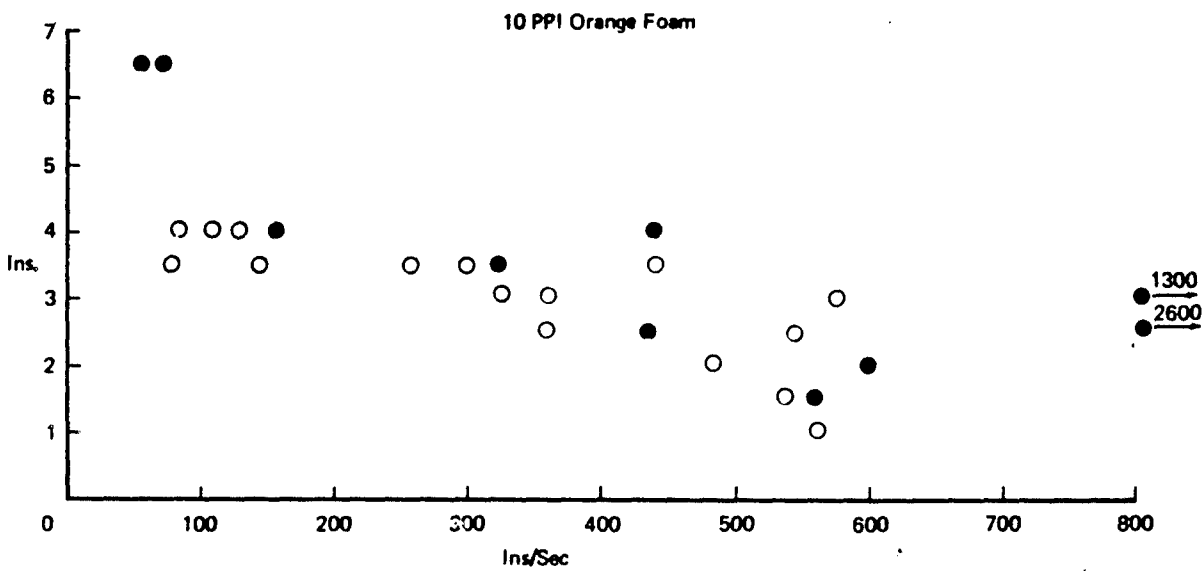
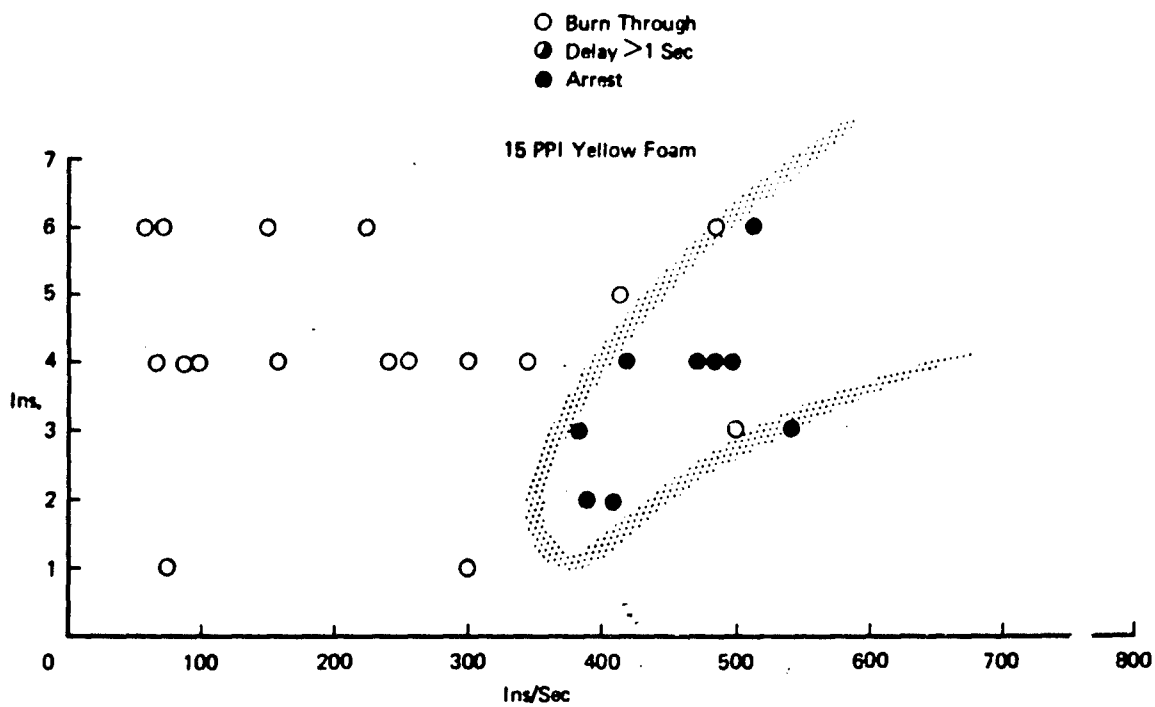


Figure A-7: 10-PPI and 15-PPI Foam Arrestor Material Dat.

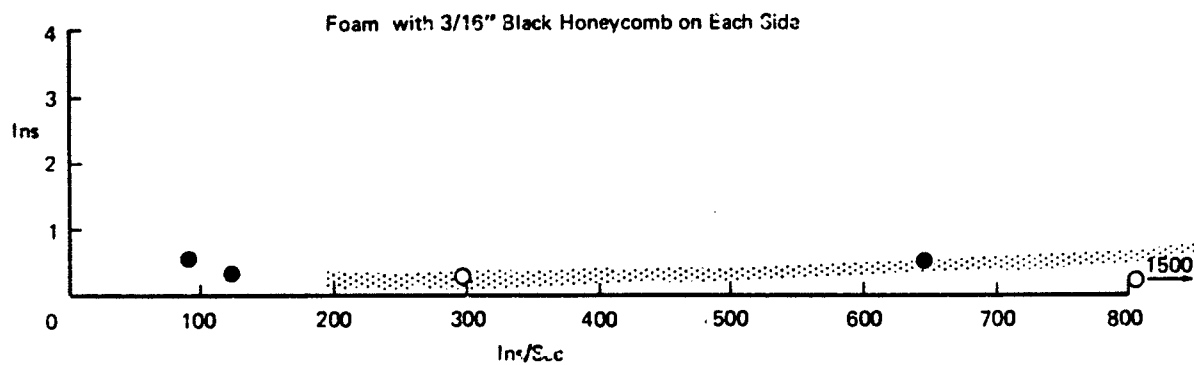
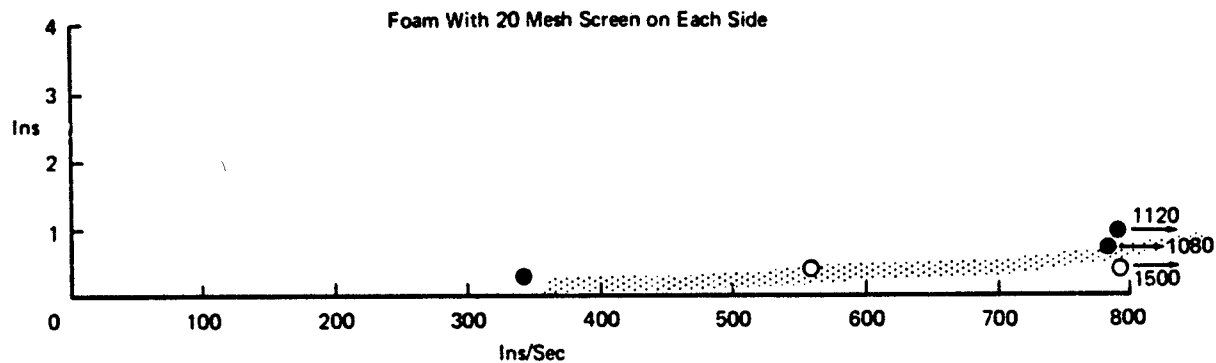
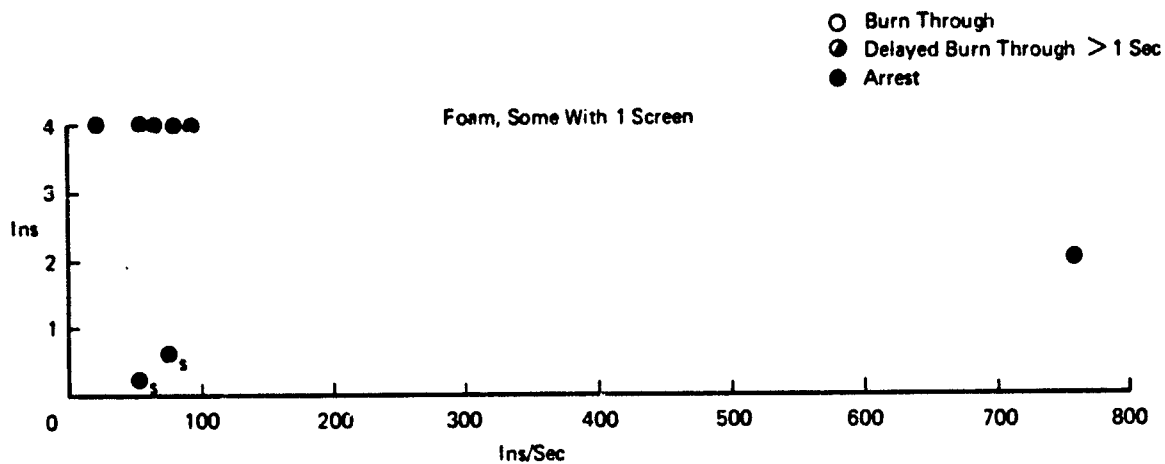


Figure A-8: Custom Material 7611XP with Various Supporting Material, Arrestor Data

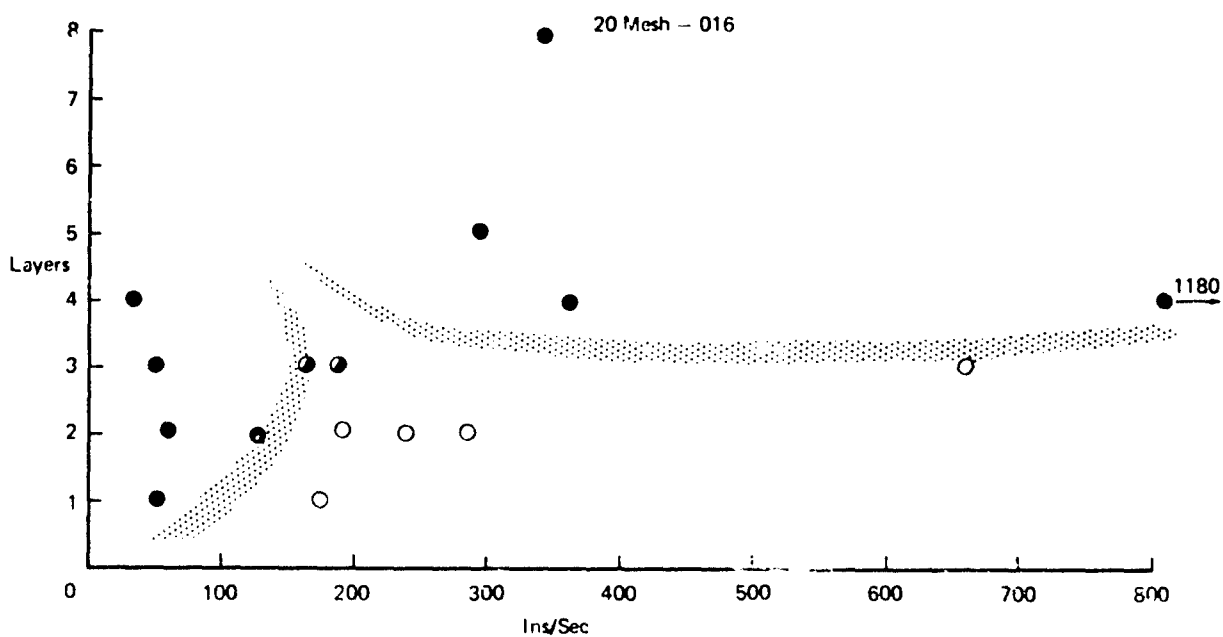
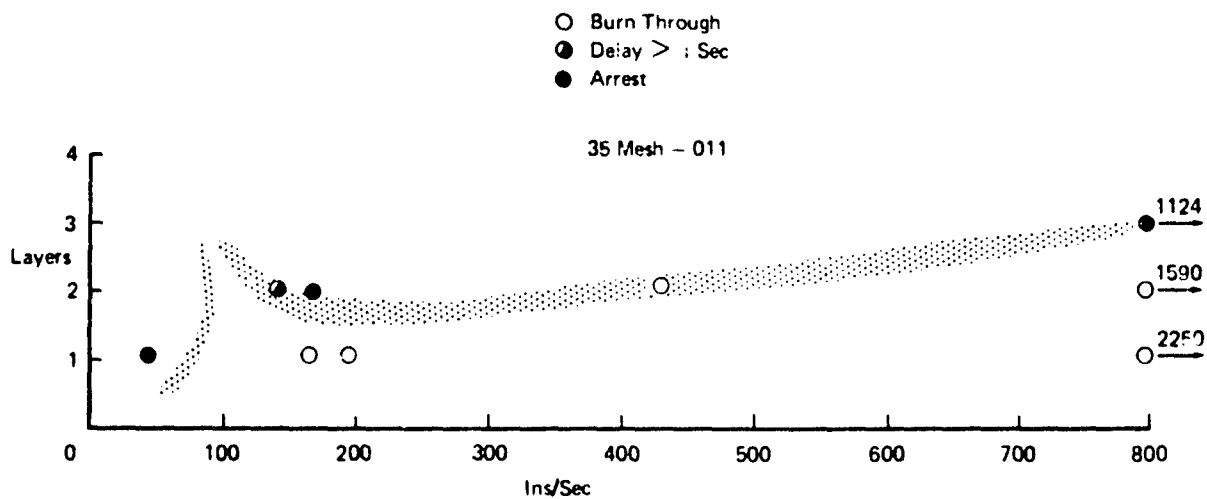


Figure A-9: 20-Mesh and 35-Mesh Stainless Steel Screen Arrestor Material Data

RUN 214
BURN THRU

25-PPJ
BLANK
BURN THRU

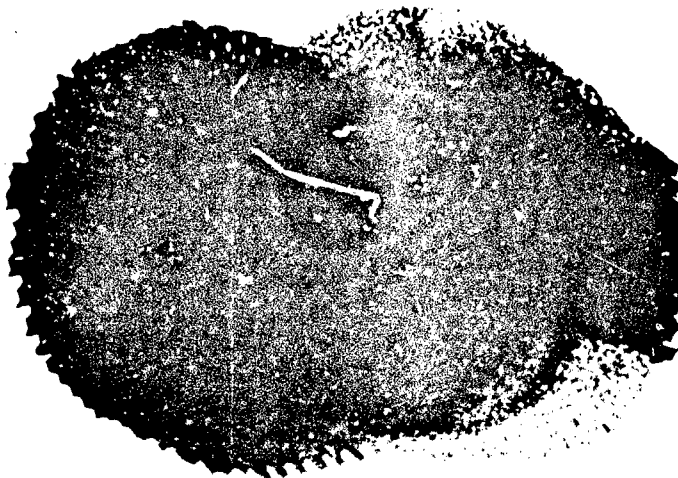
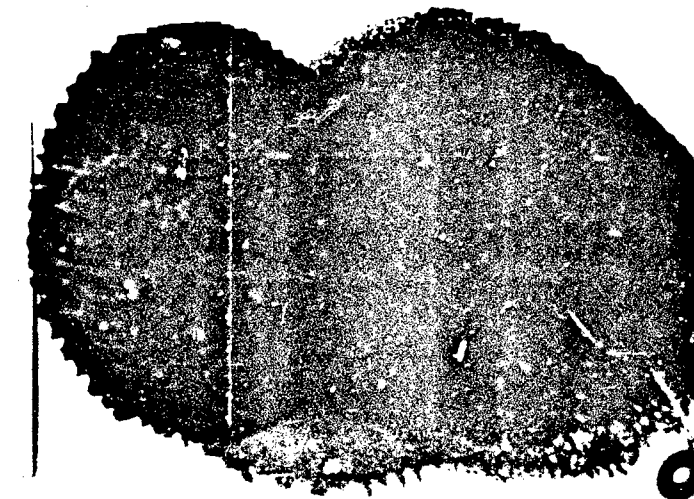


Figure A-10: 25-PPJ and Honeycomb Post Test Photograph

RUN* 132



35 MESH
WIRE
SCREEN

RUN* 132



20 MESH
WIRE
SCREEN

4

Figure A-11: 20-Mesh and 35-Mesh Stainless Steel Screen Post Test Photograph

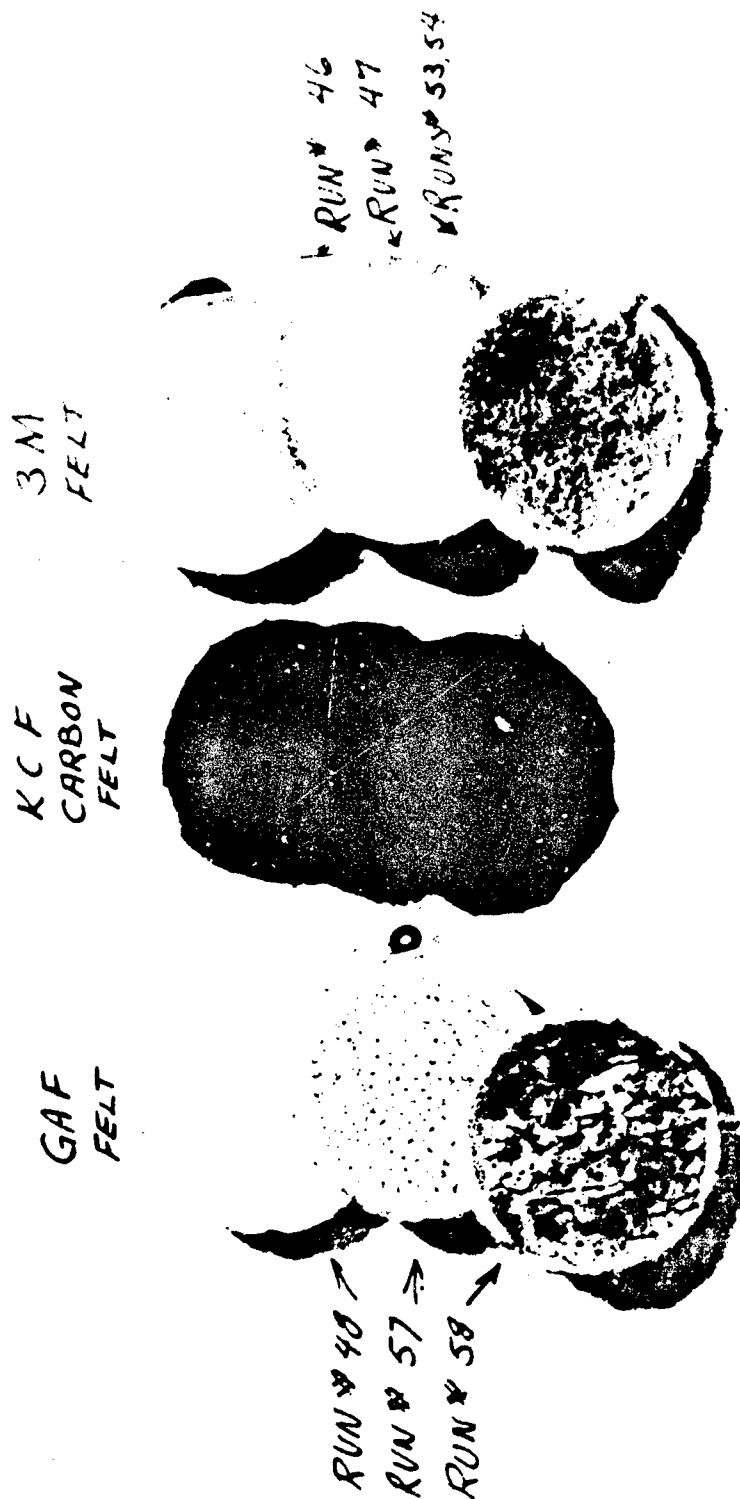


Figure A-12: GAF - FCF and 3M Felt Materials Post Test Photograph

10 PPI
ORANGE
FO.9M
↓ #196 BURN THRU

RUN #28
BURN THRU
↓
RUN #30
BURN THRU



Figure A-13: 10 PPI Foam Post Test Photograph

15 PPI
YELLOW
FOAM

RUN # 148
BURN THRU

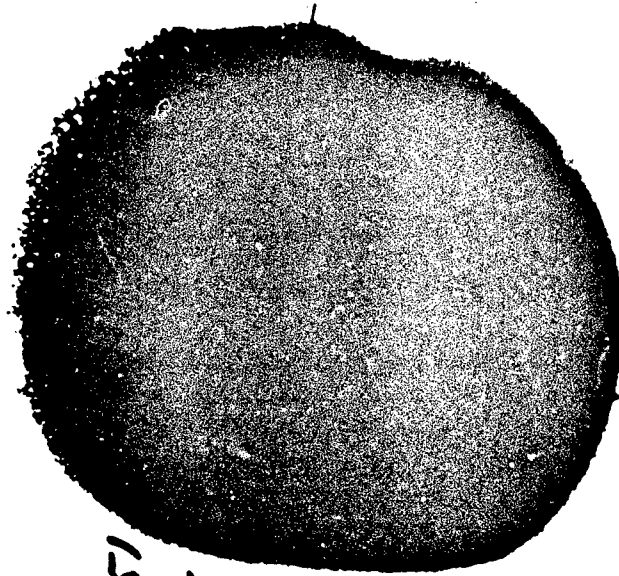


Figure A-14: 15 PPI Foam Post Test Photograph

25 PPI RED FOAM
WITH
20 MESH WIRE
SCREEN
ON
BOTH SIDES

216

ARREST

176

BURN THRU

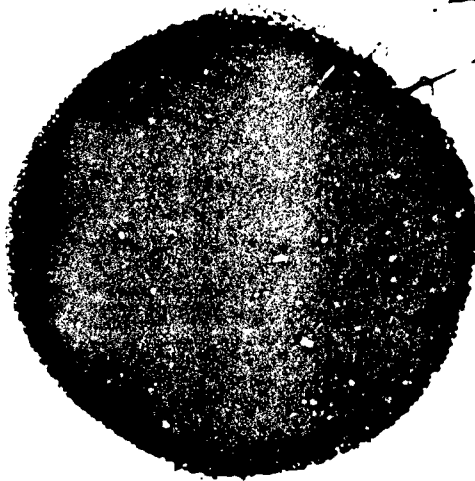


Figure A-15: 25-PPI Foam with 20-Mesh - 016 Stainless Steel Screens, Post Test Photograph

25 PPI

RED
FOAM

RUN # 197

ARREST

RUN # 198

DELAYED

BURN THRU

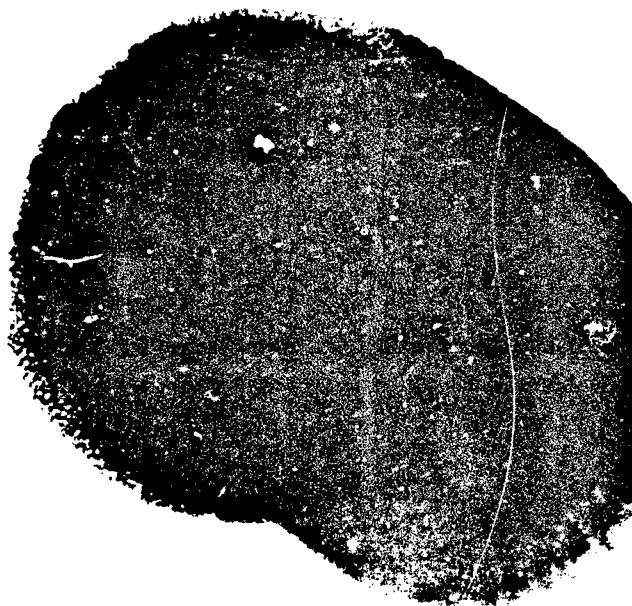
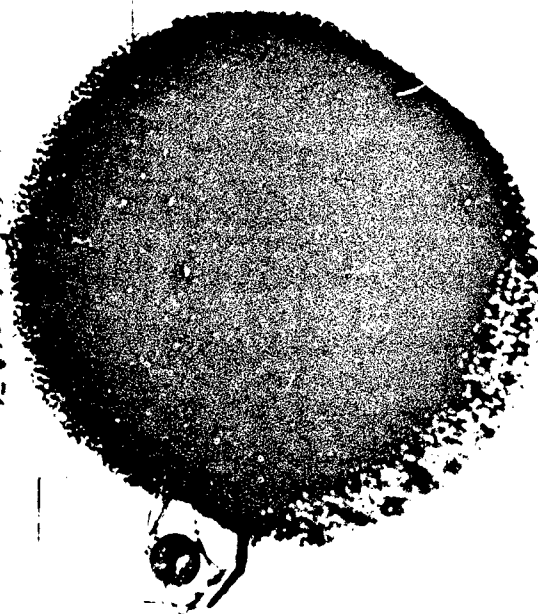


Figure A-16: 25-PPI Foam Post Test Photography

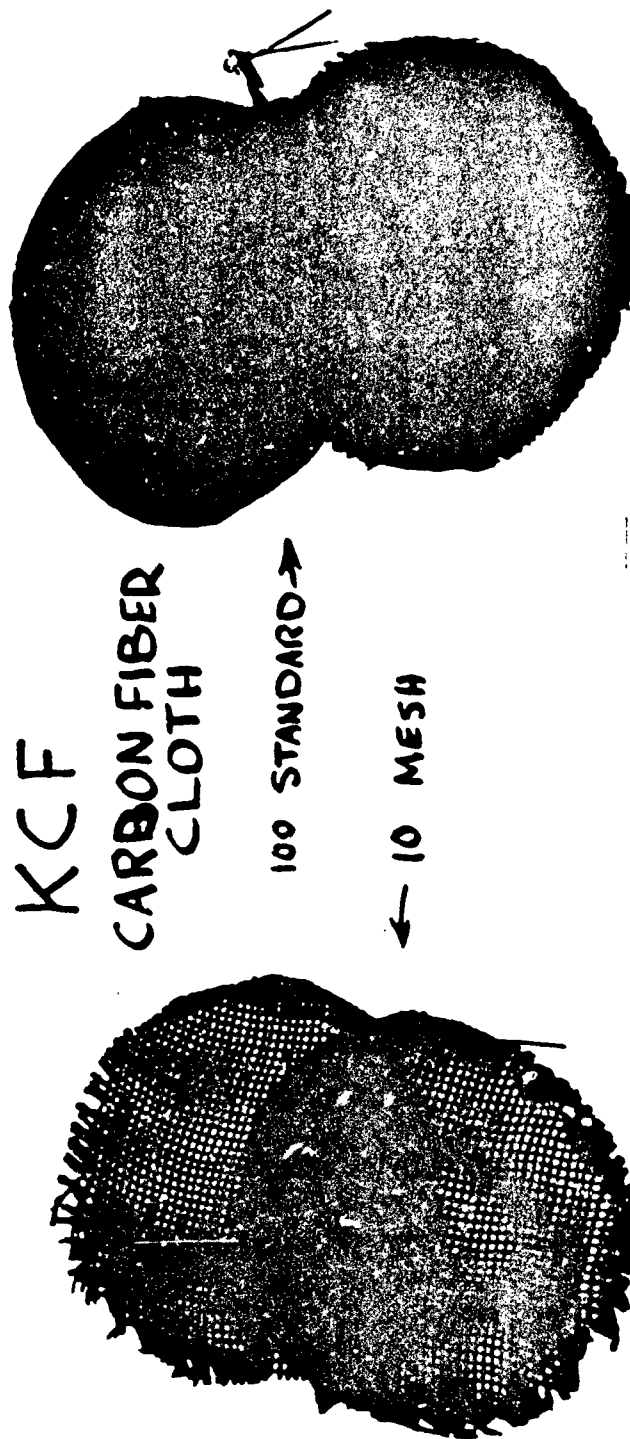


Figure A-17: KCF Carbon Fiber Cloth Screens Post Test Photograph

Table A-11: Carbon Fiber Pressure Drop Data

[illegible]

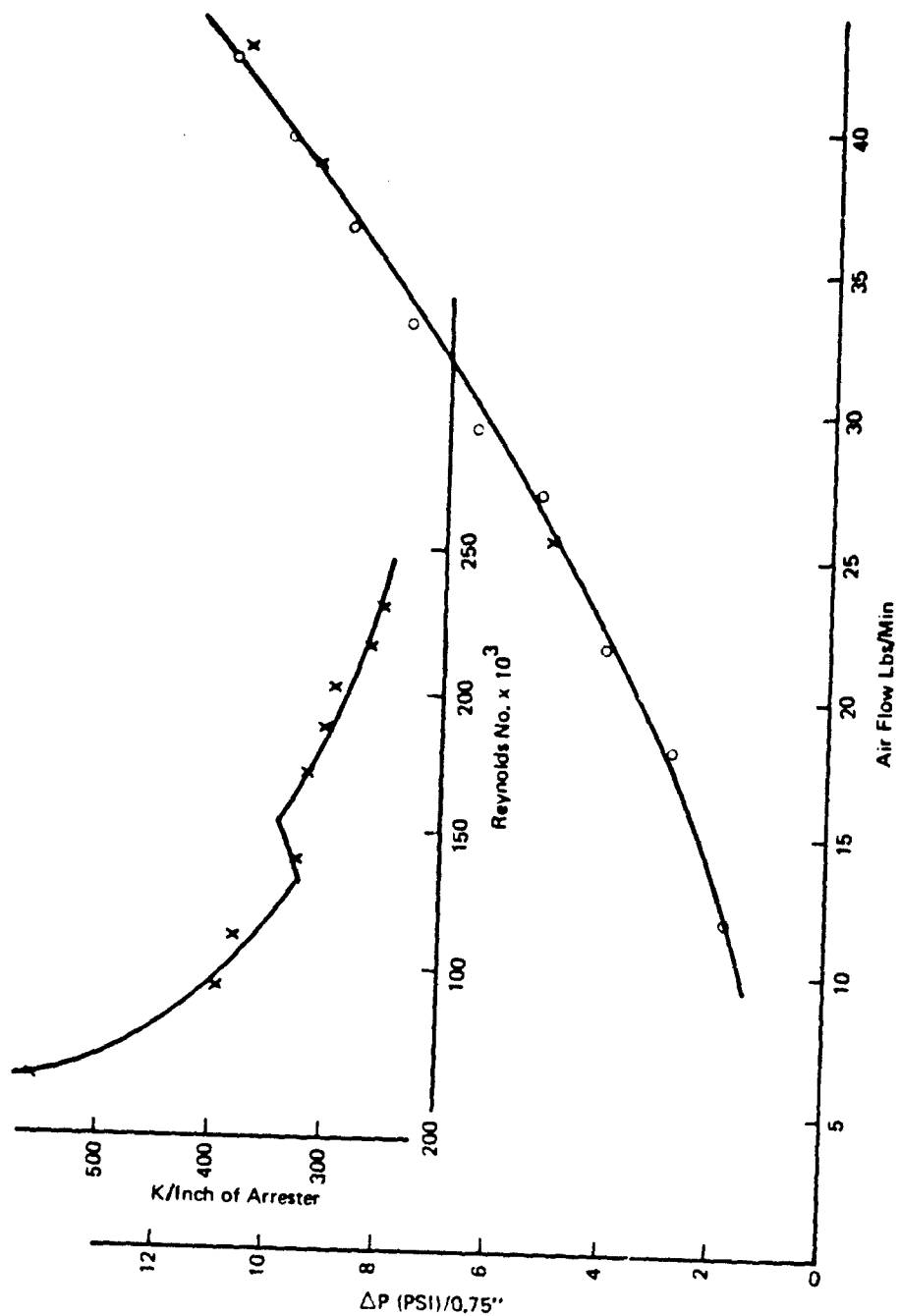


Figure A-18: Carbon Fiber ΔP Data Plots

Table A-111: 25 PPI Pressure Drop Data

[illegible]

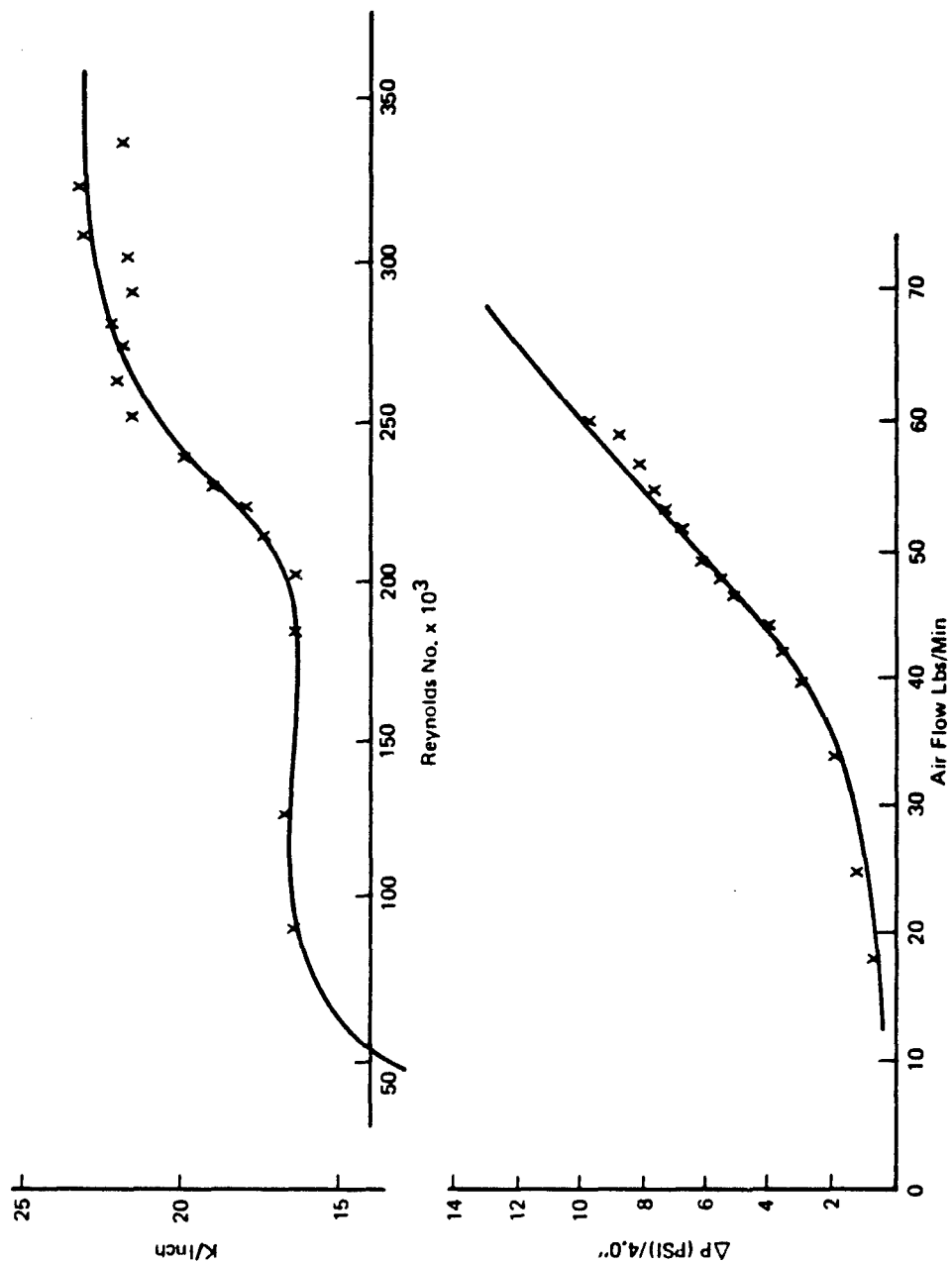
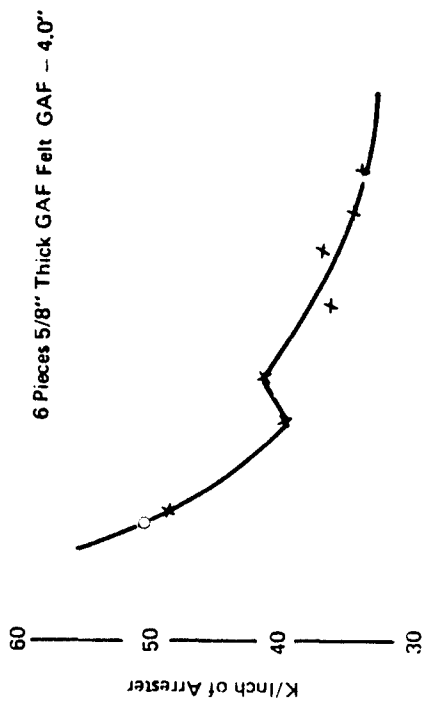


Figure A-19: 25-PPI Foam ΔP Data Plots



293

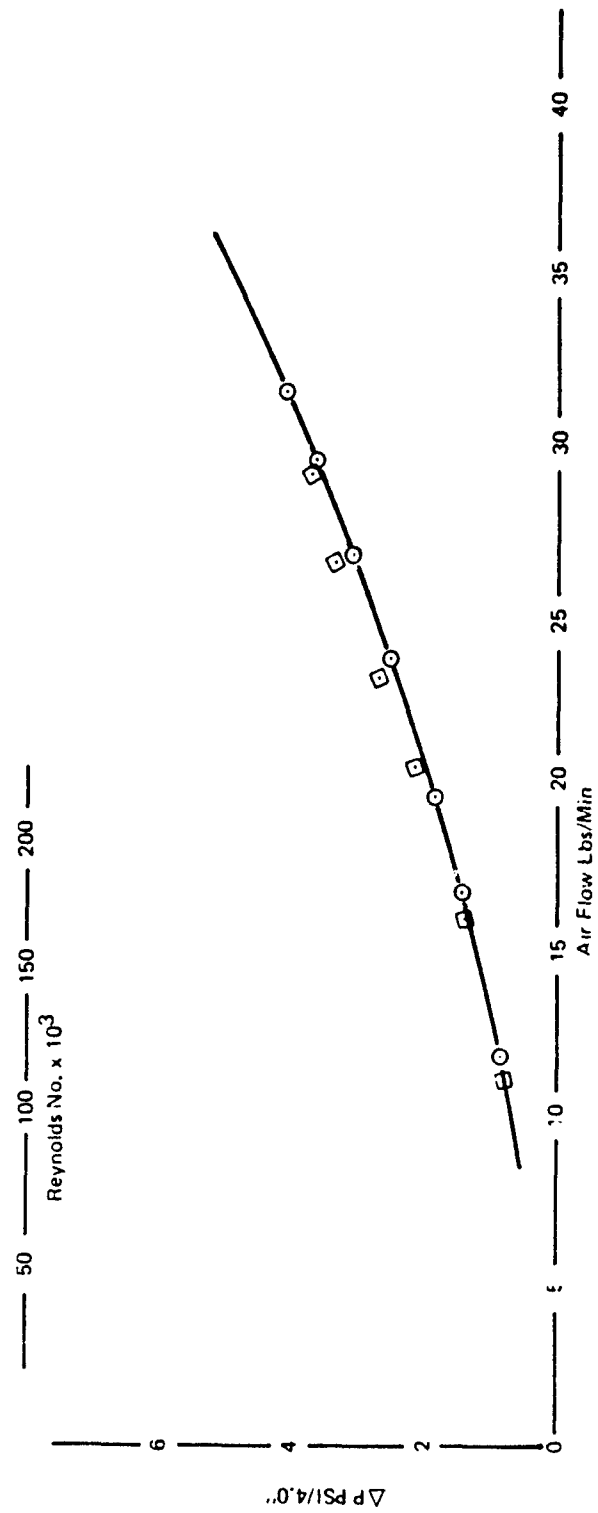


Figure A-20: GAF (Standard Felt) ΔP Data Plot:

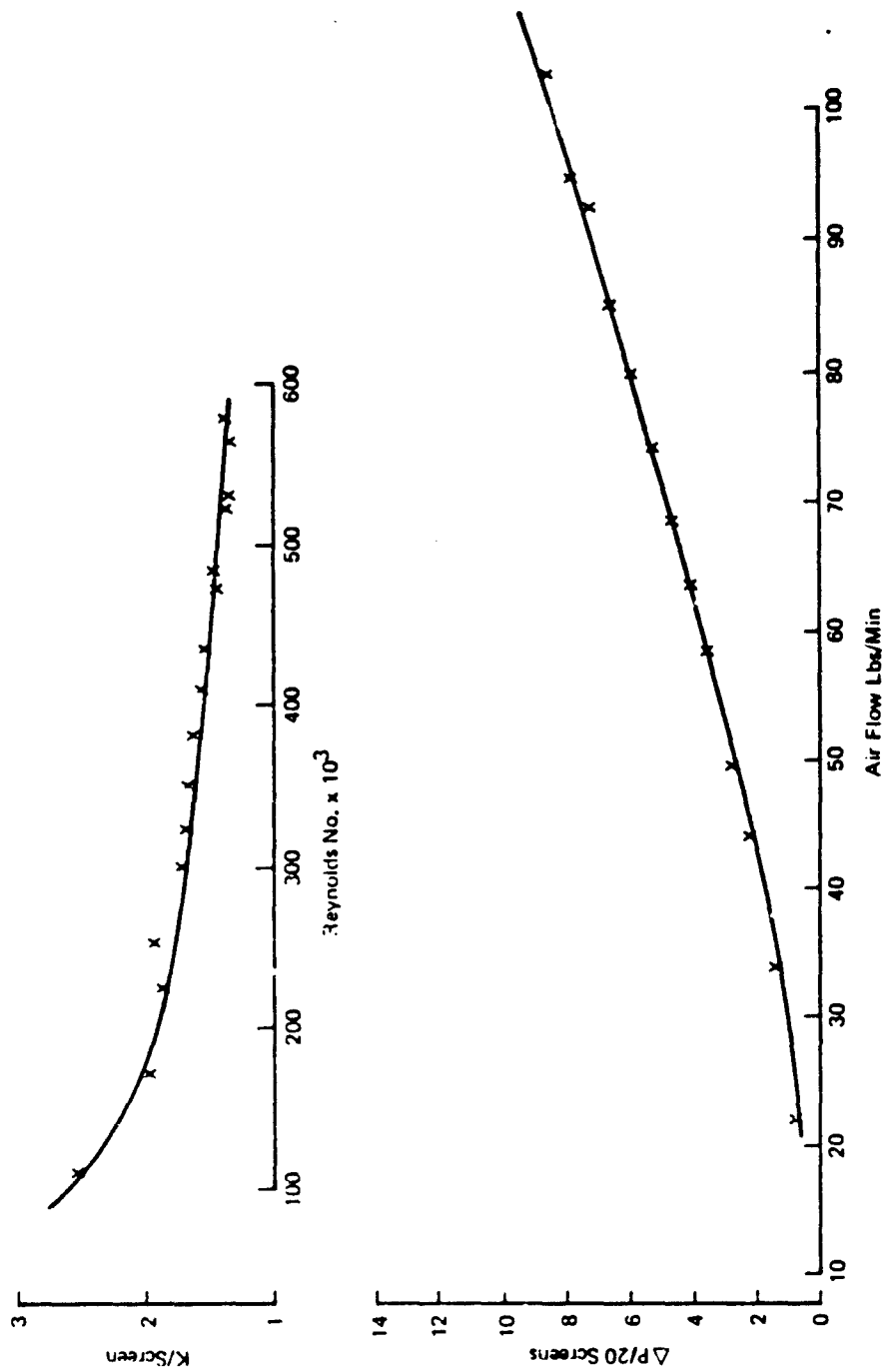


Figure A-21: 20-Mesh Stainless Steel Screen ΔP Data Plots

4

[illegible]

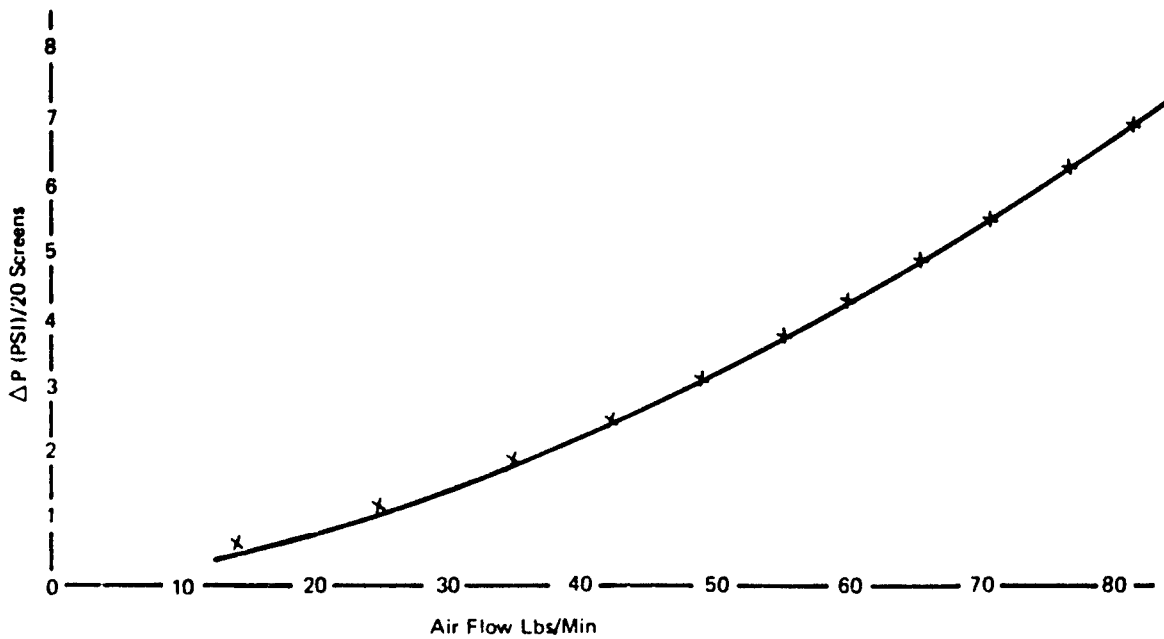
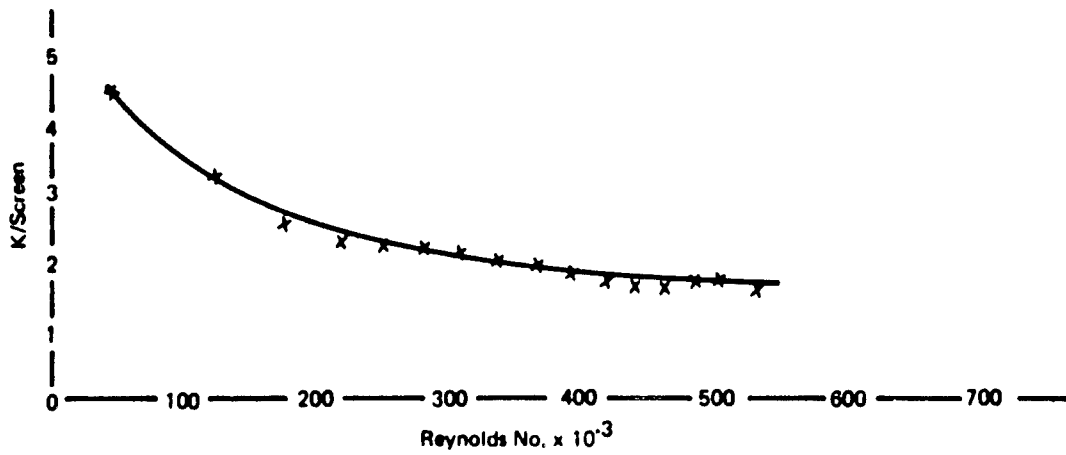


Figure A-22: 35-Mesh Stainless Steel Screen ΔP Data Plots

Table A-VII: Custom Material 7611XP Pressure Drop Data

[illegible]

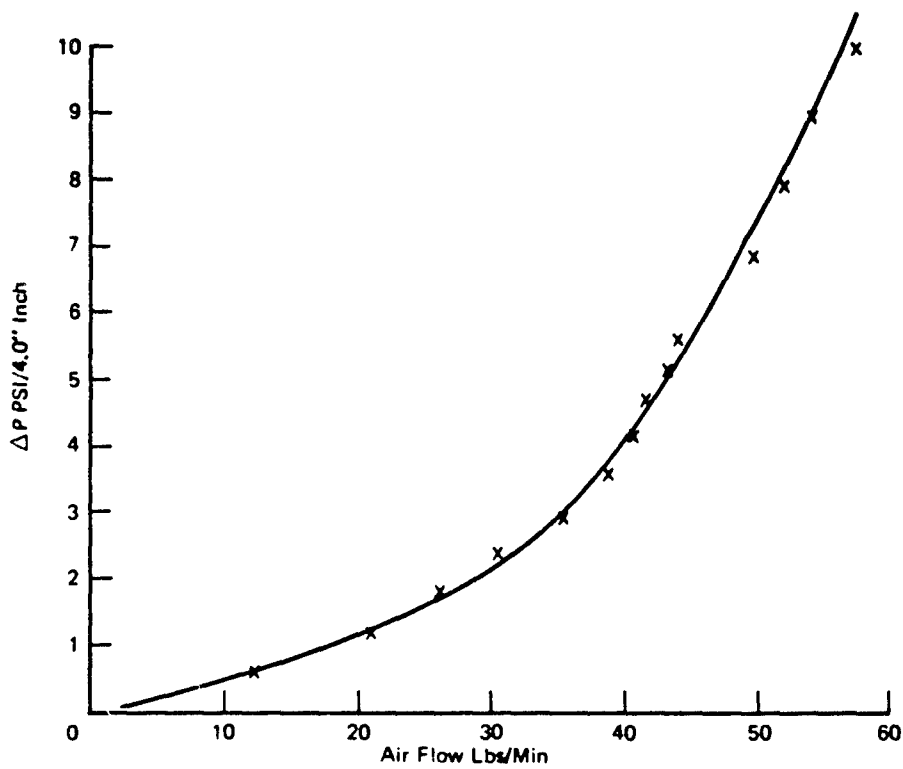
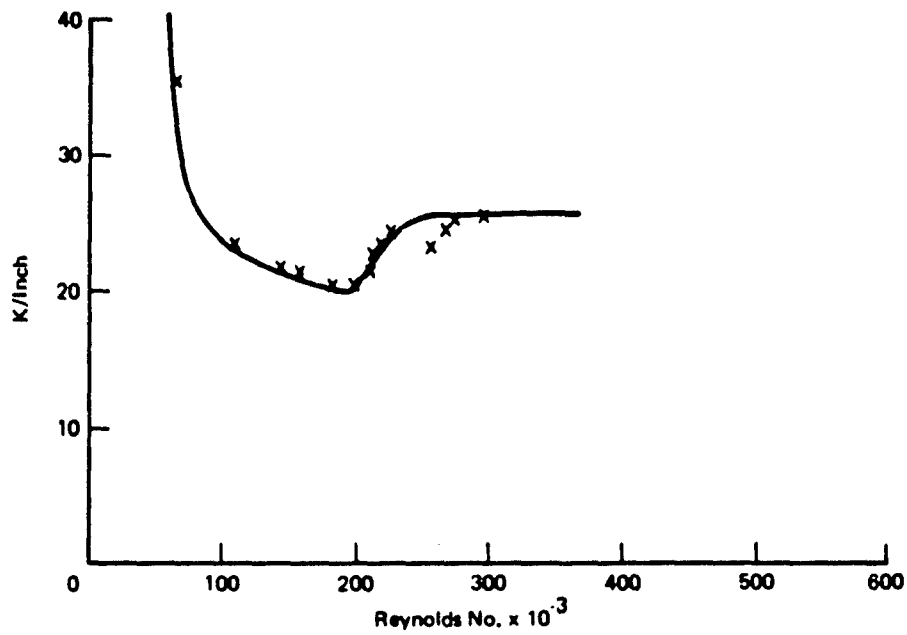


Figure A-23: Custom Material 7611XP ΔP Data Plots

Table A-VIII: 10 Oz Glass Cloth Pressure Drop Data

[illegible]

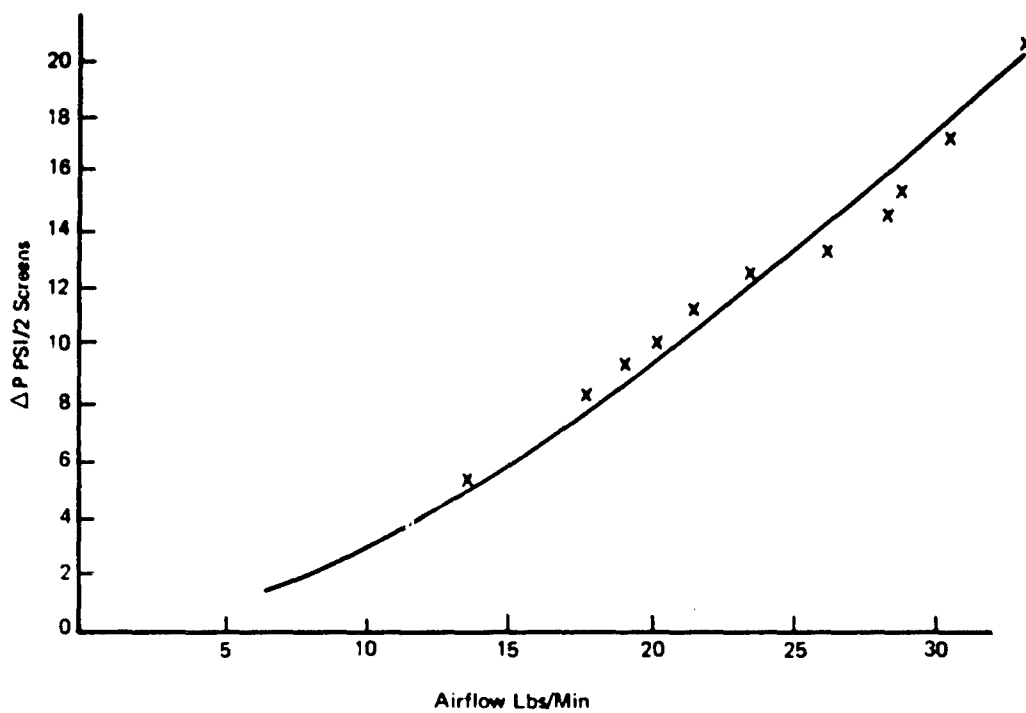
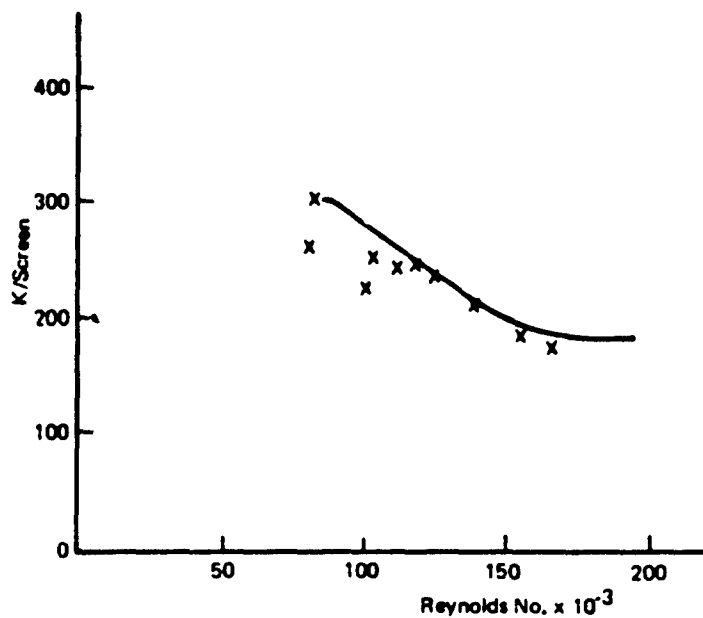


Figure A-24: 10-Ounce Glass Cloth ΔP Data Plots

Table A-IX: 3M Scotch Brite Pressure Drop Data

[illegible]

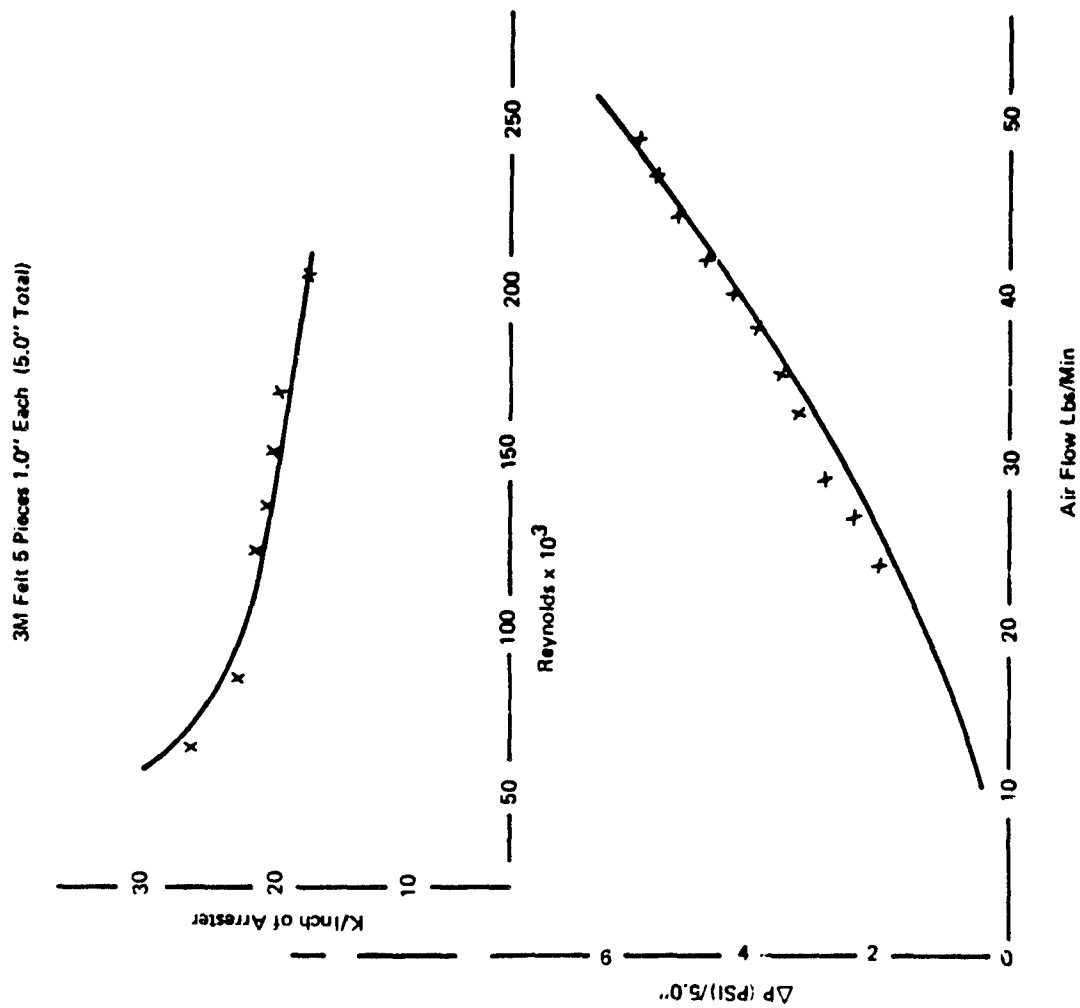


Figure A-25: 3M Scotch Brite ΔP Data Plots

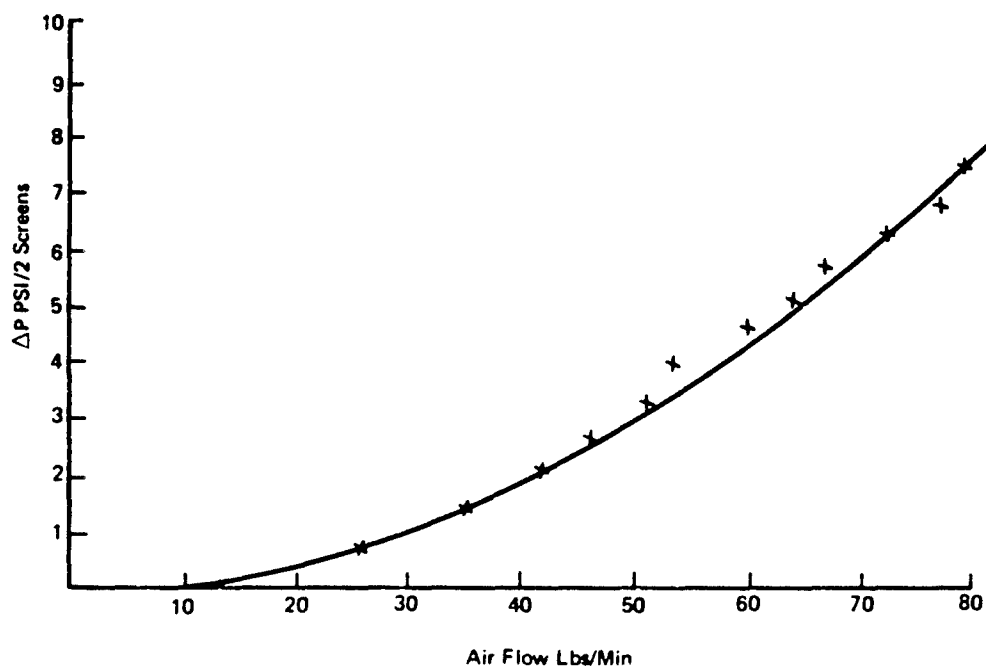
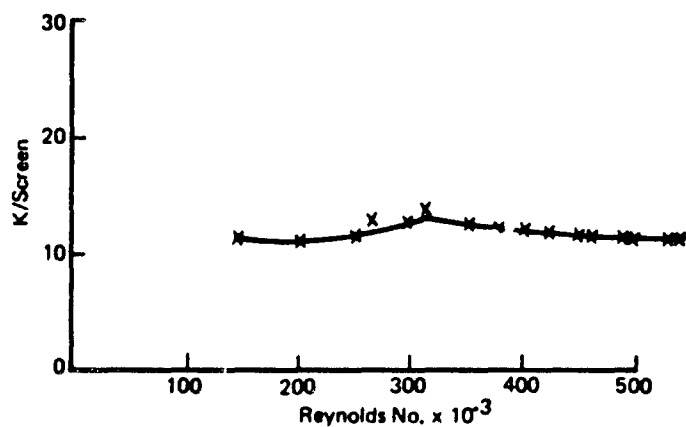


Figure A-25: KCF - 100 Carbon Fiber Cloth ΔP Data Plots

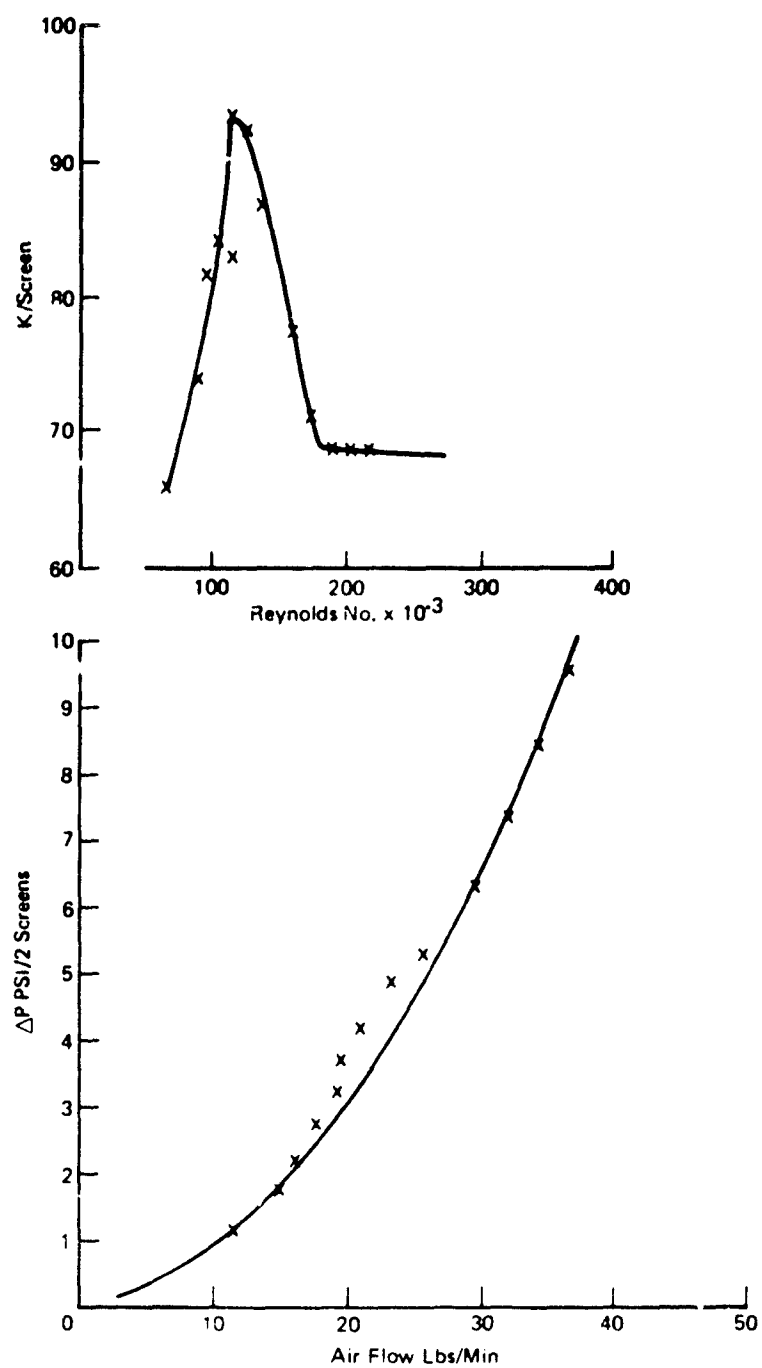


Figure 27: KCF - 100 Standard Carbon Fiber Cloth ΔP Data Plots

Table A-XII: 10-PPF Foam Pressure Drop Data

Type of Material	(1) Thickness L ins	(2) P _V psi	(3) P _S psi	(4) ΔP psi	(5) P _S (3) + 14.7 psia	(6) P _V /P _S (2)/(5)	(7) WV/T/P _S From Flow Tube Calibration	W 2.6 x (5) x (7) Lbs/Min	R _e x 10 ⁻³ 5,110 x W	K/Inch 33,800 ΔP W ² L
			M L. 2.58							
10 PPI	4.0"	.11	.52	.64	15.22	.0073	.385	15.22	78	23.4
Foam		.25	1.0	1.21	15.7	.01595	.56	22.9	117.5	19.45
Orange		.37	1.51	1.8	16.21	.0228	.68	28.6	146.5	18.6
		.45	2.02	2.4	16.72	.027	.74	32.1	164.	19.75
		.5	2.54	2.94	17.24	.029	.77	34.5	177.	20.9
		.58	3.18	3.65	17.88	.0325	.82	38.1	195.	21.3
		.6	3.6	4.04	18.3	.0328	.825	39.3	201.	22.2
		.63	4.18	4.66	18.88	.0334	.83	40.6	208.	23.9
		.65	4.6	5.1	19.3	.0337	.84	42.0	215.	24.4
		.69	5.1	5.62	19.8	.035	.85	43.8	225.	24.8
		.7	5.64	6.2	20.34	.0345				
		.72	6	6.55	20.7	.0348				
		.75	6.45	7.03	21.15	.0355				
		.76	7.18	7.77	21.88	.0348				
		.76	7.46	8.08	22.16	.0345				
		.8	8.08	8.8	22.78	.0351				
		.8	8.5	9.15	23.2	.0345				
		.8	9.0	9.7	23.7	.0338				
		.82	9.5	10.15	24.2	.034	.835	52.5	269.	31.1
		.85	10.05	10.8	24.75	.0344				
		.9	10.6	11.3	25.3	.0355				
		.97	12.5	13.3	27.2	.0356				
		1.02	15.2	16.0	29.9	.034	.835	65.	333.	32.

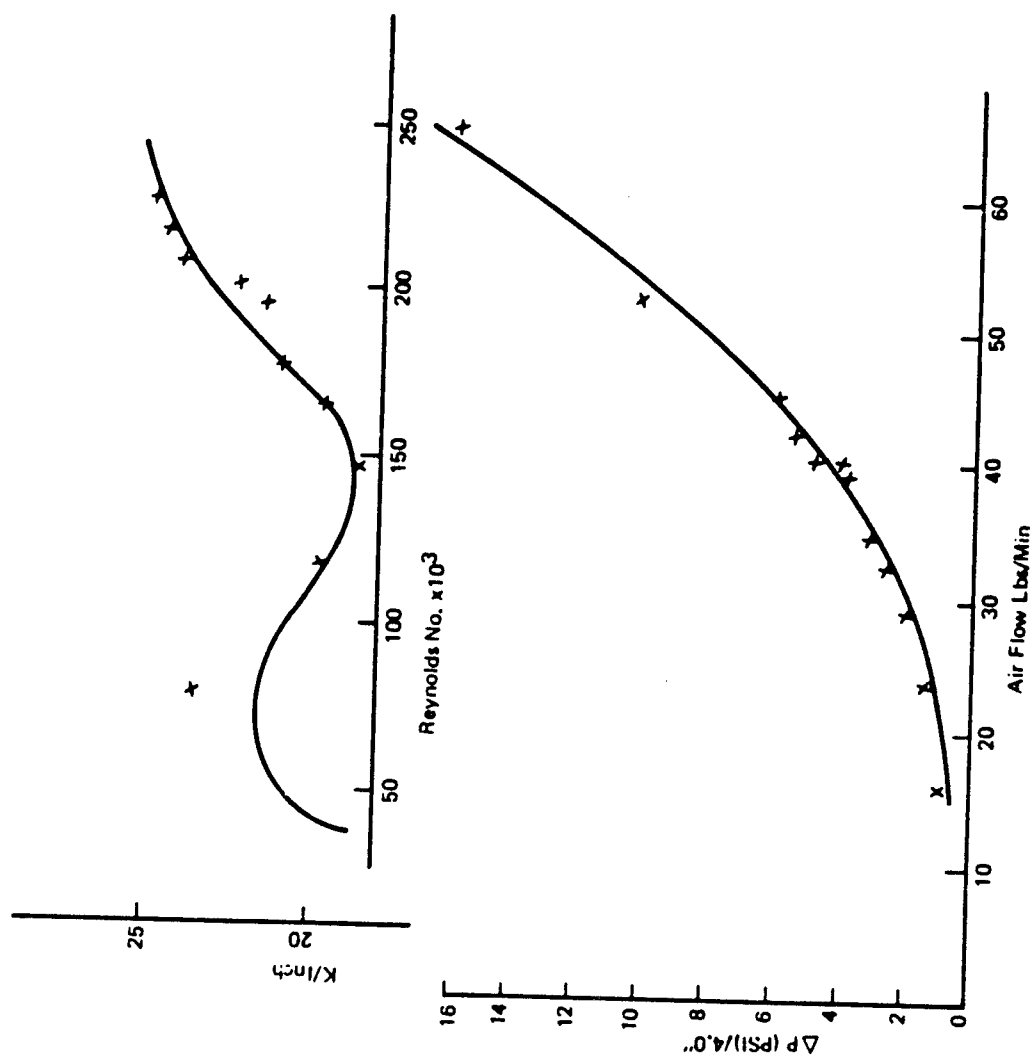


Figure A-28: 10-PPI Foam ΔP Data Plots

Table A-XIII: Hough Industries HL 1106 and HL 1107 Pressure Drop Data

Type of Material	① Viscosity cP Ins	② P _V psi	③ P _S psi	④ ΔP psi	⑤ P _S psi ③ + 4.7	⑥ P _V /P _S ②/⑤	⑦ WV/T/PS From Flow Tube Calibration	W 2.6 x ⑤ x ⑦ Lbs/Min	R _e x 10 ³ 5,880 x W	K/Inch 19,248 ΔP W ² L
		.06	0.5	0.49	15.2	.0032	.26	10.27	60.38	8.9
H. L.		.06	1.	1.04	15.7	.0032	.255	10.4	61.15	18.5
1110		.06	1.53	1.6	16.23	.0037	.278	11.7	68.8	22.49
10	≥ 0.1	.1	1.95	2.05	16.65	.006	.35	15.2	89.37	17.1
Screens		.12	2.45	2.51	17.15	.007	.38	16.95	99.66	16.82
		.12	2.97	3.07	17.67	.0068	.372	17.1	100.5	20.2
		.13	3.49	3.61	18.19	.00715	.381	18.	105.8	21.45
		.15	4.1	4.25	18.8	.00793	.403	19.7	115.8	21.
		.2	4.7	4.89	19.4	.0103	.46	23.2	136.4	17.48
		.2	5.13	5.32	19.83	.0101	.45	23.2	136.4	19.
		.21	6.05	6.2	20.75	.01012	.45	24.3	142.8	20.21
		.23	6.98	7.19	21.68	.01065	.464	26.1	153.5	20.31
		.3	8.1	8.12	22.8	.0135	.525	31.1	182.8	16.16
		.37	9.1	9.2	23.8	.0156	.565	35.	205.8	14.45
		.45	9.95	10.13	24.65	.0183	.61	39.	229.3	12.82
H.L.		.06	.5	0.51	15.2	.0033	.26	10.25	60.2	9.34
1106		.06	1.	1.08	15.7	.00383	.28	11.4	67.	15.99
6	≥ 0.1	.07	1.5	1.6	16.2	.00432	.298	12.6	74.	19.39
Screens		.12	2.1	2.18	16.8	.00715	.38	16.6	97.61	15.23
		.15	2.6	2.72	17.3	.00866	.42	18.9	111.13	14.66

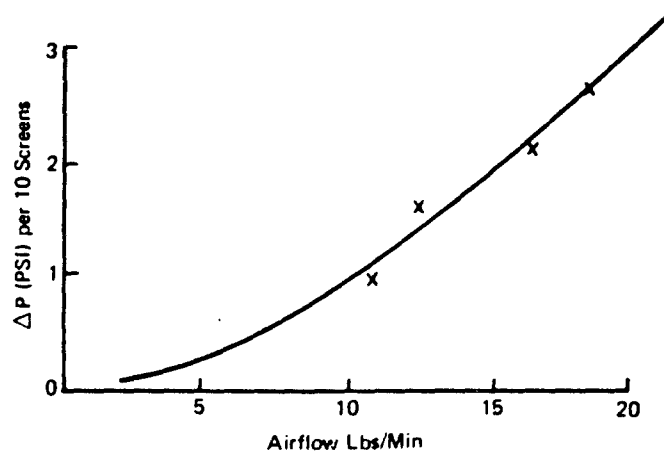
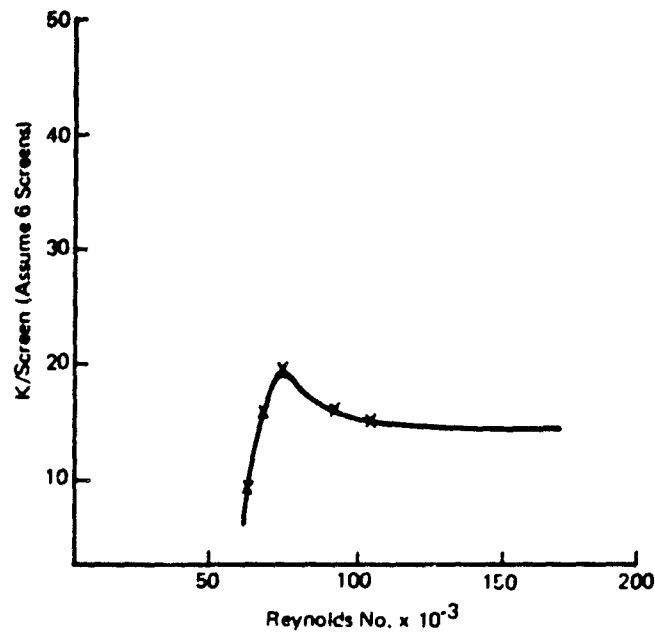


Figure A-29: Hough Industries HL 1106 ΔP Data Plots

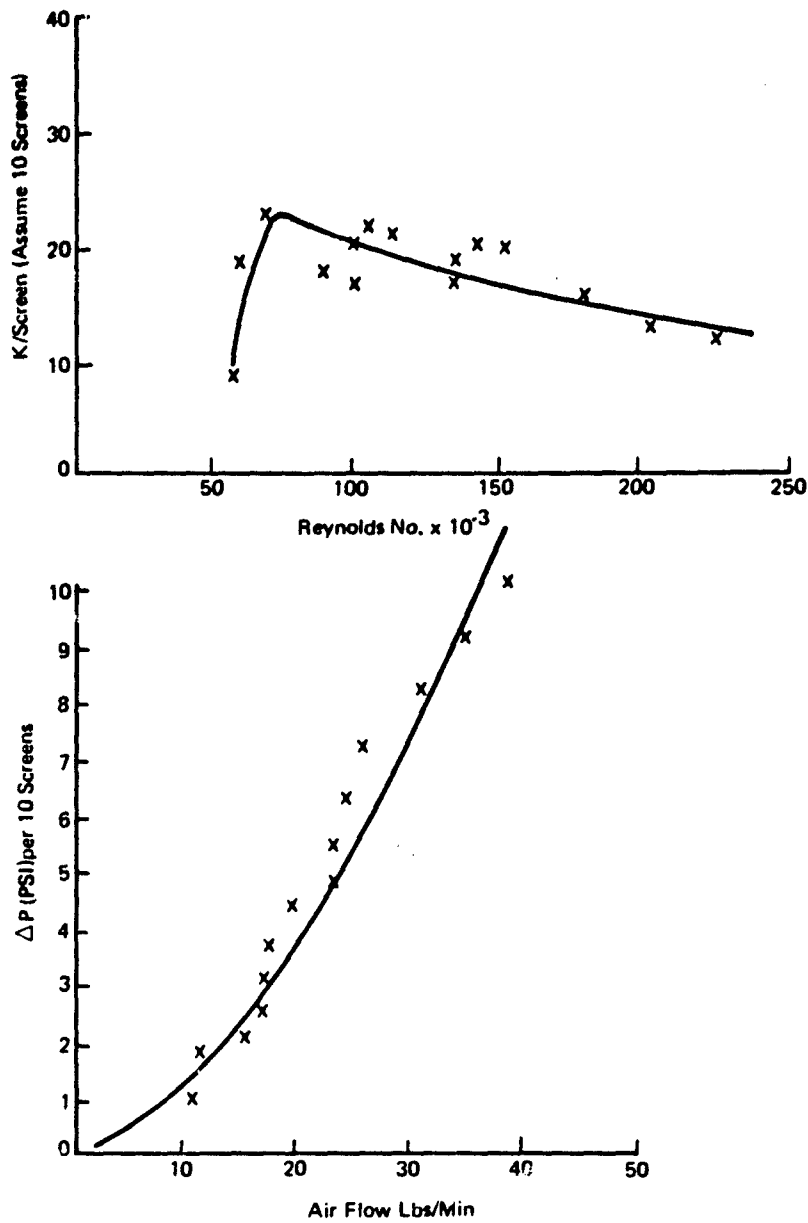


Figure A-30: Hough Industries HL 1110 ΔP Data Plots

Table A-XIV: 25 PPI Research Foam Pressure Drop Data

[illegible]

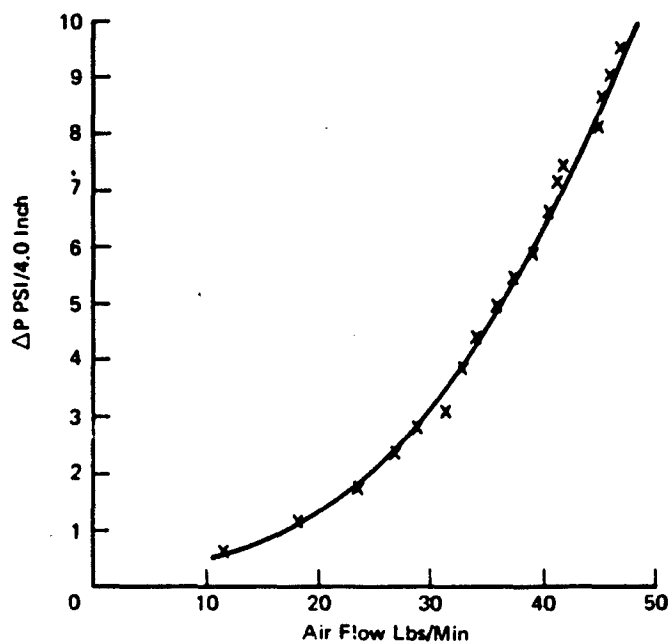
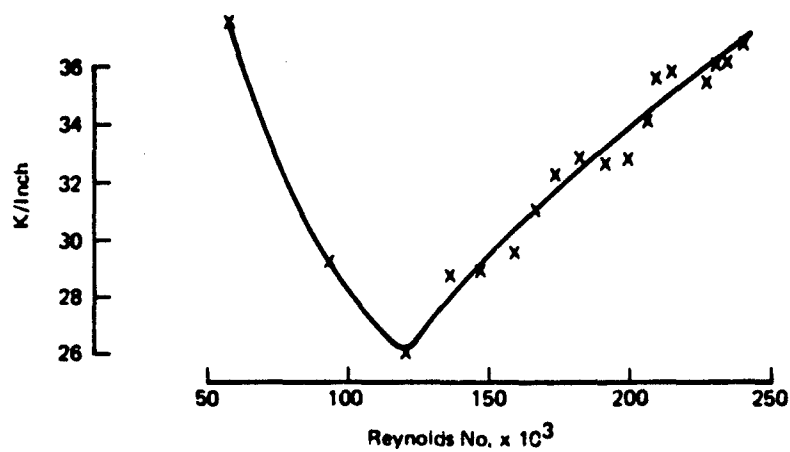


Figure A-31: 25-PPI Research Foam ΔP Data Plots

Table A-XV: Variable Geometry Tank Test Data, Runs 001 through 024

Material	Thickness (in.)	Run No.	Combustion Volume Vc (ft ³)	Vr/Vc	Combustion Pressures		Pc/Po	Ignition Mode		Arrest	
					Initial Po PSIA	Final Pc PSIA		Spark	Incendiary	Yes	No
25 PPI Red	4.0	001	.955	10.26	14.86	17.86	1.2	x		x	
		002	x		14.86	28.86	1.95	x			x
		003	x		14.76	17.76	1.203	x		x	
	7.5	004	.955	10.8	14.74	17.76	1.203		Disk .046	x	
		005	x		14.71	20.71	1.407		0.5 .046	x	
	11.2	006	x	11.31	14.7	15.95	1.085		.5 .046	x	
		007	x		14.71	18.21	1.238		1 .046	x	
	9.2	008	x	11.18	14.67	19.67	1.34		1 .046	x	
	7.5	009	x	10.8	14.45	16.95	1.173		< 1 .046	x	
		010	x		19.39	25.89	1.335		< 1 .046		x
		010		1.146	19.39	64.39	3.32		< 1 .046		x
	11.2	011	x	11.31	19.39		1.257		< 1 .046		x
		011		1.022	19.39		2.96				x
	6.0	012	x	10.60	14.61	21.61	1.48		< 1 .046	x	
	4.0	013	x	10.26	14.61	21.11	1.44		< 1 .046		x
	3.8	014	x	10.26	15.4	21.9	1.47		< 1 .046		x
		014		.84	15.4	50.4	3.27				x
	6.0	015	x	10.60	15.36	24.36	1.56		< 1 .046		x
		015		.91	15.36	50.36	3.28				x
	10.0	016	.955	11.31	15.35	22.35	1.455		< 1 .046		x
		016									x
		017	.955	11.31	15.82	22.32	1.41		1.75 .046	x	
	7.5	018	.955	11.31	15.82	17.52	1.11				
	6.0	019	.955	10.8	15.86	22.86	1.42		1 .046	x	
	4.0	020	.955	10.26	15.85	26.35	1.66		> 1 .046	x	
		021	.955	10.26	17.8	27.3	1.535		> 1.5 .045		x
		021		.85	17.8	65.2	3.67				x
	7.5	022	x	10.8	17.76	27.26	1.54		≈ 1 .045		x
		022		.73	17.76	71.76	4.04				x
	11.2	023	x	11.31	17.7	25.3	1.43		.2 .045		x
		023		.75	17.7	65.2	3.69				x
		024	x	11.31	16.6	22.1	1.35		.31 .045		x
		024		.75	16.6	59.1	3.57				x

Table A-XV: (Continued) Runs 025 through 045

Material	Thickness (in.)	Run No.	Combustion Volume V _c (ft ³)	Vr/Vc	Combustion Pressures		Pc/Po	Ignitic Mode		Arrest	
					Initial Po PSIA	Final Pc PSIA		Spark	Incendiary	Yes	No
25 PPI, Red	10.0	025	955	11.25	15.62				.5 Ω .045		
		026			15.50	22.00	1.417		.2 Ω .045	x	
	4.0	027		11.29	14.59	17.09	1.17		.5 Ω .045	x	
		028	1.955	5.01	14.8	32.3	2.18		.3 Ω .045		x
		028		.538	14.8	66.8	4.51				x
	11.2	029	2.03	5.32	14.81	25.81	1.742		.5 Ω .045		x
		029		.662	14.81	55.31	3.73				x
		030	1.529	7.06	14.81	24.31	1.64		.3 Ω .045	x	
	8.0 Used	031	1.529	6.94	14.81	26.01	1.75		.2 Ω .045		x
		031		.683	14.81	59.81	4.038				x
	8.0	032	1.529	6.94	14.92	28.62	1.918		.5 Ω .045	x	
	4.7	033	1.529	6.63	14.92	26.12	1.75		.1 Ω .045	x	
	7.5	034	1.529	6.73	15.9	28.4	1.78		.5 Ω .045		x
		034		.638	15.9	66.9	4.21				x
		035	1.529	6.73	15.4	27.9	1.81		.1 Ω .046	x	
	4.5	036	1.529	6.62	15.1	29.4	1.947		.6 Ω .046		x
		036		.56	15.1	71.6	4.74				x
	11.2	037	1.529	7.06	16.1				.5 Ω .046	x	
	11.2 8 New 3.2 Used	038	1.529	7.06	17.58	23.88	1.358		.8 Ω .046		x
		038		.65	17.58	63.58	3.62				x
15 PPI, Yellow	7.5	039	1.529	6.73	15.58	30.58	1.96		.3 Ω .046		x
		039		.583		64.08	4.39				x
	11.2	040	1.529	7.06	14.51	20.51	1.41		.3 Ω .046		x
		040		.65	14.51	49.51	3.41				x
	4.2	041	1.427	6.87	14.5	26.5	1.83		.8 Ω .046	x	
	2.6	042	1.41	6.92	14.47	25.97	1.794		.4 Ω .046	x	
	1.9	043	1.372	7.09	14.46	22.46	1.552		.3 Ω .046	x	
	4.2	044	1.427	6.87	15.72	28.22	1.8		.5 Ω .046		x
		044		.506	15.72	65.72	4.18				x
		045	1.928	5.1	14.73	34.73	2.35		.1 Ω .046		x
		045		.542	14.73	60.23	4.087				x

Table A-XV: (Continued) Runs 046 Through 069

Material	Thickness (in.)	Run No.	Combustion Volume Vc (ft ³)	Vr/Vc	Combustion Pressures		Pc/Po	Ignition Mode		Arrest	
					Initial Po PSIA	Final Pc PSIA		Spark	Incendiary	Yes	No
3:1 Felt, 5 Layer	4.4 Nom	046	1.419	6.95	14.75	41.05	2.78		x		x
		046		.53		61.15	4.14				x
3:1 Felt, 10 Layer	8.5 Nom	047	1.351	7.7	14.76	34.76	2.355		x	x	
3:1 Felt, 8 Layer	7.2	048	1.303	7.95	14.76	29.26	1.98		x	x	
3:1 Felt, 8 Layer	7.1	049	1.303	7.95	15.73	30.734	1.95		.7Ω .045	x	
3:1 Felt, 5 Layer	4.8	050	1.49	6.8	15.75	30.75	1.952		1.2Ω .045	x	
25 PPI	11.2	051	1.520	7.05	14.75	24.75	1.698		.4 Ω .045	x	
3:1 Felt, 8 Layer	7.2	052	1.511	6.73	15.75	44.25	2.81		.7 Ω .045		x
		052		0.57		61.25	3.88				x
25 PPI, Red	11.2	053	1.529	7.10	15.72	32.22	2.05		.7 Ω .046	x	
25 PPI, Red	7.5	054	1.523	6.73	15.71	44.02	2.8		.3 Ω .046	x	
25 PPI, Red	4	055	1.472	6.65	14.72	41.02	2.79		.4 Ω .046		x
25 PPI, Red	7.5	056	1.529	6.73	15.72	42.22	2.68		.2 Ω .046		x
		055		.425		61.22	3.89				x
25 PPI, Red		057	1.529	6.73	14.8	38.6	2.61		1.2 Ω .046	x	
25 PPI, Red	11.2	058	1.529	7.1	16.81	36.3	2.16		1 Ω .046	x	
25 PPI, Red		059	1.529	7.1	17.81	41.3	2.32		1 Ω .046	x	
25 PPI, Red		060	1.529	7.1	19.79	46.3	2.34		.4 Ω .046		x
		060		0.65		71.29	3.6				x
25 PPI, Red		055	1.472	0.52		62.22	4.23				x
25 PPI, Red	4.5	061	1.942	5.15	15.26	30.76	2.01		.3 Ω .046	x	
25 PPI, Red		062	1.942	5.15	15.76	33.56	2.13		.7 Ω .046	x	
25 PPI, Red		063	1.942	5.15	15.8	34.3	2.17		1.5 Ω .046	x	
25 PPI, Red		064	1.942	5.15	17.73	39.73	2.24		.3 Ω .046	x	
25 PPI, Red	2.0	065	1.525	6.55	15.715	38.22	2.43		.5 Ω .046	x	
25 PPI, Red		066	1.525	6.51	16.7	19.95	1.194		.2 Ω .046	x	
25 PPI, Red		067	1.525	6.55	17.64	31.14	1.765		.2 Ω .046	x	
Quartz Fiber	4 Layers	068	1.529	6.05	14.65	32.65	2.23		0 Ω .046		x
		068		.575		70.35	4.81				
15 PPI, Yellow	2.0 Nom	069	1.525	5.55	14.65	20.4	1.492		0.5 Ω .046		x
				.56		59.15	4.04				

Table A-XV: (Continued) Runs 070 through 091

Material	Thickness (in.)	Run No.	Combustion Volume Vc (Ft ³)	Vr/Vc	Combustion Pressures		Pc/Po	Ignitic Mode		Arrest	
					Initial Po PSIA	Final Po PSIA		Spark	Incendiary	Yes	No
15 PPI, Yellow	7.5 Nom.	070	1.529	6.74	14.63	24.63	1.683		.1 Ω .046		x
		070		0.59		54.13	3.7				
25 PPI, Red	2.0	071	1.525	6.32	14.73	19.98	1.36		.4 Ω .046		x
		071		0.49		36.23	2.46				
25 PPI, Red		072	1.525	6.32	14.73	20.48	1.39		.6 Ω .046		x
		072		0.49		53.23	3.61				
25 PPI, Red		073	1.525	6.32	14.73	26.48	1.79		.4 Ω .046	x	
25 PPI, Red	4.5	074	1.529	6.63	14.73	28.23	1.91		.4 Ω .046		x
25 PPI, Red		074		0.55		52.98	3.6				
"		075	1.529	6.75	15.2	28.7	1.88		.2 Ω .046	x	
Glass Cloth (2)	1.25	075	1.56	6.75	14.71	43.46	2.95		.4 Ω .046		x
" Honeycomb		076		0.48		75.46	5.13				
Glass Cloth (1)		077	1.53	6.26	14.71	40.46	2.75		.7 Ω .046		x
" Honeycomb		077		0.48		83.71	5.69				
25 PPI 20 Mesh Screen	4.5	078	1.529	6.63	15.23	31.23	2.05		.3 Ω .046	x	
20 Mesh Wire Screen	0.1	079	1.485	6.22	14.73				.4 Ω .046		x
	(5 Layers)	079		0.44		69.73	4.73				
25 PPI w/20 Mesh Screen	4.5	080	1.529	6.63	16.36	31.11	1.9		.7 Ω .046	x	
25 PPI w/20 Mesh Screen		081	1.529	6.62	17.86	20.86	1.17		1 Ω .046	x	
25 PPI w/20 Mesh Screen		082	1.529	6.63	17.86	24.36	1.36		.8 Ω .046	x	
GAF Felt 2A	6.0	083	2.03	4.91	14.68	63.68	4.337		.4 Ω .046	x	
GAF Felt 2A	3.0	084	2.03	4.659	14.39	57.64	4.005		.3 Ω .046		x
				0.448		40.39	2.806				
GAF Felt 2A	6.0	085	2.03	4.91	16.72	39.72	2.375		.2 Ω .046	x	
GAF Felt 2A		085	2.03	4.91	18.73	93.23	4.977		.4 Ω .046	x	
GAF Felt Std (8 Layers)		087	2.03	4.91	18.73	82.98	4.43		.6 Ω .046	x	
GAF Felt Std (4 Layers)	3.0	088	2.03	4.56	14.74	45.74	3.103		.4 Ω .046	x	
GAF Felt Std (4 Layers)		089	2.03	4.66	15.75	98.75	6.27		.2 Ω .046		x
				0.448		49.75	3.158				
3.1 Felt (3 Layers)		090	2.03	4.66	14.74	65.74	4.46		.2 Ω .046	x	
3.1 Felt (3 Layers)		091	2.03	4.66	15.74	34.74	2.207		.1 Ω .046		x
				0.443		66.74	4.24				

Table A-XV: (Continued) Runs 092 through 115

Material	Thickness (in.)	Run No.	Combustion Volume Vc (ft ³)	Vr/Vc	Combustion Pressures		Pc/Po	Ignition Mode		Arrest	
					Initial Po PSIA	Final Pc PSIA		Spark	Incendiary	Yes	No
3:1 Felt (5 Layers)	6.0	092	2.03	4.88	18.82	112.32	5.97		25Ω .045		x
				0.5	55.0	69.82	3.71				
3:1 Felt (5 Layers)		093	2.03	4.88	15.82	101.32	6.4		11Ω .046	x	
3:1 Felt (5 Layers)		094	2.03	4.83	17.83	99.32	5.57		20Ω .045	x	
GAF 2A		095	2.03	4.88	18.82	110.57	5.875		40Ω .015	x	
GAF Std		096	2.03	4.8P	18.81	128.31	6.5		20Ω .016	x	
GAF 2A	3.0	097	2.03	4.66	14.81	97.31	6.57		40Ω .016		x
				0.498		66.81	3.16				
GAF 2A	4.5	098	2.03	4.67	14.81	89.01	6.06		20Ω .046	x	
GAF Std	3.0	099	2.03	4.66	14.80	101.80	6.88		20Ω .046	x	
3:1 Felt (3 Layer)		100	2.03	4.66	15.80	23.30	1.47	x			x
				0.498		75.30	4.76				
3:1 Felt (5 Layer)	4.5	101	2.03	4.67	14.30	24.80	1.67	x			x
				0.45		62.80	4.24				
GAF 2A		102	2.03	4.67	14.80	23.35	1.577	x			x
				0.45		63.80	4.3				
3:1 Felt (5 Layer)	6.0	103	2.03	4.88	14.82	22.82	1.538	x		x	
3:1 Felt (5 Layer)		104	2.03	4.98	15.75	26.75	1.698	x		x	
GAF 2A		105	2.03	4.88	14.73	25.75	1.746	x		x	
GAF 2A		106	2.03	4.88	16.11	27.11	1.683			x	
3:1 Felt (5 Layer)		107	2.03	4.88	18.62	32.62	1.75	x		x	
GAF 2A		108	2.03	4.8P	18.67	29.67	1.59	x			x
				0.504		74.67	4.00				
25 PPI	4.0	109	2.03	4.67	14.67	97.17	6.62		20Ω .046		x
				0.45		40.17	1.575				
25 PPI	8.0	110	2.03	4.85	14.57	44.07	3.0		20Ω .045		x
25 PPI		111	2.03	4.85	14.57	23.32	1.6	x		x	
25 PPI		112	2.03	4.85	14.57	90.57	6.216		20Ω .045	x	
25 PPI	6.0	113	2.03	4.87	14.58	62.08	4.258		20Ω .045	x	
25 PPI		114	2.03	4.87	16.58	98.58	5.945		40Ω .045		x
				0.502		43.83	2.643				
25 PPI		115	2.03	4.87	16.58	22.83	1.377	x			x
				0.502		61.58	3.714				

Table A-XV: (Continued) Runs 116 through 124

Material	Thickness (in.)	Run No.	Combustion Volume Vc (ft ³)	Vr/Vc	Combustion Pressures		Pc/Po	Ignition Mode		Arrest	
					Initial Po PSIA	Final Pc PSIA		Spark	Liendary	Yes	No
25 PPI w/20 Mesh Screen	4.0	116	2.03	2.91	14.58	18.58	1.27		.30 .046		x
			2.03	0.514		46.58	3.2				
25 PPI		117	2.03	2.91	14.57	61.07	4.2		.20 .046		x
			2.03	0.514		29.37	2.03				
Quartz Fiber (10 Layers)	10 Layers	118	2.03	4.92	14.58	112.08	7.68		.20 .046		x
			2.03	0.518		75.58	5.18				
Quartz Fiber		119	2.03	4.92	14.63	62.13	4.24	x			x
			2.03	0.518		73.63	5.03				
25 PPI w/Screen	4.0	120	2.04	4.9	14.63	74.63	5.10		.20 .046	x	
25 PPI Foam		121	2.03	4.9	14.63	18.38	1.25	x			x
				0.685		33.38	2.3				
25 PPI Foam	8.0	122	2.03	4.86	18.63	128.63	6.9		.20 .046		x
				0.574		97.88	5.254				
25 PPI Foam w/10 Layers of Quartz Fiber	4.0	123	2.03	4.9	14.63	66.63	4.55		.30 .046		x
				0.696		49.63	3.39				
25 PPI Foam 8" Dia.	8.0	124	2.03	4.73	17.17	86.77	4.88				
25 PPI Foam 8" Dia.		125	x	4.73	18.81	28.06	1.49	x			x
				0.703		49.56	5.27				
25 PPI Foam 8" Dia.	11.0	126	2.03	4.73	18.82	27.57	1.46	x			x
				0.703		74.32	3.95				
25 PPI Foam 8" Dia.		127	x	4.73	16.81	23.57	1.40	x		x	
				0.703							
25 PPI 8" Dia. 4 Layer w/ 20 Mesh	8.0	128	2.03	4.73	16.81	103.56	6.16		.040 .046	x	
		129	2.03	4.73	18.81	136.31	7.25		.040 .046		x
				.703		75.06	4.00				
3M Std 5 1/2" Long 8" Dia.	5 1/2	130	2.03	4.73	18.81	71.06	3.77	x			x
		131	2.03	4.73	18.81	27.56	1.47	x			x
	8.0			0.703		51.31	2.72				
3M Std 8" Dia.		132	2.03	4.73	17.277	24.78	1.43	x			x
				0.703		66.27	3.93				
		133	2.03	4.73	16.265	23.77	1.46	x			x
				0.703		45.0	2.77				
25 PPI Foam 12.5" Dia.	11.0	134	2.03	5.32	15.755	19.005	1.205				

Table 4-XV: (Continued) Runs 135 through 160

Material	Thickness (in.)	Run No.	Combustion Volume V _c (ft ³)	Vr/Vc	Combustion Pressures		Pc/Po	Ignition Mode		Arrest	
					Initial Po PSIA	Final Pc PSIA		Spark	Incendiary	Yes	No
	11.0	135	2.03	5.32	14,746	34.50	2.33		0.2Ω .046	x	
	8.0	136	2.03	5.22	15.74	36.00	2.29		0.5Ω .046	x	
		137	2.03	5.22	18,739	52.49	2.80		1.0Ω .049		x
				0.703		57.49	3.06		0.2Ω .07		
	6.0	138	2.03	5.15	14,735	33.49	2.27				
	8.0	139	2.03	5.22	17,237	38.49	2.23		0.3Ω .09	x	
	4.0	140	2.03	5.08	14,724	35.22	2.39		0.2Ω .099	x	
	6.0	141	2.03	3.15	16,726	40.48	2.41		0.7Ω .099	x	
		142	2.03	5.15	18,725	95.48	2.43		0.4Ω .049		
		143	2.03	5.15	20,731	51.98	2.51		0.2Ω .049		x
				0.828		68.48	3.30				
3M Std Felt 17.5" Dia.		144	2.03	5.15	14,730	31.98	2.17		0.2Ω .049		x
				0.828		45.48	3.08				
	8.0	145	2.03	5.22	14,735	33.74	2.29		0.2Ω .099	x	
	7.5	146	2.03	5.20	16,739	39.99	2.39		0.2Ω .049	x	
		147	2.03	5.20	18,788	50.74	2.71		.049		x
		148	2.03		20.9	70.1	2.69		0.2Ω .046		
				0.83	20.9	69.9	3.34				
25 PPI + 20-Screen	4.0	149	2.03	4.82	16.9	47.7	2.83		.1Ω .046	x	
		150	2.03	4.82	16.9	50.7	2.69		.1Ω .046	x	
	2.0	151	2.03	4.76	14.9	26.15	1.76		.1Ω .046	x	
	4.0	152	2.03	4.82	20.9	54.65	2.61		.2Ω .046	x	
	2.0	153			18.7	48.45	2.59		.5Ω .046	x	
		154			20.7	69.95	3.38		.3Ω .046	x	
	1.0	155			18.7	58.7	3.14		.4Ω .046	x	
		156			20.75	61.75	2.98		.5Ω .046	x	
25 PPI Aft 4 Mesh Screen	11.0	157	2.03		17.76	23.51	1.32	x		x	
		158	2.03		22.77	27.27	1.20	x		x	
						68.52	3.01				
		159	2.03	4.82	20.77	24.52	1.18	x			x
				0.72	20.77	52.50	2.53				
	4.0	160			14.79	18.54	1.25	x		x	

Table A-XV: (Continued) Runs 161 through 183

Material	Thickness (in.)	Run No.	Combustion Volume V _c (ft ³)	V _r /V _c	Combustion Pressures		P _c /P _o	Ignition Mode		Arrest	
					Initial P _o PSIA	Final P _c PSIA		Spark	Incendiary	Yes	No
	4.0	161			16.3	20.05	1.23	x		x	
		162			18.79	23.04	1.23	x			x
						62.54	3.32				
	2.0	163			15.79	19.79	1.253	x		x	
25 PPI Atr 4 Mesh		164			16.79	Data Not Obtained	3.65	x			x
						61.79	1.56				
F/A 6.5%	4.0	165			17.79	27.79	1.29		0.6Ω .046	x	
F/A 6.5%		166			20.80	26.75	1.25		0.3Ω .046	x	
F/A 6.5%	2.0	167			17.80	22.3	1.33		1.0Ω .046	x	
F/A 5.5%	6.0	168	2.03		16.80	22.3	1.33		0.3Ω .046	x	
F/A 6.5%		169	2.03		18.80	25.05	1.86		0.5Ω .046	x	
F/A 6.5%		170	2.03		20.90	38.9	1.43				
F/A 6.5%		171	8.04		17.90	25.65	3.06				
						54.9	1.36		0.4Ω .046	x	
25 PPI Foam Ito. 4 Mesh F/A 6.5%	2.0	172	2.03	5.01	20.91	28.41	1.69		0.2Ω .046	x	
F/A 3.5%	4.0	173	2.03	5.08	14.91	25.36	2.22		0.2Ω .046	x	
F/A 3.5%		174	2.03	5.08	18.88	41.98	2.09		0.2Ω .046	x	
F/A 3.5%	2.0	175	2.03	5.01	20.88	43.13	3.19		0.1Ω .046		x
				0.787		66.63	2.13				
F/A 3.5%		176	2.03	5.01	16.88	33.88	2.67		0.5Ω .046	x	
				0.787		45.13	3.55		0.4Ω .046		
F/A 3.5%	4.0	177	2.03	5.08	20.87	74.12	2.03				
F/A 3.5%	2.0	178	2.03	5.01	14.87	30.12	3.71				
				0.787		55.12	1.49	x			x
Quartz Fiber	10 Layers	179	2.03	4.80	14.81	22.06	3.16				
				0.72		46.81	2.60				
Quartz Fiber	15 Layers	180	2.03	4.80	14.82	20.57	2.47	x			
				0.72		38.57	1.35				
	20 Layers	181	2.03	4.80	14.82	20.77	1.34	x			
				0.72		36.57	5.3				
	25 Layers	182	2.03	4.80	14.82	19.81		x	0.2Ω .046		
		183		4.80	14.81	78.56					

Table A-XV: (Continued) Runs 184 through 204

Material	Thickness (in.)	Run No.	Combustion Volume Vc (Ft ³)	Vr/Vc	Combustion Pressures		Pc/Po	Ignition Mode		Arrest	
					Initial Po PSIA	Final Pc PSIA		Spark	Incendiary	Yes	No
	15 Layers	184	2.03	4.80	14.80	63.55	4.29		0.2Ω .046		x
	20 Layers	185	2.03	0.72		48.3	3.26				
	(10 Used)				14.80	73.55	4.96		0.3Ω .046		x
	25 Layers	186	2.03	4.80	17.80	94.8	5.32		0.2Ω .046		x
	(All Used)					43.3	2.43				
15 Quartz 4 S/S Screen	15 + 20 Mesh	187	2.03	4.80	14.78	67.95	4.60		0.3Ω .046	x	
10 Quartz 4 SS 20 Mesh		188	2.03	4.80	14.78	62.03	4.20				
5 Quartz 4 SS 20 Mesh		189	2.03	4.80	14.78	52.78	3.57		0.3Ω .046		x
				0.72		64.27	4.35				
10 Quartz 4 S/S		190	2.03	4.80	16.70	77.02	4.59		0.3Ω .046		x
				0.72		58.52	3.49				
15 Layers 4 Screens		191	2.03	4.80	17.76	82.01	4.61		0.3Ω .046	x	
10 Layers 4 Screens (Used)		192	2.03	4.80	15.75	66.25	4.21		0.3Ω .046		x
				0.72		54.75	3.48				
15 Quartz 4 20 Mesh S/S		193	2.03	4.80	18.75	-	-		0.4Ω .046	x	
		194	2.03	4.80	18.75	85.0	4.53		0.5Ω .046	x	
30 Quartz 2 No. 4 Mesh		195	2.03	4.80	20.21	108.71	5.38		0.3Ω .046		x
				0.72							
		196	2.03	4.80	20.21	29.71	1.47	x			x
				0.72		55.96	2.77				
20 Mesh S/S	10 Layers	197	2.03	4.80	14.72	36.72	2.49		0.3Ω .046		x
				0.72		48.48	3.29				
25 PPI Quartz 4.0	10 Layers	198	2.52	3.90	14.72	63.72	4.33		0.4Ω .046	x	
25 PPI Quartz 1.75	10 Layers	199	2.69	3.52	14.72	59.97	4.07		0.4Ω .046	x	
25 PPI Quartz 4.0	10 Layers	200	2.52	3.90	18.72	90.47	4.83		0.4Ω .046	x	
25 PPI 20 Mesh S/S 2 Screens	2.0	201	2.67	3.57	16.72	60.47	3.62		0.4Ω .046	x	
3M STD S/S 20 Mesh 2 Screens	4.0	202	2.52	3.90	14.72	31.97	2.17		0.4Ω .046		x
				0.69		43.97	2.99				
15 PPI S/S 20 Mesh 2 Screens	4.0	203	2.03	5.32	14.72	30.72	2.09		0.3Ω .046		x
				0.88		39.22	2.66				
Quartz S/S 20 Mesh 2 Screens	15 Quartz	204	2.03	4.98	20.72	103.27	4.98		0.3Ω .046	x	

Table A-XVI:
Data Correlation of Volume Relationships

Combustion Volume $V_C \text{ Ft}^3$	Nominal V_R/V_C
1.0	10.0
1.5	6.6
2.0	5.0

Symbol		
Spark	Incendiary	
△	○	Burn Through
▲	●	Arrest
▲	⊙	Delayed Burn Through

Note: The relief orifice A_R is presented in the data as a percentage of the tube cross sectional area

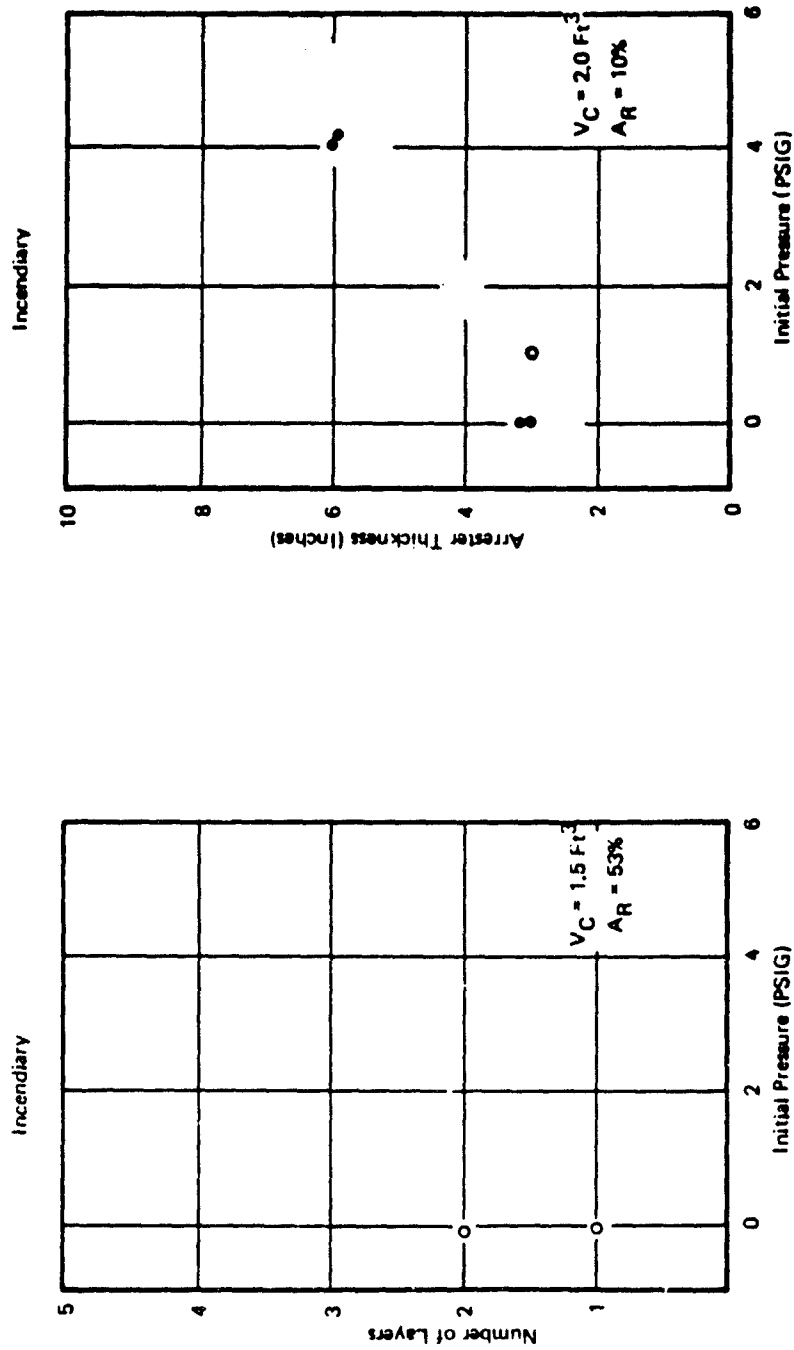
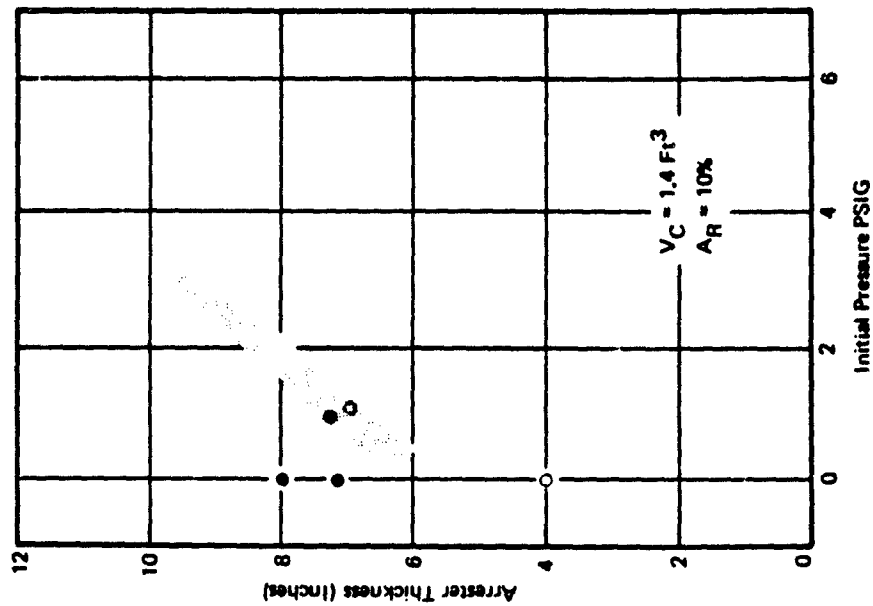


Figure A-32: Arresters Thickness Versus Initial Pressure Data Plots for 10 Oze Glass Cloth and GAF Felt (Standard) Material

Incendiary



Incendiary

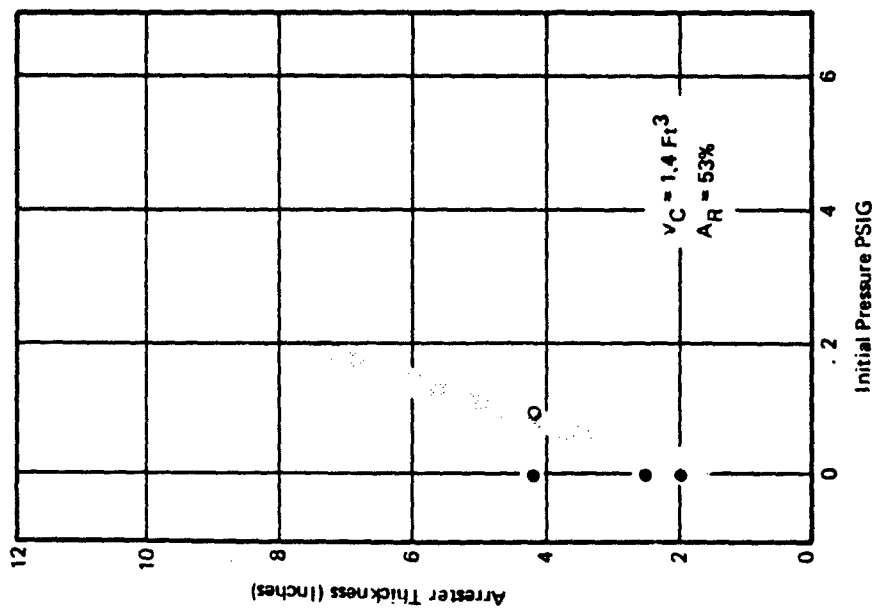


Figure A-33: Arrestor Thickness Versus Initial Pressure Data Plots for 3M Scotch Brite

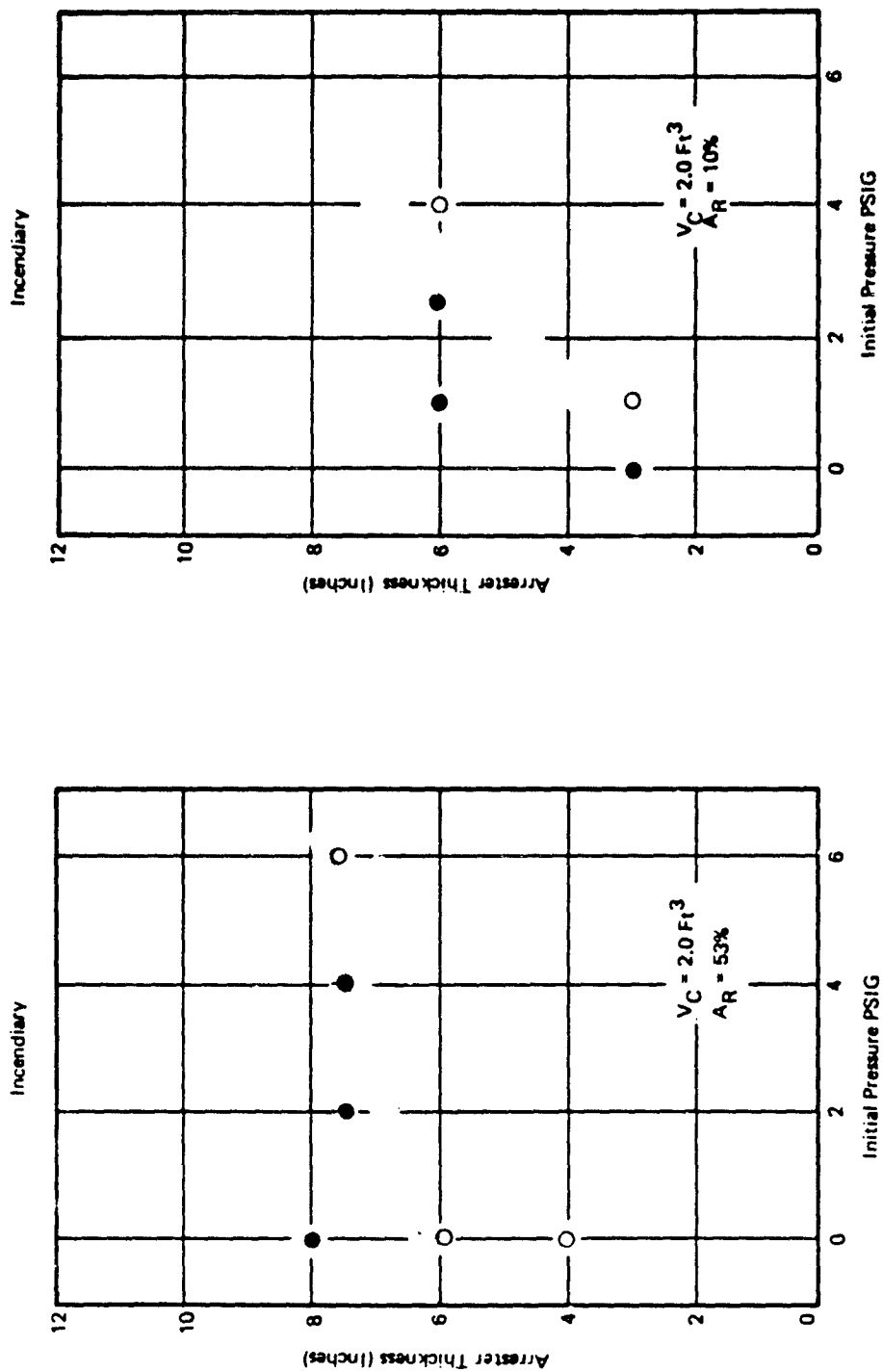


Figure A-34: Arrestor Thickness Versus Initial Pressure Data Plots for 3M Scotch Brim

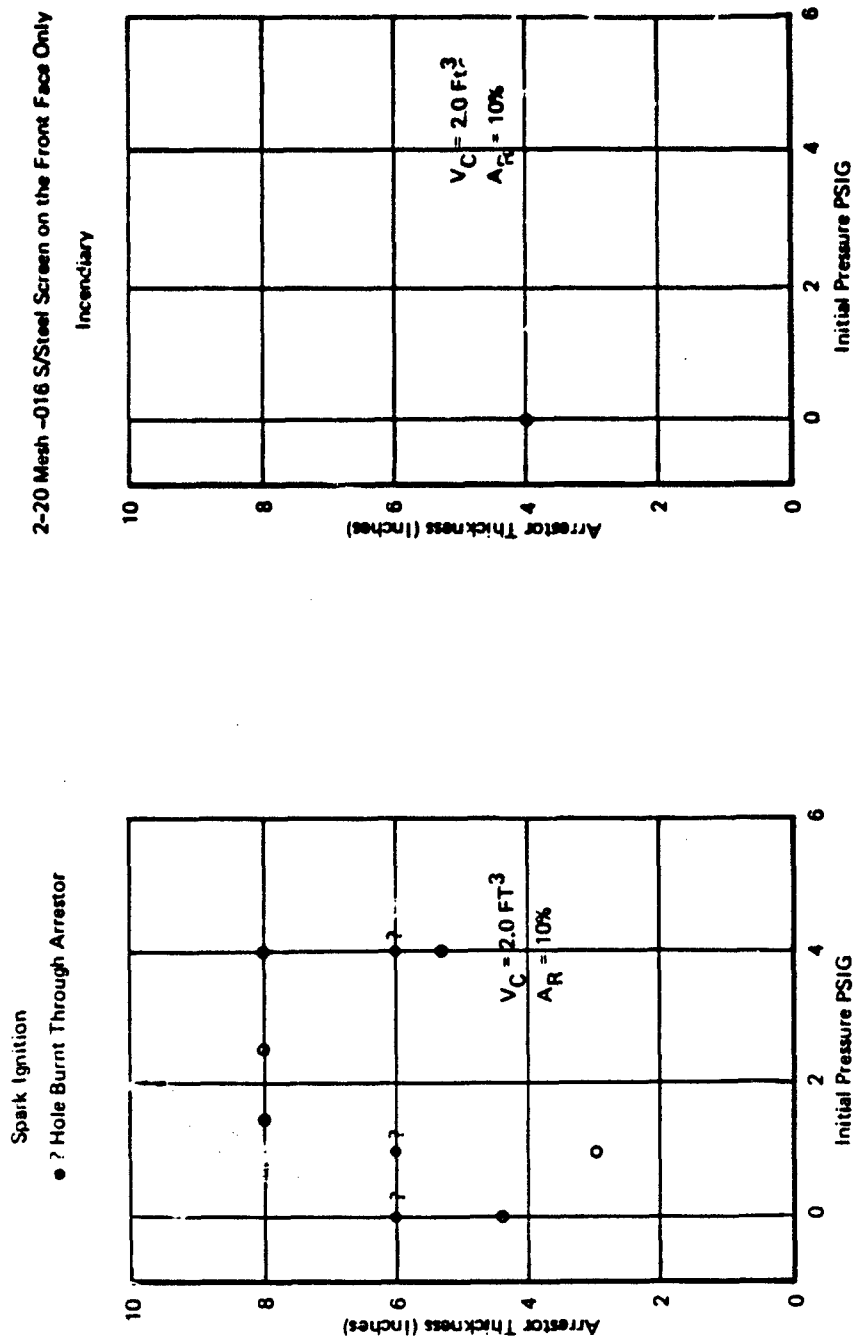


Figure A-35: Arrestor Thickness Versus Initial Pressure Data Plots for 3M Scotch Brite.

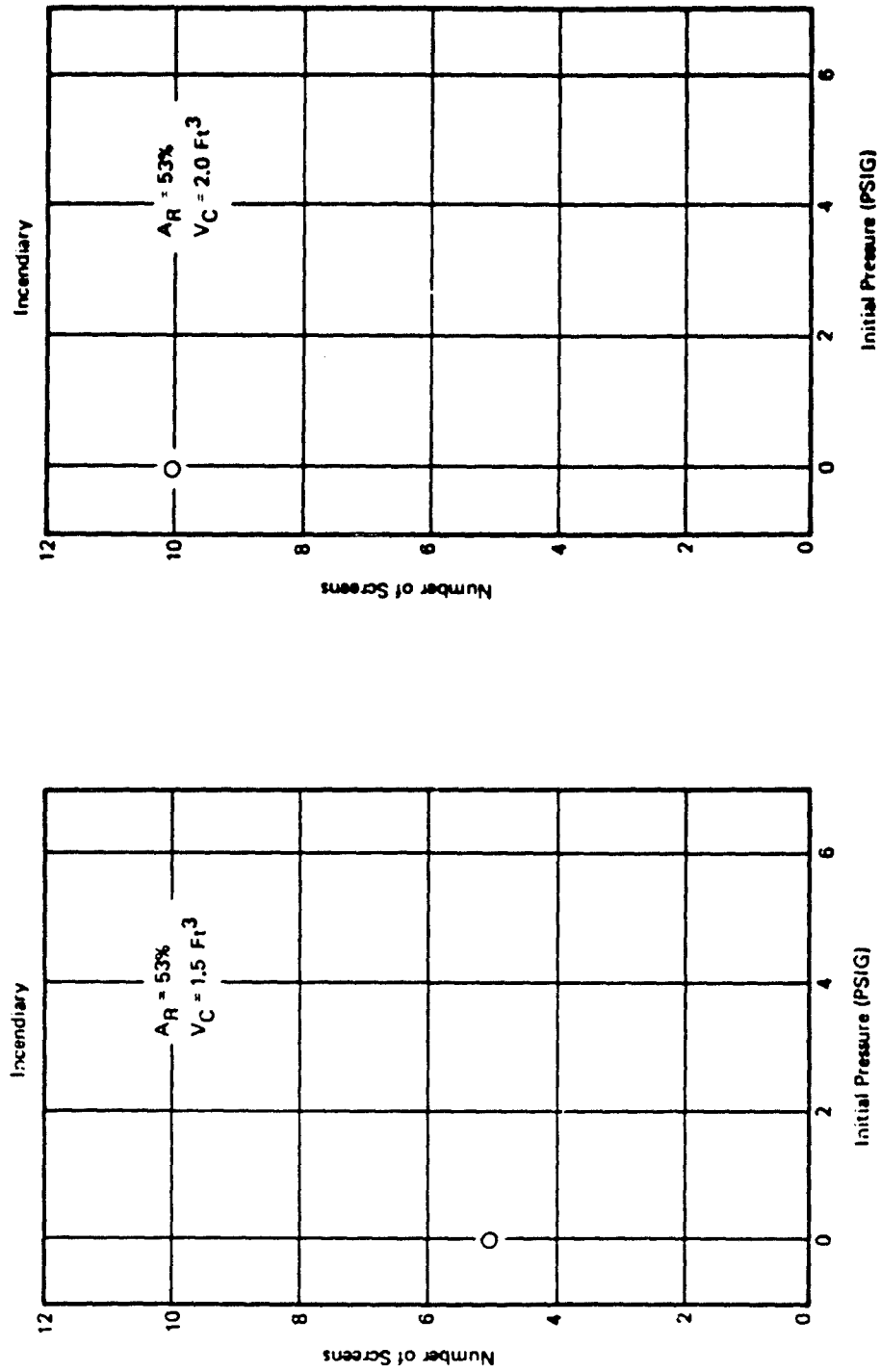


Figure A-36: Arrestor Thickness Versus Initial Pressure Data Plots for 20-Mesh 016 Stainless Steel Screen

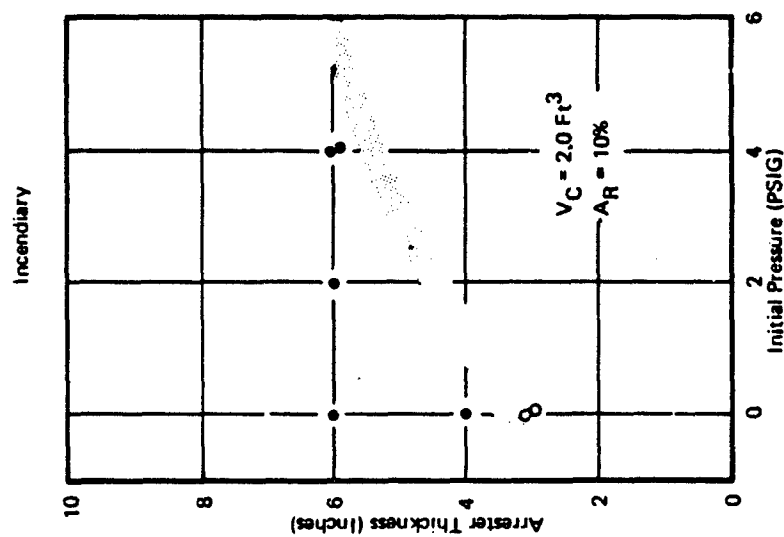
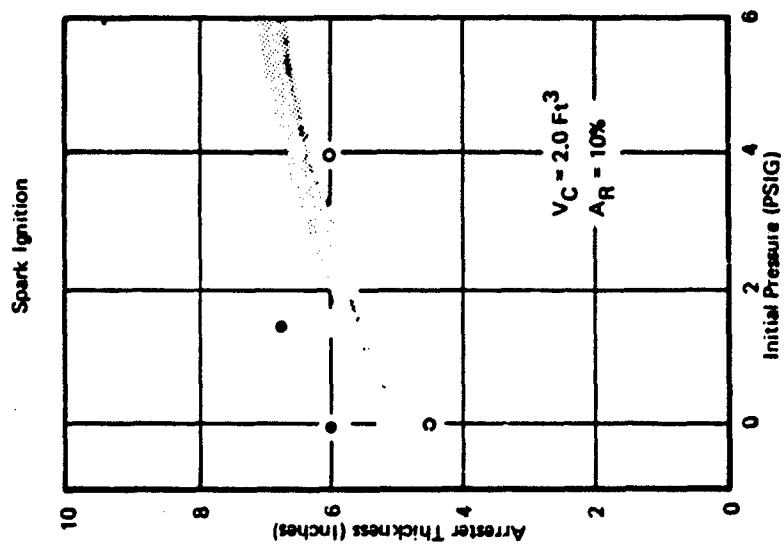


Figure A-37: Arrestor Thickness Versus Initial Pressure Data Plots for GAF Felt (Type 2A)

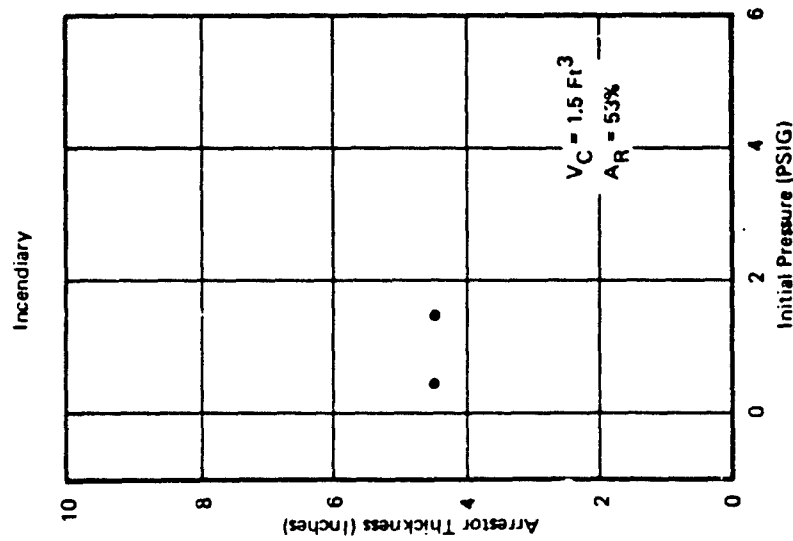
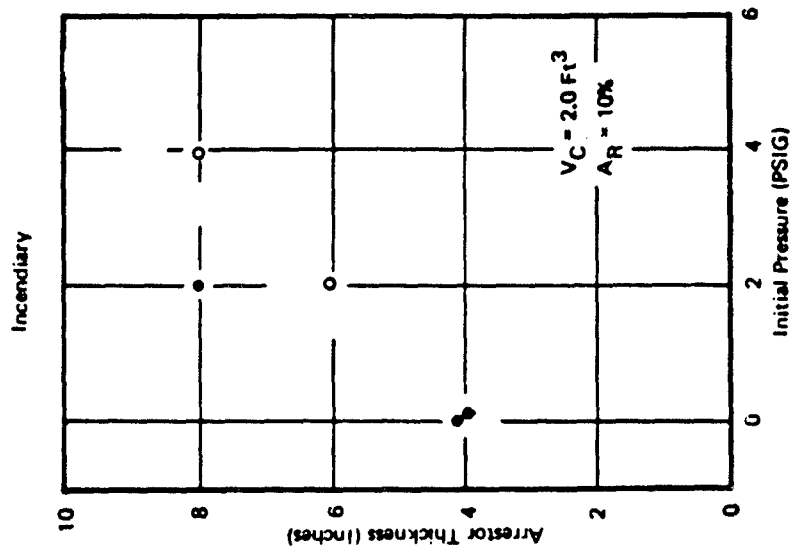


Figure A-38: Arrestor Thickness Versus Initial Pressure Data Plots for 25-PPI Foam with Two Layers of
—016 Stainless Steel Wire Screen on Each Side

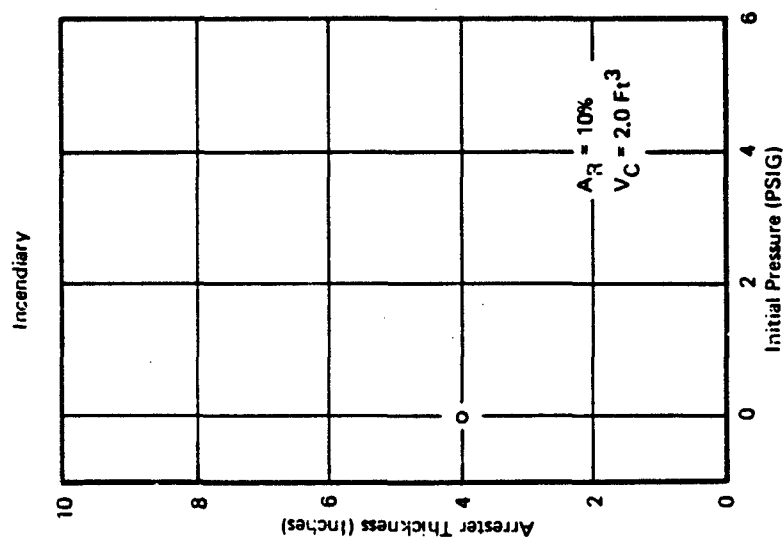
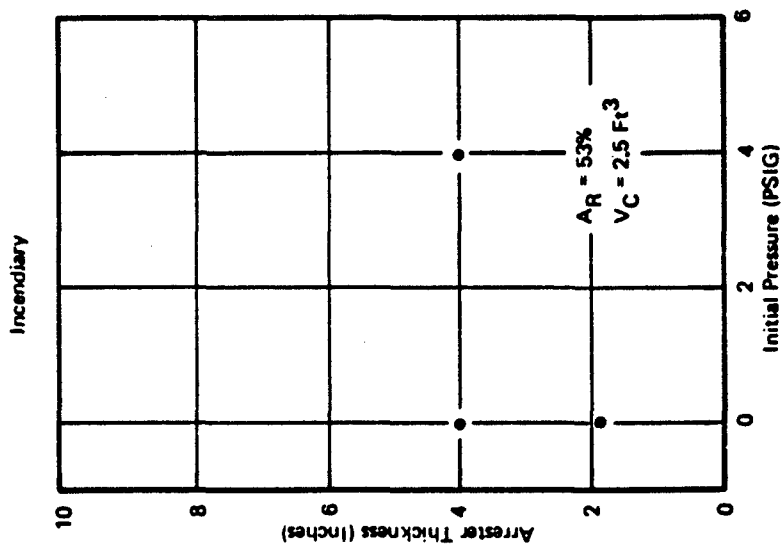


Figure A-39: Arrestor Thickness Versus Initial Pressure Data Plots for Quartz Fiber Type 594/38-9073,
10 Layers on the Front Face with 25-PPI Foam and 4-Mesh Support Screen

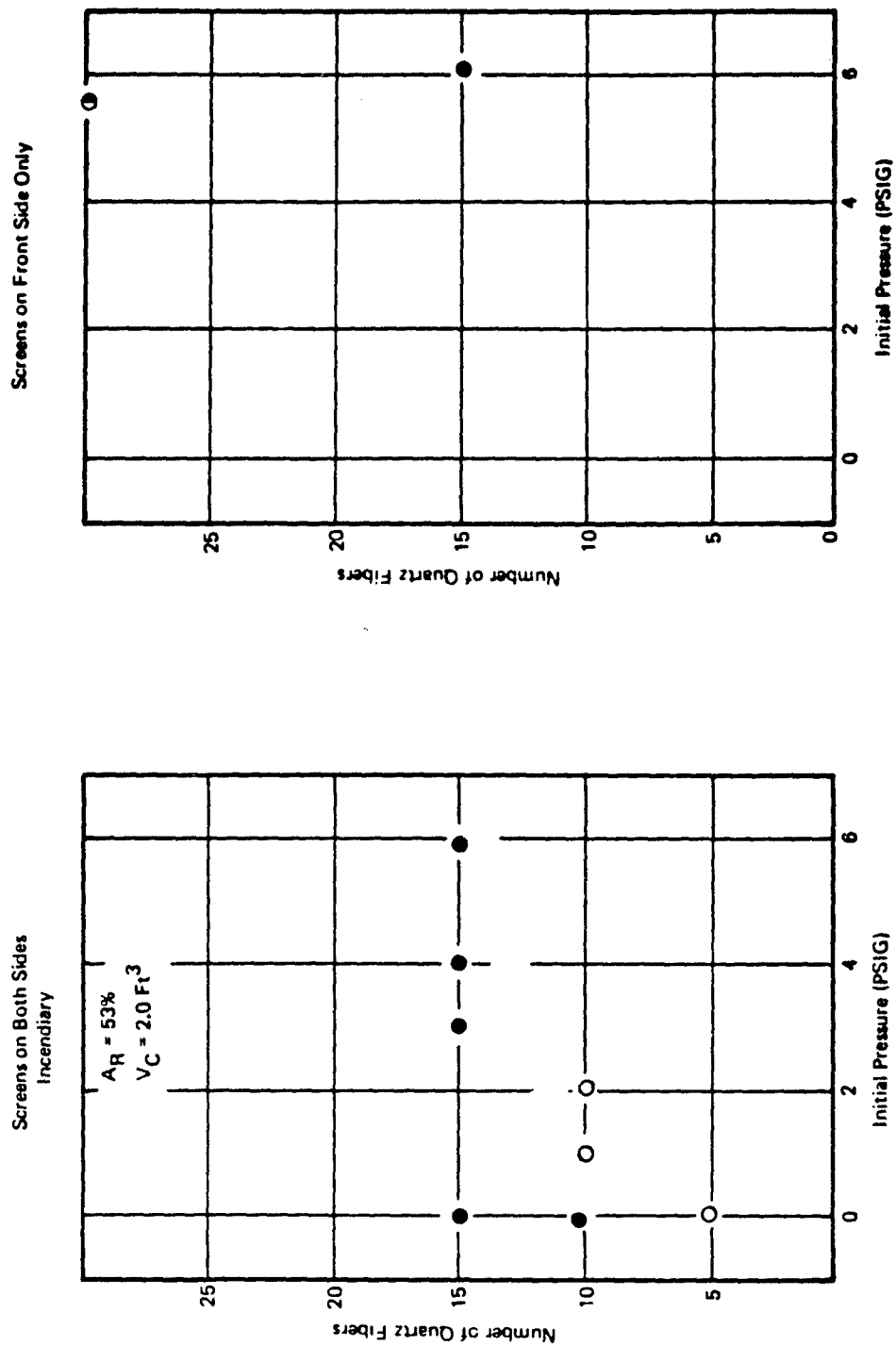


Figure A-40: Arrestor Thickness Versus Initial Pressure Data Plots for Quartz Fiber Type 594/38-9073 10 Layers with 2 Layers of 20-Mesh -016 Stainless Steel Wire Screen

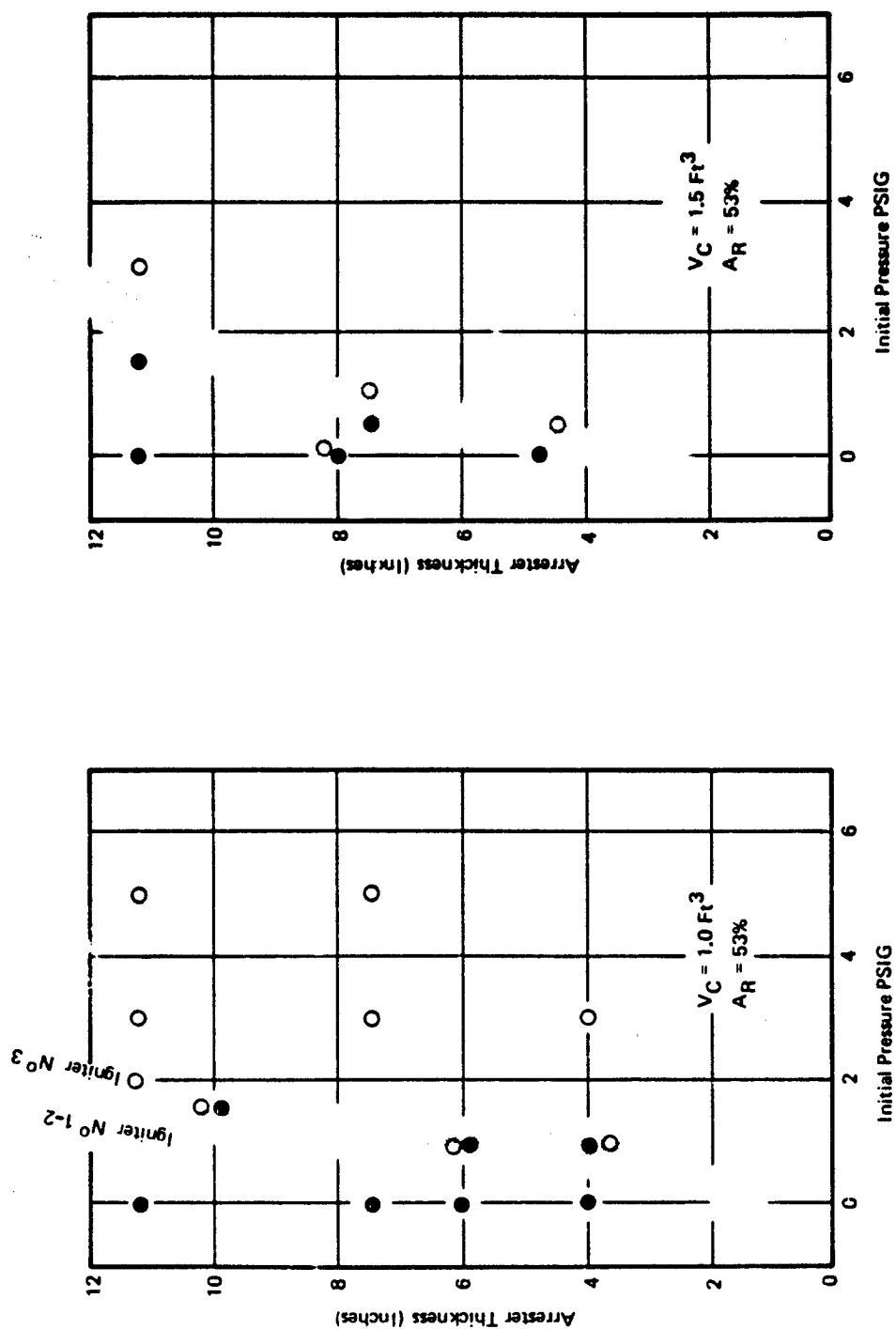


Figure A-41: Arrestor Thickness Versus Initial Pressure Data Plots for 25-PPI Foam

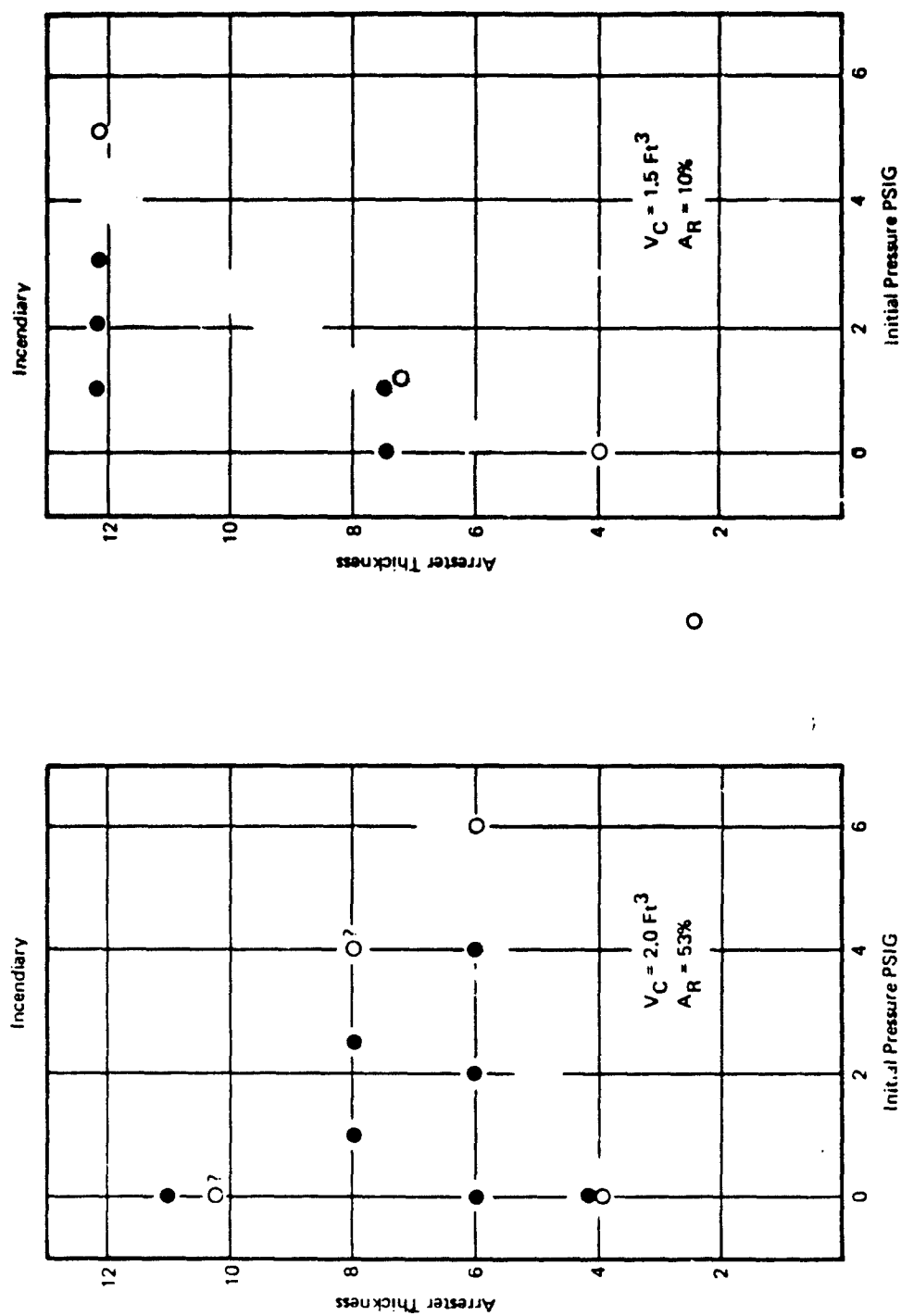


Figure A-42: Arrestor Thickness Versus Initial Pressure Data Plots for 25-PPI Foam

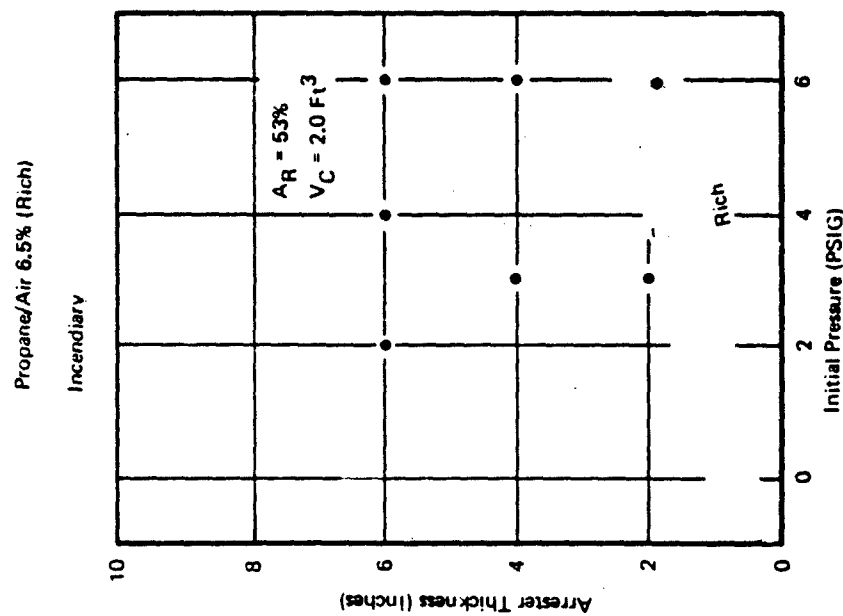
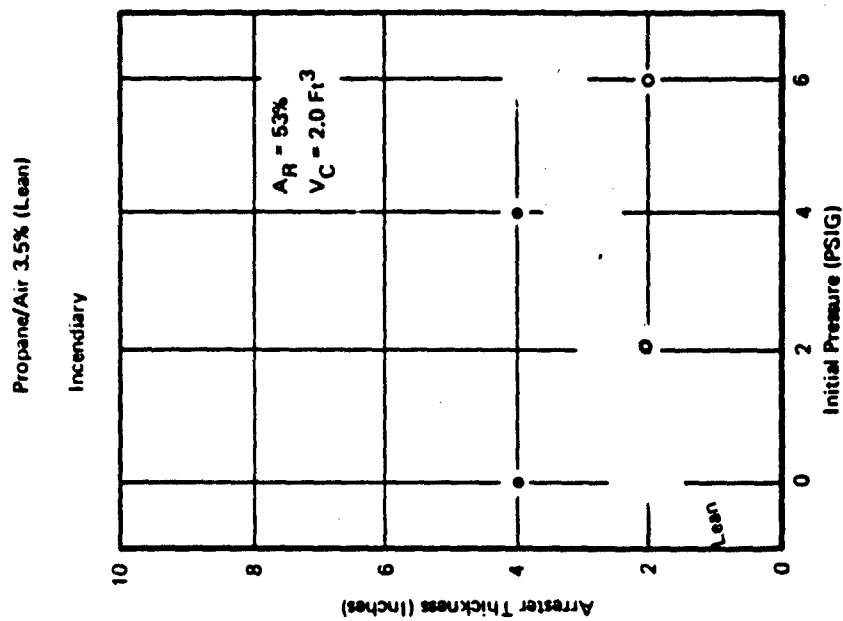


Figure A-43: Arresters Thickness Versus Initial Pressure Data Plots for 25-PPI Foam

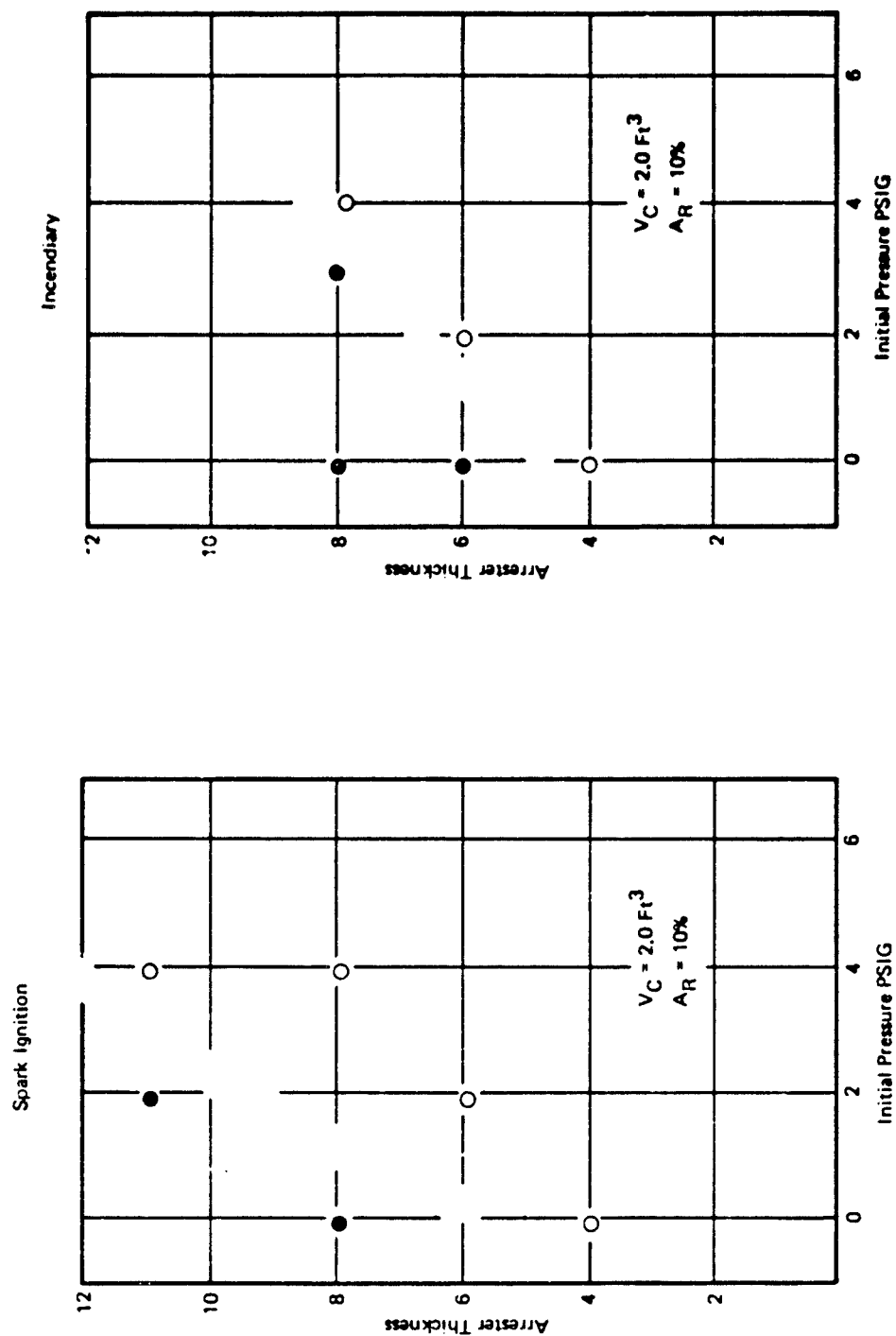


Figure A-44: Arrestor Thickness Versus Initial Pressure Data Plots for 2S-PPI Foam

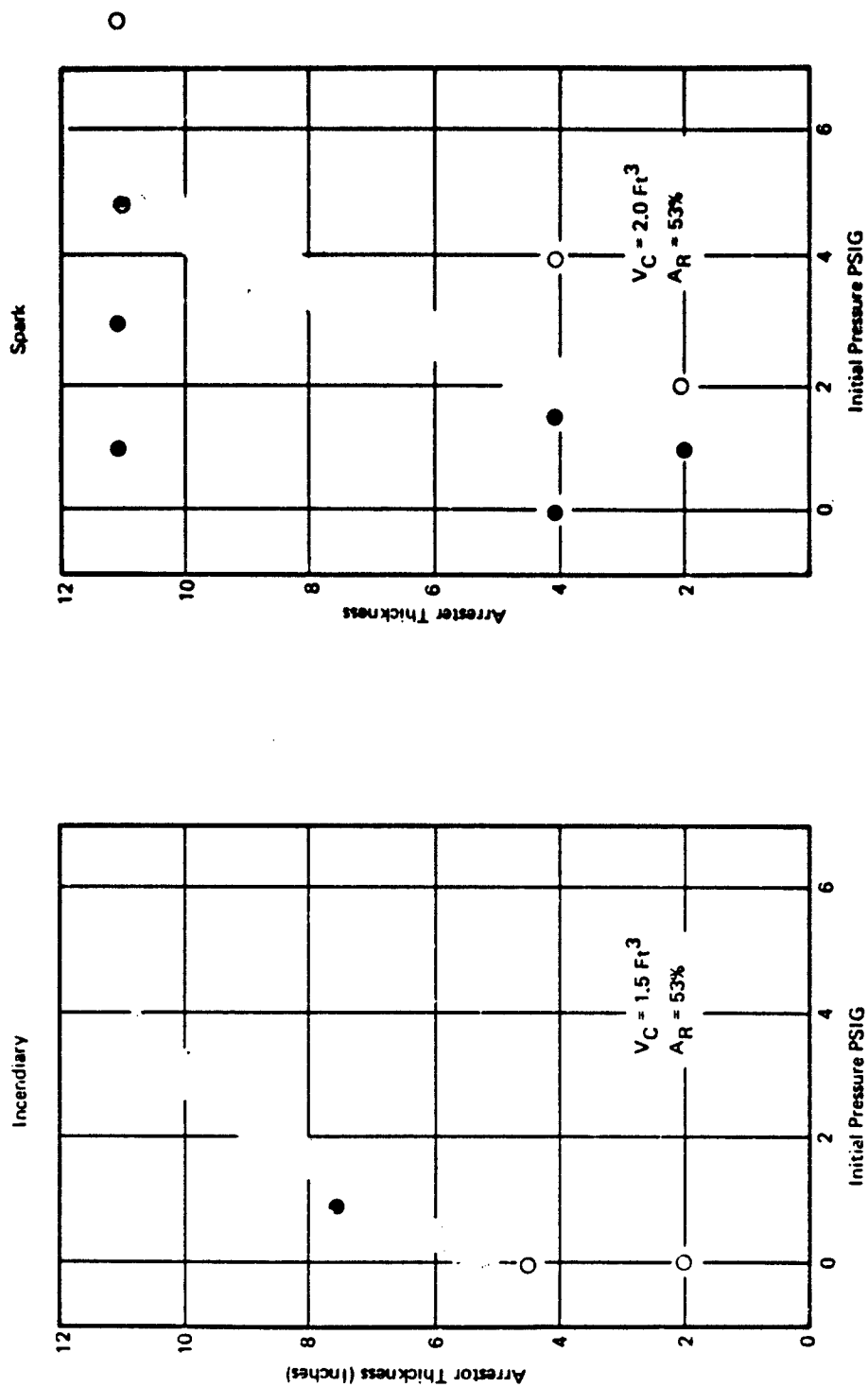


Figure A-45: Arrestor Thickness Versus Initial Pressure Data Plots for 25-PP1 Foam Wetted with JP5

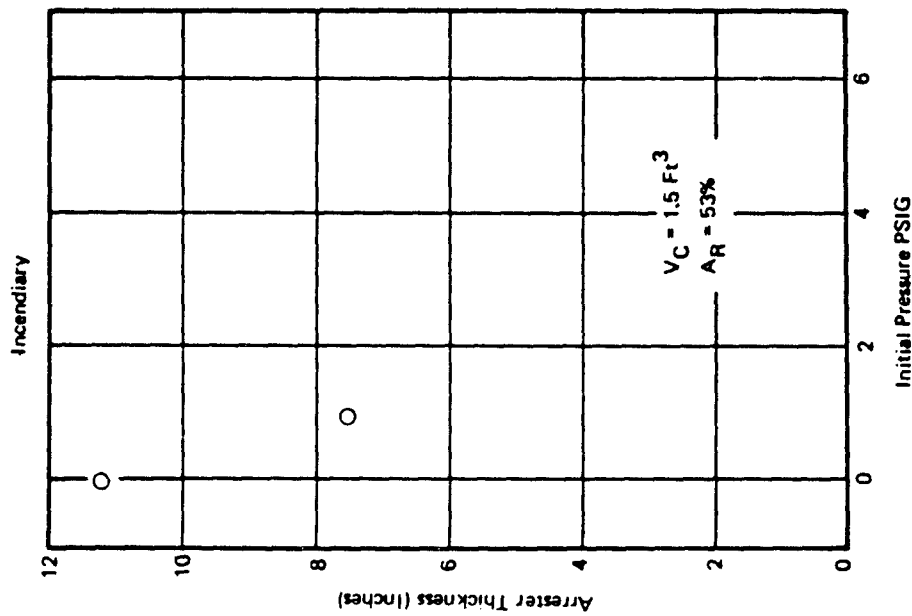
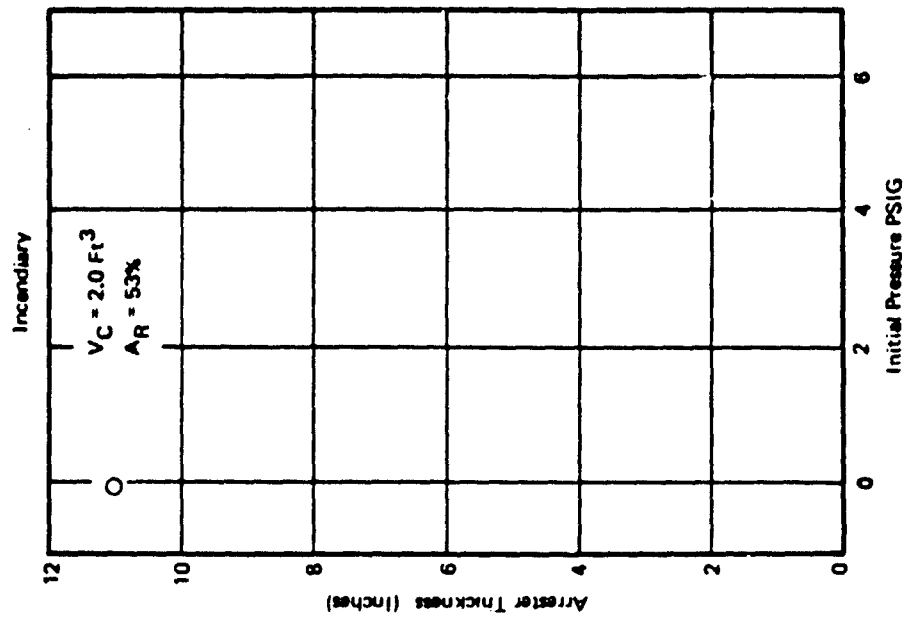


Figure A-46: Arrestor Thickness Versus Initial Pressure Data Plots for 15-PP1 Foam

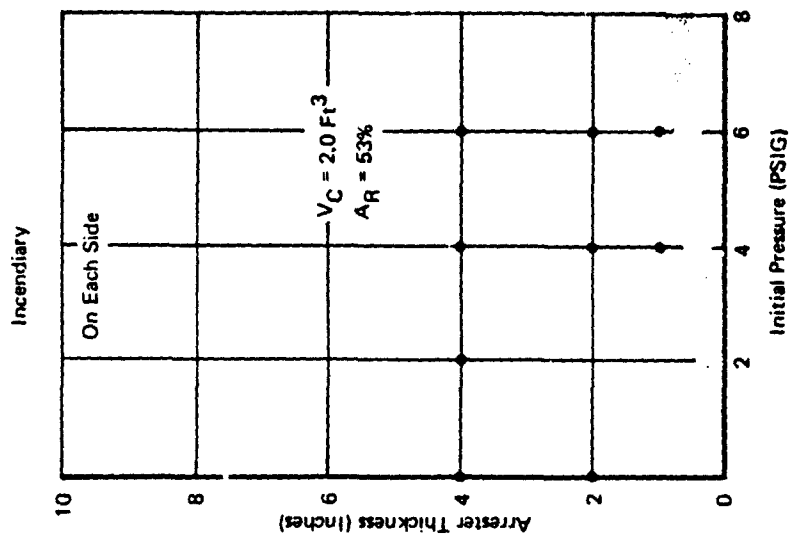
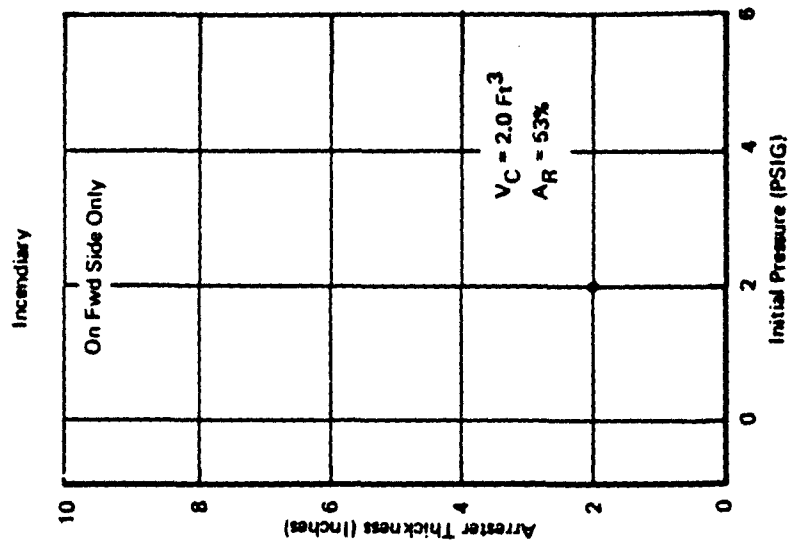


Figure A-47: Arrester Thickness Versus Initial Pressure Data Plots for 25-PPI Foam with 2 Layers of 20-Mesh
—016 Stainless Steel Wire Screen

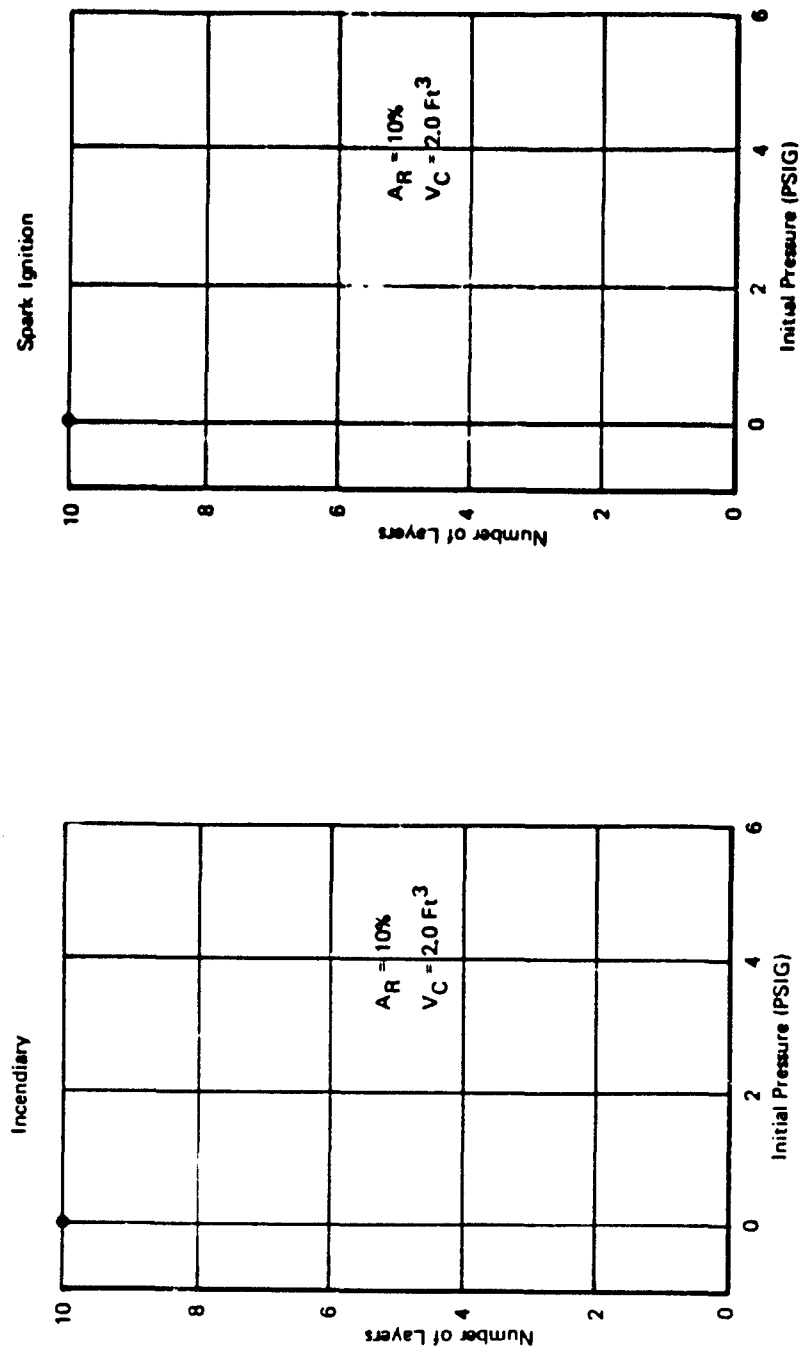


Figure A-48: Arrestor Thickness Versus Initial Pressure Data Plots for Quartz Fiber Type 594/38-9073 with 4-Mesh Support Screen

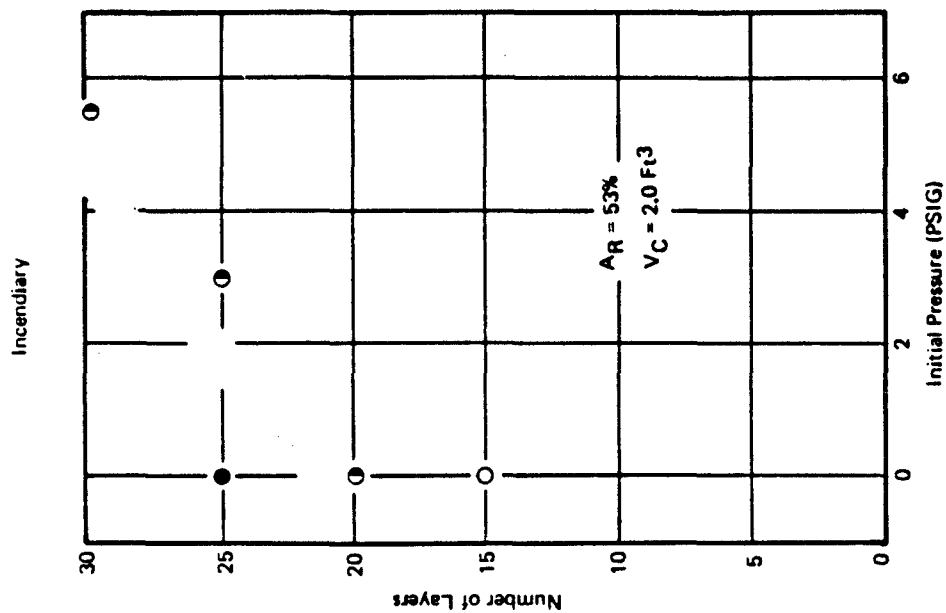
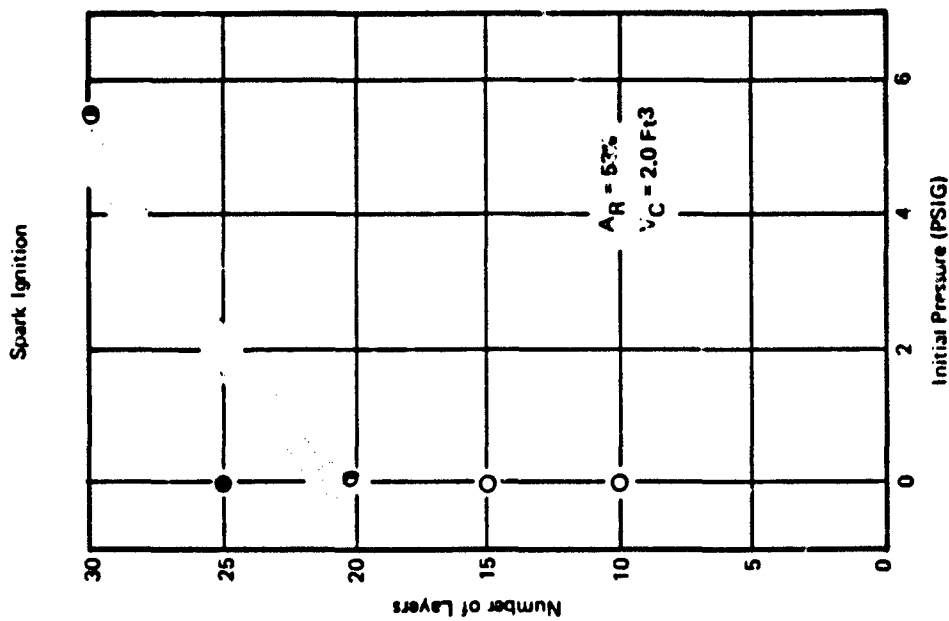


Figure A-49: Arrestor Thickness Versus Initial Pressure Data Plots for Quartz Fiber Type 594/38-9073 with 4-Mesh Support Screen

These Data Summarize Figures A-41, A-42 and A-43

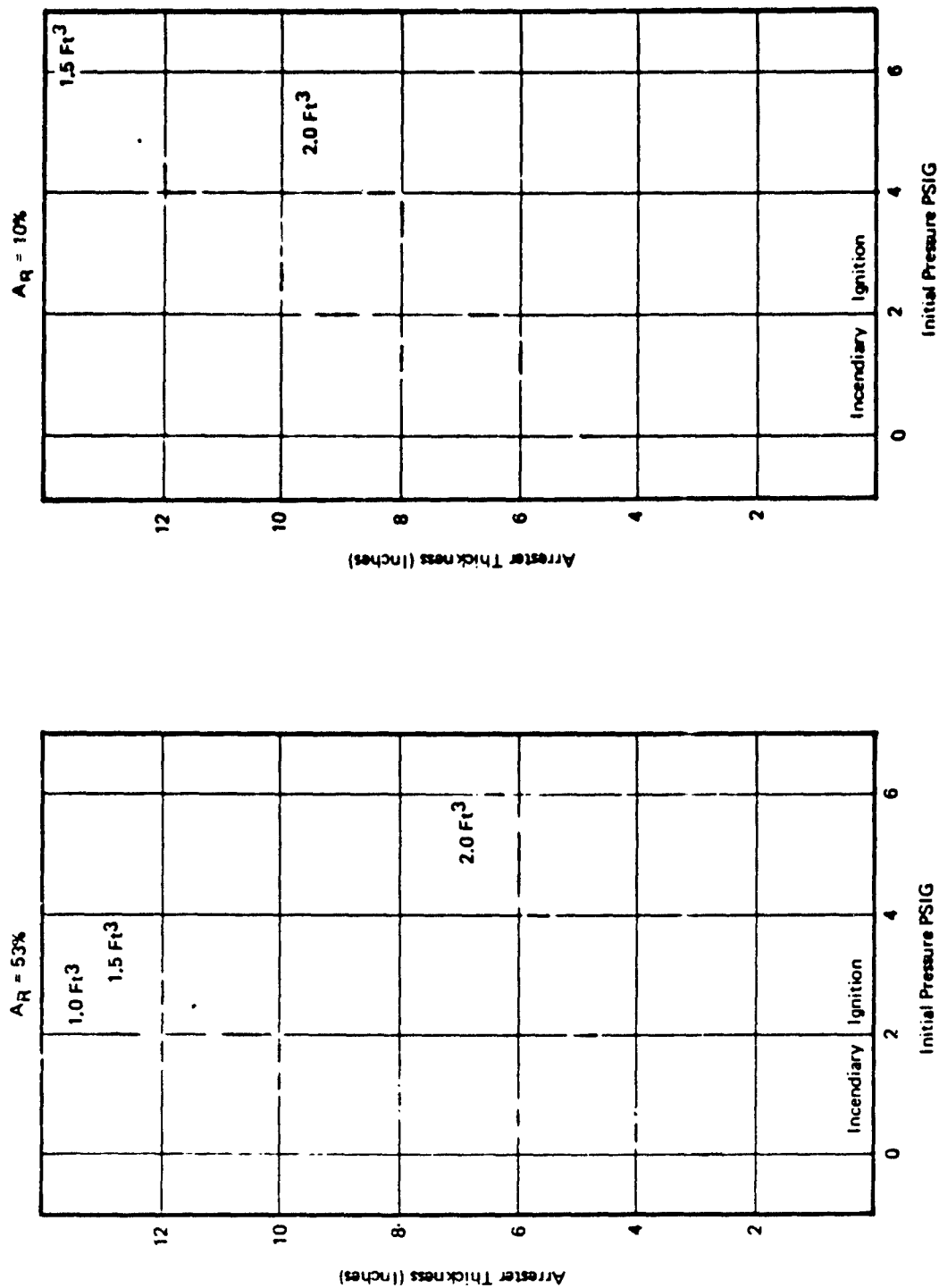


Figure A-50: Variation of 25-PPI Foam Arrester Thickness with Combustion Volume

**Dynamic Model Data 10% Orifice
Spark Ignition**

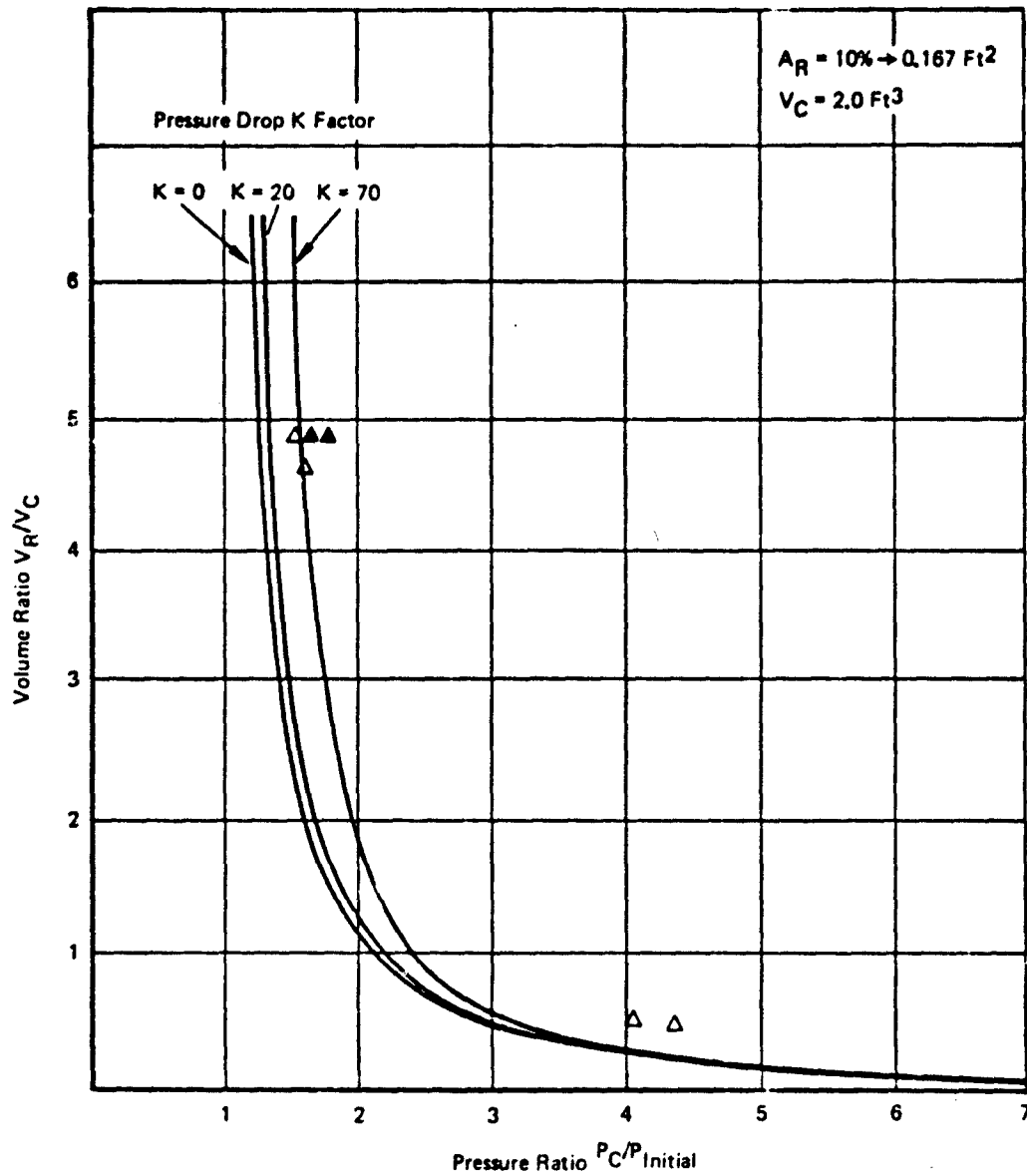


Figure A-51: Volume Ratio Versus Pressure Ratio Data Plots for GAF Felt Type 2A

Dynamic Model Data 10% Orifice
Incendiary Ignition

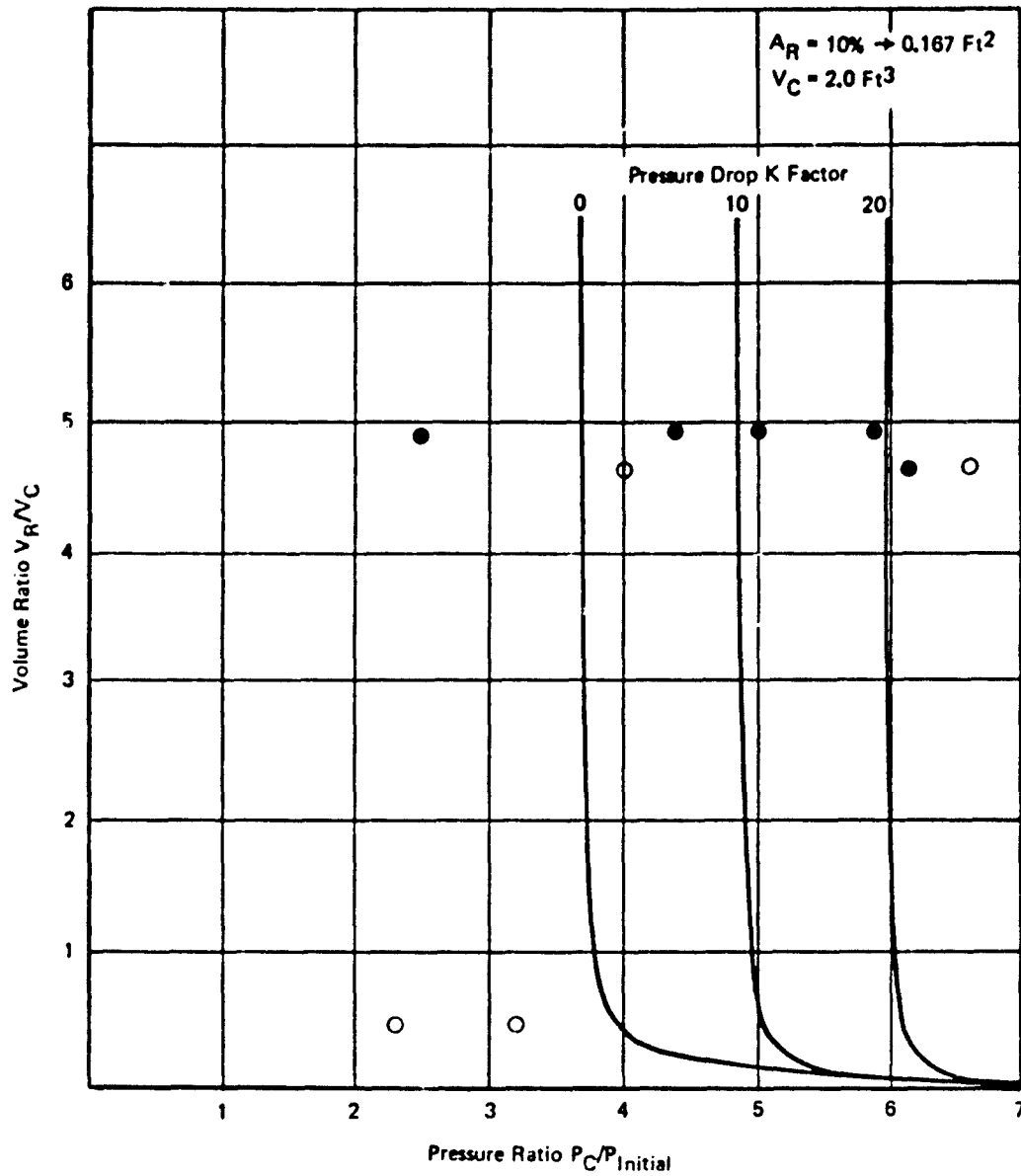


Figure A-52: Volume Ratio Versus Pressure Ratio Data Plots for GAF Felt Type 2A

**Dynamic Model Data 10% Orifice
Incendiary Ignition**

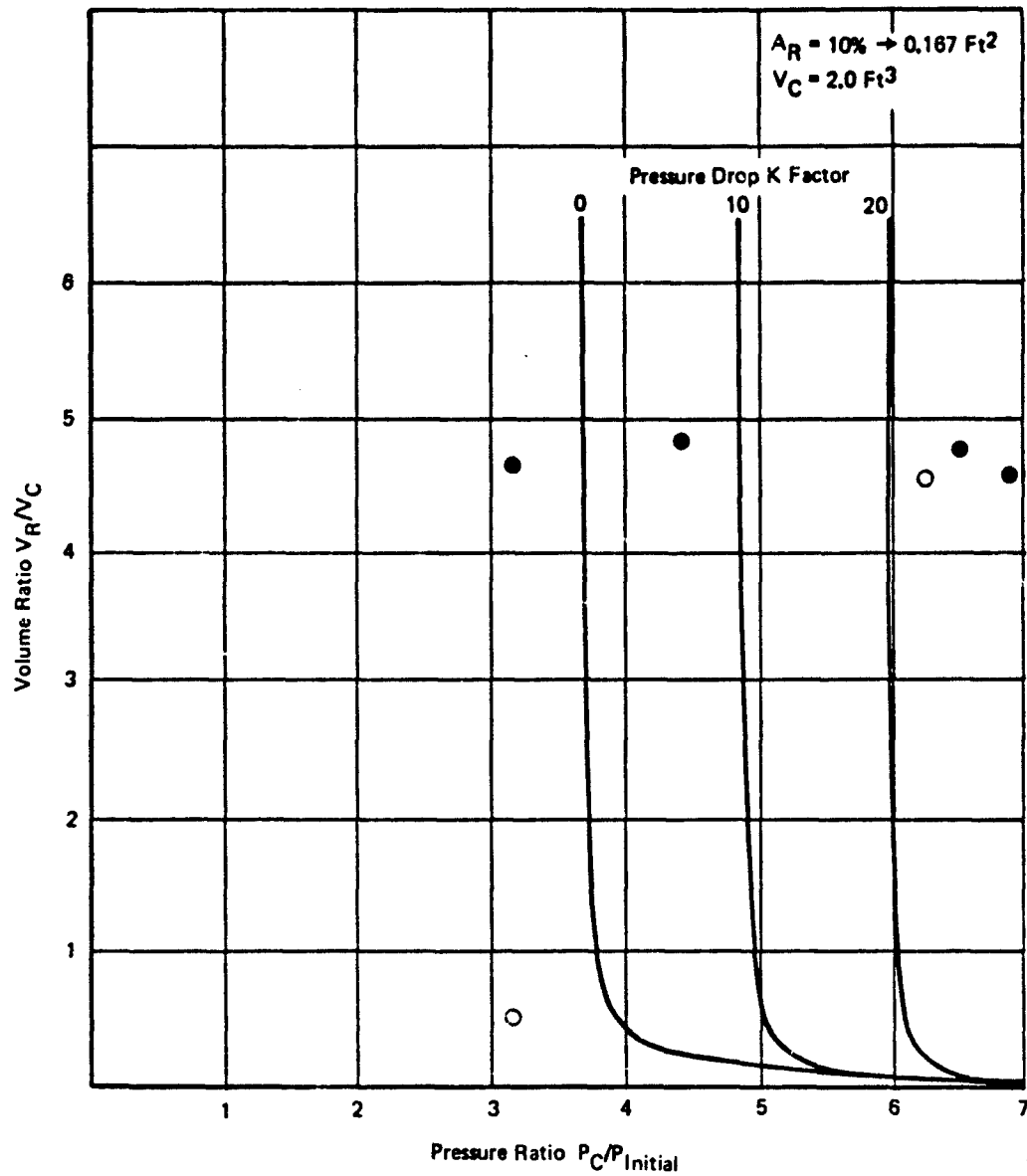
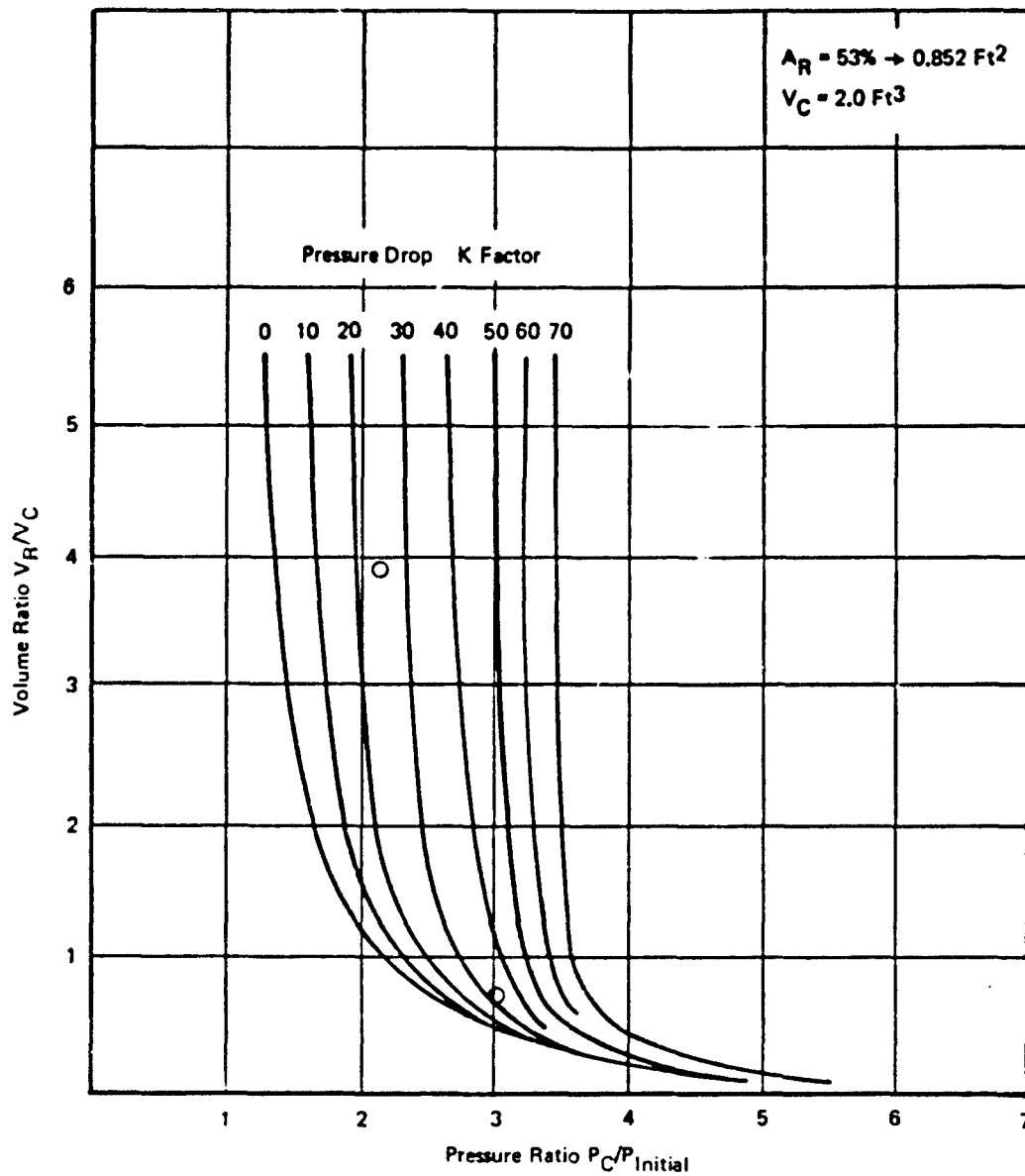


Figure A-53: Volume Ratio Versus Pressure Ratio Data Plots for GAF Felt Standard

*Dynamic Model Data 53% Orifice
Incendiary Ignition*



*Figure A-54: Volume Ratio Versus Pressure Ratio Data Plots for 3M Felt with Two 20-Mesh
-016 Stainless Steel Screens on Front Face Only*

**Dynamic Model Data 10% Orifice
Spark Ignition**

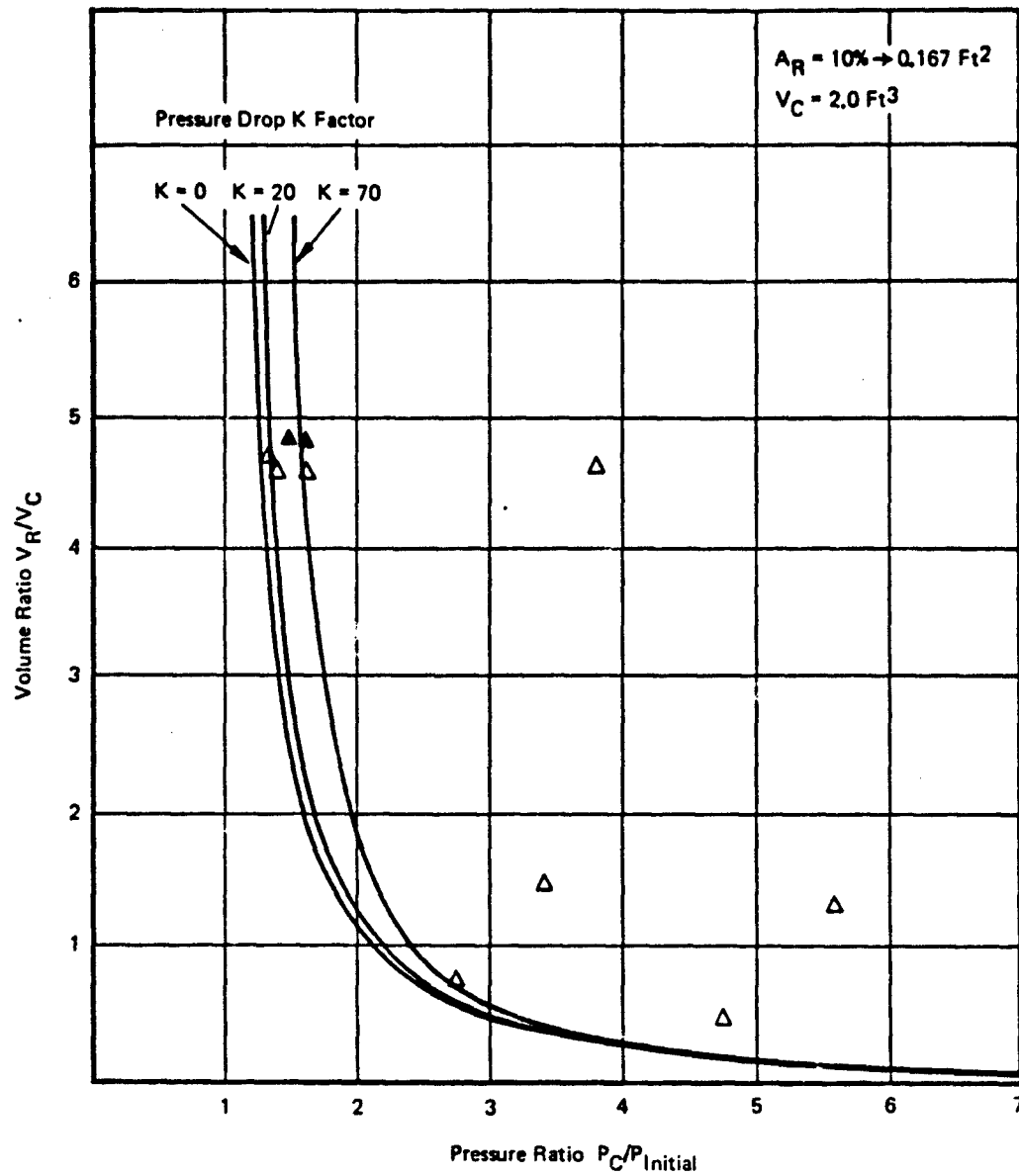


Figure A-55: Volume Ratio Versus Pressure Ratio Data Plots for 3M Felt Scotch Brite

*Dynamic Model Data 10% Orifice
Incendiary Ignition*

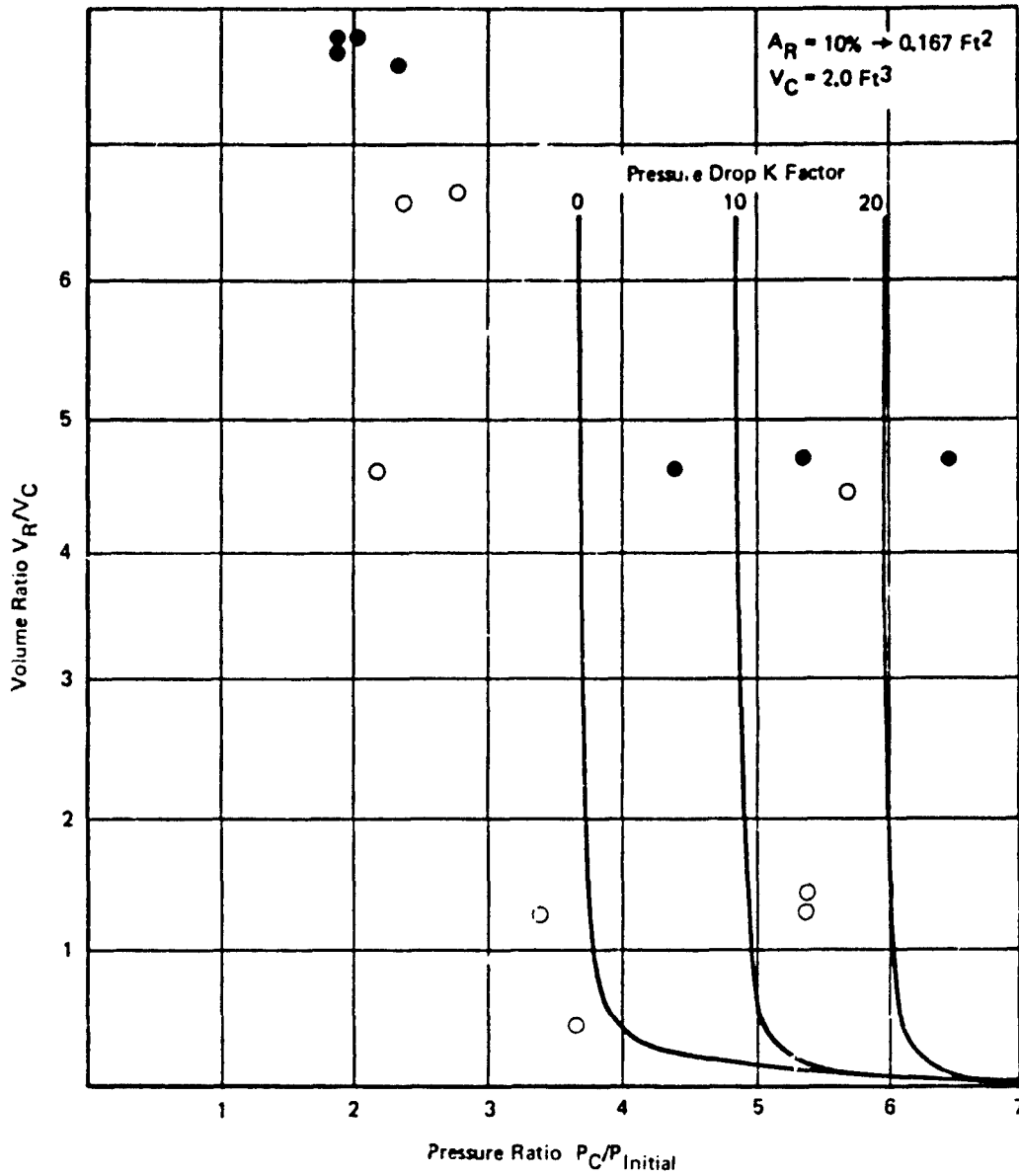


Figure A-56: Volume Ratio Versus Pressure Ratio Data Plots for 3M Felt Scotch Brite

Dynamic Model Data 53% Orifice
Incendiary Ignition

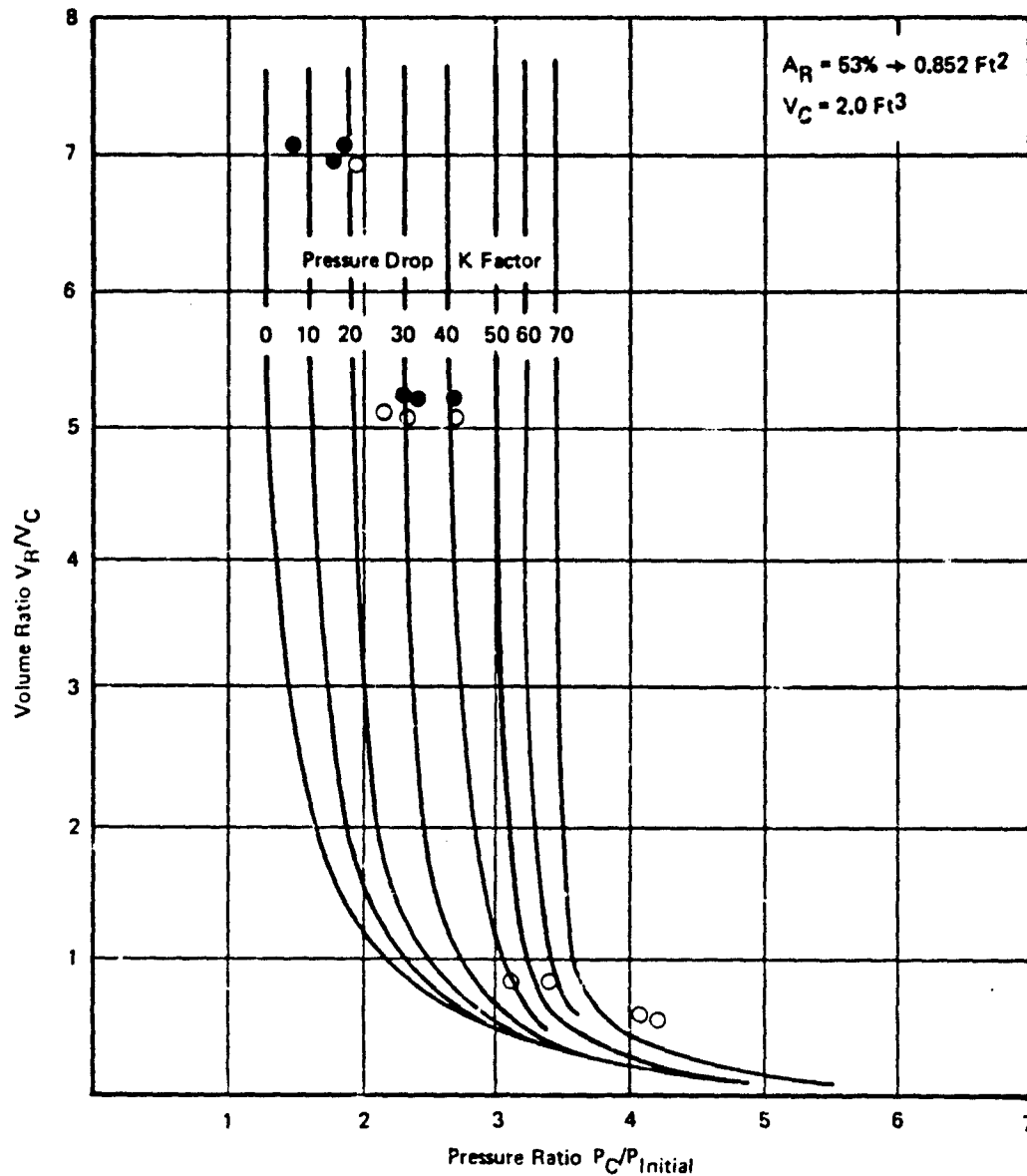


Figure A-57: Volume Ratio Versus Pressure Ratio Data Plots for 3M Felt Scotch Brite

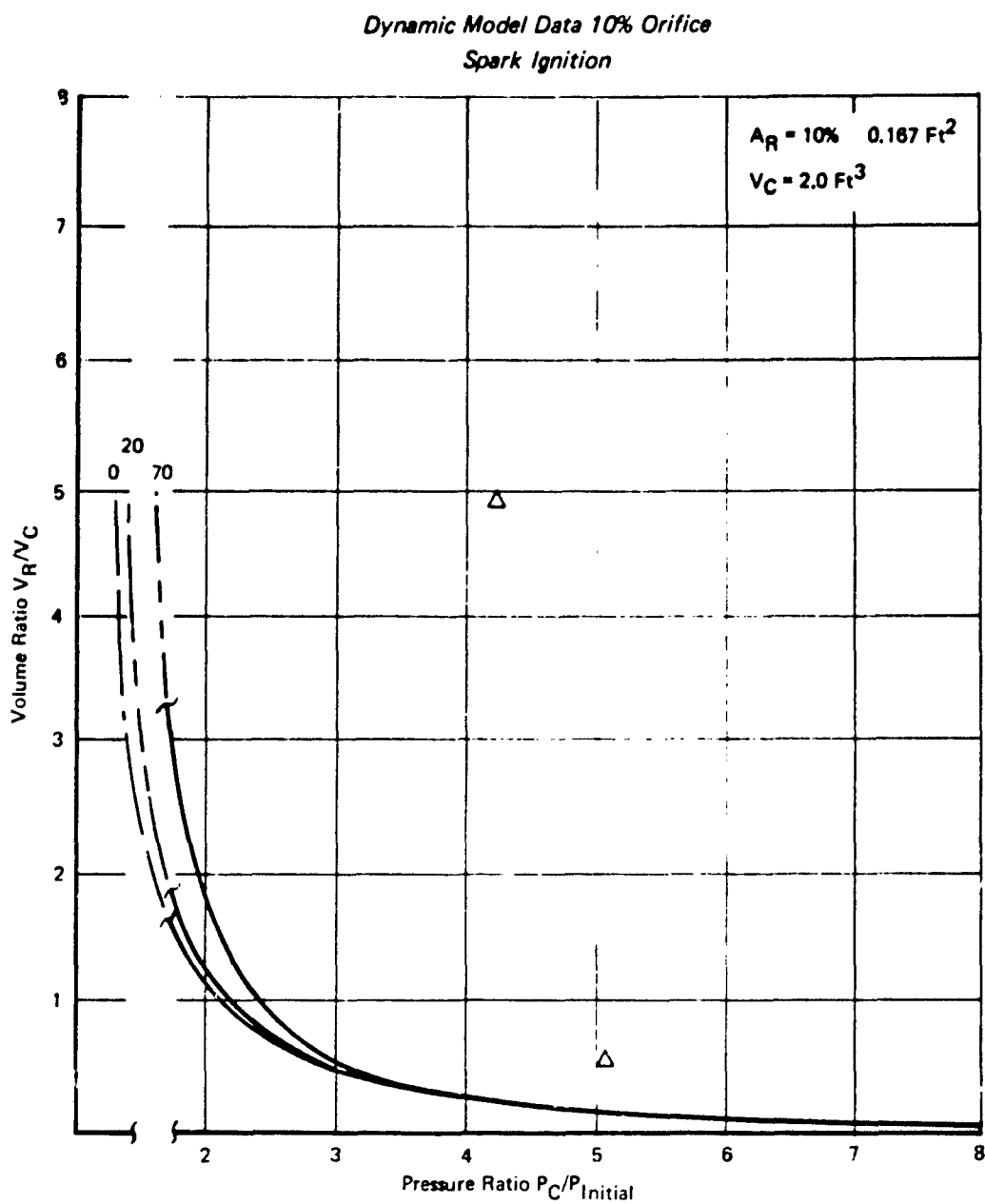


Figure A-58: Volume Ratio Versus Pressure Ratio Data Plots for Quartz Fiber 594/38-9073 with 4-Mesh Retaining Screen

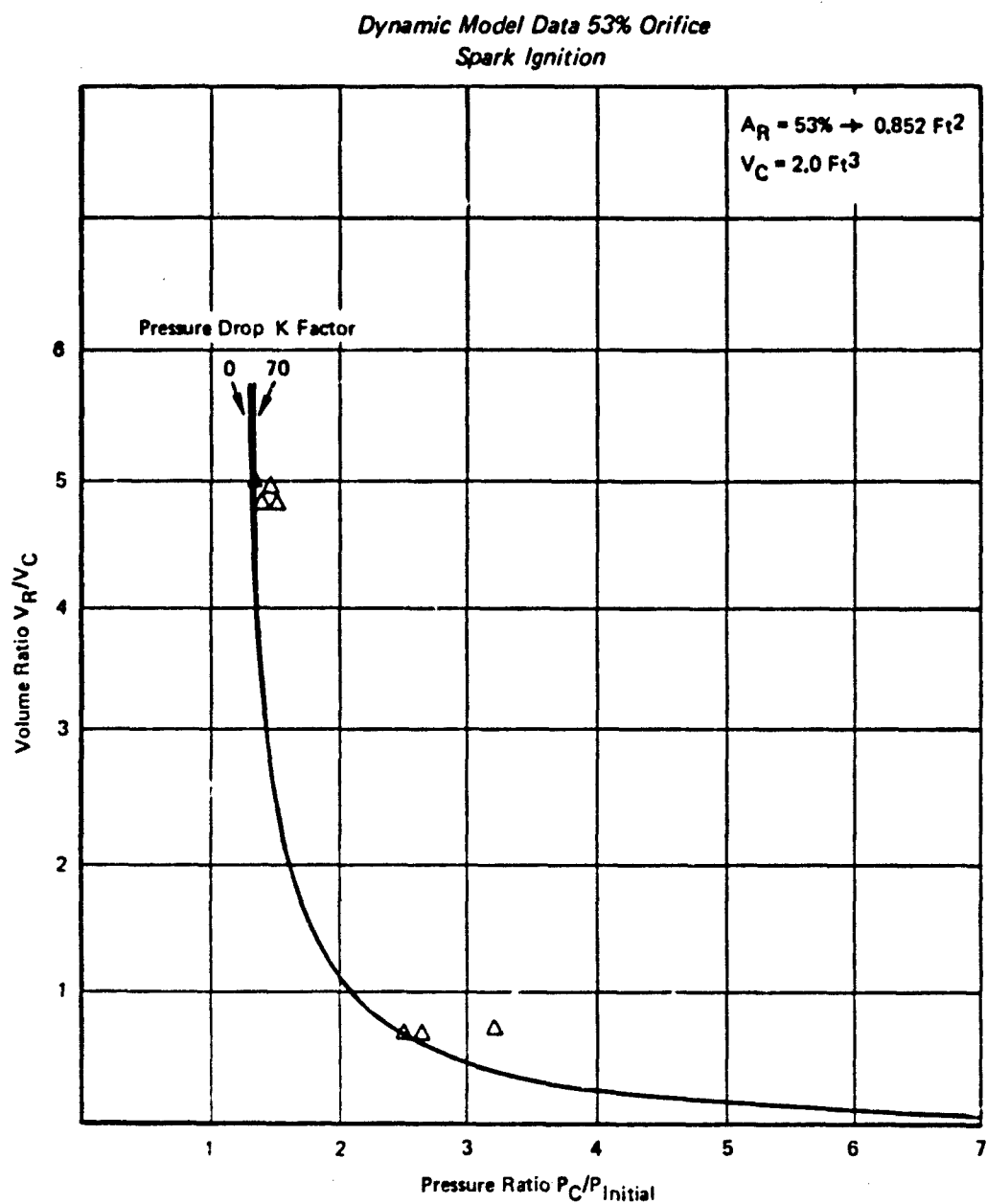
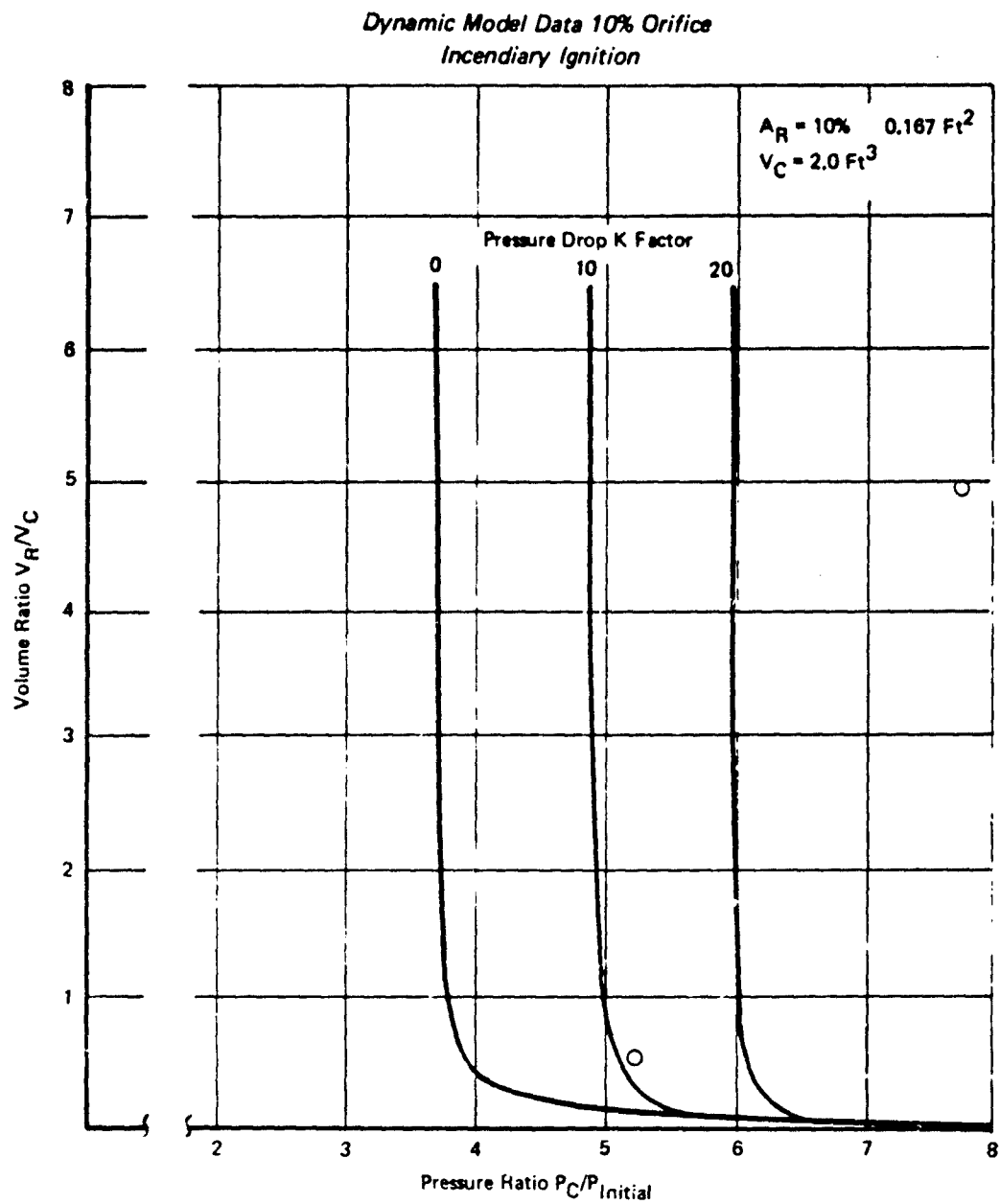
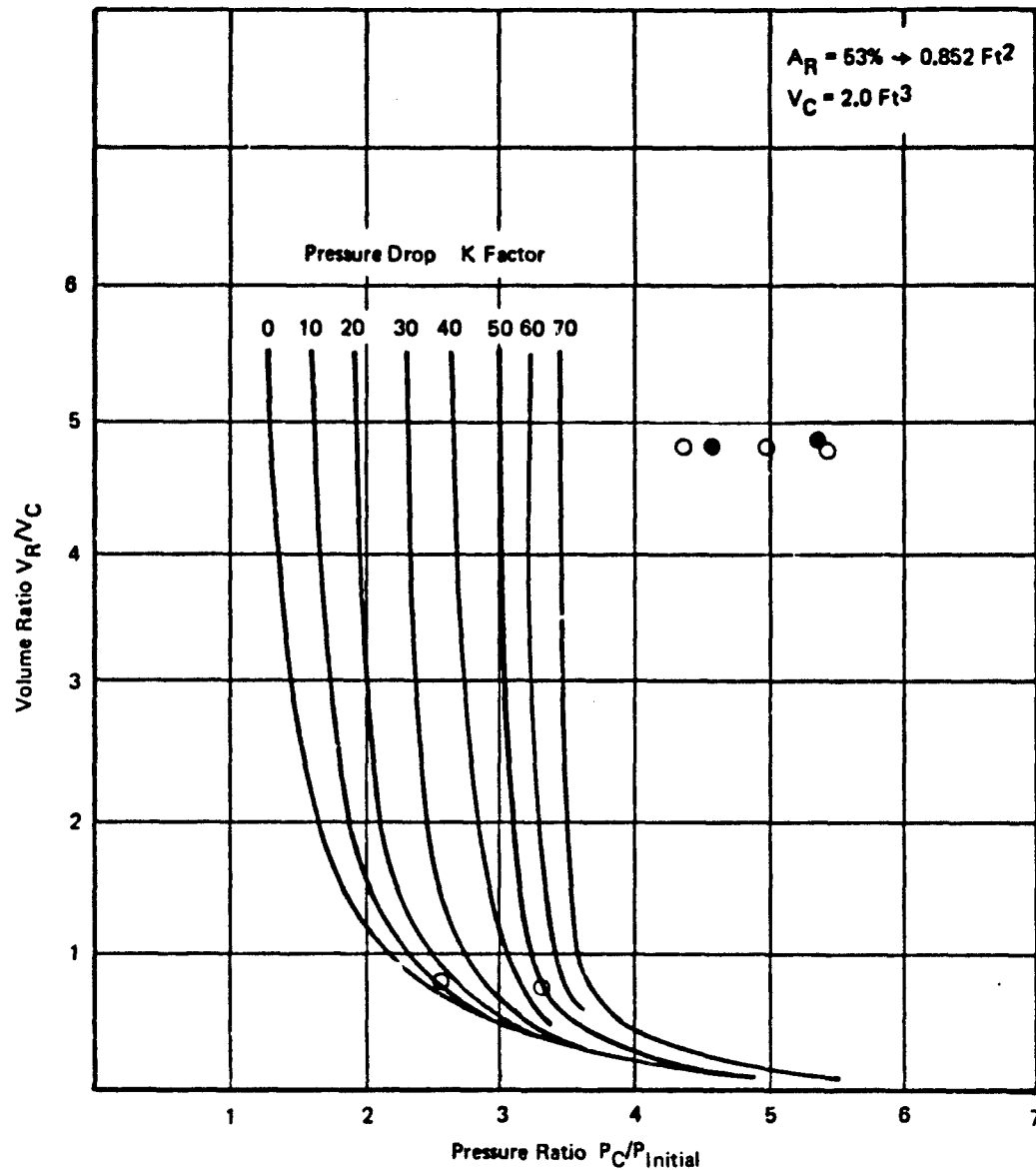


Figure A-59: Volume Ratio Versus Pressure Ratio Data Plots for Quartz Fiber 594/38-9073
with 4-Mesh Retaining Screen



*Figure A-60: Volume Ratio Versus Pressure Ratio Data Plots for Quartz Fiber 594/38-9073
with 4-Mesh Retaining Screen*

**Dynamic Model Data 53% Orifice
Incendiary Ignition**



**Figure A-61: Volume Ratio Versus Pressure Ratio Data Plots for Quartz Fiber 594/38-9073
with 20-Mesh Retaining Screen**

**Dynamic Model Data 53% Orifice
Incendiary Ignition**

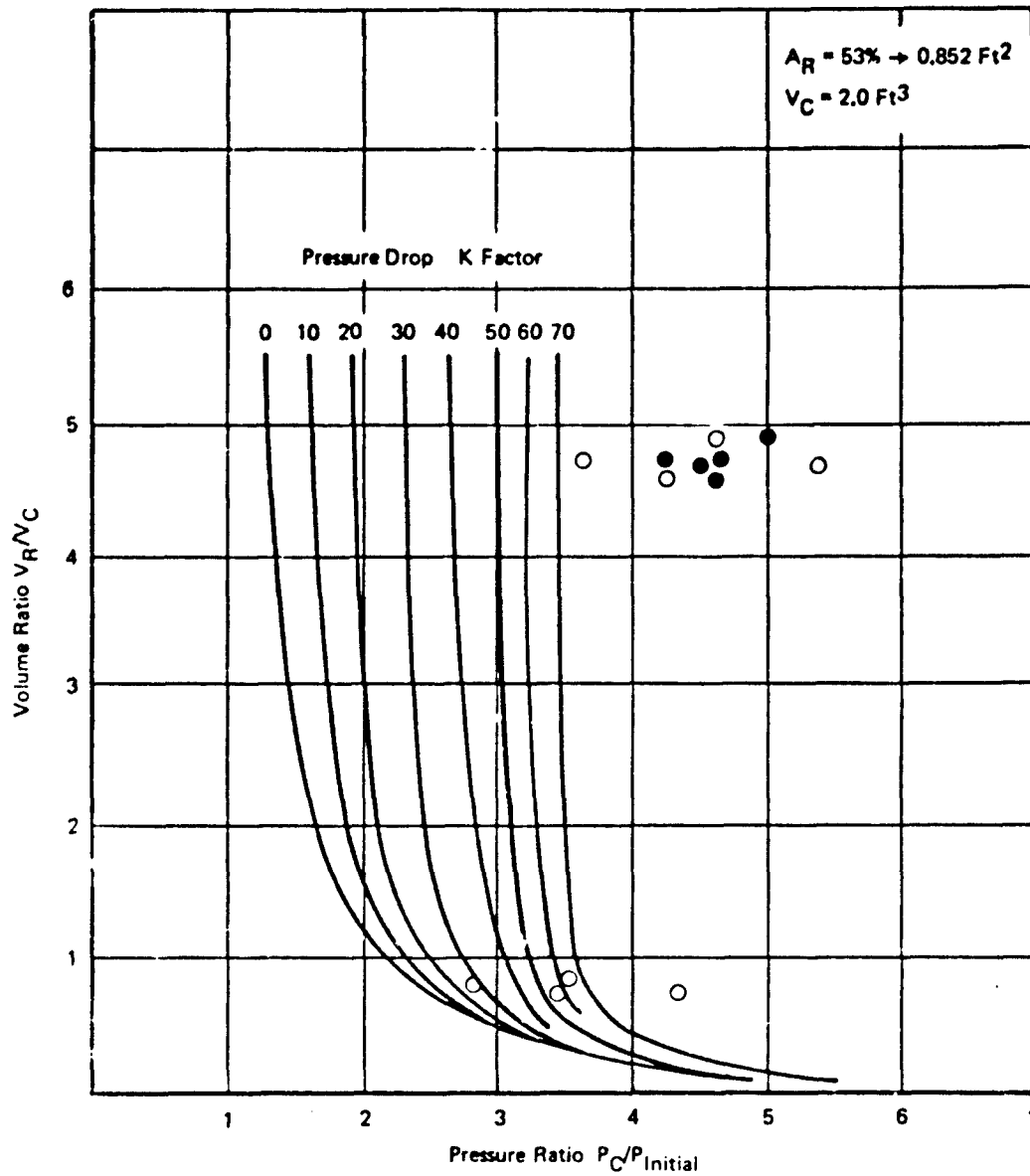
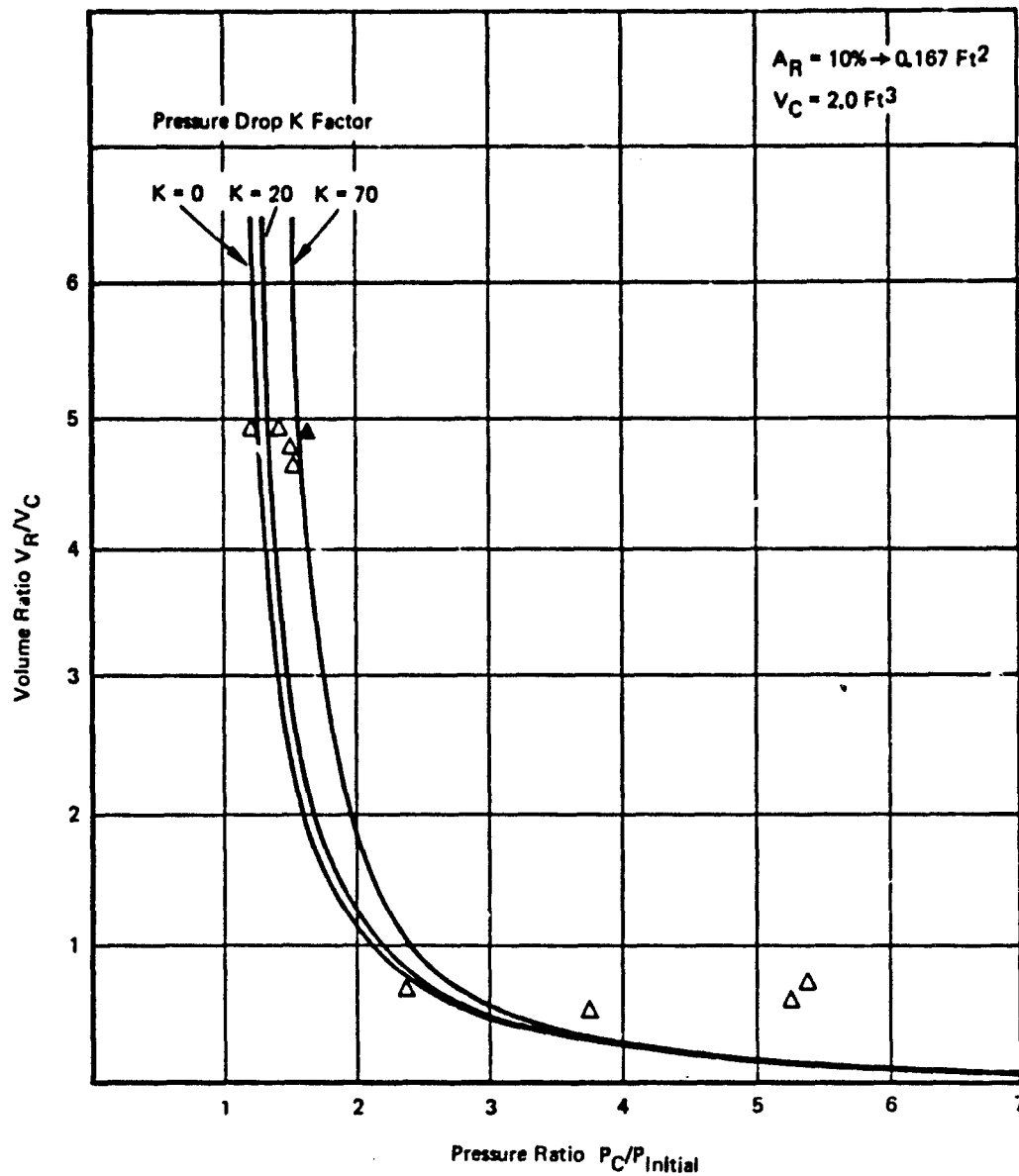


Figure A-62: Volume Ratio Versus Pressure Ratio Data Plots for Quartz Fiber 594/38-9073
594/38-9073 with Two Layers of 20-Mesh -016 Stainless Steel Screen

**Dynamic Model Data 10% Orifice
Spark Ignition**



*Figure A-63: Volume Ratio Versus Pressure Ratio Data Plots for 25-PPI Foam
with 4-Mesh Retaining Screen*

Dynamic Model Data 53% Orifice
Spark Ignition

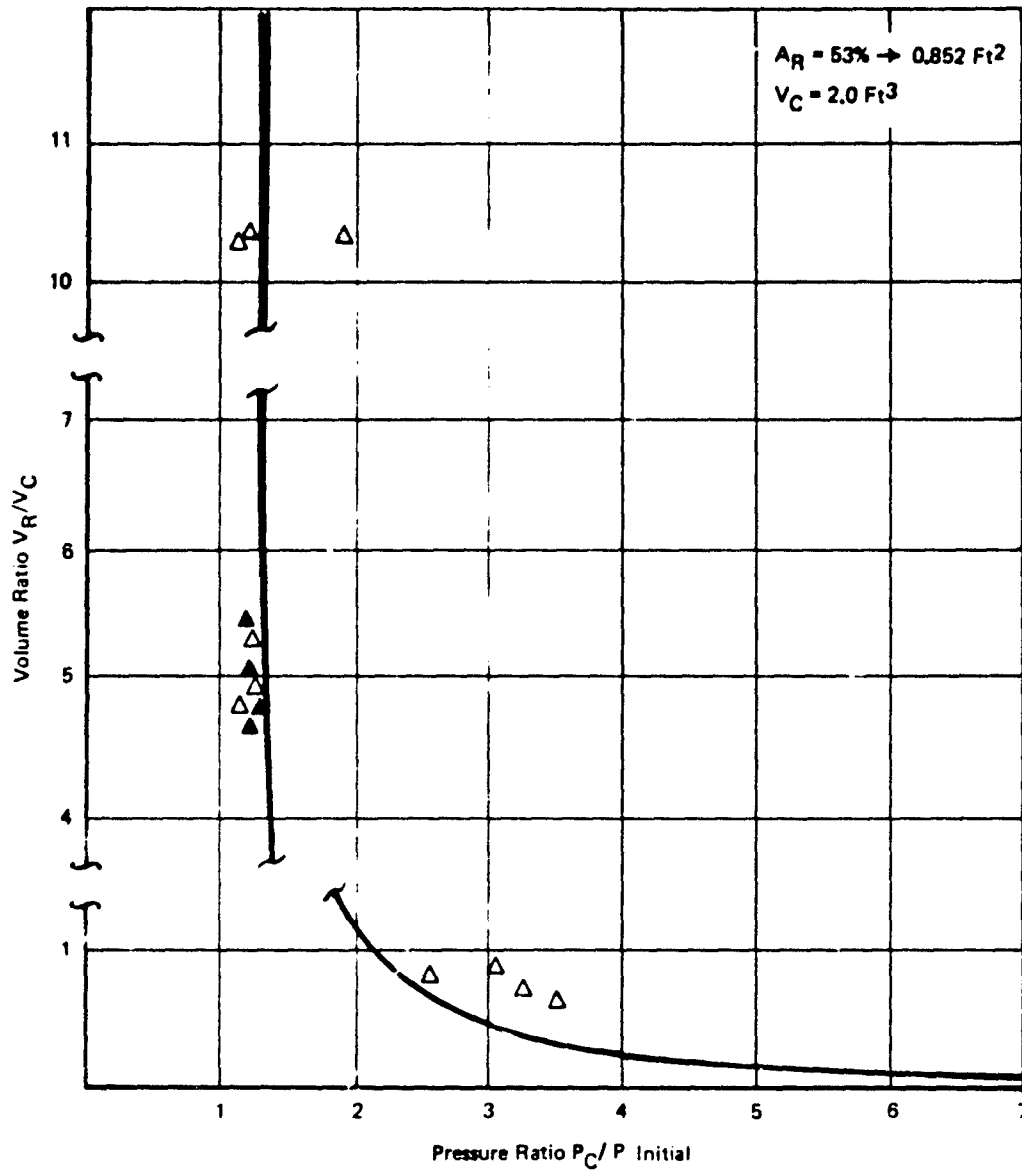
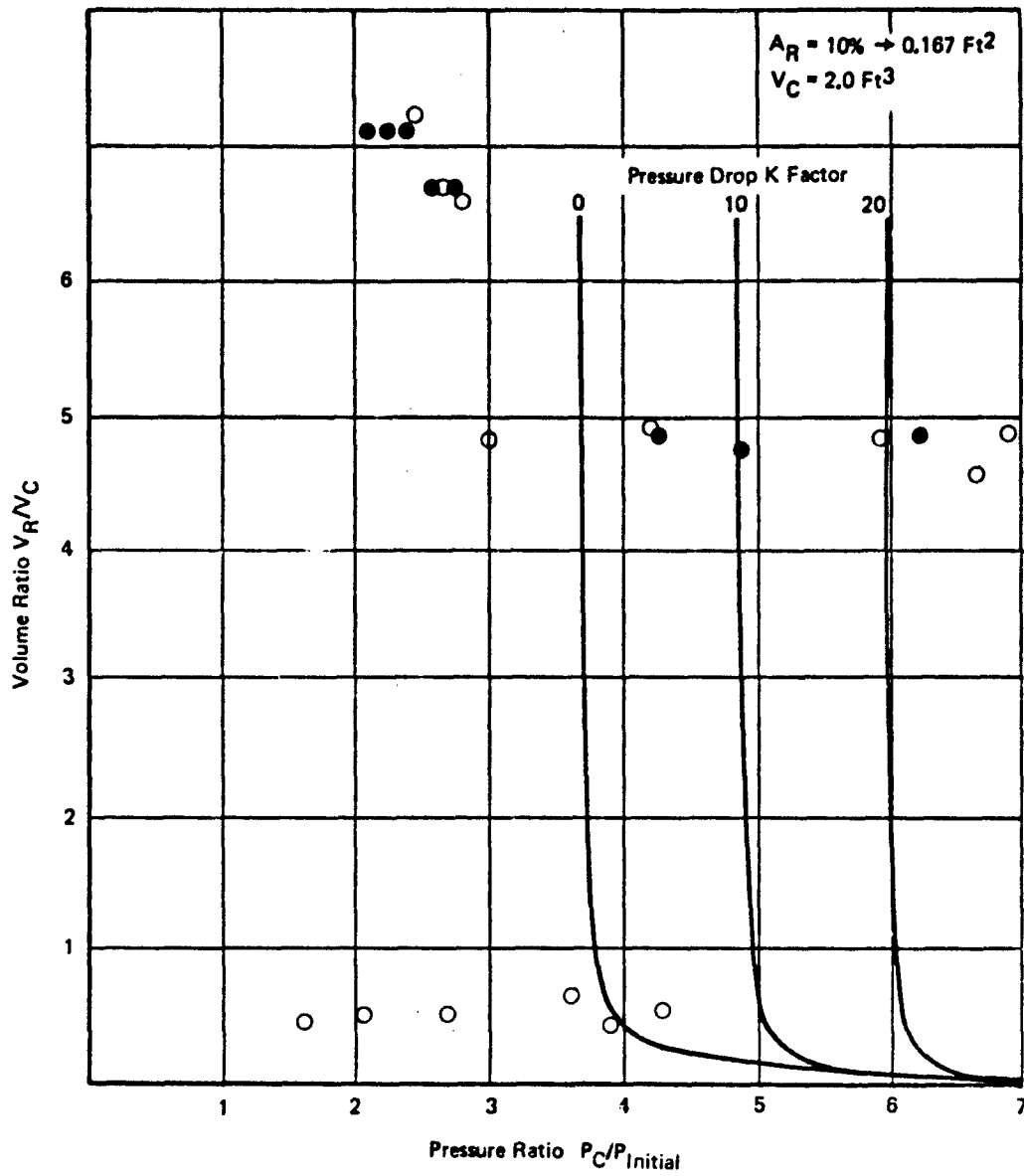


Figure A-64: Volume Ratio Versus Pressure Ratio Data Plots for 25-PPI Foam with 4-Mesh Retaining Screen

**Dynamic Model Data 10% Orifice
Incendiary Ignition**



**Figure A-65: Volume Ratio Versus Pressure Ratio Data Plots for 25-PPI Foam
with 4-Mesh Retaining Screen**

*Dynamic Model Data 53% Orifice
Incendiary Ignition*

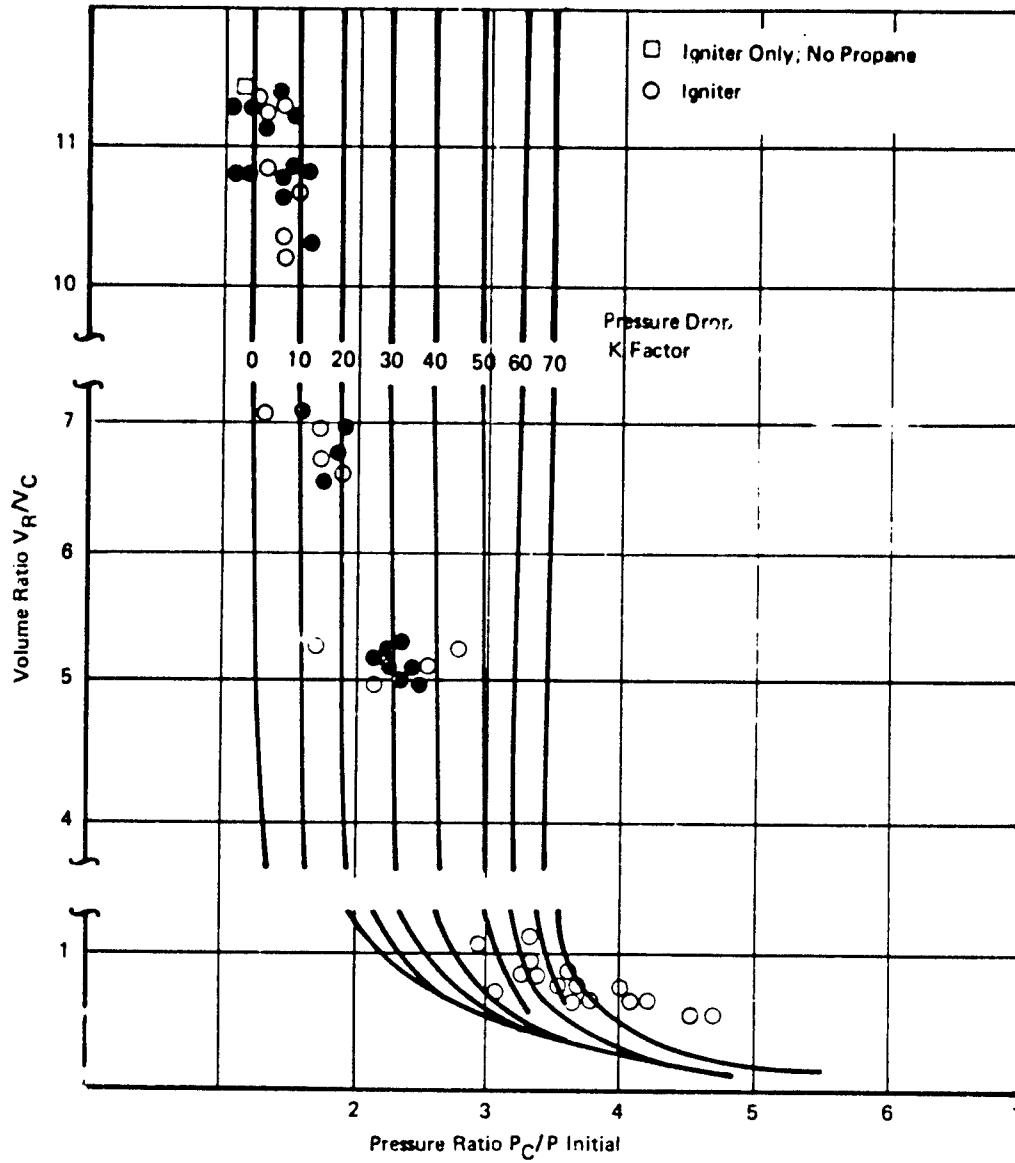


*Figure A-66: Volume Ratio Versus Pressure Ratio Data Plots for 25-PPI Foam
with 4-Mesh Retaining Screen*

**Dynamic Model Data 53% Orifice
Incendiary Ignition**

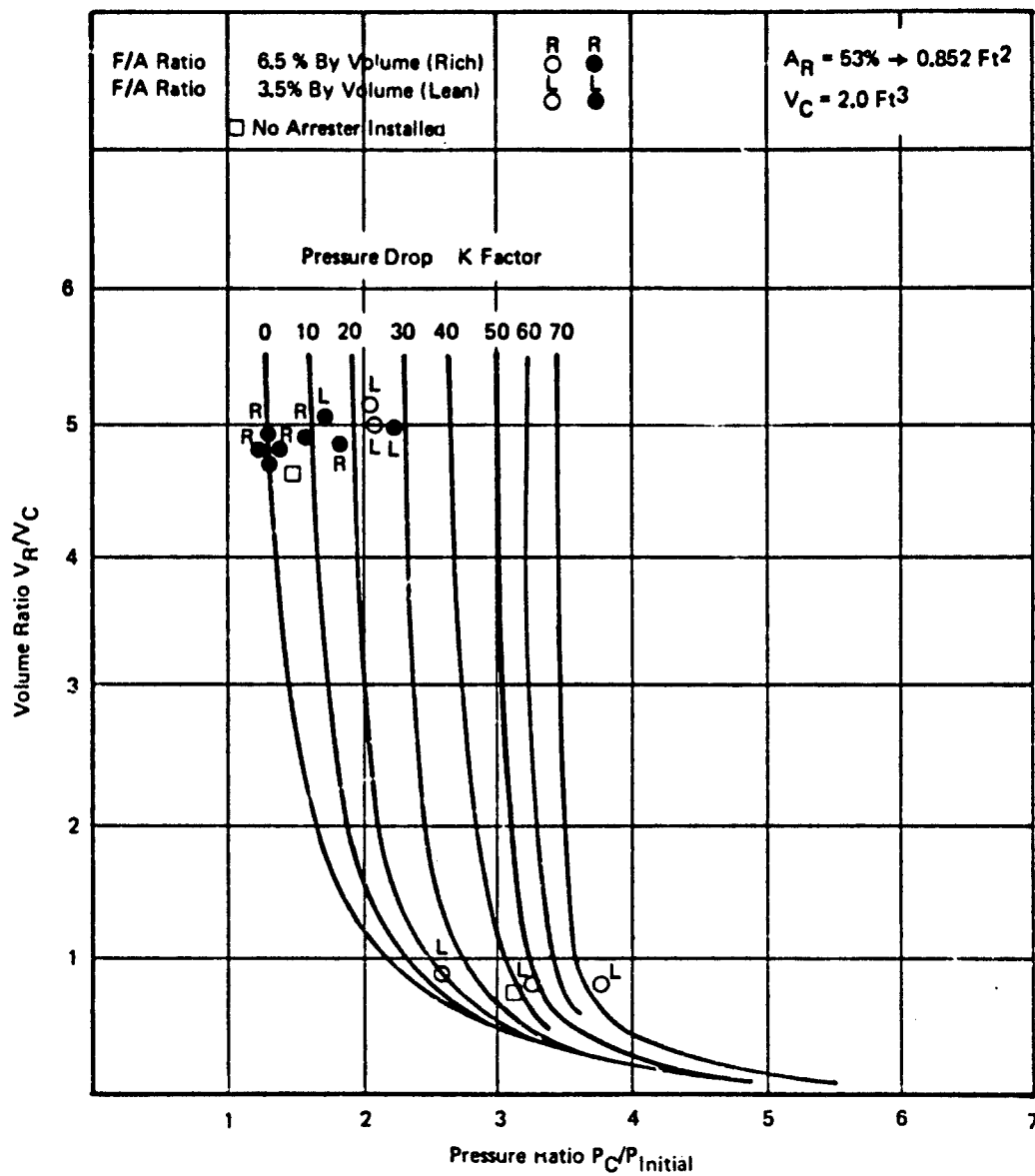


Figure A-67: Volume Ratio Versus Pressure Ratio Data Plots for 25-PPI Foam with 4-Mesh Stainless Steel Retaining Screen, Various F/A Ratios

*Dynamic Model Data 53% Orifice
Incendiary Ignition*

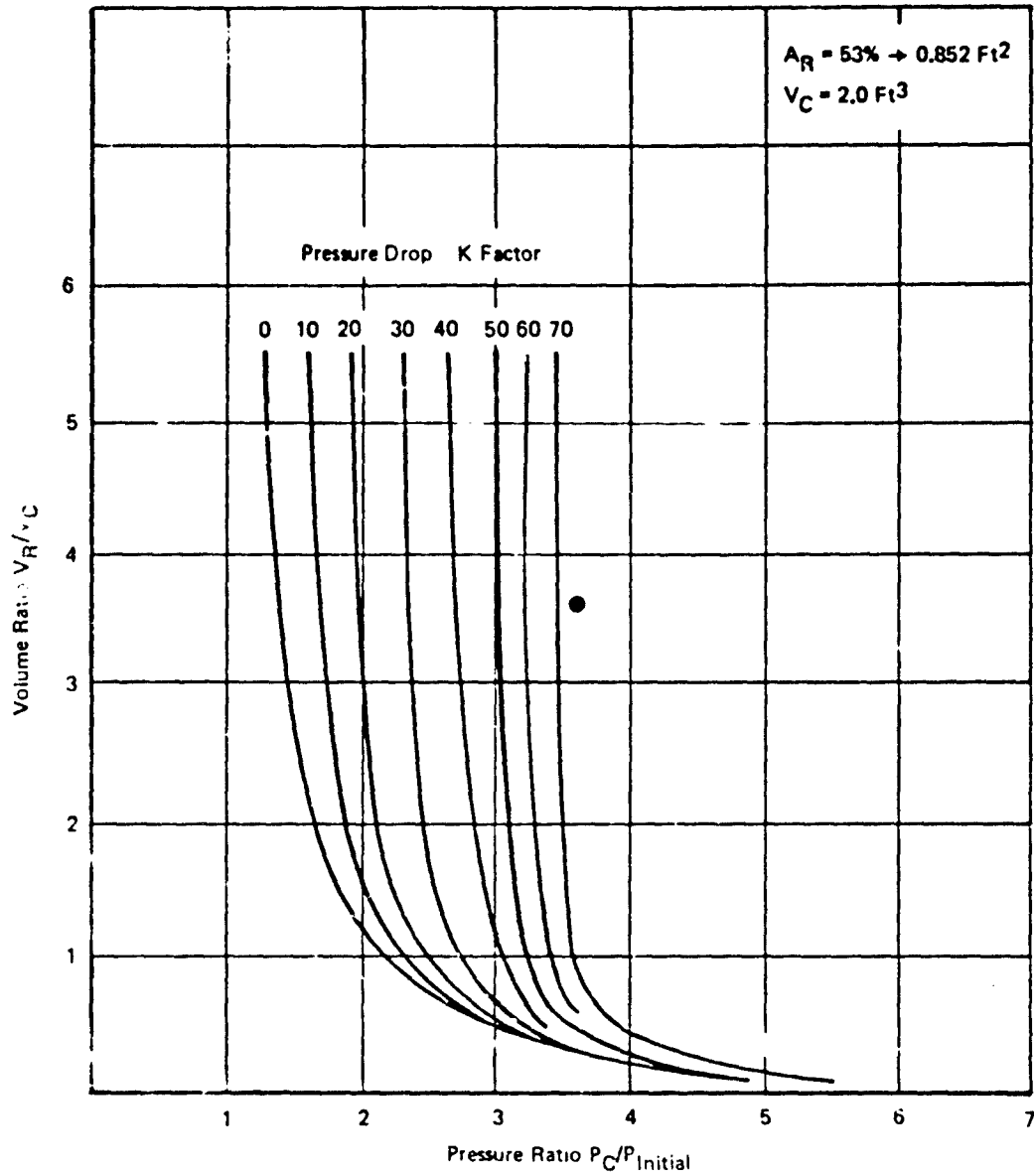


Figure A-68: Volume Ratio Versus Pressure Ratio Data Plots for 25-PPI Foam with 20-Mesh -016 Stainless Steel Screen - Two Layers on the Front Face Only

**Dynamic Model Data 10% Orifice
Incendiary Ignition**

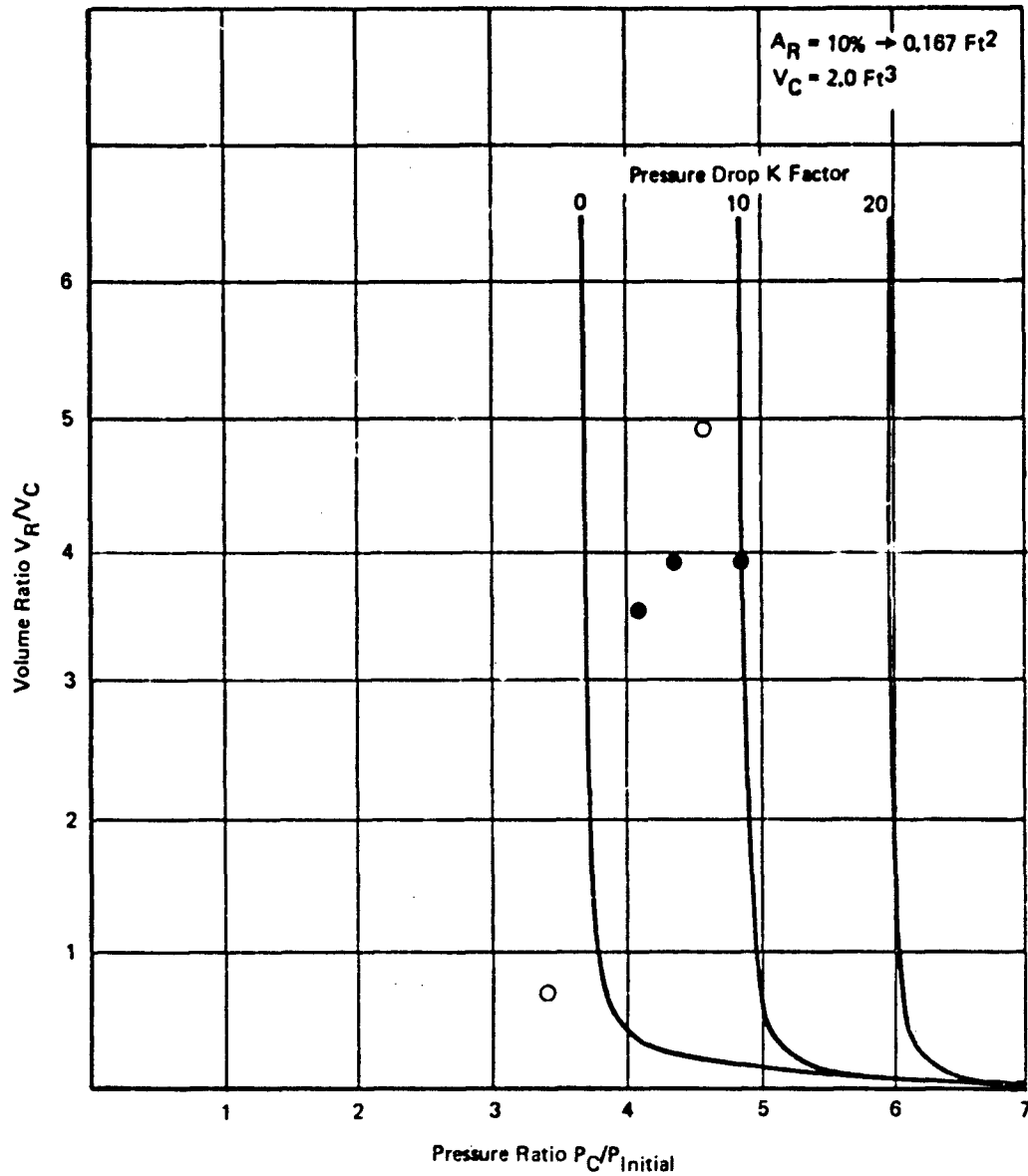


Figure A-69: Volume Ratio Versus Pressure Ratio Data Plots for 25-PPI Foam with 10 Layers of Quartz Fiber Type 594/38-9073 on the Front Face - 4-Mesh Support Screen

Dynamic Model Data 10% Orifice
Incendiary Ignition

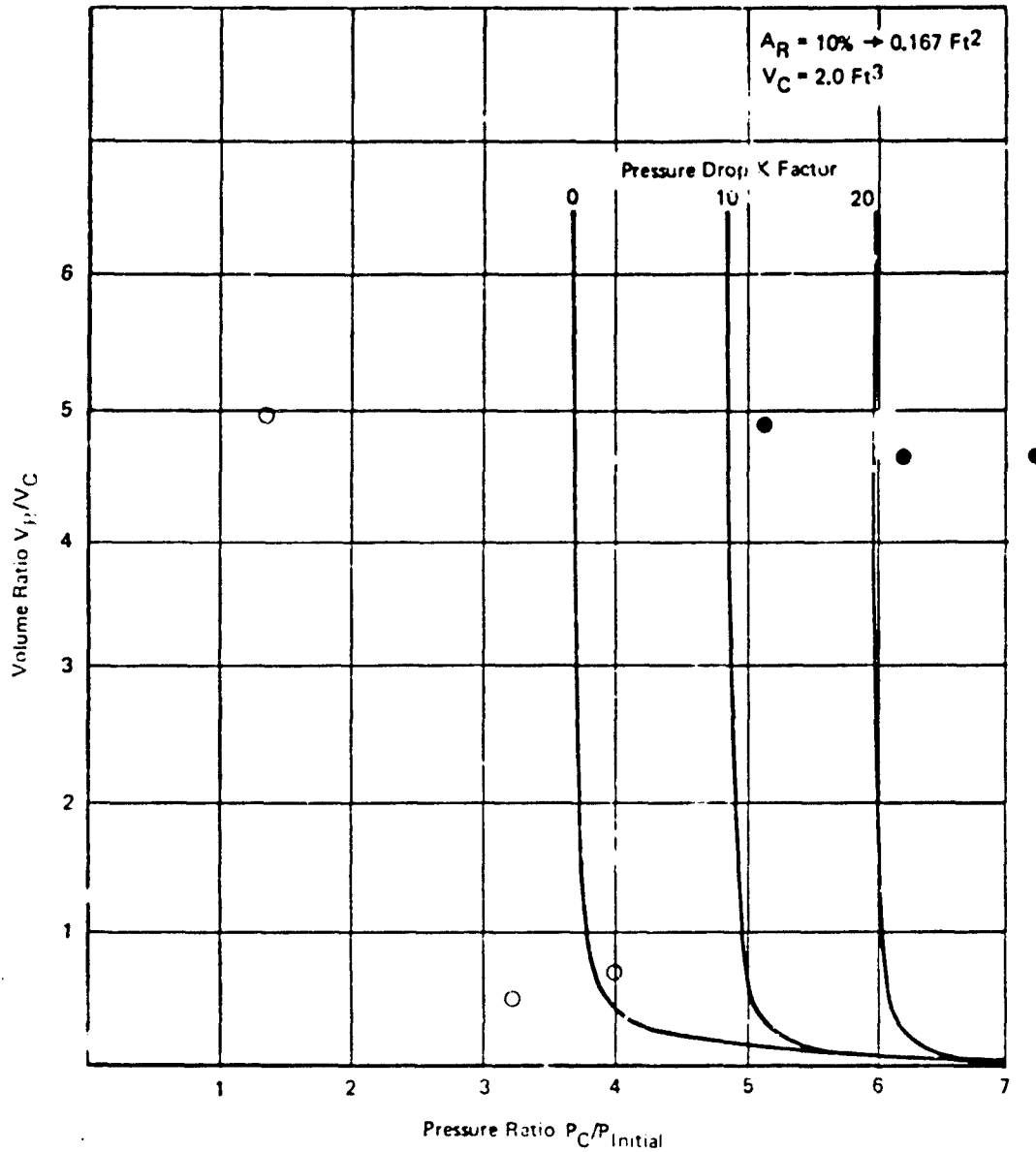
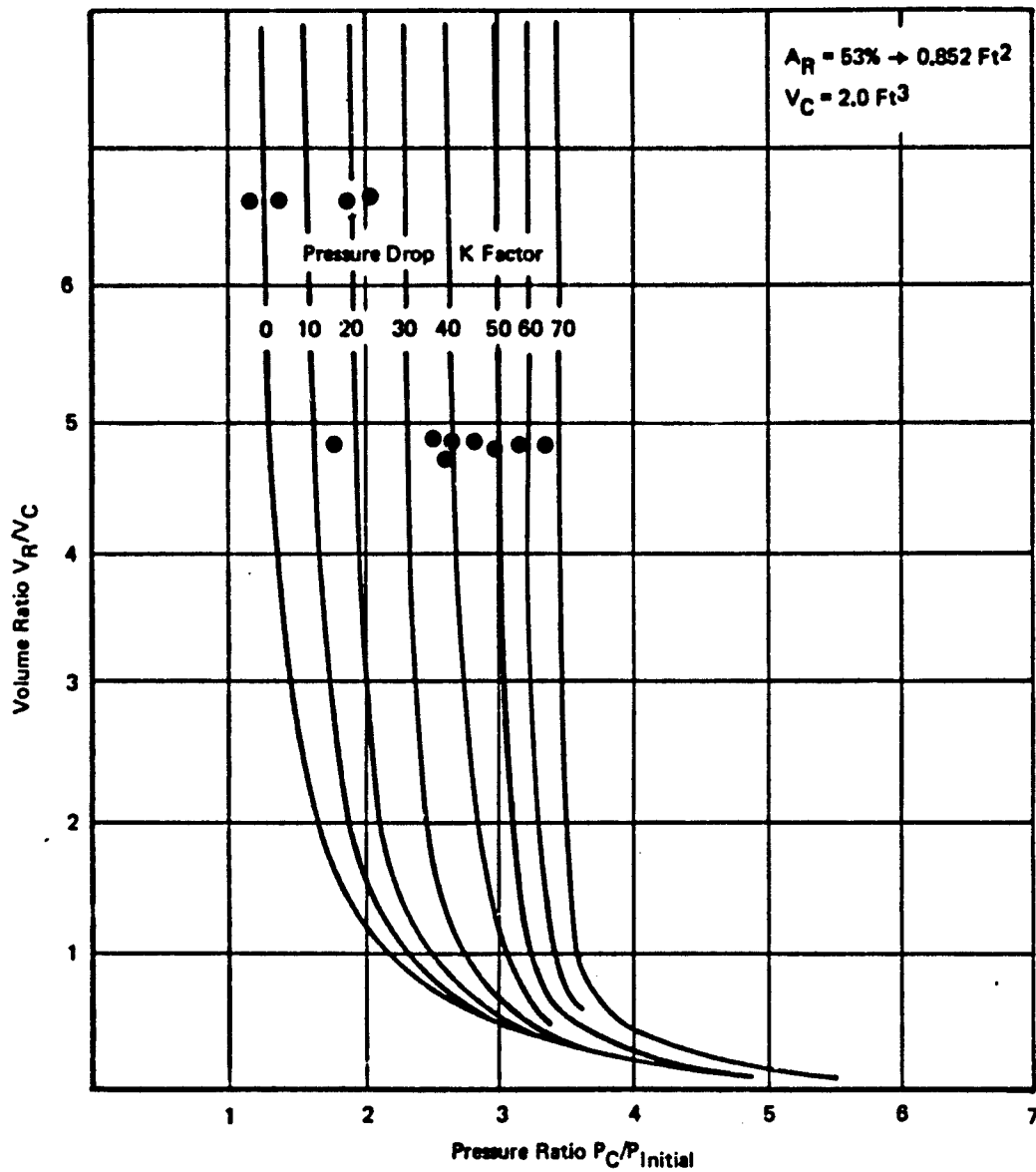


Figure A-70: Volume Ratio Versus Pressure Ratio Data Plots for 25-PPI Foam with Two Layers of Stainless Steel Screen on Each Side

**Dynamic Model Data 53% Orifice
Incendiary Ignition**



**Figure A-71: Volume Ratio Versus Pressure Ratio Data Plots for 25-PPI Foam
with Two Layers of Stainless Steel Screen on Each Side**

**Dynamic Model Data 53% Orifice
Incendiary Ignition**

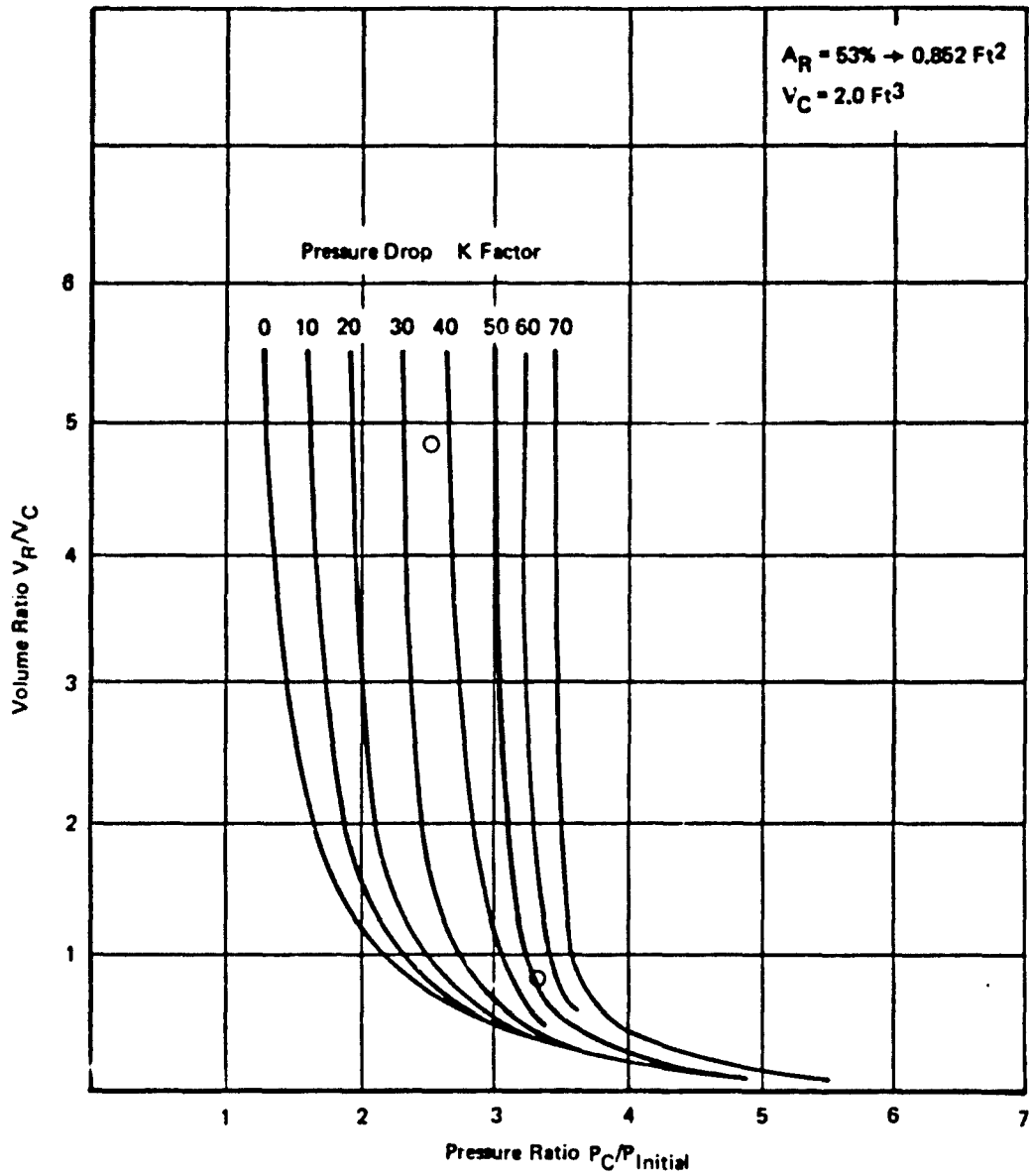


**Figure A-72: Volume Ratio Versus Pressure Ratio Data Plots for 20-Mesh
-016 Stainless Steel Screen**

**Dynamic Model Data 53% Orifice
Incendiary Ignition**

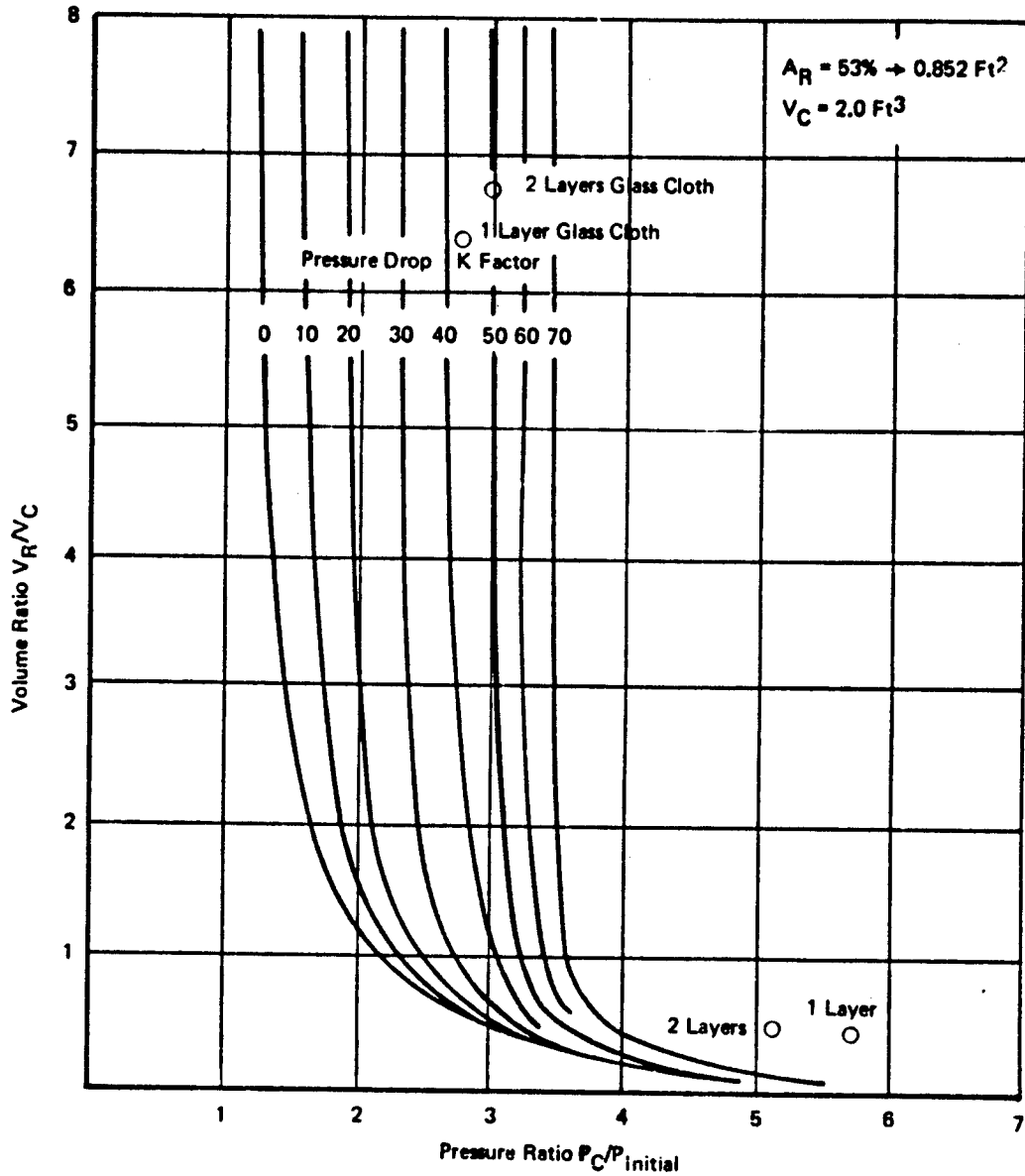


**Figure A-73: Volume Ratio Versus Pressure Ratio Data Plots for 10-Ounce Glass Cloth
with 3/16 HRH 327 Honeycomb 1 1/4 Inch Thick**

Dynamic Model Data 53% Orifice
Incendiary Ignition

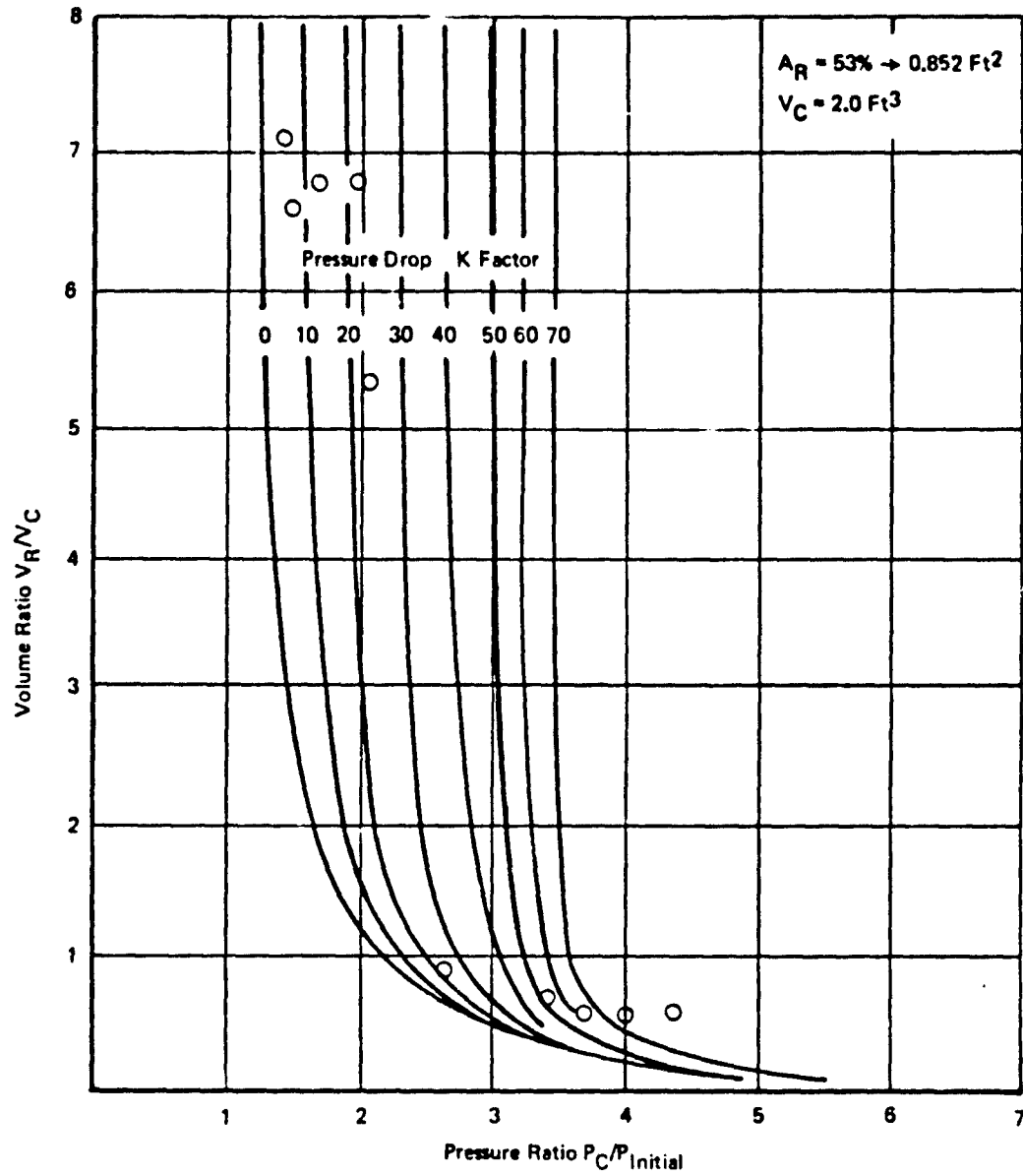
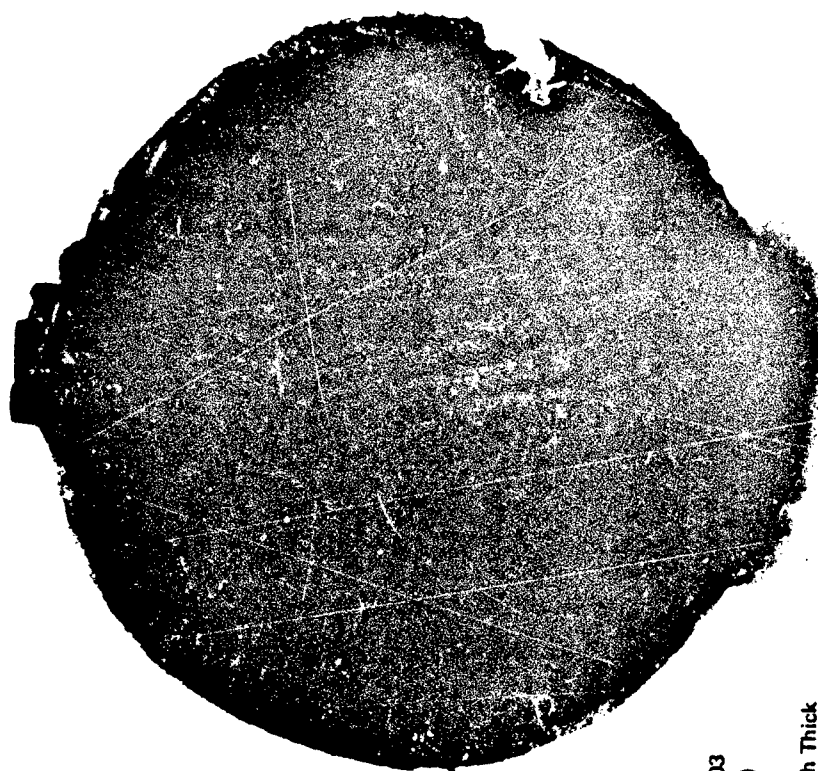
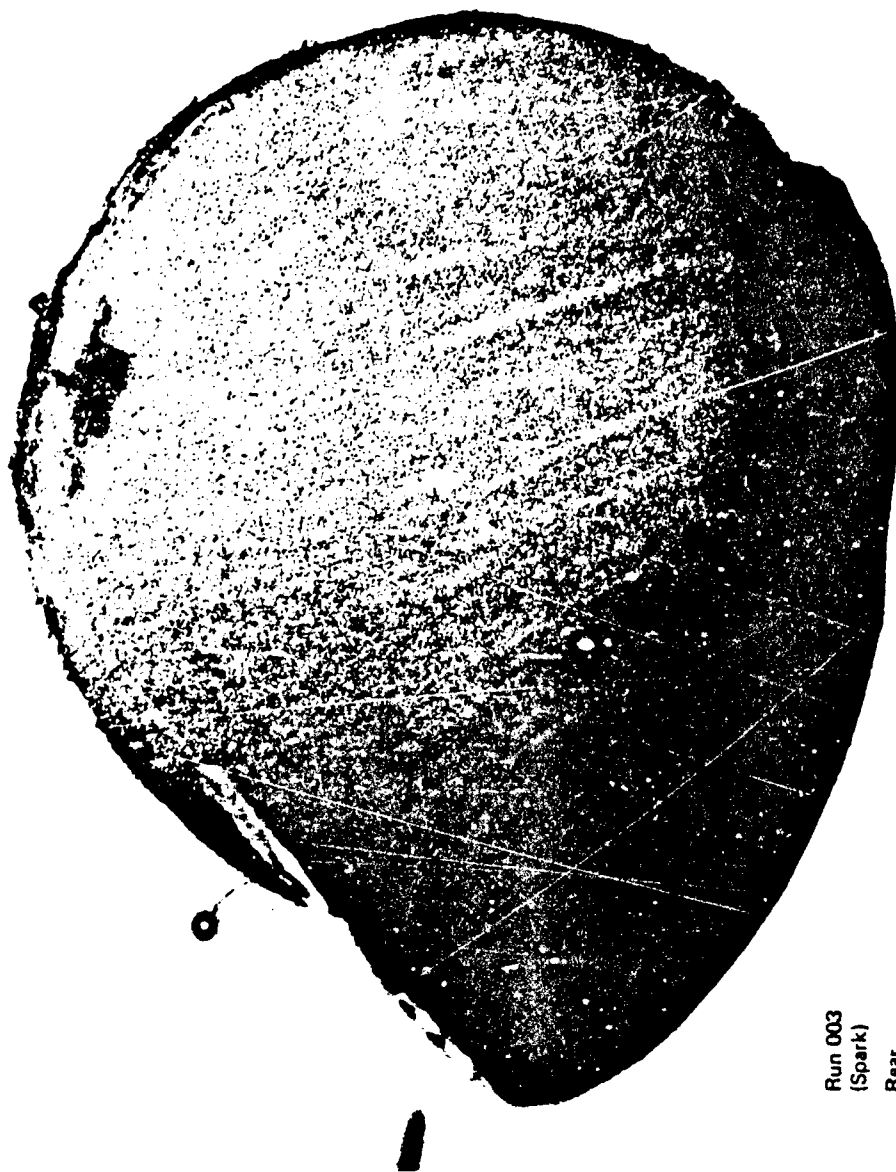


Figure A-74: Volume Ratio Versus Pressure Ratio Data Plots for 15-PPI Yellow Foam



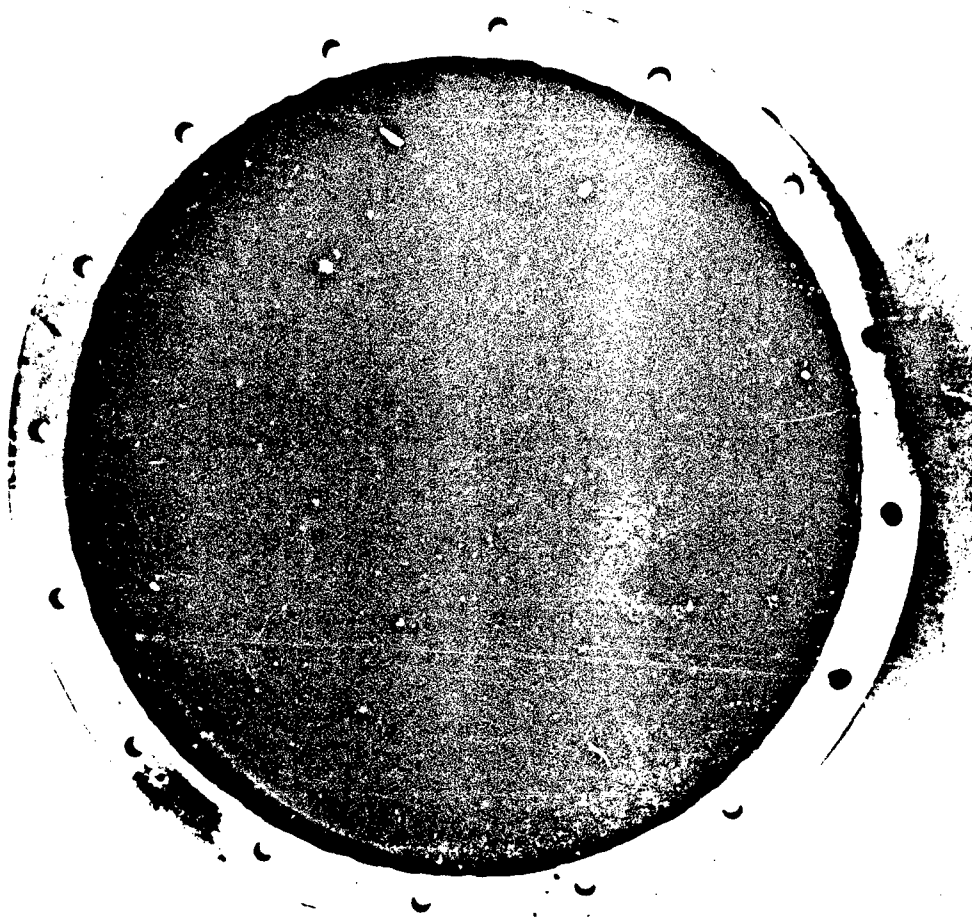
Run 003
(Spark)
Front
4.0 Inch Thick

Figure A-75: 25-PPI Foam Combustion Face, Run 003



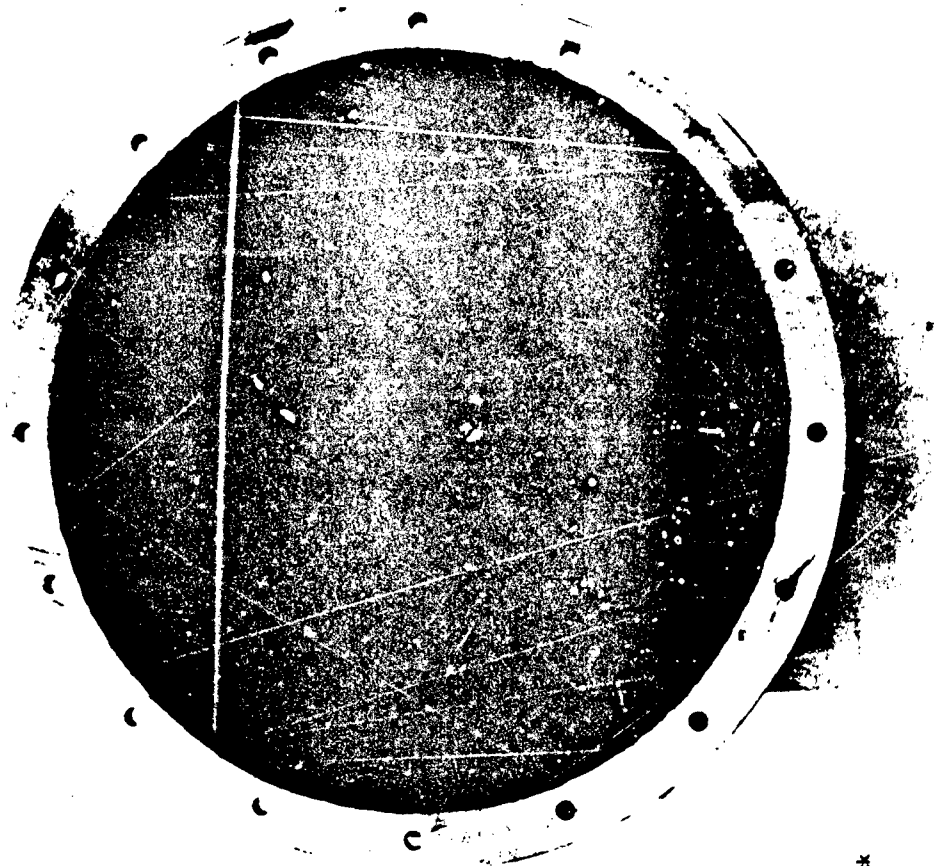
Run 003
(Spark)
Rear
4' 0 Inch Thick

Figure A-76: 25-PPI Foam Relief Face, Run 003



Run 005
Front
7' 5 Inch Thick

Figure A-77: 25-PPI Foam Combustion Face, Run 005



Run 006
Rear
7.5 Inch Thick

Figure A-78: 25-PP1 Foam Relief Face, Run 005

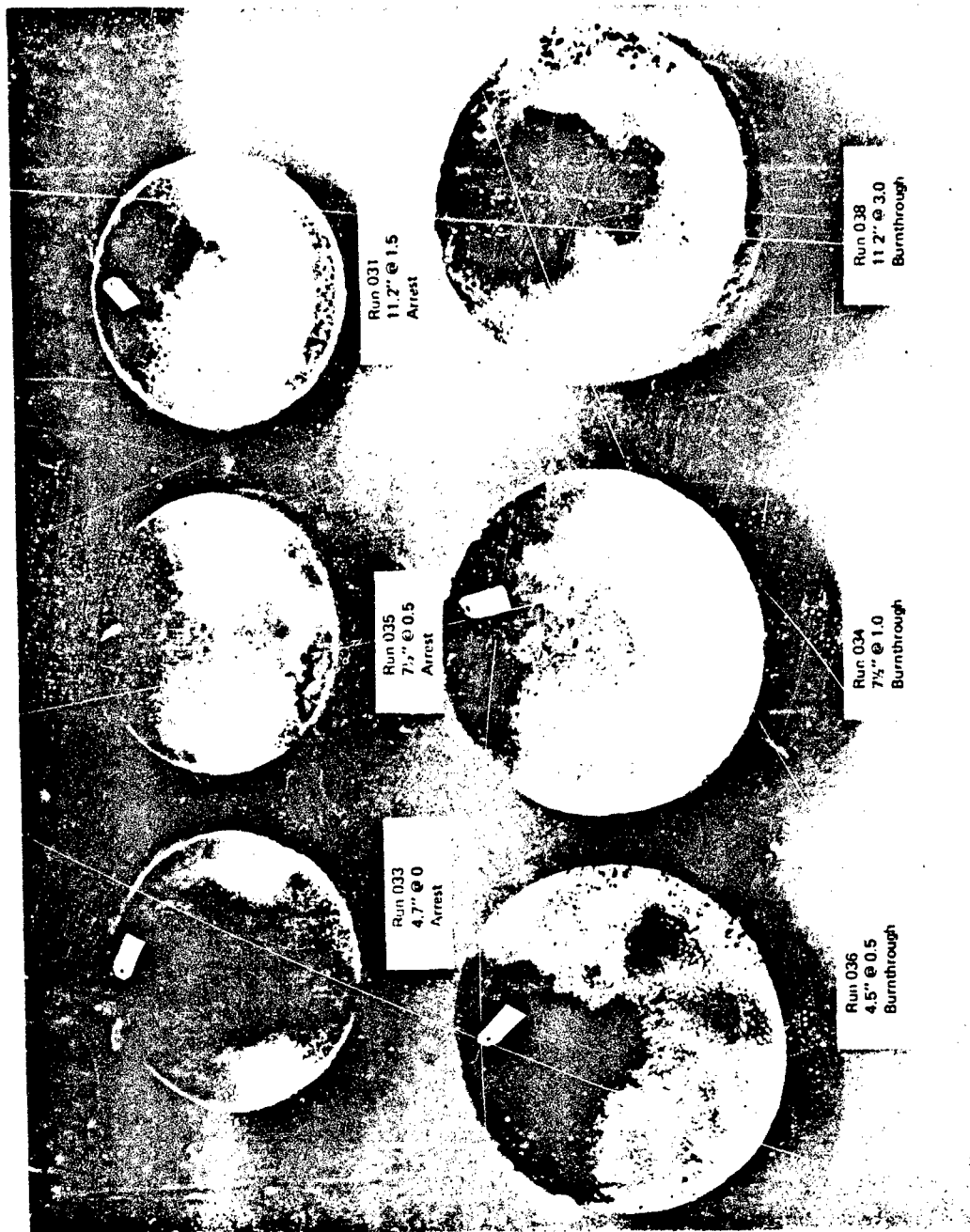


Figure A-79 : 25-PPI Foam Combustion Faces, Runs 033, 034, 035, 036, 037, and 038

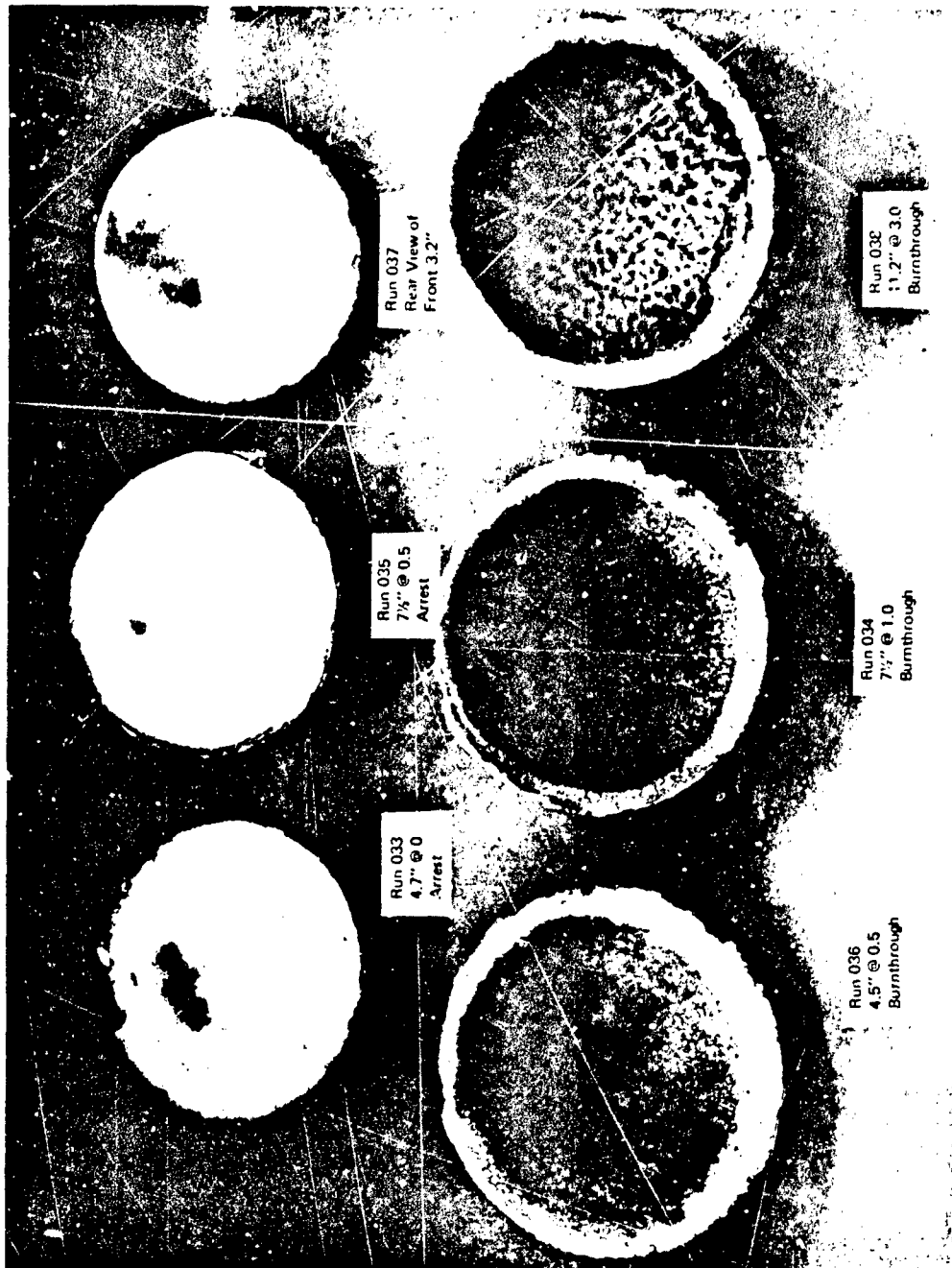


Figure A-80: 25-PPI Foam Relief Faces, Runs 033, 034, 035, 036, 037, and 038

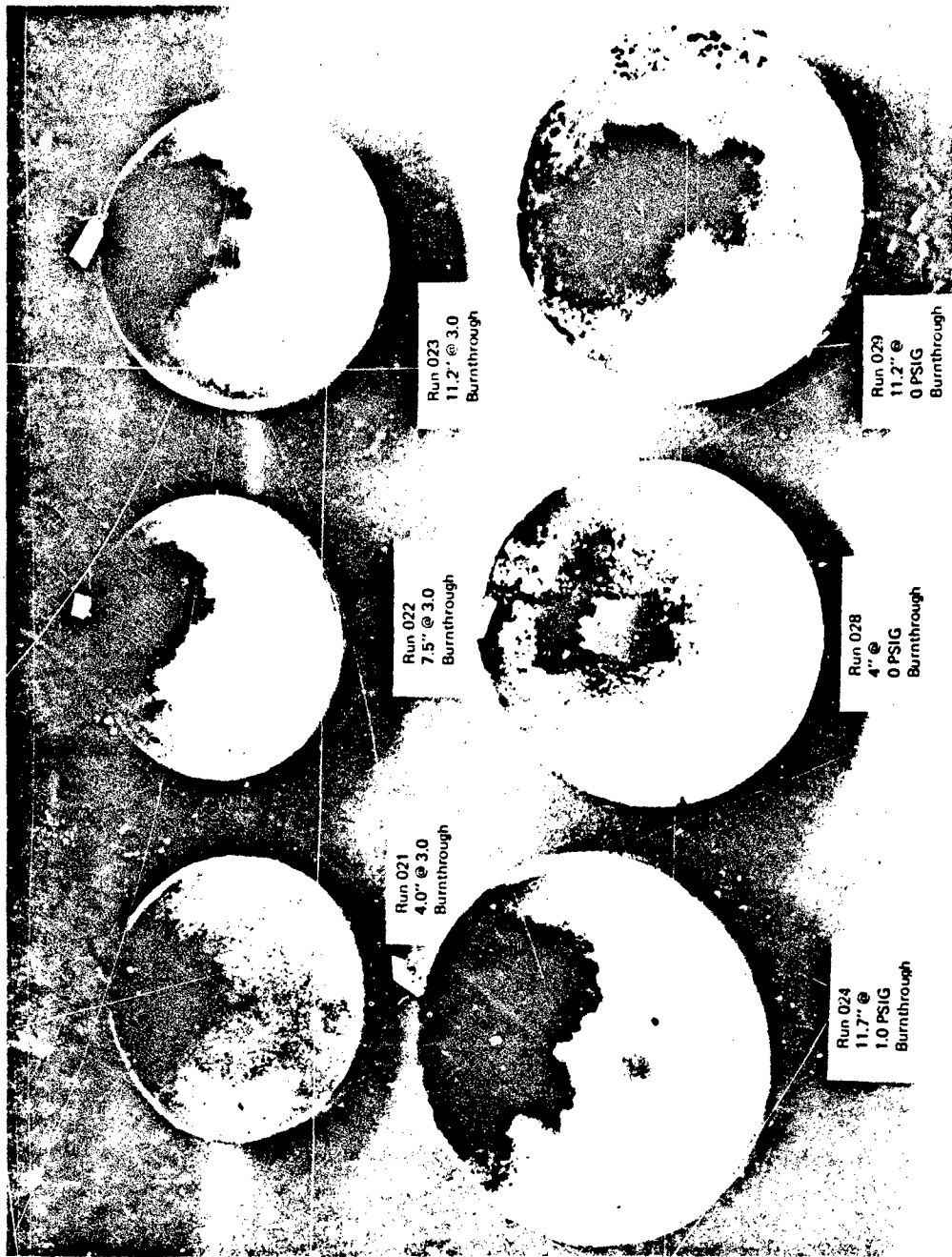


Figure A-81: 25-PPI Foam Combustion Faces, Runs 021, 022, 023, 024, 028, and 029

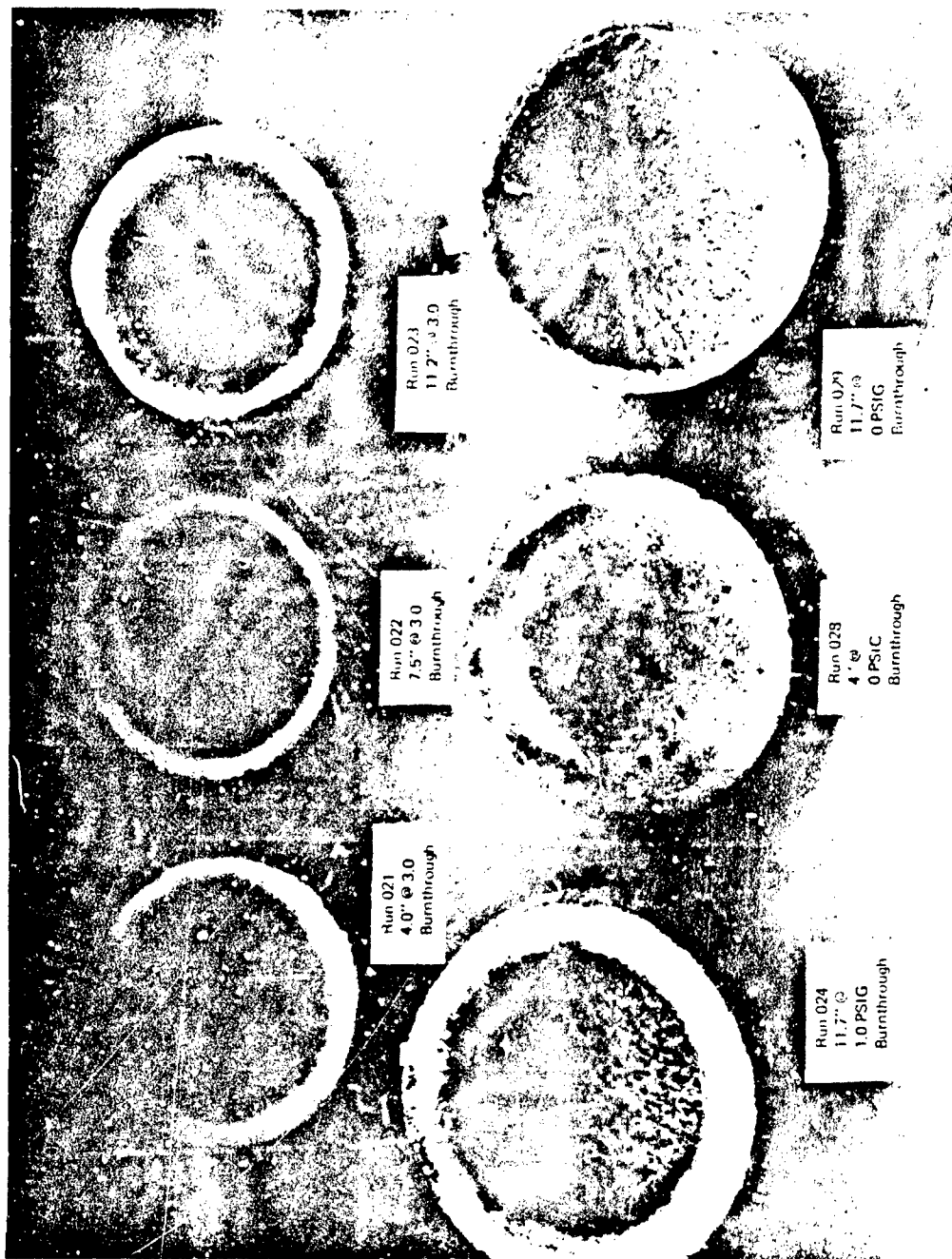


Figure A-82: 25-PPI Foam Relief Faces, Runs 021, 022, 023, 024, 028, and 029



Figure A-83: 25-PPI Foam Combustion Faces, Runs 014, 015, 016, 017, 019 and 020

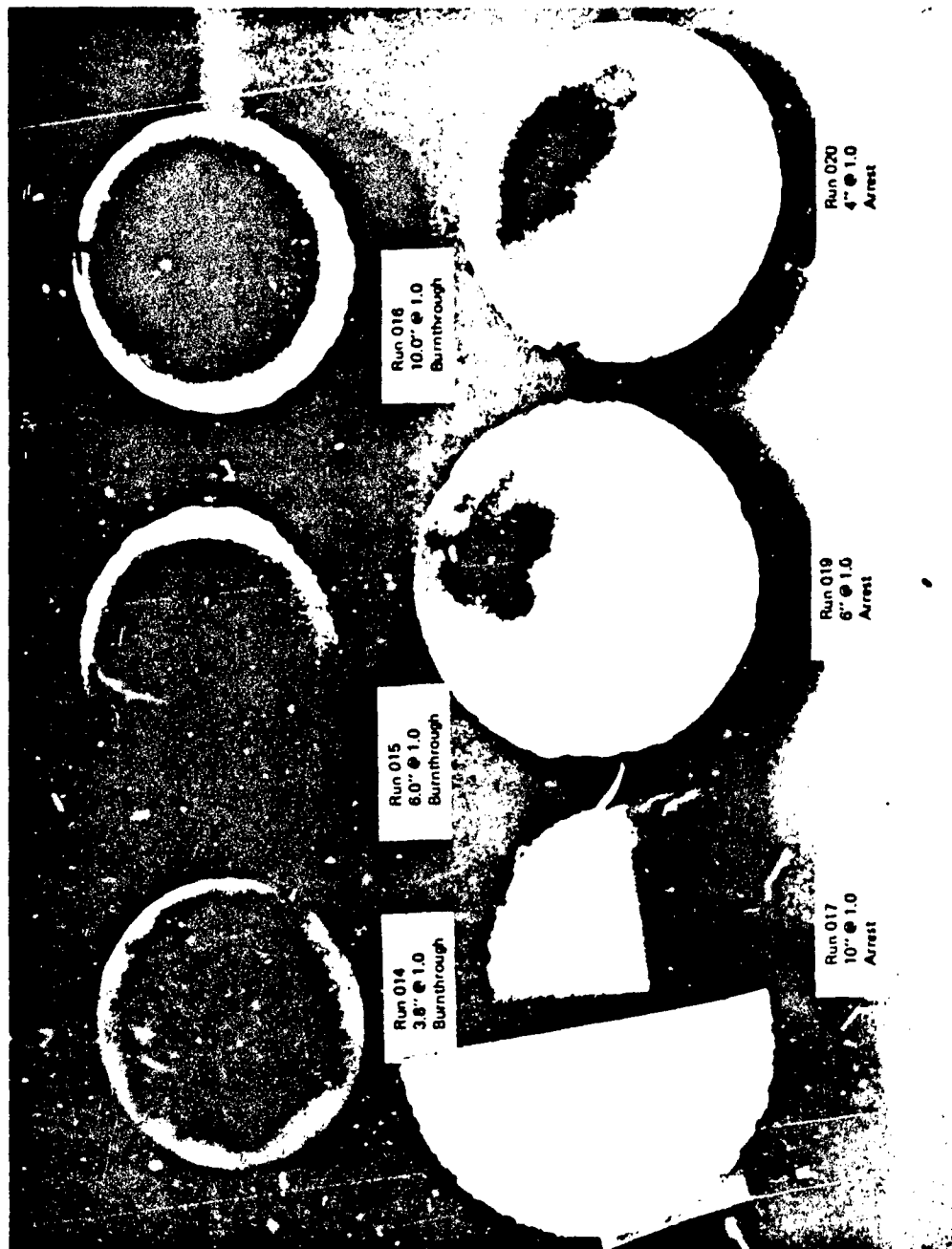


Figure A-84: 25-PPI Foam Relief Faces, Runs 014, 015, 016, 017, 019, and 020

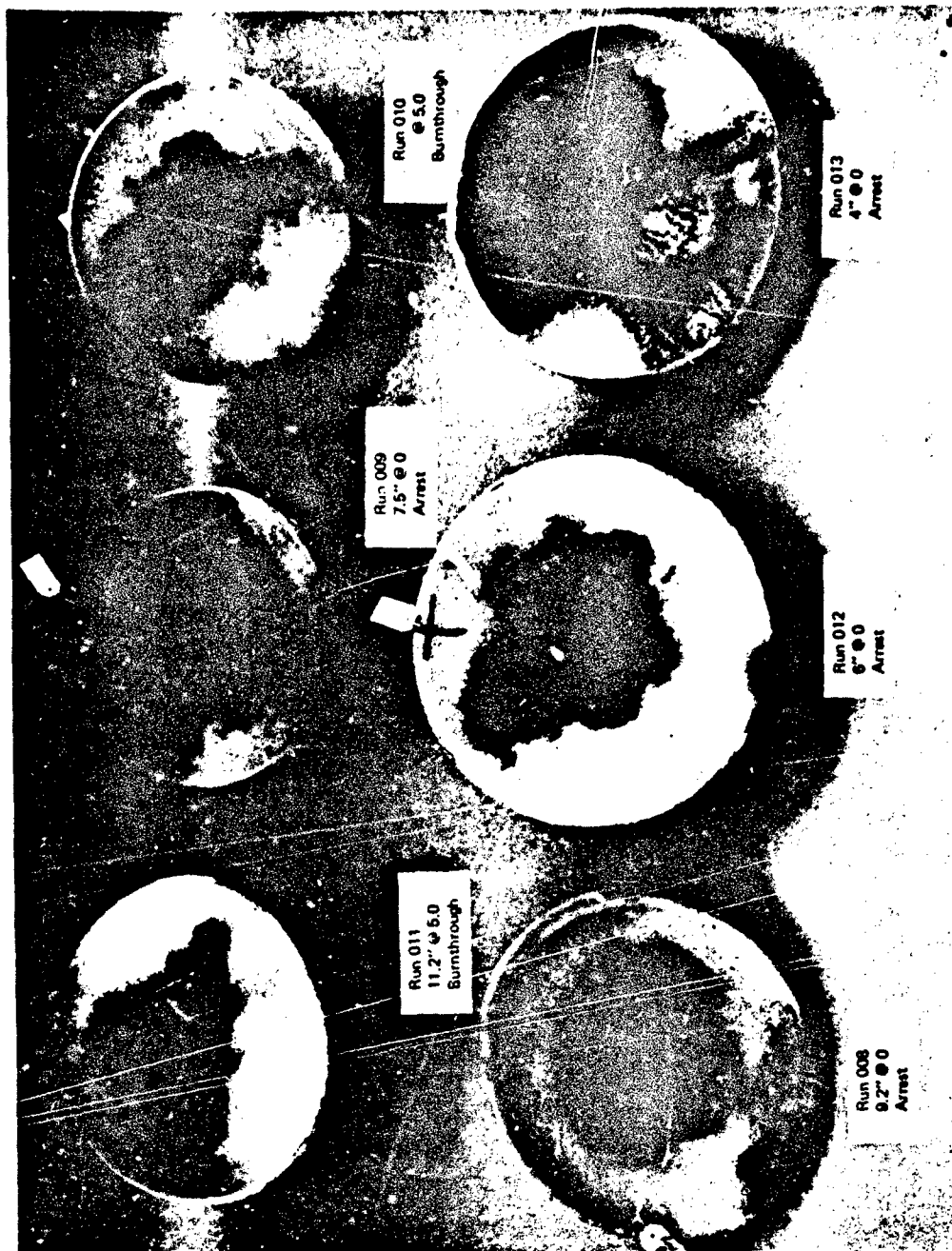


Figure A-85: 25-PPJ Foam Combustion Facies, Runs 008, 009, 010, 011, 012, and 013

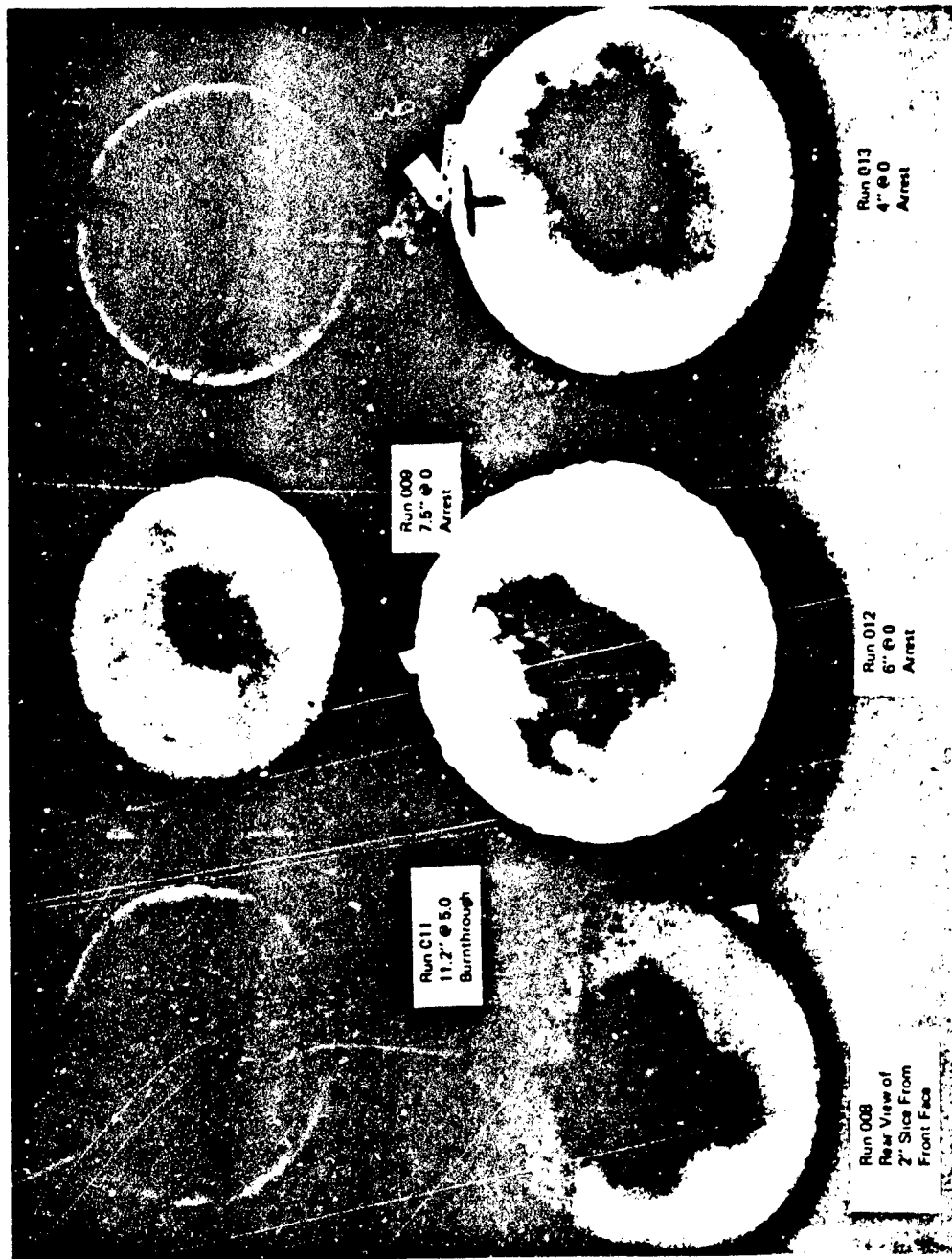


Figure A-86: 25-PPI Foam Relief Faces, Runs 008, 009, 010, 011, 012, and 013

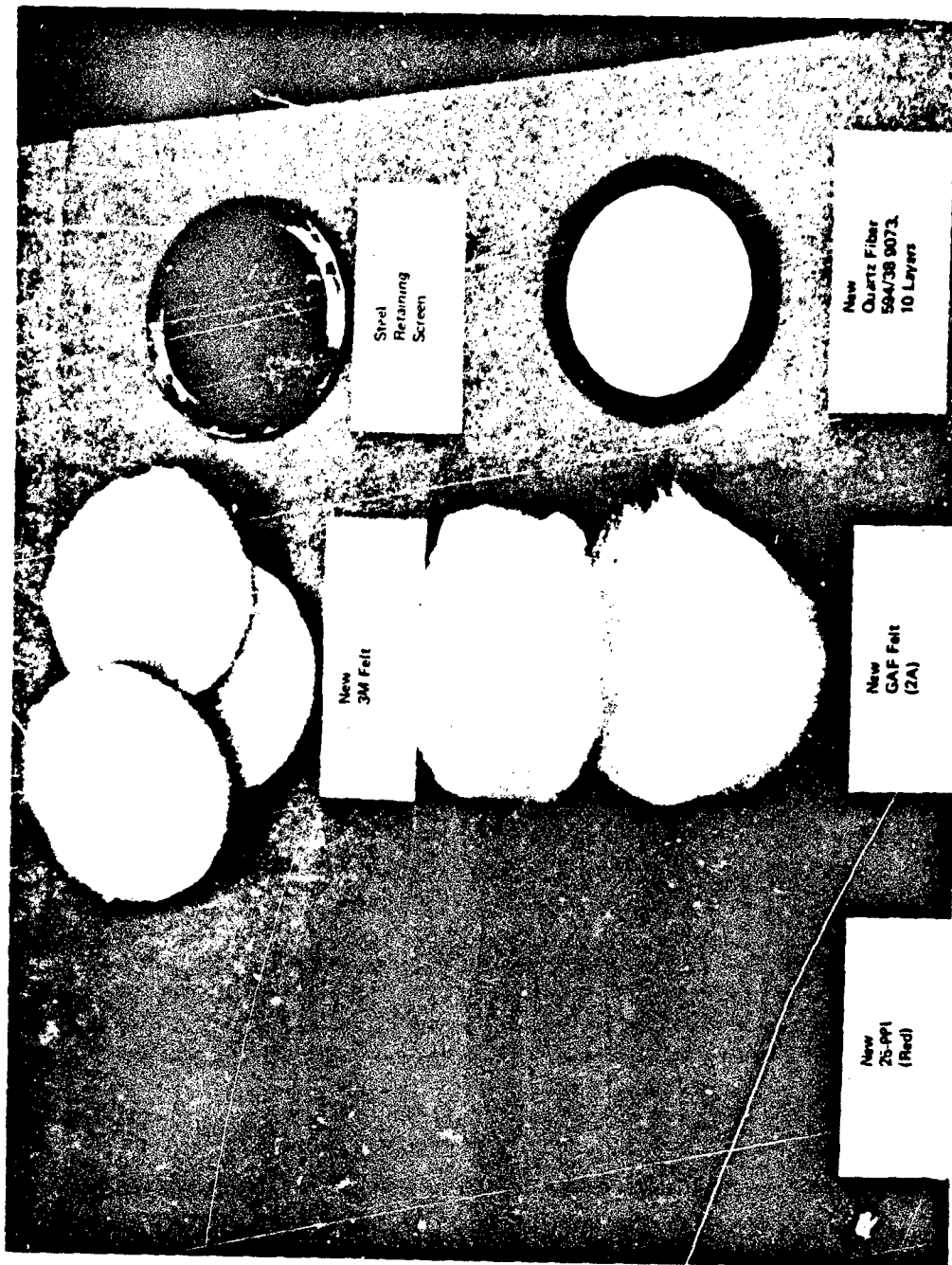


Figure A-97: Various Test Samples (Prior to Test)

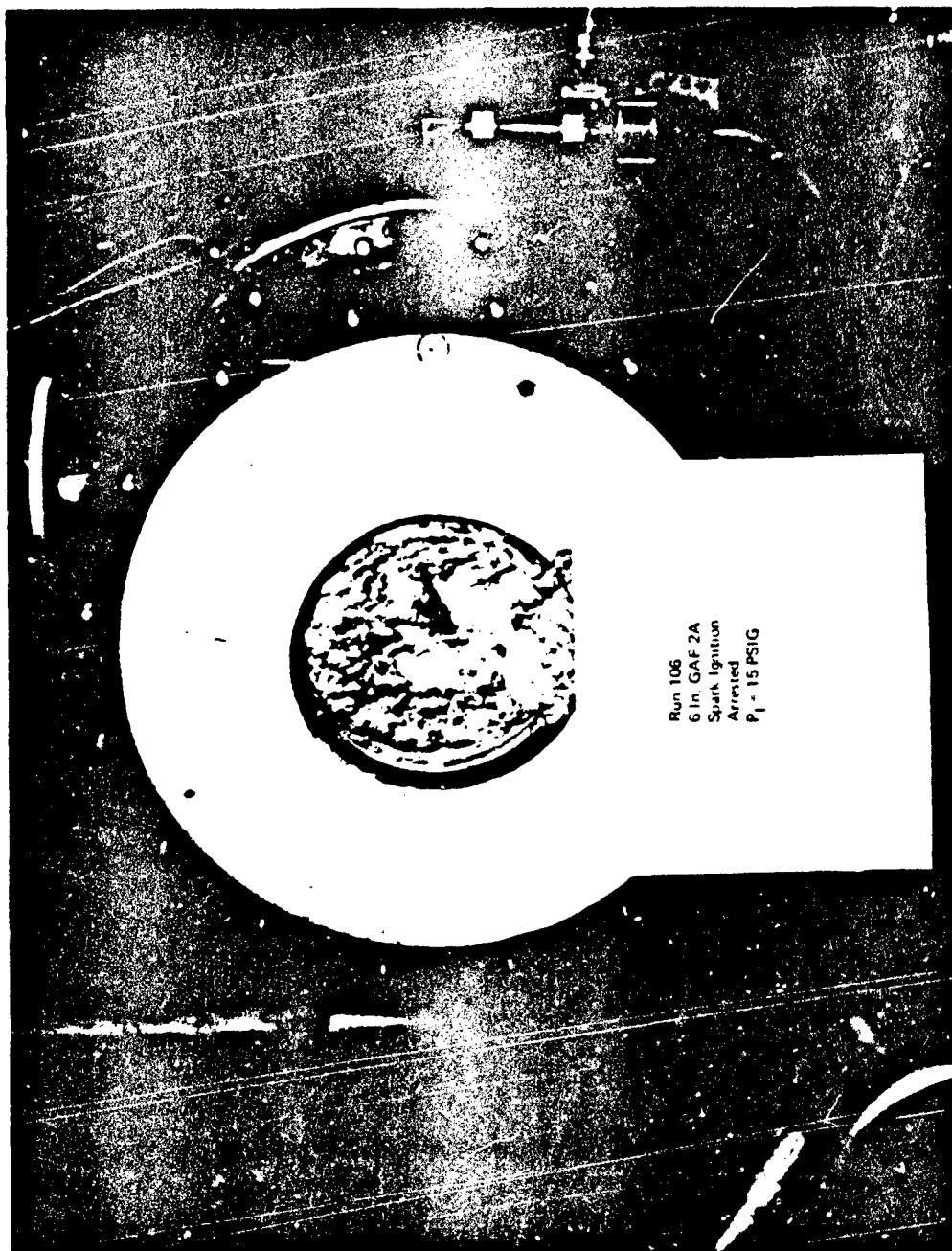


Figure A-88: GAF Felt (Type 2A) Following Combustion

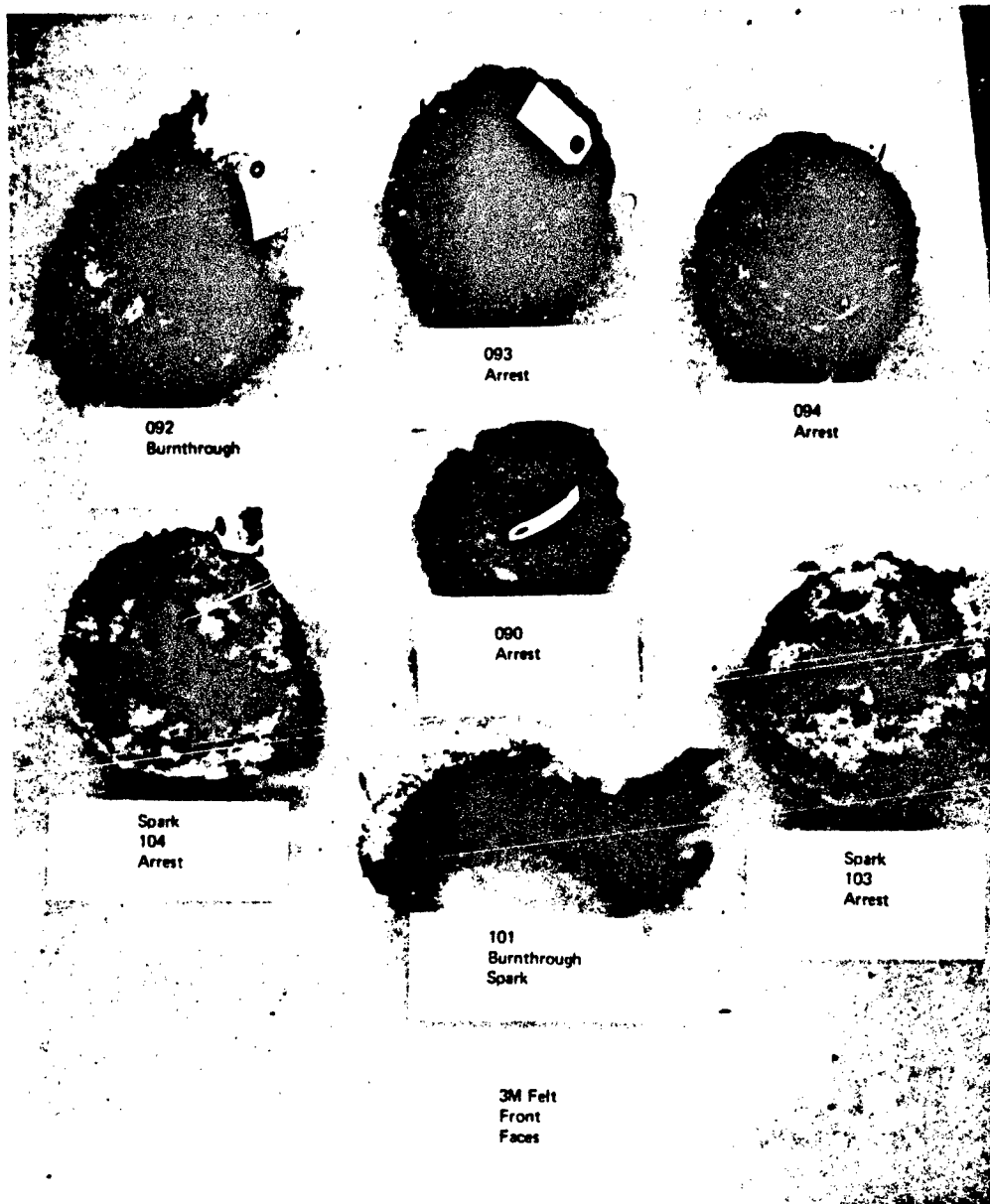


Figure A-89: 3M Scotch Brite Combustion Faces

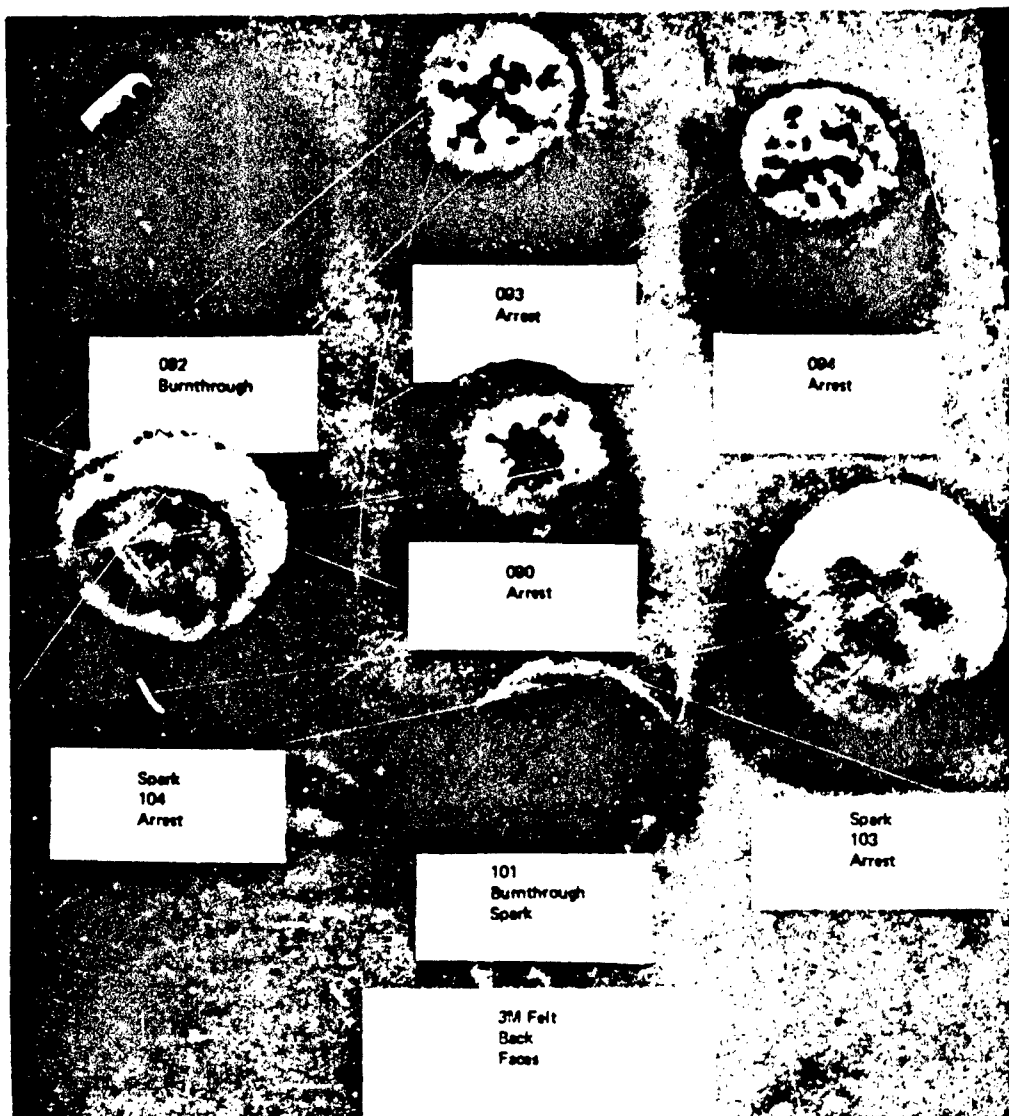


Figure A-90: 3M Scotch Brite Relief Faces

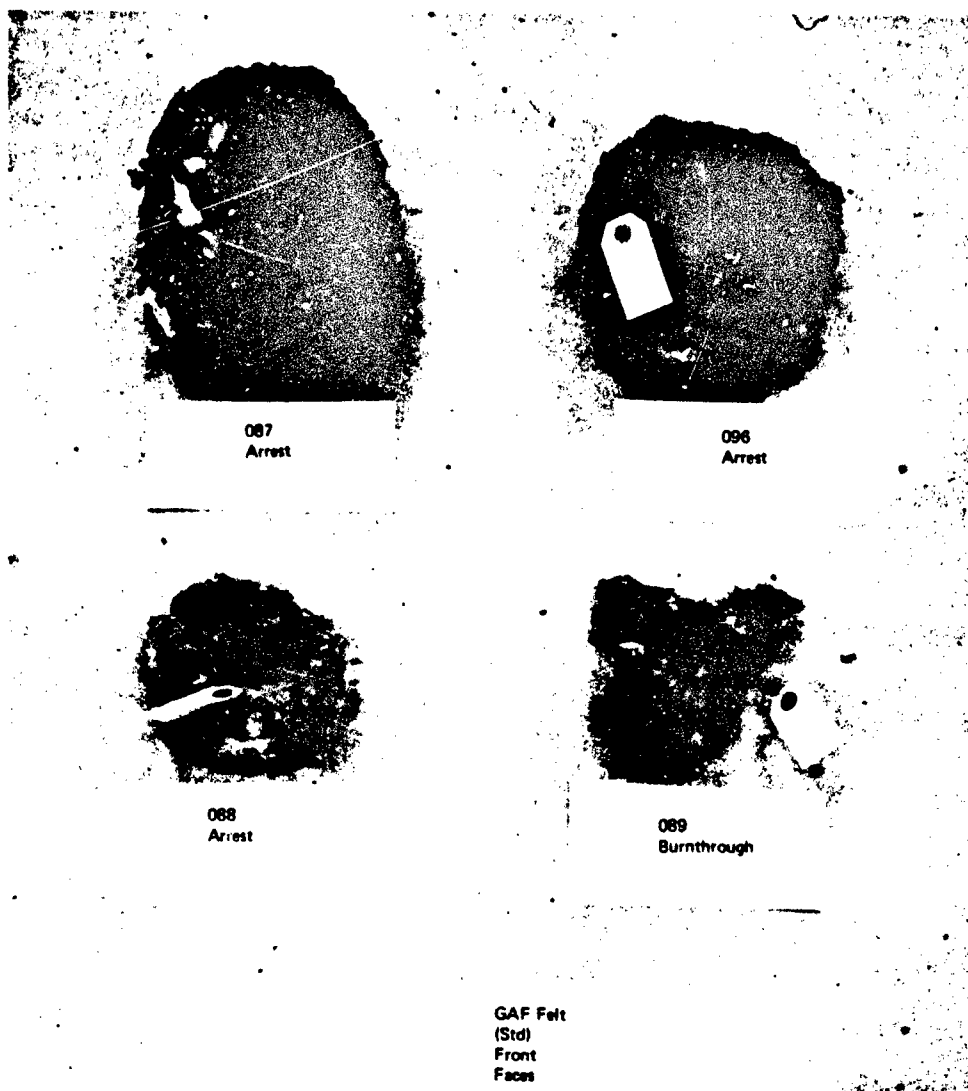


Figure A-91: GAF Felt (Standard) Combustion Faces

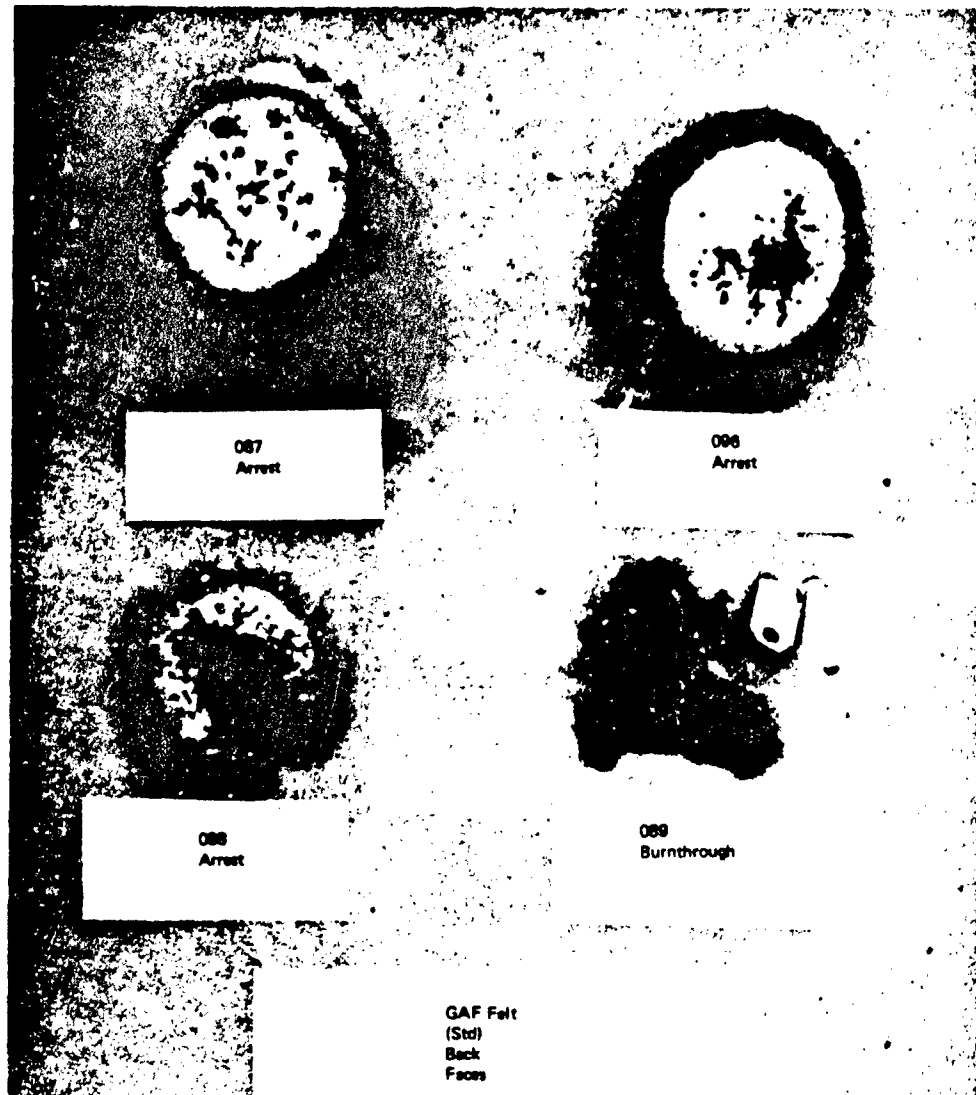


Figure A-92: GAF Felt (Standard) Relief Faces

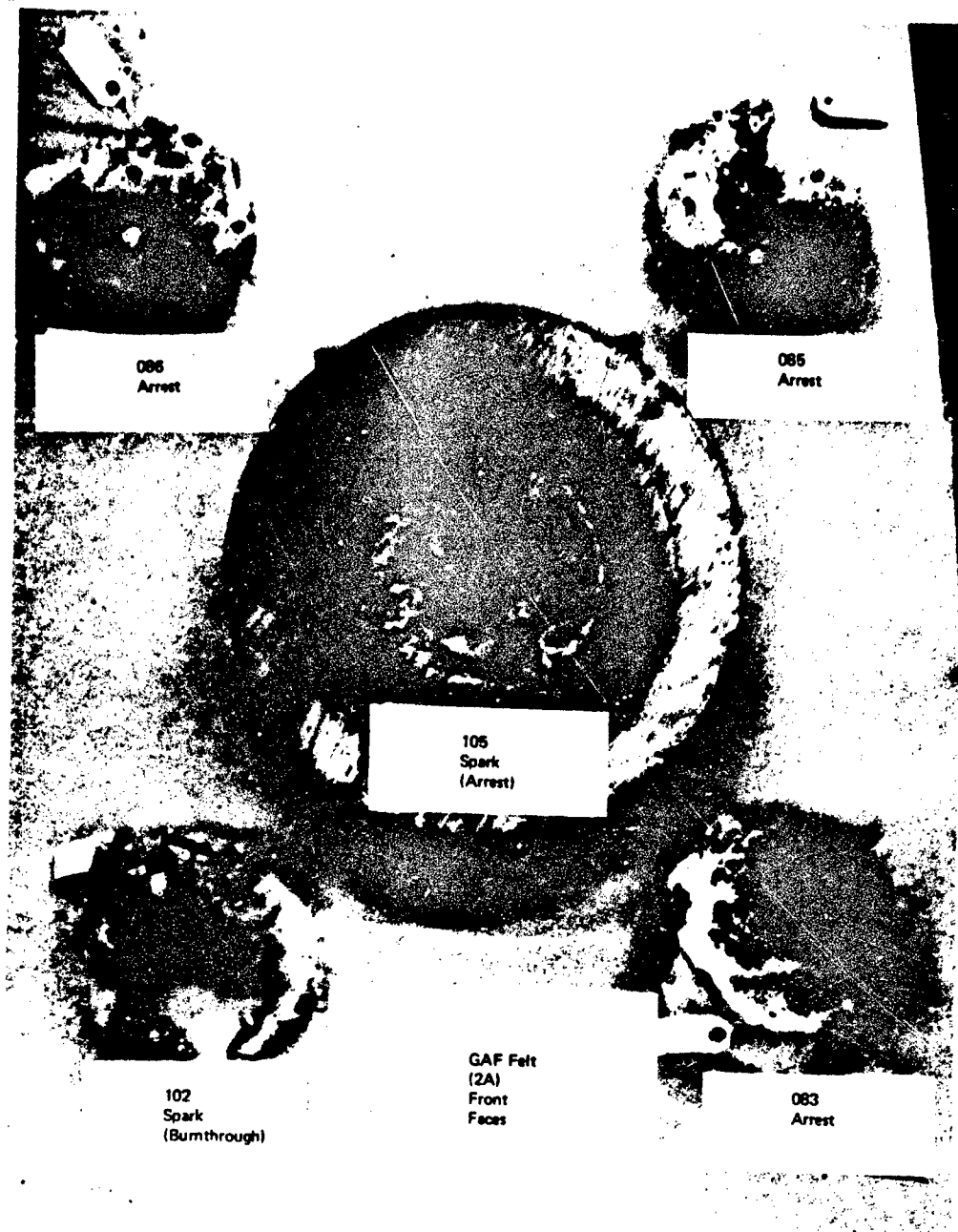


Figure A-93: GAF Felt (Type 2A) Combustion Faces

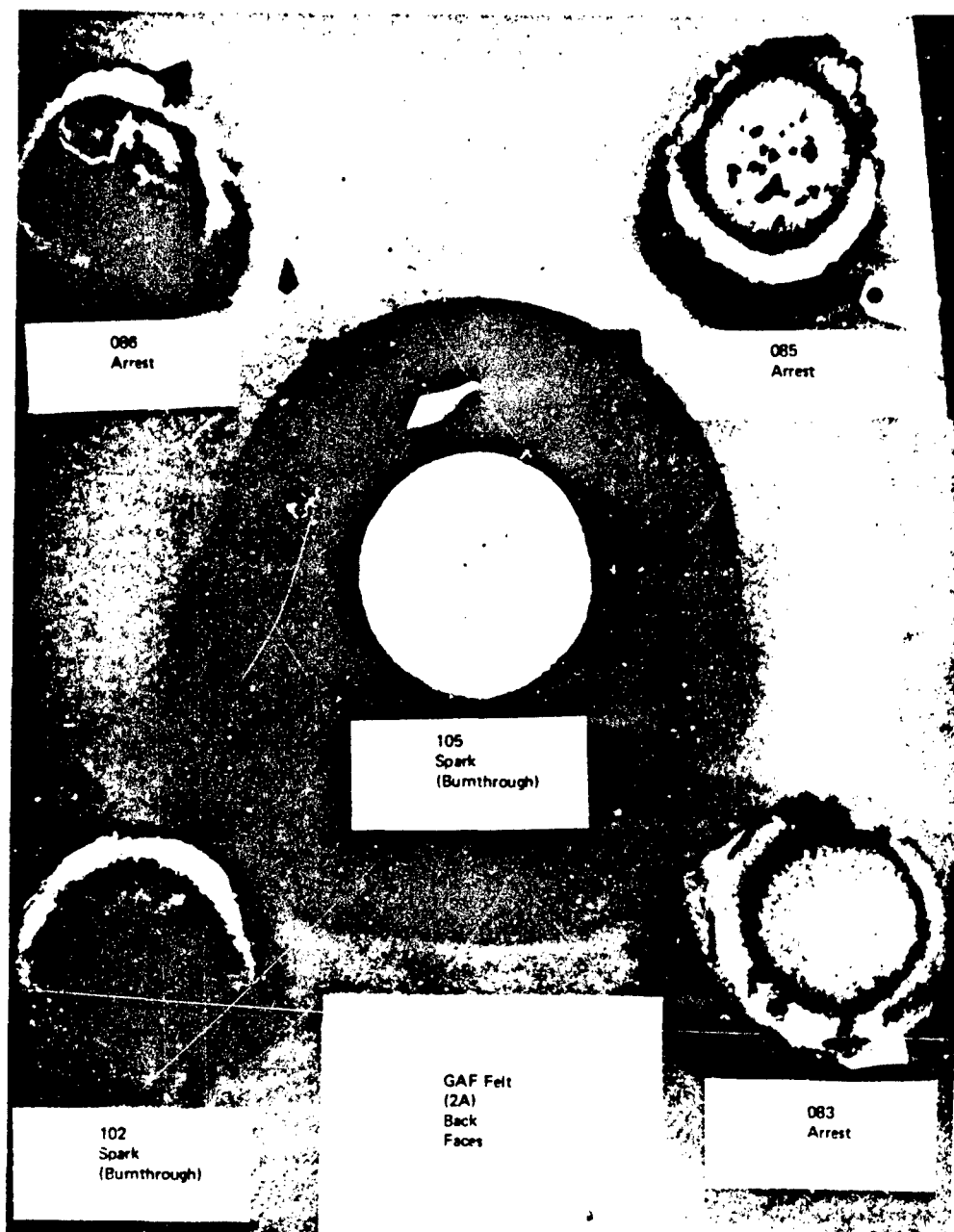
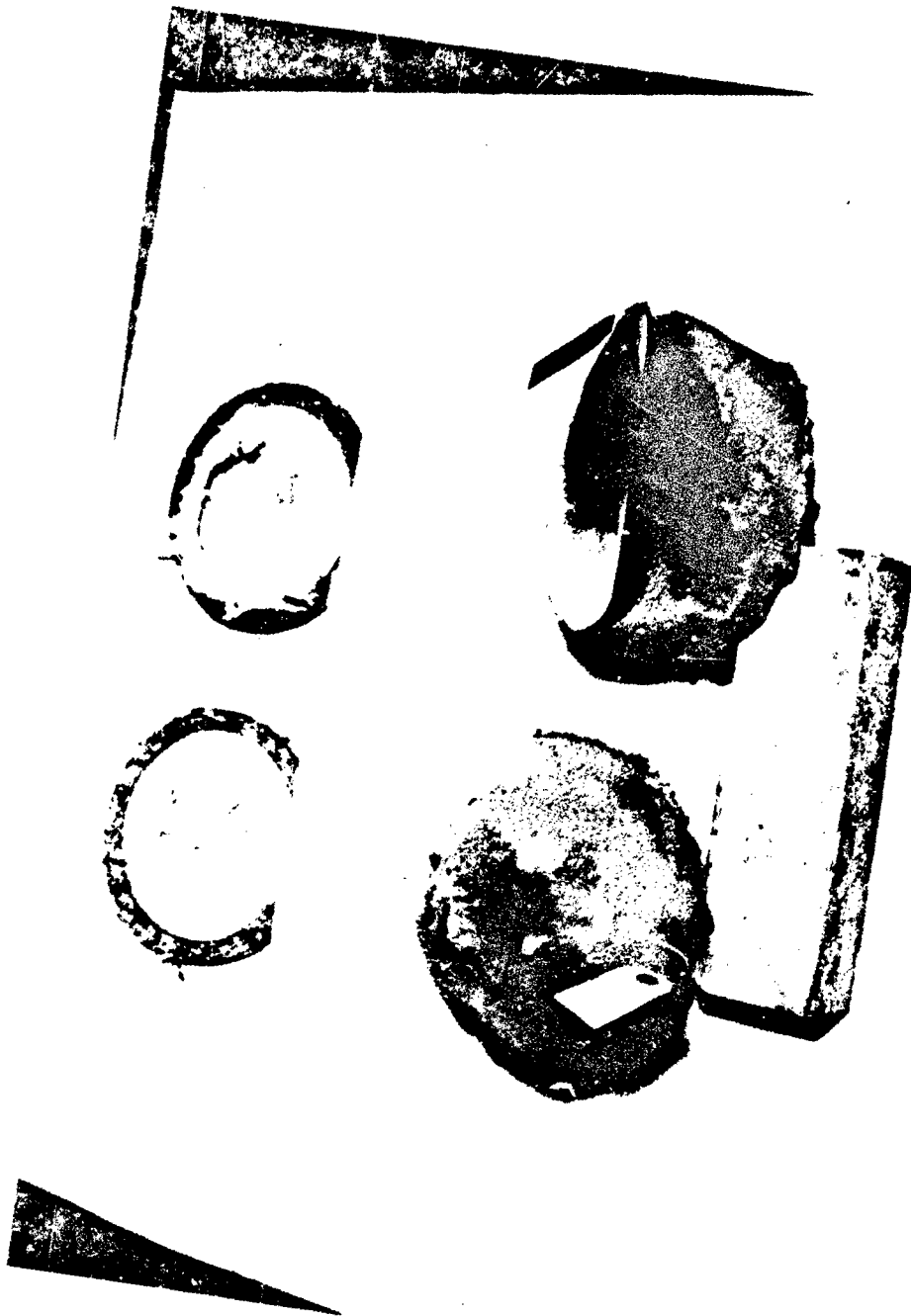


Figure A-94: GAF Felt (2A) Relief Faces



*Figure A-95: Quartz Fiber Type 594/38-9073 10 Layers and 25-PP1 Foam Backed
with Two Layers of Stainless Steel, 20-Mesh -016 Screen*

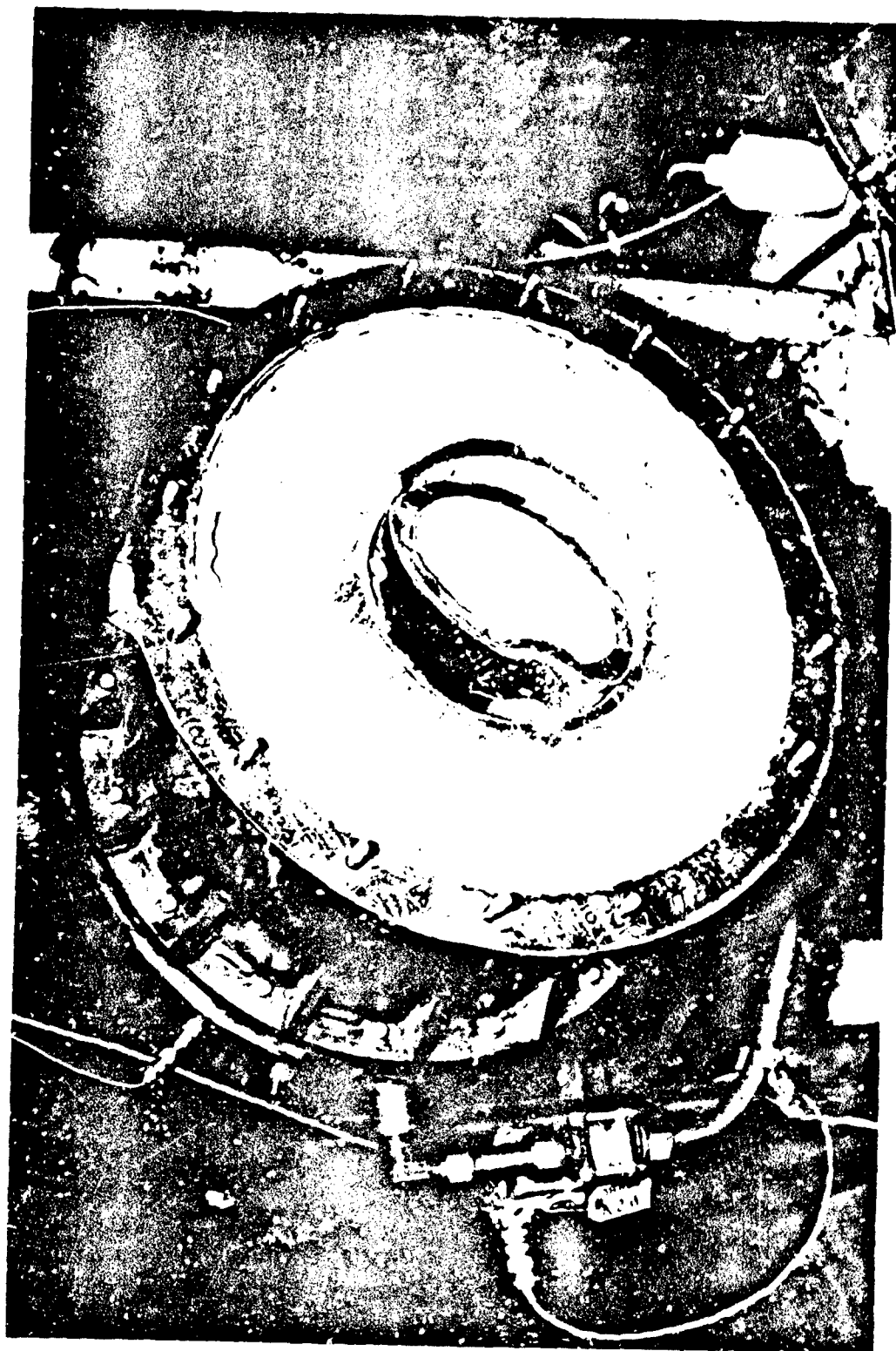


Figure A-96: Quartz Fiber Type 594/38-9073 10 Layers Backed with 25-PPJ Foam
(Note: Foam Burnt Away)

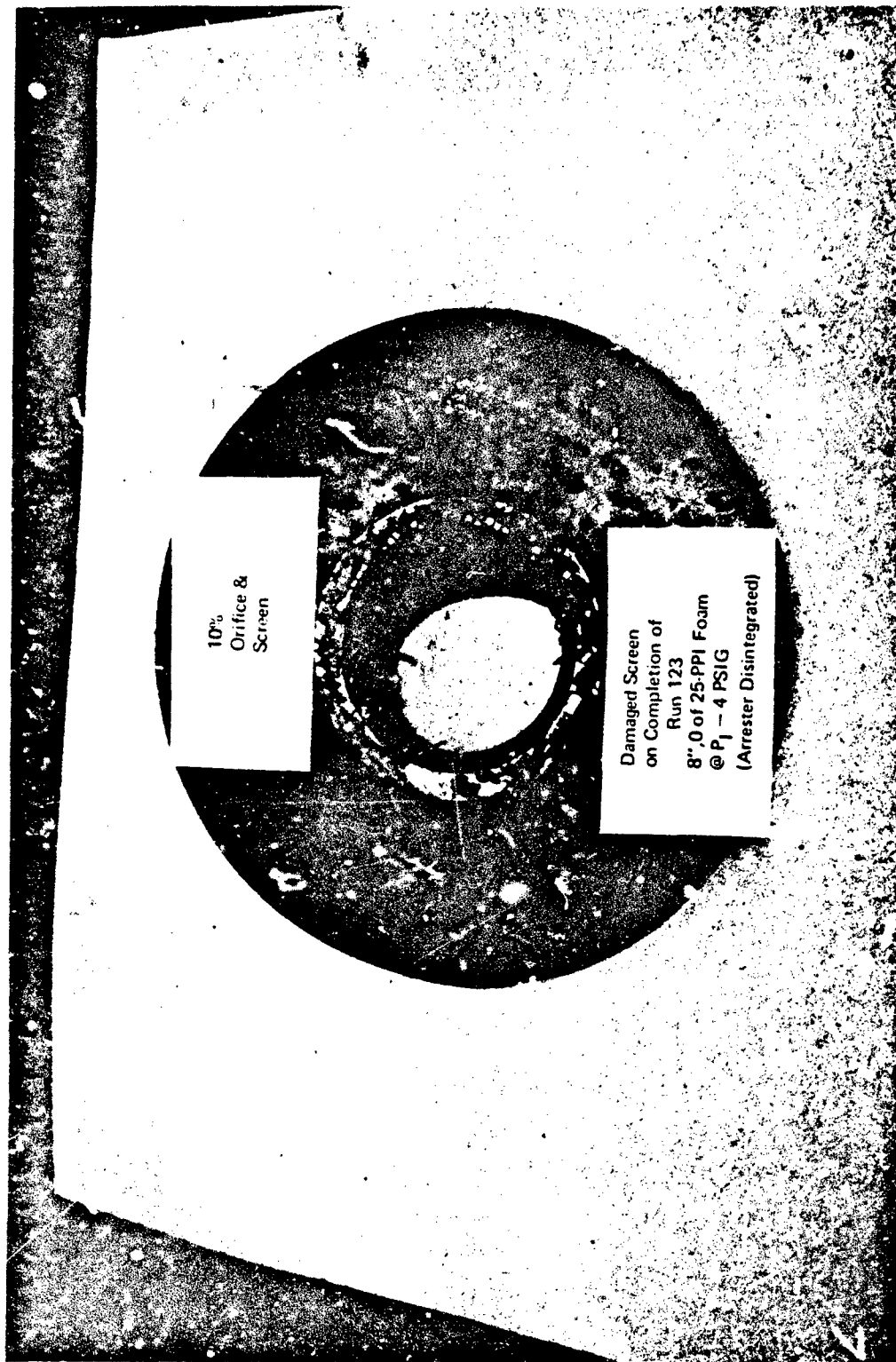
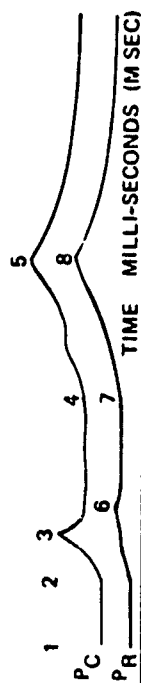


Figure A-97: Damaged 4-Mesh Support Screen on Completion of Run 123

Table A-XVII: Variable Geometry Tank Burn Time Data, Runs 1 through 23



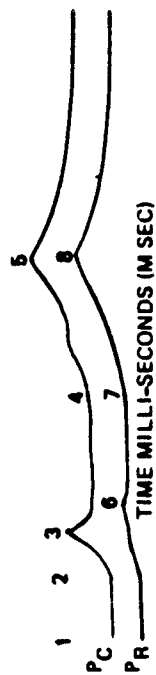
Material	Thickness	Orifice	1-2	2-3	3-4	4-5	2-6	6-7	7-8	2-4	2-7	Run
25 PPI	4.0	52	5	112	-	-	112	-	Spark	Ignition	-	001
25 PPI	4.0	52	165	164	-	-	164	-	Spark	Ignition	-	002
25 PPI	4.0	52	10	158	-	-	158	-	Spark	Ignition	-	003
25 PPI	7.5	52	17	114	-	-	114	-	Spark	Ignition	-	004
25 PPI	7.5	52	38	8	-	-	9	-	-	-	-	005
25 PPI	11.2	52	71	144	-	-	144	Igniter	Short	Spark	Ignition	006
25 PPI	11.2	52	32	4	-	-	14	-	-	-	-	007
25 PPI	9.2	52	48	7	-	-	16	-	-	-	-	008
25 PPI	7.5	52	38	88	-	-	88	Typical	Spark	Ignition	Data	009
25 PPI	7.5	52	136	8	310	126	17	300	126	318	317	010
25 PPI	11.2	52	30	5	Oscillograph Out	-	21	142	128	-	163	011
25 PPI	6.0	52	35	5	-	-	17	-	-	-	-	012
25 PPI	4.0	52	68	6	-	-	7	-	-	-	-	013
25 PPI	3.8	52	76	5	31	113	12	24	113	36	36	014
25 PPI	6.0	52	67	4	12	89	9	7	89	16	16	015
25 PPI	10	52	90	8	-	-	19	Three Second Delay to Burn Through				016
25 PPI	10	52	70	6	-	-	12	-	-	-	-	017
25 PPI	7.5	52	30	1	-	-	2	Incendiary Only Into Air				018
25 PPI	6.0	52	30	8	-	-	16	-	-	-	-	019
25 PPI	4.0	52	20	6	-	-	10	-	-	-	-	020
25 PPI	4.0	52	29	6	33	80	8	31	80	39	39	021
25 PPI	7.5	52	166	7	48	102	19	35	102	55	54	022
25 PPI	11.2	52	45	7	248	174	20	235	174	255	255	023

Table A-XVII:: (Continued) Runs 24 through 46



Material	Thkness	Orifice	TIME MILLI-SECONDS (M SEC)												Run
			1-2	2-3	3-4	4-5	5-6	6-7	7-8	8-9	9-10	10-11	11-12	12-13	
25 PPI	11.2	52	116	9	-	-	-	17	-	-	-	-	-	-	024
25 PPI	10.0	52	Mistfire 40 Amp Fuses Inadvertently Used, Did Not Fire												025
25 PPI	10.0	52	33	7	-	-	-	18	-	-	-	-	-	-	026
25 PPI	4.0	52	98	8	-	-	-	14	-	-	-	-	-	-	027
25 PPI	4.0	52	37	8	4	49	10	2	49	12	12	12	12	12	028
25 PPI	11.2	52	27	10	20	124	20	16	119	30	30	30	30	30	029
25 PPI	11.2	52	27	8	-	-	19	-	-	-	-	-	-	-	030
25 PPI	8.0	52	52	6	15	58	18	4	58	21	21	21	21	21	031
25 PPI	8.0	52	30	9	-	-	16	-	-	-	-	-	-	-	032
25 PPI	4.7	52	95	8	-	-	16	-	-	-	-	-	-	-	033
25 PPI	7.5	52	57	7	48	104	20	33	104	55	55	55	55	55	034
25 PPI	7.5	52	33	6	-	-	19	-	-	-	-	-	-	-	035
25 PPI	4.5	52	25	7.5	5	58	10	4	58	12.5	12.5	12.5	12.5	12.5	036
25 PPI	11.2	52	No Data Lamp Failure												037
25 PPI	11.2	52	15	27	419	177	33	414	177	446	446	446	446	446	038
15 PPI	7.5	52	36	6	43	103	18	29	103	49	49	49	49	49	039
15 PPI	11.2	52	36	6	257	173	21	243	173	263	263	263	263	263	040
3M	4.2	52	30	8	-	-	15	-	-	-	-	-	-	-	041
3M	2.7	52	97	8	-	-	16	-	-	-	-	-	-	-	042
3M	1.9	52	35	8	-	-	14	-	-	-	-	-	-	-	043
3M	4.2	52	80	7	20	73	15	12	73	27	27	27	27	27	044
3M	4.2	52	31	8.5	69	81	18	60	81	77.5	77.5	77.5	77.5	77.5	045
3M	4.4	10	36	10	96	80	50	56	80	106	106	106	106	106	046

Table A-XVII: (Continued) Runs 47 through 69



Material	Thickness	Orifice	1-2	2-3	3-4	4-5	5-6	6-7	7-8	2-4	2-7	Run
3 M	8.5	10	32	13	—	—	39	—	—	—	—	047
3 M	7.2	10	34	12	—	—	25	—	—	—	—	048
3 M	7.1	10	76	11	—	—	25	—	—	—	—	049
3 M	4.8	10	30	12	—	—	24	—	—	—	—	050
25 PPI	11.2	10	34	13	—	—	60	—	—	—	—	051
3 M	7.2	10	28	10	55	50	46	19	50	65	65	052
25 PPI	11.2	10	28	13	—	—	50	—	—	—	—	053
25 PPI	7.5	10	28	16	—	—	64	—	—	—	—	054
25 PPI	4.0	10	108	10	0	39	—	0	40	10	10	055
25 PPI	7.5	10	34	17	156	80	63	109	80	173	172	056
25 PPI	7.5	10	104	11	—	—	66	—	—	—	—	057
25 PPI	11.2	10	32	13	—	—	57	—	—	—	—	058
25 PPI	11.2	10	36	10	—	—	45	—	—	—	—	059
25 PPI	11.2	10	72	10	444	153	69	387	153	454	456	060
25 PPI W	4.5	52	36	8.5	—	—	28	—	—	—	—	061
25 PPI W	4.5	52	28	8.5	—	—	30	—	—	—	—	062
25 PPI W	4.5	52	36	11	—	—	20	—	—	—	—	063
25 PPI W	4.5	52	197	11	—	—	21	—	—	—	—	064
25 PP: W	2.0	52	40	6	—	—	19	—	—	—	—	065
25 PPI W	2.0	52	230	50	—	—	50	—	—	—	—	066
25 PPI W	2.0	52	94	9	—	—	18	—	—	—	—	067
Quatze Fiber W	4 Layers	52	88	7	3	51	11	0	51	10	11	068
15 PPI W	2.0	52	32	6	32	79	14	25	79	38	39	069

Table A-XVII: (Continued) Runs 70 through 92



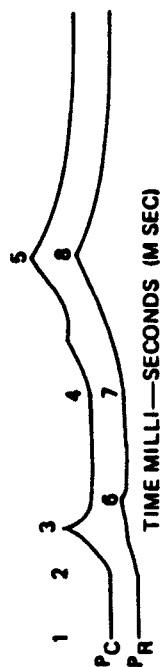
Material	Thickness	Orifice	1-2	2-3	3-4	4-5	5-6	6-7	7-8	2-4	2-7	Run
15 PPI W	7.5	52	34	8.5	77	113	20	66	113	85.5	86	070
25 PPI W	2.0	52 3%	26	4	34	76	18	20	76	38	38	071
25 PPI W	2.0	52 3 1/2%	30	3	23	105	12	14	105	26	26	072
25 PPI W	2.0	52 4%	32	8	—	—	22	—	—	—	—	073
25 PPI W	4.5	52 3 1/2%	93	10	34	95	19	23	95	44	42	074
25 PPI W	7.5	52 3 1/2%	32	10	—	—	20	—	—	—	—	075
2 Glass Cloth Honeycomb	1.25	52	34	4	3	30	7	0	30	4	7	076
1 Glass Cloth Honeycomb	1.25	52	32	7.5 7	27	23	117	07	24	9.5	11	077
25 PPI	4.5	52	29	8	—	—	17	—	—	—	—	078
20 M S/S	5 Layers	52	14	—	—	—	—	—	—	94	94	079
25 PPI	4.5	52	35	10	—	—	19	—	—	—	—	080
20 M S/S-2	4.5	52	31	109	—	—	109	Look Like Spark Ignition	—	—	—	081
25 PPI	4.5	52	14	32	—	—	40	Another	Funny Ignition	—	—	082
20 M S/S-2	4.5	52	16	26	—	—	73	—	—	—	—	083
GAF Felt 2A	6.0	10	16	32	180	50	63	157	50	222	220	084
GAF Felt 2A	3.0	10	16	32	—	—	83	—	—	—	—	085
GAF Felt 2A	6.0	10	14	30	—	—	92	—	—	—	—	086
GAF Felt 2A	6.0	10	13	30	—	—	100	—	—	—	—	087
GAF (Std)	6.0	10	15	26	—	—	107	Look Like Spark Ignition	—	—	—	088
GAF (Std)	3.0	10	17	48	—	—	77	39	30	116	116	089
GAF (Std)	3.0	10	16	26	90	30	91	—	—	—	—	090
3 M Felt	3.0	10	10	30	—	—	85	15	57	103	100	091
3 M Felt	3.0	10	14	58	45	57	78	40	32	120	118	092
3 M Felt	6.0	10	83	9	111	32	—	—	—	—	—	093

Table A-XVII: (Continued) Runs 93 through 115



Material	Thickness	Orifice	1-2	2-3	3-4	4-5	2-6	6-7	7-8	2-4	2-7	Run
3M	6.0	10	28	10.5	-	-	87	-	-	-	-	003
3M	6.0	10	35	12	-	-	87	-	-	-	-	004
GAF	6.0	10	21	8	-	-	105	-	-	-	-	005
GAF	6.0	10	30	8	-	-	126	-	-	-	-	006
GAF	3.0	10	30	8.5	80	35	53	38	36	88.5	88	007
GAF	4.5	10	29	8.5	-	-	84	-	-	-	-	008
GAF	3.0	10	25	9.0	-	-	66	-	-	-	-	009
Std	3.0	10(S)	20	110	10	55	110	10	55	120	120	100
3M	4.5	10(S)	25	90	40	55	112	18	55	130	130	101
GAF	4.5	10(S)	20	92	274	112	120	248	112	366	368	102
3M	6.0	10(S)	18	97	-	-	118	-	-	-	-	103
3M	6.0	10(S)	17	97	-	-	124	-	-	-	-	104
GAF	6.0	10(S)	19	90	-	-	124	-	-	-	-	105
GAF	6.0	10(S)	22	90	-	-	128	-	-	-	-	106
3M	6.0	10(S)	23	90	-	-	120	-	-	-	-	107
GAF	6.0	10(S)	19	100	-	-	128	-	-	-	-	108
25 PPI	4.0	10	23	10	97	39	54	55	39	107	109	109
25 PPI	8.0	10	11	31	186	42	105	120	42	226	225	110
25 PPI	8.0	10(S)	17	97	-	-	122	-	-	-	-	111
25 PPI	8.0	10	96	10	-	-	96	-	-	-	-	112
25 PPI	6.0	10	11	28	-	-	64	-	-	-	-	113
25 PPI	6.0	10	23	10	613	104	67	550	104	623	617	114
25 PPI	6.0	10(S)	24	96	29	69	114	10	69	125	124	115

Table A-XVII: (Continued) Runs 116 through 138



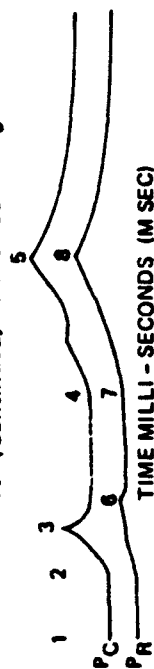
Material	Thickness	Orifice	1-2	2-3	3-4	4-5	5-6	6-7	7-8	2-4	2-7	Run
25 PPI	4 Ins	10	Burn	Through	Incendiary	Burn	No - Good	(Spark Type Ignition)				116
25 PPI	4 Ins	10	13	35	925	210	80	880	210	960	960	117
Screens	10 Layers	10	32	9	—	—	25	Immediate Burn Through (Loud Crack Heard)				118
10 Layers	10 Layers	10 (S)	—	—	—	—	—	Immediate Burn Through				119
25 PPI	4 Ins	10	88	10	—	—	58	—	—	—	—	120
Screens	4 Ins	10 (S)	21	95	119	55	120	93	55	214	213	120
25 PPI	8 Ins	10	33	9	12	6	16	3	6	21	19	122
25 PPI	4 Ins	10	15	66	292	150	113	245	150	358	358	123
Quartz	10 Layers	10	30	8	—	—	80	—	—	—	—	124
25 PPI	8 Ins	10 (S)	20	102	154	70	125	120	70	256	245	125
25 PPI	11 Ins	10 (S)	16	86	10	40	> 95	—	40	96	95	126
25 PPI	11 Ins	10 (S)	16	92	—	—	130	—	—	—	—	127
25 PPI	8 Ins	10	26	8	—	—	95	—	—	—	—	128
Screens	8 Ins	10	27	9	19	38	25	3	38	28	25	129
25 PPI	5 1/4 Ins	10 (S)	30	98	—	45	—	—	45	92	92	130
Screens	8.0 Ins	10 (S)	20	96	275	157	124	249	157	371	373	131
3 M (Std)	8.0 Ins	10 (S)	25	94	60	45	116	38	45	154	154	132
3 M (Std)	8.0 Ins	10 (S)	22	97	284	151	116	267	152	381	383	133
25 PPI	11.0 Ins	51 (S)	30	85	—	—	85	—	—	—	—	134
25 PPI	11.0 Ins	51	37	11	—	—	24	—	—	—	—	135
25 PPI	8.0 Ins	51	90	10	—	—	21	—	—	—	—	136
25 PPI	8.0 Ins	51	30	8.5	94	87	22	81	87	102.5	103	137
25 PPI	6.0 Ins	51	30	10	—	—	22	—	—	—	—	138

Table A-XVII: (Continued) Runs 139 through 164



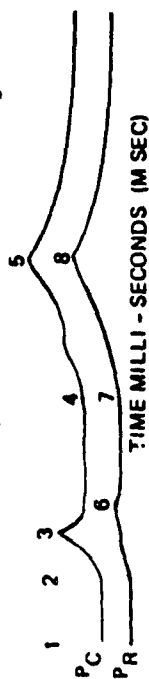
Material	Thickness	Orifice	1-2	2-3	3-4	4-5	2-6	6-7	7-8	2-4	2-7	Run
25 PPI	8.0	51	30	9	-	-	19	-	-	-	-	139
25 PPI	4.0	51	30	10	-	-	21	-	-	-	-	140
25 PPI	8.0	51	180	9	-	-	21	-	-	-	-	141
25 PPI	8.0	51	18	10	-	-	19	-	-	-	-	142
25 PPI	6.0	51	87	9	496	130	20	486	130	506	506	143
3 M (Std)	6.0	51	29	10	50	64	19	42	64	80	61	144
3 M (Std)	8.0	51	68	8	-	-	23	-	-	-	-	145
3 M (Std)	7.5	51	30	7	-	-	18	-	-	-	-	146
3 M (Std)	7.5	51	111	6	-	-	17	-	-	-	-	147
3 M (Std)	7.5	51	28	6.5	58	75	22	44	75	64.5	66	148
25 PPI	4.0	51	37	7.5	-	-	18	-	-	-	-	149
20-016 Scr	4.0	51	26	8.0	-	-	17.5	-	-	-	-	150
25 PPI	2.0	51	28	10.0	-	-	17.0	-	-	-	-	151
20-016 Scr	4.0	51	21	8.5	-	-	19	-	-	-	-	152
25 PPI	2.0	51	27	8.0	-	-	19	-	-	-	-	153
20-016 Scr	2.0	51	29	8.0	-	-	22	-	-	-	-	154
25 PPI	1.0	51	32	6.0	-	-	15	-	-	-	-	155
25 PPI	1.0	51	26	6.0	-	-	22	-	-	-	-	156
20-016 Scr	11.0	51 (S)	27	85	-	-	85	-	-	-	-	157
25 PPI	11.0	51 (S)	38	92	83	115	92	83	115	175	175	158
25 PPI	11.0	51 (S)	24	96	456	178	96	456	178	552	552	159
25 PPI	4.0	51 (S)	50	88	-	-	88	-	-	-	-	160
25 PPI	4.0	51 (S)	29	99	-	-	99	-	-	-	-	161
25 PPI	4.0	51 (S)	41	92	60	116	92	60	116	152	152	162
25 PPI	2.0	51 (S)	40	88	-	-	88	-	-	-	-	163
25 PPI	2.0	51 (S)	Burn	Through	Data	Available	Only					164

Table A-XVII: (Continued) Runs 165 through 184



Material	Thkness	Orifice	TIME MILLI - SECONDS (M SEC)										Run
			1-2	2-3	3-4	4-5	5-6	6-7	7-8	2-4	2-7		
25 PPI	4.0	Rich 6.5 51	33	6-14	-	-	24	-	-	-	-	165	
25 PPI	4.0	Rich 6.5 51	27	6-22	-	-	30	-	-	-	-	166	
25 PPI	2.0	Rich 6.5 51	23	6	-	-	40	-	-	-	-	167	
25 PPI	6.0	Rich 6.5 51	22	5	-	-	35	-	-	-	-	168	
25 PPI	6.0	Rich 6.5 51	44	5-21	-	-	31	-	-	-	-	169	
25 PPI	6.0	Rich 6.5 51	38	12	-	-	23	-	-	-	-	170	
No Arrester		Rich 6.5 51	33	3	5	41	8	41	8	8	8	171	
25 PPI	2.0	Rich 6.5 51	82	7	-	-	35	-	-	-	-	172	
25 PPI	4.0	Lean 3.5 51	28	10	-	-	19	-	-	-	-	173	
25 PPI	4.0	Lean 3.5 51	30	9.5	-	-	19	-	-	-	-	174	
25 PPI	2.0	Lean 3.5 51	62	9.5	63	70	23	48	70	72.5	71	175	
25 PPI	2.0	Lean 3.5 51	32	9.0	283	108/132	21	284	98/143	302	305	176	
25 PPI	4.0	Lean 3.5 51	88	6.0	-	-	22	-	-	-	-	177	
25 PPI	2.0	Lean 3.5 51	25	9.0	49	75	19	40	75	58	59	178	
Quartz	10 Layers	51 (S)	40	73.0	35	150	86	22	150	108	108	179	
Quartz	15 Layers	51 (S)	30	82.0	370	257	100	354	257	452	454	180	
Quartz	20 Layers	51 (S)	30	80	1,035	282	95	1,020	292	1,115	1,115	181	
Quartz	25 Layers	51 (S)	28	83	-	-	11	-	-	-	-	182	
Quartz	25 Layers	51	26	8	-	-	28	-	-	-	-	183	
Quartz	15 Layers	51	137	9	7	50	7	7	50	16	7	184	

Table A-XVII: (Continued) Runs 185 through 204



Material	Thickness	Orifice	1-2	2-3	3-4	4-5	5-6	6-7	7-8	8-9	9-10	Run
Quartz	20 Layers	51	28	9	—	—	27	1,534	227	1,562.5	1,562	185
Quartz	25 Layers	51	29	8.5	1,554	227	28	—	—	—	—	186
S/S & Quartz	15 Layers	51	30	9	—	—	26	—	—	—	—	187
S/S & Quartz	4 S/S Screen	51	31	8	—	—	23	—	—	—	—	188
S/S & Quartz	5 Layers	51	36	8	7	7	Immediate Burn Through	—	—	—	—	189
S/S & Quartz	4 S/S Screen	51	104	8	11	45	19	0	45	19	19	190
S/S & Quartz	10 Layers	51	32	8.5	—	—	29	—	—	—	—	191
S/S & Quartz	4 S/S Screen	51	70	9	11	57	24	0	57	20	24	192
S/S & Quartz	15 Layers	51	20	118	—	—	118	—	—	—	—	193
S/S & Quartz	4 S/S Screen	51	33	8	—	—	24	—	—	—	—	194
S/S & Quartz	15 Layers	51	33	8	—	—	39	—	—	—	—	195
S/S & Quartz	4 S/S Screen	51	25	92	763	199	100	755	199	855	855	196
S/S & Quartz	30 Layers	51 (S)	90	8.5	15	68	9	14	68	23.5	23	197
S/S & Quartz	10 Screens	51	31	9	—	—	30	—	—	—	—	198
S/S & Quartz	4.0"	51	65	10.5	—	—	31	—	—	—	—	199
S/S & Quartz	10 Layers	51	35	9	—	—	40	—	—	—	—	200
S/S & Quartz	4.0"	51	24	9	—	—	21	—	—	—	—	201
S/S & Quartz	2 Screens	51	115	10	70	80	23	57	80	80	80	202
S/S & Quartz	4.0" 3 M	51	32	8	73	88	19	62	88	81	81	203
S/S & Quartz	2 Screens	51	27	7	—	—	32	—	—	—	—	204

Table A-XVIII: Fuselage Tank Test Data Summary Runs 1 through 9

Run No.	Material	Condition	Void Configuration	Percent Void			Ambient PSIA			Bomb Pressures (PSIG)			Initial PSIA			Ignition Mode	P _{C1} Peak Pressure nSecs	F/A Ratio
				Wet	Dry		Pb1	Pb2	Pb3	Pb1	Pb2	Pb3	Pb1	Pb2	Pb3			
1	25 PPI		LW	X		33	14.77	75		100			14.77	18.5	X		170	4.7
														17.9				
														17.5		2.26		
2	25 PPI		LW	X		30	14.77	107		103			14.77	17.9	X		155	4.7
														17.6				
														18.2				
3	25 PPI	X	LW			33	14.77	106		110			14.77	17.3	X		170	4.7
														17.5				
														17.5		2.26		
4	25 PPI	X	LW			30	14.67	100		94			14.67	6.8	X		590	4.7
														6.8				
														6.8				
5	25 PPI	X	LW			30	14.67	108		105			14.67	10	X		157	4.7
														9.9				
														9.8		1.68		
6	25 PPI	X	LW			16.5	14.56	102.5		110			14.56	6.8	X		176	4.7
														6.8				
														6.8				
7	25 PPI	X	LW			40	14.56	107		109			14.56	21.1	X			4.7
														20.8				
														20.7		2.42	176	
8	25 PPI	X	LW			33	14.67	100		92			14.67	11.6		X	104	4.7
														11.8				
														11.8		1.79		
9	25 PPI	X	LW			16.5	14.68	108		98			14.68	2.4		X	60	4.7
														2.4				
														2.5		1.16		

Table A-XVIII: (Continued) Runs 10 through 17

Run No.	Material	Condition		Void Configuration	Percent Void	Ambient PSIA			Bomb Pressures (PSIG)			Initial PSIA			Ignition Mode			Time to PC ₁ Peak Pressure mSecs	F/A Ratio Vol %
		Wet	Dry			PB ₁	PB ₂	PB ₃	PB ₁	PB ₂	PB ₃	Initial PSIA	ΔP Initial PSIA	ΔP Final PSIA	Spark	Indirect Fire	Gun Fire		
10	25 PPI	X		LW	18.5	14.66	-	-	-	-	14.68	2.4	2.4	X	-	1.17	-	Air Only No Propane	
11	25 PPI	X		LW	18.5	14.68	-	-	-	-	14.68	-	-	X	-	-	-	4.7	
11A	25 PPI	X		LW	18.5	14.68	107	106	96	14.68	3.5	3.5	3.5	X		1.23	185	4.7	
12	25 PPI	X		LW	40	14.79	100	99	86	14.79	11.5	11.1	11.3	X		1.76	82	4.7	
13	25 PPI	X		LW	45	14.79	106	104	83	14.79	22.8	22.7	22.5	X		2.54	40	4.7	
14	25 PPI		X	LW	33	14.79	104	98	97	14.79	6.1	6.0	6.0	X		1.42	38	4.7	
15	25 PPI	X		LW	39	14.84	106	106	102	14.84	13.5	13.5	14.0	X		1.96	54	4.7	
16	25 PPI	X		LW	33	14.84	104	-	94	14.84	11.0	10.8	11.0	X		1.75	132	4.7	
17	25 PPI		X	LW	33	14.84	-	-	-	14.84	-	-	-	X		-	-	4.7	

Table A-XVIII: (Continued) Runs 18 through 28

Run No.	Material	Condition	Void Configuration	Percent Void	Ambient PSIA			Bomb Pressures (PSIG)			Initial Pressures			Ignition Mode	Time to PC ₁ Peak Pressure in Secs	F/A Ratio
					PB ₁	PB ₂	PB ₃	PB ₁	PB ₂	PB ₃	Initial PSIA	Final PSIA	ΔP Rise PSIA			
18	25 PPI	X	LW	33	14.84	110	105	14.84	110	105	14.84	7.1	7.1	X	1.47	4.7
19	25 PPI	X	LW	38	14.84	102	96	14.84	101	96	14.84	9.6	9.5	X	1.64	4.7
20	3M	X	LW	38	14.82	103	88	14.82	101	88	14.82	8.1	8.0	X	1.54	4.7
21	3M	X	LW	39	14.82	103	88	14.82	101	88	14.82	7.9	7.9	X	1.54	4.7
22	GAF	X	LW	39	14.71	104	70	14.71	100	70	14.71	8.3	8.5	X	1.66	4.7
23	25 PPI W/ SS Screen	X	LW	38	14.55	98	70	14.55	98	70	14.55	8.1	8.0	X	1.55	4.7
24	25 PPI W/ SS Screen	X	LW	39	14.55	98	70	14.55	102	70	14.55	8.1	8.2	X	1.55	4.7
25	25 PPI W/ 10 Layer Q	X	LW	38	14.55	100	70	14.55	99	70	14.55	7.2	7.0	X	1.49	4.7
26	25 PPI	X	LW	39	14.7	64.5	71	14.7	75	71	14.7	7.0	7.1	X	1.48	3.5
27	25 PPI	X	LW	39	14.7	64.5	71	14.7	75	71	14.7	7.1	7.1	X	1.48	3.5
28	25 PPI	X	LW	39	14.7	102	84	14.7	98	84	14.7	8.1	8.1	X	1.55	6.5

Table A-XVIII: Fuselage Tank Test Data Summary

Run No.	Material	Condition		Void Configuration	Percent Void	Ambient PSIA			Bomb Pressures (PSIG)			Initial Pressure		Spark	Ignition Mode		P/P in	Time to PC ₁ Peak Pressure m Sec	F/A Ratio Vol %
		Wet	Dry			PB1	PB2	PB3	PB1	PB2	PB3	P Initial	P Final		Gun Fire	Incendary			
29	25 PPI X			LW	39	14.7	107	101	14.7	107	101	14.7	7.9		X		1.54	18	5.5
													8.0						
													8.0						
30	25 PPI X W/Q Fiber			LW	39	14.7	95	104	14.7	103	103	14.7	6.7		X		1.44	16	4.7
													7.0						
													6.9						
31	25 PPI X W/Q Fiber			LW	39	14.7	100	93	14.7	93	93	14.7	6.4		X		1.43	27	6.5
													6.4						
													6.4						
32	25 PPI X W/Q Fiber			LW	39	14.7	75	88	14.7	80	90	14.7	6.3		X		1.42	18	3.5
													6.3						
													6.3						
33	3M Felt X			LW	39	14.7	67	75	14.7	84	84	14.7	7.2		X		1.50	71	3.5
													7.3						
													7.3						
34	3M Felt X			LW	39	14.7	88	95	14.7	100	100	14.7	8.3		X		1.48	67	4.7
													8.3						
													8.4						
35	3M Felt X			LW	39	14.7	101	98	14.7	92	92	14.7	8.7		X		1.50	58	6.5
													8.4						
													8.6						

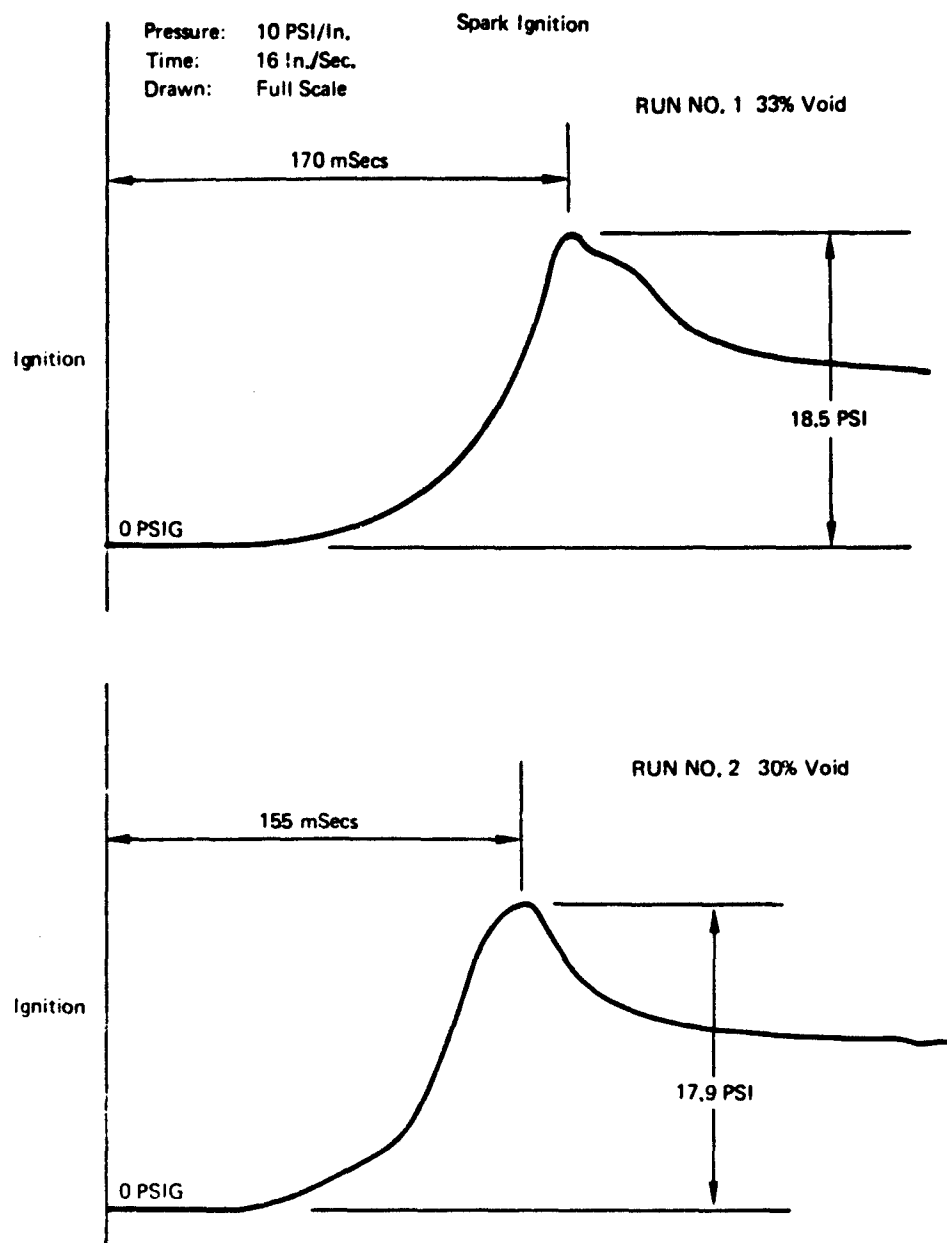


Figure A-98: Typical Fuselage Tank Pressure Traces, Line Well Configuration, 25-PPI Dry

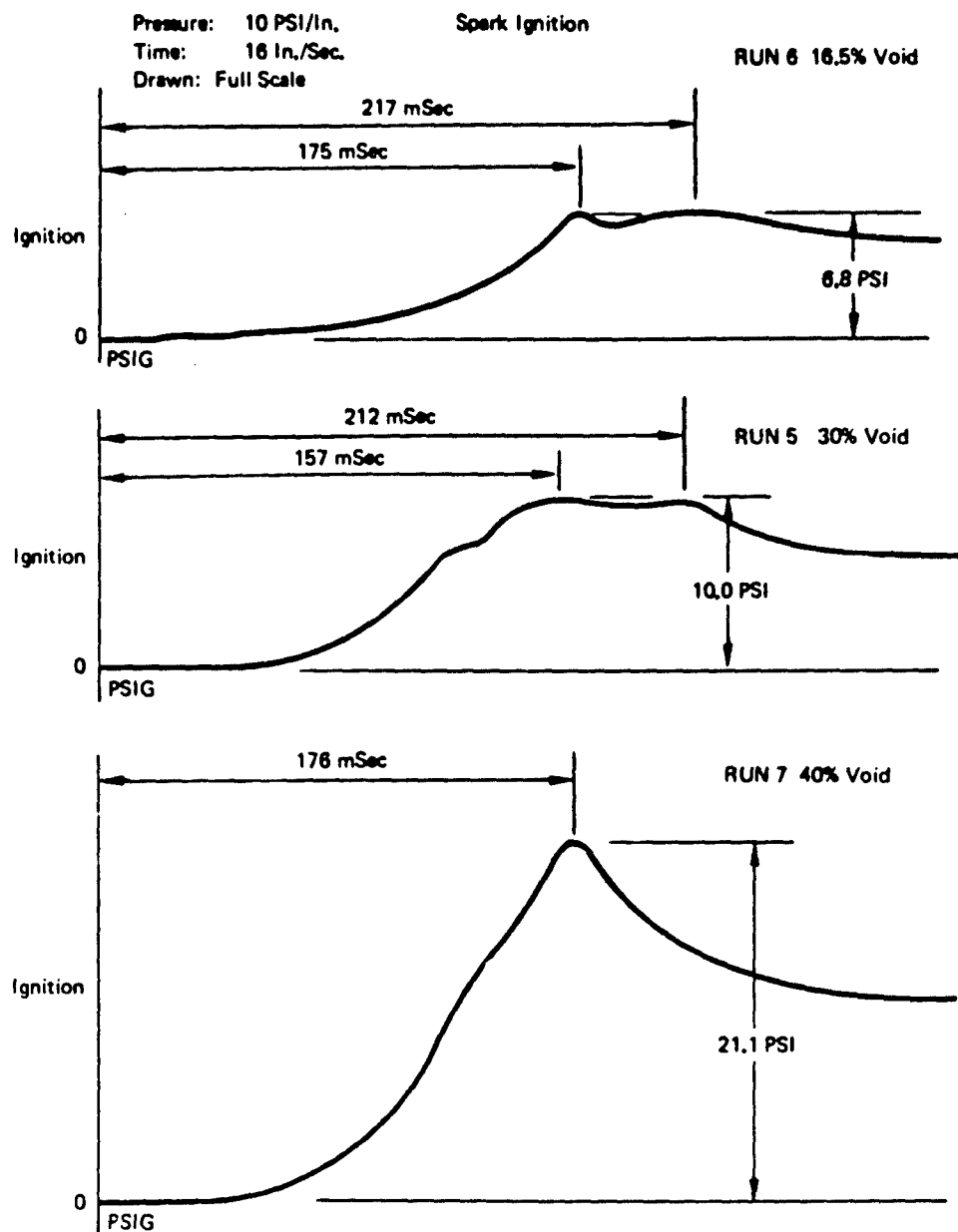


Figure A-99: Typical Fuselage Tank Pressure Traces, Lined Wall Configuration,
25-PPI Wet With JP5

Pressure: 10 PSI/in.
Time: 18 in./Sec.
Drawn: Full Scale

Incendiary Ignition

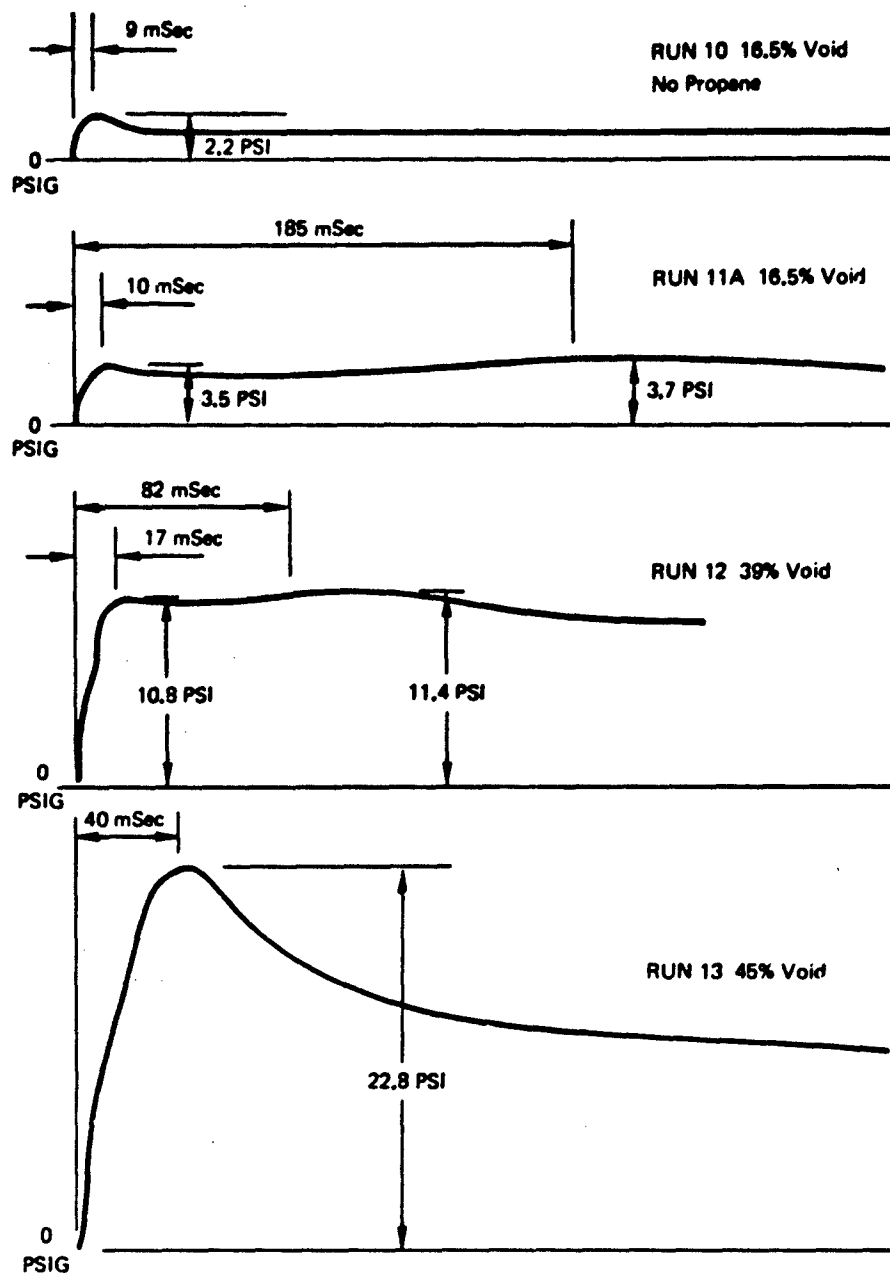


Figure A-100: Typical Fuselage Tank Pressure Traces, Lined Wall Configuration, 25-PPI Wet With JP5

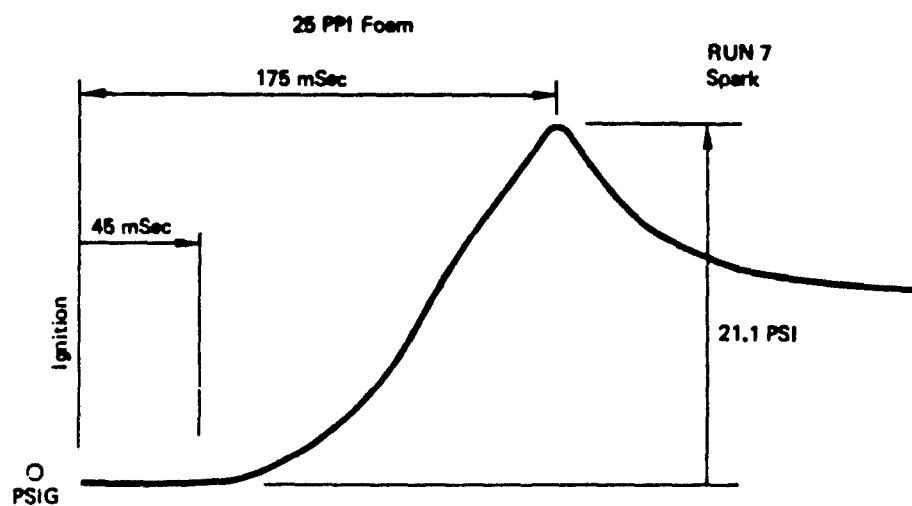
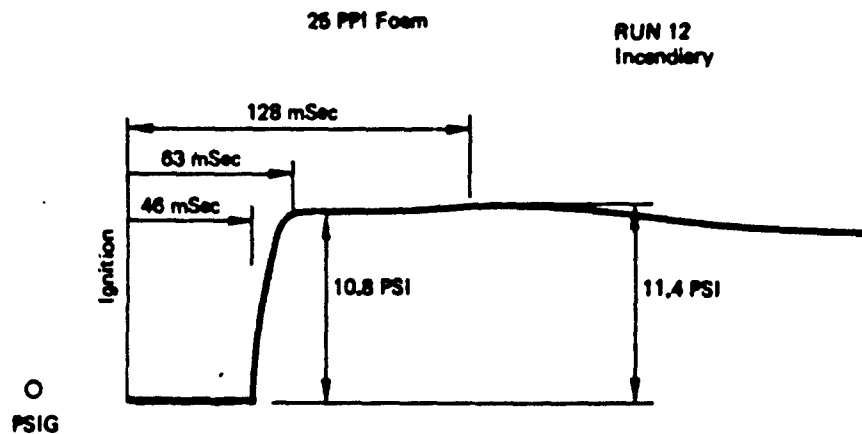


Figure A-101: Typical Pressure Traces for 39% Void Fuselegs Tank
(Lined Wall) Wet with JP5

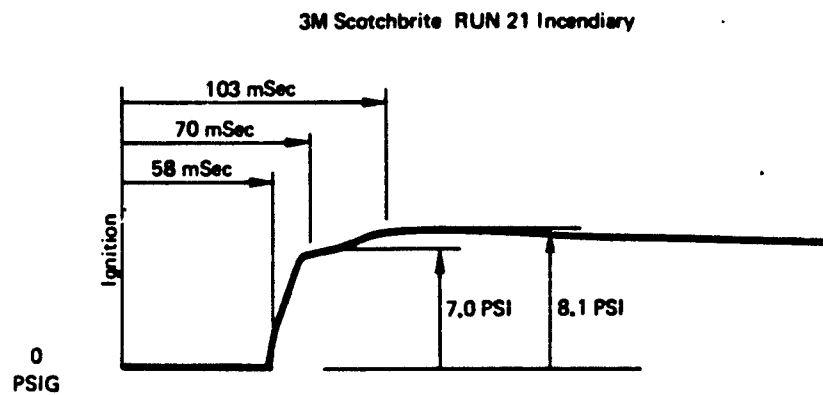
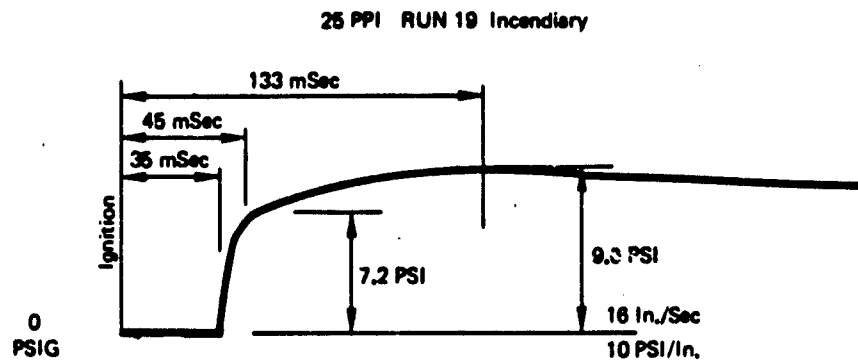


Figure A-102: Typical Pressure Traces for 39% Void Fuselage Tank (Lined Wall) (Dry)

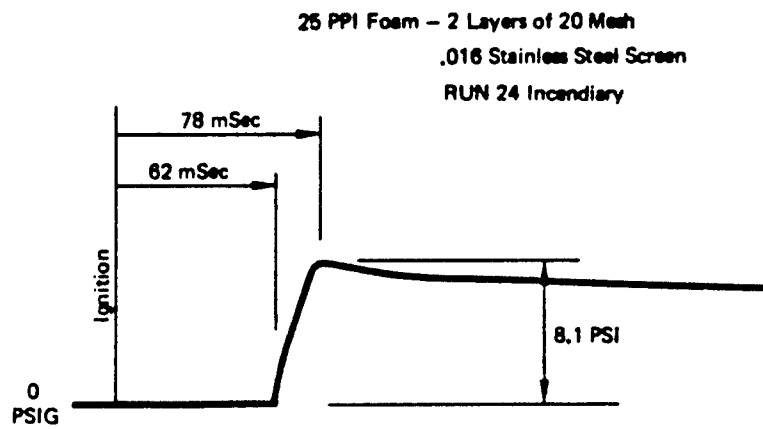
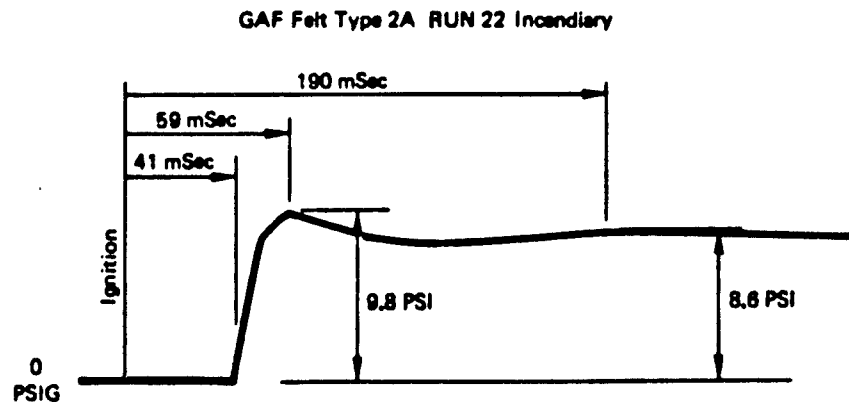
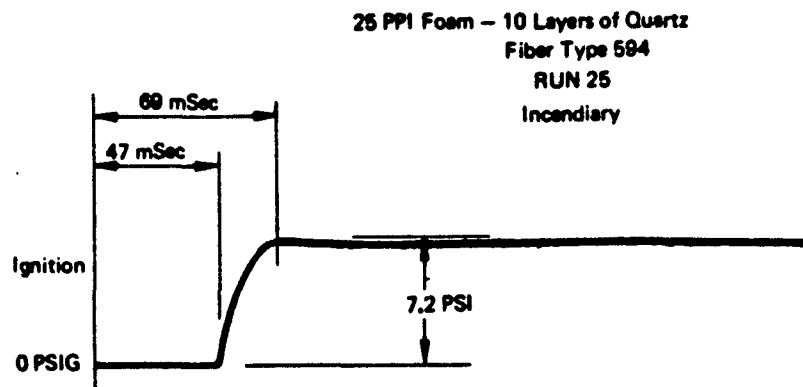


Figure A-103: Typical Pressure Traces for 39% Void Fuselage Tank (Lined Wall) (Dry)



*Figure A-104: Typical Pressure Traces for 39% Void Fuselage Tank,
Lined Wall, Dry*

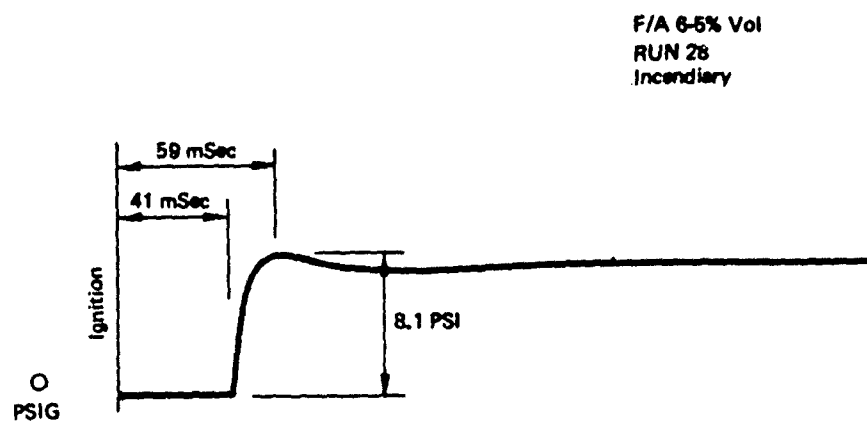
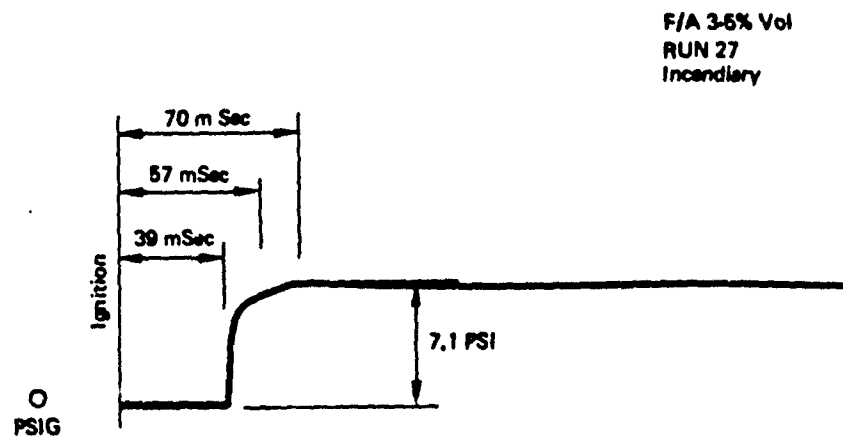
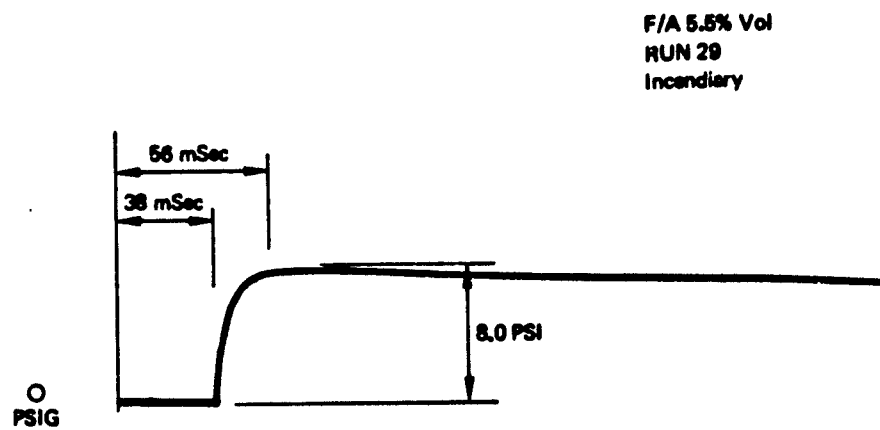


Figure A-105: Typical Pressure Traces for 39% Void Fuselage Tank,
Lined Wall, 25-PPI (Wet)



*Figure A-106: Typical Pressure Traces for 39% Void Fuselage Tank,
Lined Wall, 25-PPI (Wet)*

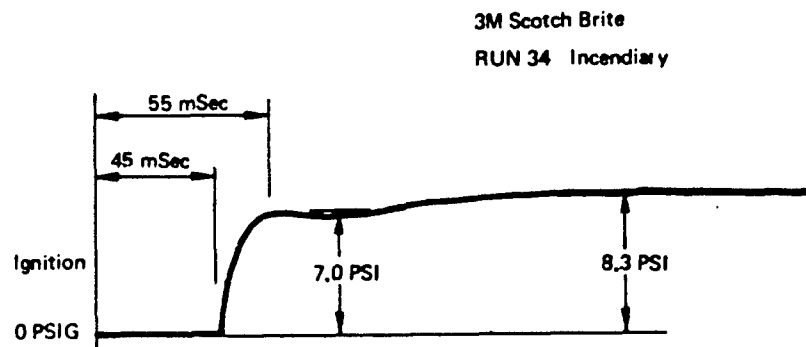
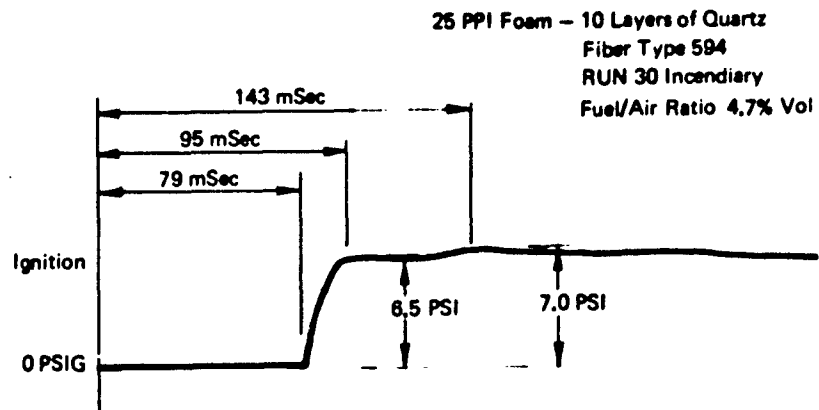
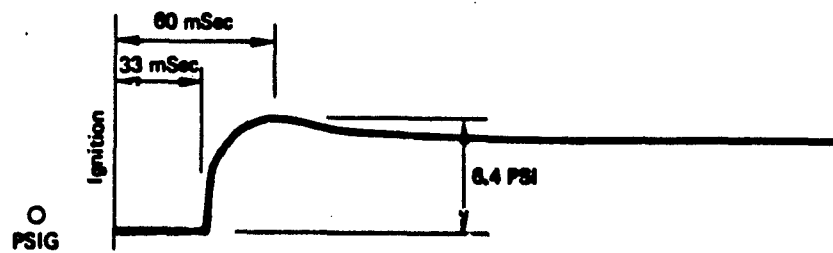


Figure A-107: Typical Pressure Traces for 39% Void Fuselage Tank,
Lined Wall, Wet with JP5

25 PPI Foam - 10 Layers of Quartz
Wet with JP-5 Fiber Type 594

RUN 31
Incendiary
F/A 6.5% Vol



RUN 32
Incendiary
F/A 3.5% Vol

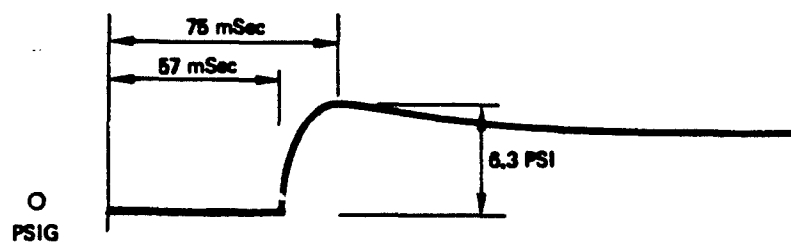
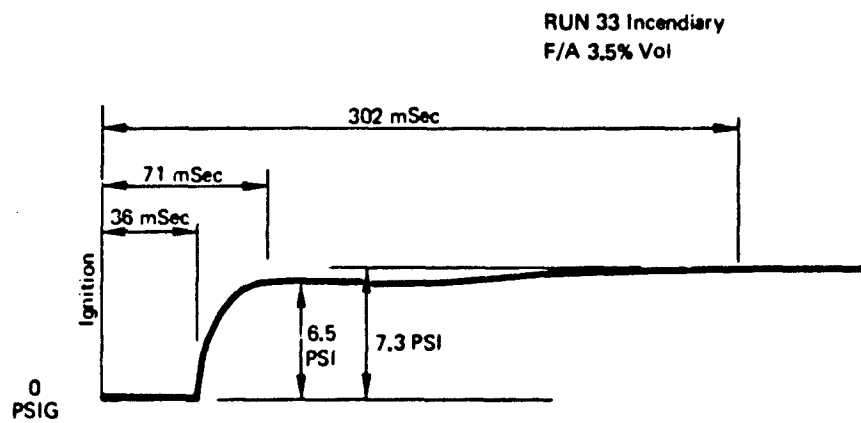


Figure A-108: Typical Pressure Traces for 39% Void Fuselage Tank,
Lined Wall, 25-PPI Foam - 10 Layers of Quartz



- 3M Scotch Drite
- Wet with JP5

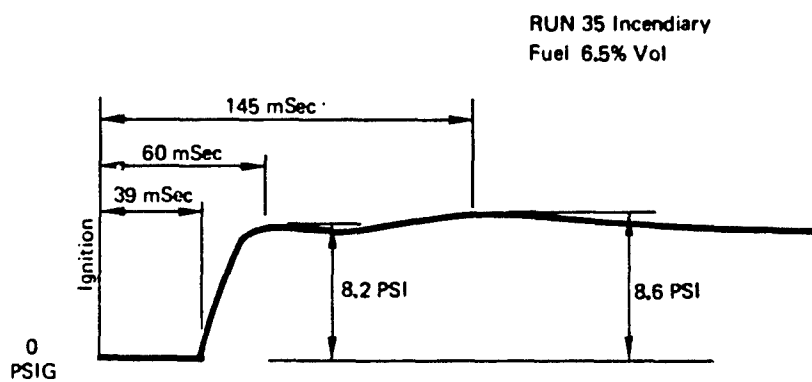


Figure A-109: Typical Pressure Traces for 39% Void Fuselage Tank, Lined Wall

APPENDIX B
TASK II TEST DATA

Preceding page blank

Table D-1:

Run No.	Material	Condition	Void Configuration		Percent Void	Ambient PSIA			Bomb Pressures (PSIG)			Initial Pressure			Ignition Mode		Time to PC ₁ Peak Pressure in Secs
						Pressure PSIA			PSIG			PSIA			Soak	Gun Fire	
						PB ₁	PB ₂	PB ₃	PB ₁	PB ₂	PB ₃	P ₁	P ₂	P ₃			
			Wet	Dry													
36	25 PPI	X		TW	40	14.7	89	100	98	14.7	8.7	8.2	8.7	X	1.58	130	
37	25 PPI	X		TW	40 + 6.65 Relief Void	14.73	92	103	101	14.73	8.6	8.4	8.4	X	1.58	170	
38	25 PPI	X		TW	40 + 8.9 Relief Void	14.73	89	104	100	14.73	9.0	8.8	9.0	X	1.60	200	
39	25 PPI	X		TW	50	14.73	85	100	99	14.73	13.4	13.3	13.3	X	1.90	93	
40	25 PPI	X		TW	50 + 6.66 Relief Void	14.70	90.5	104	100	14.73	10.1	10.26	10.27	X	1.70	132	
41	25 PPI	X		TW	30	14.70	100	102	83	14.70	6.9	6.7	6.9	X	1.45	197	
42	25 PPI	X		TW	30 + 11.1 Relief Void	14.70	91	100	97	14.70	7.3	7.4	7.5	X	1.51	188	

Table B-1: (Continued)

Run No.	Material	Condition		Void Configuration	Percent Void		Ambient PSIA			Bomb Pressures (PSIG)			Initial PSIA			Initial Pressure		Ignition Mode		Time to PC ₁ Peak Pressure in Secs
		Wet	Dry	TW	30 + 11.1 Relief Void	14.70	115	132.5	123.5	19.70	12.6	X	1.64	167						
															PB ₁	PB ₂	PB ₃	ΔP	Spark	
43	25 PPI	X		TW																
44	25 PPI	X		TW																
45	25 PPI	X		TW																
46	25 PPI	X		TW																
47	25 PPI	X		TW																
48	25 PPI	X		TW																

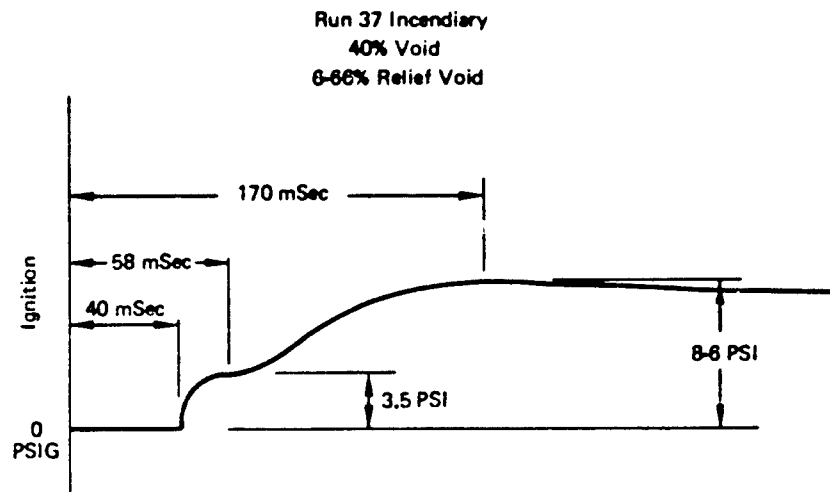
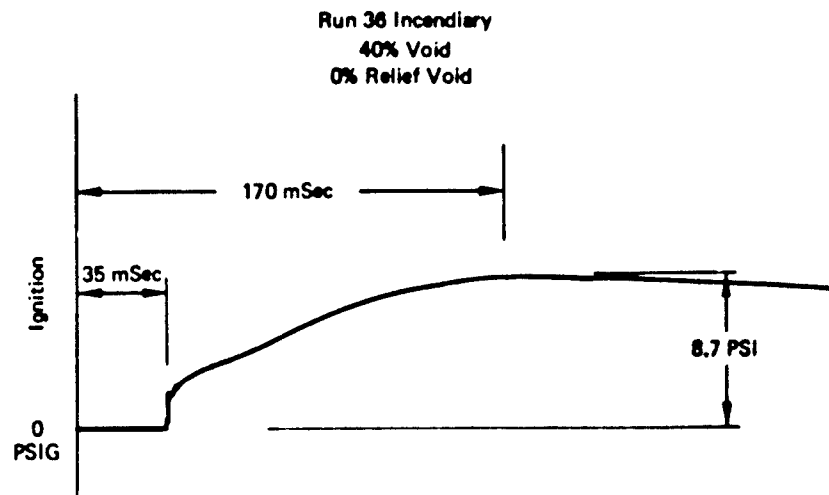


Figure B-1: Typical Pressure Traces for Fuselage Tank (Top Wall), Runs 36 and 37

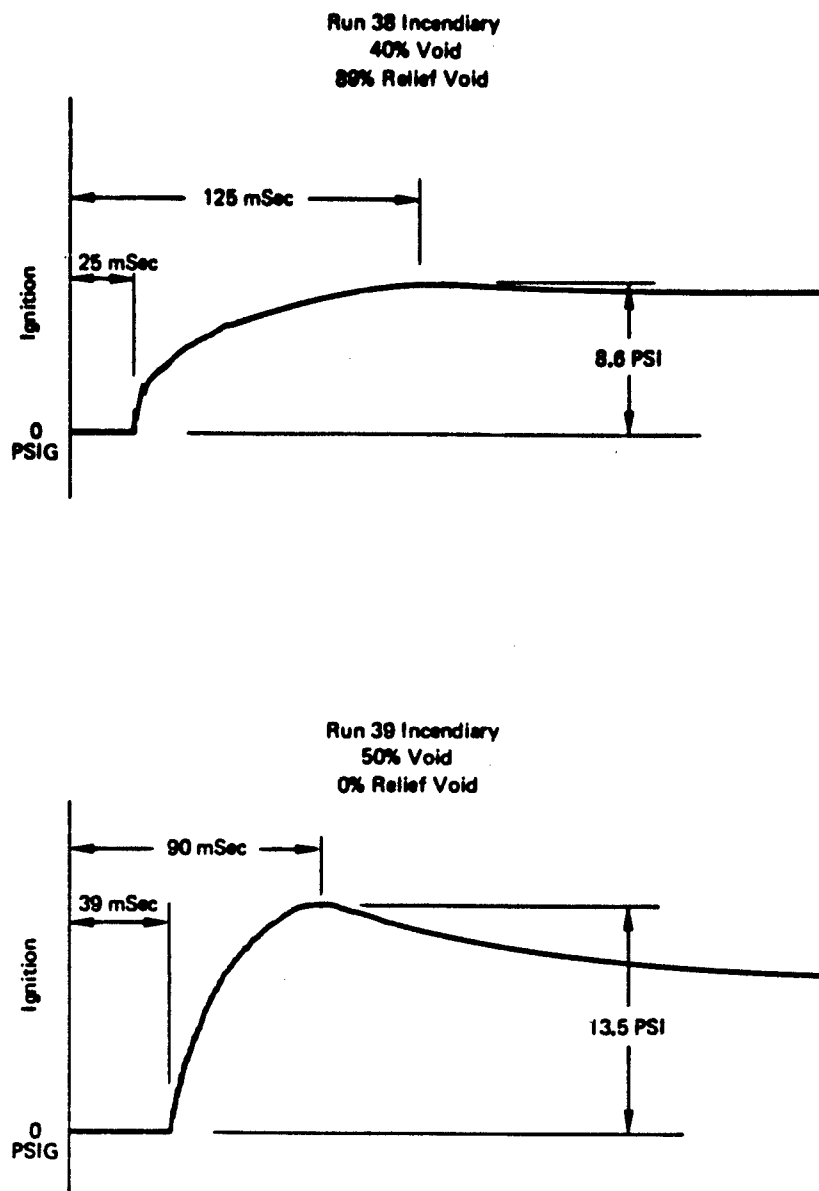


Figure B-2: Typical Pressure Traces for Fuselage Tank (Top Wall), Runs 38 and 39

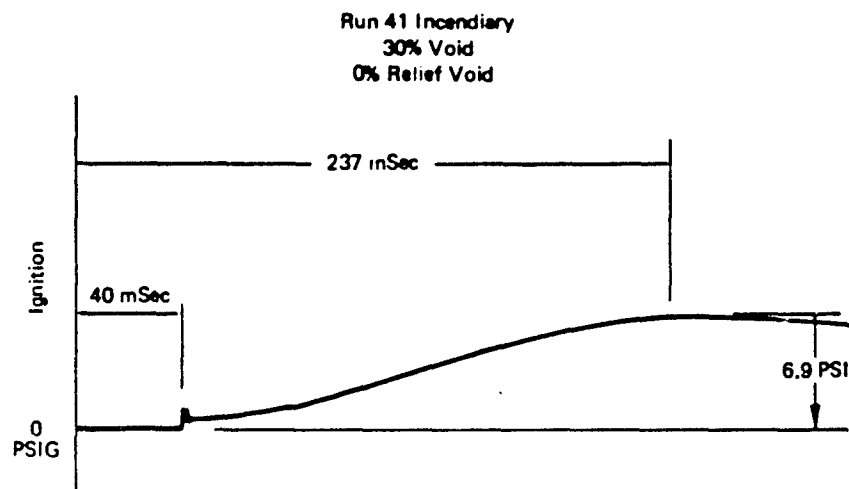
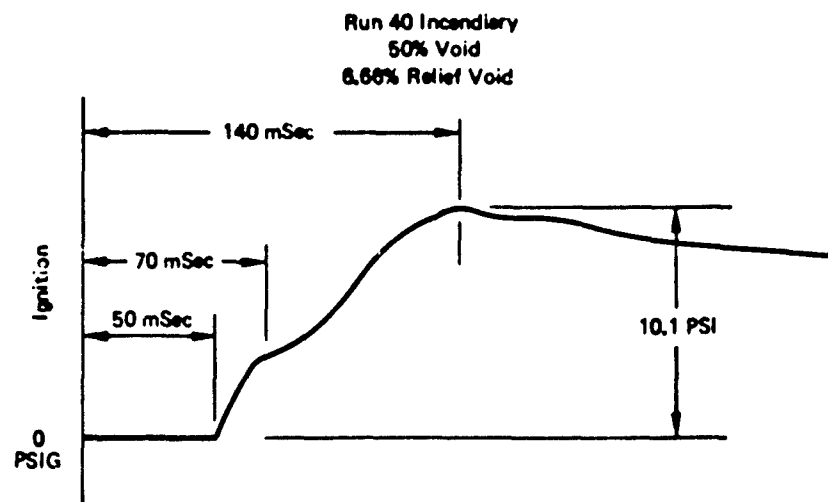


Figure B-3: Typical Pressure Traces for Fuselage Tank (Top Wall), Runs 40 and 41

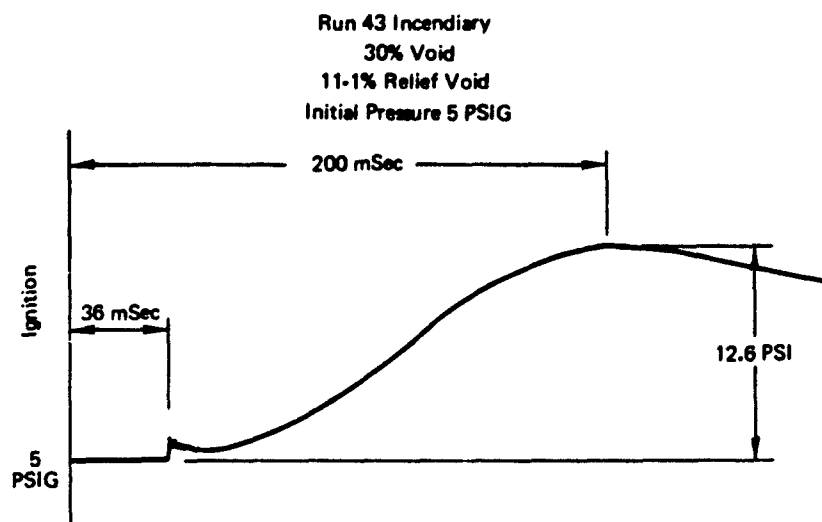
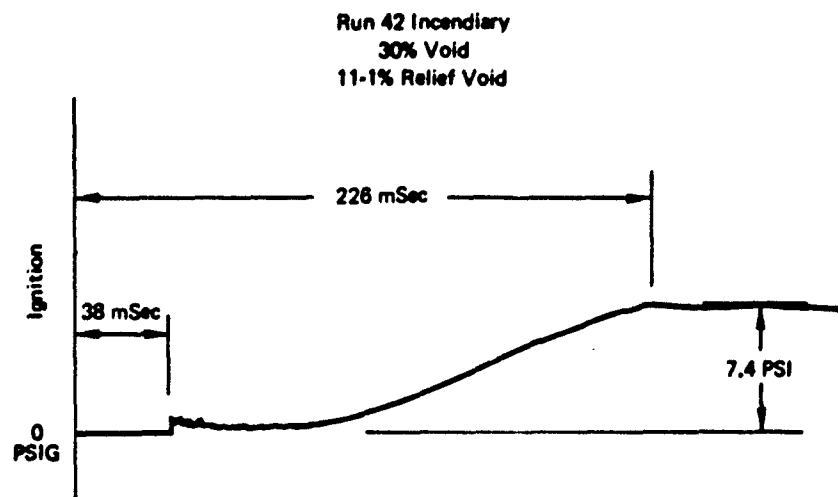


Figure B-4 Typical Pressure Traces for Fuselage Tank (Top Wall), Runs 42 and 43

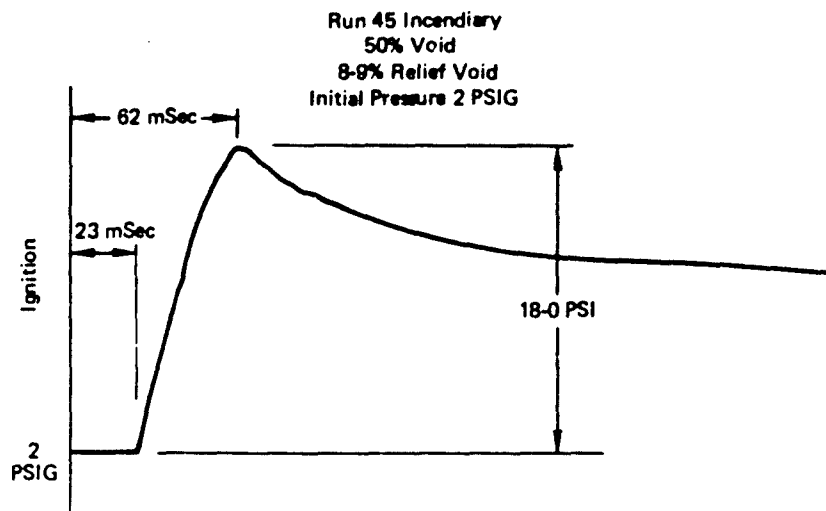
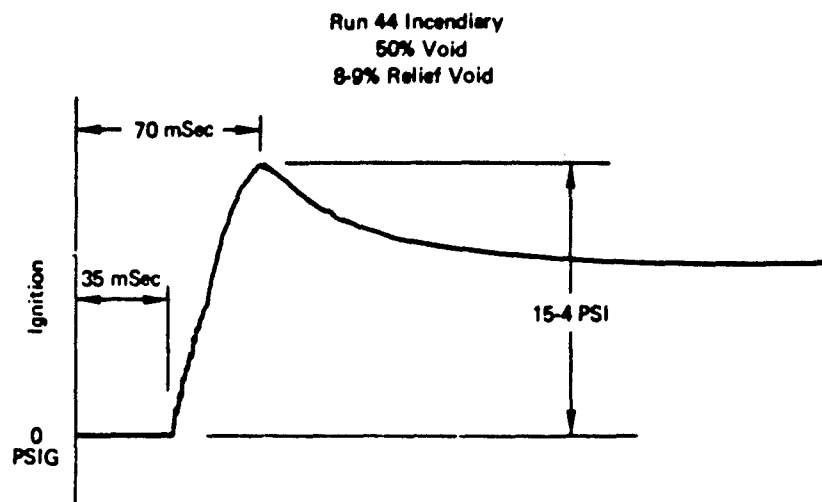


Figure D-5: Typical Pressure Traces for Fuselage Tank (Top Wall) Runs 44 and 45

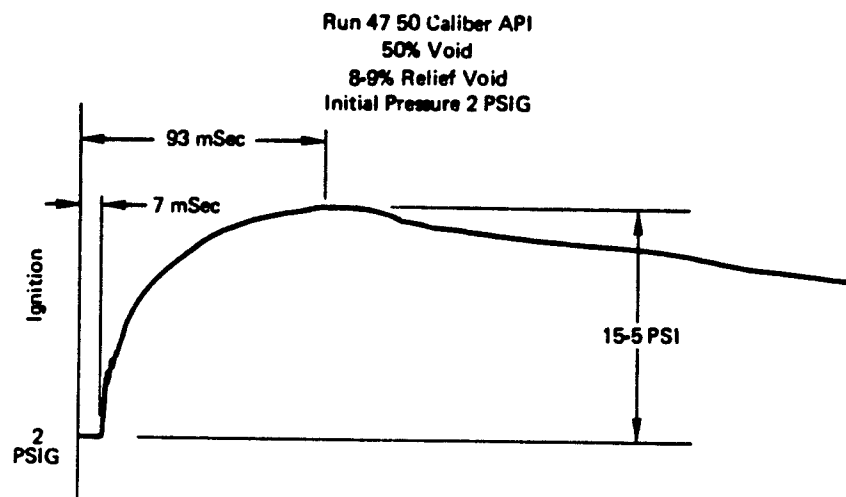
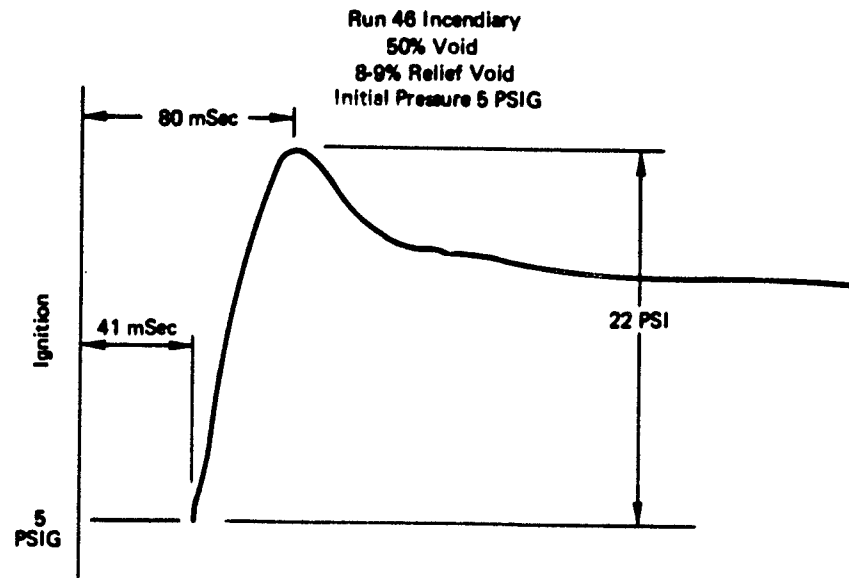


Figure D-6: Typical Pressure Traces for Fuselage Tank (Top Wall), Runs 46 and 47

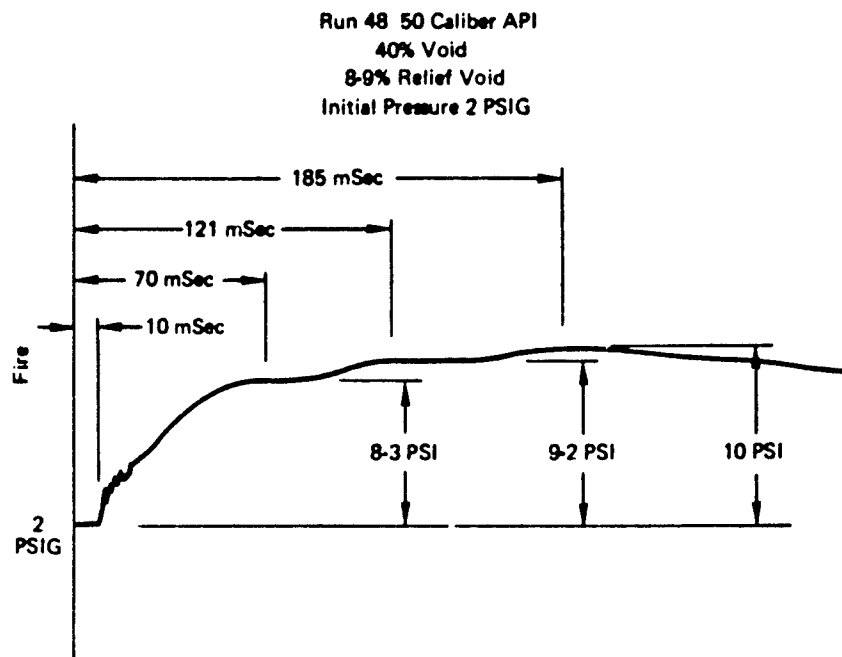


Figure B-7: Typical Pressure Traces for Fuselage Tank (Top Wall), Run 48

Table B-II: Small Wing Tankage

Run No.	Material	Condition	Void Configuration	Ambient PSIA			Bomb Pressures (PSIG)			Initial Pressures						Final Pressures ΔP Rise			Ignition Mode		Time to PC ₁ Peak Pressure mSecs
				Percent Void			Pressure PSIA			P Initial PSIA						Spark	Gun Fire				
				Wet	Dry		PB ₁	PB ₂	PB ₃	PC ₁₁	PC ₁₂	PC ₁₃	PC ₁₄	PC ₁₅	PC ₁₆						
49	25 PPI	X	VTW	57	Misfired	82.5	91.0	80.5	-	-	-	-	-	-	-	X	-	-	-	-	
49A	25 PPI	X	VTW	57	Misfired	98.0	103.5	92.0	-	-	-	-	-	-	-	-	X	-	-	-	-
49B	25 PPI	X	VTW	57	14.67	110.0	105.0	91.0	14.67	2.6	2.3	2.3	2.3	2.5	3.0	X	1.172	455	-	-	
50	25 PPI	X	Egg Crate	36	-	-	-	-	14.97	-	-	-	-	-	-	-	X	-	-	-	-
50A	25 PPI	X	Egg Crate	36	14.97	97.5	103.5	88.5	14.97	1.6	-	-	-	-	-	-	X	1.11	40	-	-
51	25 PPI	X	Egg Crate	62	14.71	104.5	100.0	85.5	14.71	2.1	2.1	3.0	2.3	2.2	6.2	X	1.14	200	-	-	-
52	25 PPI	X	VTW	76	14.71	-	-	-	14.71	-	-	Misfired	-	-	-	-	X	-	-	-	-
52A	25 PPI	X	VTW	76	14.71	-	-	-	14.71	-	-	Misfired	-	-	-	-	X	-	-	-	-
52B	25 PPI	X	VTW	76	14.71	-	-	-	14.71	-	-	Misfired	-	-	-	-	-	-	-	-	-
52C	25 PPI	X	VTW	76	14.71	-	-	-	14.71	-	-	Misfired	-	-	-	-	-	-	-	-	-
52D	25 PPI	X	VTW	76	14.71	-	-	-	14.71	-	-	Misfired	-	-	-	-	-	-	-	-	-
52E	25 PPI	X	VTW	76	14.77	107	95	88	14.77	5.7	2.1	2.4	2.4	2.3	2.3	X	1.39	115 MS	8 MS	-	-
53	25 PPI	X	VTW	73.6	14.78	100.0	83.5	101.5	14.78	9.75	9.0	10.50	10.0	9.0	9.0	X	1.60	680	-	-	-
54	25 PPI	X	VTW	79	14.83	105	108	102	14.83	5.3	2.3	2.3	2.3	2.3	2.3	X	1.30	41	7 MS	-	-
55	25 PPI	X	VTW	81.7	14.84	103.5	104	96.5	14.84	Cell 1 15.5	Cell 2 3.2	Cell 3 3.2	Cell 4 4.6	Cell 5 3.3	Cell 6 3.3	X	2.04	147	-	-	-
56	25 PPI	X	VTW	79	14.86	94	95	66	14.86	11.4	2.7	2.5	3.0	2.5	2.7	X	1.77	44	88	-	-
57	25 PPI	X	VTW	79	14.86	131	133	117	18.86	24.2	7.7	7.6	8.4	7.7	7.7	X	2.07	43	84	-	-
58	25 PPI	X	VTW	79	14.80	104.5	104	89.5	14.80	2.4	2.4	2.2	2.2	2.1	2.2	X	1.16	-	-	-	-
59	20 Layers Quartz	X	VTW	80	14.80	107.5	108.5	87.5	14.80	32.4	2.4	2.5	2.3	2.2	2.2	X	3.16	102	-	-	-
60	25 PPI	X	Egg Crate	62	14.82	135.5	139	130.5	18.82	7.7	6.0	6.0	6.0	6.0	6.0	X	1.26	4	4 MS	-	-
61	25 PPI	X	Egg Crate	70	14.78	98.5	102	100	14.78	3.0	1.5	1.3	1.3	1.3	1.3	X	1.20	5	5 MS	-	-
62	25 PPI	X	Egg Crate	80	14.72	101.0	100.5	86	14.72	3.2	2.2	2.2	2.2	2.3	2.3	X	1.22	165	-	-	-
63	25 PPI	X	Egg Crate	70	14.73	-	-	-	14.73	-	-	Misfired	-	-	-	X	-	-	-	-	-
63A	25 PPI	X	Egg Crate	70	14.73	100.5	103.5	101.5	14.73	2.5	2.2	2.2	2.1	X	2.1	X	1.17	-	-	-	-
64	25 PPI	X	Egg Crate	70	14.72	85.5	91.5	75	14.72	3.0	2.0	2.1	2.2	2.3	2.2	X	1.20	29	29 MS	-	-
65	25 PPI	X	Egg Crate	63	14.68	105.5	101.0	90.0	14.68	-	-	No Indication of Pressure Rise	-	-	-	X	-	-	-	-	-
66	25 PPI	X	Egg Crate	71	14.66	103.75	105.0	100.0	11.66	4.2	2.3	2.3	2.3	2.4	2.4	X	1.29	69	-	-	-
67	25 PPI	X	Egg Crate	71	14.73	117	129.5	111	13.73	11.3	14.8	16.4	12.9	12.0	12.5	X	1.605	175	-	-	-
68	25 PPI	X	VTW	76.5	14.70	98.5	99.0	87.0	13.3	9.7	10.8	13.4	9.3	17.0	-	X	1.90	130	-	-	-
69	25 PPI	X	VTW	79.0	14.69	99.0	104.0	93.5	14.69	17.2	4.0	4.0	20.3	4.2	4.0	X	2.17	103	-	-	-
70	25 PPI	X	VTW	76.5	14.74	112.0	131.5	131.0	18.74	11.7	3.0	3.0	3.5	3.1	3.0	X	1.63	78	-	-	-
71	25 PPI	X	VTW	76.5	14.75	122.5	118.5	111.5	18.75	30.4	4.3	4.4	29.7	4.5	4.4	X	2.62	59	-	-	-

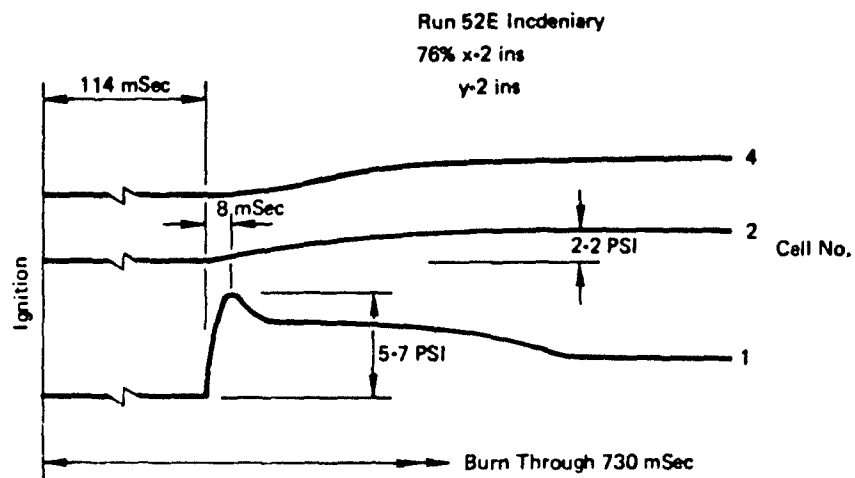
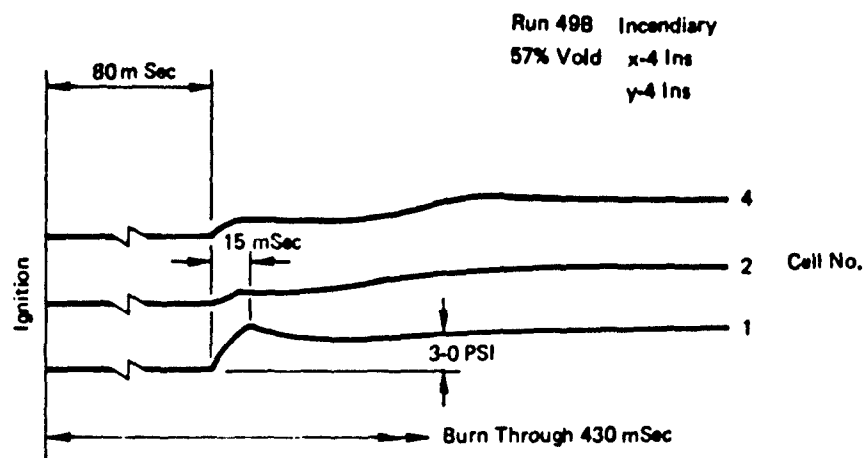


Figure B-8: Typical Small Wing Tank Pressure Trace, Voided Top Wall, Runs 49B and 52E

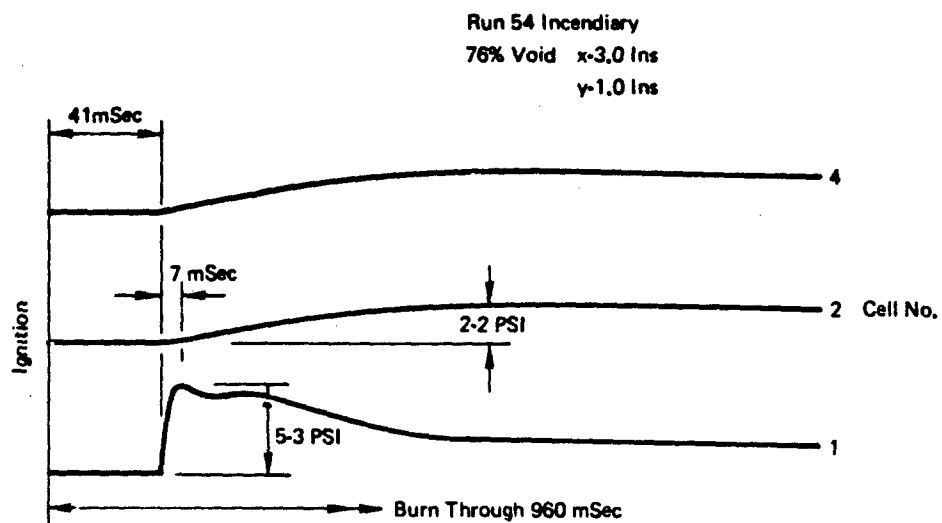
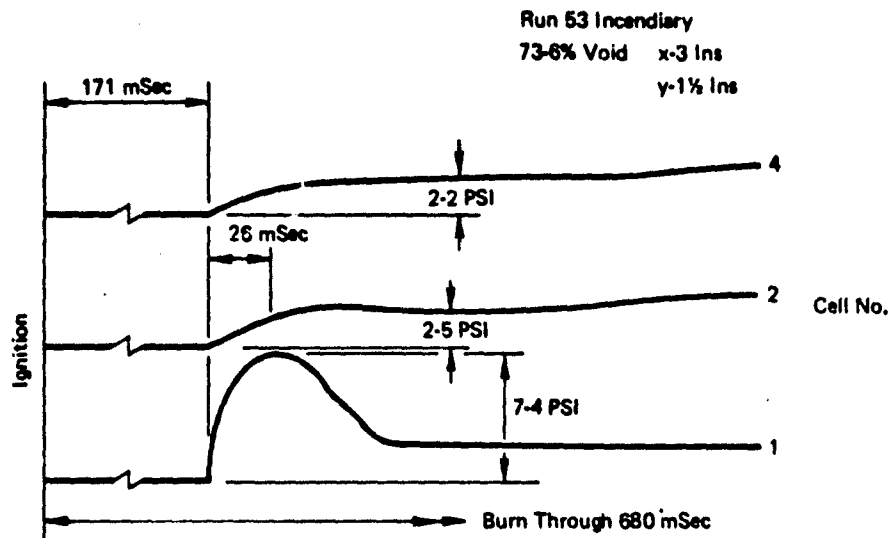


Figure B-9: Typical Small Wing Tank Pressure Traces Voided Top Wall, Runs 53 and 54

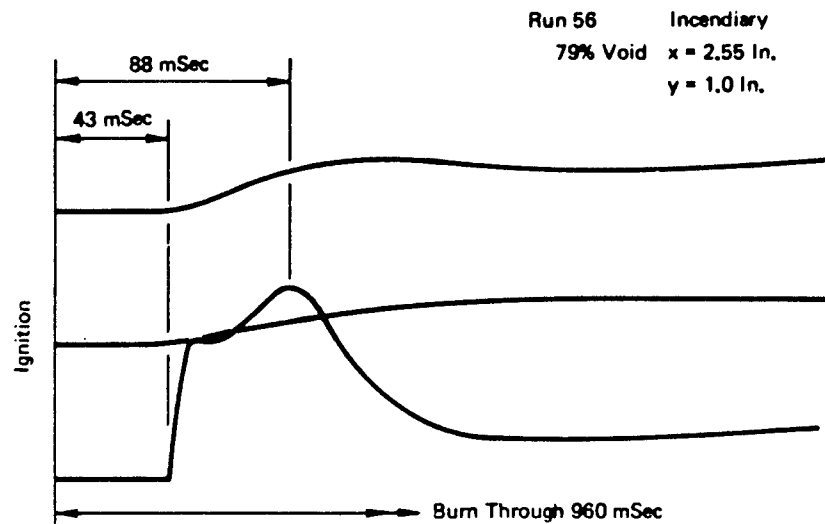
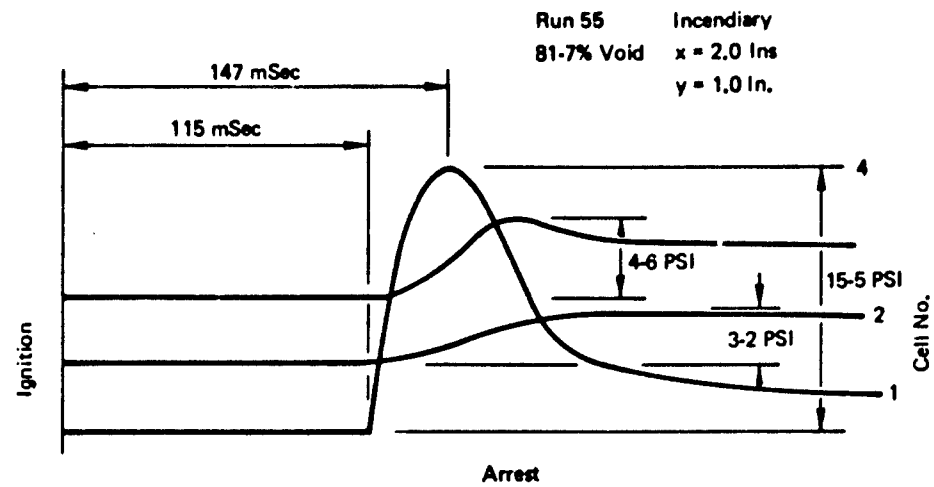


Figure B-10: Typical Small Wing Tank Pressure Traces, Voided Top Wall, Runs 55 and 56

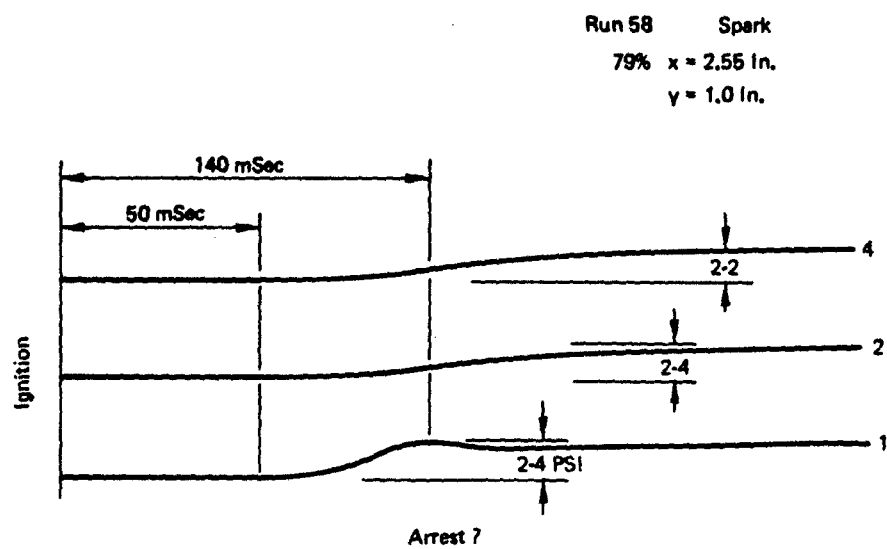
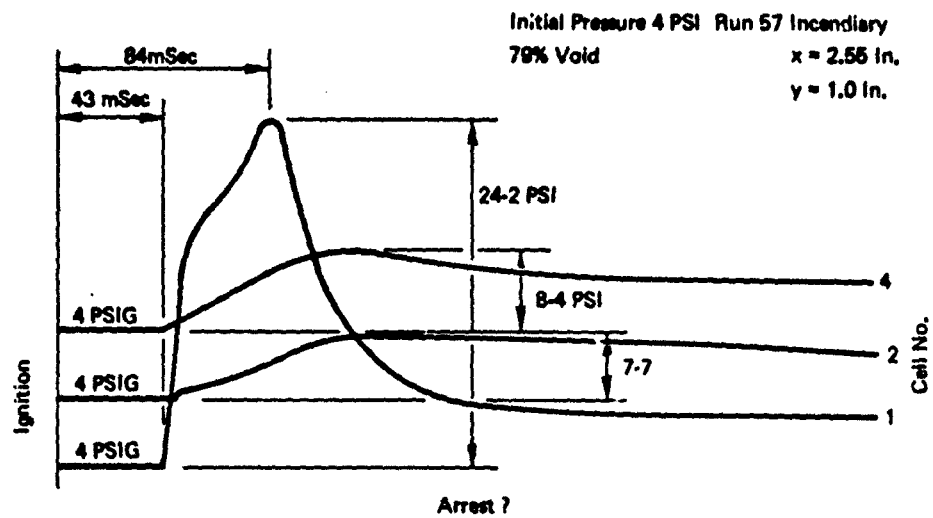


Figure B-11: Typical Small Wing Tank Pressure Traces, Voided Top Wall, Runs 57 and 58

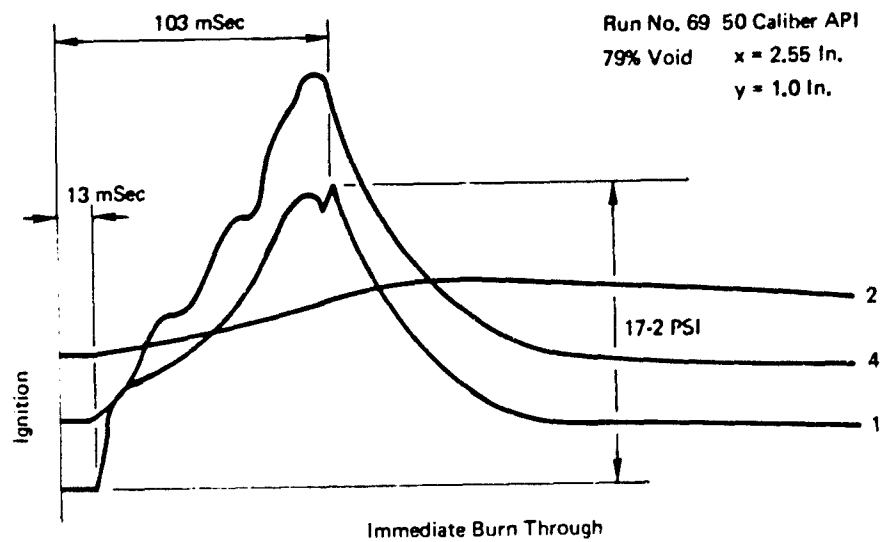
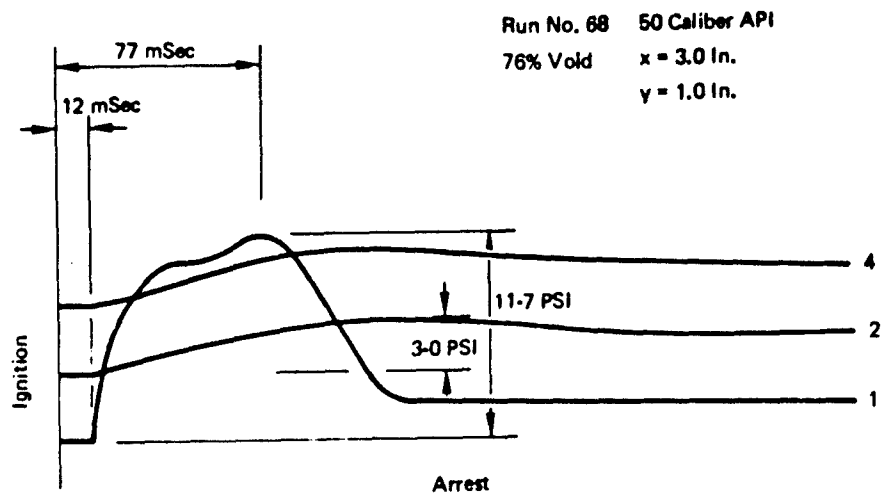


Figure B-12 : Typical Small Wing Tank Pressure Traces, Voided Top Wall, Runs 68 and 69

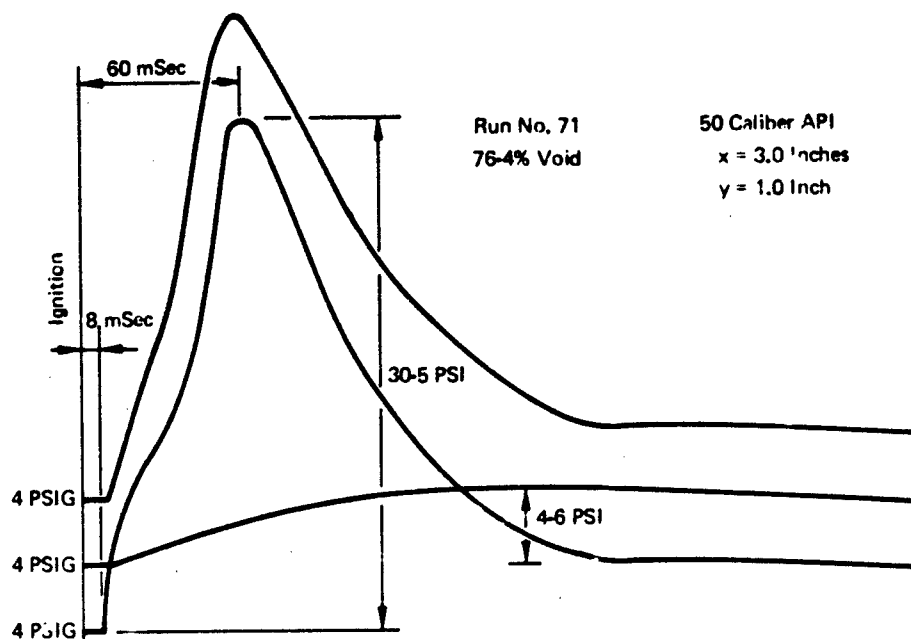
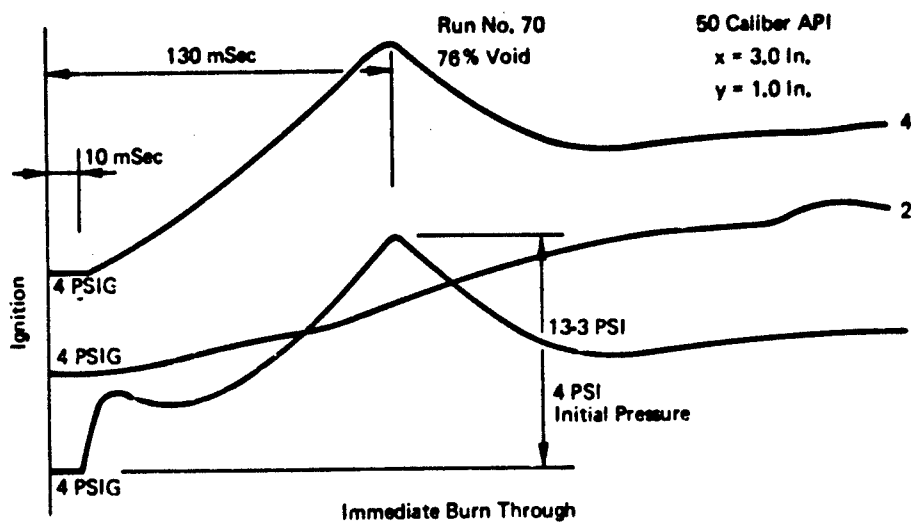


Figure B-13: Typical Small Wing Tank Pressure Traces Voided Top Wall, Runs 70 and 71

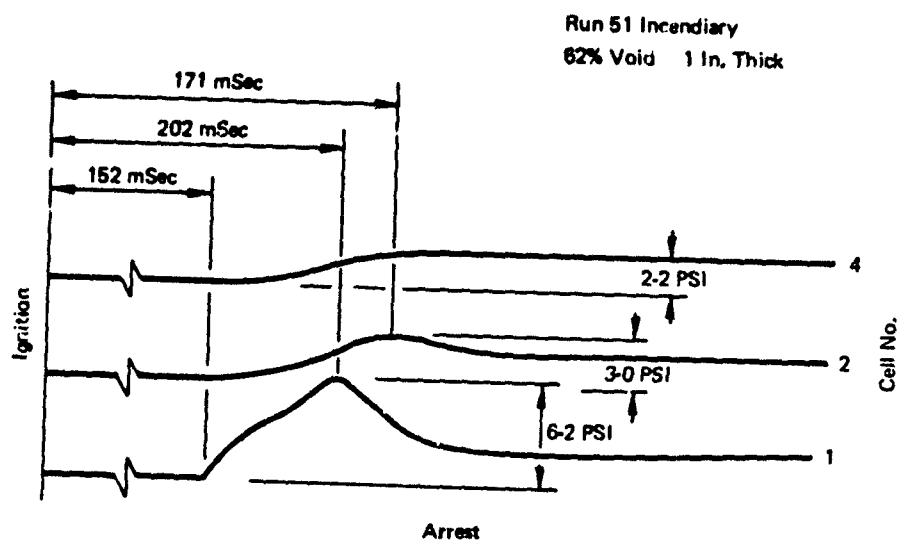
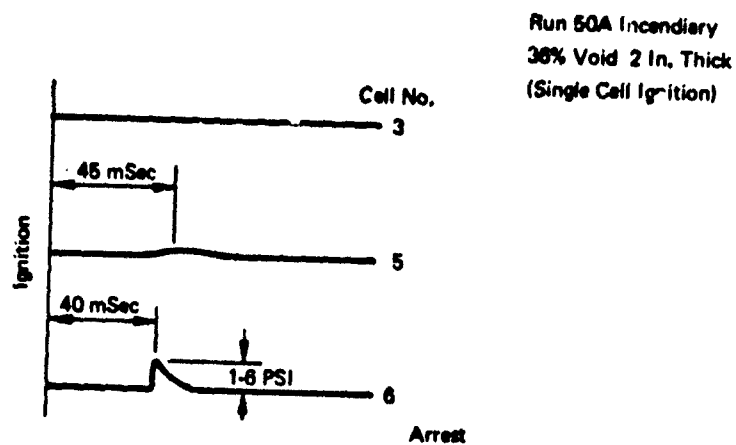


Figure B-15: Typical Small Wing Tank Pressure Traces, Egg Crate Configuration, Runs 50A and 51

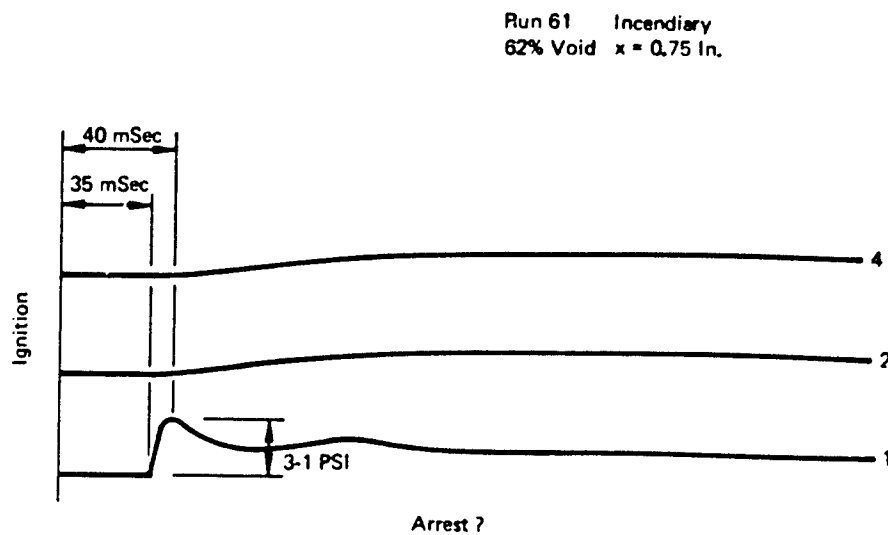
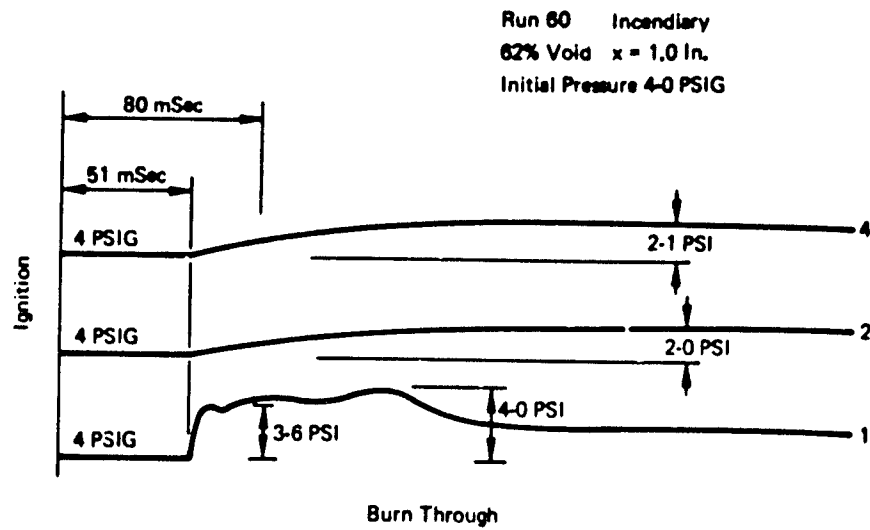


Figure B-16: Typical Small Wing Tank Pressure Traces, Egg Crate Configuration, Runs 60 and 61

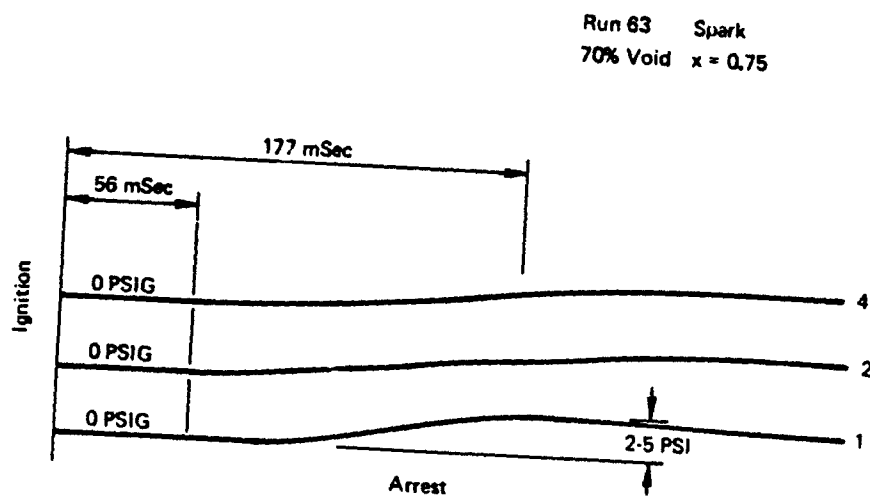
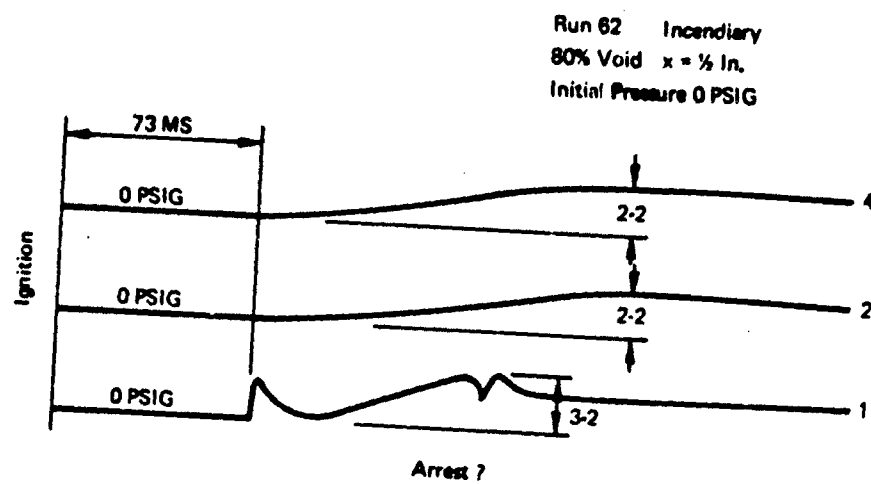


Figure B-17: Typical Small Wing Tank Pressure Traces Egg Crate Configuration, Runs 62 and 63

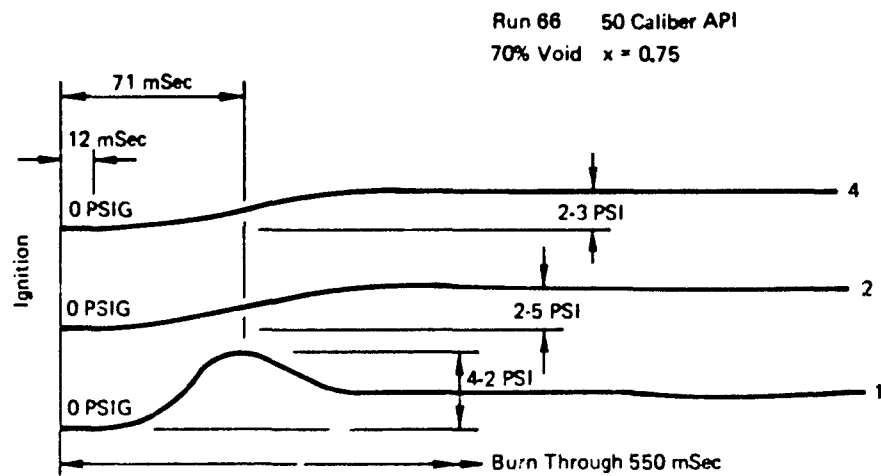
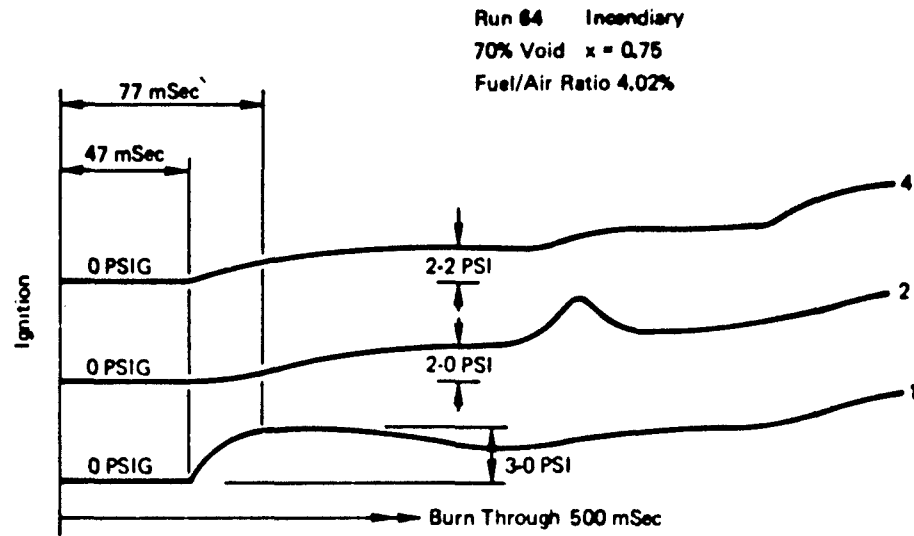


Figure B-18: Typical Small Wing Tank Pressure Traces, Egg Crate Configuration, Runs 64 and 66

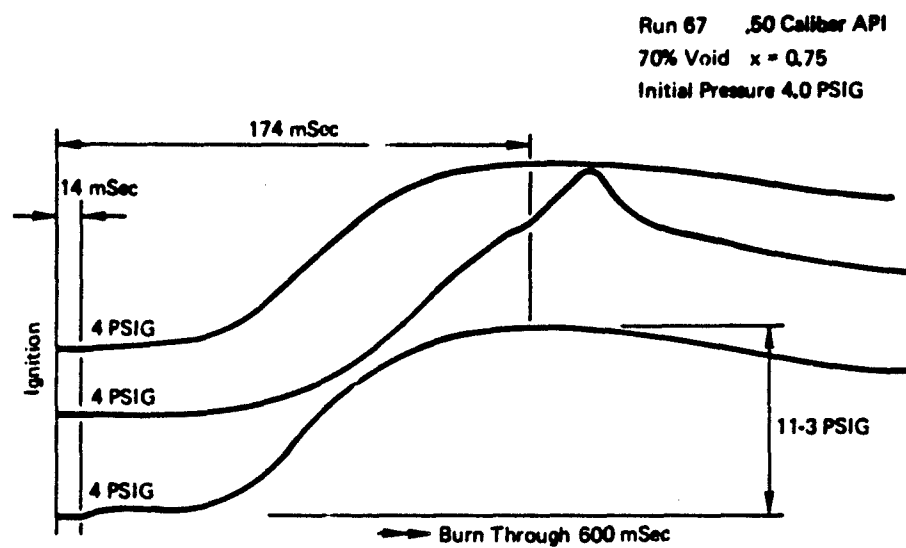


Figure B-19: Typical Small Wing Tank Pressure Traces, Egg Crate Configuration, Run 67



STW - 1 1/2 Inch Top, 3 Inch Sides & Backs
Cell No. 1 - Test Run No. 53 (Delayed Burnthrough)

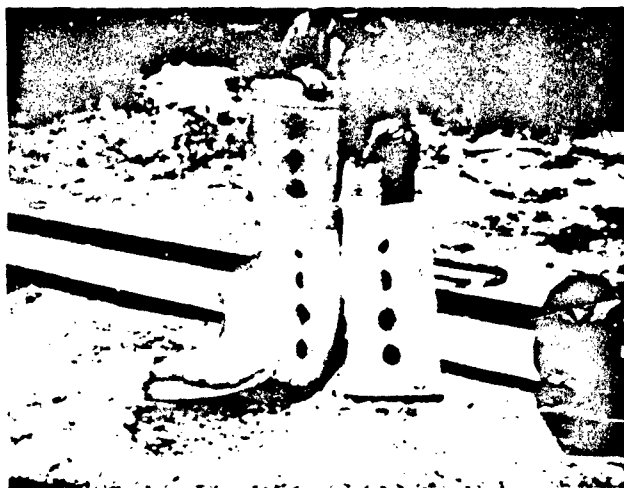
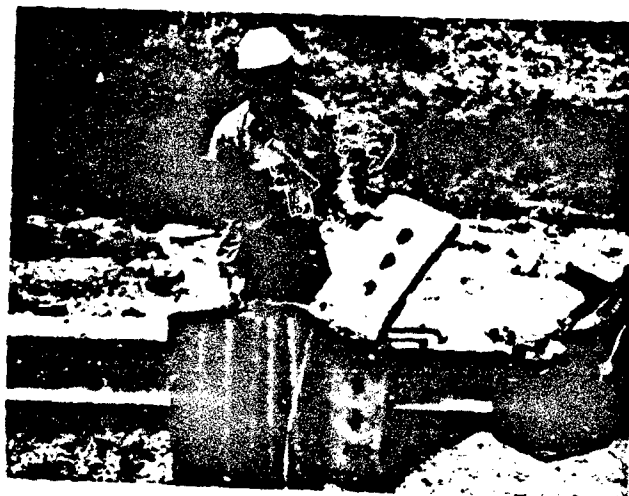


Figure B-20: Voided Top Wall (Run 53)



Ignitor Side

STW — 1-Inch Top, 2.5-Inch Sides and Backs
Cell No. 1 — Test Run No. 54 (Delayed Burnthrough)



Back Side
Holes Indicate
Burnthrough

Channels for Support Top Wall Structure

Figure B-21: Voided Top Wall (Run 54)



Run 61
3/4-Inch Egg Crate, Incendiary Ignition
Cell No. 1 - 70% Void (Burnthrough)



Run 62
1/2-Inch Egg Crate Incendiary Ignition
Cell No. 1 (Note Burnthrough holes of Cell Walls)
87% Void

Figure B-22: Egg Crate - Runs 61 and 62.

Table B-III: Large Wing Tankage

Run No.	Material	Condition	Void Configuration		Percent Void		Ambient PSIA			Bomb Pressures PSIG			Initial Pressure			Final Pressure ΔP Rise			Ignition Mode		Time to PC ₁ Peak Pressure mSecs	
			Wet	Dry	L.W.	E.G.G. CRATE	E.G.G. CRATE	L.W.	E.G.G. CRATE	E.G.G. CRATE	L.W.	E.G.G. CRATE	E.G.G. CRATE	L.W.	E.G.G. CRATE	E.G.G. CRATE	L.W.	E.G.G. CRATE	E.G.G. CRATE	L.W.		E.G.G. CRATE
72	25 PPI	x																		1.54	50.2	
73	25 PPI	x																		1.61	47.0	
73A	25 PPI	x																		1.73	171	
74	25 PPI	x																		1.81	213	
75	25 PPI	x																		1.79	131	
76	25 PPI	x																		2.37	390	
77	25 PPI	x																		1.45	150	
78	25 PPI	x																		2.36	49	
79	25 PPI	x																		2.27	216	
80	25 PPI	x																		1.84	252	
81	25 PPI	x																		1.08	211	
82	25 PPI	x																		2.19	205	
83	25 PPI	x																		2.27	283	
84	25 PPI	x																				
84A	25 PPI	x																		1.43	672	
85	25 PPI	x																				
85A	25 PPI	x																		1.52	575	
86	25 PPI	x																		2.43	132	
87	25 PPI	x																		1.44	715	

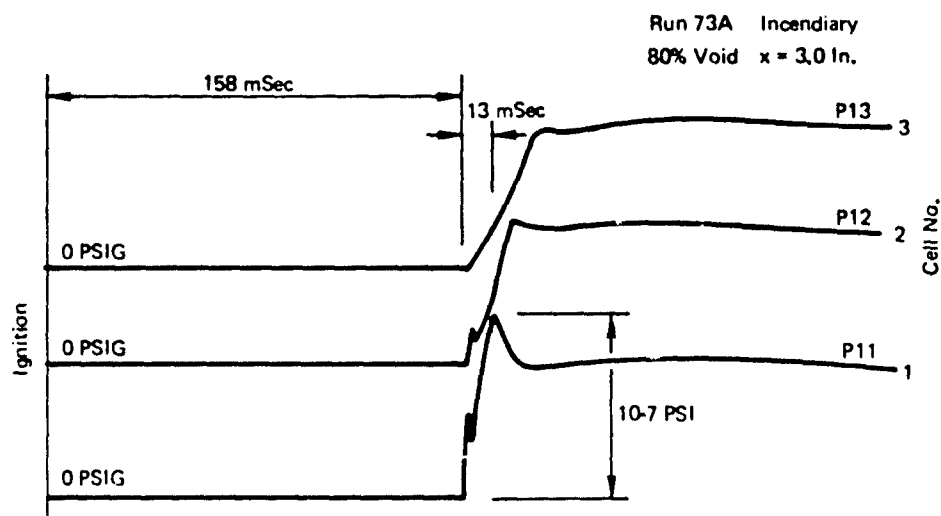
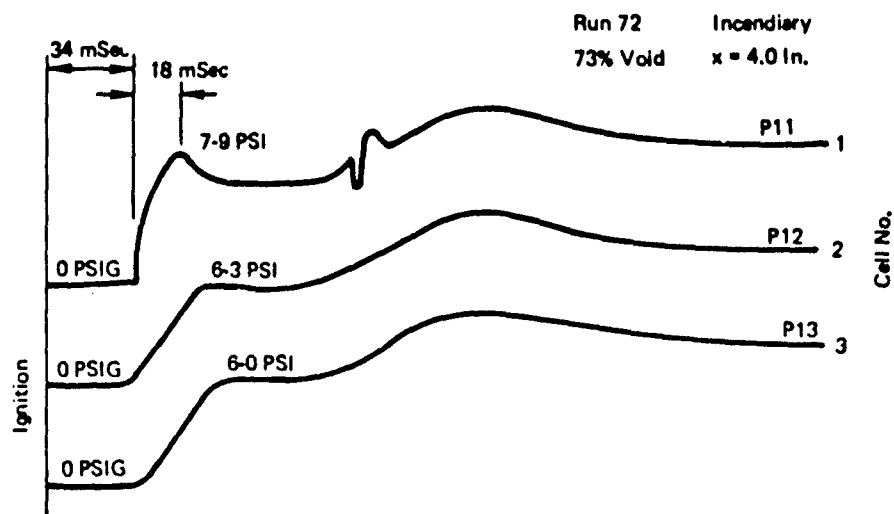


Figure B-23: Large Wing Tank Data Traces, Lined Wall (Runs 72 and 73A)

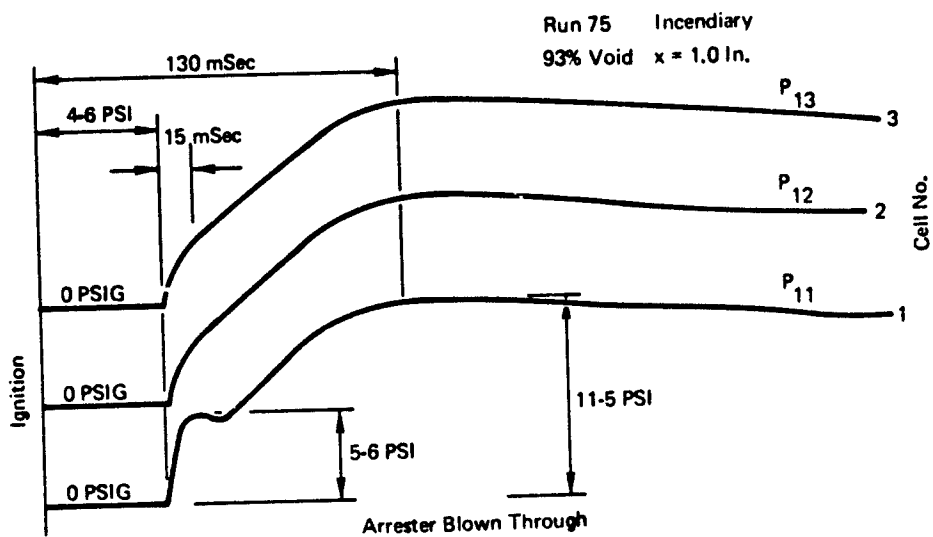
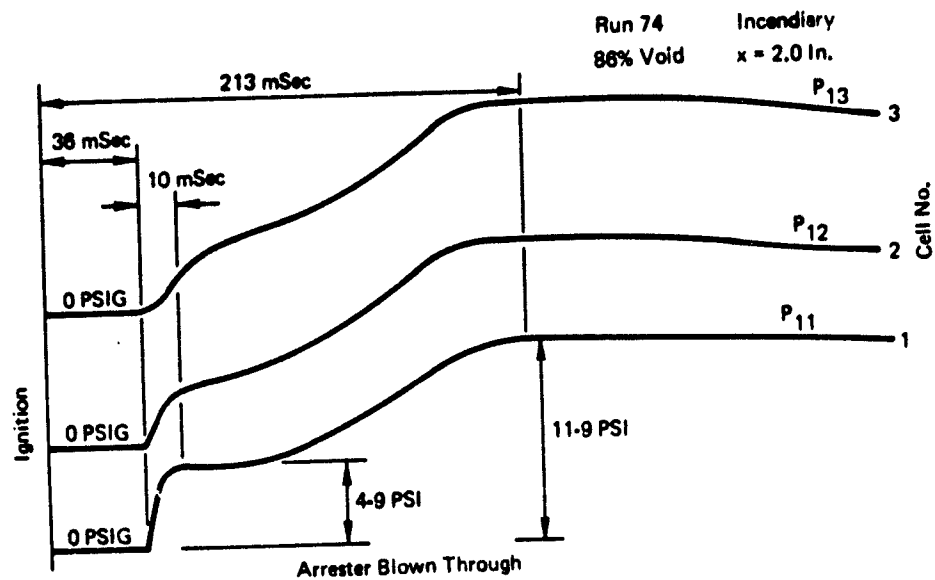


Figure B-24: Typical Large Wing Tank Pressure Traces Lined Wall (Runs 74 and 75)

Run 76 Spark Ignition
93% Void $x = 1.0$ Inch

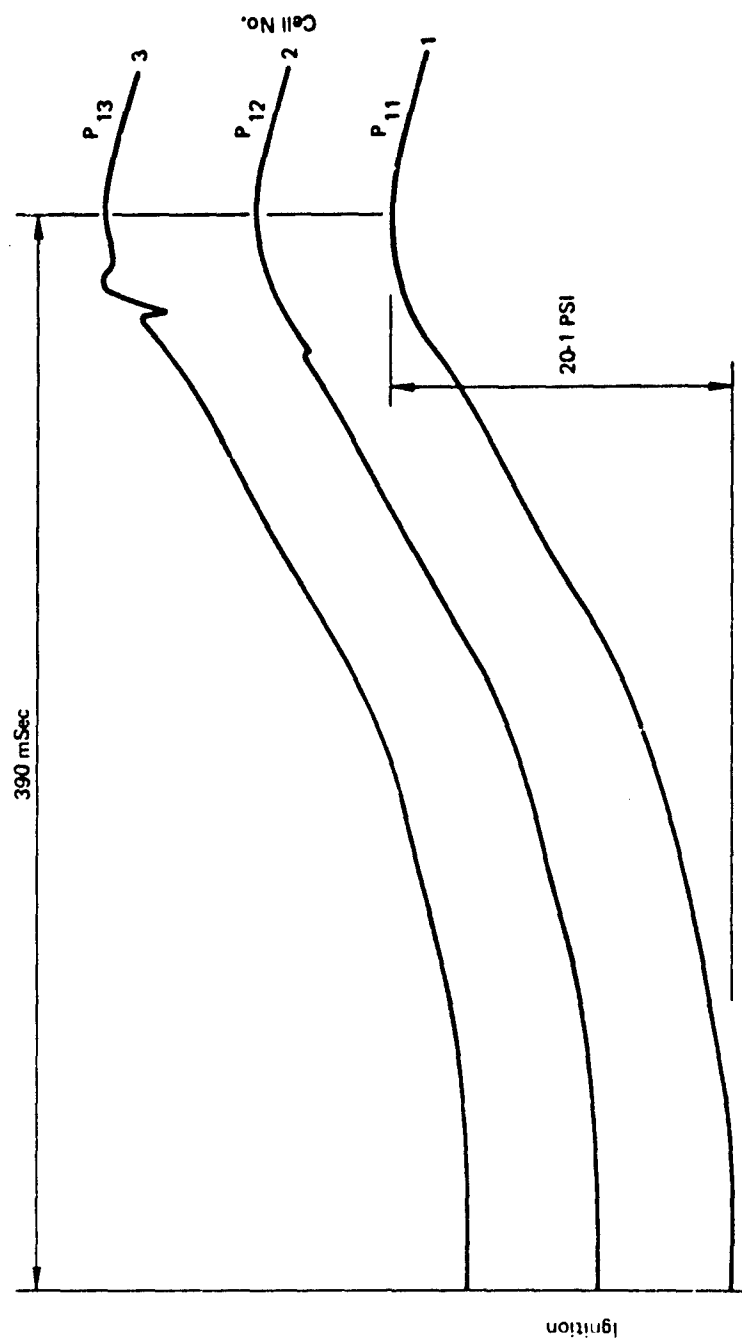


Figure 2-15 Typical Large Wing Tank Pressure Traces Lined Wall (Run 76)

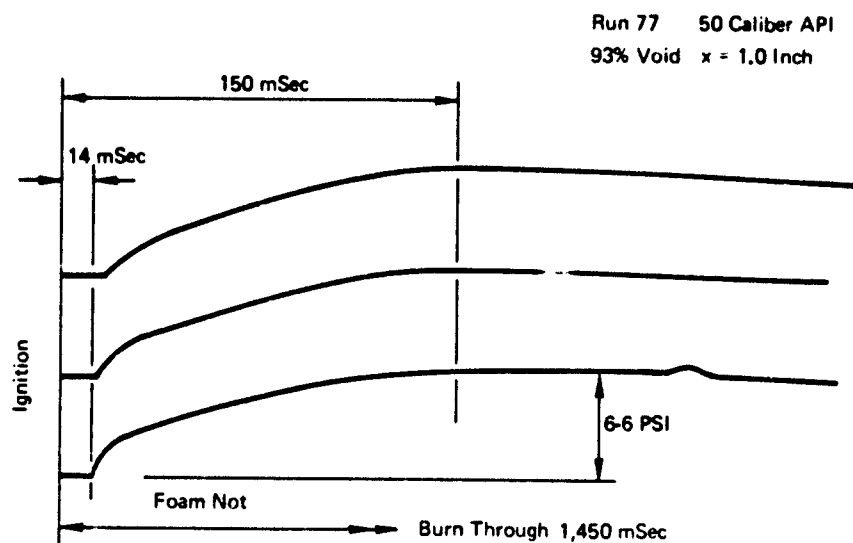


Figure B-26: Typical Large Wing Tank Pressure Traces Lined Wall (Run 77)

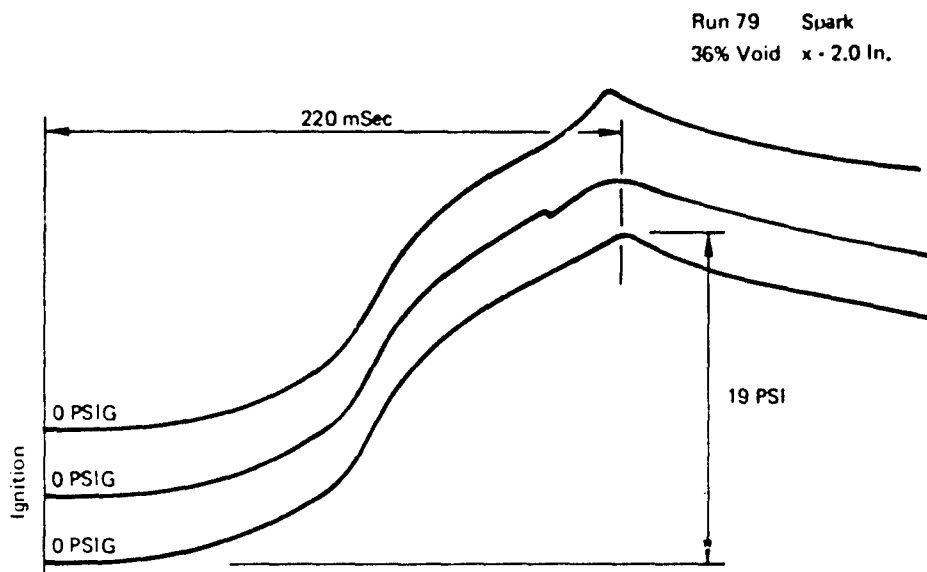
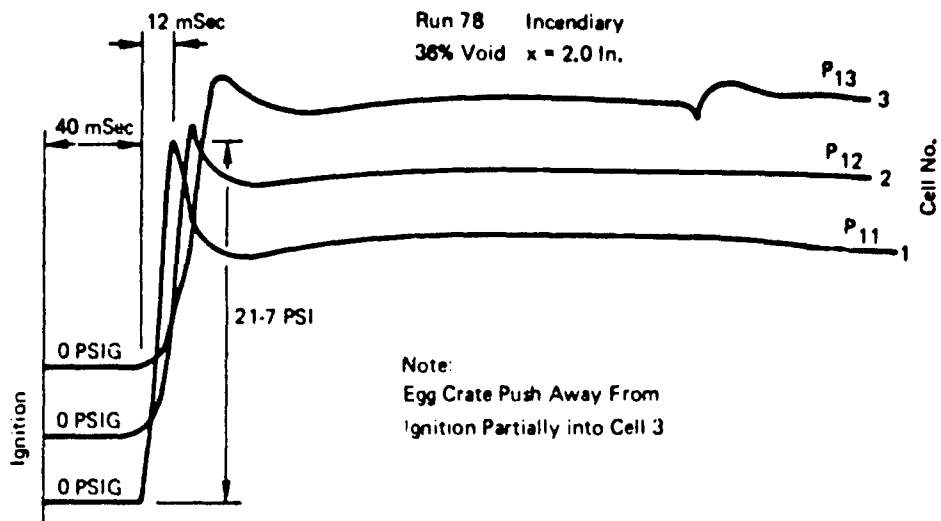
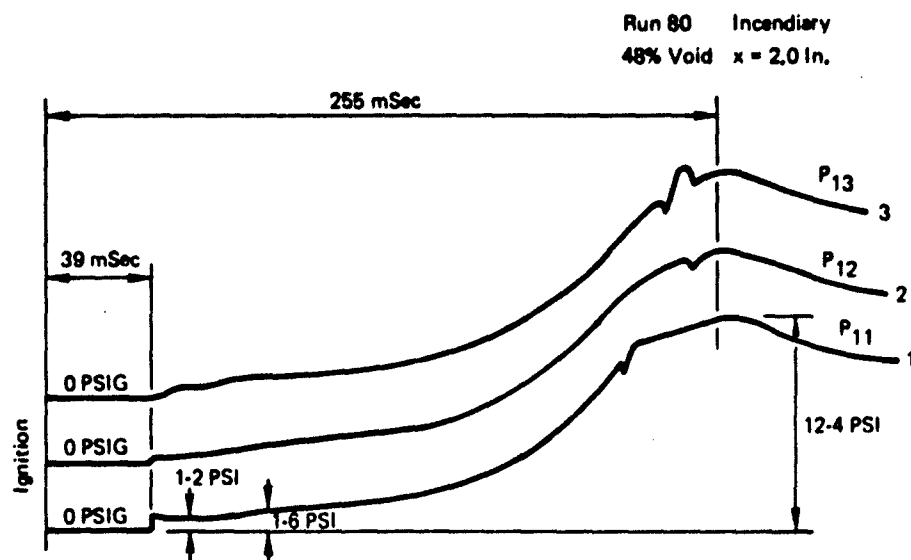


Figure B-27: Typical Large Wing Tank Pressure Traces Central Egg Crate (Runs 78 and 79)



NOTE: Run 81 was not plotted because the overpressure of 1.2 psig was considered too low to be of consequence.

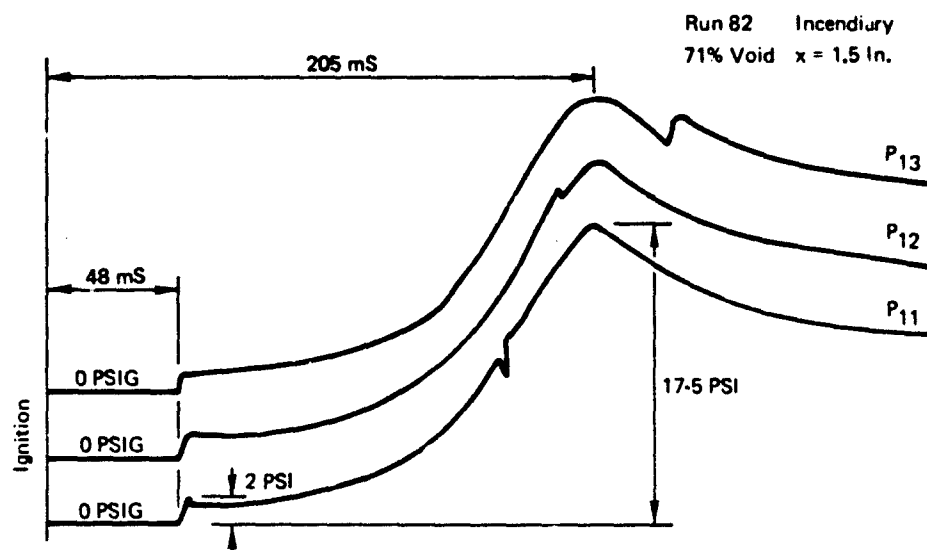


Figure B-28: Typical Large Wing Tank Pressure Traces, Total Egg Crate (Runs 80 and 82)

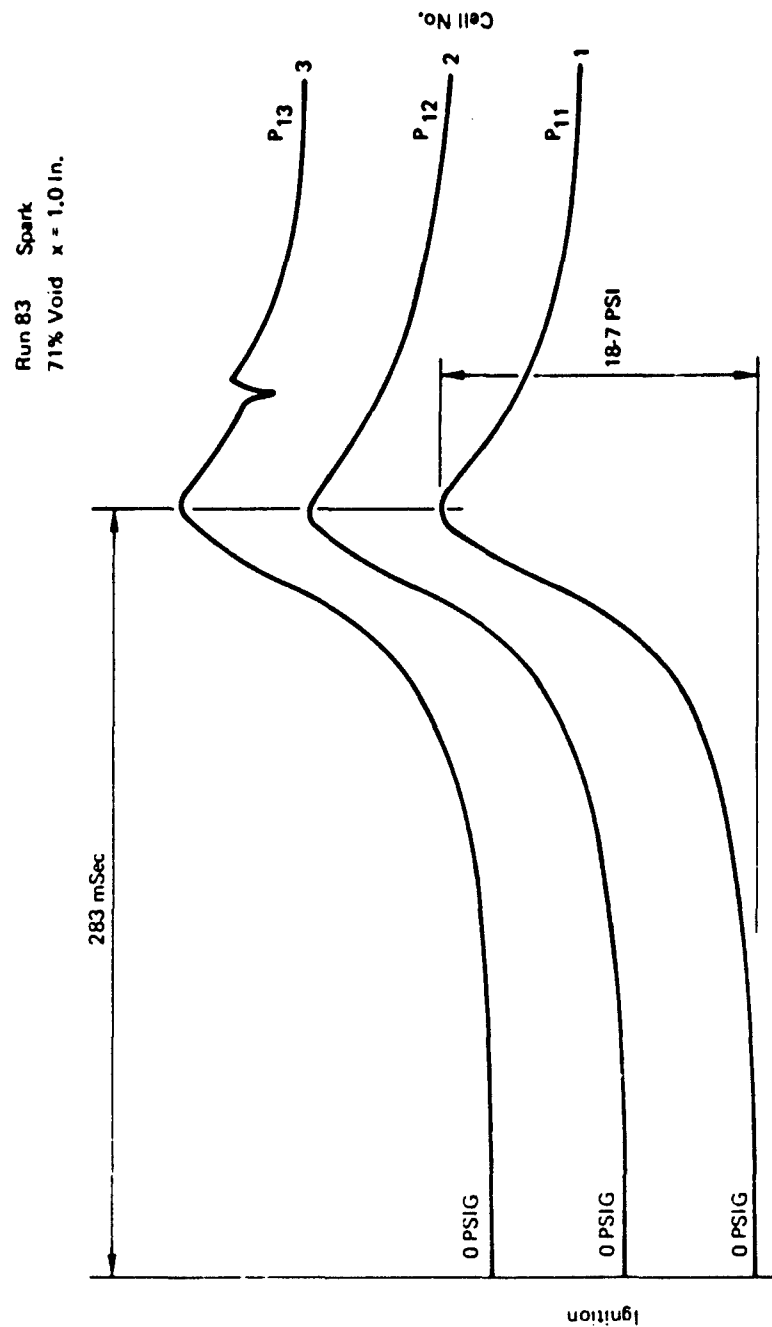


Figure D-29: Typical Large Wing Tank Pressure Traces, Total Egg Crate (Run 83)

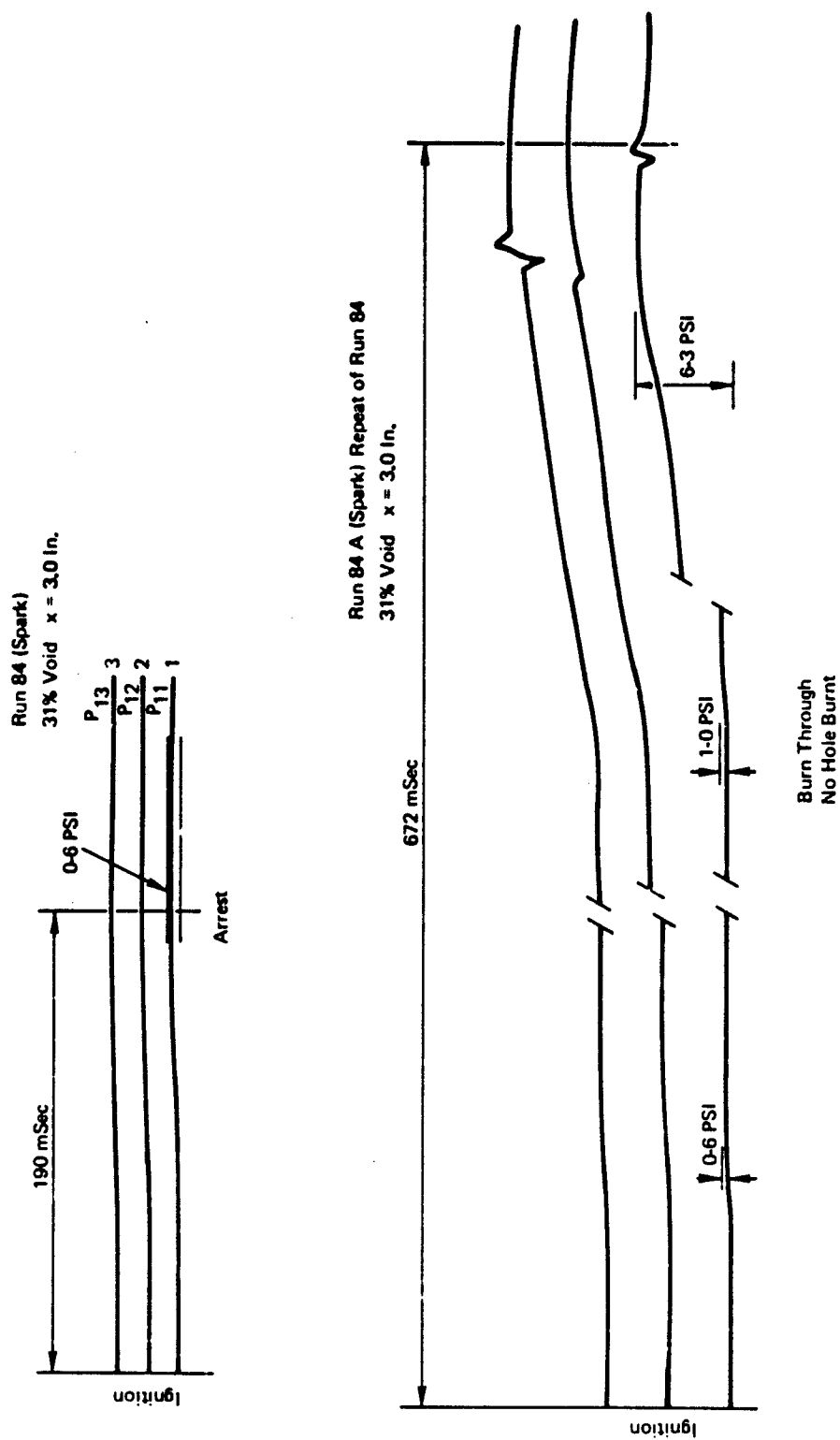


Figure E-30: Typical Large Wing Tank Pressure Traces, Total Egg Crave (Runs 84 and 84A)

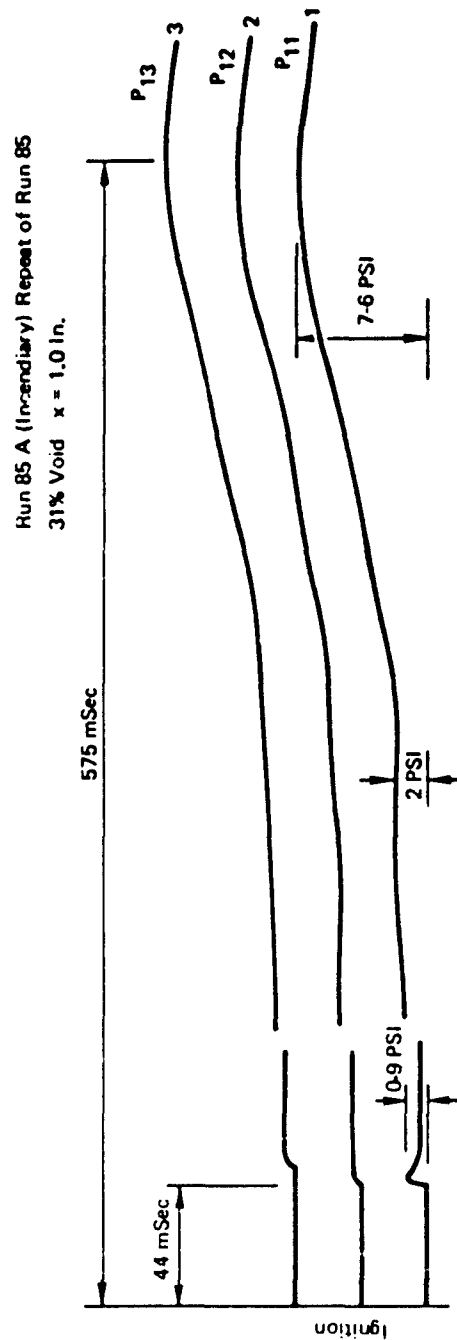
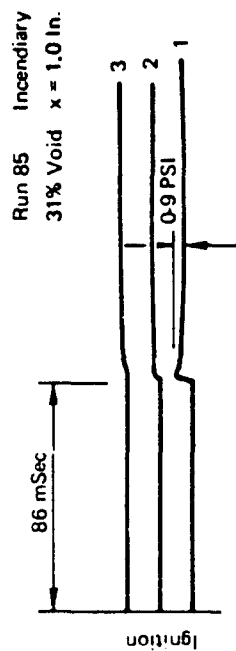


Figure B-31: Typical Large Wing Tank Pressure Traces, Total Egg Crate (Runs 85 and 85A)

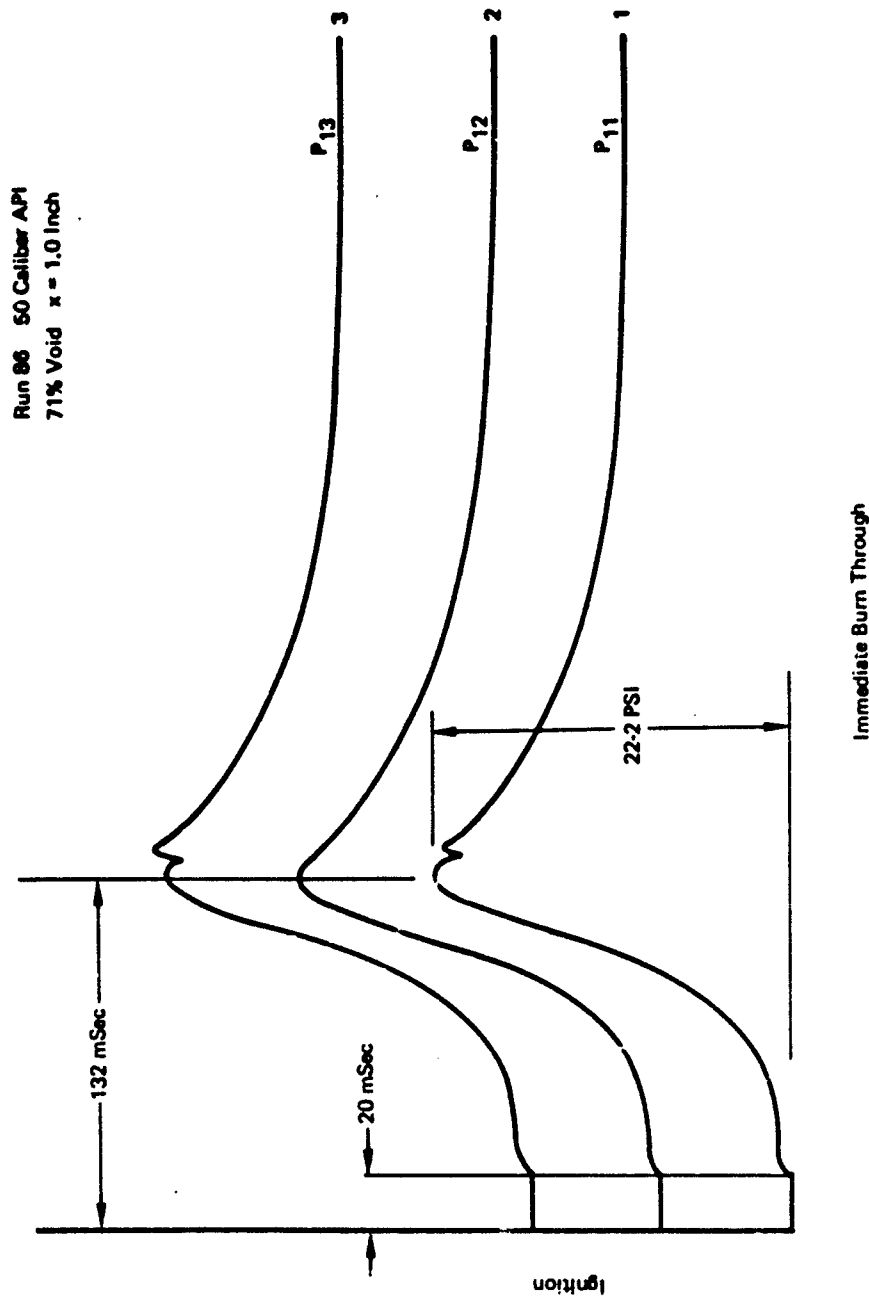


Figure B-32: Typical Large Wing Tank Pressure Trace,
Total Egg Crate Run 86

Run 87 50 Caliber API
48% Void $x = 2.0$ In.

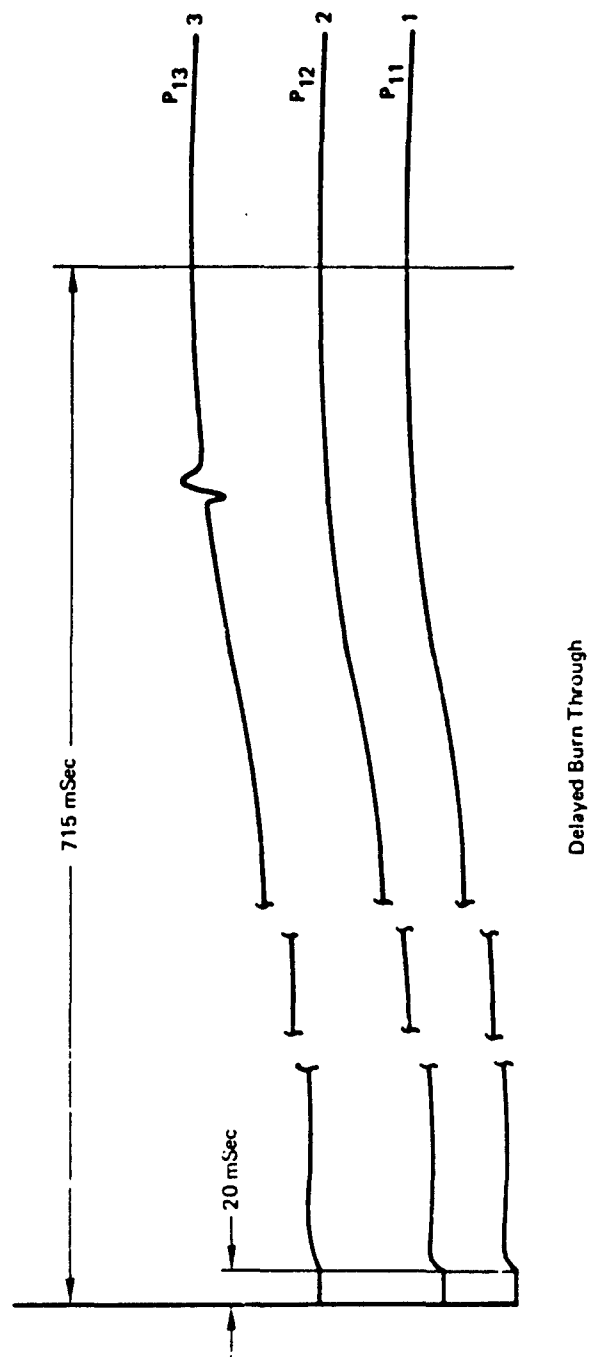


Figure B-33: Typical Large Wing Tank Pressure Trace, Run No. 87, Total Egg Crate

APPENDIX C
TASK III TEST DATA

3M Scotchbrite Felt

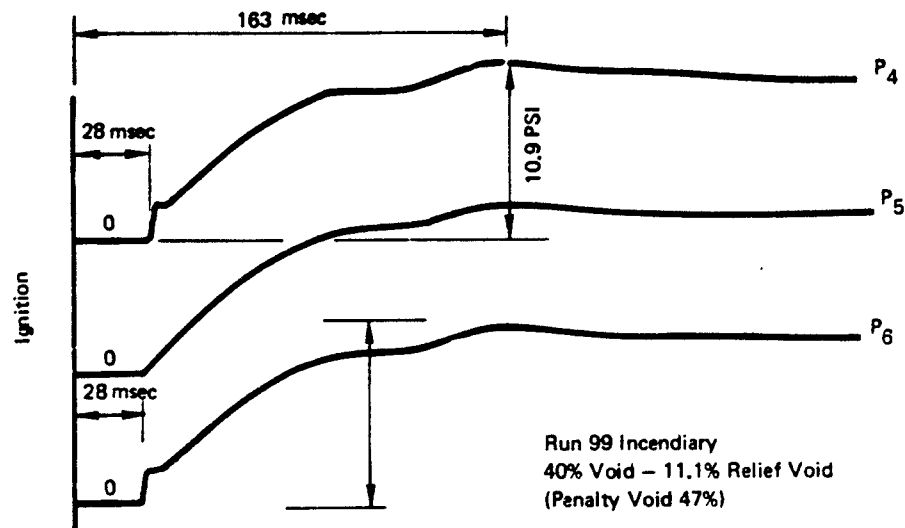
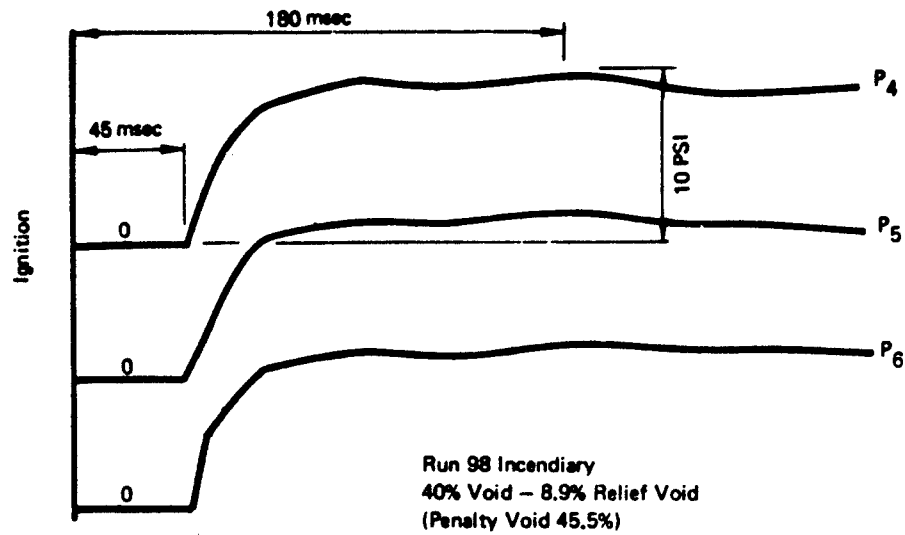


Figure C-1: Typical Pressure Traces for the Fuselage Tank Voided Top Wall Runs 98 and 99

3M Scotch Brite Felt

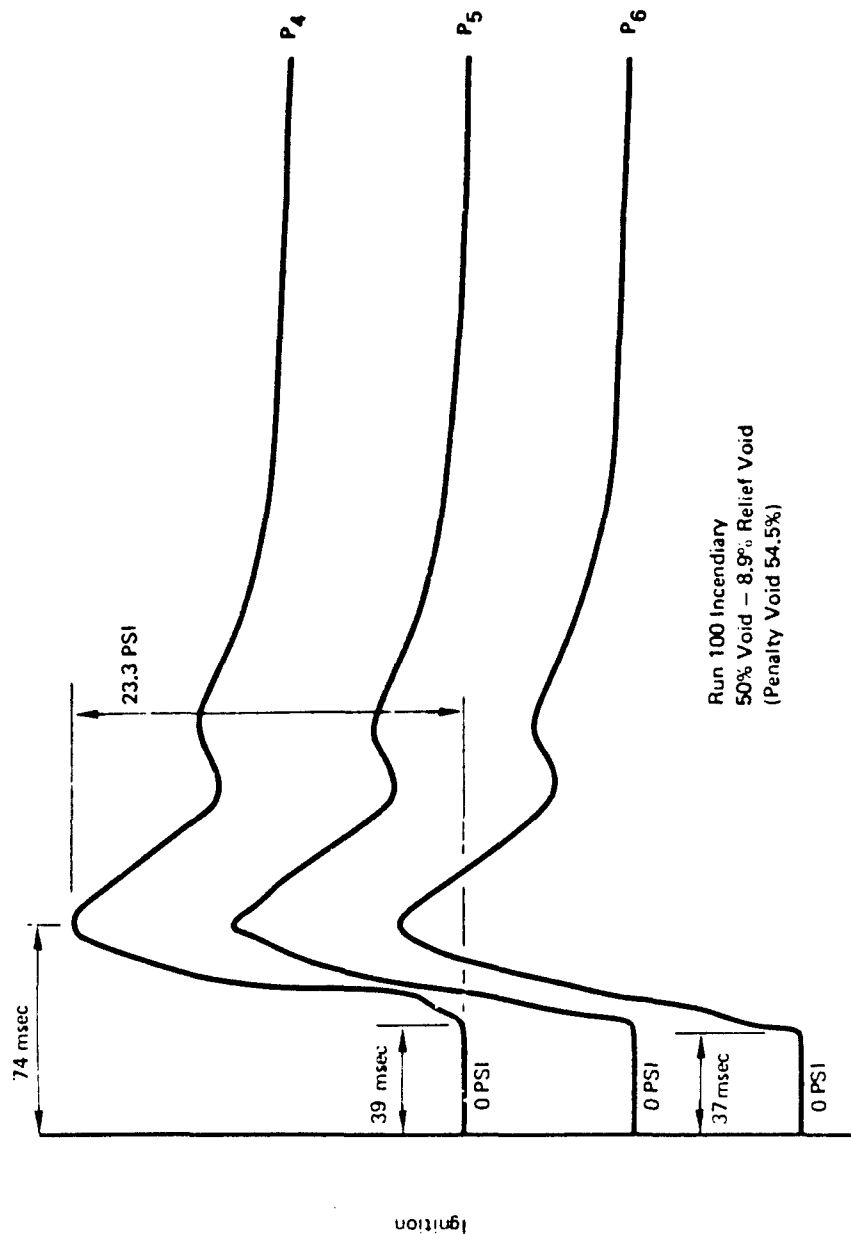


Figure C-2: Typical Pressure Trace for the Fuselage Tank Voided Top Wall - Run 100

3M Scotch Brite Felt

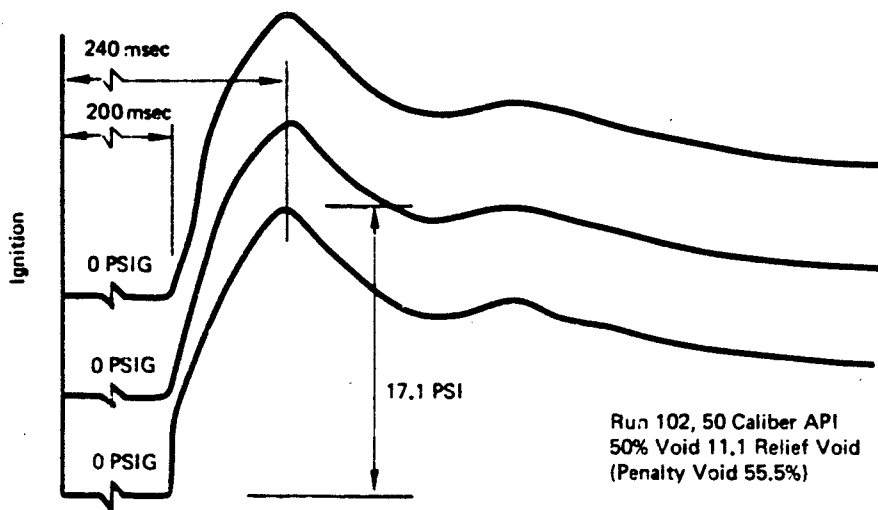
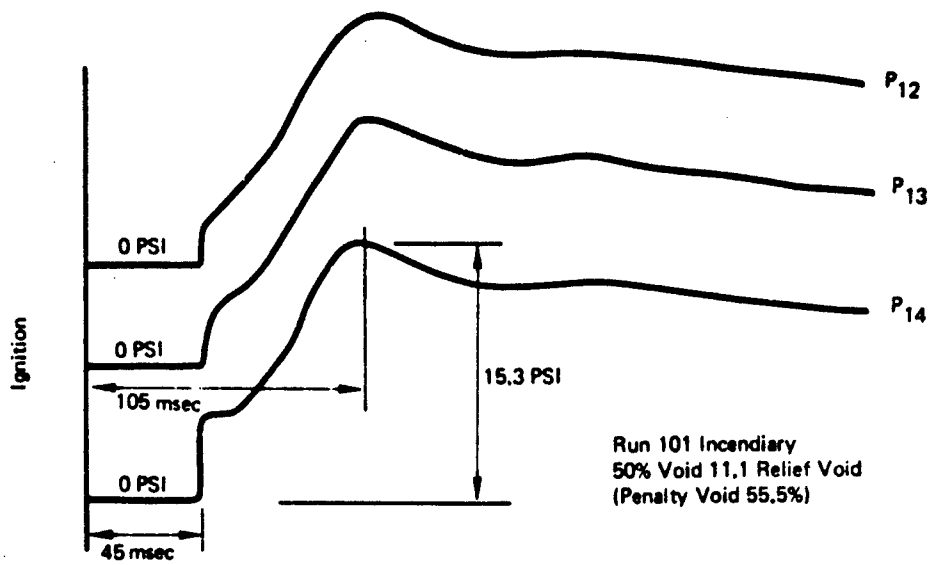


Figure C-3: Typical Pressure Trace for the Fuselage Tank Voided Top Wall
Run 101 and 102

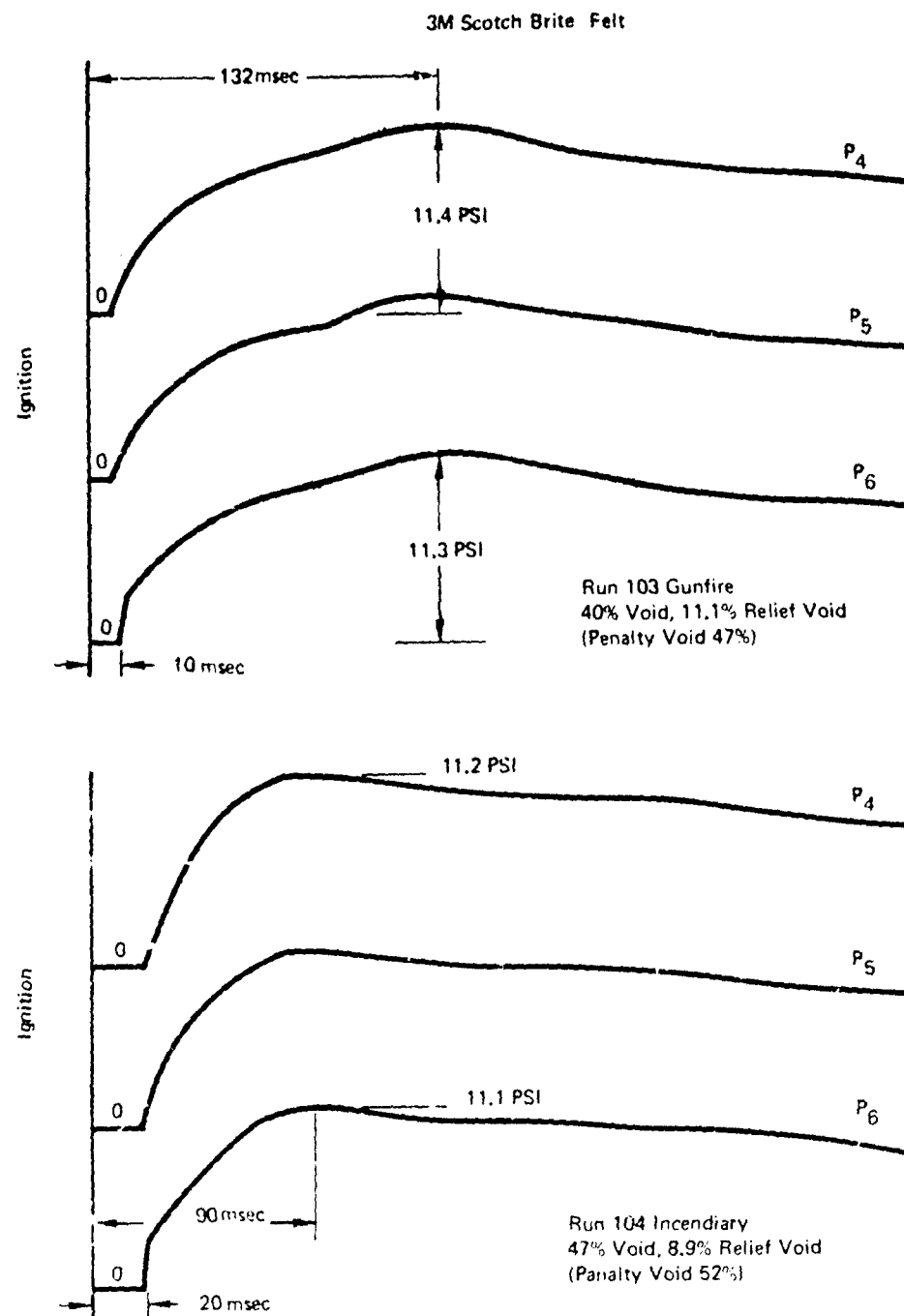


Figure C-4: Typical Pressure Trace for the Fuselage Tank Voided Top Wall
Runs 103 and 104

3M Scotch Brite Felt

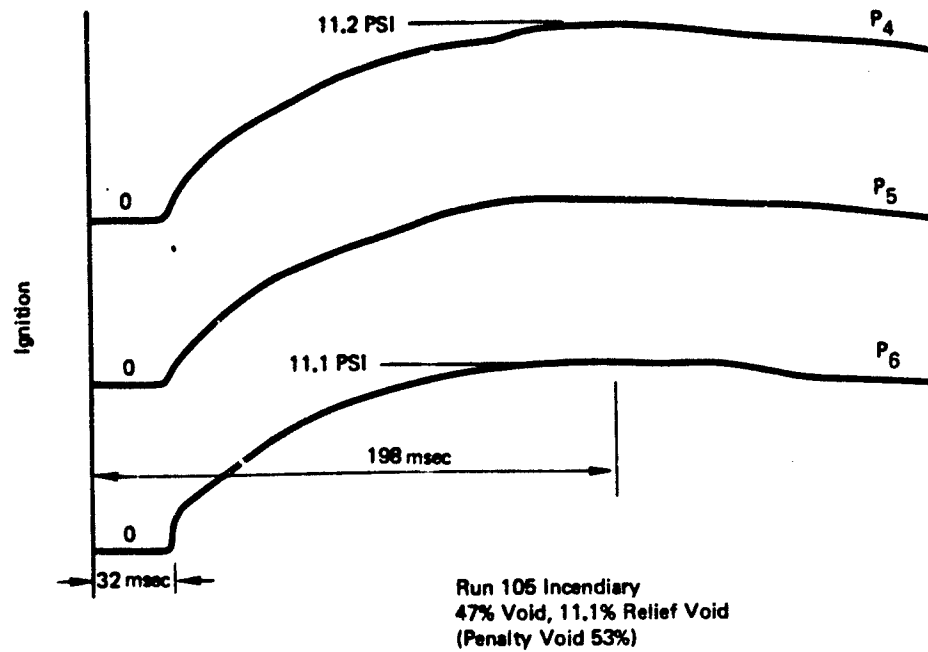


Figure C-5: Typical Pressure Trace for the Fuselage Tank Voided Top Wall Run 105

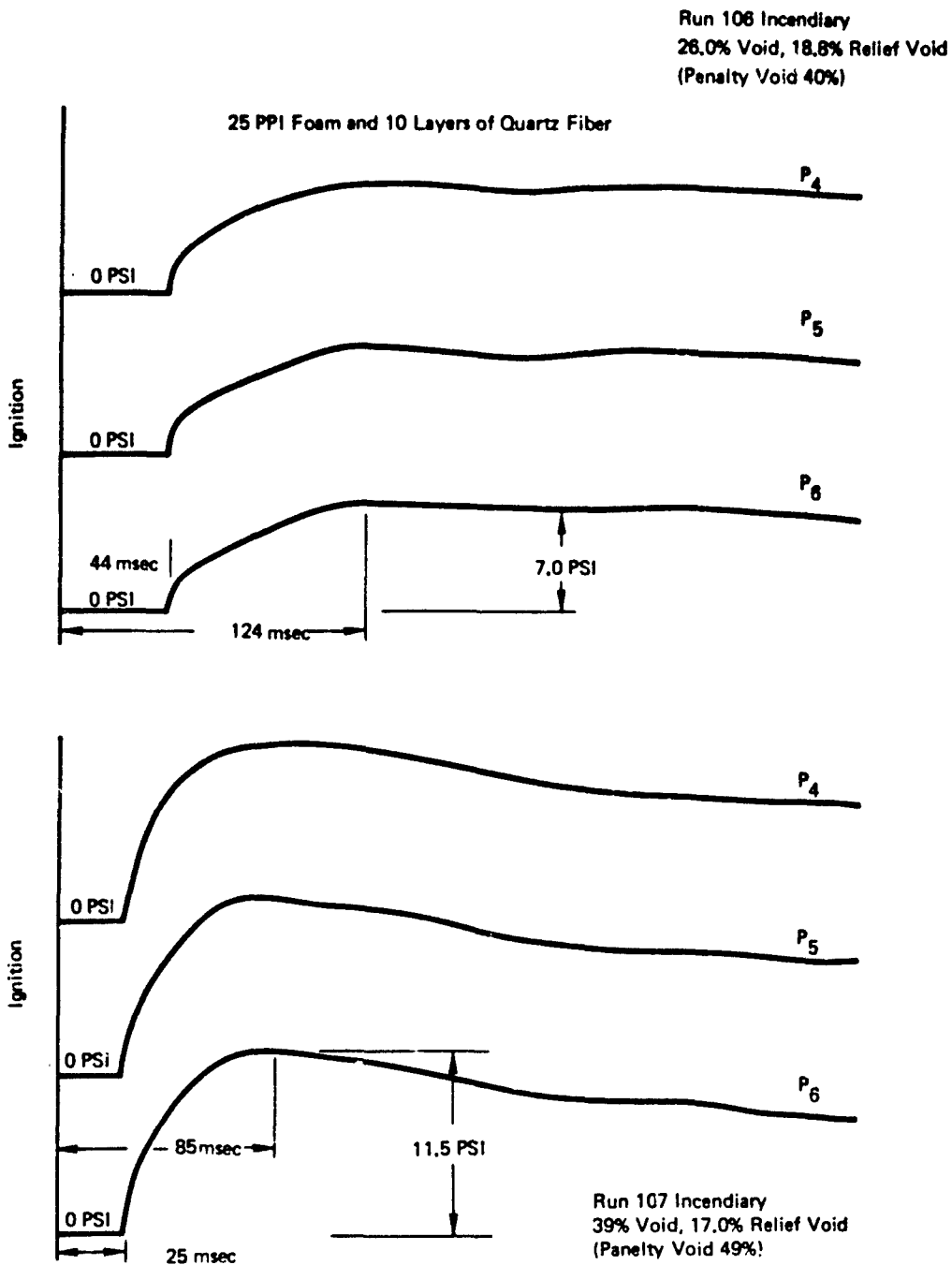
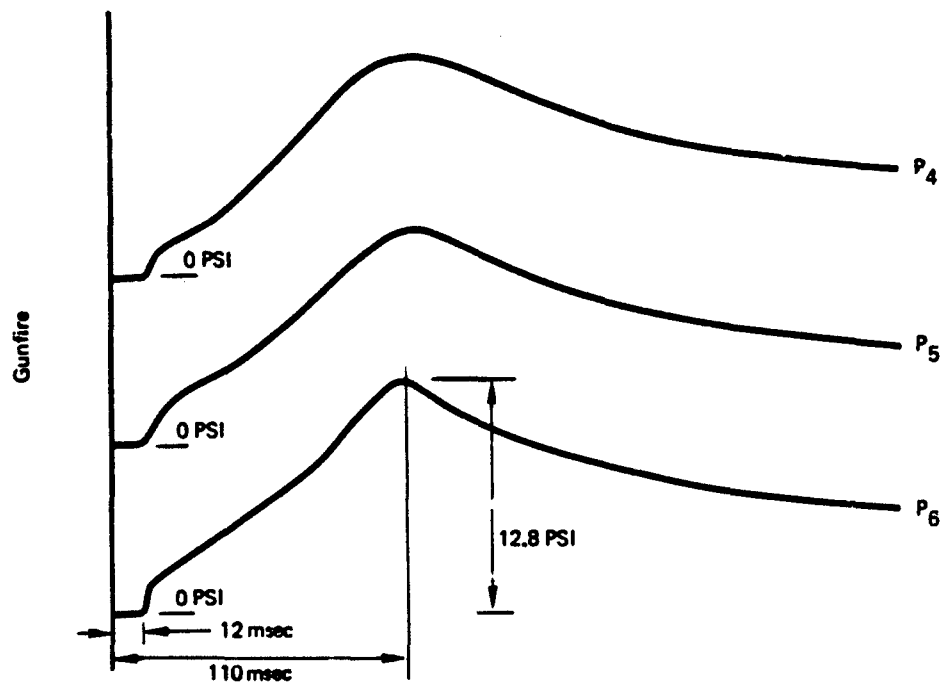


Figure C-6: Typical Pressure Traces for the Fuselage Tank Voided Lined Wall
Runs 106 and 107

25 PPI Foam and 10 Layers of Quartz Fiber



Run 108, 50 Caliber API
39% Void - 17.0 Relief Void
Penalty Void 49%

Figure C-7: Typical Pressure Traces for the Fuselage Tank Voided Lined Wall Run 108

25 PPI Foam and 10 Layers of Quartz Fiber

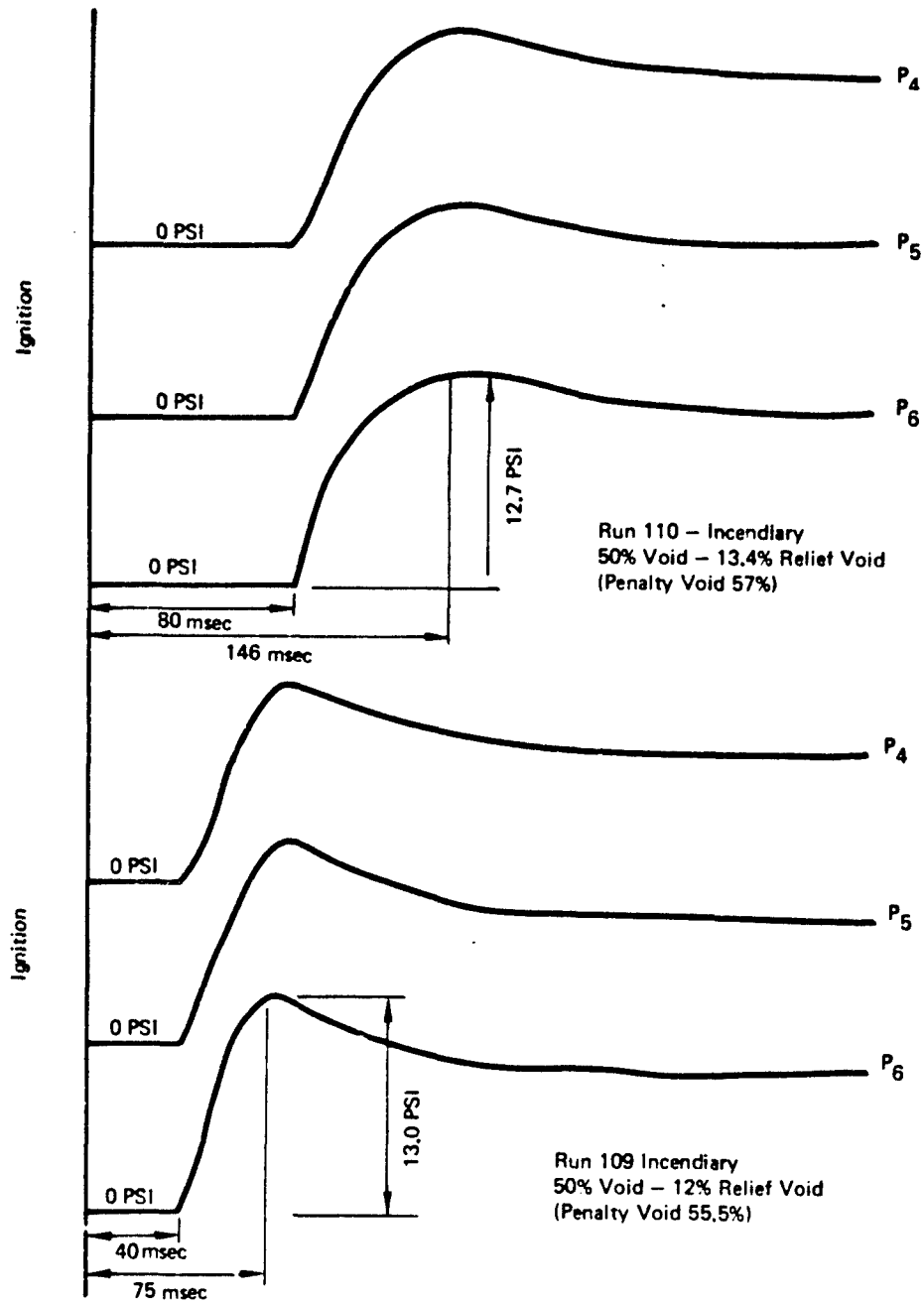


Figure C-8: Typical Pressure Traces for the Fuselage Tank Voided Top Wall
Runs 109 and 110

25 PPI Foam and 10 Layers of Quartz Fiber

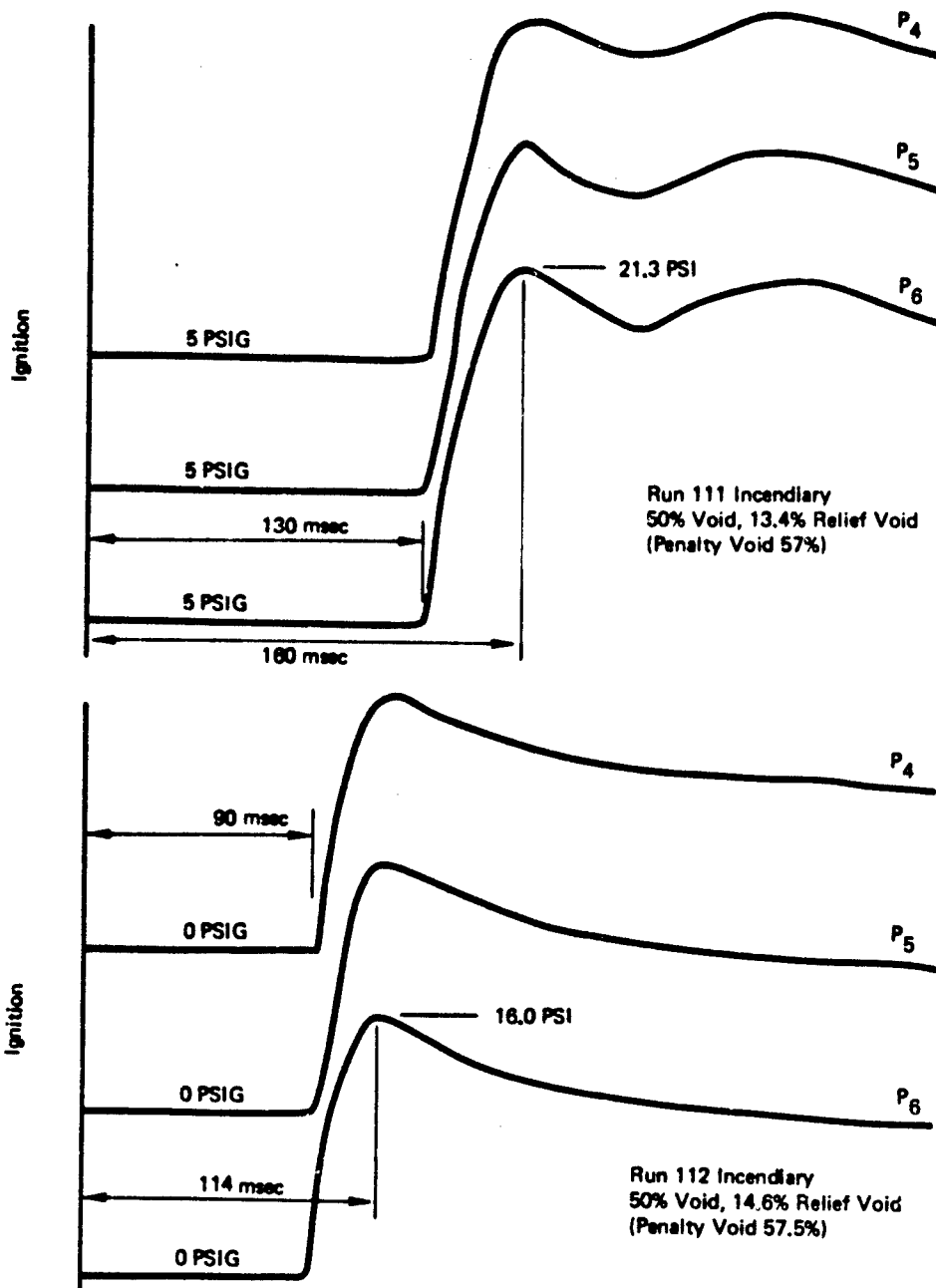
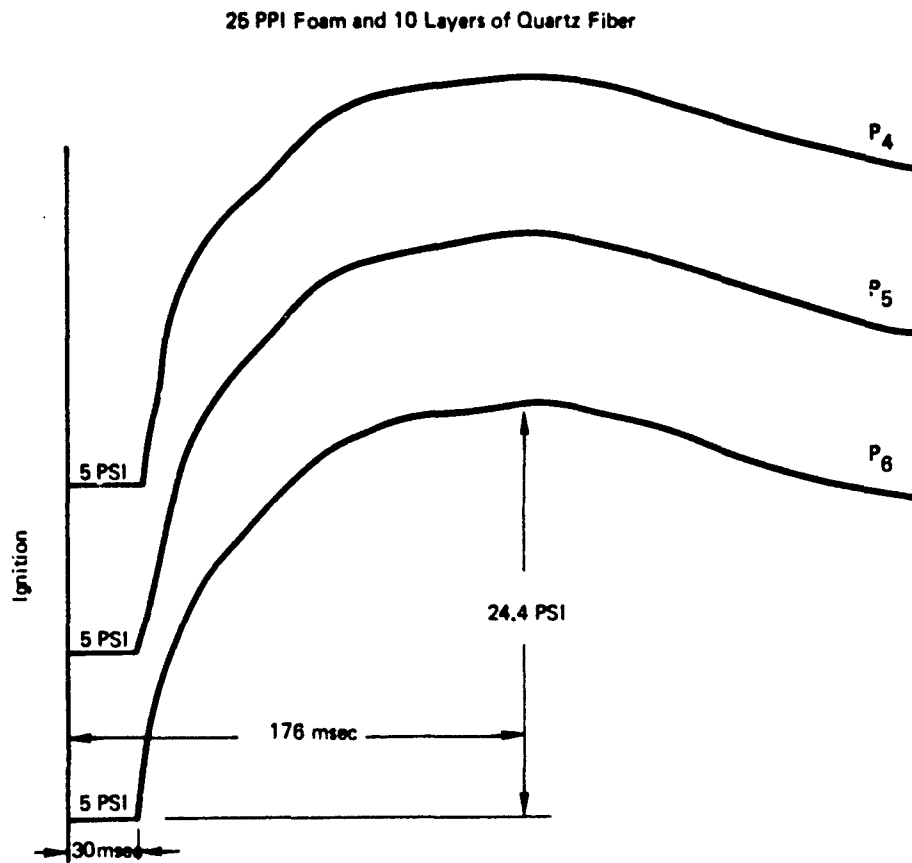


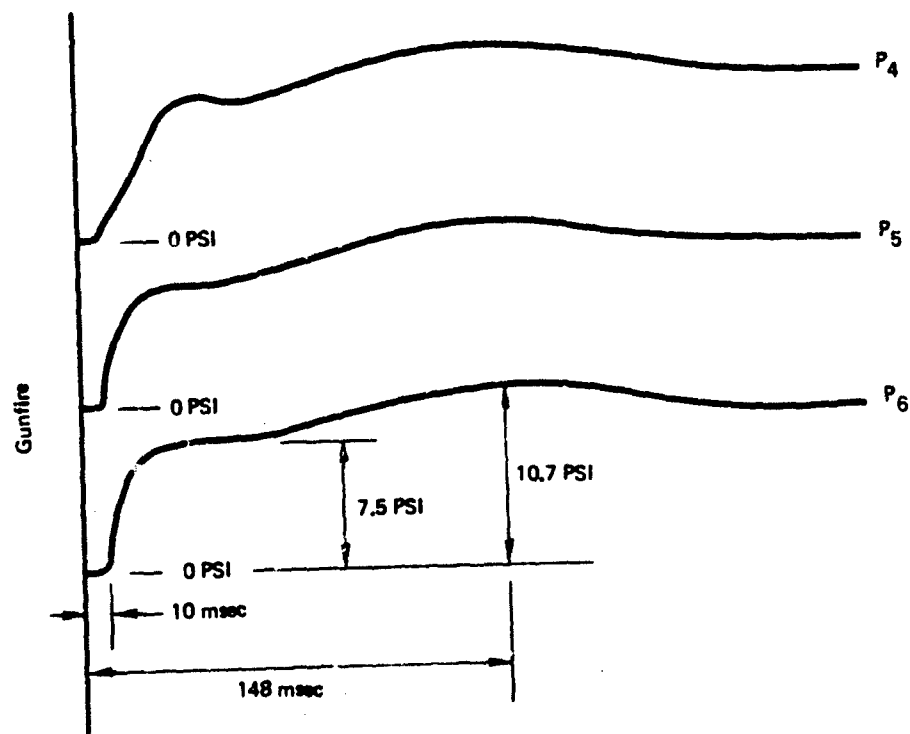
Figure C-9: Typical Pressure Traces for the Fuselage Tank Voided Top Wall
Runs 111 and 112



Run 113A Incendiary
 50% Void, 14.6% Relief Void
 (Penalty Void 57.5%)

Figure C-10: Typical Pressure Trace for the Fuselage Tank
 Voided Top Wall Run 113A

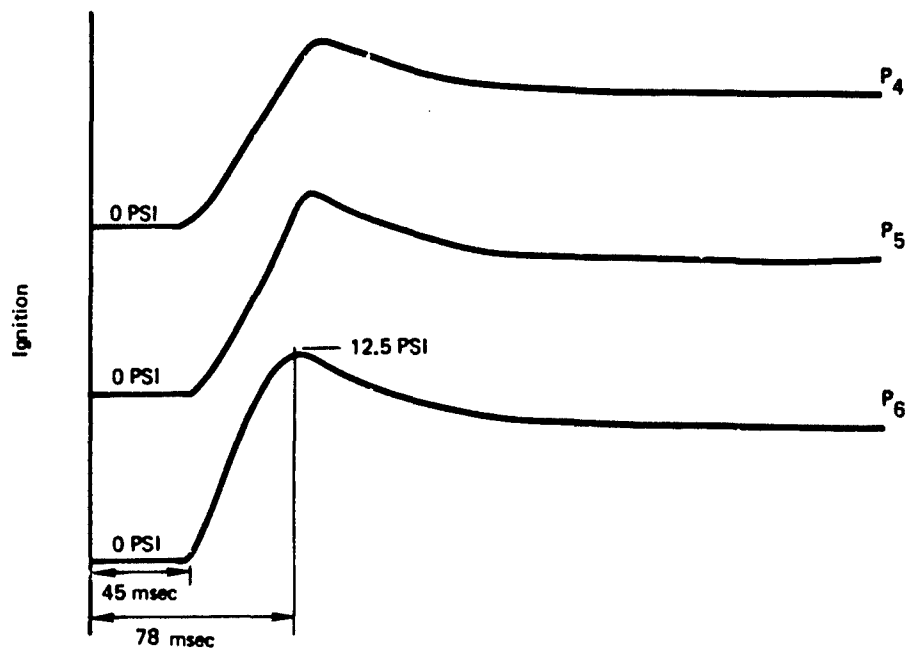
25 PPI Foam and 10 Layers of Quartz Fiber



Run 114, 50 Caliber API
50% Void, 14.6% Relief Void
(Penalty Void 57.5%)

Figure C-11: Typical Pressure Trace for the Fuselage Tank
Voided Top Wall Run 114

25 PPI Foam and 10 Layers of Quartz Fiber Backed with 2-Layers of
20 Mesh-016 Stainless Steel Screen



Run 115 Incendiary
50% Void, 12% Relief Void
(Penalty Void 55.5%)

Figure C-12: Typical Pressure Trace for the Fuselage Tank
Voided Top Wall Run 115

25 PPI Foam and 10 Layers of Quartz + Fiber Backed with 2-Layers of
20 Mesh-016 Stainless Steel Screen

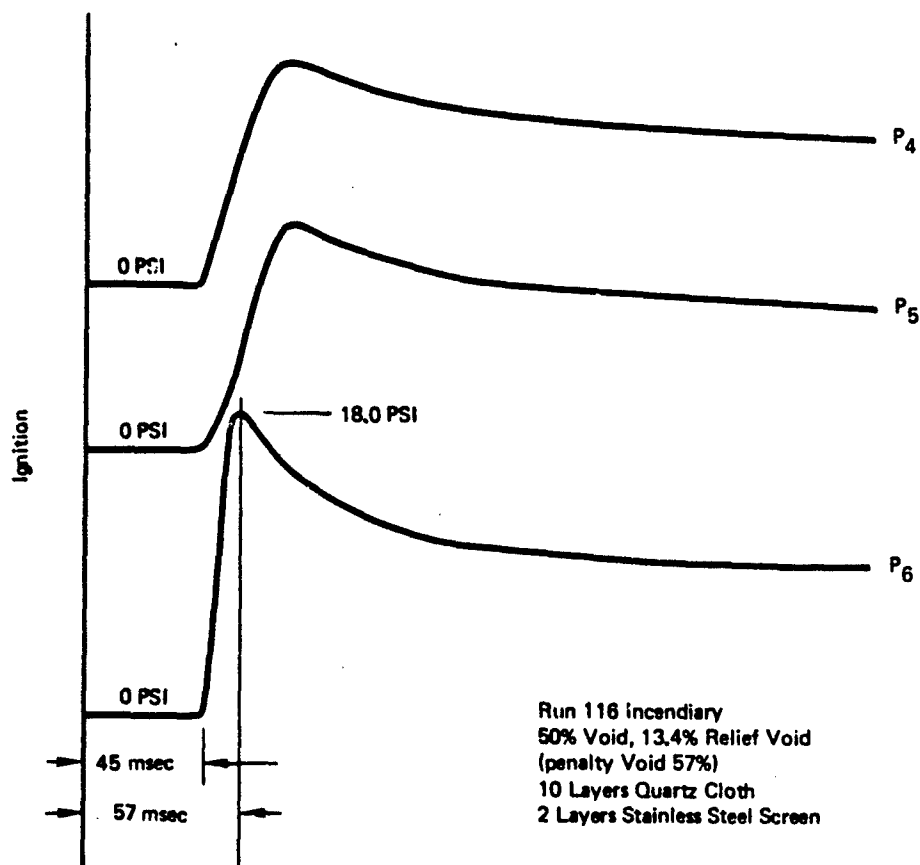
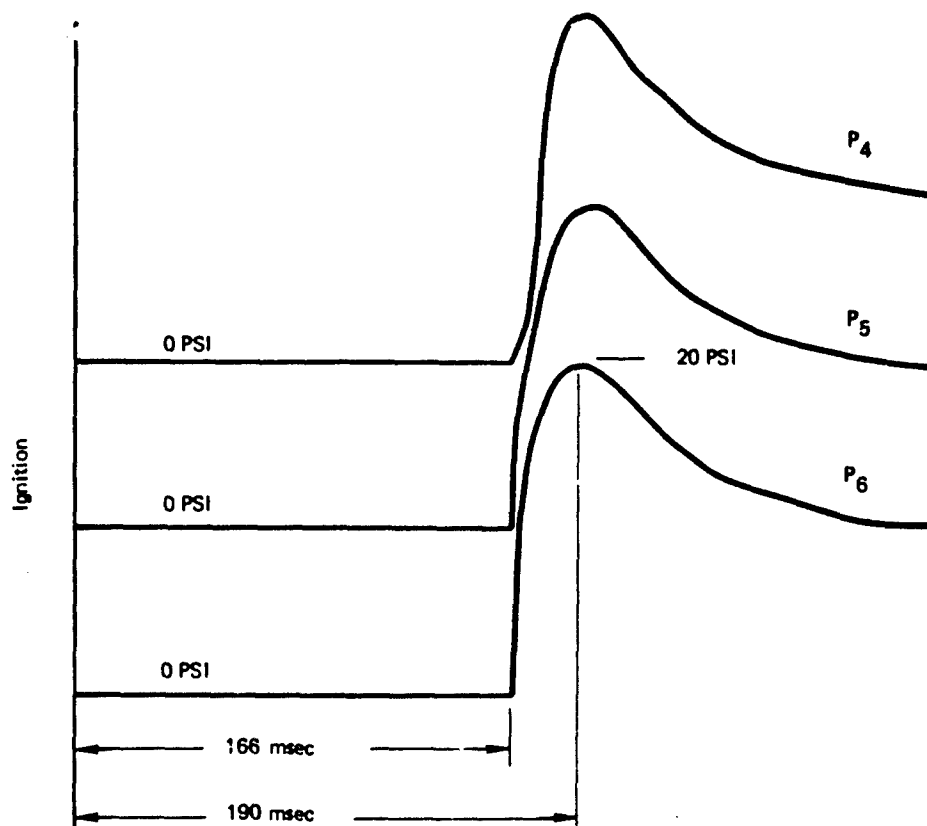


Figure C-13: Typical Pressure Trace for the Fuselage Tank
Voided Top Wall Run 116

25 PPI Foam and 10 Layers of Quartz Fiber Backed with 2 Layers of
20-Mesh-016 Stainless Steel Screen



Run 117 Incendiary
50% Void
14.6% Relief Void
(Penalty Void 57.5%)

Figure C-14: Typical Pressure Trace for the Fuselage Tank
Voided Top Wall Run 117

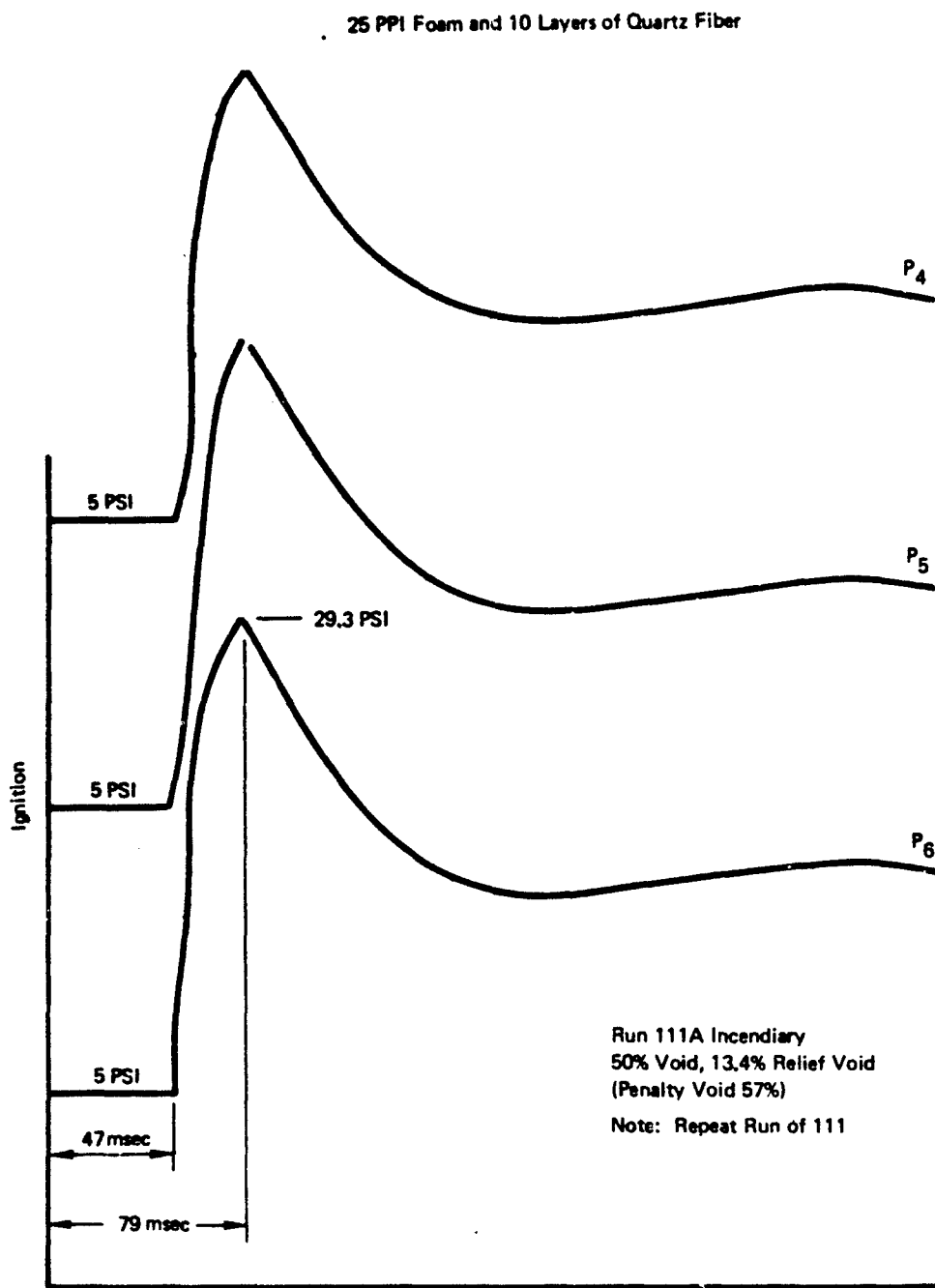


Figure C-15: Typical Pressure Trace for the Fuselage Tank
Voided Top Wall Run 111A

25 PPI Foam And 10 Layers of Quartz Fiber

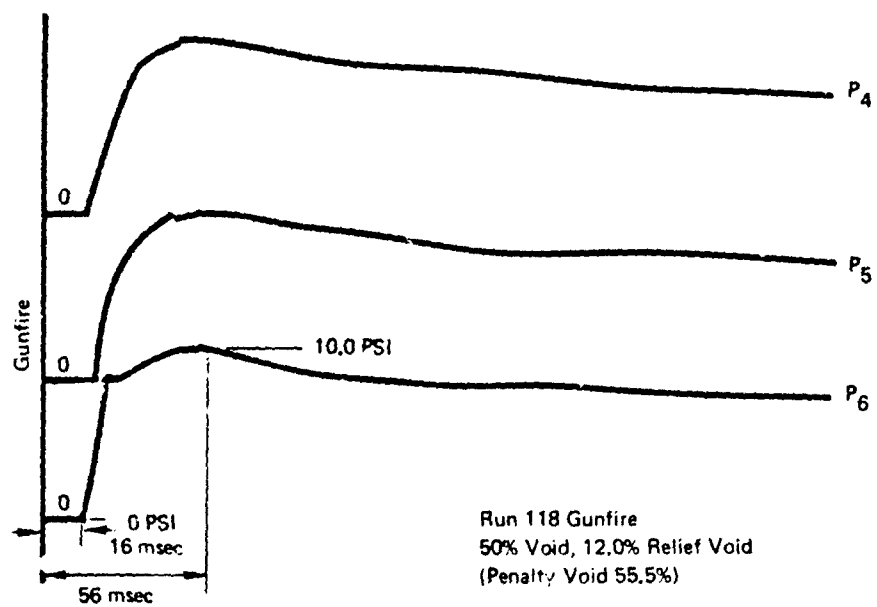


Figure C-16: Typical Pressure Trace for the Fuselage Tank
Voided Top Wall Run 118

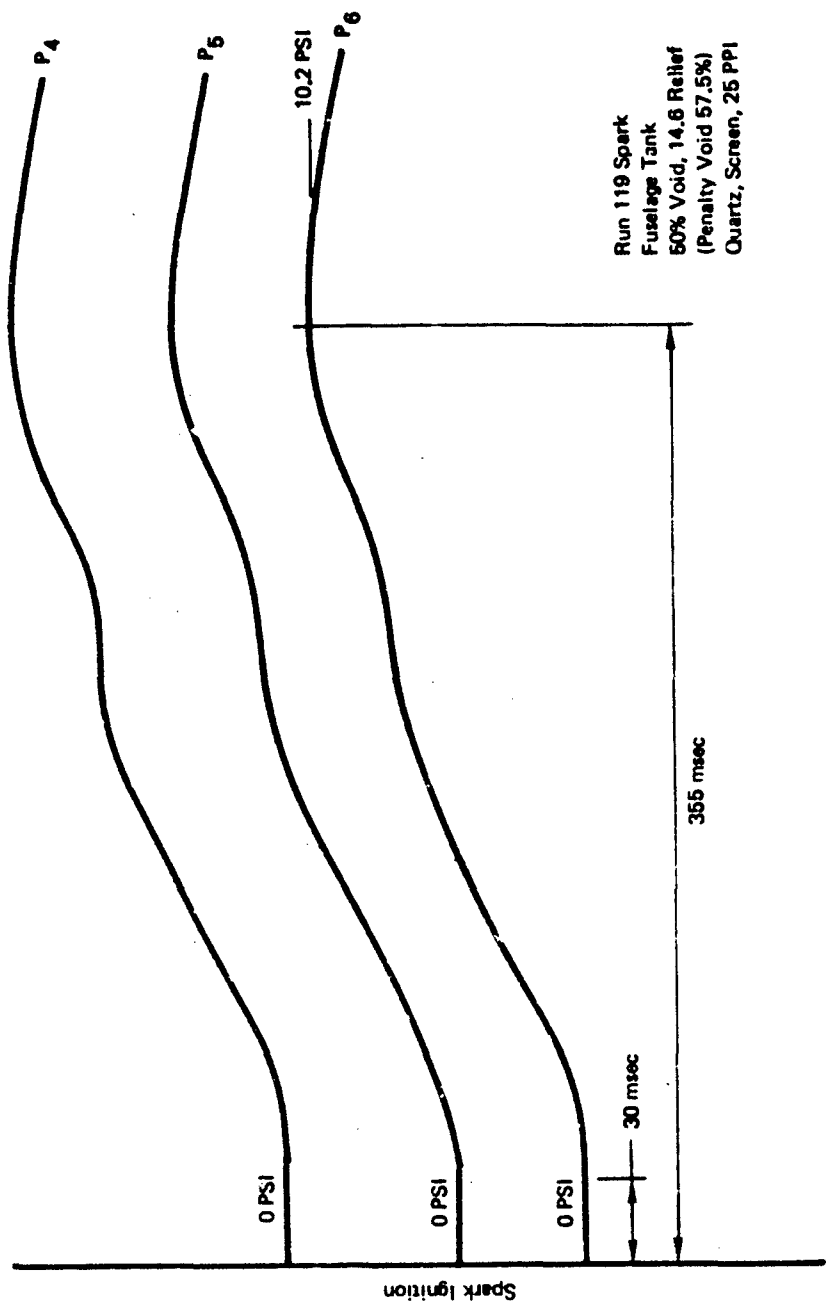


Figure C-17: Typical Pressure Trace for the Fuselage Tank
Voided Top Wall Run 119.

Table C-11: Small Wing Tankage Test Data Summary

RUN NUMBER	DATE	MATERIAL	NET WT	CONDITION	VOID CONFIGURATION	PERCENT VOID	FINAL VOID DUE TO BURNING ARRESTER			AMBIENT PRESSURE PPA			SOAK PRESSURES			INITIAL PRESSURES			IGNITION MODE			P.C.M.	TIME TO P ₁	REMARKS																																																																																																																																																																																																																																																																																																																																																																																																																																																																																																																																																																																																																																																							
							P ₁	P ₂	P ₃	P ₄	P ₅	P ₆	P ₇	P ₈	P ₉	P ₁₀	P ₁₁	P ₁₂	P ₁₃	P ₁₄	P ₁₅				P ₁₆	P ₁₇	P ₁₈	P ₁₉	P ₂₀																																																																																																																																																																																																																																																																																																																																																																																																																																																																																																																																																																																																																																																		
																								GLN FINE	GLN COARSE	GLN MEDIUM	GLN COARSE	GLN FINE	GLN MEDIUM	GLN COARSE	GLN FINE	GLN MEDIUM	GLN COARSE	GLN FINE	GLN MEDIUM	GLN COARSE	GLN FINE	GLN MEDIUM	GLN COARSE	GLN FINE	GLN MEDIUM	GLN COARSE	GLN FINE	GLN MEDIUM	GLN COARSE	GLN FINE	GLN MEDIUM	GLN COARSE	GLN FINE	GLN MEDIUM	GLN COARSE	GLN FINE	GLN MEDIUM	GLN COARSE	GLN FINE	GLN MEDIUM	GLN COARSE	GLN FINE	GLN MEDIUM	GLN COARSE	GLN FINE	GLN MEDIUM	GLN COARSE	GLN FINE	GLN MEDIUM	GLN COARSE	GLN FINE	GLN MEDIUM	GLN COARSE	GLN FINE	GLN MEDIUM	GLN COARSE	GLN FINE	GLN MEDIUM	GLN COARSE	GLN FINE	GLN MEDIUM	GLN COARSE	GLN FINE	GLN MEDIUM	GLN COARSE	GLN FINE	GLN MEDIUM	GLN COARSE	GLN FINE	GLN MEDIUM	GLN COARSE	GLN FINE	GLN MEDIUM	GLN COARSE	GLN FINE	GLN MEDIUM	GLN COARSE	GLN FINE	GLN MEDIUM	GLN COARSE	GLN FINE	GLN MEDIUM	GLN COARSE	GLN FINE	GLN MEDIUM	GLN COARSE	GLN FINE	GLN MEDIUM	GLN COARSE	GLN FINE	GLN MEDIUM	GLN COARSE	GLN FINE	GLN MEDIUM	GLN COARSE	GLN FINE	GLN MEDIUM	GLN COARSE	GLN FINE	GLN MEDIUM	GLN COARSE	GLN FINE	GLN MEDIUM	GLN COARSE	GLN FINE	GLN MEDIUM	GLN COARSE	GLN FINE	GLN MEDIUM	GLN COARSE	GLN FINE	GLN MEDIUM	GLN COARSE	GLN FINE	GLN MEDIUM	GLN COARSE	GLN FINE	GLN MEDIUM	GLN COARSE	GLN FINE	GLN MEDIUM	GLN COARSE	GLN FINE	GLN MEDIUM	GLN COARSE	GLN FINE	GLN MEDIUM	GLN COARSE	GLN FINE	GLN MEDIUM	GLN COARSE	GLN FINE	GLN MEDIUM	GLN COARSE	GLN FINE	GLN MEDIUM	GLN COARSE	GLN FINE	GLN MEDIUM	GLN COARSE	GLN FINE	GLN MEDIUM	GLN COARSE	GLN FINE	GLN MEDIUM	GLN COARSE	GLN FINE	GLN MEDIUM	GLN COARSE	GLN FINE	GLN MEDIUM	GLN COARSE	GLN FINE	GLN MEDIUM	GLN COARSE	GLN FINE	GLN MEDIUM	GLN COARSE	GLN FINE	GLN MEDIUM	GLN COARSE	GLN FINE	GLN MEDIUM	GLN COARSE	GLN FINE	GLN MEDIUM	GLN COARSE	GLN FINE	GLN MEDIUM	GLN COARSE	GLN FINE	GLN MEDIUM	GLN COARSE	GLN FINE	GLN MEDIUM	GLN COARSE	GLN FINE	GLN MEDIUM	GLN COARSE	GLN FINE	GLN MEDIUM	GLN COARSE	GLN FINE	GLN MEDIUM	GLN COARSE	GLN FINE	GLN MEDIUM	GLN COARSE	GLN FINE	GLN MEDIUM	GLN COARSE	GLN FINE	GLN MEDIUM	GLN COARSE	GLN FINE	GLN MEDIUM	GLN COARSE	GLN FINE	GLN MEDIUM	GLN COARSE	GLN FINE	GLN MEDIUM	GLN COARSE	GLN FINE	GLN MEDIUM	GLN COARSE	GLN FINE	GLN MEDIUM	GLN COARSE	GLN FINE	GLN MEDIUM	GLN COARSE	GLN FINE	GLN MEDIUM	GLN COARSE	GLN FINE	GLN MEDIUM	GLN COARSE	GLN FINE	GLN MEDIUM	GLN COARSE	GLN FINE	GLN MEDIUM	GLN COARSE	GLN FINE	GLN MEDIUM	GLN COARSE	GLN FINE	GLN MEDIUM	GLN COARSE	GLN FINE	GLN MEDIUM	GLN COARSE	GLN FINE	GLN MEDIUM	GLN COARSE	GLN FINE	GLN MEDIUM	GLN COARSE	GLN FINE	GLN MEDIUM	GLN COARSE	GLN FINE	GLN MEDIUM	GLN COARSE	GLN FINE	GLN MEDIUM	GLN COARSE	GLN FINE	GLN MEDIUM	GLN COARSE	GLN FINE	GLN MEDIUM	GLN COARSE	GLN FINE	GLN MEDIUM	GLN COARSE	GLN FINE	GLN MEDIUM	GLN COARSE	GLN FINE	GLN MEDIUM	GLN COARSE	GLN FINE	GLN MEDIUM	GLN COARSE	GLN FINE	GLN MEDIUM	GLN COARSE	GLN FINE	GLN MEDIUM	GLN COARSE	GLN FINE	GLN MEDIUM	GLN COARSE	GLN FINE	GLN MEDIUM	GLN COARSE	GLN FINE	GLN MEDIUM	GLN COARSE	GLN FINE	GLN MEDIUM	GLN COARSE	GLN FINE	GLN MEDIUM	GLN COARSE	GLN FINE	GLN MEDIUM	GLN COARSE	GLN FINE	GLN MEDIUM	GLN COARSE	GLN FINE	GLN MEDIUM	GLN COARSE	GLN FINE	GLN MEDIUM	GLN COARSE	GLN FINE	GLN MEDIUM	GLN COARSE	GLN FINE	GLN MEDIUM	GLN COARSE	GLN FINE	GLN MEDIUM	GLN COARSE	GLN FINE	GLN MEDIUM	GLN COARSE	GLN FINE	GLN MEDIUM	GLN COARSE	GLN FINE	GLN MEDIUM	GLN COARSE	GLN FINE	GLN MEDIUM	GLN COARSE	GLN FINE	GLN MEDIUM	GLN COARSE	GLN FINE	GLN MEDIUM	GLN COARSE	GLN FINE	GLN MEDIUM	GLN COARSE	GLN FINE	GLN MEDIUM	GLN COARSE	GLN FINE	GLN MEDIUM	GLN COARSE	GLN FINE	GLN MEDIUM	GLN COARSE	GLN FINE	GLN MEDIUM	GLN COARSE	GLN FINE	GLN MEDIUM	GLN COARSE	GLN FINE	GLN MEDIUM	GLN COARSE	GLN FINE	GLN MEDIUM	GLN COARSE	GLN FINE	GLN MEDIUM	GLN COARSE	GLN FINE	GLN MEDIUM	GLN COARSE	GLN FINE	GLN MEDIUM	GLN COARSE	GLN FINE	GLN MEDIUM	GLN COARSE	GLN FINE	GLN MEDIUM	GLN COARSE	GLN FINE	GLN MEDIUM	GLN COARSE	GLN FINE	GLN MEDIUM	GLN COARSE	GLN FINE	GLN MEDIUM	GLN COARSE	GLN FINE	GLN MEDIUM	GLN COARSE	GLN FINE	GLN MEDIUM	GLN COARSE	GLN FINE	GLN MEDIUM	GLN COARSE	GLN FINE	GLN MEDIUM	GLN COARSE	GLN FINE	GLN MEDIUM	GLN COARSE	GLN FINE	GLN MEDIUM	GLN COARSE	GLN FINE	GLN MEDIUM	GLN COARSE	GLN FINE	GLN MEDIUM	GLN COARSE	GLN FINE	GLN MEDIUM	GLN COARSE	GLN FINE	GLN MEDIUM	GLN COARSE	GLN FINE	GLN MEDIUM	GLN COARSE	GLN FINE	GLN MEDIUM	GLN COARSE	GLN FINE	GLN MEDIUM	GLN COARSE	GLN FINE	GLN MEDIUM	GLN COARSE	GLN FINE	GLN MEDIUM	GLN COARSE	GLN FINE	GLN MEDIUM	GLN COARSE	GLN FINE	GLN MEDIUM	GLN COARSE	GLN FINE	GLN MEDIUM	GLN COARSE	GLN FINE	GLN MEDIUM	GLN COARSE	GLN FINE	GLN MEDIUM	GLN COARSE	GLN FINE	GLN MEDIUM	GLN COARSE	GLN FINE	GLN MEDIUM	GLN COARSE	GLN FINE	GLN MEDIUM	GLN COARSE	GLN FINE	GLN MEDIUM	GLN COARSE	GLN FINE	GLN MEDIUM	GLN COARSE	GLN FINE	GLN MEDIUM	GLN COARSE	GLN FINE	GLN MEDIUM	GLN COARSE	GLN FINE	GLN MEDIUM	GLN COARSE	GLN FINE	GLN MEDIUM	GLN COARSE	GLN FINE	GLN MEDIUM	GLN COARSE	GLN FINE	GLN MEDIUM	GLN COARSE	GLN FINE	GLN MEDIUM	GLN COARSE	GLN FINE	GLN MEDIUM	GLN COARSE	GLN FINE	GLN MEDIUM	GLN COARSE	GLN FINE	GLN MEDIUM	GLN COARSE	GLN FINE	GLN MEDIUM	GLN COARSE	GLN FINE	GLN MEDIUM	GLN COARSE	GLN FINE	GLN MEDIUM	GLN COARSE	GLN FINE	GLN MEDIUM	GLN COARSE	GLN FINE	GLN MEDIUM	GLN COARSE	GLN FINE	GLN MEDIUM	GLN COARSE	GLN FINE	GLN MEDIUM	GLN COARSE	GLN FINE	GLN MEDIUM	GLN COARSE	GLN FINE	GLN MEDIUM	GLN COARSE	GLN FINE	GLN MEDIUM	GLN COARSE	GLN FINE	GLN MEDIUM	GLN COARSE	GLN FINE	GLN MEDIUM	GLN COARSE	GLN FINE	GLN MEDIUM	GLN COARSE	GLN FINE	GLN MEDIUM	GLN COARSE	GLN FINE	GLN MEDIUM	GLN COARSE	GLN FINE	GLN MEDIUM	GLN COARSE	GLN FINE	GLN MEDIUM	GLN COARSE	GLN FINE	GLN MEDIUM	GLN COARSE	GLN FINE	GLN MEDIUM	GLN COARSE	GLN FINE	GLN MEDIUM	GLN COARSE	GLN FINE	GLN MEDIUM	GLN COARSE	GLN FINE	GLN MEDIUM	GLN COARSE	GLN FINE	GLN MEDIUM	GLN COARSE	GLN FINE	GLN MEDIUM	GLN COARSE	GLN FINE	GLN MEDIUM	GLN COARSE	GLN FINE	GLN MEDIUM	GLN COARSE	GLN FINE	GLN MEDIUM	GLN COARSE	GLN FINE	GLN MEDIUM	GLN COARSE	GLN FINE	GLN MEDIUM	GLN COARSE	GLN FINE	GLN MEDIUM	GLN COARSE	GLN FINE	GLN MEDIUM	GLN COARSE	GLN FINE	GLN MEDIUM	GLN COARSE	GLN FINE	GLN MEDIUM	GLN COARSE	GLN FINE	GLN MEDIUM	GLN COARSE	GLN FINE	GLN MEDIUM	GLN COARSE	GLN FINE	GLN MEDIUM	GLN COARSE	GLN FINE	GLN MEDIUM	GLN COARSE	GLN FINE	GLN MEDIUM	GLN COARSE	GLN FINE	GLN MEDIUM	GLN COARSE	GLN FINE	GLN MEDIUM	GLN COARSE	GLN FINE	GLN MEDIUM	GLN COARSE	GLN FINE	GLN MEDIUM	GLN COARSE	GLN FINE	GLN MEDIUM	GLN COARSE	GLN FINE	GLN MEDIUM	GLN COARSE	GLN FINE	GLN MEDIUM	GLN COARSE	GLN FINE	GLN MEDIUM	GLN COARSE	GLN FINE	GLN MEDIUM	GLN COARSE	GLN FINE	GLN MEDIUM	GLN COARSE	GLN FINE	GLN MEDIUM	GLN COARSE	GLN FINE	GLN MEDIUM	GLN COARSE	GLN FINE	GLN MEDIUM	GLN COARSE	GLN FINE	GLN MEDIUM	GLN COARSE	GLN FINE	GLN MEDIUM	GLN COARSE	GLN FINE

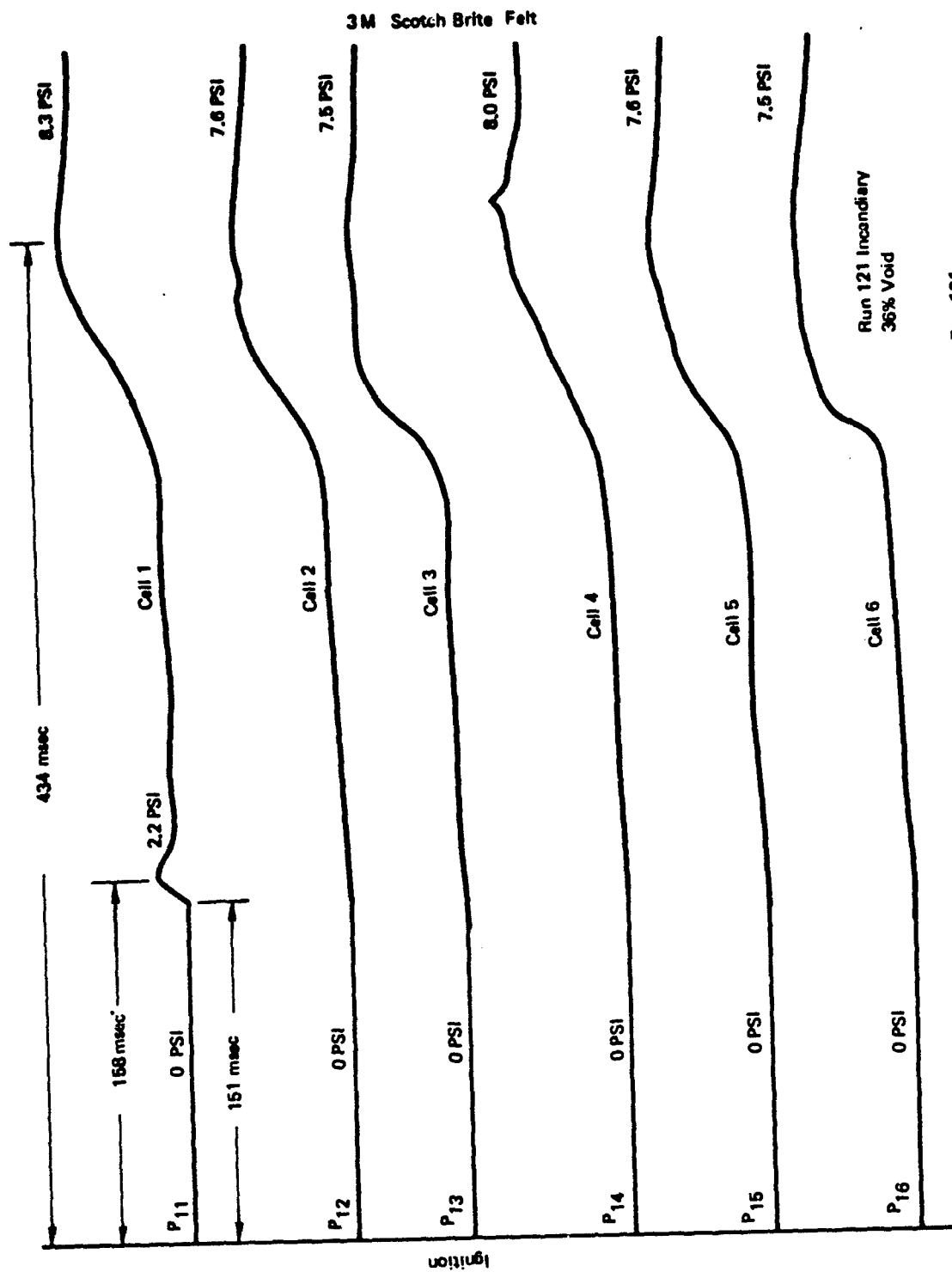


Figure C-18: Typical Pressure Traces for the Small Wing Tankage Egg Crate Run 121

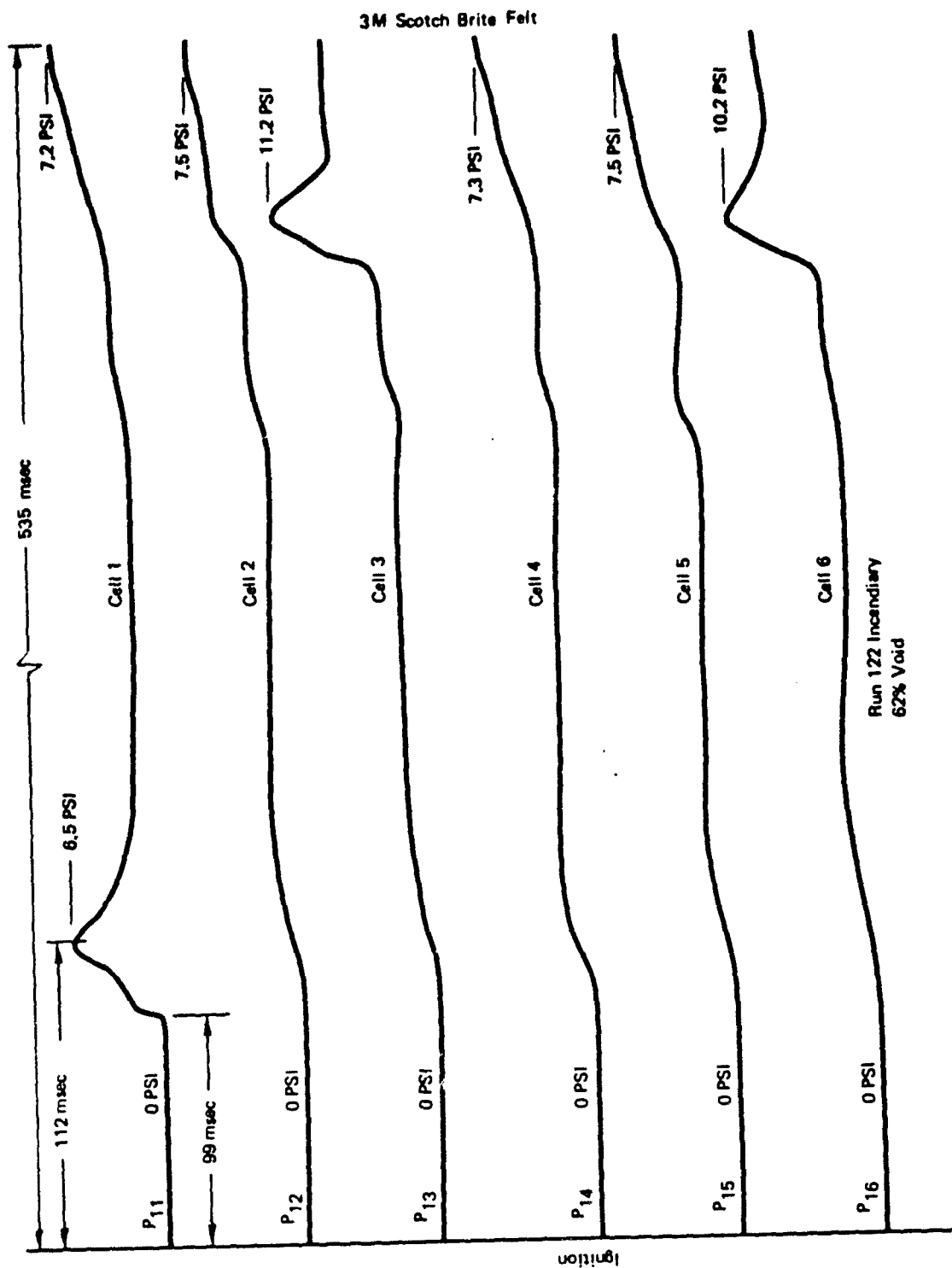


Figure C-19: Typical Pressure Trace for Small Wing Tankage Egg Crate Run 122

Run 122 Incendiary
62% Void

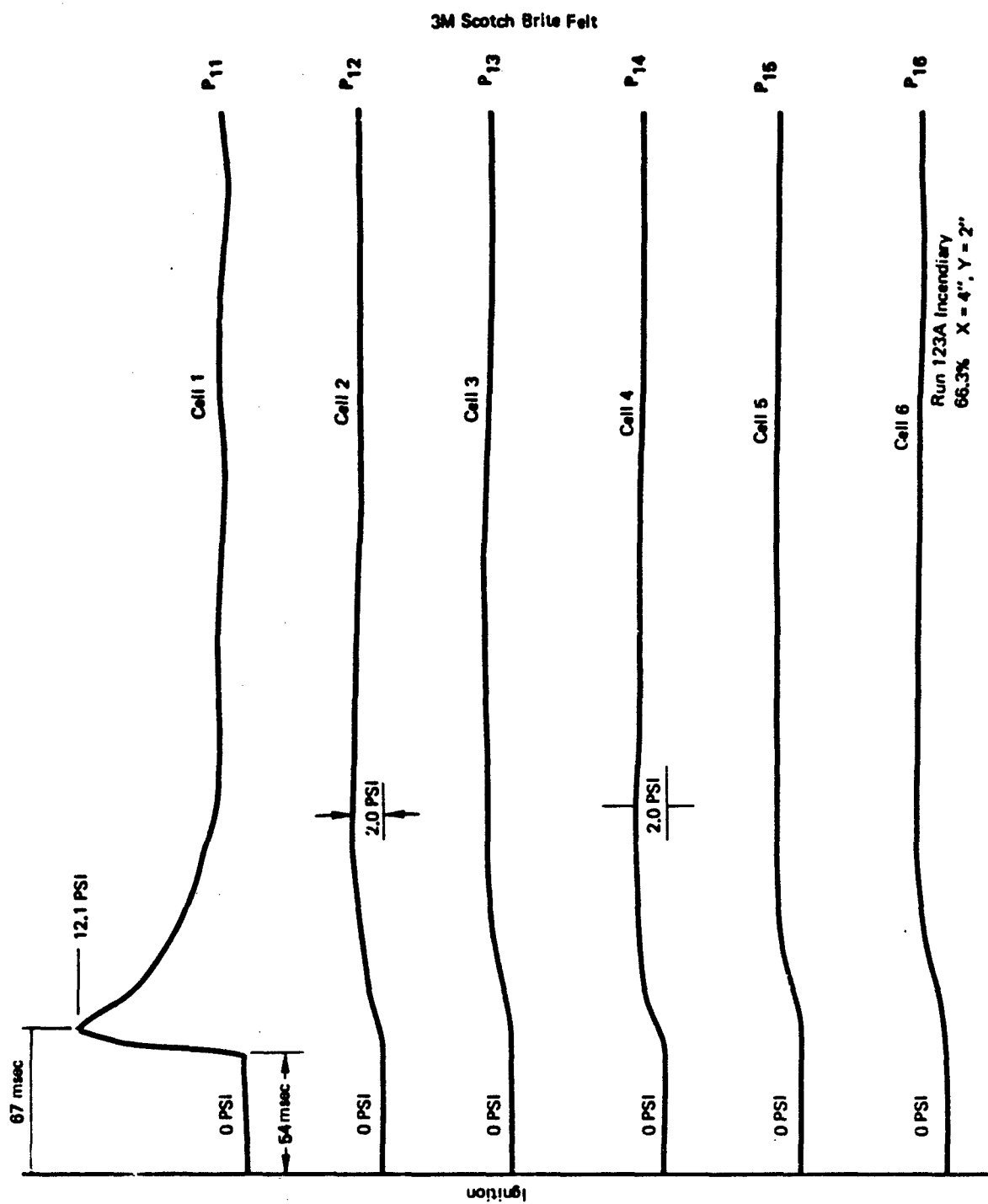


Figure C-20: Typical Pressure Trace for Small Wing Tank Voided Top Wall Run 123A

Run 123A Incendiary
66.3% X = 4", Y = 2"

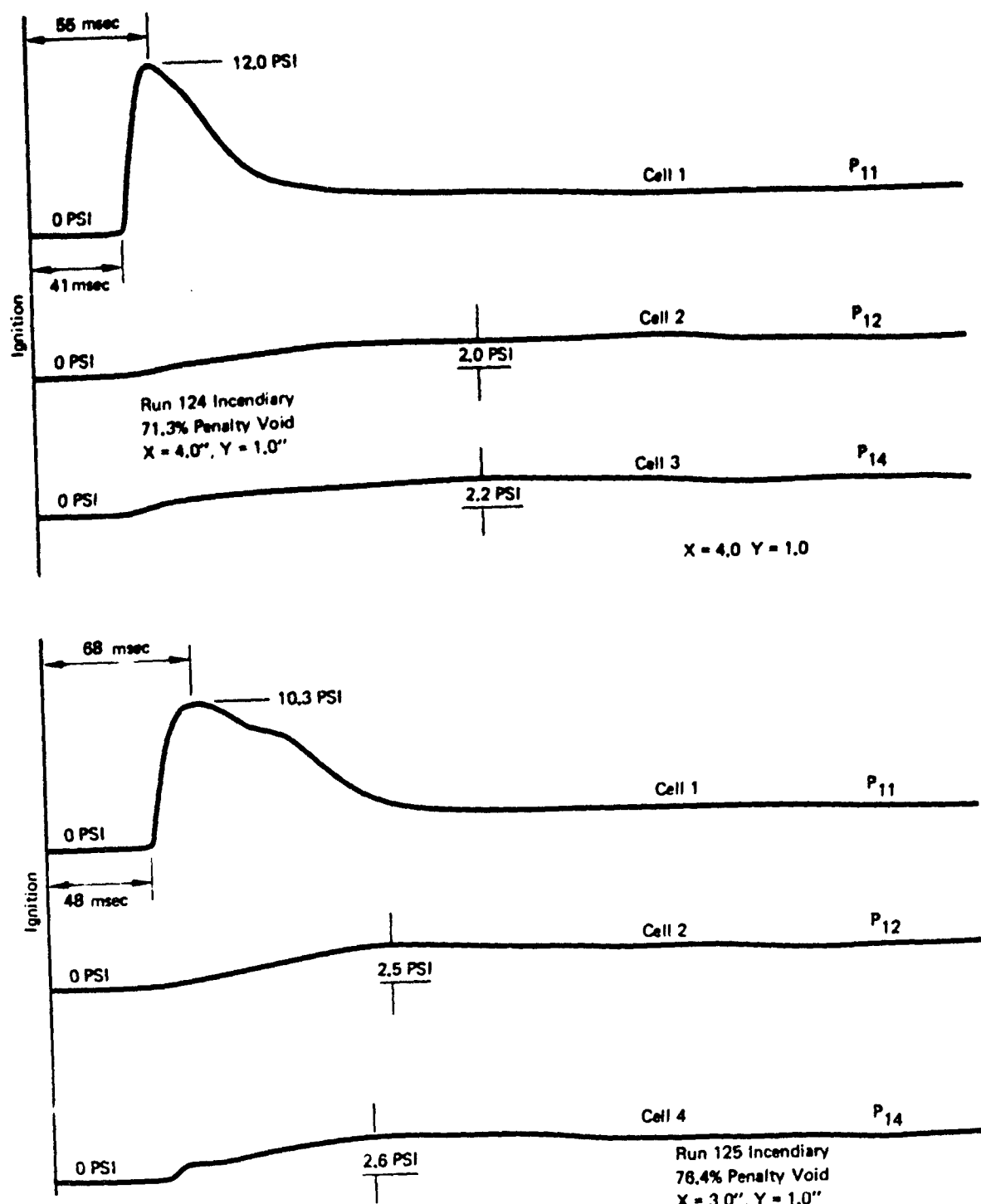
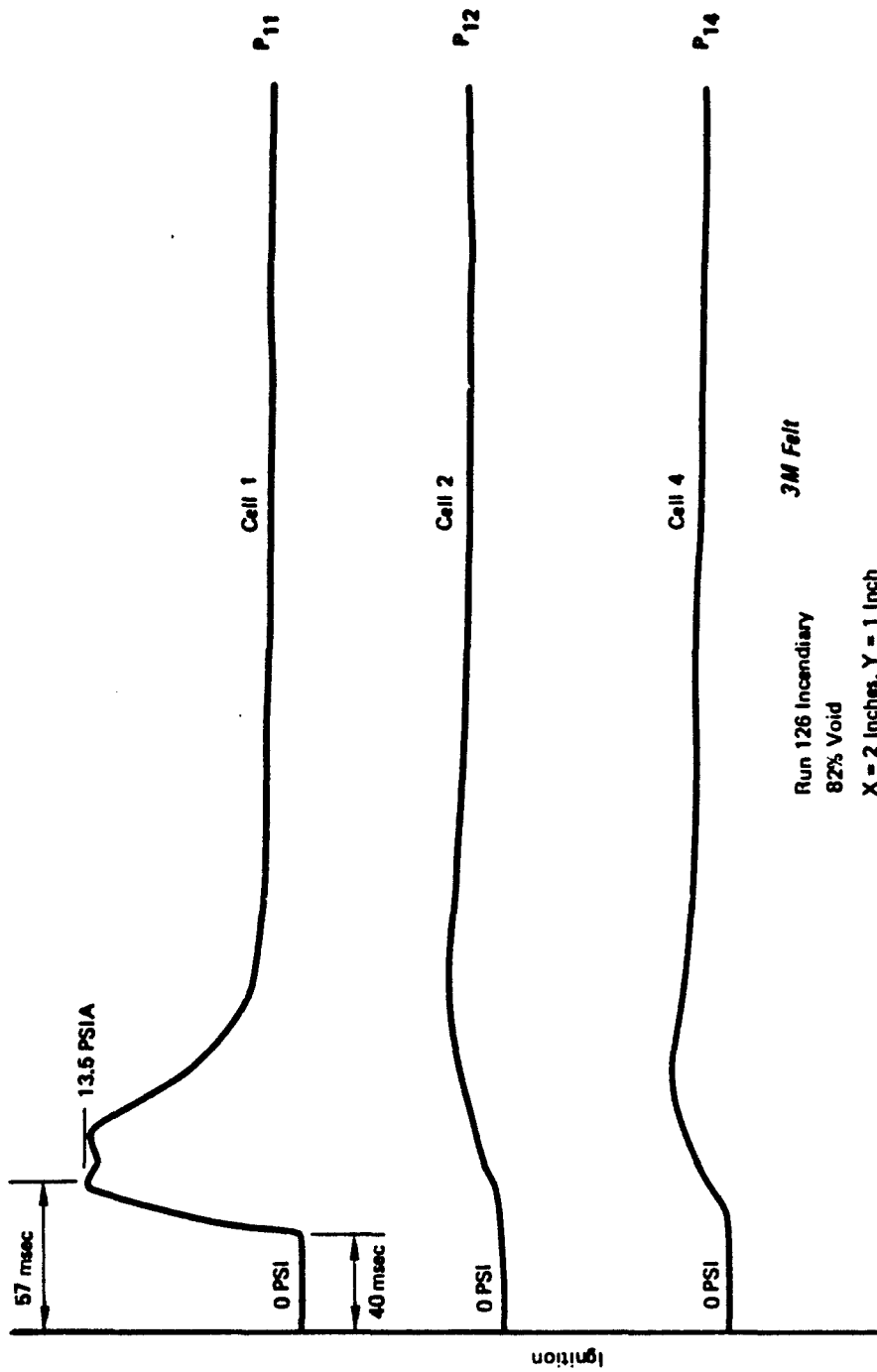


Figure C-21: Typical Pressure Trace for Small Wing Tank – Run 124 and 125 – 3M Felt – Voided Top Wall



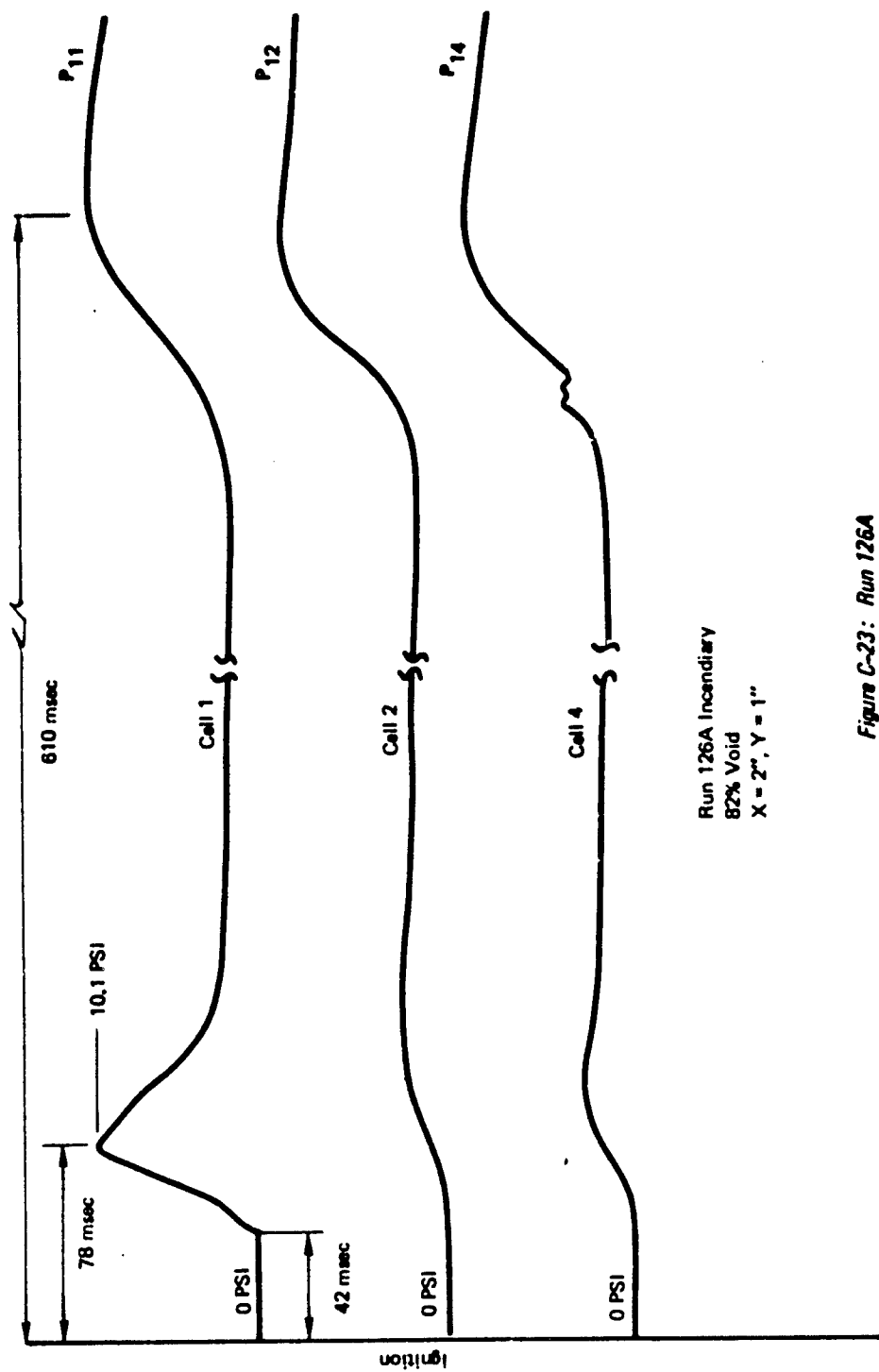
3M Felt

Run 126 Incendiary

82% Void

X = 2 Inches, Y = 1 Inch

Figure C-22: Typical Pressure Trace for Small Wing Tank Voided Top Wall
Run 126



Run 126A Incendiary
82% Void
X = 2", Y = 1"

Figure C-23: Run 126A

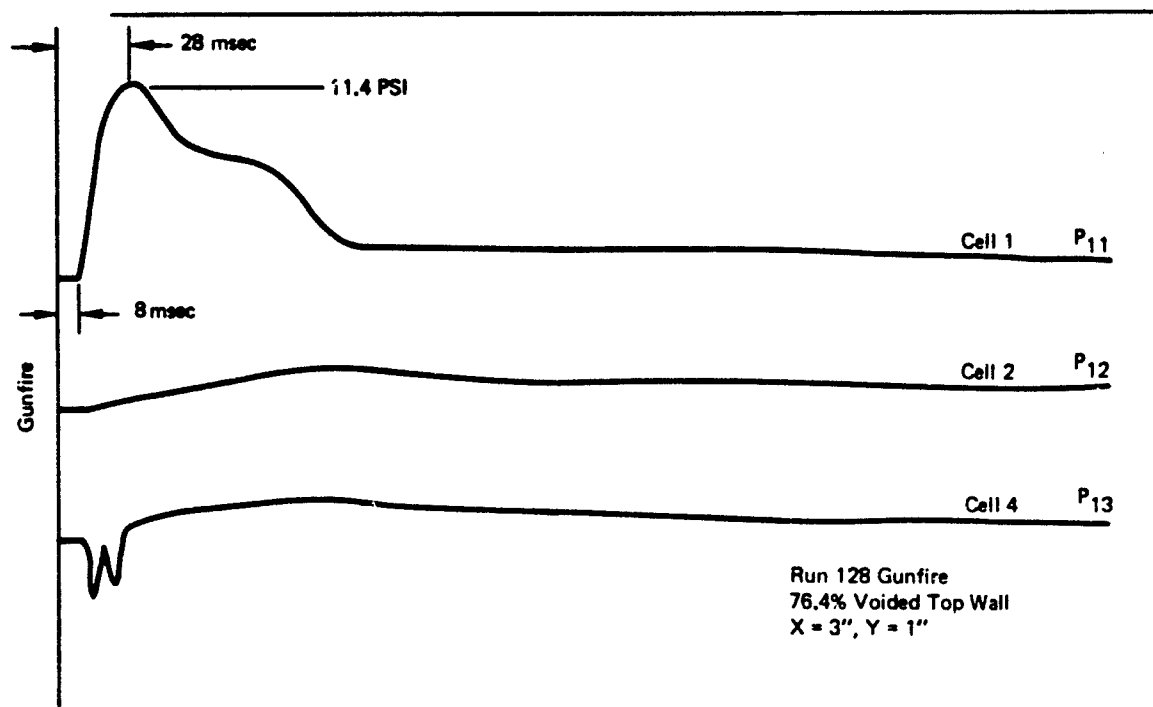
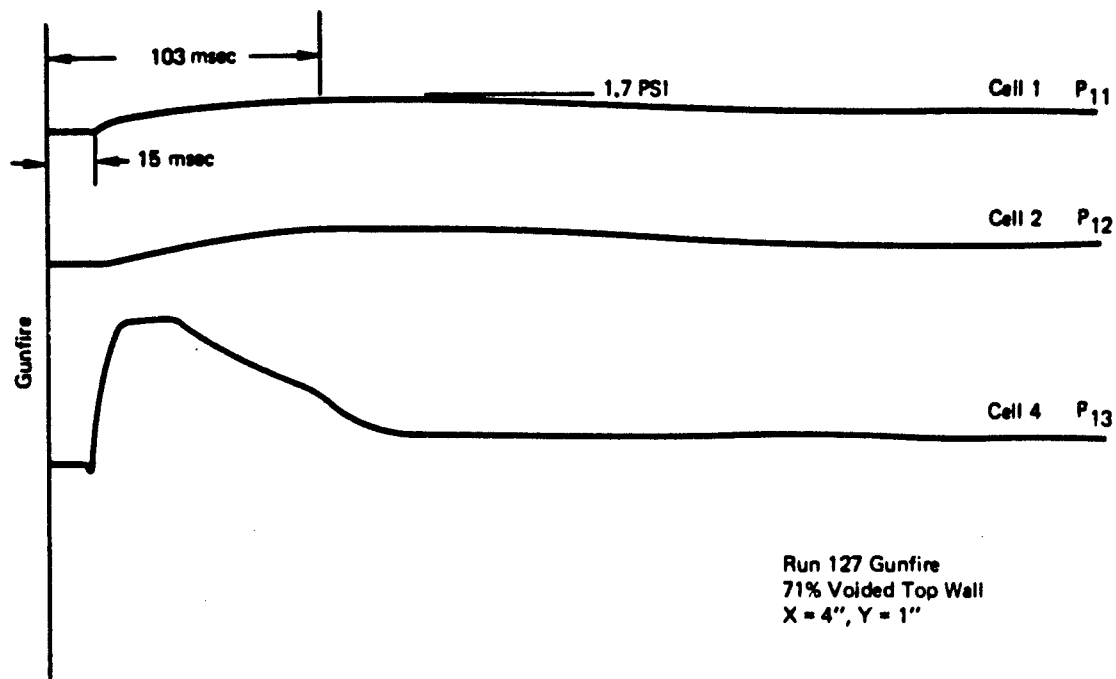


Figure C-24: Typical Pressure Trace for Small Wing Tank –
Run 127 and 128 – 3M Felt – Voided Top Wall

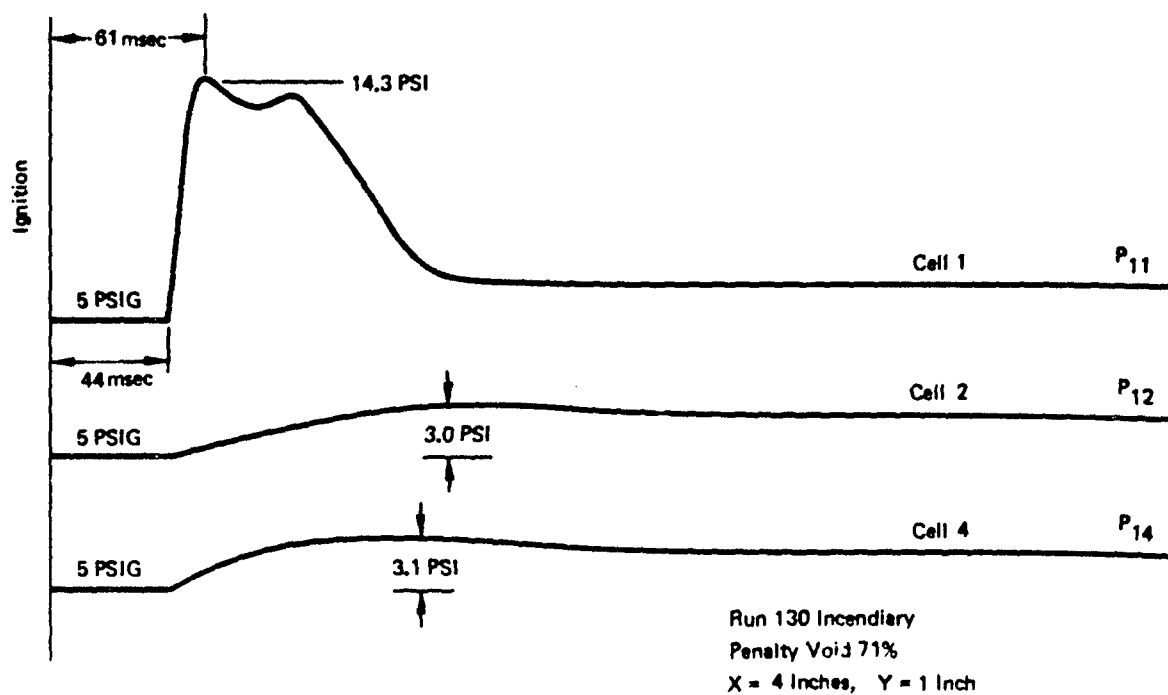
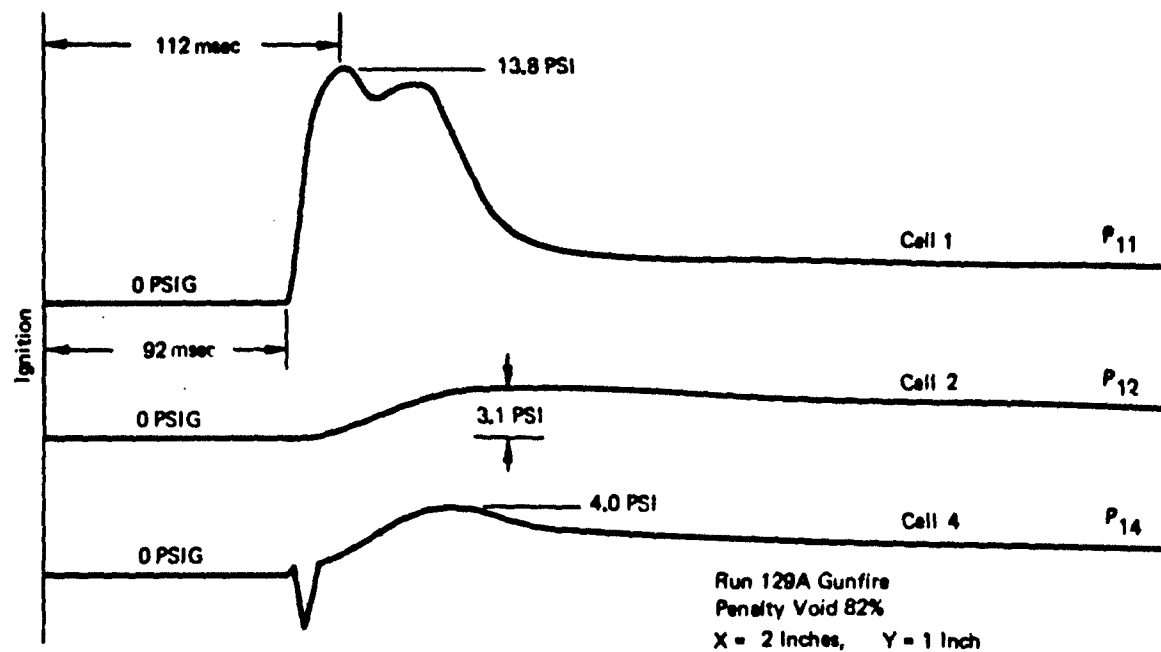


Figure C-25: Typical Pressure Trace for Small Wing Tank Run 129 and 130 3M Felt Voided Top Wall

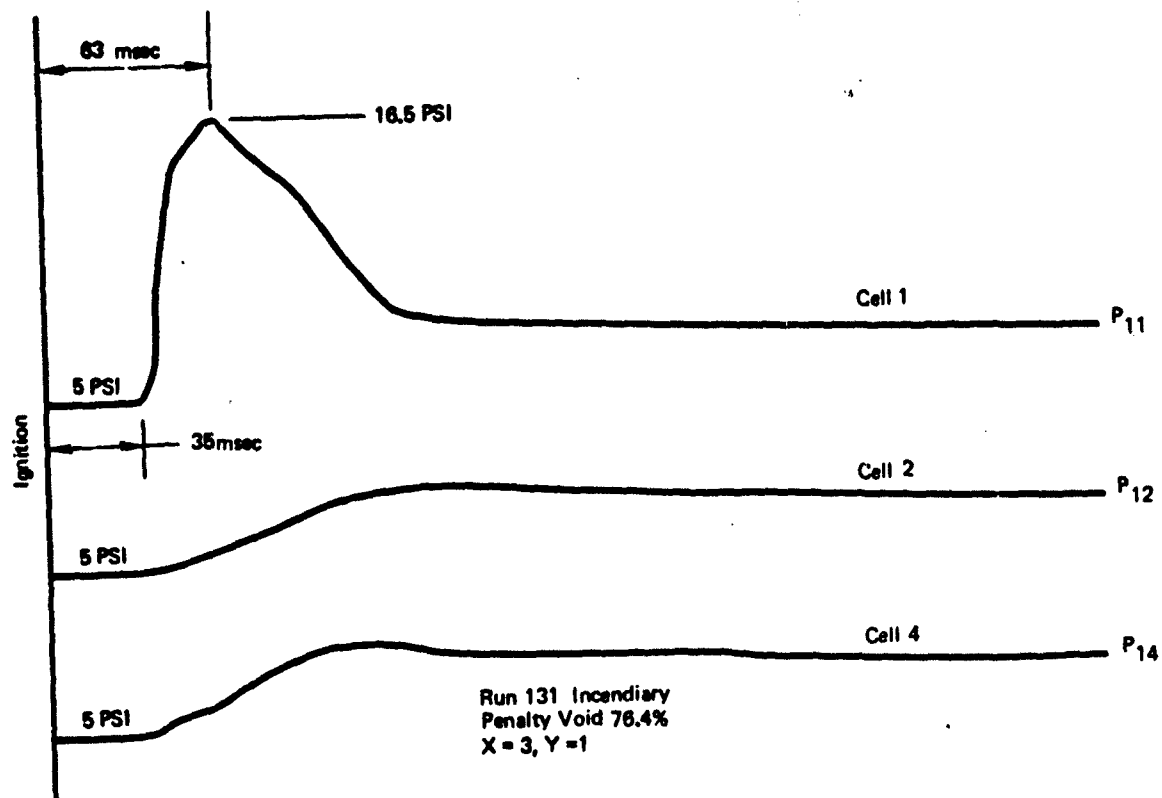


Figure C-26: Typical Pressure Trace for Small Wing Tank Run 131 3M Felt Voided Top Wall

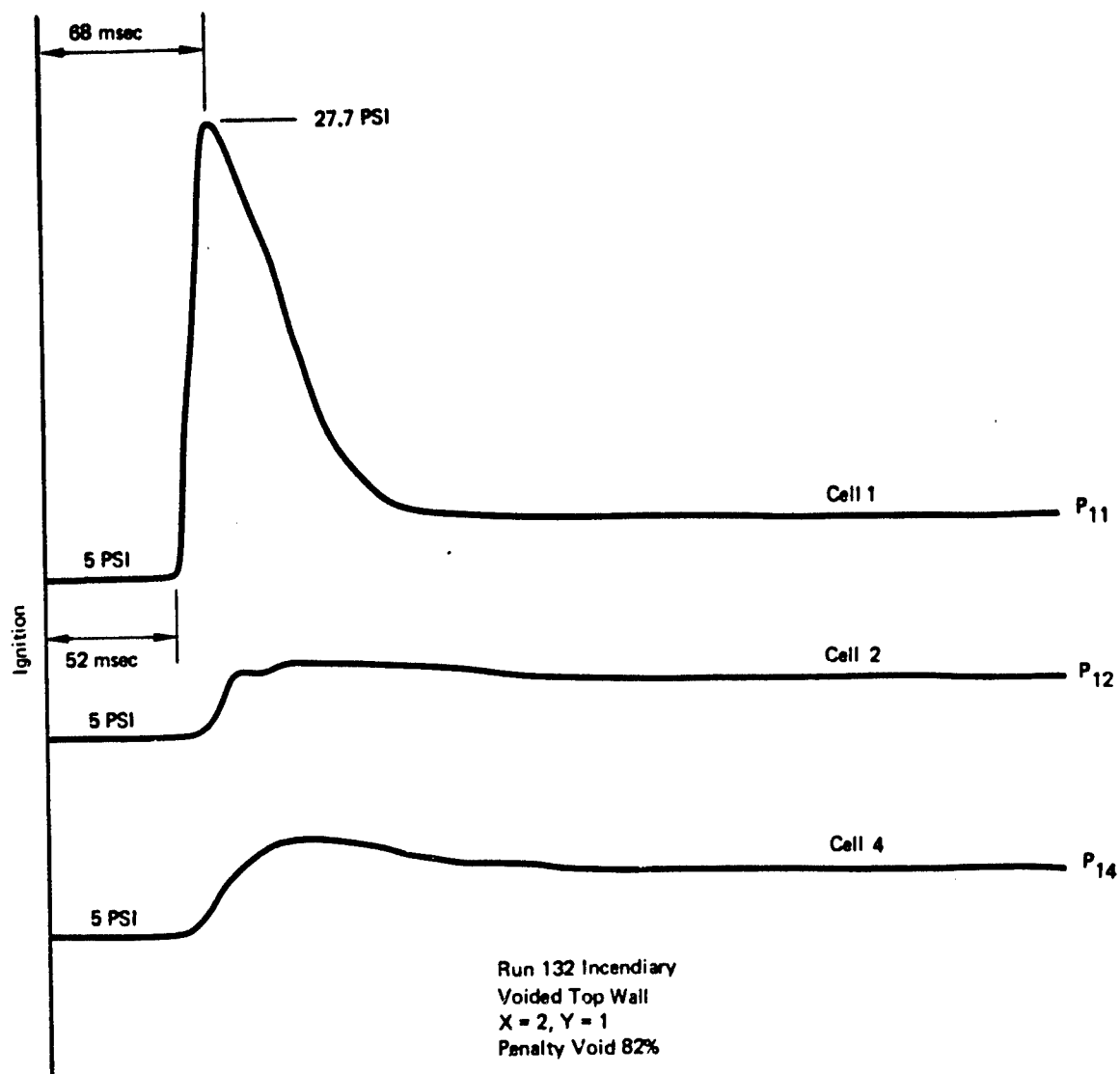


Figure C-27: Typical Pressure Trace for Small Wing Tank Run 132 3M Felt Voided Top Wall

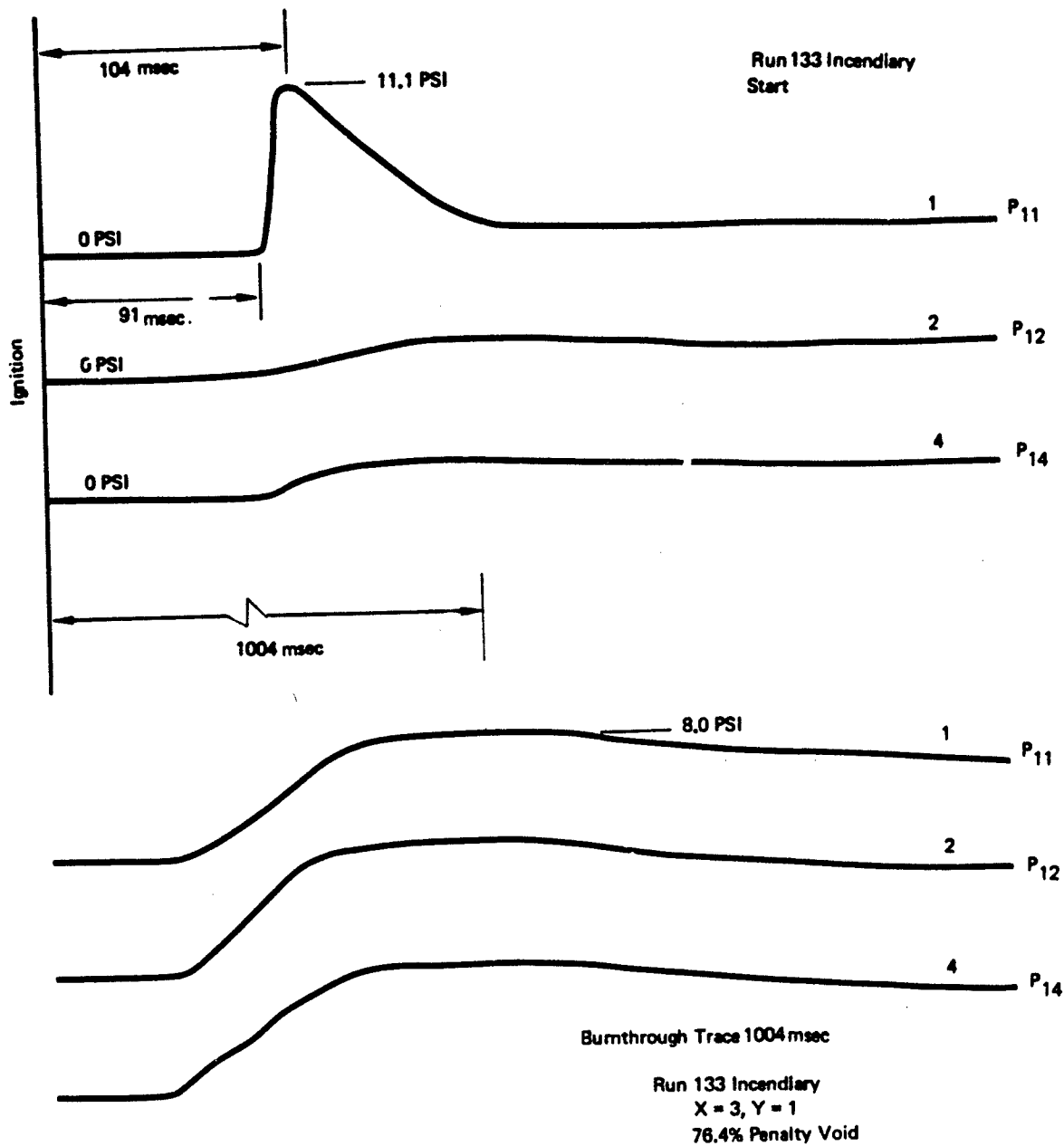


Figure C-28: Typical Pressure Trace for Small Wing Tank Run 133 25 PPI + Quartz Voided Top Wall

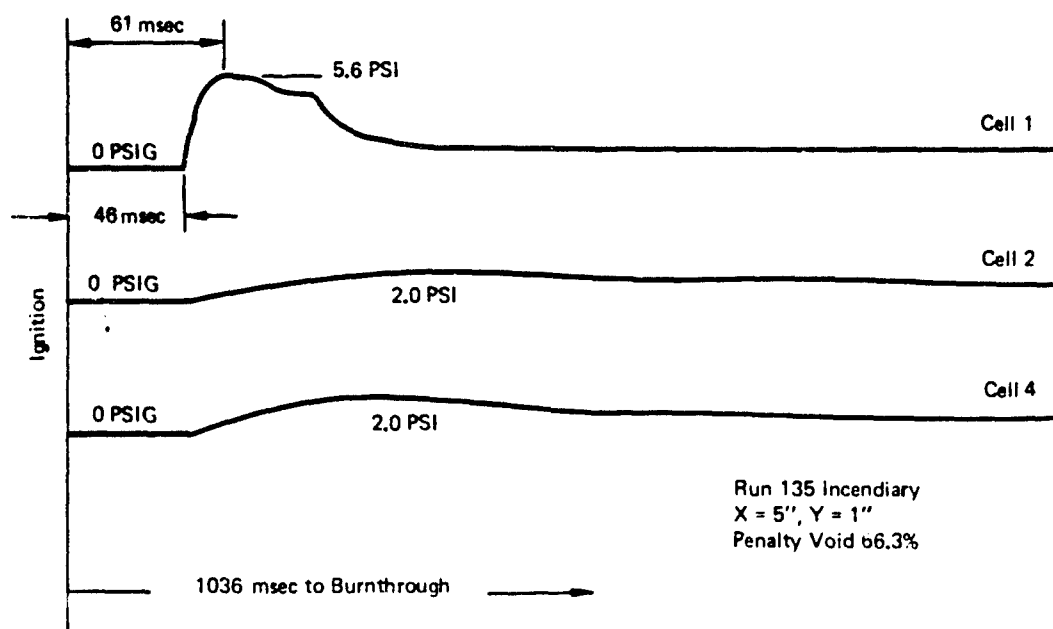
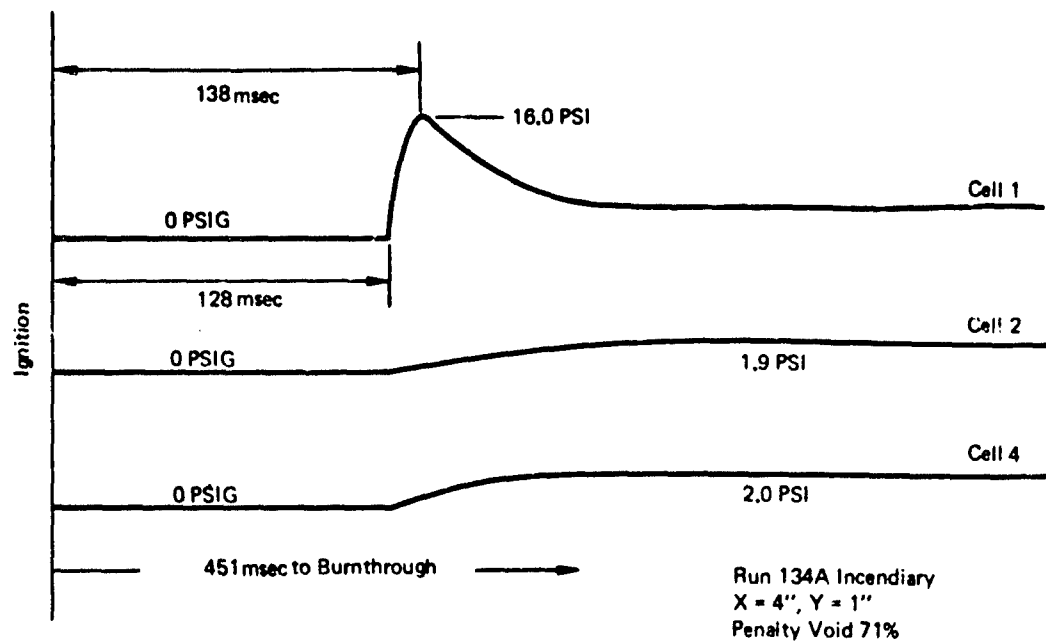


Figure C-29: Typical Pressure Trace for Small Wing Tank – Run 135 and 136
25 PPI + Quartz Voided Top Wall

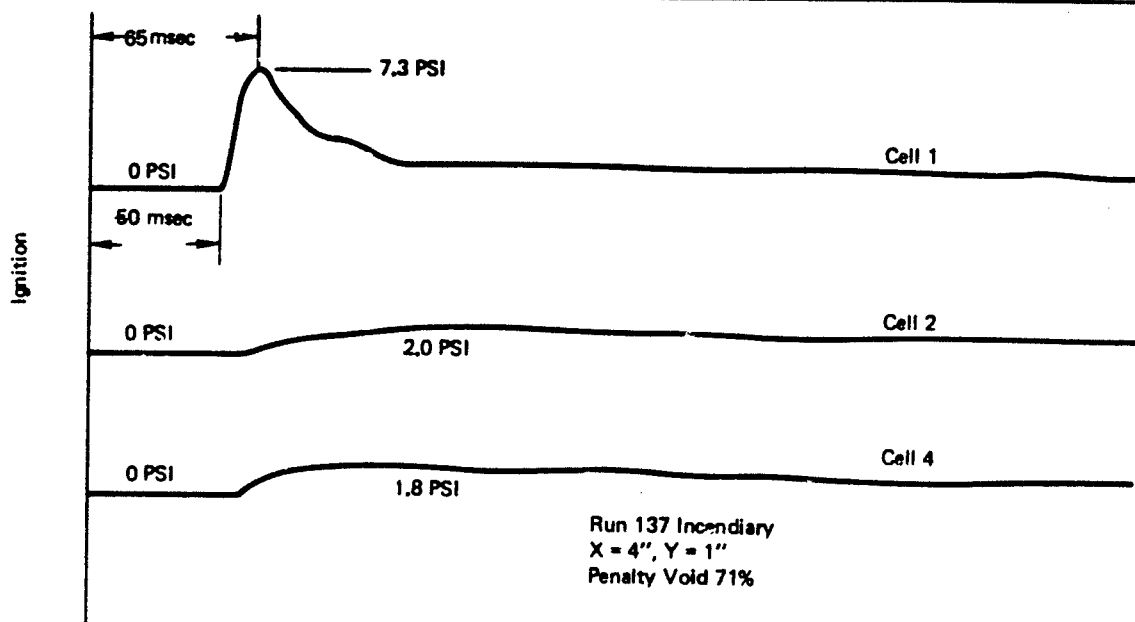
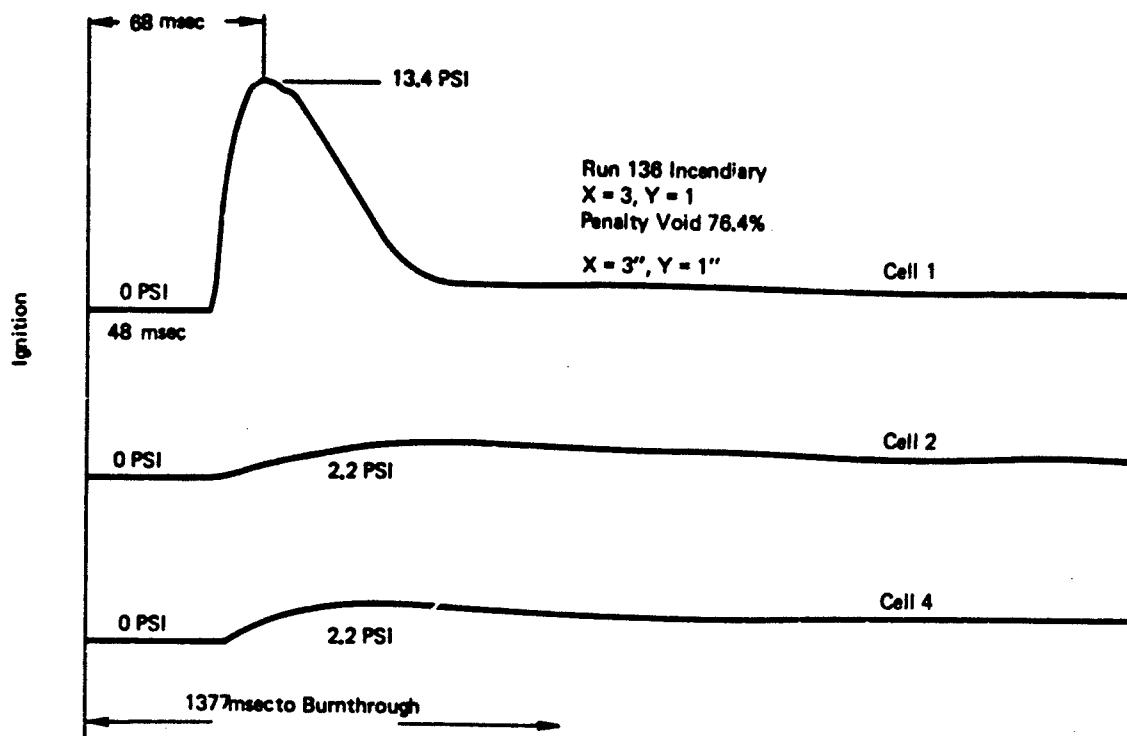


Figure C-30: Typical Pressure Trace Small Wing Tank Voided Top Wall -
25 PPI Foam + 2 Layers Stainless Steel Screen

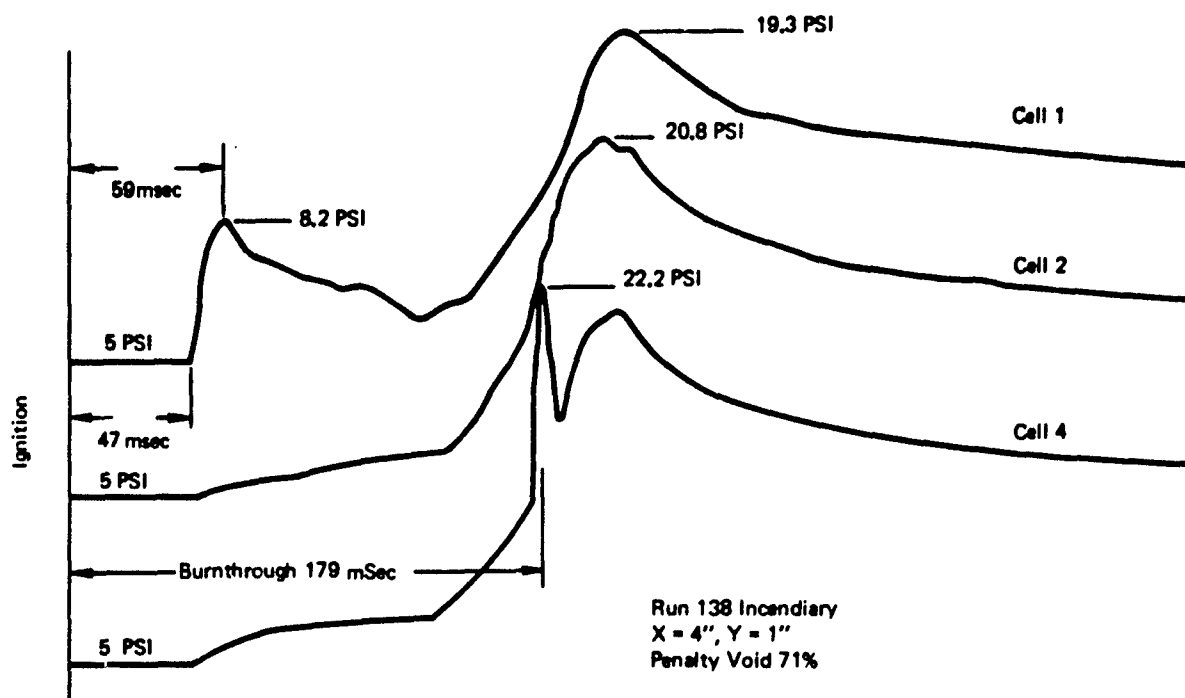


Figure C-31: Typical Pressure Trace Small Wing Tank V.T.W.
25 PPI Foam + 2 Layers Screen

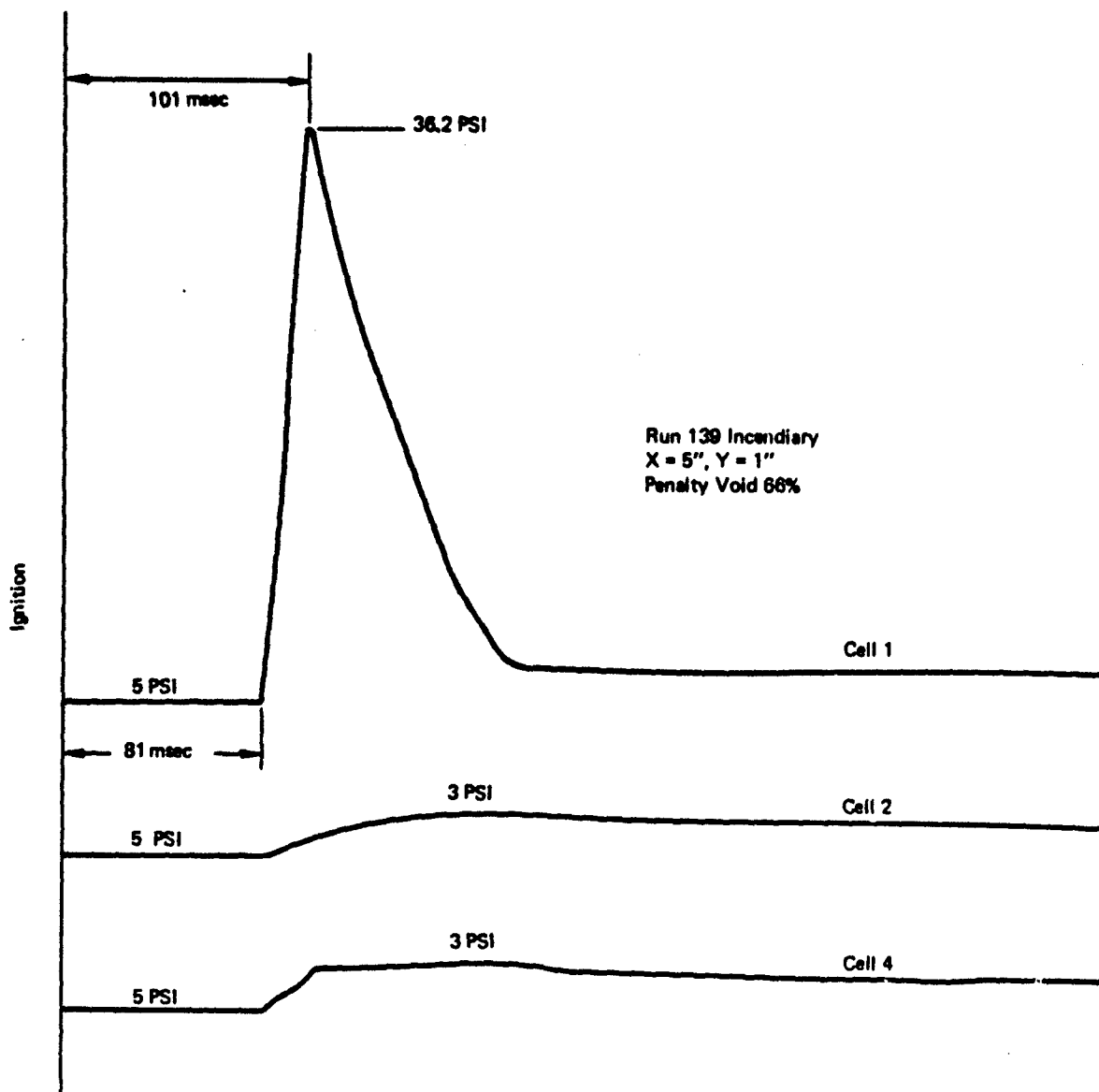


Figure C-32: Typical Pressure Trace Small Wing Tank V.T.W.
25 PPI Foam + 2 Layers Screen

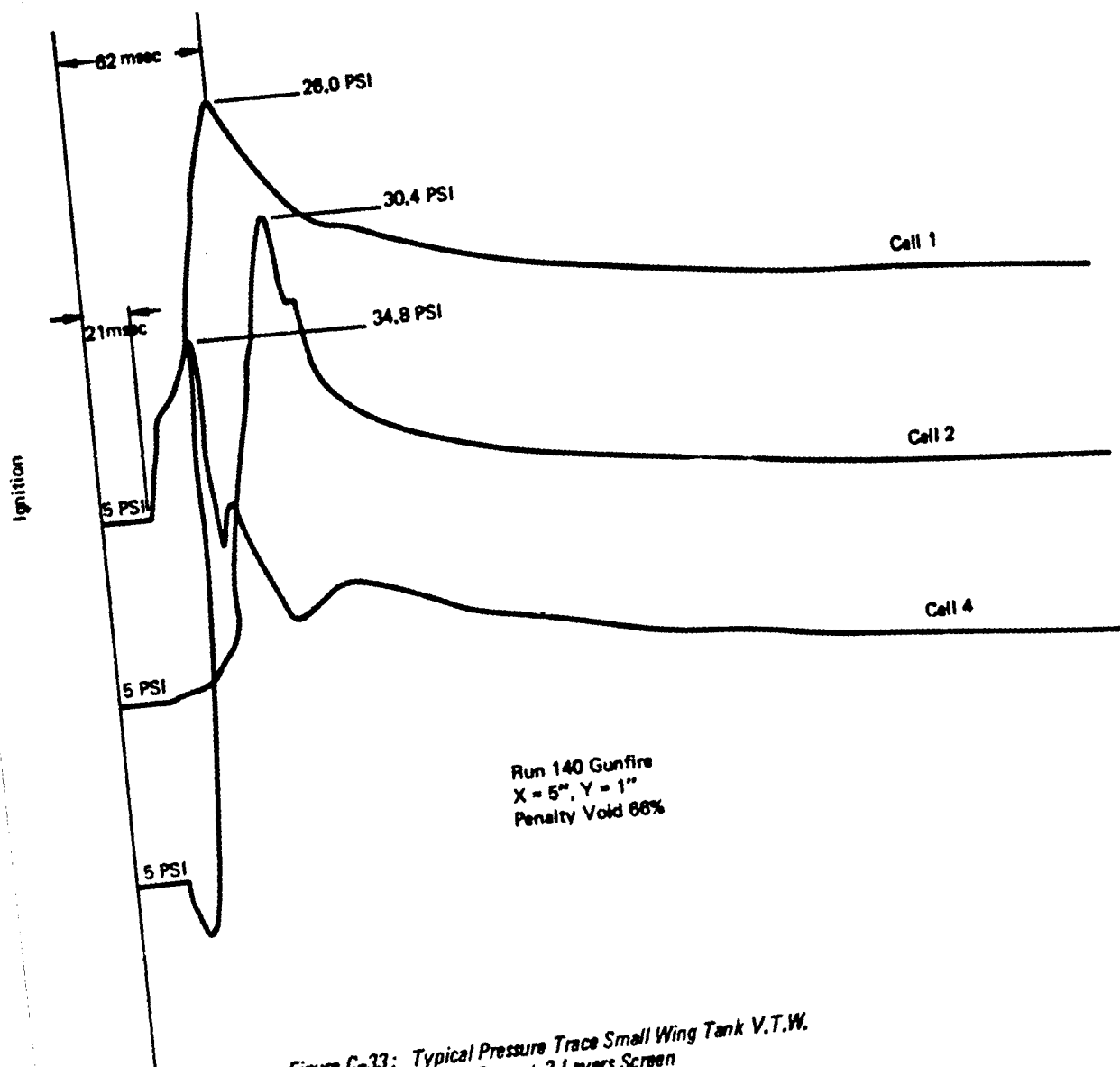


Figure C-33: Typical Pressure Trace Small Wing Tank V.T.W.
25 PPI Foam + 2 Layers Screen

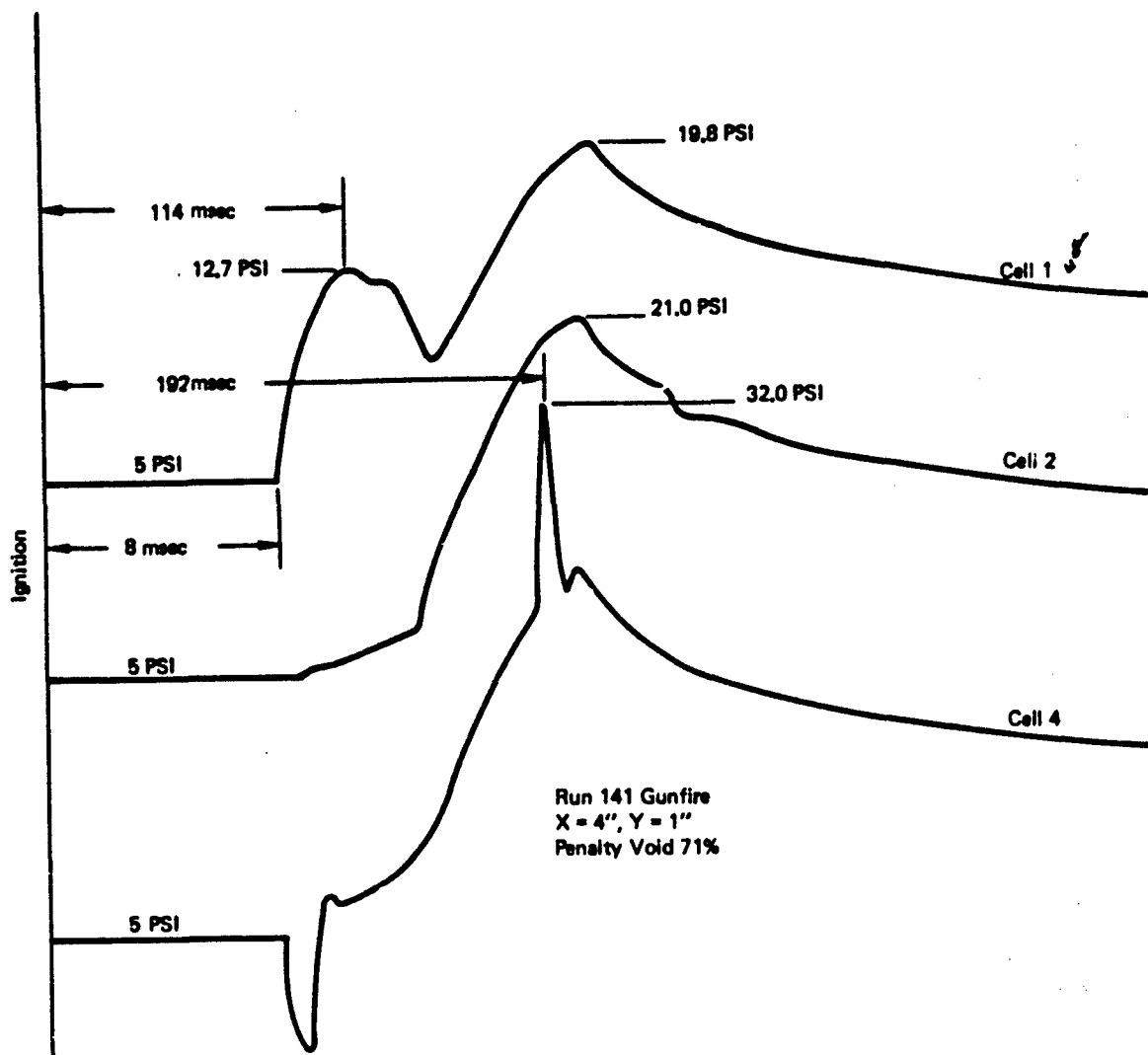


Figure C-34: Typical Pressure Trace Small Wing Tank V.T.W. -
25 PPI Foam + 2 Layers Screen

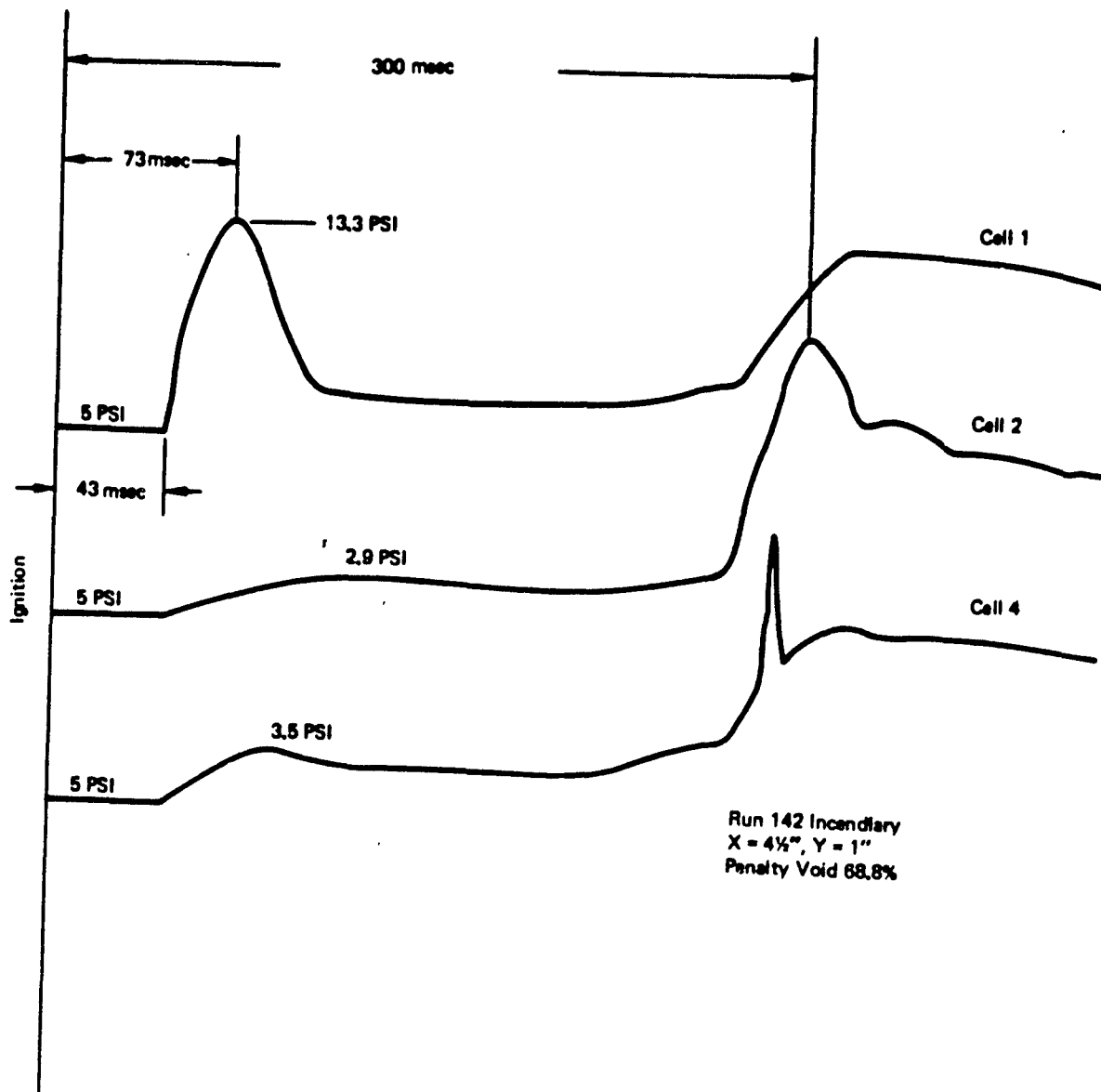


Figure C-35: Typical Pressure Trace Small Wing Tank V.T.W. -
25 PPI Foam + 2 Layers Screen

[illegible]

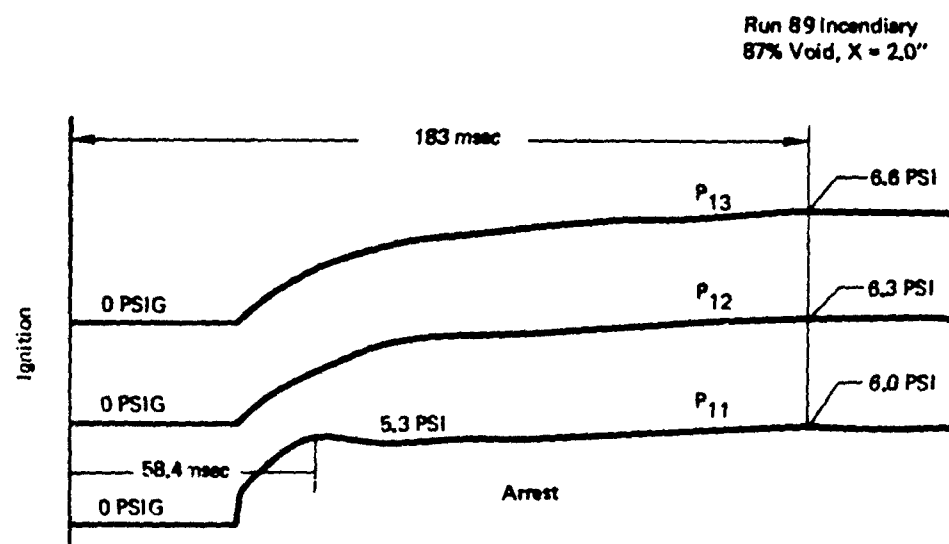
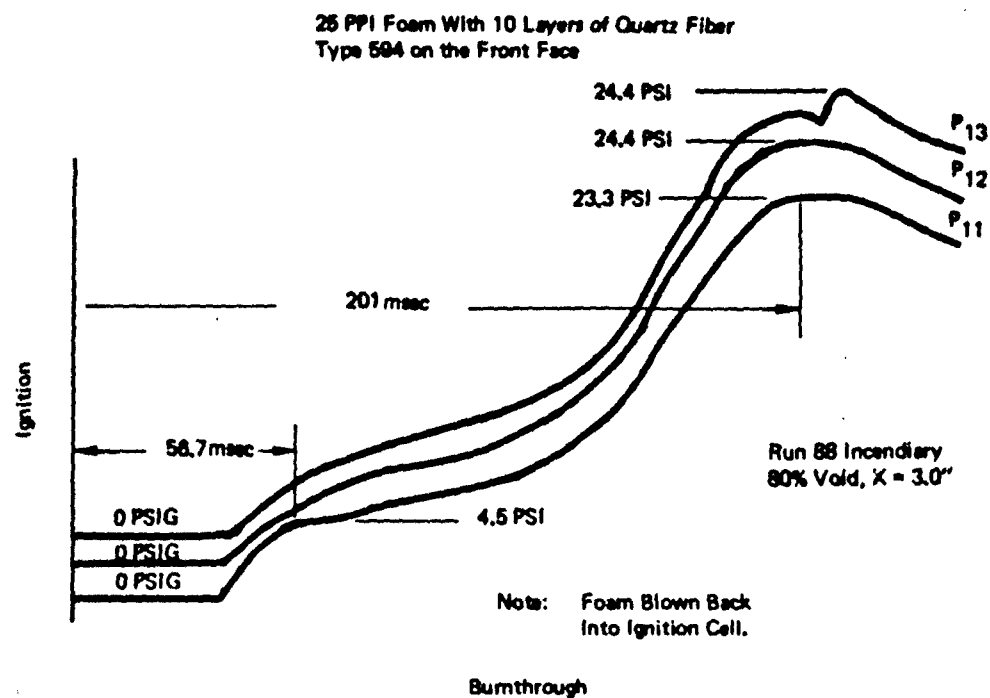
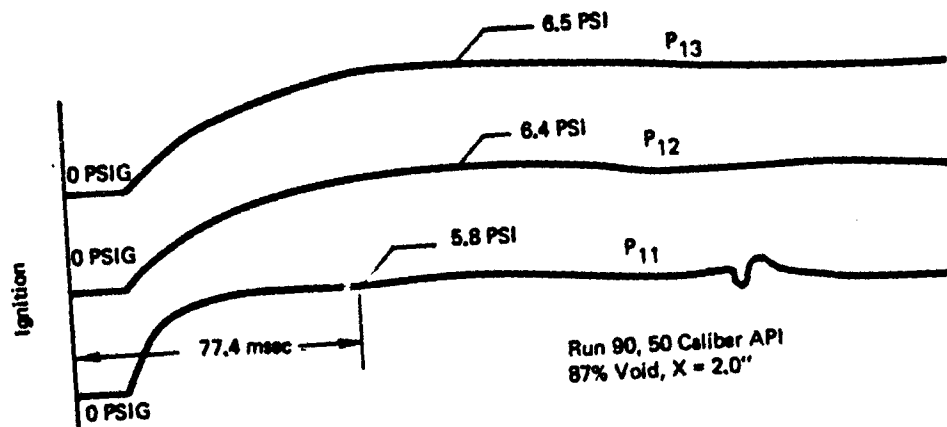


Figure C-36: Typical Pressure Traces for Large Wing Tank
Lined Well - Runs 88 and 89

25 PPI Foam With 10 Layer of Quartz Fiber
Type 594 on the Front Face



Run 90 (Continued)

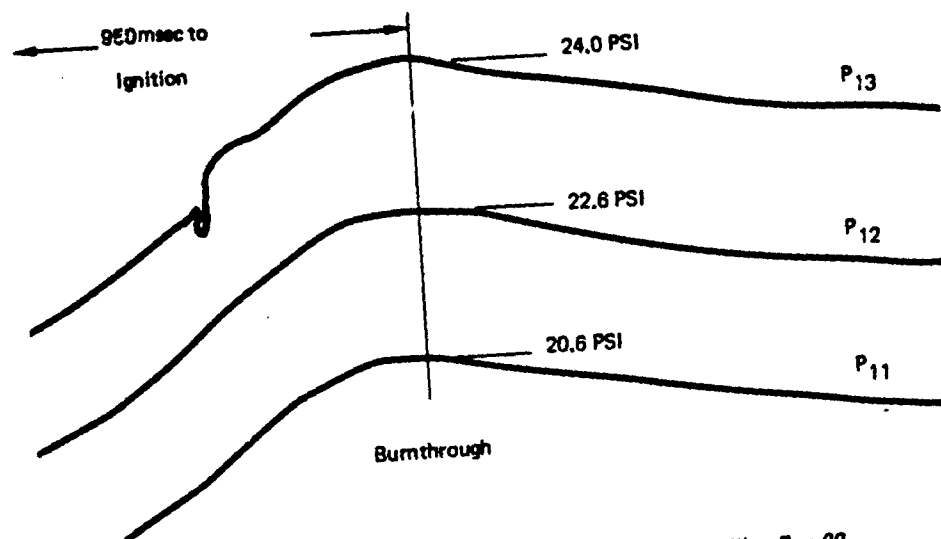


Figure C-37: Typical Pressure Traces for Large Wing Tank (Lined Wall) - Run 90

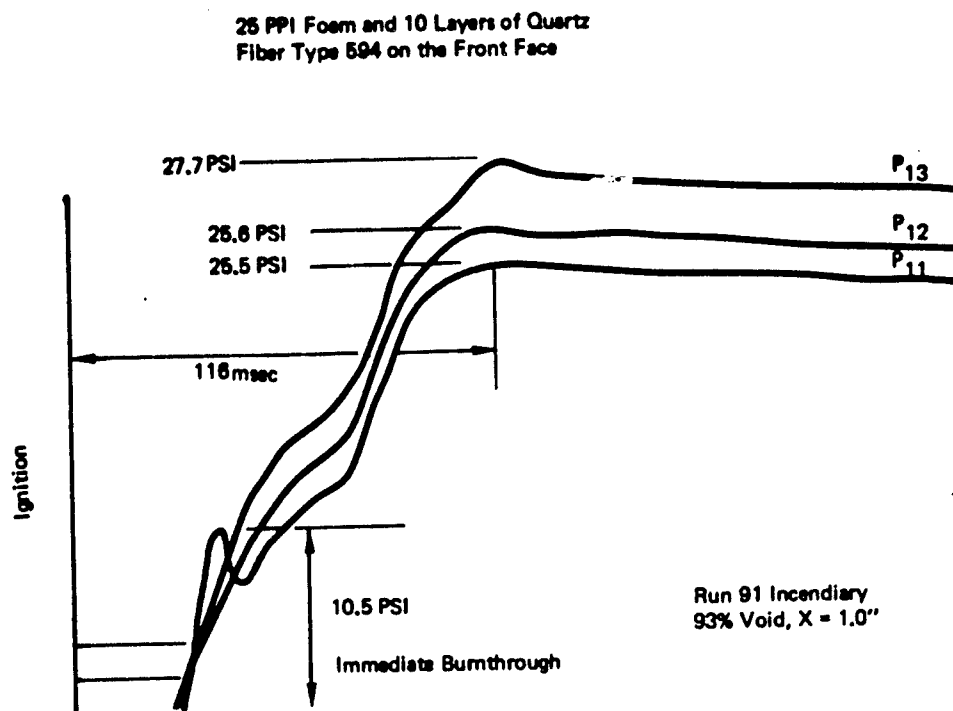


Figure C-38: Typical Pressure Traces for Large Wing Tank Lined Wall
Run 91

3M Scotch Brite Felt

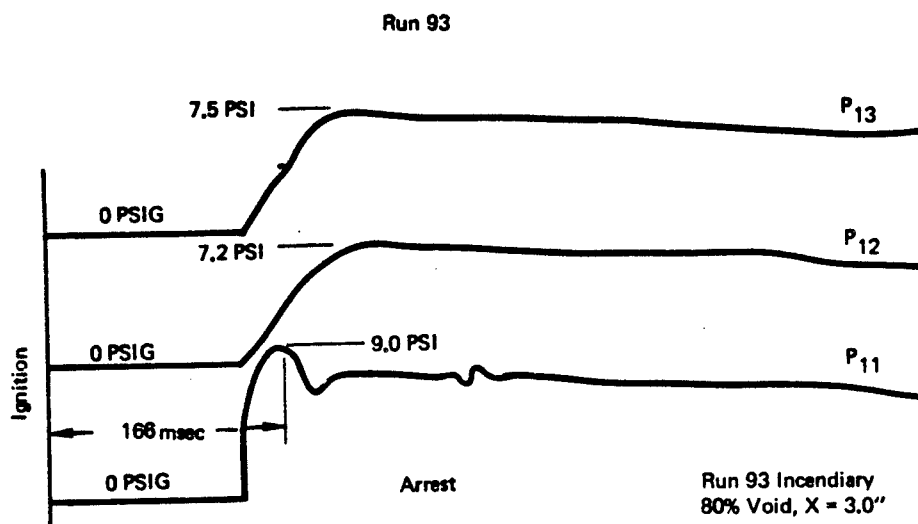
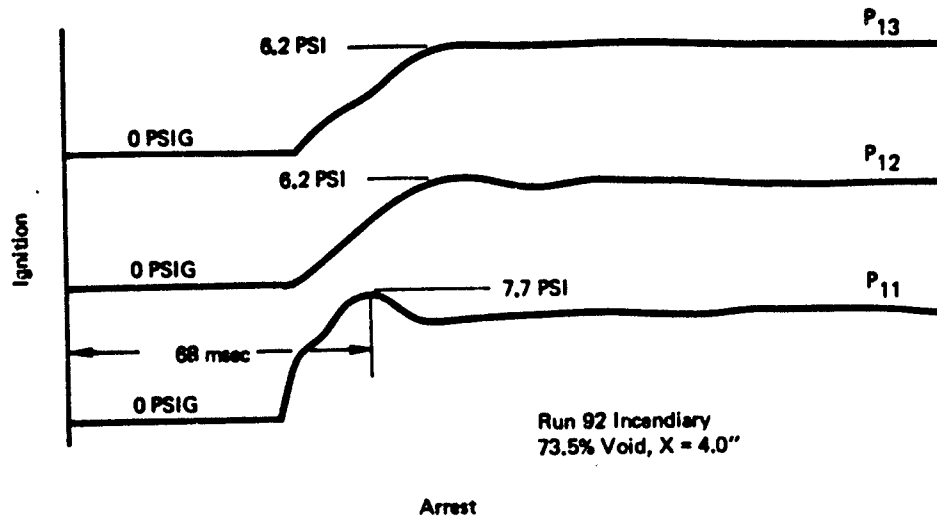


Figure C-39: Typical Pressure Traces for Large Wing Tank Lined Wall –
Runs 92 and 93

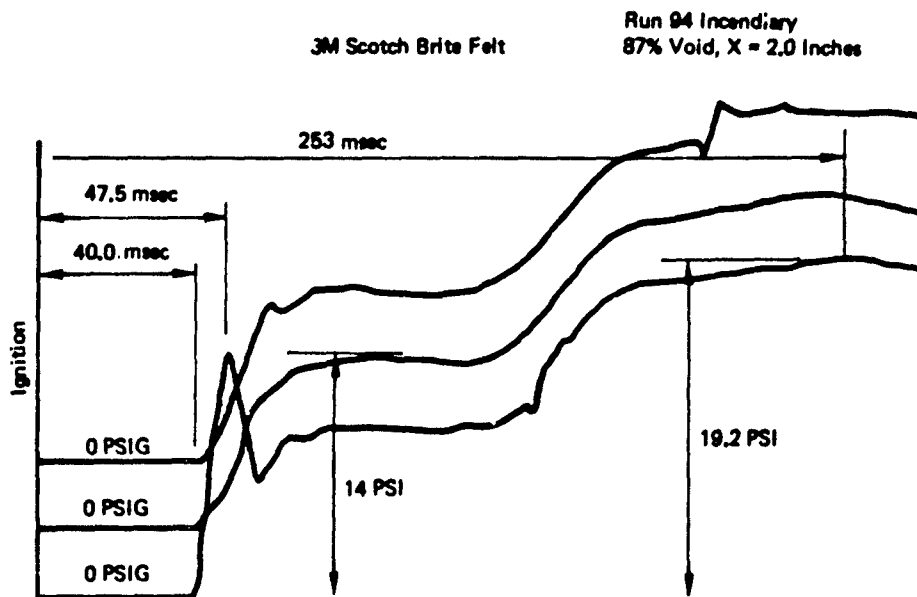


Figure C-40: Typical Pressure Traces for Large Wing Tank Lined Wall - Run 94

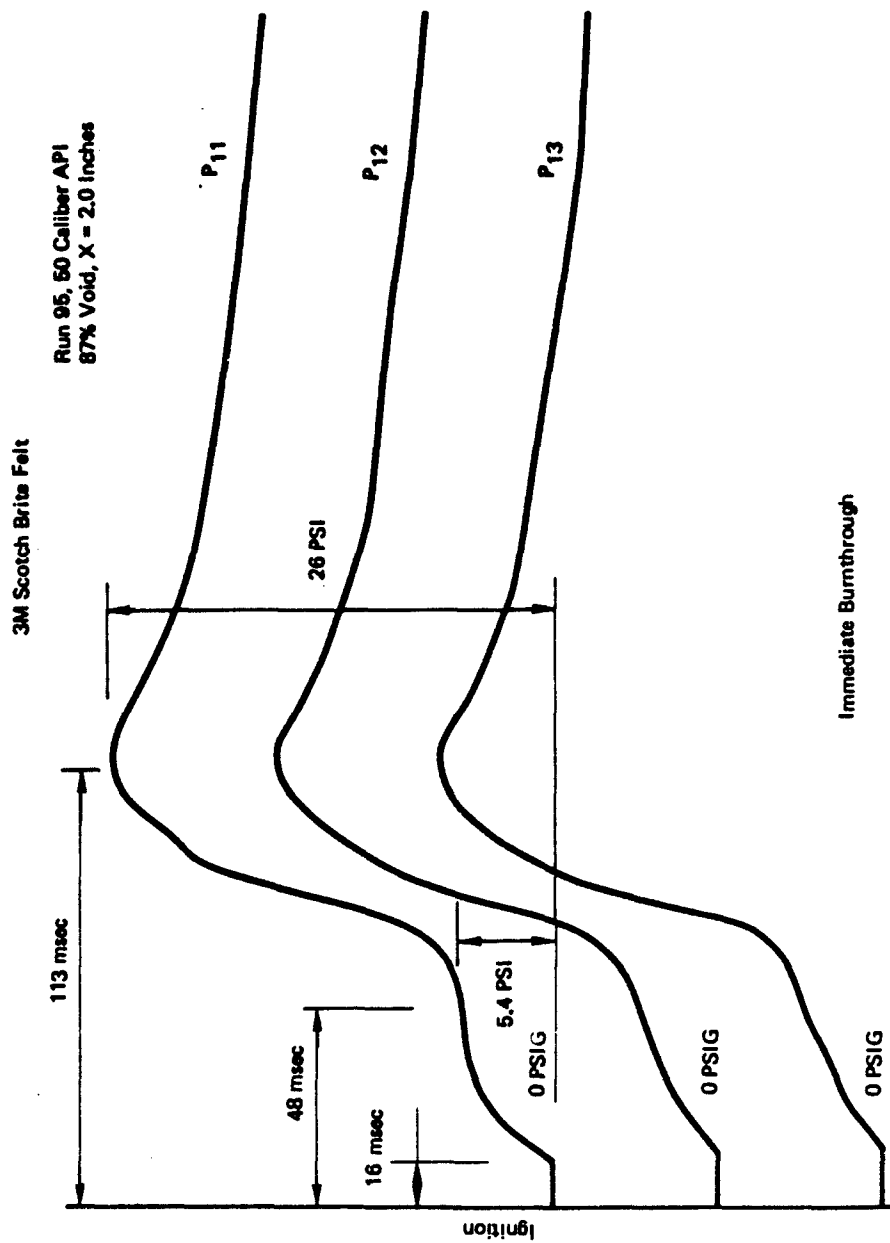


Figure C-41: Typical Pressure Traces for Large Wing Tank Lined Wall - Run 95

2 Layers of 20 Mesh-016 Stainless Steel Screen with 10 Layers of
Quartz Fiber Type 594 on the Front Face

Run No. 96 Incendiary
99% Void, $X = 0.25$

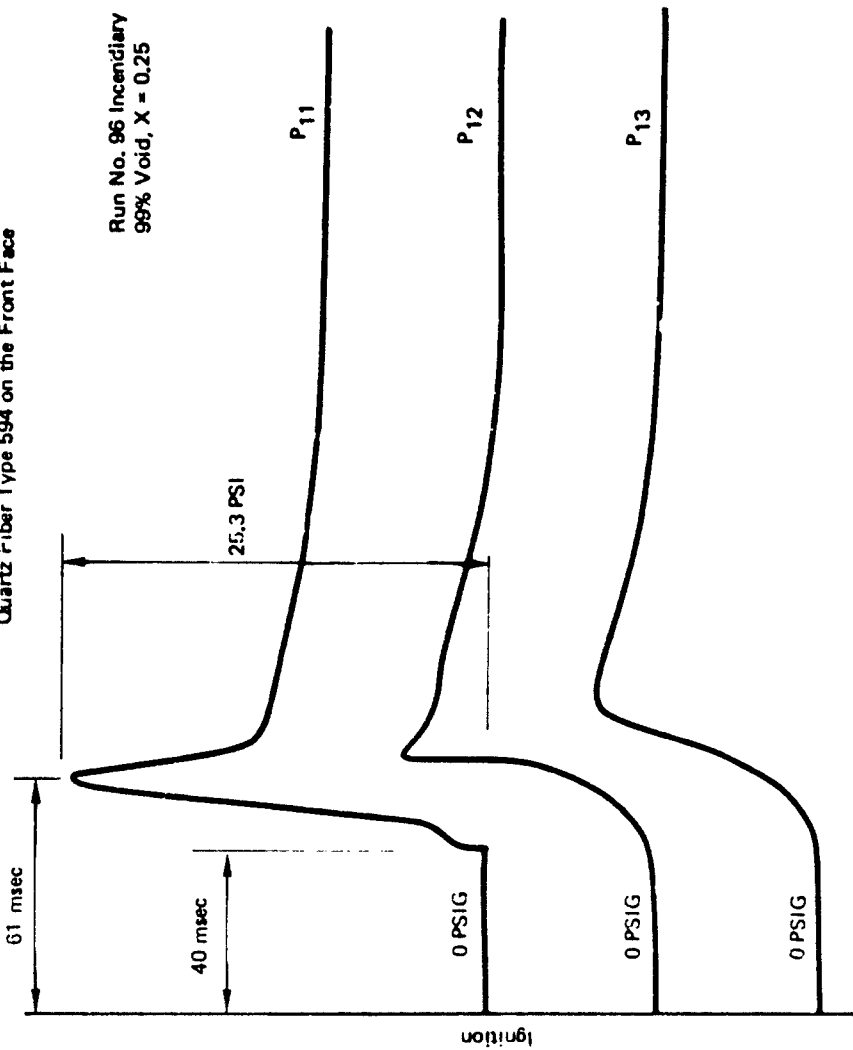


Figure C-42: Typical Pressure Traces for Large Wing Tank Lined Wall - Run 96

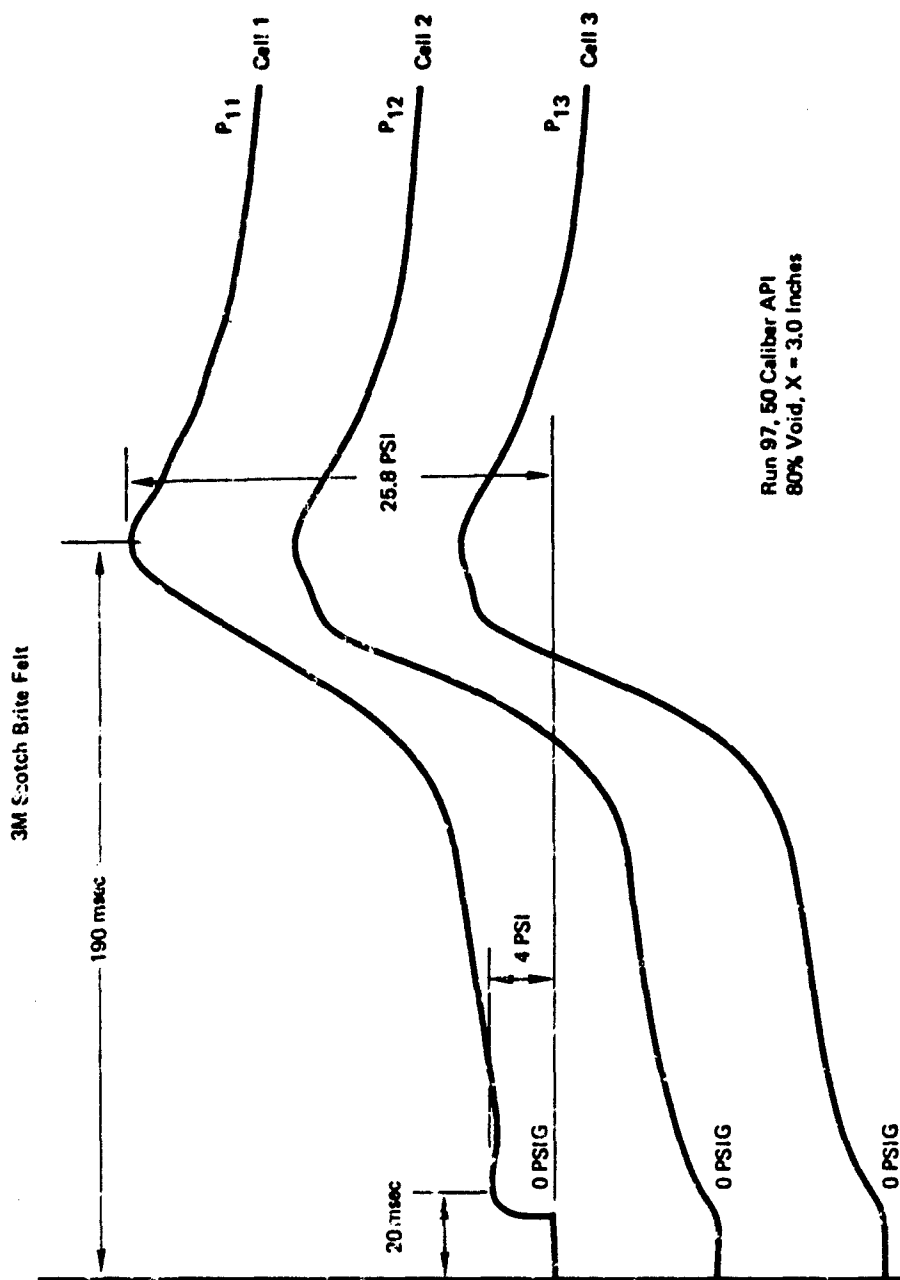


Figure C-43: Typical Pressure Traces for Large Wing Tank Lined Wall - Run 97

REFERENCES

1. Advanced Flame Arrester Materials and Techniques for Fuel Tank Protection AFAPL-TR-72-12, Quentin C. Malmberg, Edwin W. Wiggins, Contract F33615-71-C-1191, Project No. 3048, March 1972
2. Evaluation of a Reticulated Polyurethane Foam as a Flame Arrester in Airplane Vent Systems, D6-58406-1, Russell Laustsen, et al, May 1969 (The Boeing Company)
3. Incendiary Gunfire Simulation Techniques For Fuel Tank Explosion Protection Testing, AFAPL-TR-73-50; A.J. Ferrenberg, E.E. Ott; July 1973
4. Unique Fibrous Flame Arresters Materials for Explosion Protection, Ralph L. Hough and Marold W. Lavy, Technical Report AFAPL-TR-72-108, December 1972
5. Prediction of Flame Velocities of Hydrocarbon Flames, Report 1158 NACA, Gordon L. Digger and Dorothy M. Simon
6. Organ-pipe Oscillations in a Flame Filled Tube, Abbott A. Putnam and William R. Dennis
7. Gaseous and Dust Explosion Venting, Part I and 2, H. R. Maisey, A.M.I.E.E., Chemical and Process Engineering, October 1965
8. Technical Data on Fuel, H. M. Spiers
9. Space Lattice Wing Base Development Program, D-180-15047-1, Boeing Aerospace Company June, 1972
10. Air Force Technical Order T.O. 11A-1-34, Military Explosives
11. Combustion Flames and Explosions of Gases, Bernard Lewis and Guenther von Elbe
12. The Dynamics and Thermodynamics of Compressible Flow, Ascher H. Shapiro, page 206
13. Fluid Flow Through Randomly Packed Columns and Fluidized Beds, Sabri Ergun and A. A. Corning, Industrial and Engineering Chemistry, Vol. 41, June 1949, Page 1179